

# Annual Report

## Photovoltaic Subcontract Program FY 1992

K. A. Summers, Coordinator



National Renewable Energy Laboratory  
1617 Cole Boulevard  
Golden, Colorado 80401-3393  
Operated by Midwest Research Institute  
For the U.S. Department of Energy  
under Contract No. DE-AC02-83CH10093

Prepared under Task No. PV310101

March 1993

**MASTER**

## NOTICE

This report was prepared as an account of work sponsored by an agency of the United States government. Neither the United States government nor any agency thereof, nor any of their employees, makes any warranty, express or implied, or assumes any legal liability or responsibility for the accuracy, completeness, or usefulness of any information, apparatus, product, or process disclosed, or represents that its use would not infringe privately owned rights. Reference herein to any specific commercial product, process, or service by trade name, trademark, manufacturer, or otherwise does not necessarily constitute or imply its endorsement, recommendation, or favoring by the United States government or any agency thereof. The views and opinions of authors expressed herein do not necessarily state or reflect those of the United States government or any agency thereof.

Printed in the United States of America

Available from:

National Technical Information Service

U.S. Department of Commerce

5285 Port Royal Road

Springfield, VA 22161

Price: Microfiche A01

Printed Copy A15

Codes are used for pricing all publications. The code is determined by the number of pages in the publication. Information pertaining to the pricing codes can be found in the current issue of the following publications which are generally available in most libraries: *Energy Research Abstracts (ERA)*; *Government Reports Announcements and Index (GRA and I)*; *Scientific and Technical Abstract Reports (STAR)*; and publication NTIS-PR-360 available from NTIS at the above address.

## **DISCLAIMER**

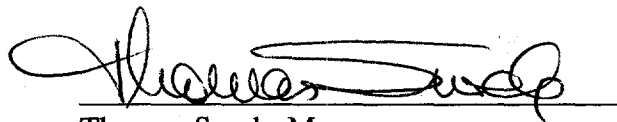
**Portions of this document may be illegible  
electronic image products. Images are  
produced from the best available original  
document.**

## PREFACE

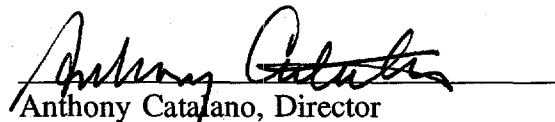
This report summarizes the fiscal year (FY) 1992 (October 1, 1991, through September 30, 1992) progress of the subcontracted photovoltaic (PV) research and development (R&D) performed under the PV Program at the National Renewable Energy Laboratory (NREL). Most of these subcontract activities were wholly implemented through NREL. In FY 1992, The U.S. Department of Energy (DOE), also assigned certain other PV subcontracting efforts to the DOE-NREL Area Office (NAO), and assigned responsibility for their technical support to the NREL PV Program. Those NAO efforts are also reported in this document. The NREL PV subcontracts are managed under the following areas: Amorphous Silicon; Polycrystalline Thin Films; Crystalline Materials and Advanced Concepts (including crystalline silicon research, high-efficiency concepts, the new ideas for photovoltaic conversion, and the university participation programs); the Photovoltaic Manufacturing Technology Project; Module and System Performance and Engineering; and PV Analysis and Applications Development. Under these areas, technical summaries of each of the subcontracted programs list approaches, major accomplishments, and future research directions. This document assists technology transfer of research results into commercial products and applications.

The NREL subcontracted PV R&D represents most of the subcontracted work that is funded by the DOE National Photovoltaics Program. The DOE National Photovoltaics Program is managed by the Photovoltaics Division under the Office of Solar Energy Conversion, which is under the Office of Utility Technologies within DOE's Conservation and Renewable Energy organization. Major program thrusts in FY 1992 continued to be implemented based on DOE's *Photovoltaics Program Plan FY 1991-FY 1995*. The mission of the National PV Program is to develop PV technology for large-scale generation of economically competitive electric power in the United States. The major challenge in fulfilling the mission is to assist industry in laying the foundation for installing at least 1000 MW of electrical capacity by the year 2000.

Approved for the NATIONAL RENEWABLE ENERGY LABORATORY



Thomas Surek, Manager  
Photovoltaic Program



Anthony Catalano, Director  
Photovoltaics Division

Notice: This publication was reproduced from camera-ready copy submitted by the individual subcontractors. The efficiency values reported by the subcontractors may not have been independently confirmed by NREL or Sandia.



## SUMMARY

The National Renewable Energy Laboratory (NREL), subcontracted photovoltaic (PV) research and development (R&D) represents most of the subcontracted work funded by the U.S. Department of Energy (DOE) National Photovoltaics Program. Most of those subcontract activities are wholly implemented through NREL. In FY 1992, DOE also assigned certain other PV subcontracting efforts to the DOE-NREL Area Office (NAO), and assigned responsibility for their technical support to the NREL PV Program. Those NAO efforts are also reported in this document. This report covers fiscal year (FY) 1992 (October 1, 1991, through September 30, 1992).

Major program thrusts in FY 1992 continued to be implemented based on DOE's *Photovoltaics Program Plan FY 1991-FY 1995*. The mission of the National PV Program is to develop photovoltaic technology for large-scale generation of economically competitive electric power in the United States. The major challenge in fulfilling the mission is to assist industry in laying the foundation for the installing at least 1000 MW of electrical capacity by the year 2000. In FY 1992, the balance of activities was readjusting according to changing DOE PV Program priorities. The DOE goal over the next few years will be to lay the groundwork for a growing U.S. PV technology and industrial base with increased emphasis on market and project development activities with industry. To accomplish this, the program's policy now embraces three relatively equal priority activities: 1) technology development and validation, 2) market conditioning, and 3) project venturing.

The NREL PV subcontracts are managed under the following areas: Amorphous Silicon; Polycrystalline Thin Films; Crystalline Materials and Advanced Concepts (including crystalline silicon research, high-efficiency concepts, the new ideas for photovoltaic conversion, and the university participation programs); the Photovoltaic Manufacturing Technology Project; Module and System Performance and Engineering; and PV Analysis and Applications Development. The subsections that follow summarize the objectives and approaches for each area. Technology transfer activities are also summarized.

There were 80 subcontracts in FY 1992 with total NREL funding of \$22.3 million. Cost-sharing by 16 industry subcontractors added another \$6.7 million to the NREL funding. Sixty percent of the NREL subcontracts was with universities, at a total funding of \$5.1 million. Procurement highlights included new awards under the polycrystalline thin films fundamental studies program; new awards for crystalline silicon materials research on impurities and defects; the initiation of the university participation program procurement; the award of the Phase 2A subcontracts under the PV Manufacturing Technology (PVMaT) Project; the initiation of PVMaT Phase 2B and Phase 3A procurements; and various module, system, and market development subcontracts, including the DOE collegiate Sunrayce 93 PV-powered car competition.

## Crystalline Materials and Advanced Concepts

High-efficiency photovoltaics, like all other approaches, need significant advances in cost-reducing technologies for production. Fortunately, we have already established that these performance levels do not require defect-free single crystal materials. Experiments in GaAs samples with controlled dislocation densities in the range from  $10^3 \text{ cm}^{-2}$  to more than  $10^7 \text{ cm}^{-2}$  show very little loss in cell performance for materials better than  $10^5 \text{ cm}^{-2}$ . The evidence suggest that even semicrystalline materials can reach efficiencies in excess of 20%, provided the density of mid-gap electronic states is held to less than  $10^{13} \text{ cm}^{-3}$ . In silicon, this corresponds to a grain diameter greater than 1 cm, assuming high-quality intragrain properties and no grain boundary passivation. Each order-of-magnitude reduction in grain boundary recombination center density achieved by passivation treatment reduces the grain diameter requirement by the same amount. Even with the advances in hydrogen passivation in silicon and sulphide surface passivation in III-V's, grain diameters of at least 100 microns appear to be the minimum acceptable target for materials with crystalline properties.

In FY 1993, NREL will continue its efforts in analysis and support of commercial silicon photovoltaic materials. This will require substantial adjustments internally in order to maintain support for associate staff hired in FY 1992 while holding to the no-growth guidance. These new individuals will assist in accelerating the response time in our Secondary Ion Mass Spectroscopy (SIMS) facility and silicon sample optical analysis and coordination. By the end of FY 1993, more than 25% of the FTEs for this project will have been shifted from research on next generation PV technology and fundamental research to activities that more directly support today's photovoltaic products. The subcontract program established in FY 1992 consists of at least seven new awards. These projects will cover three main topics including: (1) characterization of existing industrial materials to determine materials properties that may contribute to limiting solar cell performance; (2) analysis of point defect processes, such as the interaction of carbon and oxygen impurities with silicon interstitials and vacancies, which can work to the benefit or detriment of electronic properties; and (3) development of post growth processes, based on knowledge developed in the other two tasks, which enhance the electronic properties of industry's current silicon material. The combined efforts of these in-house and subcontracted projects will support Solarex, Texas Instruments, Crystal Systems, and Astropower with assistance in analysis of interactions of hydrogenation, optical anneals and other post growth processes with their materials. We will continue to provide analysis in response to requests by Siemens Solar for increased DLTS (Deep Level Transient Spectroscopy) support and by Mobil Solar for SIMS. Continued research on ingot growth strengthens the fundamental base that industry uses to guide improvements to its selected processes. However, it is unlikely that 20% efficiencies could be achieved in silicon grown by existing PV industry processes even with minor changes in growth parameters or post growth treatments. Our target, in conjunction with device optimization efforts performed by Sandia's Photovoltaic Device Fabrication Laboratory (PDFL), is to help industry boost module efficiencies to more than 16% without dramatic changes in the basic production processes. With the establishment of process design criteria for achieving this higher performance level, industry is far more likely to invest in expanded facilities.

The technology transfer of advanced GaInP multijunction technology, initiated in FY 1992, will be continued. Industrial partners have ready markets for early production for satellite power. At least two companies will acquire new metal organic chemical vapor deposition (MOCVD) systems with a per-run capacity of nearly a square meter. The prospect of availability of excess capacity in GaAs-based solar cells could bring this technology to a very competitive level relative to the mid-concentration silicon technology.

In spite of the current enthusiasm for near-term support of PV companies, the program cannot neglect the continued investigation of advanced technology needed for the next generation of product. Thin crystalline films of GaAs have already been used to reach submodule efficiencies greater than 20%. With good optical confinement, thin films of silicon can also reach this level. The approach in this task will be to continue the development of technologies needed for cost effective production of crystalline-film-based products. The vision of the project is focused on advanced flat-plate modules. However, most of the technology is immediately applicable for high-efficiency concentrator cell production. Cost reduction in the high-efficiency technologies requires a three-pronged attack. First, increasing the efficiency is still the most direct path to lower the cost of PV modules, provided that the additional device sophistication does not add cost. The focus of high efficiency cell research will be to simplify the device structures and design structures that are more tolerant of less than ideal materials. A good example is the push toward thin-cell designs in both silicon and GaAs materials. Assuming that the high-efficiency cells are limited by bulk recombination, the thin design can tolerate lower minority carrier lifetimes than thick cells. In the case of comparable bulk properties, a thin single-junction design might exceed the performance of the more complex multijunction. Either of these examples require greater sophistication in crystal growth than is applied today. The second prong is to improve the technologies for crystal growth. Production cost factors related to large-area uniformity, yield, process safety, and source utilization efficiency are, in fact, inseparable from the more esoteric scientific issues of thermal geometry, reaction chemistry, crystallographic orientation effects, spinodal decomposition, and interdiffusion. Finally, improved technology and new concepts are needed to eliminate the cost of consuming a crystalline substrate. In FY 1993 we will develop and release an RFP for re-competition of research in high-efficiency thin crystalline films. Awards for this solicitation would be made in FY 1994. A low level of effort will be maintained in research on heteroepitaxy, lateral epitaxy, lift-off techniques, and recrystallization. As indicated, a significant effort will continue in these advanced technologies; however, redirection of in-house staff and reduction in subcontractor projects will be required in order to maintain our industry support in silicon technology.

The final task covers fundamental research and advanced concepts. This includes the in-house efforts in solid state theory, in establishing new capabilities for growth and analysis of PV materials and devices, and in evaluation of new materials systems for potential photovoltaic application. The subcontract programs in University Participation and New Ideas also are included here. These are the activities that can revolutionize photovoltaics. Although it is convenient to think of these as long-term research areas, the results to date have proven to be much more immediate. For some examples, the potential impact of Dr. Lucovsky's research, under University Participation, on microcrystalline silicon is to provide a photo-stable, direct bandgap, thin-film silicon morphology. The Bragg reflector proposed under the New Ideas program opened up the possibility of reaching 30% efficiencies with single junctions and has



already yielded significant  $V_{oc}$  improvements in experimental devices. Perhaps most important, the theoretical predictions of spontaneous ordering in semiconductor alloys and initial work in the Ga-In-P system is now undergoing technology transfer to the PV industry and, as a major spin-off benefit, has opened new areas of development in photonic and quantum confinement materials and devices. While in-house efforts will continue to be reduced, new subcontracted awards will be made from the procurements in New Ideas and University Participation.

### Polycrystalline Thin Films

The objective of the Polycrystalline Thin Films Program is to develop thin-film, flat-plate modules that meet DOE's long-term goals of reasonable efficiencies (15%-20%), very low cost (near \$50/m<sup>2</sup>), and long-term reliability (30 years). The approach relies on developing solar cells based on highly light-absorbing, compound semiconductors such as CuInSe<sub>2</sub>, CdTe, and thin-film crystalline silicon. These semiconductors are fabricated as thin film (1-3  $\mu$ m thick) with minimal material and processing costs. Cell efficiencies greater than 10% have been achieved by 20 laboratories. Module efficiencies of 10%-11% have been reached by both CdTe and CIS at one square foot; nearly 10% has been reached by CIS for a 4-square-foot module.

Major progress during 1992 occurred in the CdTe technology. During the year, records were repeatedly set for laboratory cell efficiency. These records, which reached 15.8% by the end of the year (up from 12.7%) were the highest for any non-single-crystal thin-film cell of any sort (any material, any structure, including multijunctions). This was achieved using simple, single-junction cells made by a method that has already been adopted by industry (Solar Cells Inc.) for commercial development.

In parallel with these cell results, major progress occurred in CdTe module development. Early in the year, Photon Energy (now Golden Photon, see below) made its first square-foot CdTe modules, reaching 21 W (then the most for any CdTe module). They subsequently focused on shakedown tests of their pilot production at these sizes. In a more spectacular development, researchers at Solar Cells Inc. began CdTe module development at the 8-square-foot size, and within 6 months of making their first films made a module with a reported efficiency of 6.5% (47 W). This is the highest efficiency thin film module of any kind at that size.

Finally, the CdTe industrial infrastructure was bolstered by the entry of Coors, Golden Photon, (through its subsidiary, Golden Technologies). Coors purchased Photon Energy for the purpose of commercializing Photon Energy's CdTe technology in September 1992. The new company, Golden Photon, is headquartered in Golden, Colorado.

CIS progress was mixed. Siemens Solar, the technology leader, faltered in its progress toward commercial module production. Although some module efficiencies near 10% were achieved, yields peaked at about 8%. Several manufacturing issues were identified as causing this shortfall. Meanwhile, however, efficiencies at the cell level rose almost as spectacularly as those for CdTe, with a non-NREL-funded group (EuroCIS) reaching 14.8% active area for a CIS cell, and reaching 14.6% (active area) with S-Se alloys. Progress in CIS alloys with Ga and S was an important technical achievement.

ISET reached 11% (active area) efficiency using a nonvacuum method of depositing Cu-In. This replacement of a relatively expensive sputtering step with an inexpensive nonvacuum step could turn out to be one of the seminal technical achievements of the year if it is followed up with module development and manufacturing.

### Amorphous Silicon Research Project (ASRP)

Amorphous silicon photovoltaic commercial products had a 25% share of the worldwide photovoltaics market in 1991. The product is reliable, as exemplified by 10-year warranties of commercial power modules. The potential for low costs is the same as for any other thin-film photovoltaic technology, namely \$1-2/W. Gradual efficiency improvements are constantly being demonstrated. The best prototype module stable efficiencies are now 8.9%.

The near-term objective of the ASRP is to achieve 12% stable prototype module efficiency by 1994 in accordance with the goals in DOE's *Photovoltaics Program Plan FY 1991-FY1995* through better understanding and improvement of the optoelectronic properties of amorphous-silicon-based alloy materials. Additional near-term objectives are to gain an understanding of the metastability in amorphous silicon, reduce the costs to \$1/Wp, and to foster a viable amorphous silicon photovoltaic industry in the United States. A transition in emphasis did occur in FY 1990 from single-junction amorphous silicon cell and submodule research to multijunction module research, and from initial efficiency to stabilized efficiency. NREL implemented the transition in FY 1991 to focus industrial subcontractors and university subcontractors on *stabilized* efficiencies, rather than to focus on maximizing initial performance and minimizing degradation. The focus on stabilized efficiency continued in 1992.

The ASRP consists of three tasks: 1) subcontracted research, 2) NREL a-Si research, and 3) surface and interface analysis. Within the subcontracted research there are two principal activities: subcontracted multi-disciplinary research activities: and subcontracted fundamental research activities. The subcontracted multidisciplinary research activities are performed under cost-shared programs between government and industry by broad-based research teams located at the individual industrial facilities that perform focused research ranging from feedstock materials through to the development of modules. The subcontracted fundamental research activities involve basic and supporting research done by academia and research laboratories to aid the industry groups' advances of the technology base. The cost-shared subcontracted multidisciplinary research programs address issues related to all aspects of 2-terminal amorphous silicon multijunction cells and modules using same-bandgap or different-bandgap device structures. Research was performed to advance the stabilized conversion efficiency of multijunction modules having areas of at least 900 cm<sup>2</sup>, using glow discharge deposition as the primary method of fabricating the amorphous silicon films.

## **PV Manufacturing and Technology (PVMaT) Project**

The objective of the PVMaT Project is to assist the U.S. PV industry in improving manufacturing processes, accelerating manufacturing cost reductions for PV modules, increasing commercial product performance, and generally laying the groundwork for a substantial scaleup of U.S.-based PV manufacturing plant capabilities. This project is a government/industry photovoltaic manufacturing R&D effort composed of partnerships between the federal government (through the DOE) and members of the U.S. PV industry.

Phase 1 of this program, the problem identification phase, was completed early in 1991. Phase 1 competitive bidding was open to any U.S. firm with existing PV manufacturing capabilities, regardless of material or module design. Twenty-two contracts of up to \$50,000 each were awarded. Phase 2 is the process-specific solution phase of the project and addresses problems of specific manufacturers. Phase 2A, which is now under way, was open only to Phase 1 participants. Each of the seven awarded contracts is of up to 3 years in duration and is highly cost-shared between the U.S. government and U.S. industrial participants. A second, overlapping, and similar process-specific solicitation (Phase 2B) was released in June 1992, and was open to all U.S. PV manufacturing companies. Responses to this Phase 2B solicitation are being evaluated now, and subcontracted efforts are planned for later this year. A third portion of the program, called Phase 3, is also under way although slightly behind Phase 2. In Phase 3, because of the general interest to industry, some general issues related to PV module development will be studied through various teaming arrangements. The PVMaT project's ultimate goal is to ensure that U.S. industry retains and extends its world leadership role in the manufacture and commercial development of PV components and systems. The activities to date have received outstanding support, and the level of interest in participation is exceptional for this program.

## **PV Module and System Performance and Engineering Project**

The PV Module and System Performance and Engineering Project is structured to conduct state-of-the-art PV module, system, and solar radiation research; to perform engineering, testing, evaluation and analysis tasks; to provide technical results and solutions to technical issues; to develop PV standards and codes; and to maintain and enhance supporting facilities and capabilities that are consistent with DOE's new *Photovoltaics Program Plan FY 1991—FY 1995*. By keeping the project complementary to other DOE PV projects, we can ensure that project capabilities and facilities are available resources for cooperative research and utilization by the PV research and development community.

Project activities are managed through the module and the systems performance and engineering project management tasks: 1) cell and module standardized characterization performance; 2) module and system performance testing; 3) module reliability research; 4) solar radiation research; and 5) standards development.

Subcontract activities represent support for industry/utility PV power projects, domestic and international standards development and PV technology validation at the module/array and small system level.

## **PV Analysis and Applications Development Project**

In response to the opportunity presented by the transfer to NREL of additional in-house PV program funds, a new FWP entitled: Analysis and Applications Development was created in May 1992. This new FWP brings together a variety of senior NREL PV personnel to focus additional attention on the growing analytical and applications development needs of the DOE PV Program and the DOE Office of Solar Energy Conversion.

During FY 1992 activities included in-house investigations and management of subcontracted efforts (both through NREL and in support of NAO) that supported several broad analysis and applications development areas, including: *Solar 2000*, value analysis, PV demand side management (DSM) analysis, PV in buildings (PV:BONUS), PV in transportation, *Sunrayce '93*, PV market assessments, *Soltech '93*, and coordination and support of state PV collaborative and regulatory interfaces, including the PV4U industry-led effort and the newly formed Utility PV Group. An activity that emerged at the very end of FY 1992 that was supported and implemented by the analysis and applications development project was the Brazilian Rural Electrification Pilot Project.

## **Technology Transfer**

Consistent with recent DOE policy, technology transfer within NREL's PV program is defined as collaborative R&D with industry for the purpose of aiding its commercialization of products or services. An underlying theme of NREL technology transfer activities is the joint work accomplished by industry researchers and NREL researchers focused on a common R&D objective. Among government laboratories, there are seven principal tools for effecting technology transfer: subcontracted research and development, cooperative R&D, industry sponsored R&D, user facilities (at NREL), technology licenses, researcher exchanges, and information dissemination. NREL's PV program conducts its technology transfer primarily through three of the above: subcontracts, informal cooperative R&D, and information dissemination.



## TABLE OF CONTENTS

	<u>Page</u>
1.0 Introduction .....	1
1.1 Background .....	1
1.2 Key Accomplishments .....	5
1.2.1 Crystalline Materials and Advanced Concepts .....	5
1.2.2 Polycrystalline Thin Films .....	5
1.2.3 Amorphous Silicon Research Project .....	9
1.2.3 PV MaT .....	11
1.2.4 PV Module and System Performance and Engineering .....	11
1.2.5 PV Analysis and Applications Development Project .....	12
1.3 Technology Transfer .....	13
1.4 Conclusions .....	14
 2.0 Crystalline Materials and Advanced Concepts Research .....	 17
Arsine and Hydride Radical Generation for MOCVD Growth; <i>Colorado State University</i> .....	19
Influence of Self-Interstitials Injected by Phosphorus Diffusion on Defect Structures and Electronic Properties in Crystalline Silicon; <i>Duke University</i> .....	22
Fundamental Research on Post-Growth Quality Enhancement Techniques in Crystalline Silicon; <i>Georgia Institute of Technology</i> .....	26
High-Efficiency, Thin-Film Solar Cells; <i>Kopin Corporation</i> .....	30
New Approaches for High-Efficiency Solar Cells: Role of Strained Layer Superlattices; <i>North Carolina State University</i> .....	34
Detailed Non-contact Electrical and Structural Characterization of Photovoltaic Silicon Substrates; <i>North Carolina State University</i> .....	39
New III-V Cell Design Approaches for Very High Efficiency; <i>Purdue University</i> .....	43
CI-MO and MOCVD Crystal Growth Research; <i>Rensselaer Polytechnic Institute</i> .....	47
Growth Development of GaInAsP for Use in High-Efficiency Solar Cells; <i>Research Triangle Institute</i> .....	51

TABLE OF CONTENTS (continued)

	<u>Page</u>
An Inverted AlGaAs/GaAs Patterned Tunnel Junction Cascade Concentrator Solar Cell; <i>Research Triangle Institute</i> .....	55
Low-Cost, High-Efficiency Solar Cells Utilizing GaAs-on Si Technology; <i>Spire Corporation</i> .....	58
Photon and Ion Assisted Doping and Growth of II-VI Compound Thin Films; <i>Stanford University</i> .....	61
Passivation and Gettering Studies in Solar Cell Silicon; <i>The University at Albany</i> .....	65
Identification and Control of Lifetime-Reducing Defects in Polycrystalline Silicon Photovoltaic Materials; <i>University of California, Berkeley</i> .....	74
Novel Ways of Depositing ZnTe Films by a Solution Growth Technique; <i>University of Delaware, Institute of Energy Conversion</i> ....	78
Atomic Layer Epitaxy for High Efficiency Solar Cells; <i>University of Southern California, Los Angeles</i> .....	81
Optimization of Gettering Processes for Photovoltaic Silicon; <i>University of South Florida</i> .....	90
Electronic Processes in Thin Film PV Materials; <i>University of Utah</i> .....	97
3.0 Polycrystalline Thin Films .....	101
Development of Large-Area Monolithically Integrated Silicon-Film Photovoltaic Modules; <i>AstroPower, Inc.</i> .....	103
Research on Polycrystalline Thin Film CuInGaSe <sub>2</sub> Solar Cells; <i>Boeing Defense and Space Group</i> .....	107
Polycrystalline Thin Film Cadmium Telluride Solar Cells Fabricated by Electrodeposition; <i>Colorado School of Mines</i> .....	109a
Role of Polycrystallinity in CdTe and CuInSe <sub>2</sub> Photovoltaics; <i>Colorado State University</i> .....	110

TABLE OF CONTENTS (continued)

	<u>Page</u>
Non-H <sub>2</sub> Se, Ultra-Thin CIS Devices; <i>Energy Photovoltaics (EPV)</i> .....	113a
Polycrystalline CuInSe <sub>2</sub> & CdTe PV Solar Cells; <i>Florida Solar Energy Center</i> .....	114
Development of High-Efficiency CdTe and CdZnTe Solar Cells; <i>Georgia Institute of Technology</i> .....	118
High-Efficiency, Large-Area CdTe Panels; <i>Golden Photon Energy, Inc.</i> .....	122
Low-cost CuInSe <sub>2</sub> , Submodule Development; <i>International Solar Electric Technology</i> .....	126
Innovative Sputtering Techniques for CIS and CdTe Submodule Fabrication; <i>Martin Marietta Astronautics Group</i> .....	129
Research on High Efficiency, Large Area CuInSe <sub>2</sub> -Based Thin Film Modules; <i>Siemens Solar Industries</i> .....	138a
Development and Application of Computer Model for CdTe and CuInSe <sub>2</sub> Based Solar Cells; <i>Purdue University</i> .....	139
Fabrication of Stable Large Area Thin Film Cadmium Telluride Photovoltaic Modules; <i>Solar Cells, Inc.</i> .....	143
Research on Polycrystalline Thin Film Submodules Based on CuInSe <sub>2</sub> Materials; <i>Solarex Corporation, Thin Film Division</i> .....	146
Novel Thin-Film CuInSe <sub>2</sub> Fabrication; <i>University of Colorado</i> .....	150
Polycrystalline Thin-Film Materials and Devices; <i>University of Delaware, Institute of Energy Conversion</i> .....	154
Advanced Processing Technology for High Efficiency CuInSe <sub>2</sub> Solar Cells; <i>University of South Florida</i> .....	158
Thin Film Cadmium Telluride Photovoltaic Cells; <i>The University of Toledo</i> .....	162
Investigation of Polycrystalline Thin Film CuInSe <sub>2</sub> Solar Cells Based on ZnSe Windows; <i>Washington State University</i> .....	166



TABLE OF CONTENTS (continued)

	<u>Page</u>
4.0 Amorphous Silicon .....	171
Research on Amorphous-Silicon-Based Thin Film Devices; <i>Solarex Thin Film Division</i> .....	175
Research on Stable, High-Efficiency Amorphous Silicon Multi- junction Modules; <i>United Solar Systems Corporation</i> .....	179
Research on Stable, High-Efficiency Amorphous Silicon Multi- junction Modules; <i>Advanced Photovoltaic Systems</i> .....	183
Small Angle X-ray Scattering Studies of Amorphous Silicon-Based Semiconductors; <i>Colorado School of Mines</i> .....	187
Optimization of Transparent and Reflecting Electrodes for Amorphous Silicon Solar Cells; <i>Harvard University</i> .....	191
Comprehensive Research on Stability and Electronic Properties of Amorphous Silicon Alloys and Devices; <i>Iowa State University</i> .....	195
Growth Mechanisms and Characterization of Hydrogenated Amorphous Silicon Alloys Films; <i>National Institute of Standards and Technology</i> .....	198
Fundamental Studies of Defect Generation in Amorphous Silicon Alloys <sup>a</sup> , and Transport in Microcrystalline Si <sup>b</sup> , both Grown by Remote Plasma-Enhanced Chemical-Vapor Deposition; <i>North Carolina State University</i> .....	202
In Situ Characterization of Growth and Interfaces in a-Si:H Devices; <i>The Pennsylvania State University</i> .....	206
Research on Defects and Transport in Amorphous Silicon-Based Semiconductors; <i>Syracuse University</i> .....	210
Charge Transport Measurements in Hydrogenated Amorphous Silicon by Photoconductive Frequency Mixing; <i>University of California at Los Angeles</i> .....	214
Stable, High Efficiency Amorphous Silicon Solar Cells with Low Hydrogen Content; <i>Institute of Energy Conversion, University of Delaware</i> .....	218

TABLE OF CONTENTS (continued)

	<u>Page</u>
Research on Silicon-Carbon Alloys and Interfaces; <i>University of Illinois</i> .....	222
Recombination and Metastability in Amorphous Silicon Germanium Alloys; <i>University of North Carolina</i> .....	226
Microscopic Origins of Metastable Effects in a-Si:H and Deep Defect Characterization in a-Si, Ge:H Alloys; <i>University of Oregon</i> .....	230
Stability, Electronic Properties and Structure of a-Si:H and its Alloys; <i>Xerox PARC</i> .....	234
5.0 The Photovoltaic Manufacturing Technology (PVMaT) Project .....	239
Silicon-Film <sup>TM</sup> Photovoltaic Manufacturing Technology; <i>AstroPower, Inc.</i> .....	241
Continuous Roll-to-roll a-Si Photovoltaic Manufacturing Technology; <i>Energy Conversion Devices, Inc.</i> .....	246
Photovoltaic Manufacturing Technology (PVMaT) Improvements for ENTECH's Concentrator Module; <i>ENTECH, Inc.</i> .....	248
Thin EFG Octagons; <i>Mobil Solar Energy Corporation</i> .....	252
PV MaT Cost Analysis Support; <i>Research Triangle Institute</i> .....	256
PV Cz Silicon Manufacturing Technology Improvements; <i>Siemens Solar Industries</i> .....	259
Large Area, Triple-Junction, a-Si Alloy Production Scale-Up; <i>Solarex Corporation</i> .....	263
Amorphous Silicon Photovoltaic Manufacturing Technology - Phase 2A; <i>Utility Power Group</i> .....	267

## TABLE OF CONTENTS (continued)

		<u>Page</u>
6.0	Module System and Performance and Engineering Project .....	275
	National and International Photovoltaic Standards	
	<i>Solar Energy Industries Association (SEIA)</i> .....	277
	Long Term Environmental Effects on Roof-Mounted Photovoltaic Modules; <i>Southwest Technology Development Institute</i> .....	280
7.0	PV Analysis and Applications Development Project .....	283
	Design for Photovoltaics: Curriculum Development for North American Architecture School Faculty; <i>AIA/ACSA Research Council</i> .....	285
	Building-Integrated Photovoltaics; <i>Kiss Cathcart Anders Architects, P.C.</i> .....	286
	Brazilian Rural Electrification Pilot Project; <i>Siemens Solar Industries (SSI) and</i> <i>Centro De Pesquisas de Energia Eletrica (CEPEL)</i> .....	290
	Solar Resource, Utility Load Matching Assessment; <i>State University of New York at Albany</i> .....	291
	Evaluation of DSM Incentive Opportunities for Photovoltaics; <i>Center for Energy and Urban Policy,</i> <i>University of Delaware</i> .....	297
	Risk-Adjusted IRP Procedures; Reflecting the True Costs of Conventional and Solar Options; <i>University of Massachusetts</i> .....	301
8.0	List of Active Subcontracts .....	305
9.0	Photovoltaic Program FY 1992 Bibliography .....	313

## 1.0 INTRODUCTION

This report reviews subcontracted R&D activities under the NREL Photovoltaic (PV) Program from October 1, 1991, through September 30, 1992 (fiscal year [FY] 1992). Most of these subcontract activities were wholly implemented through the National Renewable Energy Laboratory (NREL). In FY 1992, The U.S. Department of Energy (DOE) assigned certain other PV subcontracting efforts to the DOE-NREL Area Office (NAO), and assigned responsibility for their technical support to the NREL PV Program. An example is PV:BONUS--Building Opportunities in the United States for Photovoltaics. That is a 5-year, \$25M (DOE), government/industry cost-shared initiative contractually administered by DOE-NAO as a financial assistance (cooperative agreement) program. Those NAO efforts are also reported in this document.

### 1.1 Background

NREL's subcontracted PV R&D represents most of the subcontracted work funded by DOE National Photovoltaics Program. The DOE National Photovoltaics Program is managed by the Photovoltaics Division under the Office of Solar Energy Conversion (which is under the Office of Utility Technologies within DOE's Conservation and Renewable Energy organization.)

Major program thrusts in FY 1992 continued to be implemented based on DOE's *Photovoltaics Program Plan FY 1991—FY 1995*. The mission of the National Photovoltaics Program is to develop photovoltaic technology for large-scale generation of economically competitive electric power in the United States. The major challenge in fulfilling the mission is to assist industry in laying the foundation for the installation of at least 1000 MW of electrical capacity by the year 2000. In FY 1992, the balance of activities was readjusted according to changing DOE PV Program priorities. The DOE goal over the next few years will be to lay the groundwork for a growing U.S. PV technology and industrial base with increased emphasis on market and project development activities with industry. To accomplish this, the program's policy now embraces three relatively equal priority activities. 1) technology development and validation, 2) market conditioning, and 3) project venturing. The new policy will continue a strong technology development program but will emphasize R&D for the technologies and companies that are positioned to achieve substantial market penetration, price reductions, and manufacturing scaleup. Program activities include continuing efforts at forming partnerships with manufacturers and utilities (the ultimate benefactors and users), with universities, and with federal and state agencies.

Under the DOE PV Program, the NREL Photovoltaic Advanced Research and Development (PV AR&D) Project sponsors fundamental and applied R&D, manufacturing development, and systems and market development in PV energy technology. The project also provides services to industry and electric utilities or other users, and it provides the leading support for the national PV program. The NREL subcontract program is responsible for most of the R&D, manufacturing technology development, and some of the systems and market development task areas under the national PV program. The implementation of the subcontract program is based on competitive public solicitations. One of the most important mechanisms is in the form of government/industry partnerships, with industry frequently sharing the cost of research with DOE.

Increasing emphasis is being directed to more closely working with industry, utilities, and other end users on PV manufacturing technology, systems, and market needs. Approaches for this increasing emphasis include mitigating barriers to PV adoption in the utility and international marketplace and project venturing with decision makers/organizations representing target market sectors for PV (i.e., utilities, buildings, transportation, and industry). As appropriate for the system and market development areas, NREL is implementing or representing DOE in activities that include education; technical assistance and training; market, economic, and financial analysis; technology characterizations; regulatory, rate, and value analysis; codes and standards assessment and development; participation involving working with customers in project development activities; and cofinancing of projects to lower costs to a level competitive with more conventional energy options. The project venturing, or "stakeholder" approach should lead to significant cost reductions while developing a strong market base for suppliers. Under project venturing, DOE is placing particular emphasis on supporting and strengthening programs that are already in place, including the Tucson Project, Project FINESSE, PV:BONUS, and Americas' 21st Century Project.

NREL's PV activities include managing subcontracted R&D projects as well as conducting research at the laboratory. The primary research activities are conducted in advanced PV material technologies, including amorphous-silicon thin-film materials; polycrystalline thin films, such as copper indium diselenide, cadmium telluride, and their alloys; and high-efficiency crystalline cells, including silicon and gallium arsenide and their alloys. Improving the way that PV devices are manufactured is vital. Two complementary approaches are pursued. One involves government/industry partnerships under the PV Manufacturing Technology (PVMaT) Project. That approach focuses on improving manufacturing processes and products, accelerating manufacturing cost reduction, and laying the foundation for increased production capacity. The second approach involves module development research to evaluate modules and module performance and suggest solutions to common module problems. System and market development rounds out the balanced approach pursued. The objective is to create the environment whereby system technology, user acceptance, and the PV industry can accommodate the continued expansion of PV into larger applications and markets. NREL subcontracts also support the continued influx of new ideas and highly qualified university research teams to expand the current limits of PV technology. Transferring research results into commercial products and applications in a timely and effective manner is another major activity of NREL's PV project.

Subcontracted R&D is a significant part of the NREL PV project — more than 50% of the project's budget is allocated yearly to subcontracts. In FY 1992, we managed 80 subcontracts with total funding of \$22.3 million. Cost-sharing by 16 industry subcontractors added an additional \$10 million to the NREL funding. Sixty percent of the NREL subcontracts were with universities, at funding of \$5.1 million. Table 1-1 shows how the subcontract budget was distributed. Figure 1-1 shows the distribution of subcontract funds by business category. Table 1-2 shows the NREL contacts for the PV subcontracts.

In summary, the PV AR&D Project activities involve conducting basic, applied; and engineering research; managing subcontracted R&D projects; performing research complementary to subcontracted work; developing state-of-the-art measurement and device capabilities; performing

PV manufacturing technology and module development; transferring results to industry, and evolving viable partnerships for PV systems and market development. This report describes the subcontracted R&D activities, many of which encompass close collaborations with NREL in-house PV researchers.

**Table 1-1. Subcontract Budget History of the NREL Photovoltaic Program<sup>a</sup>**

Notes: (a) Includes approximately 10%-15% for program management, fees, etc.  
 (b) Includes \$9 million for photoelectrochemical cell research.  
 (c) Significant effort initiated in FY 1991.  
 (d) Significant effort initiated in FY 1992.

Task Area	Fiscal Year				
	1978-1988 (\$M)	1989 (\$M)	1990 (\$M)	1991 (\$M)	1992 (\$M)
<b>Research and Development</b>					
Amorphous Silicon Thin Films	59.2	7.7	6.0	3.3	3.9
Polycrystalline Thin Films	37.1	3.7	4.6	4.5	4.5
High-Efficiency Concepts	30.63	2.0	1.9	1.3	0.9
Crystalline Silicon	22.1	0.6	0.5	0.9	0.9
New Ideas	17.6 <sup>b</sup>	0.4	0.4	0.4	0.1
University Participation	4.8	0.9	0.4	0.8	0.7
Subtotal	171.4	15.3	13.8	11.2	11.3
<b>Manufacturing Technology and System and Market Development</b>					
PV Manufacturing Technology Project	N/A	N/A	1.7	6.7	10.2
Module and System Performance and Engineering Project <sup>c</sup>	N/A	N/A	N/A	2.0	0.1
PV Analysis and Application Development Project <sup>d</sup>	N/A	N/A	N/A	N/A	0.7
Subtotal	N/A	N/A	1.7	8.7	11.0
<b>Total</b>	<b>171.4</b>	<b>15.3</b>	<b>15.5</b>	<b>19.9</b>	<b>22.3</b>

**Figure 1-1. Business category distribution of FY 1992 subcontract funds**

The chart summarizes subcontracted R&D activities under the NREL Photovoltaic Program from October 1, 1991, through September 30, 1992.

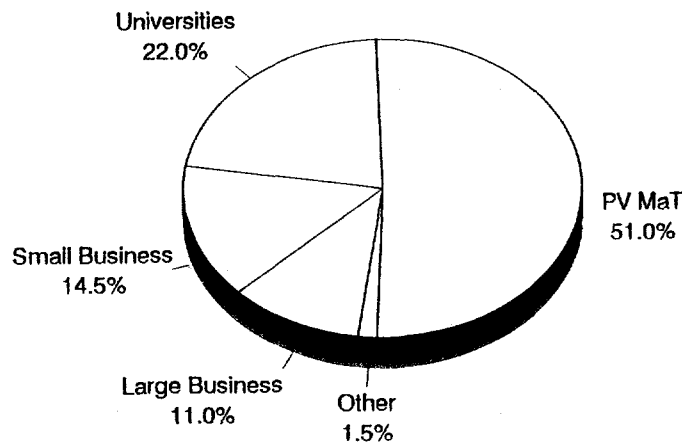


**Table 1-2. NREL Photovoltaic Program Subcontract Personnel**

Notes: (a) Area code (303).

Task Area	Contact Name	Telephone <sup>a</sup>
PV Program	Thomas Surek, Manager	231-1371
	Kathy Summers	231-1395
	Thomas Basso	231-7035
Amorphous Silicon Research Project	Werner Luft, Manager	231-1452
Crystalline Materials and Advanced Concepts (Crystalline Silicon, High Efficiency, University Participation, New Ideas)	John Benner, Manager	231-1396
Polycrystalline Thin Films Project	Kenneth Zweibel, Manager	231-7141
PV Manufacturing Technology	Ed Witt, Manager	231-1402
Module and System Performance and Engineering	Richard DeBlasio, Manager	231-1286
Analysis and Application Development Project	Roger Taylor, Manager	231-1332

## 1.2 Key Accomplishments

### 1.2.1 Crystalline Materials and Advanced Concepts Project

Crystalline silicon research continues in both subcontracts and in-house work. Awards were completed on the RFP for "Fundamental Research in Crystalline Silicon Materials". The following awards were made: North Carolina State University, G. Rozgonyi; Duke University, U. Goesele; University of South Florida, L. Jastrzebski; Georgia Institute of Technology, A. Rohatgi; University of California at Berkeley, E. Weber; and Massachusetts Institute of Technology, K. Kimmerling. "Single-grad-student" subcontracts are in process for silicon research with J. Corbett (SUNY/Albany) and S. Estreicher (Texas Tech University).

After a lapse of several years, the University Participation and New Ideas projects selected new projects for research. The Technical review of more than 100 Letters of Interest (LOIs) to the New Ideas solicitation was completed. New procedures were developed to permit the implementation of the peer review process in the University Participation Program solicitation; over 50 proposals received.

Subcontractors continue to make substantial progress in developing the pieces of cost effective production processes for high-efficiency cells. Plasma systems for in situ generation of hydride source gases, are under development by Boeing and Colorado State University. They have achieved low-temperature GaAs growth. North Carolina State University reports development of 1.9 eV bandgap, tunnel-junction interconnects for cascade cells capable of more than 1000 sun operation.

### 1.2.2 Polycrystalline Thin Films

Significant progress has been made in FY 1992 in the subcontracted research of polycrystalline thin films. The key accomplishments in both CdTe and CuInSe<sub>2</sub> solar cells and modules are listed below.

Golden Technologies, a subsidiary of Adolph Coors Company, announced an agreement September 1 to purchase Photon Energy of El Paso, Texas. Photon Energy had been a strong participant in our PV technology incubator program (our government/industry R&D partnerships) over the last 5 years. Photon Energy has been developing one of the leading CdTe PV approaches and has at times held the record for CdTe cell efficiency. Its purchase by Coors represents a big step for its CdTe technology, because it will allow the new entity (called Golden Photon) to begin pilot production of CdTe modules. This "success story" is a model of how DOE/NREL has "incubated" (with cost-shared R&D subcontracts) innovative PV technologies that have become successful enough to arouse significant U.S. corporate commercialization interest.

On November 19, 1991, NREL verified a **world record** thin-film CdTe solar cell with a total-area conversion efficiency of **14.6%** (1.08 cm<sup>2</sup>). The cell structure is MgF<sub>2</sub>/glass/TO/CdS/CdTe/graphite/Ag paste. The device parameters are  $J_{sc} = 24.41$  mA/cm<sup>2</sup>,  $V_{oc} = 0.8496$  V, and  $FF = 0.7035$ . The CdTe is deposited by the close-spaced sublimation method and



the CdS by the dip-coating method. The device was fabricated by Prof. Ting Chu and his students at the University of South Florida (USF). Prior to the deposition of the anti-reflection coating (ARC, MgF<sub>2</sub>), the cell efficiency was 13.6%. There were several devices in the efficiency range of 12% to 14.6% with a nominal cell area of 1 cm<sup>2</sup>. Optical measurements done by Prof. Jim Sites and his students at Colorado State University (CSU) estimated the reflection losses to be about 10% over the visible region of the spectrum. Based on CSU's optical analysis, a 550 Å MgF<sub>2</sub> ARC was deposited by X. Wu of NREL, which resulted in decreasing the reflection losses and improving the J<sub>sc</sub> from 23.12 mA/cm<sup>2</sup> to 24.41 mA/cm<sup>2</sup>, and in an improved efficiency. This is a truly remarkable collaborative effort between USF, CSU, and NREL that resulted in the world record efficiency. The Polycrystalline Thin-Film Project has thus accomplished a major AOP milestone (PV04 K) and a Five Year Plan (1987-91) key milestone.

During the week of June 5, 1992, we reported on a confirmed record efficiency (14.9%) for a thin film CdS/CdTe solar cell made by Ferekidis and Britt of USF. On June 26, 1992, another world record efficiency for any thin film cell was achieved by the same group from USF. NREL has measured the thin-film CdS/CdTe solar cells shown in Table 1-3.

**Table 1-3. Thin-film CdS/CdTe Solar Cells Measured by NREL**

Cell #	Efficiency	V <sub>oc</sub> (mV)	J <sub>sc</sub> (mA/cm <sup>2</sup> )	FF	Area (cm <sup>2</sup> )
6-1B-6-B	15.8%	843	25.1	74.5%	1.047
5-19B-20-C	15.7%	847	25.9	71.7%	1.090
5-19B-19-B	15.7%	851	25.1	73.4%	1.192
5-19B-10-A	15.4%	846	24.8	73.1%	1.073
5-1A-12-A	15.1%	858	23.6	74.6%	1.099
5-19A-19-A	14.9%	856	24.3	72.0%	1.109

The main factors contributing to the progress in device efficiency are the optimized solution grown CdS thin layer, and anti-reflection coating of MgF<sub>2</sub>. The 15.8% efficiency is the world record for any non-single-crystal thin film cell.

Boeing has improved its CuIn<sub>0.75</sub>Ga<sub>0.25</sub>Se<sub>2</sub> cell efficiencies. NREL measured a 13.7% ZnO/CdS/CIGS cell (0.9895 cm<sup>2</sup>, 548 mV, 36.7 mA/cm<sup>2</sup>, 68.4% FF, and 14.3% active area) and two other cells measured at NREL are quite representative of the state-of-the-art in that technology. (The EUROICIS cells were 14.8% active area, but on smaller areas of about a third of a square centimeter.) One of the better cells exhibited a relatively high FF (72.6%). Boeing is the only U.S. group doing state-of-the-art work in Ga-alloyed CIS cells. These cells have higher band gaps than CIS (very close to silicon) and have advantages in terms of 1) avoiding

light-absorption losses in the top ZnO layer, 2) having reduced losses at higher temperature (due to higher voltages), and 3) allowing for wider cells in integrated modules (fewer scribing cuts, increasing active area and yield).

International Solar Electric Technology (ISET) has produced reasonably efficient  $\text{CuInSe}_2$  solar cells using their innovative, potentially low-cost, nonvacuum method of depositing Cu and In. This is very important progress because one of the major impediments to the success of the CIS technology is the relatively high cost of existing vacuum-based (Cu,In) deposition. NREL has verified a total-area efficiency of 8.8% for a 1-cm<sup>2</sup> CIS solar cell, and 10.3% for a smaller solar cell (0.09 cm<sup>2</sup>). The active-area efficiencies for these devices are 9.5% and 11.4%, respectively. To fabricate these devices, ISET has used its low-cost, nonvacuum proprietary process for the CIS deposition. Typically, the Cu and In precursors are deposited by E-beam or sputtering methods followed by selenization. The 1-cm<sup>2</sup> device parameters are  $J_{sc} = 32.74 \text{ mA/cm}^2$ ,  $V_{oc} = 0.448 \text{ V}$ , and  $FF = 0.592$ . The cell structure is ZnO/CdS/CIS/Mo/glass. Currently, work is under way at ISET to fabricate thin-film CIS submodules using this low-cost, nonvacuum method.

Solar Cells Inc. (SCI) has continued its remarkable progress in large-area (8 ft<sup>2</sup>, 7000 cm<sup>2</sup>) thin film CdTe module efficiencies. They report making a 47-W module (about 6.5% efficiency), up from 25 W two weeks ago. The active layers (CdS/CdTe) for these modules are made in under five minutes, four minutes of which are heating up and cooling down. In addition, SCI submitted cells and mini-modules for measurement at NREL. The best cell efficiency achieved was 9.3% ( $V_{oc} = 0.783 \text{ V}$ ,  $J_{sc} = 19.2 \text{ mA/cm}^2$ ,  $FF = 0.617$ , and cell area = 1 cm<sup>2</sup>). The mini-modules had an aperture area of 75 cm<sup>2</sup>, and an aperture area efficiency of 6.0%. The patterning of these modules has not been optimized. The active cell area is only 56 cm<sup>2</sup>, corresponding to an active area efficiency on the order of 8%.

NREL verified a near 0.4 m<sup>2</sup>, 23.06 W, Photon Energy, Inc. (PEI), thin-film CdTe module measured outdoors at an insolation of 1081 W/m<sup>2</sup> and temperature of 29°C. The aperture-area efficiency of this module was 6.42%. There were 53 cells that monolithically interconnected in series. When normalized to 1000 W/m<sup>2</sup>, the power output of this module was 21.3 W. The normalized measurement of PEI was 21.6 W and aperture-area efficiency of 6.48%. This module produced more watts than any other thin-film CdTe module in the world at the time of its measurement at NREL.

NREL hosted a meeting on recycling options for CdTe and  $\text{CuInSe}_2$  PV modules. The meeting was co-sponsored by NREL, Brookhaven National Laboratory (BNL, Moskowitz), and the Electric Power Research Institute (EPRI). Besides representatives from the sponsoring organizations, members of the non-ferrous metals industry, experts in metals recycling, and members of the CIS and CdTe PV industry were present. The 2-day workshop provided some important insights into the issues associated with CIS and CdTe PV. Perhaps the most important conclusion was that many recycling options exist for both PV modules and manufacturing wastes. CIS and CdTe PV manufacturers should be able to find a number of pathways for recycling, either through 1) returning waste modules to smelters, 2) sending manufacturing waste to smelters or to existing cadmium or selenium recyclers, or 3) treating wastes on site to make them acceptable to smelters or recyclers. It was found that both the non-ferrous metals community and

the metals recycling community are used to dealing with these same materials, handle them in far larger quantities, and are willing to cooperate in recycling them economically. The workshop generated a draft report that should be finalized in the next few months. The report includes a summary of these findings as well as various recommendations for follow-on work. We are very appreciative of the 21 attendees for their serious contributions to clarifying these important issues.

During the visit by Drs. Ting and Shirley Chu, K. Ramanathan and R. Dhere of NREL fabricated an 11.3% efficiency CdS/CdTe solar cell by close-spaced sublimation (CSS). For a total area of 1.08 cm<sup>2</sup>, the relevant parameters were:  $V_{oc} = 0.8326$  V,  $J_{sc} = 22.57$  mA/cm<sup>2</sup>, and FF = 0.6. This is the best confirmed total-area efficiency for any polycrystalline thin-film solar cell fabricated at NREL. We are encouraged by the swift progress in the CSS project: deposition of the semiconductor layers started in mid-April. To date, a total of eight depositions have been made and five substrates have been processed into devices.

We received (as deliverables) four Siemens Solar 4-ft<sup>2</sup> thin-film CIS modules. The reported efficiencies of the modules range from 8.5% to 9.5% (33 W to 37 W). The module efficiencies will be baselined at NREL, and then the modules will be used for a variety of tests. The tests will include outdoor energy tests (side-by-side with CdTe, a-Si, and x-Si) conducted by K. Emery, as well as outdoor and accelerated life tests. Siemens Solar will be sending us another set of modules within a month and then company representatives will begin serious discussions with us on installing a kilowatt (kW) of modules at NREL in the near future.

ISET has reported fabricating monolithically integrated 1-ft<sup>2</sup> thin-film CIS submodules with nominal power output of 2.5 to 4.0 W. There are 18 cells connected in series. A combination of laser and mechanical scribes was used for the submodule fabrication. The modules are mainly being limited by low FF and high series resistance. Several new submodule designs are under way to improve the FF. ISET will be installing an in-line multichamber (with loadlocks) continuous sputtering system for fabrication of 1-ft<sup>2</sup> thin-film CIS submodules, using ISET's operating funds.

Solarex has successfully deposited CIS films on 8-in. x 8-in. large-area, Mo-coated, low-cost sodalime glass substrates. The films are uniform over this entire area. The CIS film is deposited by first growing the Cu, In precursors by sputtering at room temperature. This is followed by depositing Se by evaporation. The stack is then heat treated in nitrogen at 400°C for about half an hour. Single-phase stoichiometric CIS films are obtained. This is the same method by which Solarex has made 10% active-area efficiency for small-area solar cells. Work is under way on 3-in. x 3-in. substrates for interconnects and submodule integration.

NREL confirmed that evaporated thin-film CdS/CdTe solar cells prepared under subcontract at the University of Delaware's IEC reached 11% efficiency ( $V_{oc} = 0.79$  V,  $J_{sc} = 20.1$  mA/cm<sup>2</sup>, FF = 69.4%, and cell area 0.19 cm<sup>2</sup>). Previously, the best such cell measurements on the 11% efficient cells indicated that the currents below 500 nm are lower than those obtained previously with CdS/CdTe cells prepared in other laboratories. This is indicative that the CdS layer has not been fully optimized. Further improvements can be expected when the CdS layer is improved, primarily because of reduced absorption losses in this layer.

### 1.2.3 Amorphous Silicon Research Project

NREL implemented a transition to focus industrial subcontractors and university subcontractors on *stabilized* efficiencies, rather than to focus on maximizing initial performance and minimizing degradation.

A second controlled light-soaking experiment for amorphous silicon modules was started. Amorphous silicon (a-Si) modules from four manufacturers are being subjected to light-soaking at 1-sun intensity at 50°C for 2000 hours, with annealing to 70°C in the dark after 1000 hours. Characterization is done periodically, both under a Spire 240A solar simulator and outdoors. Aperture-area efficiencies as high as 8.9% were obtained after 1000 hours of light-soaking. The power output after 1000 hours of light-soaking and subsequent partial annealing ranged from 78% to 92% of the initial power output. The performance is fitted with a stretched exponential curve obtained using the data obtained for the first 1000 hours of light-soaking. For a-Si:H/a-Si:H-type of modules, stabilized performance was reached before 1000 hours. Different-bandgap multijunction modules require longer time to reach stabilized performance.

Amorphous silicon modules have passed the PVUSA qualification tests that are based on the NREL interim qualification tests and procedures for terrestrial photovoltaic thin-film, flat-plate modules.

We awarded one contract to Advanced Photovoltaic Systems under the third government/industry 50% cost-shared partnership for amorphous silicon research. This contract completed the awards under the cost-shared government/industry procurement. The principal objectives of the cost-shared government/industry research are: 1) to conduct research on semiconductor materials and non-semiconductor materials to enhance two-terminal, multijunction, thin-film, large-area, all-amorphous-silicon-alloy device performance; 2) to develop high-efficiency, *stable*, *reproducible*, and *low-cost* multijunction photovoltaic modules based on all-amorphous materials; 3) to demonstrate in stable 12% (AM 1.5) aperture-area solar conversion efficiency for different-bandgap modules; and 4) to demonstrate in stable 10% (AM 1.5) aperture-area solar conversion efficiency for same-bandgap modules. The modules will be at least 900 cm<sup>2</sup> in area and consist of at least two integrally stacked devices using all-amorphous-silicon alloy materials.

A workshop on Amorphous Silicon Solar Cell Modeling was held on July 28-29, 1992 at NREL. It was attended by 22 researchers representing 7 universities and 3 industrial companies. The workshop increased the interest of the attendees to work with the AMPS model that will be available commercially within 6 months. Researchers can currently use the model by arrangement with Penn State university.

Improved *stabilized* efficiencies (defined here as the efficiency after 600 hours of light-soaking at 50°C) for amorphous silicon modules were measured by NREL: 8.0% efficiency for a Solarex triple-junction prototype module (795 cm<sup>2</sup> aperture area), and we project 8.1% efficiency for a United Solar Systems Corporation dual-junction prototype module (920 cm<sup>2</sup> aperture area). These expected stabilized efficiencies of 7%-8% for prototype modules are a significant improvement from the 3%-5% efficiencies of such modules produced 3 or 4 years ago and the 6%-7% from 1 to 2 years ago.

United Solar Systems Corporation, (USSC) submitted a paper that reports that there is no correlation between the mid-gap defect densities of a-SiGe:H determined by constant photocurrent measurement (CPM) and the performance and stability of corresponding solar cells. This should change the modeling of a-Si:H-based solar cells and question the assumption that better alloys can be developed solely on the basis of materials analysis. Unless tested in devices, materials that are supposedly good based on materials characteristics can still result in poor device performance.

Colorado School of Mines, in collaboration with S. Guha of USSC, confirmed that increased microvoid content of intrinsic a-Si:H layers in a cell leads to inferior initial and stabilized performance. This finding is important since many materials researchers report that they have found materials with improved parameters that actually have increased microvoid content. These findings suggest that materials with increased void content may not perform well in solar cells, even if the other stabilized material parameters are improved in such materials.

The Institute of Energy Conversion (IEC) at the University of Delaware developed, in collaboration with Pennsylvania State University, a charge-defect equilibrium model that concludes that the light-induced dangling bond defect is formed in an exothermic reaction with negative entropy and free energy changes. This model suggests that the annealed state is unstable, and can only be maintained when there is a lack of free charge. IEC was able to prepare a-SiGe:H alloys with very low defect densities as measured by the University of Oregon. IEC has suggested that a-SiGe:H with inferior properties are not due to increased mid-gap defect densities, but rather because of a deterioration of electron transport.

Syracuse University reviewed most drift mobility measurements and concluded that in all a-SiGe:H alloys, there is a deterioration of the electron mobility. This suggests that while different quality alloys can be prepared, Ge-alloying causes an intrinsic degradation of electron transport.

The University of North Carolina reported that the electroluminescence in thick p-i-n junctions, when normalized for the current density, does not degrade upon light-soaking. The radiative lifetime does not shorten with photo-degradation at a temperature below 200 K. An attempt was made to describe these phenomena using a hopping transport model that includes Coulomb interaction.

The University of Oregon reported drive level (photo) capacitance results suggesting changes in the deep tail state region of a-Si:H upon light-soaking. In high-quality a-SiGe:H samples, these states may also be important. High mid-gap defect densities of states coexist in these a-SiGe:H alloys with sharp Urbach parameters. This questions the validity of certain defect equilibrium models (Stutzmann, Smith and Wagner).

Xerox reported very strong field dependencies of the conductivity of doped layers below 100 K. The conductivities are virtually temperature independent. An analysis of compensated a-Si:H sample shows 6 orders of magnitude decrease of the carrier mobilities with increased compensation. These very large decreases in mobility cannot be rationalized in terms of gap states and are attributed to potential fluctuations of the bandedges.

#### **1.2.4 PV Manufacturing Technology (PVMaT) Project**

The PVMaT project is a government/industry PV manufacturing R&D project composed of partnerships between the federal government (through the U.S. DOE) and members of the U.S. PV industry. It is designed to assist the U.S. PV industry in improving manufacturing processes, accelerating manufacturing cost reductions for PV modules, increasing commercial product performance, and generally laying the groundwork for a substantial scale up of U.S.-based PV manufacturing plant capabilities.

Phase 1 of this program, the problem identification phase, was completed early in 1991. Phase 1 competitive bidding was open to any U.S. firm with existing PV manufacturing capabilities, regardless of material or module design. Twenty-two contracts of up to \$50,000 each were awarded. Phase 2 is the process-specific solution phase of the project and addresses problems of specific manufacturers. Phase 2A, which is now under way, was open only to Phase 1 participants. Each of the seven awarded contracts is of up to 3-years in duration and is highly cost-shared between the U.S. government and U.S. industrial participants. A second, overlapping, and similar process-specific solicitation (Phase 2B) was released in June 1992, and was open to all U.S. PV manufacturing companies. Responses to this Phase 2B solicitation are being evaluated now, and subcontracted efforts are planned for later this year. A third portion of the program, called Phase 3, is also under way although slightly behind Phase 2. In Phase 3, because of the widespread interest to industry, some general issues related to PV module development will be studied through various teaming arrangements. The PVMaT project's ultimate goal is to ensure that U.S. industry retains and extends its world leadership role in the manufacture and commercial development of PV components and systems. The activities to date have received outstanding support, and the level of interest in participation is exceptional for this program.

#### **1.2.5 PV Module and System Performance and Engineering Project**

The PV module and system performance and engineering project is structured to conduct state-of-the-art PV module system research; solar radiation research; and engineering, testing, evaluation, and analysis tasks. The project also provides technical results and solutions to technical issues, develops PV standards and codes, and maintains and enhances supporting facilities and capabilities that are consistent with DOE's *Photovoltaics Program Plan (FY 1991—FY 1995)*, and are complementary to other DOE PV projects, we can ensure that project capabilities and facilities are available resources for cooperative research and utilization by the PV R&D community.

Overall project activities are managed through the module and systems performance and engineering project management task and organized to address project objectives through the following five primary tasks: 1) cell and module standardized characterization performance; 2) module and system performance testing; 3) module reliability research; 4) solar radiation research; and 5) standards development. Subcontract activities represent support for industry/utility PV power projects, domestic and international standards codes development, and PV technology validation at the module/array level of operation.

At the end of FY 1992, all subcontracts had been negotiated under the RFP No. RF-1-11061, "Amorphous Silicon Utility/Industry Photovoltaic Power Project." The objective of the project is to advance the performance of amorphous silicon photovoltaic modules and validate the performance at both the module and system levels. All subcontracts consist of a Phase I for module development and validation and a Phase II for system deployment and validation. At the end of FY 1992, two subcontracts were awarded and four were in the approval cycle. Subcontracts were negotiated with Integrated Power Corporation, Energy Conversion Devices, Solarex, Utility Power Group, Energy Photovoltaics, and Advanced Photovoltaic Systems. The delay (approximately 1 year) in negotiations and awards resulted from additional contractual complexities needed to satisfy the Source Selection Official's determination. Under this project, the earliest possible system deployment date is in the summer of 1993 by Integrated Power Corporation. This 15-kW(ac) system will use modules from United Solar Systems Corporation (USSC) and will be installed in the service territory of the New York Power Authority to augment power requirements for charging batteries for the New York Transit Authority.

Two contracts with USSC and Solar Cells Inc. for module/array technology validation were initiated. The Solar Cells Inc. activity (in support of the PV USA EMT-3 technology validation requirement) included installing a unique array support structure at NREL's outdoor test site. The CdTe modules selected are required to pass the module qualification tests before delivery to NREL for deployment at the 1-kW level. The USSC 1.0-kW amorphous silicon system has been delivered to NREL and installed, with operation completed in late 1992.

Management and administration of the IEC/TC82 and U.S.TAG included meetings of working groups and the development of an omnibus document for qualification testing of crystalline silicon flat-plate modules. This document is being readied for publication by the IEC central office.

### **1.2.6 PV Analysis and Applications Development Project**

In response to the opportunity presented by the transfer to NREL of additional in-house PV program funds, a new FWP entitled Analysis and Applications Development was created in May 1992. This new FWP brings together a variety of senior NREL PV personnel to focus additional attention on the growing analytical and applications development needs of the DOE PV Program and the DOE Office of Solar Energy Conversion.

During FY 1992 activities included in-house investigations and management of subcontracted efforts (both through NREL and in support of the DOE NAO) that supported several broad analysis and applications development areas, including: *Solar 2000*, value analysis, PV-DSM analysis, PV in buildings (PV:BONUS), PV in transportation, *Sunrayce '93*, PV market assessments, *Soltech '93*, and coordination and support of state PV collaborative and regulatory interfaces, including the PV4U industry-led effort and the newly formed Utility PV Group. An activity that emerged at the very end of FY 1992 that was supported and implemented by the analysis and applications development project was the Brazilian Rural Electrification Pilot Project.

### **1.3 Technology Transfer**

Consistent with recent DOE policy, technology transfer within NREL's PV Program is defined as collaborative R&D with industry to aid industry in the commercialization of products or services. An underlying theme of NREL technology transfer activities is the joint work accomplished by industry researchers and NREL researchers focused on a common R&D objective. Among government laboratories, there are seven principal tools for effecting technology transfer: subcontracted R&D, cooperative R&D, industry sponsored R&D, user facilities (at NREL), technology licenses, researcher exchanges, and information dissemination. NREL's PV program conducts its technology transfer primarily through three of the above: subcontracts, informal cooperative R&D, and information dissemination.

#### **Subcontracts with Industry**

In FY 1992, NREL had 7 PVMaT cost-shared subcontracts to industry totaling 10.2 million dollars. The industry contribution to these research projects totals about 6.3 million dollars. Technically knowledgeable NREL research managers participate in the definition, evaluation, award, and negotiation of statements of work submitted by industry researchers in R&D proposals. Following subcontract awards, NREL subcontract managers direct and evaluate research progress; they made numerous site visits to subcontractor facilities in FY 1992 to review research progress. A fundamental assumption of NREL's PV Program is that technology development done by industry researchers circumvents the obstacles to technology transfer that are intrinsic in technology development done by NREL in-house research.

#### **Informal Cooperative R&D**

NREL in-house researchers frequently perform informal cooperative R&D with their industrial counterparts working under NREL subcontracts. These interactions have been virtually ongoing since NREL (SERI) PV research started in 1977. The majority of these informal cooperative R&D activities involves performance measurements and materials analysis performed with NREL's large and unique set of capabilities for photovoltaic efficiency and materials analysis. Informal cooperative R&D, as distinguished from formal cooperative research and development agreements (CRADAs), are a natural complement to NREL's subcontracted PV program. CRADAs, as authorized by the National Competitiveness Technology Transfer Act of 1989, are formal agreements signed by the NREL director and his industrial counterpart for the conduct of joint research projects involving both NREL and industrial researchers. No CRADAs were signed in FY 1992. Informal cooperative R&D in FY 1992 included the analysis of more than 10,000 samples of materials, devices, or modules. More than 100 companies worked with NREL researchers in this fashion. The following list from 1 month's activities (not at all a complete listing for the year) illustrates the large, small, PV, and non-PV companies working with NREL researchers: AstroPower, Mobil Solar, Golden Photon, Martin Marietta, Siemens Solar, ISET, Spectrolab, Chorus Corporation, Spire Corporation, Solarex Corporation, Energy Photovoltaics, SCI, APS, USSC, Public Service Company of Colorado, Utility Power Group, Photcomm, Photon Energy, Tideland, MEMC Electronic Materials, and EPRI.



## Information Dissemination

During FY 1992, there were various conferences, meetings, or workshops organized with the help of PV program staff members. These events include the 22nd IEEE PV Specialists Conference and the International Solar Energy Society Conference. Other workshops were the Photovoltaic Performance and Reliability Workshop and one entitled Role of Point Defects and Defect Complexes in Silicon Device Fabrication. These gatherings provide important opportunities for industry researchers to exchange technical information with NREL and NREL-subcontracted university researchers. These information dissemination activities do contribute to progress for industry researchers; one measure of progress is the joint publications of NREL and industry researchers that describe the outcome of their joint research endeavors. A small sampling taken from the conference proceedings of the 22nd IEEE Photovoltaic Specialists Conference showed NREL researchers publishing in conjunction with researchers from Spectrolab Inc., Boeing, ISET, Photon Energy Inc., AT&T Microelectronics, and Varian Research Center.

### 1.4 Conclusions

This report reviews the FY 1992 subcontracted R&D activities under the NREL Photovoltaic Program. Most of these activities were wholly implemented through NREL. In FY 1992, DOE assigned responsibility for their technical support to the NREL PV Program. Those NAO efforts are also reported in this document.

Major PV program thrusts in FY 1992 continued to be implemented based on DOE's *Photovoltaics Program Plan FY 1991—FY 1995*. The mission of the National Photovoltaics Program is to develop photovoltaic technology for large-scale generation of economically competitive electric power in the United States. The major challenge in fulfilling the mission is to assist industry in laying the foundation for the installation of at least 1000 MW of electrical capacity by the year 2000. In FY 1992, the balance of activities was readjusted to changing DOE PV Program priorities -- now three relatively equal priority activities - 1) technology development and validation, 2) market conditioning, and 3) project venturing.

In summary, the NREL PV program involves conducting basic, applied and engineering research; managing subcontracted R&D projects; performing research complementary to subcontracted work; developing state-of-the-art measurement and device capabilities; performing PV manufacturing technology and module development; transferring results to industry, and evolving viable partnerships for PV systems and market development. The subcontracts described in this report include many activities that encompass close collaborations with NREL in-house PV researchers. Further, the implementation of the subcontract program is based on competitive public solicitations. One of the most important subcontract mechanisms is in the form of government/industry partnerships, with industry frequently sharing the cost of research with DOE. More than 50% of the NREL PV program budget is allocated yearly to subcontracts. In FY 1992, we managed 80 subcontracts with total funding of \$22.3 million. Cost-sharing by 16 industry subcontractors added an additional \$10 million to the NREL funding. Sixty per cent of the NREL subcontracts were with universities, at funding of \$5.1 million.

The subcontract activities of the NREL PV program are summarized under the following sections: 2.0 Amorphous Silicon, 3.0 Polycrystalline Thin Films, 4.0 Crystalline Materials and Advanced Concepts, 5.0 Photovoltaic Manufacturing Technology Project, 6.0 Module and System Performance and Engineering, and 7.0 PV Analysis and Applications Development Project. The sections include a brief overview including the objectives, approaches, and some key developments. Following that are technical summaries of the subcontract activities in that area. The summary sections were provided by the subcontractors themselves or were compiled from various project reports submitted by the subcontractors. Section 8.0 lists FY 1992 subcontracts, and Section 9.0 lists major subcontractor reports.



## 2.0 CRYSTALLINE MATERIALS AND ADVANCED CONCEPTS

John Benner (Manager)

The project supports the time-phased development of the analytical capabilities and advanced technologies needed to assist the photovoltaics industry in developing high-efficiency products for evolving markets. In FY 1992, this project addressed this goal by pursuing three objectives: 1) assist the photovoltaics industry on current production problems through analysis and optimization of silicon crystal growth and post-growth cell fabrication processes, as well as continuation of technology transfer of the NREL-developed GaInP solar cell; 2) develop cost-effective materials preparation technologies for advanced thin crystalline films of silicon, gallium arsenide (GaAs) and other compound semiconductors for ultra-high-efficiency concentrator cells and next generations of flat-plate modules; and 3) support fundamental and exploratory research to assure the continued source of new ideas for future products.

Experimental and theoretical evidence indicates that crystalline photovoltaic materials will be needed for advanced solar cells designed to reach the upper range of the *Photovoltaics Program Plan FY 1991 - FY 1995* efficiency goals, namely approaching flat-plate module efficiencies of 20% in the near-term and exceeding 25% in the long term. Although most of the program's efforts are focused on manufacturing issues and cost reduction for lower efficiency technologies, the crystalline technologies path to high efficiency serves two important purposes. First, high efficiency is the program's hedge should the targets for the balance of system costs prove too low. Second, it is generally accepted that utilities seek high-efficiency technologies in all power generation options and thus will prefer, and potentially demand, high-efficiency modules for their photovoltaic applications as well.



**Title:** Arsine and Hydride Generation for MOCVD Growth

**Organization:** Electrical Engineering Department, Colorado State University, Fort Collins, Colorado

**Contributors:** G. J. Collins, principal investigator; D. M. Shaw, B. G. Pihlstrom, and J. Lurkins

## Objectives

The objective of this program is to develop the capability to generate in-situ arsine and hydride radicals from lower toxicity solid precursor sources of arsenic. These techniques are then applied to the deposition of arsenic containing semiconductors. The emphasis is on the toxicity reduction of the starting material as well as the reduced deposition temperature due to the reactivity of the hydride radicals. These hydrogenated species are generated with microwave excited hydrogen plasmas. To date good quality GaAs films have been deposited and characterized. However, initial attempts to grow AlGaAs have yielded films of very low quality due to high levels of oxygen. We speculate that the hydrogen plasma etching of the quartz tube in the arsine generator is the source of the oxygen.

## Microwave Plasma Source

The in-situ generation of arsenic hydrides is accomplished by reacting an upstream microwave hydrogen plasma with solid arsenic located 2-3 cm downstream of the microwave cavity. The arsenic gasification region is intentionally air cooled and measurements of the external temperature shows no increase from room temperature during plasma gasification. The arsine generator employs a 120 W/2.45 GHz microwave source coupled to a 10 mm diameter, 15 cm long quartz tube via an Evanson microwave cavity<sup>1</sup> and is shown in Figure 1. The hydrogen flow rate through the tube ranges from 10-50 sccm. Arsenic hydrides at flow rates of 0.5-0.6 sccm are generated by etching the solid arsenic placed downstream of the cavity, which are then transported to a low pressure reactor, providing arsenic precursors for epitaxial film growth.

## GaAs Film Growth Studies

Initial GaAs film growth studies incorporated trimethylgallium (TMGa) as the group V precursor. The films grown were of good quality, however, they contained high levels ( $10^{19}$ - $10^{20}$  cm<sup>-3</sup>) of carbon, as well as silicon and oxygen ( $10^{17}$ - $10^{18}$  cm<sup>-3</sup>.) We speculate the oxygen and silicon contamination is the result of plasma etching of the quartz wall in the arsine generator. Complete results of these studies have been published<sup>2,3</sup>.

Triethylgallium (TEGa) was then used as the group V precursor in order to lower the carbon levels in the deposited films<sup>4</sup>. The films are grown at V/III ratios of 8-12, and at temperatures of 370-415 °C. Using TEGa lowers the carbon levels

by about two orders of magnitude to the  $10^{17}$ - $10^{18}$   $\text{cm}^{-3}$  range.

The resulting films are n-type, with silicon as the apparent doner. We speculate the Si doping is the result of plasma etching of the quartz wall of the arsine generator, as in the case of the TMGa films. Hall mobility of the deposited films range from a low of  $300 \text{ cm}^2 \text{ V}^{-1} \text{ s}^{-1}$  to  $550 \text{ cm}^2 \text{ V}^{-1} \text{ s}^{-1}$ . Resistivity of the films ranges from  $5 \times 10^{-4}$  to  $2 \times 10^{-3}$  ohm-cm. Oxygen levels in the TEGa films are similar to the levels in the TMGa films.

#### AlGaAs Film Growth Studies

We have begun studying the growth of AlGaAs films using the in-situ arsine generator. The gallium precursor is TEGa, and the aluminum source is dimethylaluminum hydride (DMALH.) To date, the films have been of low quality, with the expected high oxygen content.

#### Conclusions and Future Work

In-situ generation of arsenic hydrides has been accomplished. The benefits of in-situ arsenic hydride generation are increased safety and lower deposition temperature due to higher reactivity of the hydrides. The arsenic hydrides have been used to deposit good quality GaAs films containing carbon, silicon, and oxygen contaminants. Recently, we have started work on AlGaAs film deposition, which will lead to GaAs/AlGaAs heterostructures. Additional future work includes finding ways to lower the oxygen output and increase the arsine output of the generator.

#### References

1. K. Evanson, Rev Sci. Instr. 36, 294 (1965).
2. B. G. Pihlstrom, T. Y. Sheng, L. R. Thompson, and G. J. Collins, Appl. Phys Lett. 60 (1992).
3. B. G. Pihlstrom, L. R. Thompson, D. M. Shaw, A. D. Simone, T. Y. Sheng, J. Lurkins, and G. J. Collins, J. Elec. Mat., to be published.
4. G. B. Stringfellow, Organometallic Vapor-Phase Epitaxy: Theory and Practice (Academic Press, Inc., San Diego, 1989).

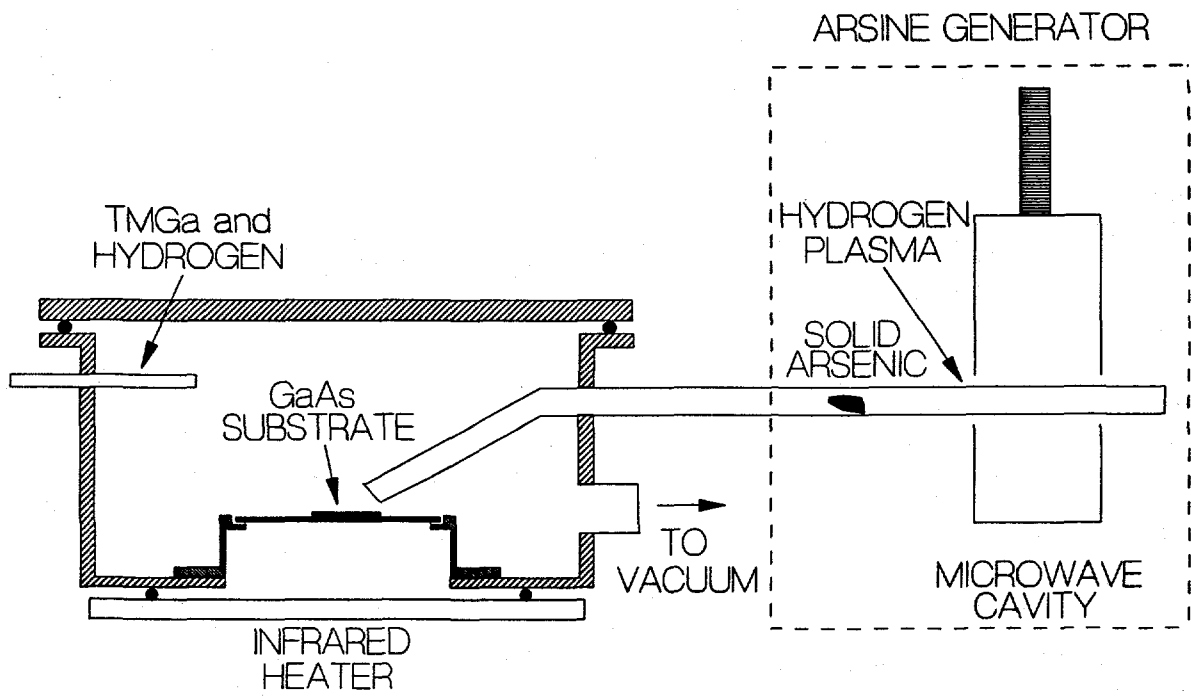


Figure 1. Schematic of MOCVD system showing attached microwave plasma arsine generator.



**Title:**           **Influence of Self-Interstitials Injected by Phosphorus Diffusion on Defect Structures and Electronic Properties in Crystalline Silicon**

**Organization:**   School of Engineering, Duke University, Durham, North Carolina

**Contributors:**   T. Y. Tan and U. Goesele, principal investigators;  
W. J. Taylor, post-doc; and R. Gafiteanu, graduate student

## **Introduction**

Single crystalline and polycrystalline silicon solar cells are the most widely used commercial photovoltaic solar cells. The NREL's Crystalline Silicon Materials Research Program aims to assist in the development of new processing and characterization techniques to improve the quality of commercial silicon substrates to produce 16% to 18% commercial solar cells. Our efforts will address both processing (phosphorus diffusion) and characterization ( $L_D$  measurement).

The minority carrier diffusion length ( $L_D$ ) is an essential materials parameter influencing the efficiency of crystalline silicon solar cells. In polycrystalline silicon, hydrogen passivation is frequently used to stabilize the electrically active defects and increase  $L_D$ , but the results are still far from that of single crystalline float zone silicon, where  $L_D$  is on the order of 500 $\mu$ m. Assuming that the grains in polysilicon are large, the effects of grain boundaries can be safely ignored (especially after  $H_2$  passivation). The remaining defects possibly causing this low  $L_D$  in polycrystalline silicon are dislocations, dissolved metallic impurities and point defect agglomerates, involving typically one or more of the following constituents: silicon self-interstitials or vacancies, carbon and oxygen.

Intrinsic point defects, self-interstitials, and vacancies, are present in non-equilibrium concentrations during crystal growth or during the formation of the  $n^+p$  junctions by high concentration phosphorus diffusion. These non-equilibrium concentrations affect several processes which have a direct or indirect influence on  $L_D$ . We therefore are concentrating our efforts on obtaining a better understanding of the processes associated with phosphorus in-diffusion. Specifically, we are investigating the injection of self-interstitials by phosphorus diffusion and the resulting changes in defect structures and the associated electronic properties in dislocations and precipitates

The first year objectives include experimental work on phosphorus in-diffusion (testing a variety of diffusion sources, substrates, and diffusion conditions), numerical modeling of this process to allow prediction of self-interstitial supersaturation profiles in both low and high dislocation density silicon, achieving the capability to use wafer bonding as a means of generating dislocations to allow subsequent studies on their electrical properties (EBIC), and bringing on-line a spatially resolved diffusion length measurement machine (ELYMAT). We have made significant progress in all areas.

## **Phosphorus Diffusion Experimentation and Modeling**

A basic process in the fabrication of all crystalline silicon solar cells is the diffusion of high concentration phosphorus into boron doped substrate to produce  $n^+p$  junctions. In-diffusion of a high concentration of phosphorus into silicon is known to be associated with

a self-interstitial supersaturation (which causes the classic kink-and-tail profile). These interstitials diffuse into the bulk silicon and may influence a variety of processes, such as nucleation and climb of dislocations, nucleation and growth of precipitates, and gettering of metallic impurities. The precipitates of interest in polycrystalline silicon involve oxygen ( $\text{SiO}_2$ ) and carbon (either  $\text{SiC}$  or  $\text{SiO}_2\text{C}_x$ ), all of which involve volume changes, and hence, either compressive or tensile strain. Thus, in addition to the unsatisfied bonds at the precipitate/matrix interface affecting electronic properties, the strain may also play a role. In order to understand the effects of these self-interstitials on the electronic properties in the bulk, we must first have an understanding of their presence (supersturations) throughout the bulk. Since self-interstitials can not be detected analytically, we will combine experimental phosphorus in-diffusion profiles with a numerical model of the phosphorus in-diffusion process (which includes the interaction between phosphorus and self-interstitials and predicts self-interstitial profiles).

We have begun our experimental work by studying several parameters involved in phosphorus in-diffusion: phosphorus spin-on glass vendor and concentration, and spin-on conditions (spin-on glass coverage, pre anneals, lag-time between application and diffusion). Initial tests were performed at  $900^\circ\text{C}$  for 30 minutes on CZ silicon, to avoid any complications which dislocations may present. Results of this study indicate that a one-hour lag time between evaporation of spin-on glass solvents and diffusion may be better (more consistent results) than immediate diffusion. Longer lag time (24 hours) produces poor results. We have also investigated two means of measuring the diffusion profile: spreading resistance profiling and electrochemical etch profiling. Both techniques rely heavily upon the experience of the researcher. It appears that at this time in our group, spreading resistance profiling provides more consistent results.

The second round of experiments involved both single and polycrystalline silicon. We have obtained polycrystalline samples from a variety of vendors, including Mobil Solar, Solarex, Osaka Titanium, Wacker Silso, Heliodynamica and HEM. A primary objective of this experiment is to determine whether a high density of dislocations in polycrystalline silicon will prevent a self-interstitial supersaturation from spreading throughout the entire thickness of the material. These results can assist in obtaining an estimate for the diffusivity of silicon self-interstitials. (See Chapter 2 of reference <sup>1</sup>)

The numerical modeling is based upon the pair diffusion model of Orlowski<sup>2</sup>. We have included both self-interstitials and vacancies in the model, and obtain reasonable correlation to phosphorus in-diffusion data. The predicted profiles for self-interstitials indicate that within 30 minutes at  $900^\circ\text{C}$ , supersaturations extend a considerable distance into the bulk.

### Dislocation Generation

In order to investigate the influence of the injected self-interstitials on the electrical properties of dislocations and oxide-silicon interfaces, we wish to develop techniques to consistently create these defects. Two model systems are under study. Oxidation of silicon allows one to generate a distribution of stacking faults at the wafer surfaces, which are surrounded by *edge* dislocations of Burger's vector  $1/3 \langle 111 \rangle$ . By controlling the misalignment when bonding two (100) silicon wafers, however, one can create a defined planar array of misfit *screw* dislocations with Burgers vector  $1/2 \langle 110 \rangle$ . Because of volume considerations at the dislocation core, we believe that the screw dislocation, particularly when dissociated, is difficult to passivate with hydrogen. When subjected to a subsequent self-

interstitial supersaturation during a phosphorus in-diffusion, these screw dislocations are expected to grow via a climb process. This summer, we were able to obtain a stable array of misfit screw dislocations via the wafer bonding technique, see Fig. 1. We are currently preparing new samples for the phosphorus diffusion and electrical characterization (EBIC) steps.

The wafer bonding technique can also be used to study the electrical properties of the silicon/oxide interface. The oxides produced by wafer bonding may either be a continuous film or be an array of oxide precipitates distributed in a defined pattern and size range. The electrical activity of both types will be examined before and after self-interstitial injection.

### Minority Carrier Lifetime Measurement

One means of testing the electrical properties of samples is with the ELYMAT<sup>3,4</sup> machine, which utilizes a silicon/electrolyte (3%HF) contact on both sides of a sample. This contact not only behaves as a Schottky diode, but also passivates the surface so that surface recombination effects are minimized. HeNe laser light passes through the electrolyte at the front surface, and introduces carriers which are then collected at the back surface. By comparing the voltages at the front and back surfaces,  $L_D$  can be derived. The laser light can be scanned across the surface of the wafer to obtain spatial variations in  $L_D$ . The system is now operational in our lab, and we are working with it to eliminate the primary causes of uncertainty in measurements, and to develop confidence in measurement repeatability. This system offers the potential of rapid, non-destructive evaluation of material prior to processing, where costs are still low. Furthermore, the spatial resolution of the technique, and the ability to measure voltages at both front and back surfaces allows monitoring of processing conditions (i.e. "is lifetime severely altered in the vicinity of contacts?").

### Modeling Precipitate Growth and Shrinkage

During the high concentration phosphorus in-diffusion, the generated self-interstitials enter the bulk and can there affect precipitation behavior. The common precipitants in solar-grade silicon are oxygen and carbon. Precipitation of these species involves changes in volume, which introduces strain. The excess free energy associated with this strain has a significant impact on precipitation behavior, and therefore can not be ignored. Typically, this strain must be relieved, either by emission of silicon self-interstitials, absorption of vacancies, or absorption of (small) carbon atoms. We addressed this topic in a previous project,<sup>1</sup> and are continuing theoretical work in this area to facilitate our understanding of the growth or dissolution of oxygen microprecipitates during solar cell processing. The interaction between precipitates and prismatic dislocation loops,<sup>5</sup> general models for strain relief during precipitation,<sup>6</sup> the interaction between oxygen and carbon during precipitation<sup>7</sup> and the likelihood of SiC precipitation in silicon<sup>8</sup> have all been addressed.

### References

- 1.) U. Gösele, T. Y. Tan, B. P. R. Marioton, W. J. Taylor, and W.-S. Yang, Final Report for Solar Energy Research Institute Subcontract # XL-8-18097-1 (1992).
- 2.) M. Orlowski, Appl. Phys. Lett. **53**, 1323 (1988).
- 3.) V. Lehmann, and H. Föll, J. Electrochem. Soc. **135**, 2831 (1988).

- 4.) H. Föll, V. Lehmann, G. Zoth, F. Gelsdorf, and B. Göttinger, in *Analytical Techniques for Semiconductor Materials and Process Characterisation*, edited by B. O. Kolbesen, D. V. McCaughan, and W. Vandervorst (Electrochem Soc., Pennington, 1989)
- 5.) W. J. Taylor, U. Gösele, and T. Y. Tan, *J. Appl. Phys.* **72**, 2192 (1992).
- 6.) W. J. Taylor, U. M. Gösele, and T. Y. Tan, Submitted to *Mat. Chem. and Phys.*
- 7.) W. J. Taylor, U. Gösele, and T. Y. Tan, To be submitted to *Appl. Phys. Lett.*
- 8.) W. J. Taylor, T. Y. Tan, and U. Gösele, Submitted to *Appl. Phys. Lett.*

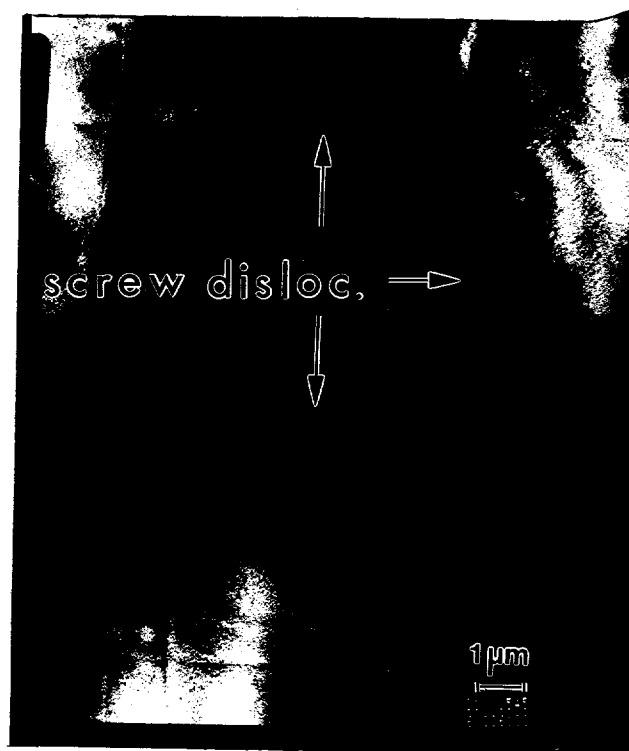


Figure 1. A transmission electron microscope micrograph of the screw dislocation network produced by the wafer bonding method.

**Title:** Fundamental Research on Post-Growth Quality Enhancement Techniques in Crystalline Silicon

**Organization:** Georgia Institute of Technology, Atlanta, Georgia 30332

**Contributors:** A. Rohatgi, Z. Chen, W. A. Doolittle, J. Salami, and P. Sana

### Objective

The objective of this research is to develop a basic understanding of various post-growth quality enhancement processes and apply them to fabricate high efficiency polycrystalline silicon solar cells. In this report major emphasis is placed on phosphorus gettering, aluminum treatment and PECVD coatings for achieving high efficiency polysilicon cells.

### Phosphorus and Aluminum Gettering of Cast Polysilicon

In this study phosphorus diffusion on the front and aluminum treatment on the back were used as the main gettering steps, which also form the  $n^+$ -emitter and  $p^+$ -back surface field, respectively. Thus, gettering is an integral rather than additional part of the cell process sequence. Prior to fabricating the high efficiency cells, baseline experiments were conducted to optimize the gettering conditions. A  $0.8 \Omega\text{-cm}$  p-type cast polycrystalline silicon from Osaka Titanium Co. (OTC) was used in this investigation.

Phosphorus gettering was performed at  $930^\circ\text{C}$  for 25 minutes, using solid sources. In order to take advantage of this intense phosphorus gettering, without paying the penalty of heavy doping effects in the emitter, a controlled etch-back technique was used to partially etch the  $n^+$ -region. A  $\text{HNO}_3\text{:HF:H}_2\text{O}$  [1000:1:100] etch was used in our process sequence to increase the emitter sheet resistance in the range  $16 \Omega/\square$  to  $80 \Omega/\square$  by varying the etch time. The cells with high emitter sheet resistance of  $80 \Omega/\square$  gave the highest  $V_{oc}$ ,  $J_{sc}$  and cell efficiency while the cells with  $16 \Omega/\square$  emitter gave the lowest efficiency. No attempts were made to increase the sheet resistance beyond the  $80 \Omega/\square$  because the grid design used in this study was not suitable for greater than  $100 \Omega/\square$  sheet resistance. Aluminum gettering was performed by evaporating  $1\text{-}2 \mu\text{m}$  thick Al on the back of the cells followed by a high temperature drive-in for 35 minutes. Oxide passivation was done during the Al drive-in to simplify and maintain the cost effectiveness of the process sequence. In an earlier study it was found that  $850^\circ\text{C}$  is the optimum drive-in temperature for the OTC cast polysilicon. After a  $1.2 \mu\text{m}$  thick Al evaporation on the back, wafers were slowly inserted in a furnace maintained at  $850^\circ\text{C}$  with oxygen ambient in order to grow  $\sim 100 \text{ \AA}$  thick passivating oxide on top of the  $n^+$  emitter region on the front. After about 5 minutes of oxide growth, gas ambient was switched to nitrogen for an additional 30 minute Al drive-in. The temperature was ramped down to  $400^\circ\text{C}$  and then forming gas was switched on for two hours. Some cells were also fabricated without the oxide passivation or without the Al layer during the drive-in process to quantify the merit of oxide passivation and Al treatment on polycrystalline cells. It is shown that Al treatment forms Back Surface Field (BSF) and improves bulk lifetime from  $10 \mu\text{sec}$  to  $24 \mu\text{sec}$  but it reduces Back Surface Reflection (BSR) from 85% to 69% and gives high  $J_0$  ( $\geq 10^{-12} \text{A/cm}^2$ ) because of the rough Al-Si alloyed back surface. Aluminum treatment contributed to about 1% (absolute) increase in cell efficiency, Figure 1. Front oxide passivation resulted in an additional  $\sim 1\%$  (absolute) increase in the efficiency of these properly gettered polysilicon cells. Oxide passivation reduced  $J_0$  by a factor of two and increased  $J_{sc}$  by  $1 \text{ mA/cm}^2$ .

## Effects of PECVD SiO<sub>2</sub>/SiN AR Coating On Polysilicon Solar Cells

Application of a novel plasma enhanced chemical vapor deposition (PECVD) of SiN and SiO<sub>2</sub> double layer coating, followed by rapid thermal anneal (RTA), gave remarkable improvements in cell parameters of 9-10% efficient unpassivated polysilicon cells without AR coating. Table I shows 60% increase in J<sub>sc</sub>, 24 mV improvement in V<sub>oc</sub> and greater than 60% increase in cell efficiencies. Detailed analysis showed that these improvements resulted not only from good antireflection property of PECVD SiO<sub>2</sub>/SiN, but also from defect and surface passivation effects on polysilicon cells. The passivation effects were studied by internal quantum efficiency (IQE) measurements and PC-1D modeling. It is found that the PECVD SiO<sub>2</sub>/SiN followed by RTA can passivate both surface and bulk defects in polysilicon cells. Significant reduction in front surface recombination velocity (S<sub>f</sub>) and minority carrier lifetime (τ) in bulk were observed in Osaka Titanium polysilicon. Measured IQE data and PC-1D modeling showed, that S<sub>f</sub> decreased from 2x10<sup>5</sup> to 5x10<sup>4</sup> cm/s and τ increased from 10 to 20 μsec, due to the PECVD coating. The calculated improvements in J<sub>sc</sub> and V<sub>oc</sub> due to antireflection properties, surface passivation, and bulk passivation due to PECVD SiO<sub>2</sub>/SiN coating are listed in Table II.

## Fabrication of High Efficiency Polysilicon Solar Cells Using Al and Phosphorus Gettering

A combination of optimum phosphorus and aluminum gettering, oxide passivation, and ZnS/MgF<sub>2</sub> double layer antireflection coating resulted in record 17.7% efficient polycrystalline silicon solar cells under one sun illumination, tested and verified by NREL, Figure 2.

After matching the measured cell parameters of the 17.7% efficient polycrystalline cell using PC-1D model, attempts were made to change the cell design and material properties to provide guidelines for achieving even higher efficiencies. Figure 3 shows that increase in the carrier lifetime from 25 to 100 μsec increases the absolute efficiency by less than 0.5% for this cell with unpassivated BSF. Therefore additional gettering will not help this cell much unless BSF or BSRV are improved. Model calculations revealed that some gettering was very important for these polycrystalline cells because efficiency increases rapidly in the lifetime range of 5 to 25 μsec. Beyond τ = 40 μsec relative improvement in cell efficiency becomes very small. Model calculations show that even with the increase in bulk lifetime value up to 1 msec, an efficiency of only 18.6% can be realized with this cell structure. Figure 3 also shows that front surface texturing alone, using slats or grooves with a pitch of 100 μm and slat angle of 60°, can raise the efficiency of this cell to 18.5%. Finally, Figure 3 demonstrates that a combination of reduced BSRV, increased base doping from 10<sup>16</sup> cm<sup>-3</sup> to 9x10<sup>16</sup> cm<sup>-3</sup>, without sacrificing lifetime, and front surface texturing can produce ≥20% efficient polycrystalline silicon cells. Attempts are being made to incorporate some of these modifications.

## References

- (1) A. Rohatgi, P. Sana, J. Salami, "Record High Efficiency Solar Cell On Cast Polycrystalline Silicon", to be published in the proceedings of 11th European Photovoltaic Solar Energy Conference, Montreux, Switzerland, 1992.
- (2) P. Sana, J. Salami, and A. Rohatgi, "Fabrication and Analysis of High Efficiency Polycrystalline Silicon Solar Cells", to be published in IEEE Transactions of Electron Devices.

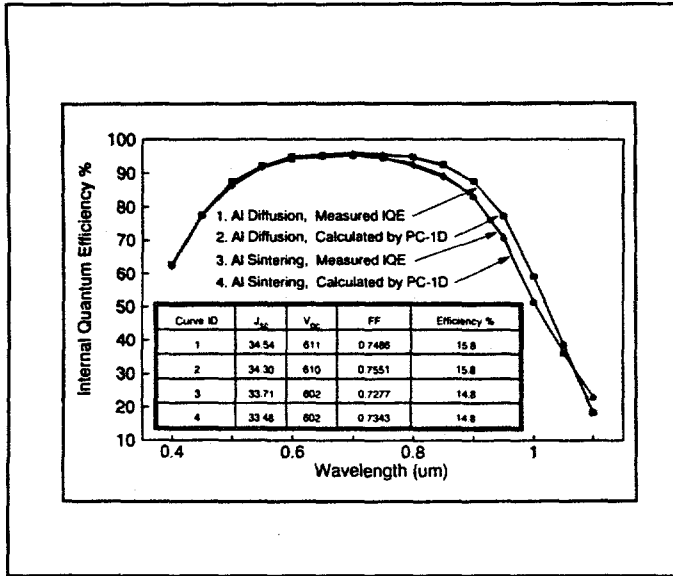


Figure 1. A comparison of measured and modelled IQE and cell data for Al diffused and Al sintered cells

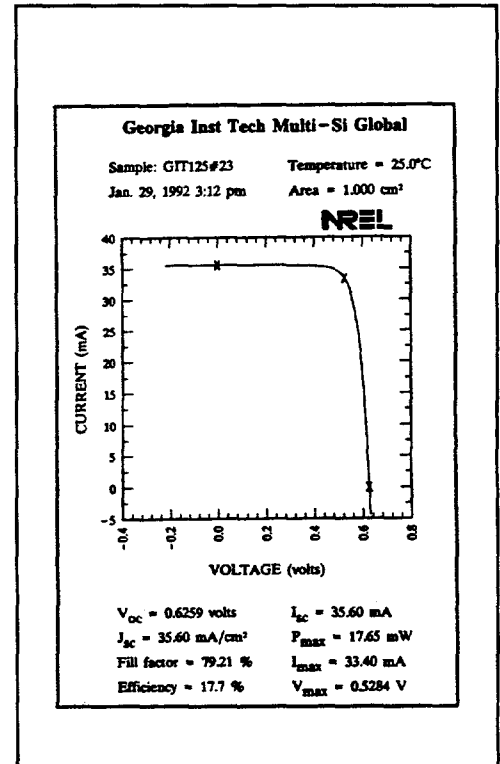


Figure 2. Light I-V data of the 17.7% efficient OTC polysilicon cell.

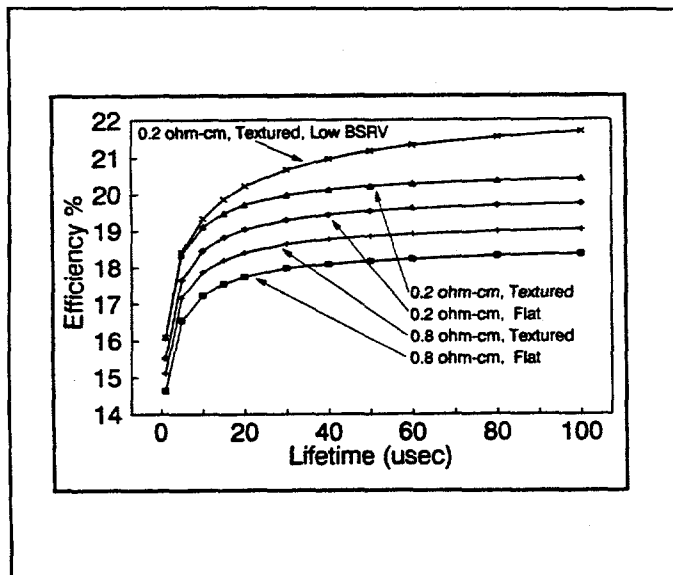


Figure 3. Model calculation for achieving greater than 20% efficient polysilicon cell.

**Table I.** The effects of PECVD SiO<sub>2</sub>/SiN coating and rapid thermal annealing on unpassivated cell parameters

ID	J <sub>sc</sub> (mA)	V <sub>oc</sub> (mV)	FF	Eff(%)
before AR coating	21.7	587	0.77	9.85
after AR coating	31.72	599	0.64	12.26
AR coating+RTA	34.54	611	0.75	15.81

**Table II.** PC-1D calculated J<sub>sc</sub> and V<sub>oc</sub> due to antireflection, surface/bulk passivations and positive charge effect, respectively.

ID	J <sub>sc</sub> (mA)	V <sub>oc</sub> (mV)	net effect on J <sub>sc</sub> and V <sub>oc</sub>	parameters used in PC-1D
uncoated	21.84	586		S <sub>f</sub> =2E5, τ=10
antireflection effect	31.39	596	9.55mA, 10mV	S <sub>f</sub> =2E5, τ=10
surface passivation effect	33.08	602	1.69mA, 6mV	S <sub>f</sub> =5E4, τ=10
bulk passivation effect	33.61	608	0.53mA, 6mV	S <sub>f</sub> =5E4, τ=20



**Title:** High-Efficiency Thin-Film Solar Cells

**Organization:** Kopin Corporation  
Taunton, Massachusetts

**Contributors:** R.P. Gale, principal investigator; B.D. Dingle, J.V. Gormley,  
R.W. McClelland

### **Objectives**

The objectives of this research program are to investigate thin-film GaAs-GaInP cells using the CLEFT technique and to determine the process to enable overgrowth of GaAs films using organometallic chemistry.

### **GaInP Growth and Characterization**

The application of the CLEFT thin-film technique to GaInP/GaAs solar cells and organometallic overgrowth was investigated. Growth experiments were carried out using tertiarybutylphosphine (TBP) as the group 5 source, resulting in GaInP layers grown latticed matched to GaAs. The layers had good surface morphology and exhibited strong room-temperature photoluminescence (PL).

Baseline GaInP layers grown in one of our research reactors exhibited less than 100 arc-sec of mismatch to GaAs substrates, with a full width at half maximum (FWHM) of 80 arc-sec as measured by double-crystal X-ray diffraction. The layers were In-rich. The surfaces were specular. The room-temperature PL intensity was 3200 mV/mW @654 nm. N-type samples measured by transient PL at NREL showed 6 ns bulk lifetime for  $5E17 \text{ cm}^{-3}$  Si doping.

Growth conditions developed for the best surface and most narrow X-ray FWHM were at 680° C and 40 torr pressure. The In:Ga ratio was 2.36, and the V:III ratio was 36 using TBP. These conditions resulted in a growth rate of 4.4 um/hr.

These conditions did not guarantee quality material, however. We were growing layers with very low minority-carrier lifetimes, causing poor solar cell performance. Samples of GaInP, GaAs, and GaInAs were grown and sent to NREL's SIMS facility for characterization. The analysis performed by S. Asher of NREL indicated excess indium at the GaInP/GaAs interface. The problem was traced to the indium source, which was changed to improve the growth. In addition, pressure was counterbalanced in the manifold to reduce potential composition fluctuations upon flow injection.

### **GaInP Cell Development**

Solar cell structures have been grown and fabricated using the growth parameters for GaAs and GaInP previously determined. Homojunction cells with GaInP window and BSF were fabricated, resulting in series-resistance limited cell efficiencies above 19% AM1.5.

Various cell structures were grown to test the effects of the cell components on cell performance. The components tested included emitter thickness and composition, and back-surface field. The best cell performance resulted from structures with a 0.2 um GaAs emitter under a GaInP window, accompanied by a GaInP back-surface field layer. The

external quantum efficiency and illuminated IV curves for one of these cells are shown in Figures 1 and 2.

The quantum efficiency is improved from our earlier cell experiments, but indicates several areas for cell current collection improvement. The peak efficiency is 0.88 at 530 nm, and drops off to about 0.7 at the band edge. This shape suggests that the GaAs base material quality could be improved. Postulating that the GaInP back-surface field (BSF) layer was causing a problem with the base layer, we grew the same structure without the GaInP BSF layer. Cells fabricated without the heterojunction BSF exhibited poorer red response, indicating that the GaInP BSF was beneficial for current collection. Further tests are underway.

The efficiency of these cells is also limited by the fill factor. As seen in Figure 2, the low fill is due to a series resistance in the cell. Emitter thickness strongly affected both current collection and fill factor, pointing to additional optimization of the emitter for higher efficiencies. However, the interfaces between the GaInP and the GaAs layers is not well characterized, and may contribute to the cell resistance.

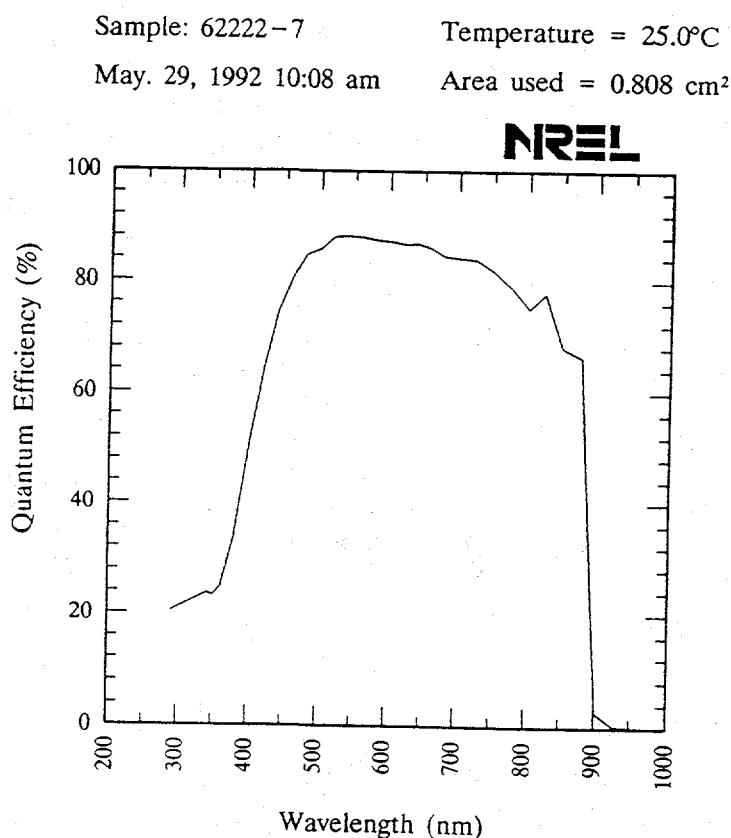
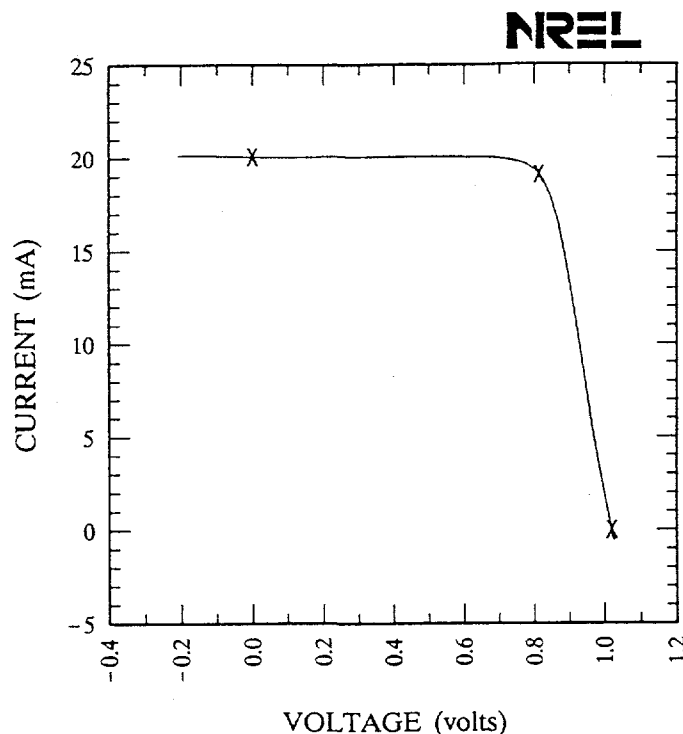


Figure 1. External quantum efficiency of a GaInP/GaAs solar cell. The cell was measured with 5.0 mA light bias, and zero voltage bias.

Sample: 62222-7  
Jun. 1, 1992 3:53 pm

Temperature = 25.0°C  
Area = 0.808 cm<sup>2</sup>



$V_{oc} = 1.020$ volts	$I_{sc} = 20.11$ mA
$J_{sc} = 24.89$ mA/cm <sup>2</sup>	$P_{max} = 15.55$ mW
Fill factor = 75.82 %	$I_{max} = 19.13$ mA
Efficiency = 19.2 %	$V_{max} = 0.8130$ V

Figure 2. I-V curve for the cell of Figure 1, under simulated AM1.5 illumination.

GaInP emitters were investigated by the growth and fabrication of heterojunction cells. These cells had 0.1 and 0.2  $\mu\text{m}$  GaInP emitters grown directly on the GaAs base, with GaInP BSF layers. The cells exhibited current loss in the short-wavelength spectrum, indicative of either absorption in the emitter or high surface recombination at the emitter-contact layer interface.

### Organometallic Overgrowth

Conditions for the in situ overgrowth by OMCVD were determined and continuous GaAs layers were grown over a separation mask layer. To enhance the overgrowth ratio and inhibit heterogeneous nucleation, HCl was added to the reactor during growth. Several of these layers have subsequently been successfully cleaved from their substrates.

Overgrowth conditions were investigated using a screening experiment. Controlled factors were the arsine flow (50 to 100 sccm), HCl flow (400 to 1200 sccm), TMGa flow (6 to 12 sccm), growth temperature (540 to 640 C), and growth pressure (90 to 130 torr). Responses were the overgrowth ratio, growth rate, and nucleation on the overgrowth mask

The experimental objective was screening, using a fractional-factorial design. Overgrowth ratios from 0 to 2 were observed with layers growing at from 0.4 to 9  $\mu\text{m}/\text{hour}$ . Nucleation was measured in areas away from the overgrowth lines.

Nucleation, overgrowth ratio, and growth rate were modeled over the parameter space. Overgrowth ratio turned out to be a complex function of all five factors (independent variables in the matrix). The linear terms were not as significant as the interactions. The maximum overgrowth occurred near the high value of the five factors, but the interesting result was that with the interactions, all of the factors had an impact on the overgrowth ratio. This result is somewhat counter productive as the objective of the screening experiment was to eliminate factors from further consideration.

Growth rate of GaAs on the witness bulk piece was most affected by the HCl flow, decreasing for the higher flow conditions. This decrease even dominated the size of the increase in growth rate with the doubling of the TMGa flow.

Nucleation on the mask was relatively rare in the matrix, being driven by increases in reactor pressure and temperature as much as by reduction in HCl flow. Since the only nucleation occurred at low values for HCl flow, temperature, and TMGa flow, nucleation was not a constraint on the overgrowth conditions.

During analysis of the above experiment, one promising set of growth conditions were repeated several times using full 3" GaAs wafers prepared for overgrowth. Continuous films of GaAs were overgrown on three wafers, demonstrating feasibility of this step. The layers were successfully separated from their substrate using the CLEFT process, demonstrating the application of overgrowth using OM chemistry with HCl.

**Title:** New Approaches for High Efficiency Solar Cell: Role of Strained Layer Superlattices

**Organization:** Electrical and Computer Engineering Department  
North Carolina State University  
Raleigh, North Carolina 27695-7911

**Contributors:** S.M. Bedair and N.A. El-Masry

### **Objective**

The object of the research is to address current problems that are hindering progress toward achieving high efficiency cascade solar cells. During the last year our efforts were directed towards the growth and fabrication of  $p^+$ -AlGaAs/ $n^+$ -GaInP heterojunction tunnel diodes with  $E_g \approx 1.9$  eV suitable for high concentration solar cells.

### **Approach**

We present a new approach to fabricate a heterostructure tunnel diode in the  $p^+$ -AlGaAs/ $n^+$ -GaInP material system with  $E_g \approx 1.9$  eV and with performance suitable for 1000 suns solar concentration. The tunnel diode was epitaxially grown at low temperature using the Atomic Layer Epitaxy growth mode approach. In the ALE growth mode the growth conditions were optimized to achieve high doping levels rather than to maintain a monolayer per ALE cycle. Carbon was chosen as the p-type dopant of AlGaAs for several reasons. First, carbon is reported to have the lowest diffusion properties compared with other p-type dopants such as Zn or Be<sup>1</sup>. Second, high doping levels in the  $10^{20}/\text{cm}^3$  range were achieved both in GaAs and AlGaAs<sup>2,4,5</sup>. Third, using the Atomic Layer Epitaxy technique, carbon is readily extracted from the decomposition products of the organometallic without the need of any new dopant source<sup>3,4,5</sup>. For the  $n^+$  side of the junction, GaInP was preferred to AlGaAs due to the difficulty of achieving  $n^+$ -AlGaAs in  $10^{19}/\text{cm}^3$  range due to the presence of high concentration of DX centers<sup>6</sup>. Selenium was used for  $n^+$ -type dopant because it has relatively shallow donor levels<sup>7</sup>. This AlGaAs and GaInP combination allows the highest doping levels, both  $p^+$  and  $n^+$ , to be achieved in these high band gap films ( $E_g \approx 1.9$  eV).

### **$p^+$ -AlGaAs**

For the AlGaAs layer, the ALE growth mode at 600 °C consisted of the simultaneous exposure of the substrate to the TMG and TMA fluxes followed by rotation to the AsH<sub>3</sub> side to complete one cycle. The composition of Al<sub>x</sub>Ga<sub>1-x</sub>As was controlled by the TMA / (TMA + TMG) molar ratio in the column III stream and was adjusted to give  $x \approx 36\%$  determined from photoluminescent measurement. The p-type carrier concentration in AlGaAs films depends on

several factors, among which the exposure time to column III sources was the most important one in our growth method. P-type carrier concentration as high as  $1 \times 10^{20}/\text{cm}^3$  was achieved when exposure times to column III and V fluxes are 0.8 and 0.3 sec, respectively. The time for one complete cycle was 3.1 sec and the growth rate was about 5 monolayers per cycle.

### **n<sup>+</sup>-GaInP**

For GaInP, due to the high Se vapor pressure, a low growth temperature ( 460 °C ) was used to achieve high levels of doping<sup>8</sup>. The substrate was exposed to TMG and TMI on the column III side for 0.3 sec, moved to the column V side and kept there under PH<sub>3</sub> and H<sub>2</sub>Se for 3.3 - 6.3 sec resulting in a growth rate of about 0.5 monolayer per cycle. A long exposure time to PH<sub>3</sub> of several seconds was required during this low temperature ALE growth mode. The composition of the as-grown Ga<sub>y</sub>In<sub>1-y</sub>P was controlled by the TMG / (TMG + TMI) molar ratio in the column III stream. The value of y was determined from x-ray diffraction and  $y \approx 0.51$  was achieved. Se doping levels depend on several parameters such as H<sub>2</sub>Se flow, growth temperature, exposure times and PH<sub>3</sub> flow. When these parameters are optimized, a carrier concentration of  $n \approx 5 \times 10^{19}/\text{cm}^3$  was measured by Hall technique for a GaInP film ( ~ 800 Å ) grown on a Si GaAs substrate. This is considered to be the highest n-type carrier concentration ever reported for any high band gap semiconductor film. Details of the doping process of GaInP will be reported later<sup>9</sup>.

### **p<sup>+</sup>-AlGaAs/n<sup>+</sup>-GaInP Tunnel Diode**

The tunnel diode structure shown in Figure 1 is grown on a Zn-doped p-type GaAs substrate and consists of 1000 Å p<sup>+</sup>-AlGaAs layer (  $p = 1 \times 10^{20}/\text{cm}^3$  ), 1000 Å n<sup>+</sup>-GaInP layer (  $n \sim 2 - 5 \times 10^{19}/\text{cm}^3$  ) and 5000 Å n<sup>+</sup>-type GaAs contacting layer. For electrical evaluation 2000 Å Au was deposited on the back side of the p-type GaAs substrate, 1000Å AuGe / 300Å Ni / 2000Å Au were deposited on the GaAs top layer using photolithography technique. Mesas with an area  $200\mu\text{m} \times 200\mu\text{m}$  were etched using a 3-step etching method. First H<sub>3</sub>PO<sub>4</sub> : H<sub>2</sub>O<sub>2</sub> : H<sub>2</sub>O = 6 : 2 : 100 solution was used to etch the GaAs top layer followed by HCl : H<sub>2</sub>O = 1 : 1 solution to remove the n<sup>+</sup> GaInP layer. Finally H<sub>3</sub>PO<sub>4</sub> : H<sub>2</sub>O<sub>2</sub> : H<sub>2</sub>O = 6 : 2 : 100 solution was used again to etch the p<sup>+</sup> AlGaAs layer and part of the p-type GaAs substrate.

Figure 2 shows the current-voltage ( I-V ) characteristics of the tunnel diode with  $n^+ \sim 2 \times 10^{19}/\text{cm}^3$  (a) at room temperature and (b) at 120 °K. At room temperature the total resistance of the structure shown in Fig.1, including the probe resistance, the series resistances of the structure and the resistances of metal contacts, is ~ 3Ω. The peak voltage  $V_{\text{peak}}$  at which the tunneling current is maximum can be estimated by  $V_{\text{peak}} \approx (V_n + V_p)/3$  where  $V_n$  and  $V_p$  are the degeneracies on the n and p side of the tunnel diode, respectively<sup>10</sup>. The calculated values of  $V_n$  and  $V_p$  on the n and p side of the present diode are 264 mV and 140 mV, respectively. This will correspond to a peak voltage  $V_{\text{peak}}$  of about 135 mV. The measured peak voltage in Fig.2 (a) is 176 mV. The difference of those two values may be attributed to the probe resistance and resistances of the substrate and metal contacts, estimated to be about 1Ω.

At 15 A/cm<sup>2</sup>, which is the approximate current density for an AlGaAs/GaAs two junction solar cell operating at 1000 suns, the voltage drop across the tunnel junction is only ~ 17 mV.

This voltage drop is considered an upper limit since no corrections for the probe, metal contact and substrate resistance were considered. This performance of the AlGaAs/GaInP high band gap tunnel diode exceeds the best reported value of p<sup>+</sup>-GaAs/n<sup>+</sup>-GaAs tunnel junction. Such a high value of tunnel current density may be attributed to two reasons. The peak current density is very sensitive to the thickness of the depletion region of the tunnel junction<sup>11</sup> and the present tunnel junction has a very narrow depletion region because both p and n sides are very heavily doped. It should be mentioned that it is very difficult to achieve high n-type doping levels in high band gap materials due to the presence of DX centers<sup>6</sup>. A second reason may have to do with the band lineup at the AlGaAs/GaInP interface. It had been reported that the Al<sub>0.36</sub>Ga<sub>0.64</sub>As/Ga<sub>0.51</sub>In<sub>0.49</sub>P interface has a staggered band lineup and both the conduction and valence bands of AlGaAs have higher energies than those of GaInP<sup>12</sup>.

## Conclusion

In summary, a p<sup>+</sup>-AlGaAs/n<sup>+</sup>-GaInP tunnel junction was grown by ALE using C and Se for the p and n-type dopants, respectively. There is only ~ 17 mV voltage drop across this junction at 15 A/cm<sup>2</sup>, which is the expected current density for an AlGaAs/GaAs two junction solar cell at 1000 suns operation.

## References

1. N. Kobayashi, T. Makimoto and Y. Horikoshi, *Appl. Phys. Lett.*, **50**, 1435 (1987).
2. M. Konagai, T. Yamada, T. Akatsuka, K. Saito, E. Tokumitsu and K. Takahashi, *J. Cryst. Growth*, **98**, 167 (1989).
3. J.R. Gong, D. Jung, N.A. El-Masry and S.M. Bedair, *Appl. Phys. Lett.*, **57**, 400 (1990).
4. K.G. Reid, H.M. Urdianyk and S.M. Bedair, *Appl. Phys. Lett.*, **59**, 2397 (1991).
5. B.C. Chung, R.T. Green and H.F. MacMillan, *J. Cryst. Growth*, **107**, 89 (1991).
6. P.M. Mooney, *J. Appl. Phys.*, **67**, R1 (1990).
7. T. Ishikawa, T. Maeda and K. Kondo, *J. Appl. Phys.*, **68**, 3343 (1990).
8. A. Usui and H. Sunakawa in *Inst. Phys. Conf. Ser. no.83, GaAs and Related Compounds*, 129 (1986).
9. D. Jung et al ( unpublished )
10. S.M. Sze, *Physics of Semiconductor Devices*, 2nd Edition, New York: Wiley (1981), Chap.9.
11. R.E. Hayes, P. Gibart, J. Chevrier and S. Wagner, *Solar Cells*, **15**, 231 (1985).
12. M.A. Rao, E.J. Caine, H. Kroemer, S.I. Long and D.I. Babic, *J. Appl. Phys.*, **61**, 643 (1987).

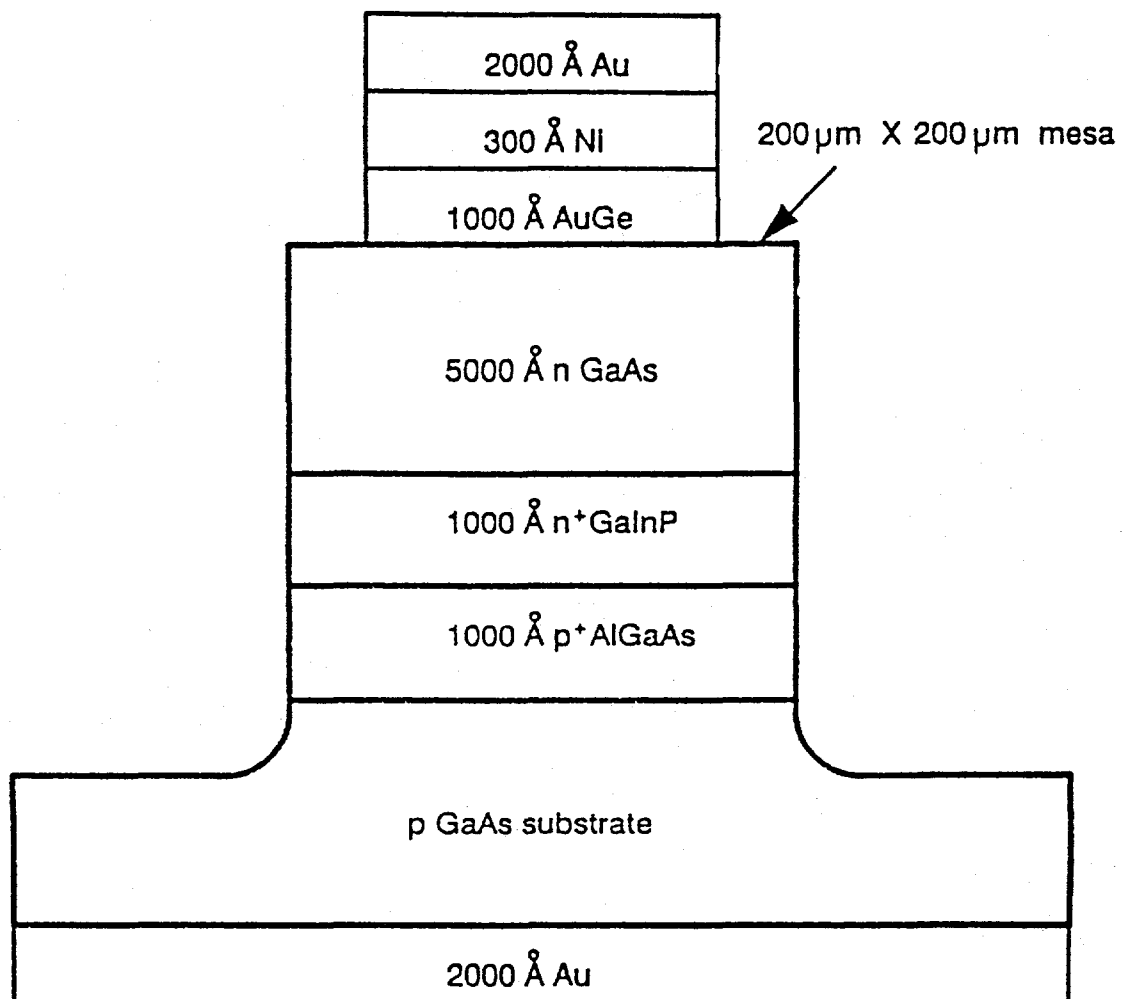


**Figure 1. Structure of the p<sup>+</sup>-AlGaAs/n<sup>+</sup>-GaInP heterojunction tunnel diode.**



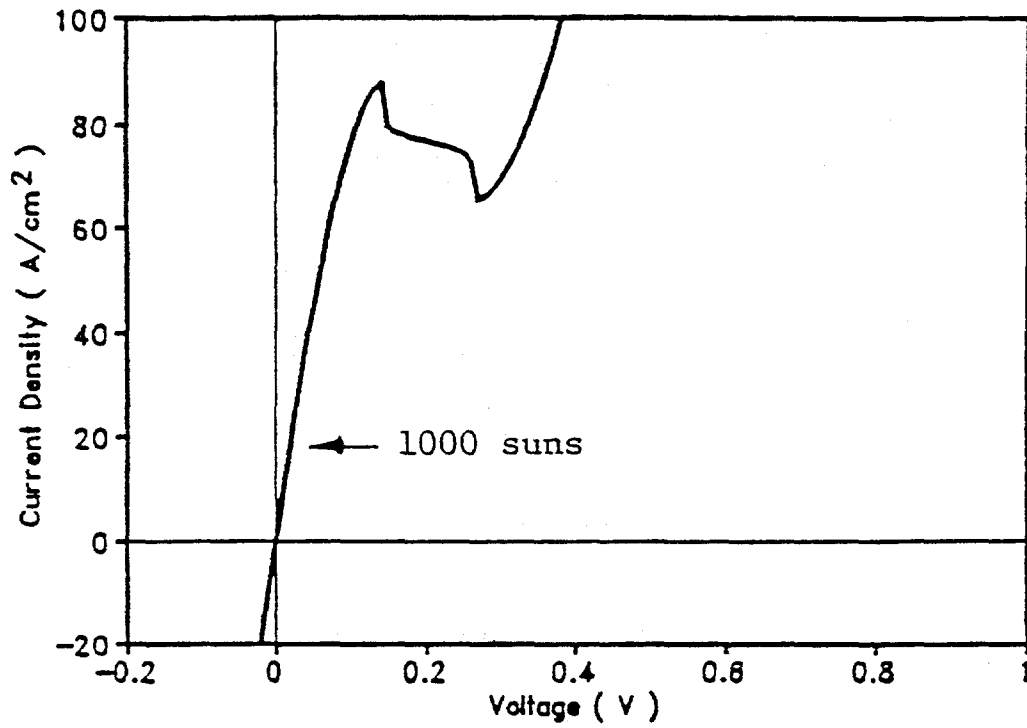


**Figure 2. I-V characteristics of AlGaAs/GaInP tunnel junction.**

**Title:** Detailed Non-contact Electrical And Structural Characterization of Photovoltaic Silicon Substrates

**Organization:** Department of Materials Science and Engineering  
North Carolina State University  
Raleigh, NC 27695-7916

**Contributors:** B. Sopori, program manager; G. A. Rozgonyi, principal investigators; A. Buczkowski, and F. Shimura

## Introduction

The overall objective of this research is to establish fundamental understanding on the nature of defects and impurities in the commercial silicon substrates and determine their effects on the photovoltaic parameters. Full wafer evaluation of silicon material for photovoltaic applications is an important part of this goal. Electrical characterization is especially suitable for this purpose since it is very sensitive to the presence of defects.<sup>1,2</sup> One of the most commonly observed electrical properties is minority carrier recombination lifetime, for which a contactless, nondestructive, and high throughput technique is especially desired. The laser excitation/microwave reflection photoconductance (LM-PC) technique meets many of these basic requirements.<sup>3-5</sup> In spite of fact that the correct interpretation of LM-PC decay curves requires a detailed understanding of the origin of carrier recombination processes, this technique supplies data which, if properly analyzed, is a rich source of information about defect properties and origin. With respect to the volume distribution of these defects, two distinct regions must be considered: the bulk of the wafer, and the potentially more highly defected (or contaminated) near-surface region. These bulk/surface nonuniformities yield a photoconductance decay which is a non-exponential function of time (especially in its initial stage), but then becomes exponential at its tail. Because of its simplicity the so called "effective" lifetime,  $\tau_{\text{eff}}$ , defined by the slope of the decay tail portion is specified.  $\tau_{\text{eff}}$  carries information about two lifetime components, namely the bulk and the surface lifetimes  $\tau_{\text{bulk}}$  and  $\tau_{\text{surf}}$ . The bulk component is controlled by the concentration of recombination centers, their capture cross sections, and energy levels; whereas the surface component depends on surface recombination velocities, carrier diffusion constant and wafer thickness. It is generally possible to separate  $\tau_{\text{bulk}}$  from  $\tau_{\text{surf}}$  by an analysis of the shape of the photoconductance decay curve which results from these recombination processes.<sup>6-8</sup> Although the bulk lifetime depends on the specific electrical properties of a defect(s), it has not been widely used for more detailed defect characterization because of the availability of Deep Level Transient Spectroscopy (DLTS) based on low temperature capacitance transient measurements. Even though data analysis is much more straightforward in the conventional DLTS (c-DLTS) case, it has a limited sensitivity and cannot be successfully used for high quality materials with trace amounts of contamination. In addition, it is destructive and time consuming. Therefore, there is a great interest in establishing a procedure for a non-contact electrical characterization of defects, which does not require special sample preparation and at the same time improves the relatively low sensitivity of c-DLTS. Since the carrier recombination process monitored via contactless LM-PC is based on the same physical principles as the carrier emission observed in DLTS, it is reasonable to expect the LM-DLTS to be a complimentary tool for the classical DLTS technique.<sup>9-12</sup> Of particular current interest is the temperature range between 10°C and 300°C where the LM-DLTS approach allows direct determination of the kinetics of Fe-B and Cr-B pair interactions.<sup>13</sup>

## Experimental

Measurements were performed on Czochralski grown 10 - 20  $\Omega\text{cm}$  Si wafers using the commercially available Lifetech-88<sup>®</sup> system (Semitex Co., Ltd.) operating at a laser wavelength of 904 nm and pulse width of ~ 150 ns.

In order to illustrate the LM-PC technique possibilities four sets of experiment are presented. They include: (i) determination of surface recombination velocity and surface and bulk lifetime of an oxidized sample following etching in hydrofluoric acid, (ii) surface and bulk lifetime separation and mapping of virgin silicon wafers at room temperature, (iii) non-contact deep level energy analysis of a sample intentionally contaminated with iron, and finally (iv) dissociation and re-formation kinetics of the iron-boron complex.

## Results

The influence of surface recombination lifetime on the photoconductance decay is illustrated in Fig. 1 where the same sample, characterized with a single value of bulk lifetime, is measured several times after etching in hydrofluoric acid. The sample was initially oxidized in order to eliminate (passivate) the surface recombination process. Surface lifetime of the order of 35,000  $\mu$ s and surface recombination velocity close to 0.1 cm/s were determined for this case. The surface lifetime dramatically decreased to 37  $\mu$ s 30 min after oxide stripping. It continued to decrease as a native oxide grew and a de-passivation effect, most likely due to dissociation of hydrogen-silicon bonding, progressed. After several days the process stabilized with a surface lifetime of about 30  $\mu$ s. The same value of the time independent bulk lifetime, about 145  $\mu$ s, was recovered for all of these cases. It is evident that the level of surface contamination strongly affects the surface recombination activity, which is reflected in the shape of the decay curve in Fig. 1. Furthermore, these two lifetime components,  $\tau_{\text{bulk}}$  and  $\tau_{\text{surf}}$  can be mapped over the full wafer. Thus, both surface cleanliness and bulk defects can be monitored. A representative application of lifetime analysis in a mapping mode is presented in Fig. 2a and b, where the surface and the bulk lifetime components are independently plotted for the same quadrant of a 6 inch diameter wafer. Four ring shape regions reflecting lateral differences in wafer quality are observed for both parameters in this example. It is interesting to notice that for both the surface and bulk lifetime components, high and low values are observed in the center and outer ring, respectively. However this type of association does not exist in the second ring (counting from the center), where  $\tau_{\text{bulk}}$  undergoes a larger decrease. This effect is most likely related to the inhomogeneous, diameter dependent gettering action of oxygen precipitates and/ or other defect complexes.<sup>14</sup>

Surface and bulk lifetime component separation along with lifetime mapping is an attractive method of depth and lateral defect distribution analysis. However, full electrical characterization of defects requires a determination of defect energy, electron and hole capture cross section, and concentration. Since these parameters strongly influence the temperature dependence of the recombination lifetime, it is possible to recover them from this relation. To verify this procedure a sample contaminated with Fe during Czochralski crystal growth was studied with both c-DLTS and LM-DLTS. The theoretical lifetime based on a single trap as predicted by the Shockley-Read-Hall (SRH) theory was calculated using data determined in the c-DLTS experiment. Satisfactory agreement was not fully acceptable until a second trap level was introduced and adjustments made in some of the c-DLTS trap properties, see Fig. 3. A full set of eight fitting parameters is specified in the figure caption. It was found that only the hole capture cross sections for both identified traps could be varied within a relatively wide range without significant influence on lifetime. The influence of the other six parameters was more critical and relatively unique. High speed algorithm for automatic computer analysis of LM-DLTS is under development.<sup>15</sup>

The inherent sensitivity of the lifetime-based DLTS is much better than that of c-DLTS because at the low trap/recombination center concentration the lifetime can be easily measured, whereas the DLTS signal proportional to the trap concentration disappears. As a result, the LM-DLTS can identify defects at levels which are not detectable with classical DLTS. An example of the temperature dependence of a p-type sample contaminated with iron is presented in Fig. 4. A unique inverse temperature curve shape with a lifetime "bump" is observed in this situation due to the dissociation of iron-boron pairs. Note that after the expected initial lifetime increase with temperature the lifetime decreases again as relatively inactive shallow level Fe-B pairs dissociate creating a more active deep level of interstitial Fe. The kinetics of the Fe-B pair dissociation and re-formation is presented in Figure 4. Measurements were made three times in succession to observe

changes in  $\tau_{\text{eff}}$  within a time frame which was too short for re-formation of all of the interstitial Fe with the B. The 1st measurement was conducted starting at room temperature and then increasing to 200°C. The second measurement was after the stage cooled down to 50 °C, allowing some of the Fe to reform complex with B. A continuing decrease in the Fe-B pairs was established in the 3rd run by moving the sample to a separate hot plate at 200°C while the LM stage cooled, and then immediately measuring within the 100°C to 200°C temperature range. Again, a consistent interstitial Fe increase was observed at the contamination level lower than the detection limit of the c-DLTS.

## References

- 1 D. K. Schroder, *Semiconductor Material And Device Characterization* (John Wiley, 1990).
- 2 J. W. Orton and P. Blood, *The Electrical Characterization of Semiconductor: Measurement of Minority Carrier Properties* (Academic Press, San Diego, 1990).
- 3 F. Shimura, T. Okui, and T. Kusama, *J. Appl. Phys.* **67**, 7168 (1990).
- 4 Y. Kirino and F. Shimura, *J. Appl. Phys.* **69**, 2700 (1991).
- 5 A. Buczkowski, et al., in *Defects in Silicon II* (Eds. W. M. Bullis, et al., The Electroch. Soc., 1991), pg.107
- 6 K. L. Luke and L. J. Cheng, *J. Appl. Phys.* **61**, 2282 (1987).
- 7 A. Buczkowski, Z. Radzimski, G. Rozgonyi and F. Shimura, *J. Appl. Phys.*, **69**, 6495 (1991).
- 8 A. Buczkowski, Z. Radzimski, G. Rozgonyi and F. Shimura, *J. Appl. Phys.*, **72**, 2873 (1992).
- 9 Y. Kirino, A. Buczkowski, G. Rozgonyi and F. Shimura, *Appl. Phys. Lett.*, **57**, 2832 (1990).
- 10 A. Buczkowski, Z. Radzimski, Y. Kirino, F. Shimura, and G. Rozgonyi, *MRS Proc.*, **209**, 567 (1991).
- 11 A. Buczkowski, G. Rozgonyi and F. Shimura, *MRS. Proc.*, **261**, 235 (1992)
- 12 A. Agarwal, Z. Radzimski, A. Buczkowski, F. Shimura, and G. Rozgonyi, *MRS Proc.*, **262**, 615 (1992).
- 13 Y. Hayamizu, T. Hamaguchi, S. Ushio, T. Abe and F. Shimura, *J. Appl. Phys.*, **69**, 3077 (1991).
- 14 N. Ikeda, K. Iba, A. Buczkowski and F. Shimura, "Non-contact characterization for grown-in defects in Czochralski silicon", extended abstract, The Electrochem. Soc. Meeting, Hawaii 1993
- 15 Z. Helak, A. Buczkowski and F. Shimura, in preparation

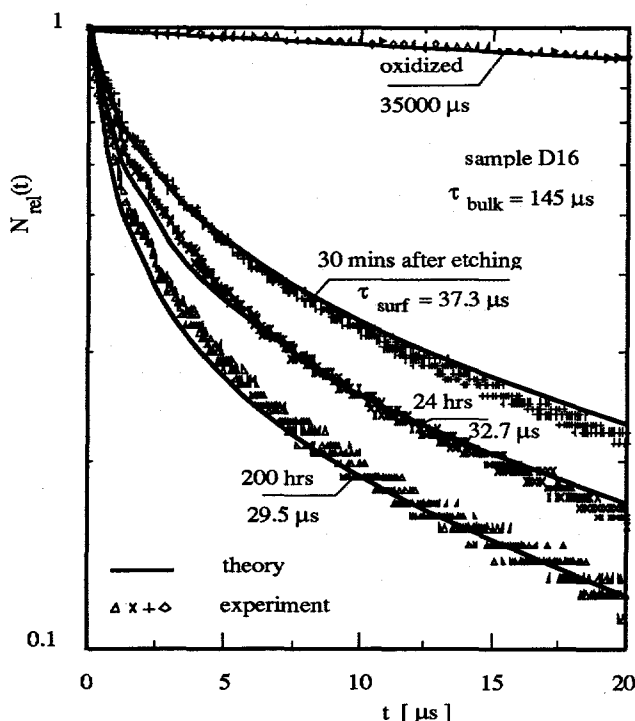
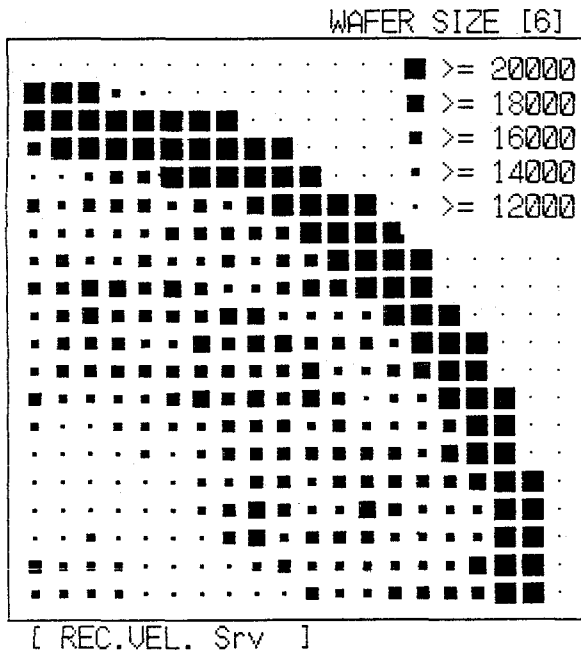


Fig.1. Influence of different surface conditions (e.g. time of the native oxide growth) on the photoconductance decay for an oxidized sample after HF oxide stripping.

(a)



(b)

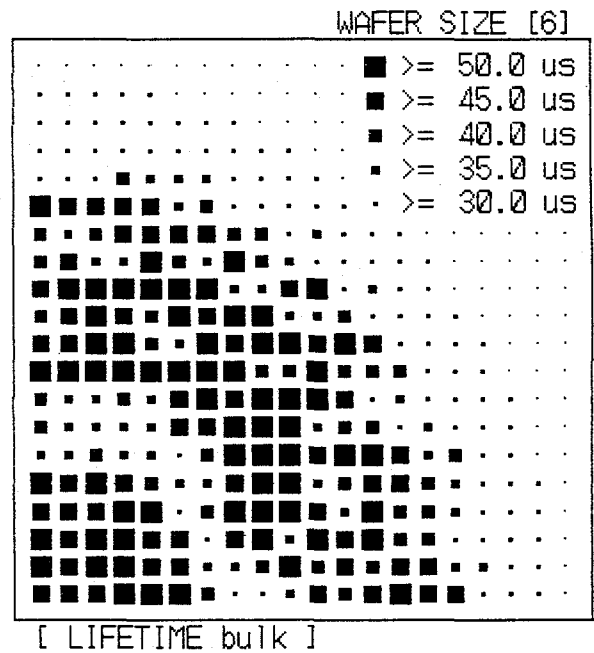


Fig. 2. Map of (a) surface recombination velocity, and (b) bulk lifetime measured at room temperature for thermally untreated CZ p-type material showing ring defects across quadrant of 6" diam wafer.

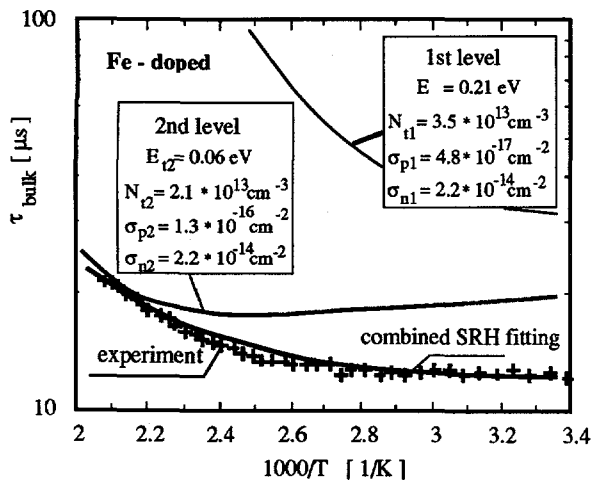


Fig. 3. Temperature dependence of the bulk recombination lifetime of an n-type iron contaminated sample. Solid lines represent the theoretical dependence for two separate deep levels fitted for the best combined agreement with LM-DLTS data.

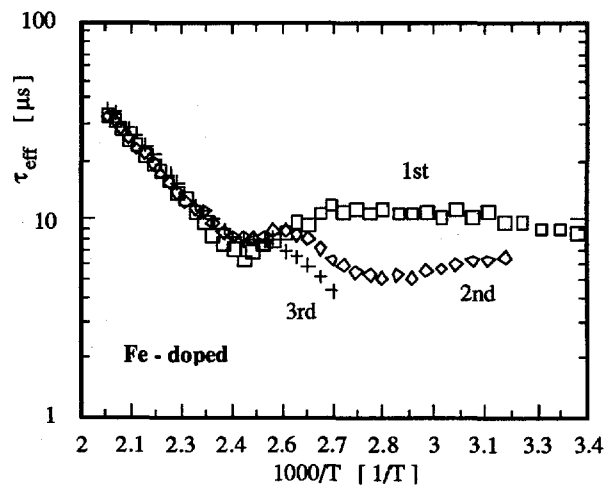


Fig. 4. Temperature dependent effective lifetime for the p-type wafer doped with iron repeated three times in quick succession as described in the text

Title: New III-V Cell Design Approaches for Very High Efficiency  
Organization: School of Electrical Engineering, Purdue University  
West Lafayette, Indiana 47907-1285  
Contributors: M. S. Lundstrom and M. R. Melloch, principal investigators; G. B. Lush,  
M. P. Patkar, and M. P. Young

### Objectives and Approach

To realize cost-effective solar cells with efficiencies exceeding 35% is an important objective of the national photovoltaics program. Cell efficiencies are progressing rapidly, but it seems unlikely that the present design approach will produce efficiencies very much above 30% under concentration. Multi-junction cells have already achieved efficiencies well above 30%, but substantial cost reductions are still required. The objective of this project is to examine new *design* approaches for achieving very high conversion efficiencies [1].

The project thrust centers on exploring new thin-film approaches specifically designed for GaAs. Research on basic studies previously conducted by our group has given us a deep understanding of the loss mechanisms that dominate in present-day cells, and it serves as the foundation for the device design research being proposed. The unconventional design approaches we are exploring also require new basic research on radiative recombination and photon recycling. The research program is, therefore, balanced to increase our basic understanding of the electro-optic characteristics of GaAs and to explore the potential of unconventional cell designs.

The project's thrust is directed at enhancing the already high efficiency of GaAs cells by exploring new, thin-film approaches designed to trap incident light and to take advantage of so-called photon recycling effects. It has long been realized that radiative recombination is not necessarily a loss mechanism; *if* the cell is thick enough and *if* the emitted photons are confined within the cell. By adopting a thin-film cell approach, designed to optically confine the photons emitted by radiative recombination within the cell, lifetimes could be enhanced by an order of magnitude - or even more. Thin-film cells might also benefit from conventional, incident light trapping, which is used with great success for silicon cells. The potential for sizeable efficiency gains along with the cell cost advantages make the thin-film approach a promising one that should be broadly applicable to III-V single- and multiple-junction cells.

### Research Results

During the past year we have continued our study of minority hole recombination in n-type GaAs and initiated a study of the optical properties of n-GaAs, including photon recycling. Thirty double heterostructure (DH) films with various electron concentrations,  $n_0$ , and active layer thicknesses,  $w$ , were grown by metalorganic chemical vapor deposition (MOCVD) by Dr. Hugh MacMillan at Varian Associates. Photoluminescence decay studies were performed and the minority carrier lifetimes have been reported [2-3]. To understand the optical characteristics, transmission measurements were done to deduce the near band edge absorption coefficient,  $\alpha(h\nu)$ , as a function of energy,  $h\nu$ , and  $n_0$ . The results of this study [4] are summarized briefly in Fig. 1. In comparing these results to those of Casey *et al.* [5], we find qualitative agreement in that the slope of the absorption edge decreases with increasing  $n_0$ , and the

absorption edge occurs at higher  $h\nu$  due to the filling of electron states in the conduction band (known as the Burstein shift). Quantitative similarity exists for  $n_0 \leq 10^{18} \text{ cm}^{-3}$  and  $h\nu < E_g$ , but significant differences occur for higher energy photons at all electron concentrations and for  $h\nu < E_g$  and  $n_0 > 10^{18} \text{ cm}^{-3}$ . These differences are attributed mostly to compensation in the material used by Casey *et al.*. Because our films do not suffer from compensation, the results for  $\alpha(h\nu)$  should be of great interest to the photovoltaic community as well as to those modeling other optoelectronic devices or studying band structure theory.

To demonstrate the effect of light-trapping on photon recycling, we observed photoluminescence decay on thin-film membranes, created by etching a hole in the substrate and on the area adjacent to the film where the substrate remained intact [6-8]. The lifetime enhancement, or the minority carrier lifetime of the membrane divided by the minority carrier lifetime of the DH with the substrate intact, was as great as ten for DH's with  $n_0 = 1.3 \times 10^{17} \text{ cm}^{-3}$ . We observed lifetimes as long as 1.2  $\mu\text{s}$  in these DH's; previously such long lifetimes had only been observed in nominally undoped GaAs. An upper limit to the  $\text{Al}_{0.3}\text{Ga}_{0.7}\text{As}/\text{GaAs}$  interface recombination velocity was deduced to be  $S < 11 \text{ cm/s}$  -- the lowest ever seen for moderately doped  $\text{AlGaAs}/\text{GaAs}$ . These results, summarized in Figure 2, show that ultra-long lifetimes are possible in moderately doped GaAs, if non-radiative recombination can be controlled, and suggest that the thin-film solar cell concept is viable.

One of the most important parameters needed in the characterization and modeling of GaAs optoelectronic devices is the radiative recombination B-coefficient. There is still much controversy over the value of B as published estimates have varied over an order of magnitude [9]. To deduce properly the value of B from lifetime measurements, one must understand photon recycling, and to properly model photon recycling, one must have correct data for  $\alpha(h\nu)$ . This work represents the first comprehensive study of recombination and absorption in n-GaAs grown by modern epitaxial techniques. We have done computer simulations to model photon recycling and combined the results of those simulations with the measured minority carrier lifetimes to deduce the B-coefficient. After accounting for non-radiative recombination, we deduce values for B which are plotted in Fig. 3. The error bars result from uncertainty in  $\alpha(h\nu)$ , the lifetimes, w, and the recycling cofactor.

These data show that B decreases significantly with increasing  $n_0$  which has been observed previously for p-type GaAs, and these data for B are consistent with the limited data available for valid comparisons in n-type GaAs [9].

## Conclusions

This past year was the second of a three-year project. We have completed a comprehensive study of recombination and absorption in n-type GaAs grown by MOCVD. We have demonstrated ultra-long lifetimes and ultra-low interface recombination velocities in moderately doped n-GaAs, indicating that the thin-film solar cell employing light-trapping and enhanced photon recycling is a viable technique for obtaining high-efficiency GaAs solar cells. The next step is the fabrication and characterization of thin-film cells. Issues to be faced include methods of separating the thin-film cell from the substrate, light-trapping techniques, and back surface optical reflectors.

## References

- [1] Greg Lush and Mark Lundstrom, "Thin film approaches for high-efficiency III-V cells," *Solar Cells*, **30**, p. 337, 1991.
- [2] G. B. Lush, H. F. MacMillan, B. M. Keyes, D. H. Levi, R. K. Ahrenkiel, M. R. Melloch, and M. S. Lundstrom, "A Study of Minority Carrier Lifetime versus Doping Concentration in N-type GaAs Grown by Metalorganic Chemical Vapor Deposition," *J. of Appl. Phys.*, **72** (4), p. 1436, 1992.
- [3] R. K. Ahrenkiel, B. M. Keyes, G. B. Lush, M. R. Melloch, M. S. Lundstrom, and H. F. MacMillan, "Minority-Carrier Lifetime and Photon Recycling in N-GaAs," *J. Vac. Sci. Technol.*, **10** (4), p. 990, 1992.
- [4] G.B. Lush, M.R. Melloch, M.S. Lundstrom, H.F. MacMillan, and S. Asher, "Concentration Dependent Absorption Coefficient in N-type GaAs Grown by Metalorganic Chemical Vapor Deposition," Submitted to *J. Appl. Phys.*, 1992.
- [5] H. C. Casey, Jr., D. D. Sell, and K. W. Wecht, "Concentration Dependence of the Absorption Coefficient for n-type and p-type GaAs Between 1.3 and 1.6 eV," *J. Appl. Phys.*, **46** (1), p. 250, 1975.
- [6] G. B. Lush, M. R. Melloch, M. S. Lundstrom, D. H. Levi, R. K. Ahrenkiel, and H. F. MacMillan, "Microsecond Lifetimes and Low Interface Recombination Velocities in Moderately Doped n-GaAs Thin Films," *Appl. Phys. Lett.*, **61** (20), 1992.
- [7] G. B. Lush, D. H. Levi, H. F. MacMillan, R. K. Ahrenkiel, M. R. Melloch, and M. S. Lundstrom, "Microsecond Lifetimes in Moderately Doped n-GaAs Thin Films." Presented at the Electronic Materials Conf., Cambridge, MA, 1992.
- [8] M. S. Lundstrom, M. R. Melloch, G. B. Lush, M. P. Patkar, M. Young, S. M. Durbin, J. L. Gray, H. F. MacMillan, B. M. Keyes, D. H. Levi, and R. K. Ahrenkiel, "Radiative Recombination and Photon Recycling in Gallium Arsenide Solar Cells," *AIP Proceedings*, 1992.
- [9] G. B. Lush, *Recombination and absorption in n-type gallium arsenide*, Ph. D. Thesis, Purdue University, August 1992.

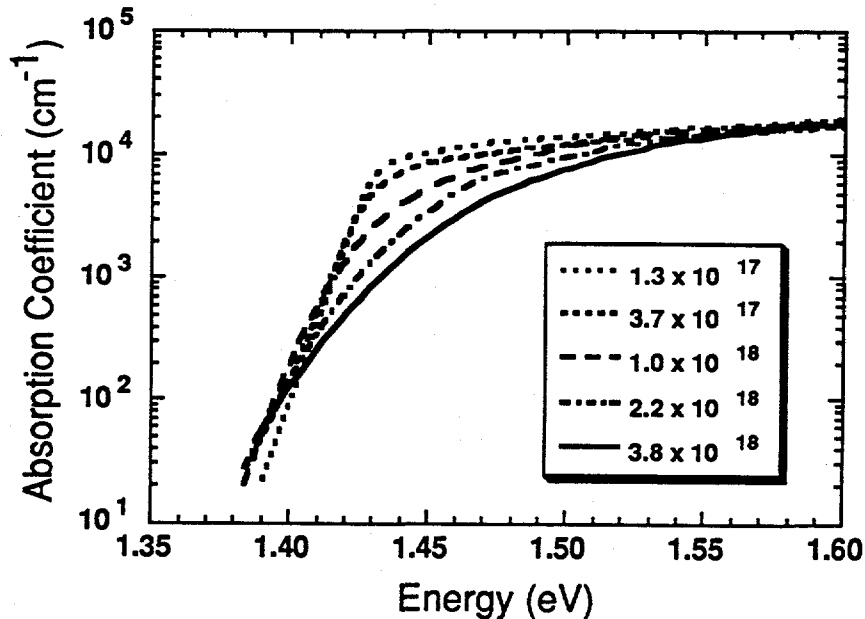


Fig. 1. Results of transmission measurements to deduce the near band edge absorption coefficient as a function of energy for  $1.3 \times 10^{17} < n_0 < 3.8 \times 10^{18} \text{ cm}^{-3}$ .



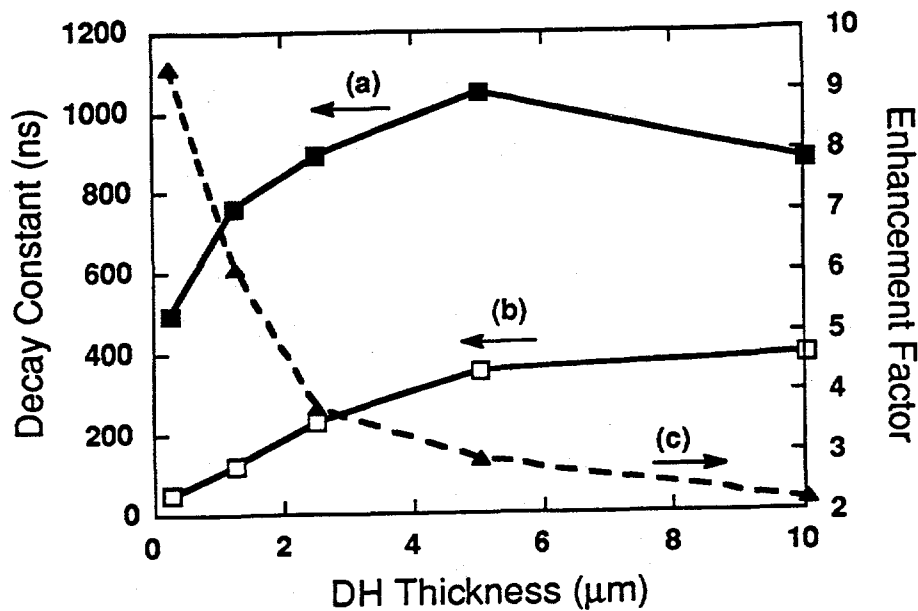


Fig. 2. Results of PL decay measurements on thin-film membranes. The lifetime was enhanced as much as nearly ten times for the thinnest DH, demonstrating how light-trapping can increase the effective radiative lifetime.

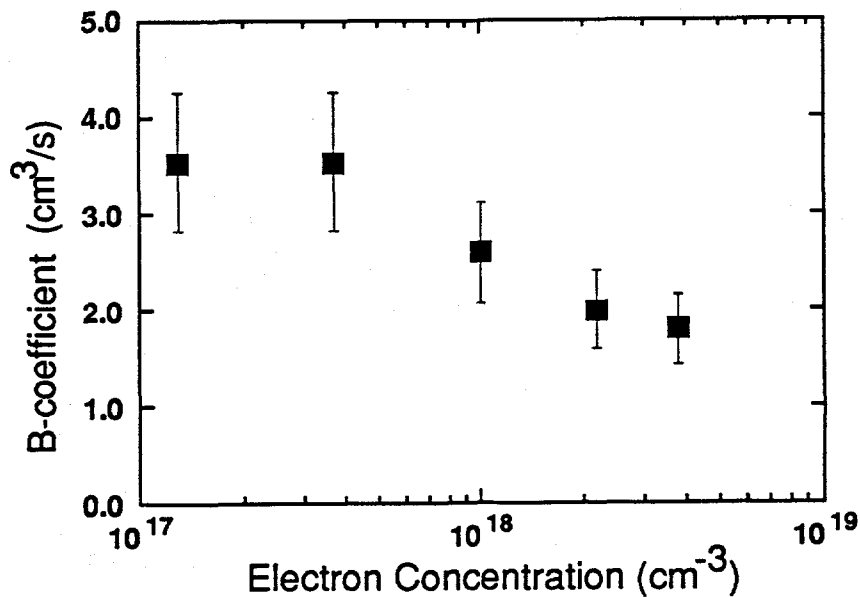


Fig. 3. Values for B deduced from PL decay measurements. The error bars result from uncertainty in  $\alpha(h\nu)$ , the lifetimes,  $w$ , and the recycling cofactor.

**Title:** CI-MO and MOCVD Crystal Growth Research

**Organization:** Department of Electrical, Computer and Systems Engineering, Rensselaer Polytechnic Institute, Troy, New York

**Contributors:** I.B. Bhat, J.M. Borrego and S.K. Gandhi, Co-Principal Investigators

The program objective is to evaluate new reactor designs with minimal convection and high source utilization efficiency, and to characterize the growth of GaAs material using novel metalorganic precursor sources.

**MOCVD Growth:** Over the past few years, we have developed an advanced computer program which has been used to design a novel reactor with a close-spaced vertical structure. During FY 1992, we extended our work in order to assess the structural and electronic properties of material grown in this reactor. Here, we have investigated the minority carrier lifetime, which is the most important measure of material quality for high efficiency solar cells. To do so, a number of  $n^+n^-n^+$  test structures have been grown on SI GaAs substrates. For these structures, the  $n^+$ -GaAs was doped to  $5 \times 10^{18} \text{ cm}^{-3}$ , whereas the  $n$ -GaAs was  $3 \times 10^{15} \text{ cm}^{-3}$ . The thickness of the  $n$ -GaAs is varied from 2.6 to 4.6  $\mu\text{m}$ . Top and bottom  $n^+$ -layers were 500  $\text{\AA}$  and 1500  $\text{\AA}$  respectively.

Minority carrier lifetime was measured by nondestructive photoconductive decay techniques using microwave reflectance at 35 Ghz. From these measurements, we have obtained a bulk lifetime of about 115 nsec for a typical run. Values as large as 900 nsec were obtained when a freshly cleaned molecular sieve trap, operated at  $-10^\circ\text{C}$ , was installed in the arsine line.

Most of our growth runs have been made at 380 Torr. To complete our study, we have made measurements of thickness uniformity over a range of system operating pressures. The results of these measurements are shown in Fig. 1, together with the computer simulation. The experimental data (points) show an improvement in uniformity at reduced pressures, whereas the simulation results (line) are independent of pressure. This lack of correspondence is due to the fact that the inlet nozzle consists of a series of discrete holes; in our simulations, the gas flow is continuous in the angular direction, and flows radially. As the gases emerge from each nozzle hole, they disperse in the radial and angular directions and merge with the gases from adjacent holes to form a continuous flow. At higher pressures there is less force on the gases in the radial direction and hence greater tendency for the gases to disperse in the angular direction. This causes a deterioration in the radial uniformity.

Computer simulations are being extended to the conceptual design of a reactor which can handle multiple slices. Initial simulations have been made, but are excessively wasteful of machine time. Work is proceeding to develop more efficient algorithms for these simulations.

**CI-MO Source Chemicals:** This task is focused on the use of new chemicals of interest for the growth of solar cell materials. Diethylgalliumchloride (DEGaCl) is a potential candidate because it has a number of unique features. First, since it is a clean burner, it can probably be used with a low V/III ratio of starting chemicals, and hence reduce both reactant cost and effluent handling

problems. Next, the GaAs formation reaction using DEGaCl is exothermic, as compared to that using trimethylgallium which is pyrolytic. As a result, it should be possible to grow GaAs in a hot wall reactor with this alkyl, with the advantages of high throughput and simplified reactor heating. This formation reaction is also reversible, so that it can be used for patterned epitaxial growth. This is an advantage in both cascade and concentrator cells, which require highly doped contact and interconnection regions.

Experiments with DEGaCl are carried out in a conventional, horizontal, induction heated OMVPE reactor. The system is operated at 80 Torr in order to obtain a reasonable partial pressure of DEGaCl (20-50 mTorr) without an excessive flow of hydrogen through the bubbler. In order to avoid condensation of DEGaCl on gas plumbing, heater tapes are used to keep all the OM lines at about 70°C. Pure arsine was used as the source chemical for arsenic. A conventional TMGa source was also used for calibration runs, from time to time.

A series of initial experimental runs were made to establish the regime for GaAs growth. The best growth was observed at 600°C, with  $P_{\text{react}} = 80$  Torr, and  $p_{\text{DEGaCl}} = 0.28$  Torr. The  $\text{AsH}_3$  pressure was varied over a wide range of V/III ratios. Results of Hall data on these samples are shown in Fig. 2. Note that this result is quite different from what would be expected with the TMGa process, where the material would normally convert to p-type around an  $\text{AsH}_3/\text{TMGa}$  ratio of 16, at a growth temperature of 700°C. Note also that  $\text{AsH}_3$  is not completely cracked at 700°C; since our experiments are at 600°C, we can expect the actual As/Ga ratio to be well under the values quoted here for the  $\text{AsH}_3/\text{TMGa}$  ratio.

A study of early papers dealing with the hydride process ( $\text{Ga-HCl-AsH}_3$ ) for GaAs indicates the same trend, i.e., the best GaAs is grown in these systems with V/III ratios approaching unity. It is tempting to propose that the DEGaCl- $\text{AsH}_3$  process is very similar to the hydride process, with GaCl as the active species. However, there are some important differences and we are in the process of developing a growth model to explain them.

A series of runs were made over the temperature range from 350° to 900°C. Growth was observed between 350-750°C, and etching over the range from 800-900°C. The etch rate varied from 0.45  $\mu\text{m/hr}$  to 6  $\mu\text{m/hr}$ , with an activation of 60 kcal/mole. By way of comparison, our previous work with trimethylgallium and arsine showed a fall off in growth (not etching) due to the desorption of Ga-species, at a rate of about 100 kcal/mole.

**Diagnostics:** Most of our conventional diagnostic tools have been used to evaluate materials grown on this program. Upgrade of these tools was carried out on a continuing basis either by extending their sensitivity and/or operating range, or by automating them for ease of data handling and acquisition.

Non-destructive techniques which we use in our laboratory have focused on the measurement of bulk properties of solar cell materials. With improvements in these materials, our interest has shifted to surface properties, which are responsible for the remaining loss mechanisms in these cells. Photorefectance (PR) is increasingly used as a non-destructive characterization tool for the study of surface fields in bulk semiconductors and related surface and interface phenomena. In many cases, PR yields more information at room temperature than PL. Based on the above

considerations, a system has been set up to acquire and analyze PR data.

In this system, an arc lamp and a monochromator are used to form the probe beam, and a light chopper and a laser are used for the modulating pump beam. A detector, followed by a current preamplifier, voltmeter and a lock-in amplifier are used to measure the probe light reflected from the sample surface. A computer is used to collect and process the data. A 1 kW Xenon arc lamp is focussed on the input slits of a high intensity monochromator, with a focal length of 0.25 meters, and a scan range of 0.4 to 1.1  $\mu\text{m}$ . The output from this monochromator, after focusing, serves as the probe beam for PR. Normal incidence of the probe beam on the test sample is obtained by using a partially reflecting mirror with a reflectivity and transmissivity of 30% each. The light reflected from the test sample is incident on a photodetector.

The electric field at the semiconductor surface is modulated by a pump beam whose intensity is much higher than the intensity of the probe beam. An Nd:YAG laser at a wavelength of 1.06  $\mu\text{m}$ , or an HeNe laser at a wavelength of 0.6238  $\mu\text{m}$ , are used for sub-band and band-to-band pumping purposes, respectively. The laser light is chopped and coupled with an optical fiber to the semiconductor sample under test. A computer program was written to measure the PR spectrum, and fit it to the Aspnes Third Derivative Functional form.

Initial studies have focused on the use of SI-GaAs, since PR measurements on this material are easy to interpret. Figure 3 shows the PR signal on SI-GaAs, before and after a rinse in dilute HCl. Analysis of the data shows a reduction in  $N_{ss}(\phi_s - \phi_{s0})$  by a factor of 1.4 due to this treatment. Here,  $N_{ss}$  is the surface state density,  $\phi_{s0}$  is the fermi level if the surface is charge neutral and  $\phi_s$  is the surface fermi level upon application of the pump beam.

A list of papers and presentations in FY 1992 now follows:

1. H. Bhimnathwala and J.M. Borrego, Solid State Electronics, 35, 1503 (1992).
2. P.B. Chinoy, J.M. Borrego and S.K. Ghandhi, Solar Energy Materials and Solar Cells, 27, 1 (1992).
3. S.D. Tyagi, K. Singh, S.K. Ghandhi and J.M. Borrego, Proc. 22nd IEEE Photovoltaic Specialists Conf., Las Vegas, NV, October 7-11, 1991.
4. P.B. Chinoy, I.B. Bhat, J.M. Borrego and S.K. Ghandhi, "Performance and Characteristics of an OMVPE Reactor for Solar Cell Materials," NREL PV AR&D Meeting, Denver, CO, May 13-15, 1992.
5. H.G. Bhimnathwala and J.M. Borrego, "Photoreflectance Characterization of LEC-Si GaAs and Fe-InP," 7th Conference on Semi-Insulating III-V Materials, Ixtapa, Mexico, April 21-24, 1992.

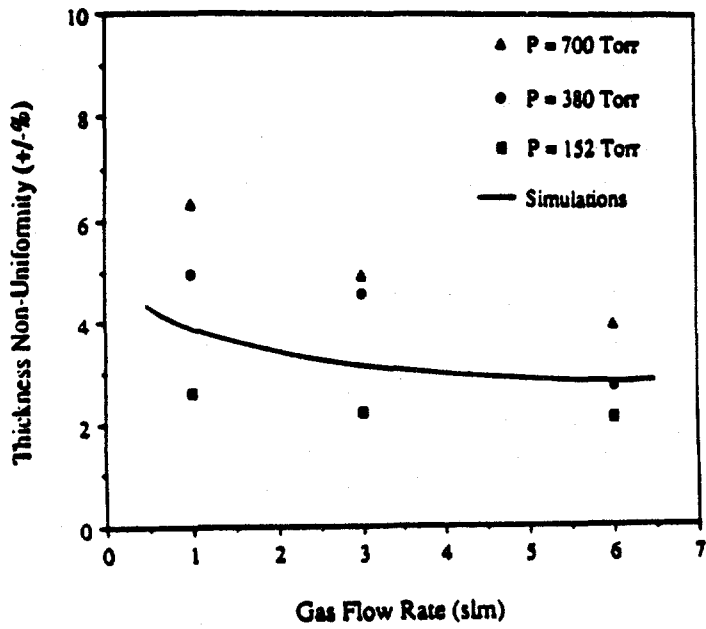


Figure 1. Thickness uniformity for various system pressures.

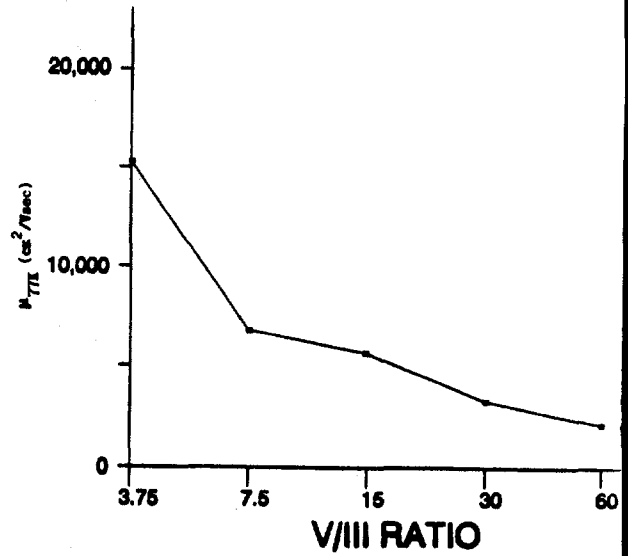


Figure 2. 77K mobility vs. V/III Ratio.

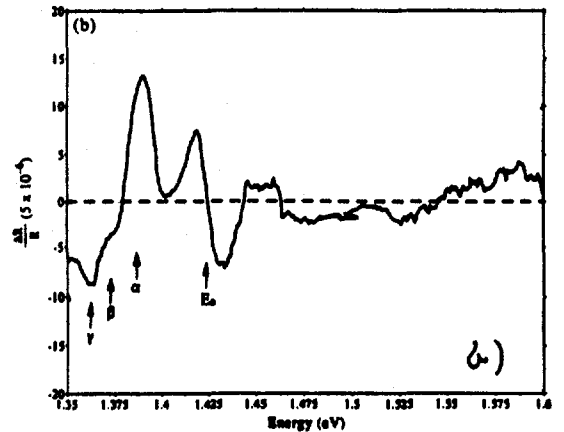
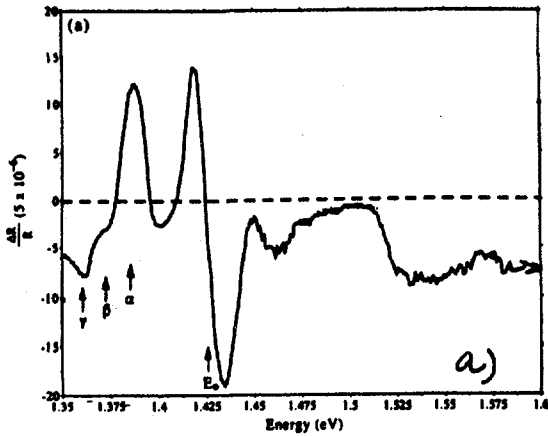


Figure 3. PR signal a) before, b) after a rinse in dilute HCl.

**Title:**                   **Growth and Development of GaInAsP for Use in High-efficiency Solar Cells**

**Organization:**       **Research Triangle Institute  
Research Triangle Park, North Carolina**

**Contributors:**       **P.R. Sharps, project leader; M.L. Timmons, R. Venkatsubramanian, R. Pickett, J.S. Hills, and J. Hancock**

## **Introduction**

The quaternary semiconductor compound GaInAsP lattice-matched to GaAs (and hence Ge) is an ideal candidate as a top junction in monolithic cascade cells. With quaternary semiconductors the lattice constant and band gap can be, within limits, varied independently. For GaInAsP lattice-matched to GaAs, the band gap spans the range from 1.42 to 1.92 eV. Such a range provides great flexibility for current matching with a low band gap junction. For the composition  $\text{Ga}_{0.84}\text{In}_{0.16}\text{As}_{0.68}\text{P}_{0.32}$ , the band gap is 1.55 eV, and junctions made from such a composition provide current matching and lattice matching with Ge junctions. Under concentrated sunlight, multiple junction cells using GaInAsP as the top junction project to a theoretical efficiency of about 35% [1].

The overall goals of the present program are:

1. to develop the necessary technology to grow 1.55 eV band gap GaInAsP layers that are lattice-matched to GaAs,
2. to demonstrate high-efficiency GaInAsP single-junction solar cells, and
3. to demonstrate GaInAsP/Ge cascade solar cells suitable for operation under concentrated (500x) sunlight.

## **Results**

Progress is being made in developing each component of the final cascade structure. The GaInAsP cell, the Ge cell, and the GaInAsP tunnel interconnect (grown on Ge) have all been demonstrated, with the results for the GaInAsP cell previously reported [2]. Work is progressing on improving the Ge cell, with the efficiencies currently being

in the 3% range. Fig. 1 shows the I-V curve for the tunnel diode interconnect. The peak current for the tunnel diode interconnect occurs at 65 mV, and is  $4.33 \times 10^3$  mA/cm<sup>2</sup>. For a GaInAsP/Ge cascade cell under 10 sun concentration, (a current density of approximately 300 mA/cm<sup>2</sup>), the voltage drop across the tunnel diode interconnect is 4.5 mV (For 100 suns, the voltage drop is 45 mV). The GaInAsP is nucleated directly on the Ge, indicating that the GaInAsP junction can be grown directly on the Ge junction, without any need for a GaAs nucleation layer on the Ge. More work needs to be done to improve the tunnel diode for use at 500 suns.

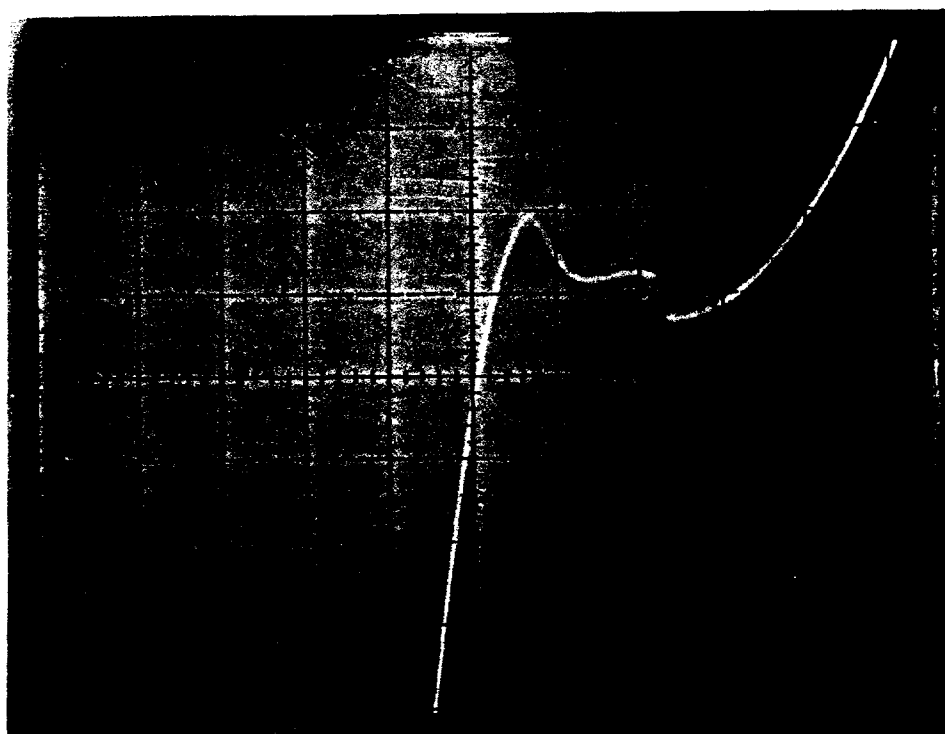


Fig. 1 Current-voltage curve for a  $p^{++}$ -GaInAsP- $n^{++}$ -GaAsInAsP tunnel diode. The x-axis scale is 0.1 V per large division, and the y-axis scale is 2 mA per large division. The area of the tunnel diode is  $9 \times 10^{-4}$  cm<sup>2</sup>. The peak current occurs at 65 mV, and the peak current density is  $4.33 \times 10^3$  mA/cm<sup>2</sup>.

A schematic for the cascade cell is shown in Fig. 2. One of these devices has recently been grown. The results have been encouraging in that cascade action in the device is definitely seen, indicating that the Ge junction and the GaInAsP tunnel diode interconnect are not degraded during the growth of the GaInAsP junction. However, further work is needed to optimize the device. It appears that a spurious junction is

developing at the GaInAsP/Ge interface, believed to be due to the diffusion of Ga and In into the Ge. Also, the two junctions are not quite-current matched, but further improvement in the Ge junction should lead to current-matched conditions.

Metal Contact		
n <sup>+</sup> -GaAs 3 x 10 <sup>18</sup> cm <sup>-3</sup> 0.5 μm	AR Coating	
n <sup>+</sup> -AlInP <sub>2</sub>	1 x 10 <sup>18</sup> cm <sup>-3</sup>	400 Å
n <sup>+</sup> -GaInAsP	1 x 10 <sup>18</sup> cm <sup>-3</sup>	0.3 μm
p-GaInAsP	1 x 10 <sup>17</sup> cm <sup>-3</sup>	3.5 μm
p <sup>+</sup> -GaInP <sub>2</sub>	1 x 10 <sup>18</sup> cm <sup>-3</sup>	400 Å
p <sup>++</sup> -GaInAsP	1 x 10 <sup>19</sup> cm <sup>-3</sup>	0.5 μm
n <sup>++</sup> -GaInAsP	1 x 10 <sup>19</sup> cm <sup>-3</sup>	0.5 μm
n <sup>+</sup> -GaInAsP	1 x 10 <sup>18</sup> cm <sup>-3</sup>	3.5 μm
n <sup>++</sup> -Ge	5 x 10 <sup>18</sup> cm <sup>-3</sup>	0.1 μm
n <sup>+</sup> -Ge	1 x 10 <sup>18</sup> cm <sup>-3</sup>	1.0 μm
p-Ge	1 x 10 <sup>17</sup> cm <sup>-3</sup>	6.0 μm
p <sup>+</sup> -Ge	1 x 10 <sup>18</sup> cm <sup>-3</sup>	0.1 μm
p-Ge	Substrate	~300 μm
Metal Contact		

Fig. 2 Schematic for the GaInAsP/Ge cascade cell.



## Conclusions

All the necessary components for a GaInAsP/Ge cascade cell have been developed. One GaInAsP/Ge cascade cell has been grown to date, and initial results have indicated the viability of such a device. Research over the next few months will focus on improving the device. Several particular issues include ensuring current matching between the two junctions, optimizing the Ge junction, and ensuring that no spurious junctions are formed at the GaInAsP/Ge interface. The thickness and doping of the  $n^{++}$ -Ge layer will need to be increased to prevent the formation of a p-Ge layer due to the diffusion of Ga and In into the Ge layer from the GaInAsP layer.

## References

1. M. W. Wanlass, J. S. Ward, K. A. Emery, T. A. Gessert, C. R. Osterwald, and T. J. Coutts, *Solar Cells* **30** (1991), 363.
2. Annual Report, Photovoltaic Program, FY1991. (March 1992), NREL/TP-410-4724. 306 pp. Available NTIS: Order No. DE92001248.

**Title:**                   **An Inverted AlGaAs/GaAs Patterned Tunnel Junction Cascade Concentrator Solar Cell**

**Organization:**       **Research Triangle Institute  
Research Triangle Park  
Research Triangle, NC 27709**

**Contributors:**       **R. Venkatasubramanian (Principal Investigator)  
M.L. Timmons, T.S. Colpitts, J.S. Hills,  
J. Hancock, and J.A. Hutchby.**

## **Objectives**

To develop inverted-growth techniques and the related technology for monolithic cascade AlGaAs/GaAs solar cells utilizing a tunnel junction for concentrator devices, based on a lattice-matched AlGaAs/GaAs material system.

## **Technical Approach**

Monolithic AlGaAs/GaAs cells based on a lattice-matched material system with a mature growth technology and near-ideal current-match of components can offer high efficiency (>30%) in concentrator-based (500 suns) terrestrial PV applications. A key impediment has been the high growth temperature for high quality AlGaAs. A successful approach has been a metal interconnect between the cells as part of the post-growth processing, and Entech cover glass to reduce obscuration losses. Alternatively, the Research Triangle Institute (RTI) inverted-growth approach first grows the AlGaAs top cell at high temperatures, and then a GaAs interconnect and bottom cell are grown at lower temperatures. The cascade structure is then removed from the parent substrate, Ge in this case, for frontside illumination.

## **Significant Results**

This project was successfully completed as planned. RTI developed a rapid multi-wafer process for etching Ge to produce thin AlGaAs/GaAs films. This can be advantageously used to develop a current-matched AlGaAs/GaAs/Si (three-junction) cell. The approach could use an AlGaAs/GaAs tunnel-interconnect cascade cell eutectic-metal-bonded (EMB) onto an Si cell. The EMB technique was developed under this program. A similar approach can be extended to a three-junction GaInP<sub>2</sub>/GaAs/Si cascade cell. RTI also developed the "cycled" organometallic vapor phase epitaxy (OMVPE) growth technique that gave enhanced conductance of GaAs tunnel junctions. RTI achieved demonstration of an inverted-grown, thin film, GaAs solar cell. NREL efficiency measurements were 14% for a demonstration sample. RTI reports that as being 17.9% active-area efficiency, and, subsequent cells are reported at 20.3% efficiency (active-area). These inverted-grown cells were eutectic metal-bonded onto silicon. RTI also obtained a thin film, inverted-grown Al<sub>0.34</sub>Ga<sub>0.66</sub>As/GaAs cascade cell they reported as 19.9% efficient at 1-sun and 21% efficient at 7-suns. This represents a milestone in the development of an AlGaAs/GaAs cascade by OMVPE utilizing a tunnel interconnect and demonstrates the proof-of-concept for the

inverted-growth approach.

## Conclusions

In summary, we have provided the first demonstration of an inverted-grown, fully processed, thin-film  $\text{Al}_{0.34}\text{Ga}_{0.66}\text{As}/\text{GaAs}$  cascade solar cell. Also, AM1.5 cell efficiency of approximately 20.3% for a thin film GaAs cell has been obtained. An inverted-grown, thin-film,  $\text{Al}_{0.34}\text{Ga}_{0.66}\text{As}/\text{GaAs}$  cascade with an efficiency of 19.9% at AM1.5 and an efficiency of 21% under 7 AM1.5 suns, has been obtained. The thin-film approach based on a sacrificial Ge substrate and the eutectic-metal-bonding onto Si, has demonstrated a minority carrier lifetime of 103 ns, the highest for a GaAs thin film on Si. Based on internal quantum efficiency measurements, an electron diffusion length of approximately 7.0  $\mu\text{m}$  has been estimated in the p-type base of an EMB thin-film GaAs cell on Si.

In conclusion, the inverted-growth approach to high-efficiency AlGaAs/GaAs cascade should allow a significant IR-transmission below GaAs bandgap. This can be used to mechanically stack the AlGaAs/GaAs cascade onto a moderately high-efficiency Si cell. The EMB scheme described in this effort can be modified to produce a 3-junction, 2-terminal, current-matched (at AM1.5, monolithic  $\text{Al}_{0.37}\text{Ga}_{0.63}\text{As}/\text{GaAs}/\text{Si}$  cascade. Efficiency under (200x) concentration for such a cascade is projected to approach 40%. Most importantly, this approach will involve rather inexpensive Si cells, and the OMVPE growth of III-V cascade on potentially cheaper, large-area Ge substrates. It is worth noting that a significant cost (70%) in the fabrication of the high-efficiency GaAs cells by OMVPE is from the GaAs substrates. Thus, the approach suggested in this program is likely to offer solutions to meet the long-term goals of NREL in the area of cost-effective, high-efficiency photovoltaics.

## Publications

1. R. Venkatasubramanian, M.L. Timmons, T.S. Colpitts, and J.S. Hills, "Advances in the Development of any AlGaAs/GaAs cascade solar cell using a patterned germanium tunnel interconnect", *Solar Cells*, 30, 345 (1991).
2. R. Venkatasubramanian, M.L. Timmons, and T.S. Colpitts, "High conductance GaAs Tunnel Diodes by OMVPE", *Proc. of MRS Symposium on Atomic Layer Growth and processing*, April 1991, Anaheim, CA.
3. R. Venkatasubramanian, M.L. Timmons, and T.S. Colpitts, "Selective plasma etching of Ge substrates for thin freestanding GaAs-AlGaAs heterostructures", *Appl. Phys. Lett.*, 59, 2153 (1991).
4. R. Venkatasubramanian, M.L. Timmons, T.P. Humphreys, B.M. Keyes, and R.K. Ahrenkiel, "High-Quality Eutectic-Metal-Bonded GaAs-AlGaAs Thin Films on Si Substrates", *Appl. Phys. Lett.*, 60 886 (1992).
5. R. Venkatasubramanian, M.L. Timmons, T.S. Colpitts, J.S. Hills, and J.A. Hutchby, "An Inverted-Growth Approach to Development of an IR-Transparent, High-Efficiency,

- AlGaAs/GaAs Cascade Solar Cell", Proc. of 22nd IEEE PVSC (IEEE Press, New York, NY, 1991), p. 93.
6. R. Venkatasubramanian, M.L. Timmons, T.S. Colpitts, and S. Asher, "Properties and Use of "Cycled" OMVPE GaAs;Zn, GaAs:Si and GaAs:Se Layers for High Conductance GaAs Tunnel Junctions", J. Elect. Mater. 21, 893 (1992).
  7. R. Venkatasubramanian, M.L. Timmons, P.R. Sharps, T.S. Copitts, J.S. Hills, J. Hancock, and J.A. Hutchby, "Development of an IR-Transparent, Inverted-Grown Thin-Film  $\text{Al}_{0.34}\text{Ga}_{0.66}\text{As}/\text{GaAs}$  Cascade Solar Cell", presented at the NREL PV AR&D 11th Review Meeting, May 14, 1992, Denver, CO.
  8. R. Venkatasubramanian, M.L. Timmons, T.P. Humphreys, "Vertical-Cavity Fabry-Perot Action in  $\mu\text{m}$ -thick, Eutectic-Metal-Bonded (EMB) AlGaAs-GaAs Films on Si Substrates", Presented at the Electronic Materials Conference June 26, 1992, Cambridge, MA.
  9. R. Venkatasubramanian, M.L. Timmons, T.S. Colpitts, and J.A. Hutchby, "An Inverted-Growth approach to Development of an IR-Transparent, High-Efficiency, AlGaAs/GaAs Cascade Solar Cell", NREL Final Subcontract Report under subcontract XM-0-18110-1.

**Title:** Low-Cost, High-Efficiency Solar Cells Utilizing GaAs-on-Si Technology

**Organization:** Spire Corporation, Bedford, Mass. 01730-2396

**Contributors:** S.M. Vernon, Principal Investigator and N.H. Karam

## **Introduction**

The overall goal of this research is to establish a technology to produce very-high-efficiency solar cells for terrestrial photovoltaic applications, using either multijunction or single-junction concepts. The approach pursued in this program involves the growth of GaAs and/or GaInP<sub>2</sub> materials onto Si substrates by the metalorganic chemical vapor deposition (MOCVD) technique. This year we have developed technology to deposit GaAs on Si using a nucleation layer of atomic-layer-epitaxy (ALE)-grown GaAs or AlAs on Si. This ensures two-dimensional nucleation, and should lead to less defects in the final GaAs layer. As an alternative, we also developed technology for depositing GaAs on sawtooth-patterned Si. Preliminary studies showed that this material can have a very low defect density ( $\approx 1 \times 10^5 \text{ cm}^{-2}$ ), as opposed to our conventionally grown GaAs on Si, which has a typical defect density of over  $1 \times 10^7 \text{ cm}^{-2}$ . Efforts of our prior-year's NREL work have resulted in the achievement of a GaAs-on-Si solar cell having a verified terrestrial efficiency world record of 21.3% at 200 suns, as shown in Figure 1.

## **GaAs-on-Si Material Studies**

We have looked at several means of reducing the dislocation density in the GaAs-on-Si layers. A promising, and unique, approach being studied makes use of the concept of restricting the nucleation area for the GaAs on Si. Lithographically patterning the Si substrate with sub-micron dimensions using holography permits the growth of planar GaAs films with greatly reduced dislocation density: preliminary results indicate a value of  $\sim 10^5 \text{ cm}^{-2}$  is achievable. Figure 2 shows a cross-sectional transmission electron micrograph of a GaAs film on sawtooth-patterned Si. The dislocation density in this film is quite low, probably about  $1 \times 10^5 \text{ cm}^{-2}$ ; the GaAs completely planarizes within approximately a half micron from the silicon.

Another dislocation-reduction technique being examined is the use of atomic-layer epitaxy (ALE) to deposit a nucleation layer, of GaAs or AlAs, that is two dimensional. Such a nucleation layer is expected to enable a thick GaAs to be subsequently grown with minimal threading dislocations propagating through the layer.

Both methods have resulted in GaAs-on-Si films showing improved minority-carrier lifetimes. Measurements at NREL indicate that these films have a lifetime of three nanoseconds; our previous best value was two nanoseconds. This 50% increase implies that solar cell efficiency should improve by several efficiency points.

Both methods have also resulted in GaAs-on-Si films having the lowest double-crystal X-ray rocking curve full width half maximum (FWHM) achieved at Spire. The FWHM value of 98 arcsec is among the best reported in the literature, and indicates the excellent structural quality of the layers.

### **Concentrator Solar Cell Studies**

The basic problem limiting the efficiency in GaAs-on-Si solar cells is the large defect density, which causes increased space-charge recombination and a reduced minority-carrier lifetime. Detailed analyses of current-voltage behavior in GaAs-on-Si cells have shown that the use of concentrated sunlight helps to overcome some of this difficulty by allowing the cell to operate in a regime where the ( $n = 1$ ) diffusion current dominates, thus leading to higher open-circuit voltages. Thus, we have been studying concentrator cells as the major vehicle for demonstrating high efficiency in GaAs-on-Si solar cells.

### **Future Directions**

Our continuing research interests include improving the efficiency of GaAs solar cells as well as reducing the defect level of our GaAs-on-Si "substrates". High-efficiency cell studies will include the development of GaInP<sub>2</sub> windows and of GaAs-GaInP<sub>2</sub> monolithic tandems, continued optimization of Bragg reflector structures, and combination of Bragg-reflector and concentrator concepts into GaAs-on-Si solar cells. GaAs-on-Si material improvements will be accomplished by continued study of substrate patterning and two-dimensional-nucleation techniques based on the use of atomic-layer epitaxy. We plan to use the newly developed GaAs-on-Si growth techniques to achieve higher efficiency in GaAs-on-Si solar cells.

### **Publications**

NREL-funded research has resulted in three articles being published in the scientific literature over the course of this past year. They are listed below:

"Growth and Characterization of Uniform AlGaAs Bragg Reflectors by LP-MOCVD," S.M. Vernon, S.P. Tobin, M.M. Sanfacon, A.L. Mastrovito, N.H. Karam, and M.M. Al-Jassim, *Journal of Electronic Materials*, 21, 335 (1992).

"High-Efficiency Concentrator Cells from GaAs on Si," S.M. Vernon, S.P. Tobin, V.E. Haven, L.M. Geoffroy, and M.M. Sanfacon, *Proc. of 22nd IEEE Photovolt. Spec. Conf., Las Vegas, NV*, Oct. 1991, 353 (1992).

"Enhanced Light Absorption in GaAs Solar Cells with Internal Bragg Reflectors," S.P. Tobin, S.M. Vernon, M.M. Sanfacon, and A.L. Mastrovito, *Proc. of 22nd IEEE Photovolt. Spec. Conf., Las Vegas, NV*, Oct. 1991, 147 (1992).

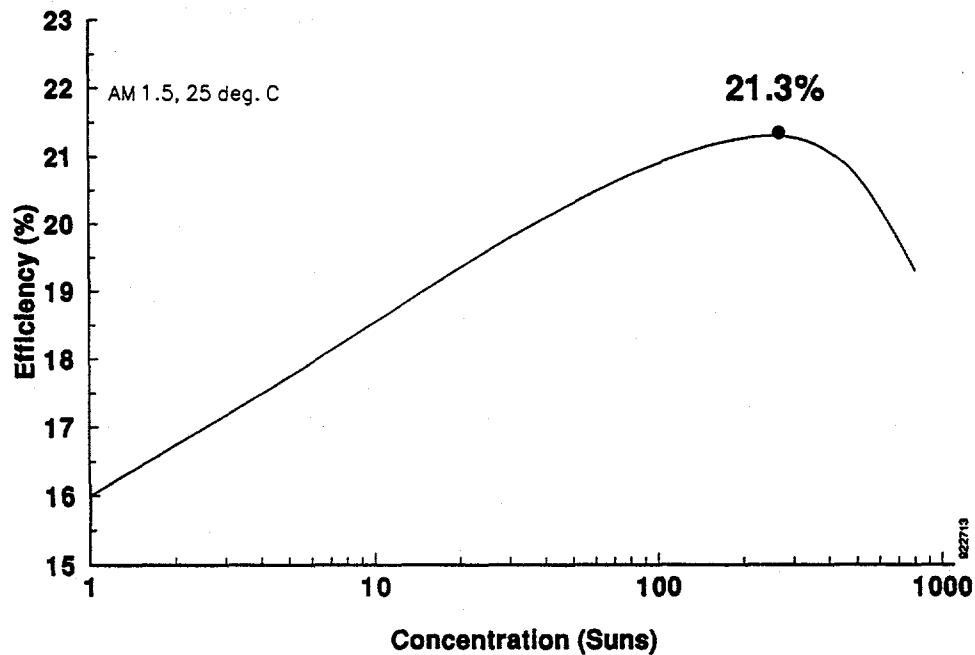


**Figure 1** Efficiency versus concentration for a GaAs-on-Si solar cell, measured at Sandia National Laboratory. The peak is at 237 suns, where the efficiency reaches 21.3%, AM1.5D.

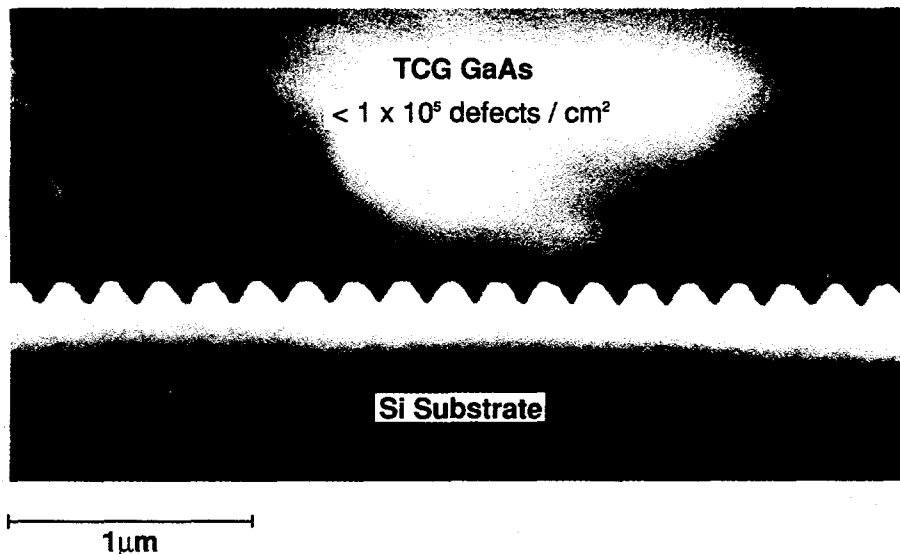


**Figure 2** Cross-sectional transmission electron micrograph of a GaAs film on sawtooth-patterned Si. The dislocation density in this film is quite low, probably about  $1 \times 10^5 \text{ cm}^{-2}$ .

**Title: Photon and Ion Assisted Doping and Growth of II-VI Compound Thin Films**

**Organization:** Department of Materials Science and Engineering,  
Stanford University, Stanford, CA 94305-2205

**Contributors:** R.H.Bube (Principal Investigator), A. L. Fahrenbruch, G. Jensen  
D. Kim, J. Mösslein, and A. Lopez-Otero

This is an investigation of the doping and growth of II-VI p-CdTe films by physical vapor deposition with co-evaporation of the dopant. Dopant incorporation by (a) photon-assisted doping (PAD) and (b) ion-assisted doping (IAD), and (c) co-evaporation of Cd<sub>3</sub>P<sub>2</sub> are compared with respect to the growth, structural, and photoelectronic properties of the deposited films. The effects of low energy electron irradiation and excess Cd flux during the deposition were also explored.

### Methods of Approach

Control of p-type doping in polycrystalline CdTe solar cells is a promising tool for minimizing series resistance loss and maximizing  $V_{oc}$  [1]. Our previous work, using IAD [2-5], focused on incorporation of the dopants and yielded carrier densities up to  $2 \times 10^{17} \text{ cm}^{-3}$  in homoepitaxial films with P as a dopant, but gave films with low minority carrier diffusion length ( $L_d$ ) [6].

We investigated PAD, in the hope that it could yield both high doping and good  $L_d$ , but we [6, 7], and other workers [8, 9, 10], could not reproduce the PAD results of Schetzina *et al.* [11,12]. However, there is consensus among most, if not all researchers, that illumination during deposition does enhance crystalline quality and that using excess Cd flux during deposition increases both doping and crystalline quality. For example, Arias *et al.* [8] found that illumination had little or no effect on doping, but that a Cd/Te flux ratio = 1.1–1.3 was necessary to incorporate and electrically activate As during the MBE growth of p-CdTe—regardless of whether the sample was illuminated or not.

We returned to IAD to find methods of increasing  $L_d$ , while maintaining the doping level. These include (1) lowering the ion energy to reduce damage and (2) using coincident low energy electron irradiation and (3) increasing the Cd/Te flux ratio slightly to increase dopant incorporation. Fig. 1 is a schematic of our deposition system. Characterization methods include measurements of resistivity, carrier density (by  $1/C^2$  vs V), and analysis of In Schottky barriers on the films. SIMS, x ray diffraction rocking curves, and photoluminescence measurements have also been made.

### Significant Results

Since we believe that the small  $L_d$  seen in the IAD samples is due to ion damage, and, in general, ion damage would be expected to increase with both the ion energy ( $E_i$ ) and ion dose ( $N_i$ ), an obvious solution is to lower  $E_i$  and/or  $N_i$ . Recent work with lower  $E_i$  has yielded promising results. Films grown with  $E_i \approx 20 \text{ eV}$  were compared with those grown at 60 eV, with all the other growth parameters held relatively constant. The representative spectral quantum efficiency curves for transparent Cr/CdTe Schottky diodes (Fig. 2), grown under similar conditions, indicate that the 20 eV films are considerably better.

Another series of films was grown to find the relationship of  $L_d$  to  $N_i$ , at  $E_i = 20$  and 60 eV. Modeling of the resulting spectral quantum efficiency data (and accounting for the spectral transmission of the Cr and the effect of the depletion layers in the diodes) yielded the  $L_d$  values plotted in Fig. 3. It can be seen that  $L_d$  decreases strongly with increasing  $N_i$  (in fact,



$L_d \propto N_i^{-1.45}$ ) at 60 eV, but that  $L_d$  values for 20 eV ions are at least a factor of 3 higher than those for 60 eV. The etch pit density for the 60 eV samples rises linearly with  $N_i$  and forms cellular patterns on the CdTe layers, indicating that the dislocation density is also rising.

Since the maximum doping  $p_{\max}$  that we can obtain with IAD decreases with decreasing  $E_i$ , we sought means to increase  $p_{\max}$  for the lower  $E_i$ , while maintaining  $L_d$ . We found that the electron flux ( $\approx 10\text{--}30$  eV), which accompanies the ion beam under certain operating conditions, increased the doping efficiency. The data for  $p$  vs.  $E_i$  shown in Fig. 4 shows that electron irradiation during growth increases  $p$  by a factor of 10 for these conditions. The electron current density is  $\approx 2 \mu\text{A}/\text{cm}^2$ , while the ion current is  $\approx 0.2 \mu\text{A}/\text{cm}^2$  for this series.<sup>1</sup> Finally, by increasing the (Cd/Te) ratio from 1.000 to 1.008, we could obtain  $p = 1 \times 10^{17} \text{ cm}^{-3}$ , and maintain  $L_d$  at  $\approx 0.35 \mu\text{m}$ , a value 3 to 5 times those obtained at 60 eV without electrons and excess Cd.

The "chemical" doping methods (in which P or As is impinged or deposited in an activated state) that have been developed in the past few years for the n- and p-type doping of CdTe thin films, appear to have a good degree of success [13–15]. In our own preliminary experiments on co-evaporation of  $\text{Cd}_3\text{As}_2$  during CdTe film growth without excess Cd, we reproducibly obtained  $p \approx 2 \times 10^{16} \text{ cm}^{-3}$  (without ionization of the dopant).

## Conclusions

Despite good doping control with IAD, the unacceptably small  $L_d$  values observed in our previous work suggested at first that the method had limited usefulness. However, the work reported here for IAD is much more promising. The use of lower ion energies (10–20 eV), electron irradiation during growth, and the use of small excess Cd fluxes has enabled us to dope CdTe up to  $p \approx 1 \times 10^{17} \text{ cm}^{-3}$ , while maintaining a respectable  $L_d$  of  $\approx 0.35 \mu\text{m}$ .

These results again emphasize the importance of micro-stoichiometry control in the deposition and doping of II-VI compounds.

Our observation of significant increases in  $L_d$  at lower ion energies and with electron flux during growth, and the reports of successful IAD doping with N for CdTe [16] and ZnSe [17] promise higher doping levels, better  $L_d$  values, and the application of these methods to polycrystalline material in the future.

## Future Work

We are refocusing our research on two areas. The first is a continuation of the IAD work to include:

- (i) Exploration of the transport properties of various photovoltaic junctions involving CdTe, using our capabilities for IAD deposition of p-CdTe.
- (ii) Exploration of the use of N radicals as a dopant for p-CdTe.
- (iii) Further exploration of the use of un-ionized  $\text{Cd}_3\text{As}_2$  as a dopant source.
- (iv) Extension to polycrystalline thin films.

The second area is the investigation of single-crystal and polycrystalline ZnTe films, grown by CSVT, for low-resistance ohmic contacts to p-CdTe and as an active component in tandem cells.

Our ultimate goal is to test the most promising technique(s) from the studies above on CdS/CdTe(/ZnTe) heterojunction solar cells based on these IAD doped single-crystal and polycrystalline CdTe films.

<sup>1</sup> As a point of comparison, the Cd-Te pair equivalent current is typically  $\approx 700 \mu\text{A}/\text{cm}^2$  and, for the PAD experiments, the photon equivalent current is  $30,000 \mu\text{A}/\text{cm}^2$ .

## Acknowledgements

We are grateful to Sally Asher at NREL for SIMS measurements, Dr. Mowafak Al-Jassim and the late John Goral of NREL for XTEM studies, and Martin Schöfthaler for EBIC measurements. This work has also benefited from facilities made available to Stanford University by the National Science Foundation through the Center for Materials Research at Stanford University.

## References

1. C.M. Fortmann, A.L. Fahrenbruch, and R.H. Bube, *J. Appl. Phys.* **61**, 2038 (1987).
2. A. Fahrenbruch, A. Lopez-Otero, P. Sharps, and R.H. Bube, *Proc. 19th IEEE Photovoltaic Spec. Conf.* (1987) p. 1309.
3. A.L. Fahrenbruch, K-F. Chien, D. Kim, A. Lopez-Otero, P. Sharps, and R.H. Bube, *Solar Cells* **27**, 137 (1989).
4. P. Sharps, A. Fahrenbruch, A. Lopez-Otero, and R. H. Bube, *Proc. 21st IEEE Photovoltaic Spec. Conf.* (1990), p. 493.
5. P. Sharps, A.L. Fahrenbruch, A. Lopez-Otero, and R.H. Bube, *J. Appl. Phys.* **68**, 6409, 1990.
6. R.H. Bube "Photon and Ion Assisted doping and growth of II-VI Compound Thin Films," NREL AR I and II, NREL Subcont. XM-0-181-4, 7/1/89-6/31/90 and 7/1/90-6/31/91.
7. A.L. Fahrenbruch et al., *Int J. Solar Energy*, **12**, (1992).
8. J.M. Arias et al., *J. Vac. Sci. Technol.* **A8**, 1025 (1990).
9. A. N. Tiwari, et al., *J. Cryst. Growth* **111**, 730 (1991).
10. C.J. Summers, private communication, 1990.
11. R.L. Harper Jr., S. Hwang, N.C. Giles, and J.F. Schetzina, D.L. Dreifus, and T.H. Myers, *Appl. Phys. Lett.*, **54** (2), 170 (1989).
12. K. A. Harris, et al., *J. Vac. Sci. Technol.* **B9**, 1752 (1991).
13. S.K. Gandhi, N.R. Taskar, and I.B. Bhat, *Appl. Phys. Lett.* **50**, 900 (1987).
14. C. Cohen-Solal, *J. Cryst. Growth* **72**, 512 (1985).
15. F. S. Turco-Sandroff, et al., *Appl. Phys. Lett.* **59**, 688 (1991).
16. N. Romeo, A. Bosio, V. Canevari, C. Spaggiari, and L. Zini, *Solar Cells* **26**, 189 (1989).
17. R.M. Park et al., *Appl. Phys. Lett.* **57**, 2127 (90).

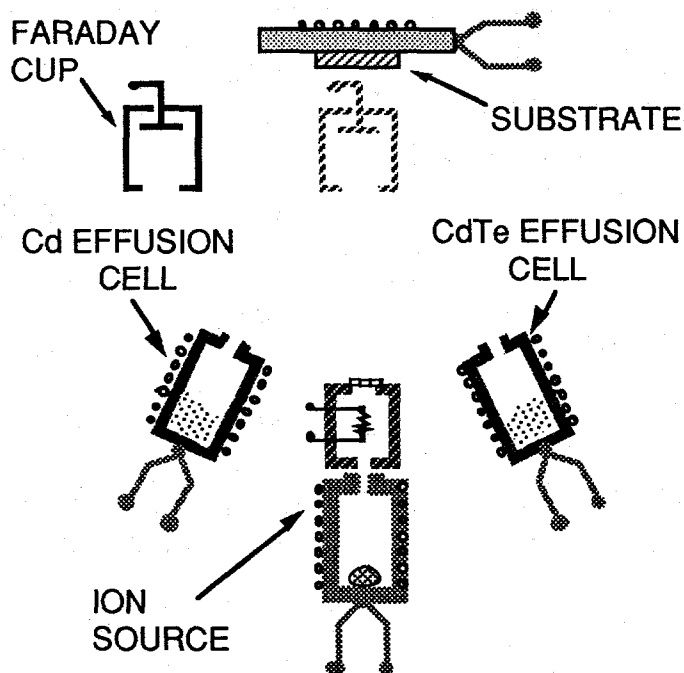


Fig. 1. IAD system. Depositions are typically homoepitaxial films  $\approx 10 \mu\text{m}$  thick on (100) single-crystal p-CdTe substrates. Chamber pressure is  $\approx 2 \times 10^{-7}$  Torr.

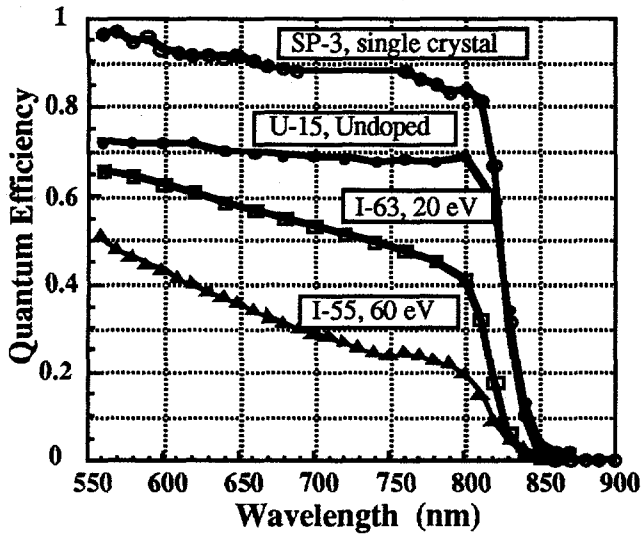


Fig. 2. Spectral quantum efficiency data for Cr/CdTe diodes. Light is incident through the Cr and the curves were corrected for the reflection and absorption of the Cr.  $T_{\text{sub}} = 400^\circ\text{C}$  and SP-3 is a single crystal control sample with  $p \approx 10^{17} \text{ cm}^{-3}$ . For I-63,  $N_i = 10^{19} \text{ cm}^{-3}$  and  $p = 5 \times 10^{16} \text{ cm}^{-3}$ . For I-55,  $N_i = 1.3 \times 10^{19} \text{ cm}^{-3}$  and  $p = 1.4 \times 10^{17} \text{ cm}^{-3}$ .

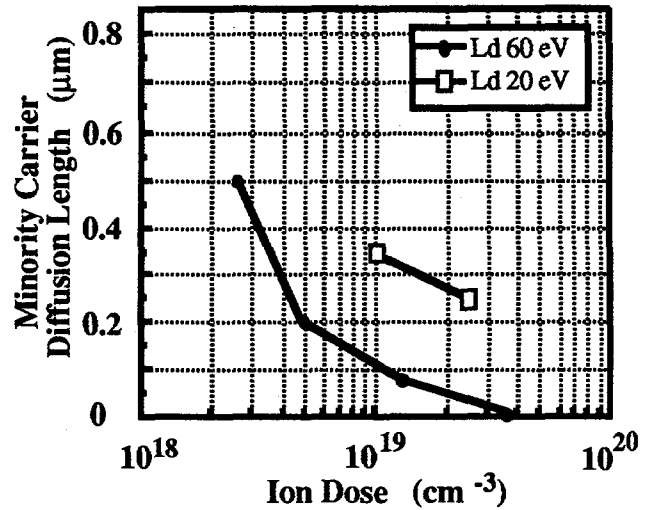


Fig. 3. Minority carrier diffusion length vs. ion dose for  $E_i = 20$  and  $60 \text{ eV}$ . Typical values for good single crystal are  $0.5 - 1 \mu\text{m}$ .

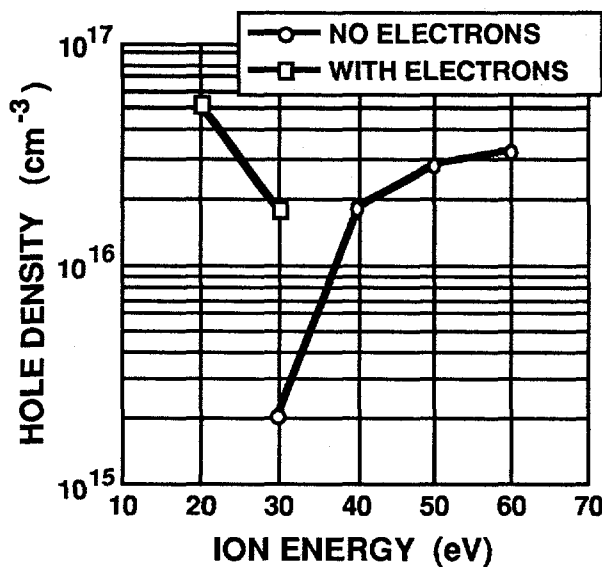


Fig. 4. Hole density vs.  $E_i$  at  $N_i = 5 \times 10^{18} \text{ cm}^{-3}$  and  $T_s = 400^\circ\text{C}$ , with and without electron irradiation.

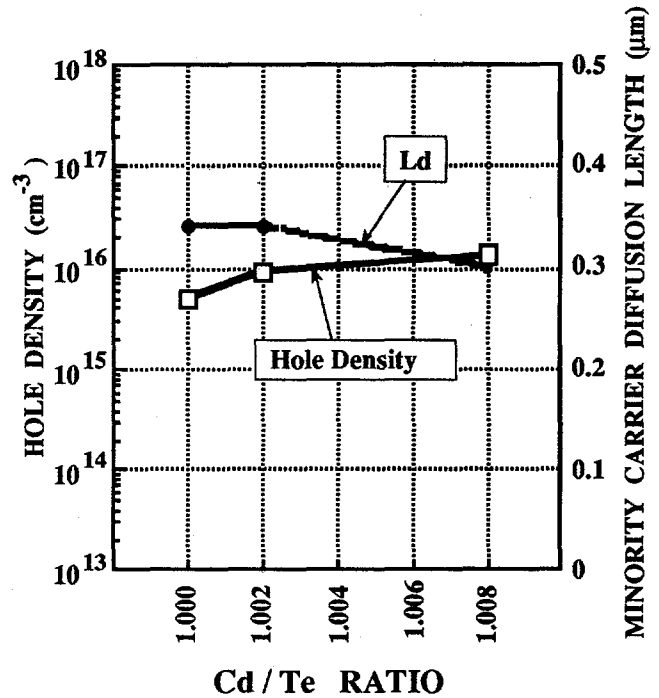


Fig. 5. Hole density and  $L_d$  vs. Cd/Te ratio for  $E_i = 20 \text{ eV}$  with electron irradiation.

**Title: Passivation and Gettering Studies in Solar Cell Silicon**

**Organization:** Institute for the Study of Defects in Solids,  
Physics Department  
The University at Albany  
Albany, N. Y. 12222

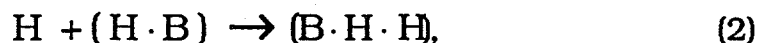
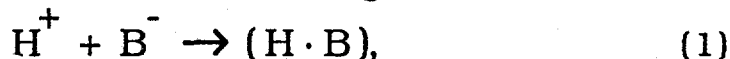
**Contributors:** J. W. Corbett, principal investigator;  
J. T. Borenstein, P. Deák, S. J. Pearton,  
D. A. Tulchinsky, I. V. Verner, and A. Yencha.  
(Not all receive support from the contract.)

This research program has two major aspects: 1) The study of hydrogen in crystalline silicon; and 2) the study of gettering in crystalline silicon. In the hydrogen studies are concerned with all aspects of hydrogen in silicon: how hydrogen is introduced into silicon (by wet-etching, boiling, plasma treatment, injection from a Kaufman source, etc.); its configurations and diffusion mechanisms; and the nature of its interactions with defects. The main emphasis has been the modeling of the diffusion profiles. The gettering studies are concerned with mechanism by which deleterious impurities are introduced into silicon and the mechanism by which these impurities can be removed from the device region, e. g., removal at an external surface or at a precipitate.

### **Hydrogen-Related Studies.**

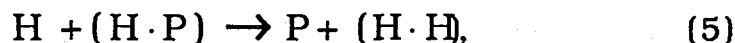
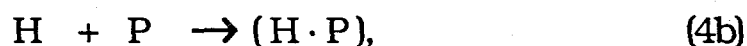
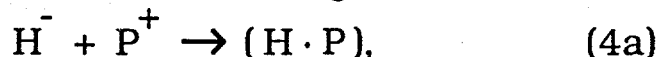
As we have discussed in prior reports, diffusion in the presence of traps does not exhibit the normal erfc profile and the common Eistein scaling; further hydrogen diffusion in silicon uniformly doped with boron has several features: 1) the plateau expected from the hydrogen exhausting the boron traps; 2) another plateau indicating multiple trapping of hydrogen by boron; and a steep exponential drop<sup>1</sup> at the surface suggesting an unsaturable trap for the hydrogen. Again, as discussed in earlier reports we established the scaling<sup>2</sup> for the profile in these cases. We also achieved a fit to the experimental profiles<sup>3</sup>. Further work on the fit is in progress<sup>4</sup>.

The model which appears to describe the diffusion processes in p-type silicon includes the following reactions:



Equation 1 reflects the Coulombic interaction between the charged boron and a charged hydrogen; the diffusion profiles suggest that the (0/+) level for hydrogen is at ca. ( $E_V + 0.3 \pm 0.1$  eV). Equations 2 & 3 describe the capture of additional hydrogens by a boron; the diffusion profiles suggest this additional capture with  $n \sim 8-16$ , and as we mentioned, we have found direct evidence for an additional, slightly bound hydrogen in C-V experiments<sup>9</sup>. Theoretical studies<sup>17, 5-6, 7</sup> have suggested that hydrogen may agglomerate without forming hydrogen molecules. We are carrying out theoretical studies<sup>8</sup> on the agglomeration process (for  $n < 8$ ) at a boron in silicon. It is not clear if the {111} platelet formation observed by Johnson *et. al.*<sup>9</sup> and by Jeng *et. al.*<sup>10</sup> occurs heterogeneously or homogeneously. Although the {111} planar defects observed could be due to the partially dissociated multivacancy defects that we have discussed earlier<sup>11</sup>, we are inclined to the view proposed by Johnson *et. al.*<sup>48</sup> that a number of hydrogens in BC-sites interact through their associated distortions to form an extended planar defect. We have performed calculations<sup>45, 46</sup> on such a defect, and find that the strain interaction will stabilize a planar defect. We further find that subsequent hydrogens will bond in the same bond axis, i.e., one on each silicon, without forming a molecule, and thereby form an incipient crack, a prototype of a defect causing the brittleness<sup>45, 46</sup> of silicon grown in hydrogen gas.

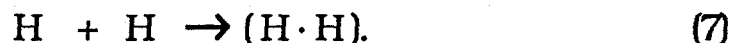
The model which appears to describe the diffusion processes in n-type silicon includes the following reactions:



Equations 4 show the reaction of a single hydrogen with the donor phosphorus; Eq. 4a describes the possibility of a Coulombic interaction. Our diffusion data does not require this reaction, i. e., we see no evidence of a negatively charged hydrogen in the range of

resistivities of 100- to 0.1  $\Omega$ -cm silicon; more specifically these diffusion profiles do not exhibit the abrupt change in character found in p-type material. Johnson et. al.<sup>12</sup> and Tavendale et. al.<sup>13</sup> have found evidence of H<sup>-</sup> in drift experiments, so the Coulombic reaction should occur. Equation 5 indicates that a second hydrogen may reactivate the phosphorus, a process which we use to explain the "partial deactivation" of the phosphorus and the fact that the diffusion profile does not show the plateau associated with impurity trapping (a plateau observed for boron-doping). The diffusion profile for 100  $\Omega$ -cm silicon (both n-type and p-type) shows the shape which is characteristic of diffusion limited by molecule formation. As the phosphorus concentration increases the slope of the profile steepens, which we interpret as reflecting impurity mediated molecule formation. There is also at shallow depths a peak in the profile which tends to increase with the impurity concentration, and it is for that reason we invoke the multi-hydrogen agglomeration at a phosphorus shown in Eq. 6. It does seem from the work of Stavola and co-workers<sup>14- 15, 16</sup> that a high percentage (e. g., >80%) of phosphorus can be deactivated with sufficient hydrogen.

We find that we can fit the simple diffusion profiles (e.g., 1  $\Omega$ -cm p-type and 100  $\Omega$ -cm n-type) with physically reasonable parameters, for example, with a 40 Å capture radius for the process in Eq. 1, and a 4 Å capture radius for those in eqs. 2 and 3, and a similar 4 Å radius for direct molecule formation:



We have also found<sup>17</sup>, however, that these parameters are not unique! For example, we have found that we can fit the molecule-formation data with comparable success for the range of variables described by the following equations:

$$R D H_0^2 = C_1, \quad (8)$$

$$R H_0 = C_2; \quad (9)$$

and for the impurity-trapping regime for the range of variable described by the equation:

$$D H_0 = C_3. \quad (10)$$

In these equations D is the diffusion coefficient, R the corresponding capture radius, and H<sub>0</sub> the (unknown) concentration of hydrogen at the surface of the silicon; C<sub>1</sub>, C<sub>2</sub>, and C<sub>3</sub> are constants. There are "invariants" associated with conservative systems<sup>18</sup> described by non-linear equations, but we know of none such as these; we have been

unable to derive these "invariants" with any generality. We do not despair of establishing the parameters unambiguously, in particular since some of the parameters may well be the same in different processes.

As we have discussed before<sup>1-4</sup>, there is considerable scatter in the published data for diffusion of hydrogen in silicon. Part of this results from the common presumption that the diffusion profile is described by the conventional erfc profile and that the Einstein relationship holds, i. e., the product of the diffusion coefficient times the diffusion time equals the square of the mean diffusion distance.

But the profiles for the molecule-forming regime and the impurity-trapping regime is not an erfc profile, nor is the Einstein relation an accurate measure of the diffusion. The breakdown of Eq. 2 is a manifestation of a broader phenomenon, namely, diffusion in a fractal lattice. The Einstein relation holds for diffusion in one-, two- and three-dimensional lattices. It does not hold for diffusion in a fractal lattice where the appropriate result<sup>19</sup> has the time raised to the power given by Eq. 11.

with

$$R = 2/(2+\delta) \quad (11)$$

with  $\delta$  a parameter equal to zero for one-dimension, equal to 0.8 for two, and equal to 1.5 for three. The origin of this deviation from the Einstein relation is the hindered motion of the random walking a fractal lattice. A hindered motion occurs in hydrogen diffusion in silicon. For example, a random array of impurities at which the hydrogen can be trapped presents a hindrance to penetration into the lattice; similarly a random distribution of diffusing hydrogen with which a hydrogen can form molecules also forms a hindrance. We have not found a derivation of the expression corresponding to Eq. 11<sup>20</sup> for these cases. For impurity trapping with a capture radius of 10 Å, a surface hydrogen concentration of  $10^{16}/\text{cm}^3$  we find  $\log(Dt) \sim 1.3 \log \langle X \rangle$  for 0.1 Ω-cm material and  $\log(DT) \sim 1.7 \log \langle X \rangle$  for 1 Ω-cm material. That is we find  $\delta = -0.7$  and  $-0.3$  for 0.1 Ω-cm and 1 Ω-cm, respectively. We presume that the change in sign in our result vs. that for diffusion on the fractal lattice relates to the different form of hindrance in the two type of random walk. In the random walk on the fractal lattice the missing sites require the diffusing particle to go further, i. e., there are sites it cannot visit; in the case that we consider if the hydrogen visits a "forbidden" site it is captured and removed from the ensemble and represents a net loss to the advance

of profile. We are continuing these studies to establish the broader picture.

We also have carried out theoretical studies to examine if boron has several trapping sites; we find<sup>21,22</sup> that it and phosphorus both do.

Sopori *et. al.*<sup>23, 24</sup> have recently reported on observations of enhanced hydrogen diffusion in the bulk of polycrystalline solar cell silicon. In the experiments, hydrogen was introduced into the p-type (B doped) 0.5 - 1 ohm cm resistivity samples through low energy (0.5 - 2 keV) implantation at temperatures in the 100C to 300C range. To observe the migrating hydrogen secondary ion mass spectroscopy (SIMS) was used, as well as cross sectional transmission electron microscopy (XTEM) to detect the decoration of grain boundaries and dislocations by the diffusing hydrogen.

At the suggestion of Dr. Sopori ( our contract monitor) we began studies of the role of hydrogen in enhancing the motion of oxygen, the silicon vacancy, and boron, the latter two with Dr. S. K. Estreicher. We have found<sup>25</sup> in theoretical studies a configuration of H-O-H which has an enhanced motion over the isolated oxygen, and indeed is a negative-U system, i. e., the motion is further enhanced by the presence of ionization. Further studies are in progress.

### **Gettering-Related Studies**

It is well known that oxygen precipitates act as gettering sites for the iron-group transition elements, i.e., for the major "fast diffusers." We have completed several studies related to these problems, including identifying<sup>41</sup> the defect created when a vacancy interacts with an iron atom. A major problem in gettering studies is the indirect nature of the measurement studying the transition element, e.g., EPR can identify the transition element if it is in the proper charge state, DLTS can identify an electrical level which may be associated with a transition element. We have begun studies using radio-active tracers to better follow the introduction and history of the transition elements. Another aspect of gettering at oxygen defects is identifying the oxygen defects of which there are a plethora of varieties<sup>26</sup>. We have carried out a number of studies<sup>27- 28, 29, 30, 31, 32, 33, 34, 35</sup> helping to clarify the nature of the electrical properties of the 450°C thermal donors, the new shallow donors, the anomalous oxygen diffusion mechanism, and the nature and structure of the core of the thermal donors, and of the thermal donors, and oxygen-related recombination centers. We anticipate exploiting this knowledge in our gettering studies.



The copper which enters the system is trapped at the boron; this trapping is consistent with the electrical measurements made by others above after polishing, although some of the early literature suggested that such trapping was not occurring for copper and boron.

Again with the concurrence of Dr. Sopori, we began studies of the gettering at Germanium sites in Si(Ge) single crystal alloys. These alloys were made available to us by IBM, and are very high quality, i.e., our channeling studies show that the Ge is on substitutional sites. We have found gettering of 3d transition element at the germanium, or rather in the germanium layer, and have shown<sup>36</sup> that these elements are in random interstitial sites.

## REFERENCES

1. B. L. Sopori: Mechanism of Enhanced Hydrogen Diffusion in Solar Cell Silicon; MRS Meeting, 4/27-5/1/92, San Francisco; Symposium on Defect Engineering.
  2. B. L. Sopori: Hydrogen Induced Defects and Defect Passivation in Silicon Solar Cells; in Defects in Semiconductors, Proceedings of the 16th International Conference on Defects in Semiconductors, Eds. G. Davies, G. G. Deleo, and M. Stavola, Materials Science Forum Vol. 83-87 (Trans Tech Publications, 1992) pp. 1531-1538.
  3. L. Korpás, J. W. Corbett, and S. K. Estreicher: New traps for H<sup>0</sup> in p-type Si, *Superlattices and Microstructures*, 10, 121 (1991).
  4. L. Korpás, J. W. Corbett, and S. K. Estreicher: New traps for H<sup>0</sup> in boron- and phosphorous-doped silicon, pp. 27-32 in the publication of ref. 2.
  5. L. Korpás, S. K. Estreicher, and J. W. Corbett: Multiple trapping of hydrogen at boron and phosphorous in silicon, to appear in *Phys. Rev. B* 46, 15 November, 1992 issue.
240. "New Traps for H<sup>0</sup> in p-type Silicon," Levente Korpás, J.W. Corbett, and S.K. Estreicher submitted to *Superlattices and micro-structures* (1991).
241. "New Traps for H<sup>0</sup> in Boron-and Phophorus-doped Silicon," Levente Korpás, J.W. Corbett, and S.K. Estreicher, to be submitted(1991).

242. "A New Way for Measuring the Ion Implantation Amorphous Critical Dose *in Situ*," Jian-zhong Yuan, Igor V. Verner, and James W. Corbett. MRS Mtg Fall 1991 Session A.
243. " Study of Amorphization Process in Silicon Irradiated by Different Ions Using *in situ* Measurements and TEM Measurements," Jian-zhong Yuan, Igor V. Verner, Sergei K. Maksimov, James W. Corbett., and Andrew J. Yench. MRS Fall Mtg 1991 Session A.
249. "Dose Rate Dependence of the Stress in Ar<sup>+</sup> Ion Implantation of Silicon, Jian-Zhong Yuan and J. W. Corbett, in *Rad Eff., Section A*. (1992).
250. "Studies of Disorder Induced by Ion Implantation into Silicon Using *in situ* Stress Measurement Technique," Jian-Zhong Yuan, James W. Corbett, Sergei N. Voronkov, and Igor V Verner, submitted to Radiation Effects, Section A (1992).
251. "Changes in the Evolution of Point Defects Related to the Formation of Porous Silicon," I. V. Verner, D. I. Shereshevskii, and N. N. Gerasimenko.
252. "Reactive Ion Etching of S(Ge) Using Fluorine-and Chlorine-Containing Plasmas," Ying Zhang, Gottlieb S. Oehrlein, and Edouard de Frésart, and James W. Corbett., to be submitted Sept. 1992.
253. "A Negative-U Hydrogen-Oxygen Complex and Its Effects on Oxygen Diffusion and Loss in Silicon." Jun Liu, J. W. Corbett, L.C. Snyder, and Péter Deák, to be submitted, Sept. 1992.
254. "Theoretical Studies of the Core Structure of the 450 deg C Thermal Donors in Silicon," Péter Deák, Lawrence C. Snyder, and J. W. Corbett, to be submitted , Oct. 1992.

---

## REFERENCES.

- 1 Exponential Diffusion Profile for Impurity Trapping at an Unsaturable Trap," D. A. Tulchinsky, J. W. Corbett, J. T. Borenstein, and S. J. Pearton, *Phys. Rev. B* 42 (1990) 11881-11883.

- 
- 22 "Effect of Multiple- trapping of Hydrogen in Silicon, "J.T. Borenstein, J. W. Corbett, and S.J. Pearton, Proc. 16-ICDS, LEHIGH, 1991.
  - 3 J. T. Borenstein, D. A. Tulchinsky, and J. W. Corbett in Proc. Fall-MRS-89, to be published.
  - 4" Diffusion Profile With Multiple-Trapping," J.T. Borenstein and J.W. Corbett, to be published..
  - 5 K. J. Chang and D. J. Chadi, *Phys. Rev. Lett.* **62** (1989) 937.
  - 6 J. W. Corbett, P. Deák, C. Ortiz, and L. C. Snyder, *J. Nucl. Materials*, in press.
  - 7 C. Ortiz, D. Deák. L. C. Snyder, and J. W. Corbett, to be published.
  - 8 L. Korpás, S. K. Estreicher, J. W. Corbett, and L. C. Snyder, to be published.
  - 9 N.M. Johnson, F.A. Ponce, R.A. Street, and R.J. Nemanich, *Phys. Rev. B* **35** (1987-1) 4166.
  - 10 S.-J. Jeng, G.S. Oehrlein, and G.J. Scilla, *Appl. Phys. Lett.* **53** (1988) 1755.
  - 11 J. W. Corbett, J. P. Karins, and T.-Y. Tan, *Nucl. Instr. & Meth.* **182/183** (1981) 457.
  - 12 N. M. Johnson and C. Herring in *Defects in Semiconductors 15*, ed. G. Ferenczi (Trans Tech, Switzerland, 1989) p. 961.
  - 13 S. J. Pearton, private communication.
  - 14 M. Stavola, S.J. Pearton, J. Lopata, and W.C. Dautremont-Smith, *Appl. Phys. Lett.* **50** (1987) 1086-1088.
  - 15 K. Bergman, M. Stavola, S.J. Pearton, and J. Lopata, *Phys. Rev. B* **37** (1988) 2770.
  - 16 K. Bergman, M. Stavola, S.J. Pearton, and T. Hayes, *Phys. Rev. B* **38** (1988) 9643.
  - 17 J. T. Borenstein, D. A. Tulchinsky, and J. W. Corbett in Proc. Fall-MRS-89, to be published.
  - 18 R. Z. Sagdeev, D. A. Usikov, and G. M. Zaslavsky, *Nonlinear Physics: From the Pendulum to Turbulence and Chaos* (Harwood Academic Publishers, New York, 1988).
  - 19 Y. Gefen, A. Aharony, and S. Alexander, *Phys. Rev. Lett.* **50** (1983) 77.
  - 20
  - 21 "New Traps for  $H^0$  in p-type Silicon,"Levente Korpás, J.W.Corbett, and S.K. Estreicher submitted to *Superlattices and micro-structures* (1991).
  - 22 "New Traps for  $H^0$  in Boron-and Phophorus-doped Silicon,"Levente Korpás,J.W.Corbett, and S.K. Estreicher,to be submitted(1991).

- 
- 23 B. L. Sopori: Mechanism of Enhanced Hydrogen Diffusion in SolarCell Silicon; MRS Meeting, 4/27-5/1/92, San Francisco; Symposium on Defect Engineering
  - 24 . B. L. Sopori: Hydrogen-Induced Defects and Defect Passivation in Silicon Solar Cells; in Defects in Semiconductors, Proceedings of the 16th International Conference on Defects in Semiconductors, Eds. G. Davies, G. G. Deleo, and M. Stavola, Materials Science Forum Vol. 83-87 (Trans Tech Publications, 1992) pp. 1531-1538.
  - 25 J. Liu, L. C. Snyder, J. W. Corbett, P. Deák, and L.C Snyder, to be published.
  - 26 See the several pertinent review articles in *Oxygen, Carbon, Hydrogen and Nitrogen in Crystalline Silicon*, eds. J. C. Mikkelsen, Jr., S. J. Pearton, J. W. Corbett, and S. J. Pennycook (MRS, Pittsburgh, 1986) and in *Defects in Electronic Materials*, eds. M. Stavola, S. J. Pearton, and G. Davies, (MRS, Pittsburgh, 1988).
  - 27 J. T. Borenstein, J. W. Corbett, M. Herder, S. N. Sahu, and L. C. Snyder, *J. Phys. C: Solid State Phys.*, **19** (1986) 2893.
  - 28 J. T. Borenstein, D. Peak, and J. W. Corbett, in *Oxygen, Carbon, Hydrogen and Nitrogen in Crystalline Silicon*, eds. J. C. Mikkelsen, Jr., S. J. Pearton, J. W. Corbett, and S. J. Pennycook (MRS, Pittsburgh, 1986)
  - 29 J. A. Griffin, H. Navarro, J. Weber, L. Genzel, J. T. Borenstein, J. W. Corbett, and L. C. Snyder, *J. Phys. C: Solid State Phys.* **19** (1986) L579.
  - 30 L. C. Snyder, J. W. Corbett. P. Deák, and R.-Zh. Wu in *Defects in Electronic Materials*, eds. M. Stavola, S. J. Pearton, and G. Davies (MRS, Pittsburgh, 1988) p. 179.
  - 31 K. Banerjee, V. A. Singh, and J. W. Corbett, *Semicond. Sci. & Tech.* **3** (1988) 542.
  - 32 L. C. Snyder, J. W. Corbett, P. Deák, and R.-Zh. Wu in *New Developments in Semiconductor Physics*, eds. G. Ferenczi and F. Beleznyay (Springer Verlag, Berlin 1988) 147-156.
  - 33 P. Deák, L. C. Snyder, J. W. Corbett, R.-Zh. Wu and A. Sályom in *Defects in Semiconductors 15*, ed. G. Ferenczi (Trans Tech, Switzerland 1989) 281.
  - 34 L.C. Snyder, P. Deák, R.-Zh. Wu, and J. W. Corbett in *Defects in Semiconductors 15*, ed. G. Ferenczi (Trans Tech, Switzerland 1989) 329.
  - 35 L. C. Snyder, P. Deák, R.-Zh. Wu, and J. W. Corbett in *Proc. Shallow Donor Conf., Linköping, Sweden, 1988*, in press.
  - 36 C. Barbero, G. S. Oehrelein, and J.W. Corbett, to be published.

**Title:** Identification and Control of Lifetime-Reducing Defects in Polycrystalline Silicon Photovoltaic Materials

**Organization:** Department of Materials Science and Mineral Engineering  
University of California, Berkeley  
Berkeley, California

**Contributors:** E. R. Weber, principal investigator; R.J. Bailey

## **Introduction**

Our efforts have concentrated so far on the identification of lifetime-limiting defects in Edge-defined Film-fed Growth (EFG) silicon ribbon, and the role of transition metal impurities in reducing minority carrier diffusion length. The electrical effects of 3d transition metals have been well known for years in Cz and FZ silicon,<sup>1</sup> but in EFG the high carbon concentration ( $10^{18} \text{ cm}^{-3}$ ) and lattice defect density silicon complicates the study of transition metals. There is the possibility that 3d transition metals exist in a variety of states: paired with acceptors, interstitially dissolved, precipitated at dislocations, grain boundaries, and twin planes, or clustered at heretofore unidentified sites.

In particular iron, a common detrimental contaminant in silicon, has been examined previously as an impurity in EFG silicon. Results show that cells with a bulk iron concentration of  $3 \times 10^{14} \text{ cm}^{-3}$  (intentionally contaminated in the melt) yielded an acceptable cell efficiency of 13%.<sup>2</sup> Information is totally lacking about the state of iron in this material, however, which is important since iron not only diffuses at room temperature but is very electrically active in its isolated interstitial state.<sup>3</sup> In moderately doped p-silicon iron is normally paired with boron at room temperature; the pair is less effective as a recombination center. It is therefore important that the properties of iron be understood with respect to its configuration. This study, therefore, is an attempt to understand the properties of iron in EFG silicon, while simultaneously observing and controlling its configurational state.

## **Experimental Results**

To determine the effects of iron on the recombination properties of the material, average diffusion length measurements (averaged over several  $\text{mm}^2$ ) were obtained using the Surface PhotoVoltage (SPV) method.<sup>3,4</sup> Iron concentration was measured as the concentration of iron-boron pairs using DLTS. Electron Beam Induced Current (EBIC) measurements were obtained on some samples, and the local diffusion length was obtained using energy-dependent EBIC.<sup>5</sup> This technique allows much greater spatial resolution than SPV for diffusion length determination.

We have found that when iron is diffused into EFG silicon at high temperature ( $1050^\circ\text{C}$  for 1hr.) and then quenched ( $\sim 1000^\circ\text{C}/\text{sec.}$ ) to avoid iron precipitation during cooling, the minority carrier diffusion length (SPV) is reduced to less than  $5 \mu\text{m}$ . This occurs in EFG samples with as-received diffusion lengths ranging from 10 to  $60 \mu\text{m}$ . This illustrates the effectiveness of a high concentration of iron-boron pairs ( $10^{15} \text{ cm}^{-3}$ ) at increasing carrier recombination.

After post-diffusion characterization, several samples were annealed at  $235^\circ\text{C}$  to precipitate the dissolved iron. The precipitation kinetics for two samples are represented in Figure 1,

which shows that the precipitation rate is much greater in a sample with a lower as-received diffusion length. The time constant for precipitation in the low diffusion length sample is approximately one third that in the high diffusion length sample. This suggests that the same electrically-active defects which limit diffusion length also act as heterogeneous nucleation sites for iron precipitation. (The precipitation rate has been shown to be a strong function of the bulk defect concentration.<sup>6</sup>) The precipitate morphologies and the exact sites for precipitation have not yet been determined, but it is clear that these sites exist in drastically different concentrations in closely separated regions of the same ribbon.

Figure 2 indicates that the SPV-measured diffusion length in sample #14 returned to its original (but low) diffusion length after iron precipitation. Figure 2 also shows, however, that the same precipitation anneal applied to sample #10, which had an as-received diffusion length of about 60  $\mu\text{m}$ , has similar results but yields a different conclusion. We see that with both samples the diffusion length is limited to about 10  $\mu\text{m}$  after iron precipitation, suggesting that a similar diffusion length-limiting mechanism is responsible in both samples.

EBIC micrographs of iron-precipitated EFG silicon show that precipitation, at least in part, proceeds heterogeneously, with dislocations and planar defects acting as preferred precipitation sites. This is illustrated in Figure 3, which is an EBIC micrograph of sample EFG25, annealed for 71 minutes after iron diffusion and quench. One sees bright EBIC contrast along the planar defect (presumably a twin boundary) and around the dislocations above it. This is typical in cases where denudation of an electrically-active impurity occurs near an impurity precipitation site. Based upon the interstitial iron diffusion coefficient at 235°C, the expected diffusion distance ( $\sqrt{4Dt}$ ) is approximately 20  $\mu\text{m}$  for 71 minutes at 235°C; this corresponds well with the EBIC image. An EBIC image of another high-diffusion length sample does not show this denudation effect. Figure 4 shows sample EFG10 after 70 minutes of iron precipitation; no denudation around the dislocations in the micrograph is visible. Point-mode diffusion length measurements of EFG10 at the points indicated show that there is little improvement in diffusion length away from the dislocations. This suggests that precipitation has occurred more locally than in EFG25, and that the precipitates are electrically active. Point mode EBIC of EFG25, indicated in Figure 3, shows a very low diffusion length away from the planar defect. This may be due to the electrical activity of unprecipitated iron, but when paired with boron, iron is relatively electrically inactive. Assuming, then, that *Fe precipitates* limit the diffusion length after lengthy precipitation anneals, the denudation observed in Figure 3 may represent a decrease of the electrically active *precipitate* concentration near the planar defect and dislocations.

Iron-diffused and precipitated EFG material was examined with High-Resolution TEM to detect the presence of precipitates at or near these defects. HRTEM examination shows no evidence of second phases at planar defects or dislocations. We conclude, therefore, that iron agglomeration at crystallographic defects does occur, but at low temperature does not lead to the formation of large second phases (which *will* occur with slower cooling rates).

### Discussion and Future Work

We have shown clear evidence that iron is a strong diffusion length limiter when intentionally diffused into EFG silicon. Although EBIC evidence indicates that iron diffuses to and agglomerates at twin boundaries and dislocations, it is unclear whether precipitation also occurs on a much more local scale. Figure 2 shows that the diffusion length remains low in all samples after lengthy precipitation anneals, for which there are two possible explanations.

The first is that unprecipitated iron-boron pairs are much more effective recombination centers than has been previously thought. Calculations based upon the measured electron capture coefficients for the Fe-B center<sup>3</sup> indicate, however, that only at a concentration of about  $10^{15}\text{cm}^{-3}$  (solubility limit at  $1050^{\circ}\text{C}$ ) can Fe-B pairs limit the diffusion length to  $10\mu\text{m}$ . We have observed persistent diffusion length reduction with Fe-B an order of magnitude lower (Figure 2). The second explanation is that iron forms small precipitates, invisible to EBIC, which subsequently limit both overall and local measured diffusion lengths. This explanation requires the presence of a high concentration of heterogeneous nucleation sites which have never been positively identified. An explanation for the formation of SiC microprecipitates has been proposed in EFG silicon,<sup>7</sup> but these defects have never been observed. These microdefects are important, because if they exist they may provide an explanation for not only the precipitation of iron and other transition metals but the relatively low as-grown diffusion length in EFG silicon.

We hope to resolve this question by attempting to decorate these microdefects with copper diffused into the material at an elevated temperature. Copper is known to precipitate preferentially at dislocations and other defects, but unlike iron cannot be quenched on interstitial sites because of its high diffusivity.<sup>1</sup> We hope that by diffusing copper into an EFG sample at  $600^{\circ}\text{C}$  and rapidly quenching to room temperature, the copper will have insufficient time to diffuse to dislocations or planar defects to precipitate, and will therefore decorate microdefects. Quenching may be essential, because copper atoms can easily diffuse to neighboring dislocations or planar boundaries during a cooling period of only a few seconds. During a quench, presumably, the copper atoms will only be able to diffuse a short distance to the nearest microdefect to precipitate, which may not even be the most energetically favorable precipitation site.

### Summary

We have shown that iron in its dissolved state (paired with boron) is electrically active and reduces the minority carrier diffusion length when iron is intentionally introduced into EFG silicon at high temperature. The rate of iron precipitation is related to the original diffusion length, suggesting that the intra-grain recombination centers in as-grown material act as nucleation sites for precipitation. The precipitates themselves are recombination active, because diffusion lengths remain low after precipitation has occurred. We show evidence that precipitation occurs at planar defects and dislocations, as well as at unidentified intra-grain sites. We hope to confirm or refute the presence of carbon-related microdefects with additional transition metal precipitation studies, by attempting to decorate the microdefects with copper.

### References

1. E. R. Weber, *Appl. Phys. A* **30**, 1 (1983)
2. B. R. Bathey, et al., in *Proceedings of the 4th International Photovoltaic Science and Engineering Conference* (Institution of Radio and Electronics Engineers Australia, Sydney, 1989), p. 117
3. G. Zoth and W. Bergholz, *J. Appl. Phys.* **67**, 6764 (1990)
4. A. M. Goodman, *J. Appl. Phys.* **32**, 2550 (1961)
5. C. J. Wu and D. B. Wittry, *J. Appl. Phys.* **49**, 2827 (1978)
6. D. Gilles, E. R. Weber and S. Hahn, *Phys. Rev. Lett.* **64**, 196 (1990)
7. J. P. Kalejs and B. Chalmers, *J. Crystal Growth* **79**, 487 (1986)

## Figures

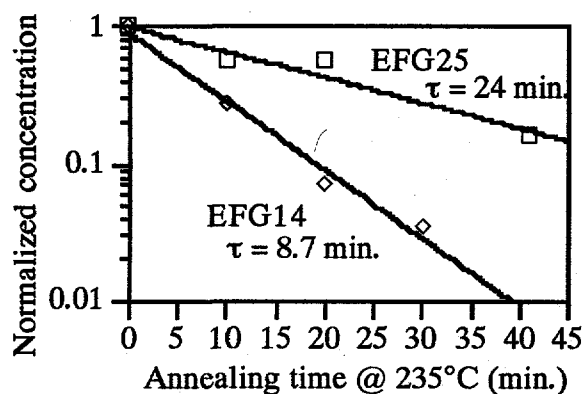


Figure 1. Unprecipitated iron concentration versus annealing time at 235°C for two EFG samples with different as-received diffusion lengths (EFG25: 45 $\mu$ m, EFG14: 10 $\mu$ m).

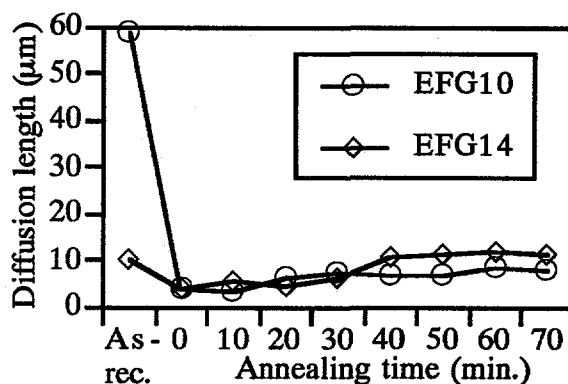


Figure 2. SPV-measured diffusion length for two EFG samples as a function of 235°C annealing time.

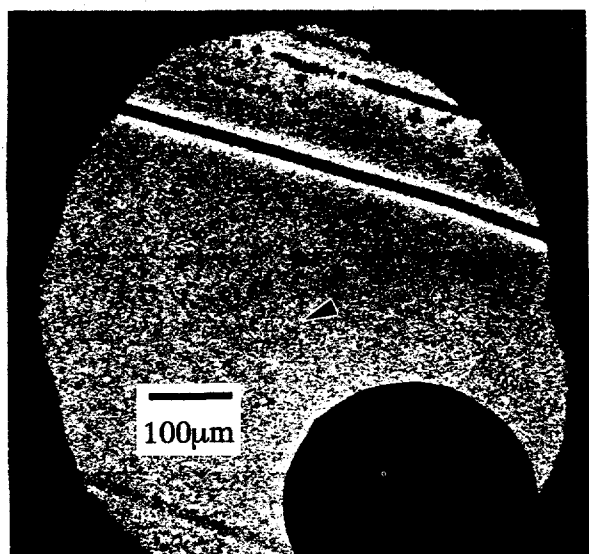


Figure 3. EBIC micrograph of EFG25 (post Fe-diffusion and anneal; starting diffusion length 45 $\mu$ m), showing bright contrast near a planar defect and dislocations, indicating iron diffusion toward the defects. The local diffusion length at the indicated mark was found to be 3.1 $\mu$ m.

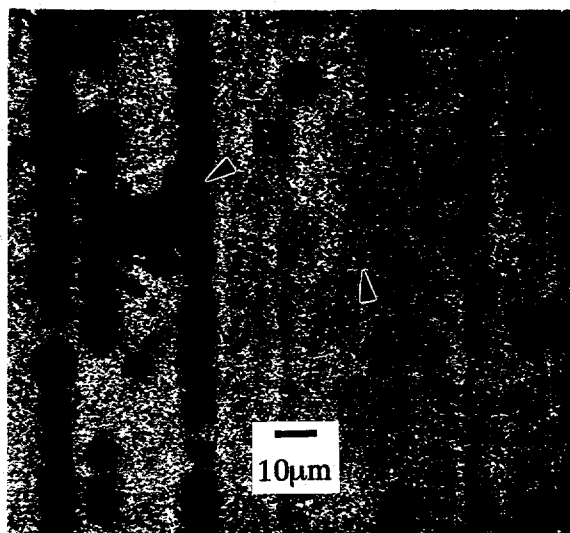


Figure 4. EBIC micrograph of EFG10 (post Fe-diffusion and anneal; starting diffusion length 59 $\mu$ m), showing no bright contrast near dislocations. The diffusion length at point A is 3.8 $\mu$ m, at point B 3.0 $\mu$ m.



**Title:** Novel Ways of Depositing ZnTe Films by a Solution Growth Technique

**Organization:** Institute of Energy Conversion  
University of Delaware  
Newark, DE 19716-3820

**Contributors:** Robert W. Birkmire, Principal Investigator;  
Anup Mondal, Brian E. McCandless and Tracey I.  
Yokimcus, Research Contributors

## Objectives

The objective of this research was to develop novel processes for the deposition of thin ( $< 500$  Å) ZnTe layers suitable as transparent ohmic contacts for CdS/CdTe solar cells. The processes developed for ZnTe deposition were also applied to deposition of other II-VI semiconductor layers for polycrystalline thin film solar cells.

## Technical Approach

In order to achieve the objectives the Institute of Energy Conversion (IEC) carried out a program of investigation and analysis to deposit ZnTe and ZnSe films according to the following research tasks.

- IEC investigated methods for depositing II-VI films using solution growth and electrochemical techniques. The processes investigated included direct ZnTe film formation on the CdTe surface and an exchange reaction with CdTe surface forming a ZnTe layer where Cd is replaced by Zn. Doping of the ZnTe film with Cu to control their resistivity was an integral part of the process.
- IEC characterized the structural, optical and electrical properties of the ZnTe films using established techniques of x-ray diffraction and total reflection and transmission measurements. Emphasis was placed on obtaining single phase films and on minimizing sub-bandgap absorption.
- IEC fabricated superstrate CdS/CdTe/ZnTe solar cells to characterize the contact properties of the ZnTe films on a working device. The properties of the devices using the ZnTe contact were compared to devices using Au or Cu/ITO as the CdTe contact. Emphasis was placed on total transmission through the device and resistivity losses due to the contact.
- IEC investigated different processes for depositing ZnSe films onto Mo/glass and CuInSe<sub>2</sub>/Mo/glass substrates. The processes investigated were solution growth, electrodeposition, and galvanic deposition. The primary difficulty encountered with the solution growth method was promoting reaction of Zn and Se on the substrate; reproducible deposits could not be achieved. Both electrochemical and galvanic

techniques met with limited success owing to the wide difference in deposition potentials of Zn and Se.

IEC deposited CdS and CdTe films by the galvanic technique to investigate the application of the deposition technology to other II-VI compounds and to demonstrate the feasibility of an all-galvanically deposited device.

## Significant Results

The Institute of Energy Conversion (IEC) investigated three processes for the deposition of ZnTe - surface exchange with CdTe where Cd is replaced by Zn from an aqueous bath to form a ZnTe layer, solution growth, and galvanic deposition from an aqueous bath. The galvanic deposition technique proved to be the only method in which ZnTe films were successfully and reproducibly formed.

Galvanic cells were constructed in solution with Zn foil used as an anode and a glass/ITO/CdS/CdTe substrate acting as a cathode. These electrodes were externally short-circuited, and their potential difference was the driving force for the electrochemical reaction. The optimal solution in which ZnTe was formed consisted of 0.1 M Cd salt and  $10^{-4}$  M  $\text{TeO}_2$ ; a Cu salt in the range of  $10^{-4}$  to  $10^{-5}$  M and triethanolamine were added for the formation of Cu-doped ZnTe films. Both temperature and pH were controlled, and deposition times of 10 to 30 minutes resulted in film thicknesses of 30 to 150 nm. The effects of agitation, temperature, and Cu doping on the ZnTe films were determined. Structural, optical and electrical film properties were characterized and CdS/CdTe/ZnTe devices were fabricated and evaluated.

The formation of ZnSe and CdS films using this galvanic deposition method was attempted, and encouraging results were achieved for the formation of CdS films on  $\text{SnO}_2$ /glass substrates. Electrochemical deposition processes for ZnSe film formation on  $\text{CuInSe}_2$ /Mo/glass substrates proved to be problematic in terms of film uniformity.

## Conclusion

An electrochemical process has been successfully developed for the reproducible deposition of ZnTe and copper-doped ZnTe films suitable as transparent ohmic contacts for CdS/CdTe solar cells. The development of this method and optimization of key processing steps in the fabrication of CdS/CdTe/ZnTe:Cu devices has allowed IEC to achieve cell performance results of  $\text{FF} > 70\%$  and  $\eta$  approximately 10%. Preliminary efforts have indicated that the deposition methods investigated are potentially feasible for the formation of other II-VI compounds for use in polycrystalline thin film solar devices and should be the focus of future work.

## References

1. R.W. Birkmire, B.E. McCandless, T.A. Yokimcus, A. Mondal, "Novel Ways of Depositing ZnTe Films by a Solution Growth" NREL Final Subcontract Report, October 1992, [NREL/TP-410-4959](#) or NTIS No. [DE92010591](#).
2. Anup Mondal, Brian E. McCandless, Robert W. Birkmire, "Electrochemical Deposition

- of Thin ZnTe Films as a Contact for CdTe Solar Cells", Solar Cells, August, 1991.
3. Anup Mondal, Robert W. Birkmire, Brian E. McCandless, "A New Method for Forming ZnTe Contacts for CdTe Cells", presented at 22nd IEEE PVSC, Las Vegas, Nevada, October 7-11, 1991.
  4. P.V. Meyers, C.H. Liu, L. Russell, V. Ramanathan, R.W. Birkmire, B.E. McCandless and J.E. Phillips, Proc. 20th IEEE PVSC, 1448 (1988).

Title: **Atomic Layer Epitaxy for High Efficiency Solar Cells**

Organization: Departments of Electrical Engineering  
and Materials Science  
University of Southern California  
Los Angeles, CA

Contributors: P. D. Dapkus, principal investigator,  
B. Y. Maa, and M. Jow

### **Introduction**

The objective of this program is to explore and develop a low temperature, large scale epitaxial process for high efficiency solar cells based upon atomic layer epitaxy (ALE). ALE has the potential for high throughput, layer thickness control and uniformity based upon the inherent saturated surface reactions involved in the process. We have previously shown that the growth rate in atmospheric pressure, thermally driven ALE is limited by the maximum temperature attainable before homogeneous gas phase reactions dominate the process and preclude the achievement of saturated monolayer growth. In this program we are exploring the use of photoassisted ALE and vacuum ALE as alternative approaches for achieving usable growth rates and high throughput. The program is structured in two phases. In the first phase, we measured the fundamental thermal and photoassisted surface reaction rates involved in the growth of GaAs using TMGa and a variety of As sources. Based upon these results a decision was made that the vacuum ALE approach was a viable approach to use for the growth of GaAs and related compounds. The second phase will concentrate upon developing VALE for the growth of high efficiency solar cells. Issues such as materials quality, reactant utilization, and throughput will be examined.

### **Progress**

During the second year of the program efforts continued on three fronts: studies of basic surface reaction rates and processes, development of a vacuum ALE system for the growth of solar cells, and the assessment of materials quality grown by ALE and photoassisted ALE. The key accomplishment of the year was the completion of the VALE reactor. This was done late in the second year and experiments were performed to verify that the approach was suitable for the growth of materials by ALE. Of significant importance was the further verification of our model of ALE surface reactions and the demonstration that ALE could be performed at higher than expected temperatures.

Finally we also demonstrated that triethylgallium could be incorporated into a photoassisted ALE process to produce very high quality GaAs materials.

#### VALE Reactor Design and Verification

The basic design of our VALE reactor is a synthesis of our work on surface reactions and Fraas' earlier work on vacuum chemical epitaxy. The basic concept is shown in Fig. 1. Growth takes place in a vacuum of approximately  $10^{-3}$  Torr. At this pressure, the molecular reactant beams have a mean free path longer than the distance in which they must travel in the vacuum - minimizing any gas phase reactions that may limit the upper temperature that can be used in ALE. The wafers are held in a small chamber that temporarily traps reactants that are not reacted in the first pass onto the substrate. These molecules then have several encounters with the surface before exiting the chamber and entering a region of high vacuum where they are pumped away. The Ga and As reactants are alternately aimed at the surface from a beam source formed by a valved inlet into the small chamber. There are no carrier gases used and the process results in all reactant molecules having several passes at the substrate. This should optimize reactant usage.

The reactants are injected into the chamber by a novel injection manifold that does not rely on continuous reactant flow to achieve uniform pulse content as is usually the case in near atmospheric pressure systems. Instead the system employs a large ballast of reactants that can be opened to the vacuum through a restricting orifice on a pulse basis. The volume of the ballast is chosen so that an exposure pulse depletes the reactant by no more than 5% during an exposure pulse. The pulsed extraction of reactants is balanced by a steady input flow whose flow rate is controlled to keep the average pressure in the vessel constant. In this way the reactants are being extracted under near constant pressure only when the exposure occurs. This design is economical in the use of reactants and precise in their delivery.

The VALE concept is unique among ALE reactor designs in that it can be extended to a multiple wafer design with little variation of the reactor design. Because the reactants can make several passes at a surface before exiting the growth region and because the surface reaction saturates, little variation on the original design is necessary to substantially increase the wafer throughput. We believe this will be required to overcome the slower growth rate inherent to ALE to make it a high throughput technique.

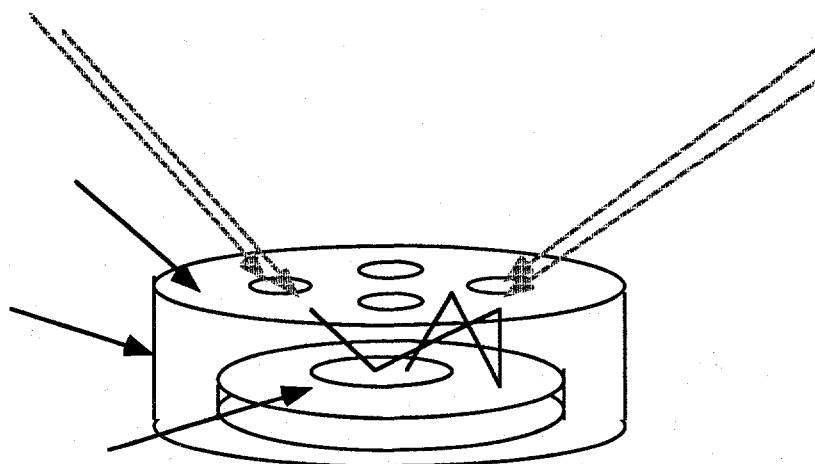


Figure 1 - Concept of Vacuum Atomic Layer Epitaxy Reactor

This reactor concept has been realized in a system that is constructed of stainless steel and equipped with a load lock entry system. In our initial experiments the system is equipped with only a Ga and an As source. Preliminary experiments have been carried out to determine the window of temperature and reactant exposures that will result in ALE growth. Figures 2 and 3 show preliminary data at one temperature (500°C) for the growth rate as a function of TBAs and TMGa exposure time. The data show clear saturation of the growth rate at one monolayer/cycle of exposure. We are now extending the range of exposures, substrate temperatures, and fluxes to determine the interplay of growth rate saturation and materials quality.

#### Surface Reaction Rates and Mechanisms

During this year we have modified our surface analytical system to include mass spectroscopy, RHEED, and a fast reactant switching manifold. This has allowed us to investigate for the first time the evolution of reaction products from surface to better understand the kinetics of the growth and the saturation mechanisms. We have performed a study of the evolution of  $\text{CH}_3$ , TMGa, and  $\text{GaCH}_3$  from the surface after exposure of an As rich surface to TMGa. The studies clearly show a strong correlation of the desorbing byproducts with the observed details of the RDS transients. In particular, we observe that during the initial exposure when the surface is largely As rich, the primary desorbing species is  $\text{CH}_3$ . As the surface approaches the Ga saturated condition, the  $\text{CH}_3$  desorption decreases and the  $\text{GaCH}_3$  increases. In figs. 4 and 5 we show the simultaneous MS and RDS transients resulting from the exposure of an As

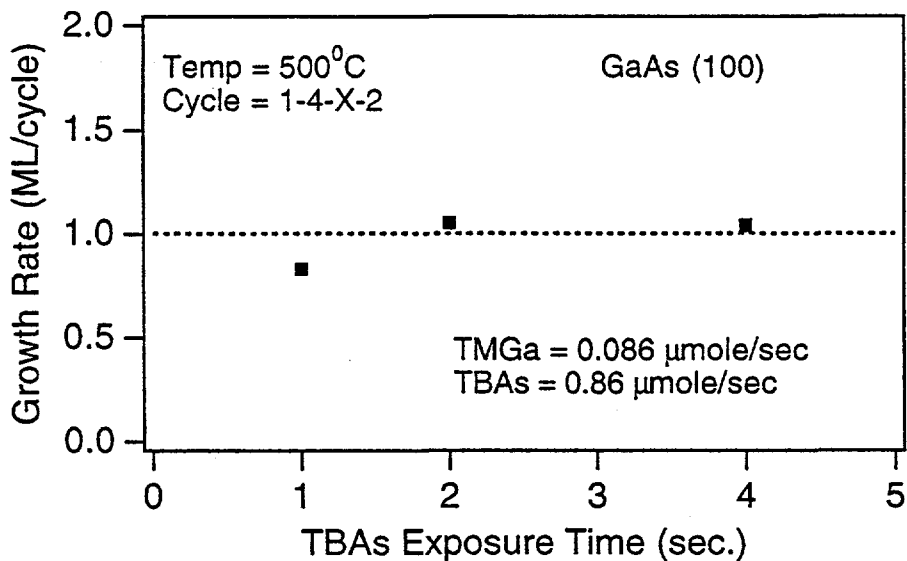


Fig. 2 Growth rate as a function of TBAs exposure.

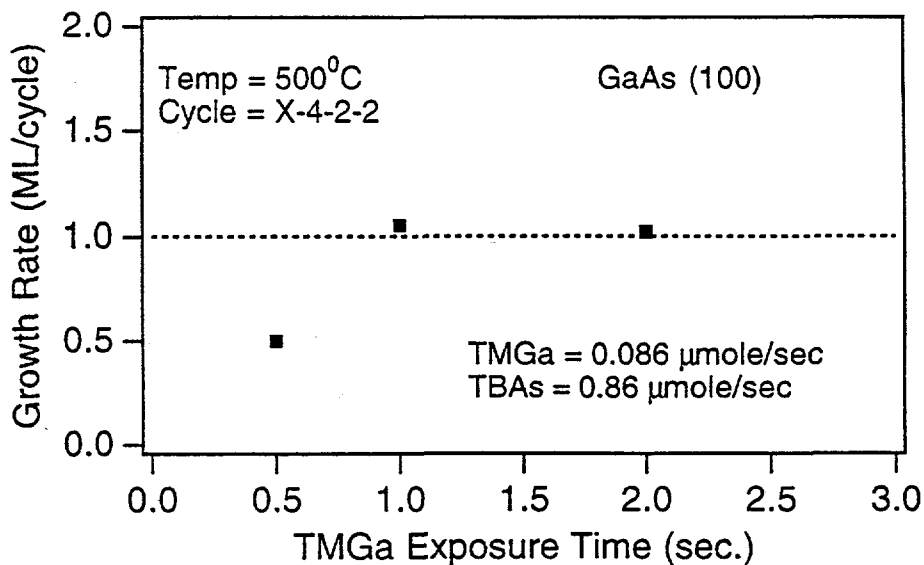


Fig. 3 Growth rate as a function of TMGa exposure.

rich surface to TMGa. In Fig. 4, we show that the  $\text{CH}_3$  transient decreases with time while the  $\text{GaCH}_3$  transient increases with time as the surface approaches saturation as indicated by the RDS signal. Similarly, we show in Fig. 5 that with repeated TMGa short nonstaurating pulses, the surface approaches saturation only after several pulses as indicated by the RDS signal. as the surface approaches saturation, the amplitude of the the  $\text{GaCH}_3$  desorption increases. These observations are consistent with our saturation model that says that the surface reaction saturates when all As sites are covered with Ga or  $\text{GaCH}_3$ . The TMGa only reacts with exposed As sites. As the surface saturates with Ga, the surface relaxes to the 4X surface by the desorption of the  $\text{GaCH}_3$  adsorbed on sites that will be empty in the final surface structure. The correlation of the  $\text{GaCH}_3$  desorption with the RDS signature of over saturation of the surface adds further credence to our model. We are now pursuing the independent verification of the process by RHEED. If this approach also confirms our model, we will have achieved a significant unification of the understanding of this process and will be in a position to further model the growth kinetics.

In the meantime, we have continued our empirical study of the kinetics by studying the dependence of the ALE reaction saturation on the controlling TMGa exposure. In particular, we are interested to know the shortest exposure time that will result in monolayer reaction saturation. In Fig 6 we show the effects of TMGa exposure time on the RDS transient. The exposure time ranges from one second exposure, as indicated by the TMGa mass spectrometer signal, at which time we know that a sufficient exposure is provided to complete a monolayer is delivered to the surface. Note that the RDS signal saturates at an amplitude that we take as indicating that the surface is saturated with Ga. The subsequent data are shown for progressively shorter exposure times. Note that the Ga surface concentration saturates at the same level for each of the exposures indicating that exposures as short as 0.2 sec are sufficient to provide enough Ga to saturate all surface sites. Note also that the reaction completion time is almost independent of the exposure time since it is governed by the desorption of reaction byproducts. In fact overexposure seems to increase the reaction completion time as indicated by the slightly slower rise time of the RDS signal for longer exposure times. These data suggest that at temperatures of  $530^\circ\text{C}$  it should be possible to considerably shorten the TMGa reaction time over that shown in the data of Fig. 5.

In addition to these studies of VALE, we have continued our studies of photoassisted ALE to determine if this was a suitable way to accelerate the growth rate of materials by ALE. The key result that we have achieved in this year is to demonstrate that low carbon content ( $<10^{15} \text{ cm}^{-3}$ ) GaAs with PL efficiency comparable to materials



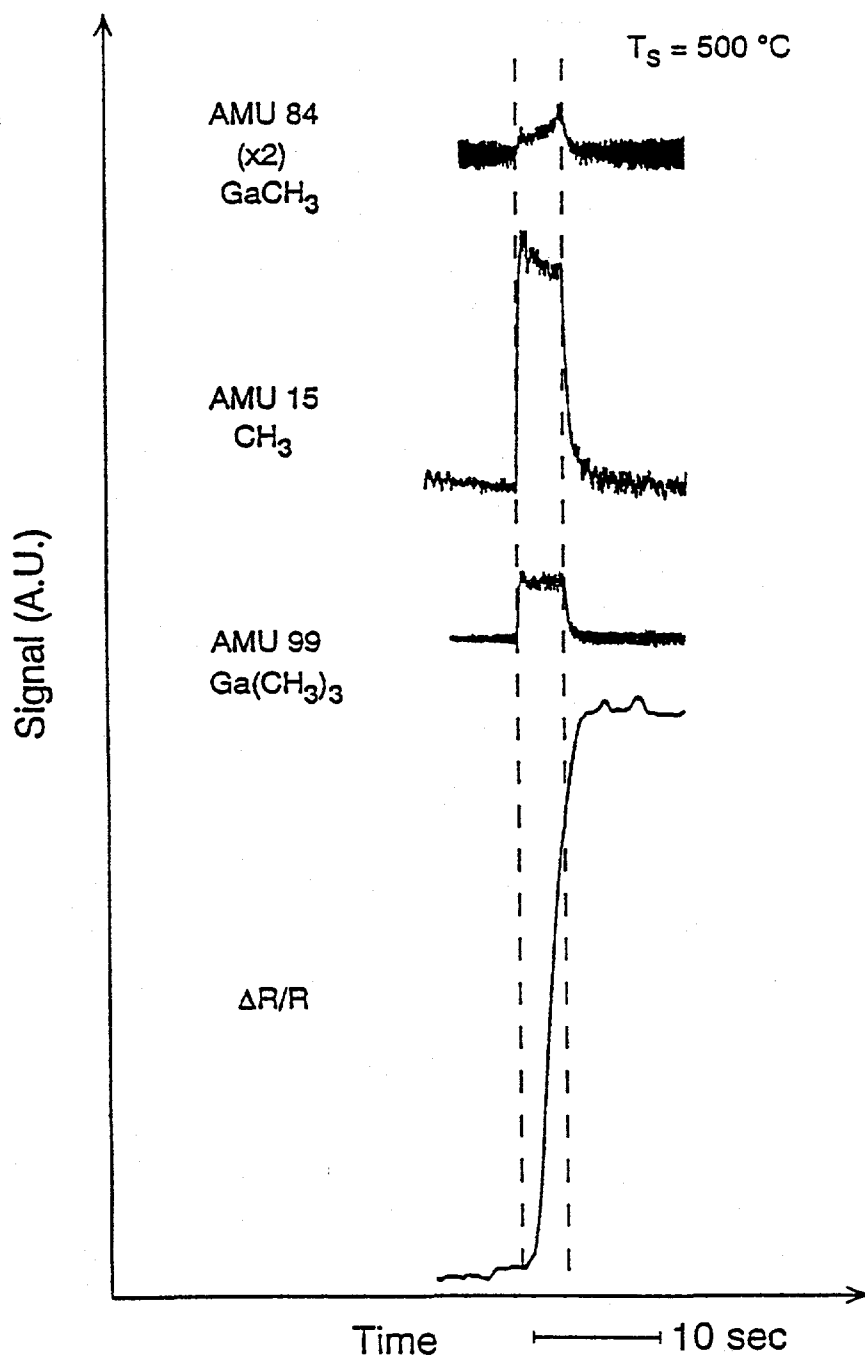


Fig. 4 - MS and RDS response of As-stabilized GaAs (001) surface to a saturating TMGa pulse showing the time dependence of the CH<sub>3</sub> and GaCH<sub>3</sub> desorbing species and the Ga dimer concentration as indicated by the RDS response.

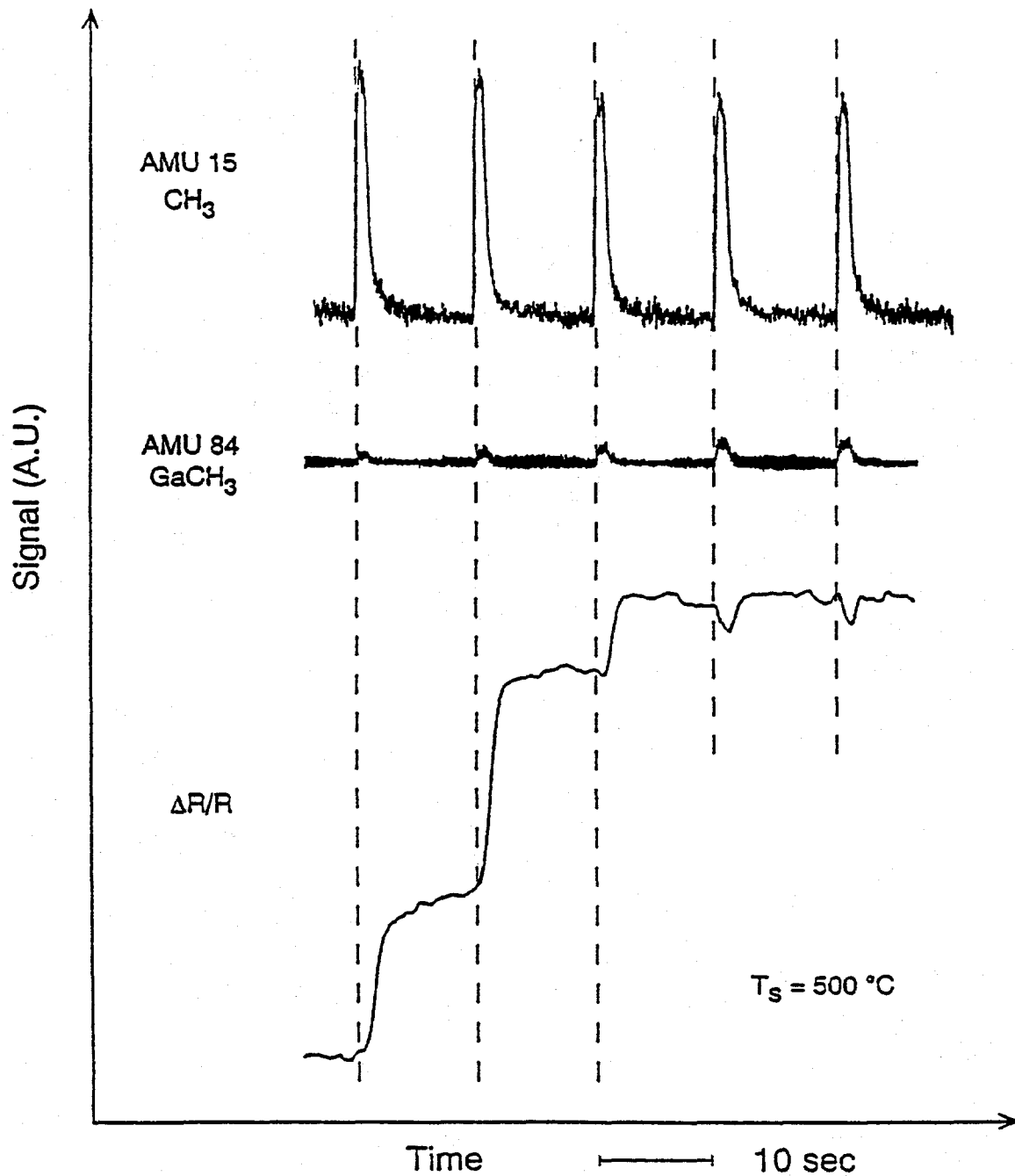


Fig. 5 - MS and RDS response of As-stabilized GaAs (001) surface to nonsaturating TMGa pulses showing the time dependence of the CH<sub>3</sub> and GaCH<sub>3</sub> desorbing species and the Ga dimer concentration as indicated by the RDS response.

530 °C, TMGa  $8 \times 10^{-5}$  Torr

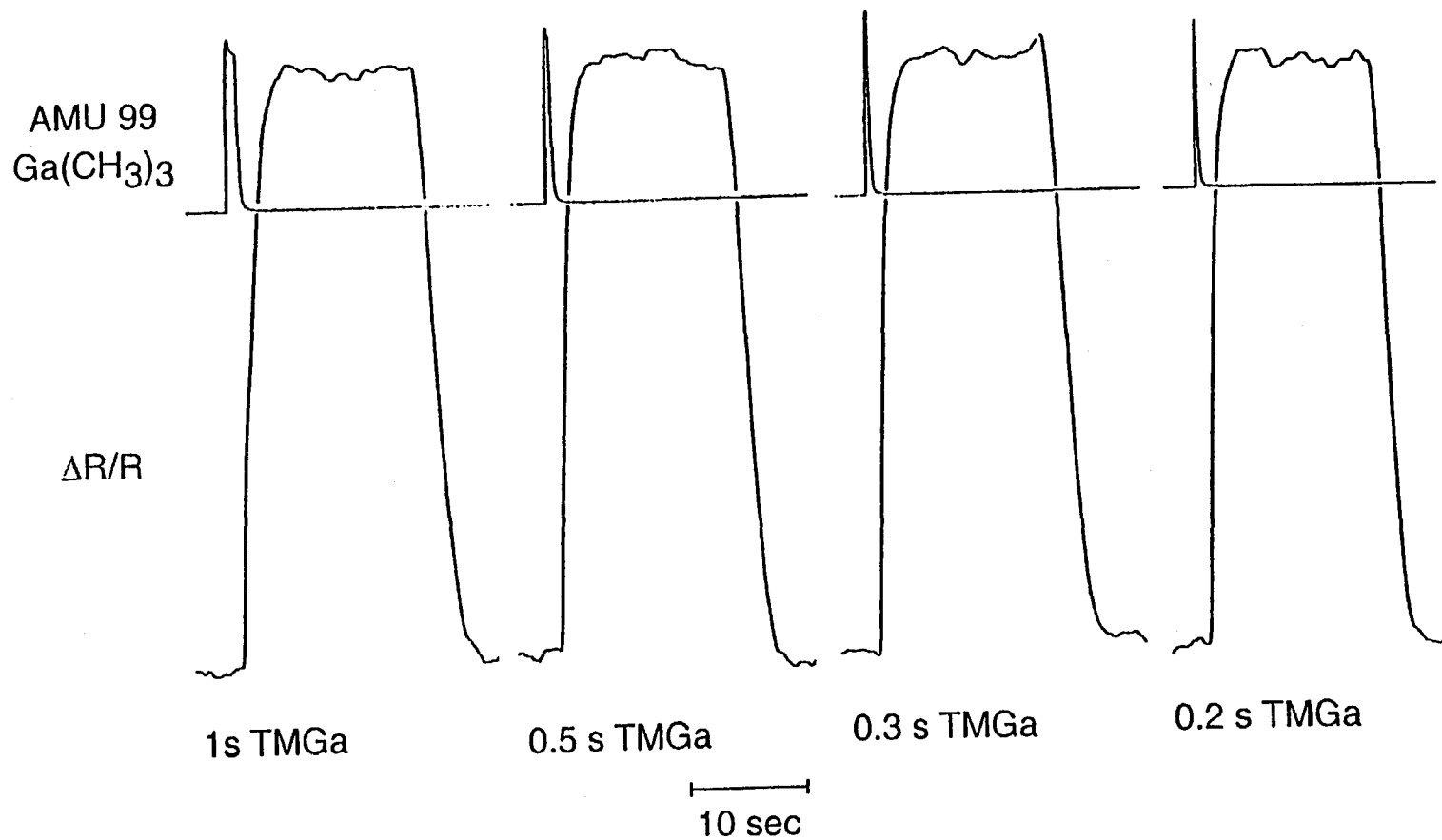


Fig. 6 - RDS response of As-stabilized GaAs (001) surface to TMGa pulse of decreasing width. Note that the RDS saturation level is independent of pulse width down to 0.2 seconds.

grown by MOCVD can be grown at temperatures as low as 350°C by using photoassisted ALE with triethylgallium. These results are the most promising achieved to date and indicate that ALE is a process in which high quality materials can be made.

### **Conclusions**

The results we have achieved this year clearly indicate that ALE is capable of producing high quality materials in volumes compatible with solar cell production. The program now turns to demonstration of high quality materials by VALE and the demonstration of ALE -grown solar cells.

**Title:** Optimization of Gettering Processes for Photovoltaic Silicon

**Organization:** University of South Florida, Tampa, Florida

**Contributors:** L. Jastrzebski, principal investigator and W. Henley

### Objective

This effort is focused on the development and optimization of gettering procedures whose application prior to and during solar cell fabrication will enhance the quality of low-cost photovoltaic poly-silicon, improve the reproducibility and homogeneity of the material, and reduce costs by allowing the use of lower quality feed material. The objective of this contract is to develop an experimental base for optimization of various gettering techniques for polycrystalline silicon and provide a foundation for the development of a comprehensive gettering model which will take into account the impurity/defect interaction and the role of temperature and atmosphere during heat treatments.

### Technical Approach

During the first five months of this contract our effort was focused on two areas:

1) Establishing a knowledge base regarding properties of available poly-silicon. This effort was initiated due to the lack of a proper data base required to judge the benefits of gettering. The majority of published values of diffusion length/lifetime are the best achieved by a given process. A proper evaluation of gettering efficiency can only take place if its effects are evaluated for the full range of available poly-silicon material quality.

2) Initiation of chlorine gettering work in association with studies of the effects of heat treatments on defect annealing and re-dissolution of heavy metal precipitates.

The surface photovoltage (SPV) technique was chosen for measurement of diffusion length/lifetime in poly-silicon.[1] The procedure used for Fe and Cr concentration determination, from SPV measurements, is based on the unique properties of Cr and Fe in p-type silicon.[2,3] In the presence of B at room temperature, Fe forms Fe-B and Cr forms Cr-B pairs. If these pairs are decomposed, then Fe and Cr become interstitial and concentrations are determined from the equations:

$$N_{\text{Fe}} = 1.05 \times 10^{16} (1/L_{\text{after}}^2 - 1/L_{\text{before}}^2) \quad (1)$$

$$N_{\text{Cr}} = 1.2 \times 10^{16} (1/L_{\text{before}}^2 - 1/L_{\text{after}}^2) \quad (2)$$

where N is in  $\text{cm}^{-3}$  and L is in  $\mu\text{m}$  ( $L_{\text{before}}$  and  $L_{\text{after}}$  are diffusion lengths prior to and after the decomposition of pairs).

Decomposition of Fe-B pairs is achieved by illumination and the decomposition of Cr-B pairs is achieved by thermal activation (200°C for 2 minutes followed by quenching to room temperature), but not by light activation. In order to determine the concentration of Fe and Cr when both are present in silicon at the same time, the light activation should be done prior to the thermal activation.

In mono-crystalline silicon with diffusion lengths around 300  $\mu\text{m}$ , the Fe and Cr detection limits are of the order of a few times  $10^9 \text{ cm}^{-3}$  (for commercial equipment, Model CMS III-A, manufactured by Semiconductor Diagnostics, Inc. of Tampa, Florida).

### Chlorine Gettering and Annealing

A new tube quartz tube, with TCA as the source of chlorine, was installed for evaluation of Cl gettering effects and annealing conditions on the diffusion length in poly-silicon. A quartz tube was chosen because of the low background heavy metal contamination levels in quartz tubes.

The tube was first cleaned by running TCA and dry oxygen at 1100°C for 4 hours, then it was conditioned by an extended dry oxidation over a few weeks. Heavy metal contamination levels in the furnace ambient were evaluated from diffusion length measurements done on IC-quality, mono-crystalline silicon wafers (10  $\Omega\text{cm}$ , p-type). For oxidation in the presence of chlorine, the diffusion lengths were around 310  $\mu\text{m}$  and Fe concentration levels were less than  $2 \times 10^{11} \text{ cm}^{-3}$ , for dry oxygen without Cl, the diffusion length was 175  $\mu\text{m}$  and the Fe level increased to  $8 \times 10^{11} \text{ cm}^{-3}$ , and for annealing done in nitrogen the diffusion length was 50  $\mu\text{m}$  and Fe was around  $8 \times 10^{12} \text{ cm}^{-3}$ . It has to be emphasized that the reduction of diffusion length is not related to the change of self-interstitial/vacancy type defects structure when material is annealed in  $\text{N}_2$ , but rather to contamination introduced from the furnace environment. Silicon wafers processed at 1200°C in nitrogen ambient in the best furnaces used by the IC industry have diffusion lengths of the order of 250  $\mu\text{m}$ .

Only dissolved heavy metals, which can diffuse to gettering sink (chlorinated surface), can be gettered from silicon matrix. To remove heavy metals which have already formed precipitates, one has to first re-dissolve the precipitates. One can expect that dissolution of the precipitates will take place when the eutectic temperature for a given heavy metal/silicon system is reached and when the concentration of heavy metals which are dissolved in the silicon is below the solubility limit at a given temperature. These temperatures are summarized in the Table 1. We believe that our temperature cycle is adequate for the dissolution of precipitates of heavy metals which are fast diffusers such as Ni, Cu, Fe, Co and Cr. Therefore, one can expect these fast diffusers to be gettered by chlorine during the oxidation.

## Results

### Diffusion Length and Fe and Cr Measurements

Poly-silicon from three suppliers was obtained for this study. The wafers were grown by three different methods: heat exchange method (HEM), casting, and EFG. Since the wafers were complementary, and this study is not designed to establish the advantage of one growth method over another, but rather ranges of variability in material properties which are encountered by various growth methods, we will refer to the growth methods as (A), (B) and (C). The measurement of diffusion lengths and Fe and Cr concentrations were done with a commercial SPV system manufactured by Semiconductor Diagnostics, Inc. (the Model CMS III-A).

High density (1200-point) maps of diffusion length were measured on the wafer grown by each method. The measured area is 12 cm by 12 cm, the measurement area for each point is 3 mm in diameter, and the distance between points is 3 mm. In all samples, the measured diffusion length was found to be independent of the background illumination (the difference in L values measured with background illumination on and off showed less than a 15% difference). This indicates that there is no significant trapping of minority carriers in this material.

For samples grown by methods (A) and (B), there is no correlation between the diffusion length values and the grain size or location. There are small grains with very good and very poor diffusion length values as well as large grains with poor and good diffusion lengths. In some cases of large grains, there are large variations of diffusion length values inside a grain. These results indicate that the material properties inside the grain control the diffusion length. This is not surprising since recombination at the grain boundaries can only reduce diffusion length inside the grains when diffusion lengths became larger than about half of the grain size.[4] The size of the majority of the grains exceeds  $280 \mu\text{m}$  ( $2L_{\text{max}} = 140 \mu\text{m}$ ).

The Fe and Cr concentrations were measured for 9 points on all wafers and the data is presented in Table 2. Other wafers, cut from the same part of the crystal, showed identical characteristics. Wafers from a different crystal showed similar characteristics in the distribution of diffusion length, but quantitative variations of diffusion length, Fe, and Cr concentrations as shown in Table 2.

For method (B), the wafers from the middle and top part of the crystal were similar and significantly better than wafers from the bottom part. The wafers obtained from a different ingot, showed significantly different values of diffusion length, Fe and Cr concentration (see Table 2).

We only had two "as-grown" samples grown by method (C). For these samples, there is a well-defined characteristic stripe pattern in the diffusion length distribution which corresponds to the grain distribution. Some grains have much higher diffusion lengths, although there is no relationship to the grain size.

The results for all three growth methods are summarized in Figures 1 and 2. The diffusion lengths for these methods cover the range from 15  $\mu\text{m}$  to 200  $\mu\text{m}$ . The best diffusion length values, around 150 to 200  $\mu\text{m}$ , were obtained for methods (B) and (C) and they are somewhat higher than those obtained for method (A) where the best value was 80  $\mu\text{m}$ . The lowest diffusion lengths are around 15  $\mu\text{m}$  and are similar for methods (A) and (C). However, method (B) gives higher minimum values (45  $\mu\text{m}$ ). The average diffusion length for all three techniques are similar. The Fe and Cr concentrations seems to follow similar trends as that of the diffusion lengths. The highest contamination level,  $3 \times 10^{14} \text{ cm}^{-3}$  was observed for method (A). The largest variations in heavy metal concentrations were observed in this material. Method (C) had areas in the samples with very high Fe concentration ( $1.4 \times 10^{14} \text{ cm}^{-3}$ ). The lowest concentrations were measured in the samples grown by method (B) where Fe and Cr concentration did not exceed  $4 \times 10^{12} \text{ cm}^{-3}$ . These results clearly indicate that reproducibility and uniformity of polycrystalline silicon properties are a serious problem for all investigated growth methods.

### **Chlorine Gettering and Annealing**

Initial experiments were focused on the effects of chlorine gettering and annealing on material from supplier (A). The results are summarized in Table 2. The measurements clearly show that TCA gettering improves the diffusion length by about 50% which corresponds to a reduction by a factor of two amount of recombination centers (assumes only one type of recombination centers). In order to quantitatively evaluate relative changes induced by processing, we will assume that the capture cross-section of the recombination center is similar to that for a Fe-B pair.[2] This analysis is not designed to determine the absolute amount of recombination centers in the samples, but rather to monitor changes caused by processing. The results are summarized in Table 3. There is significant improvement due to chlorine gettering. In the case of annealing in nitrogen and dry oxidation, the observed decrease of diffusion length, and the increase of recombination centers, is probably related to contamination introduced from the furnace ambient. The calculated increase in the average number of recombination centers for the poly-silicon wafers, and the mono-crystalline control wafers annealed in  $\text{O}_2$  and  $\text{N}_2$ , is similar.

### **Summary**

The results obtained during the first five months of this contract clearly demonstrate that meaningful evaluation of gettering in photovoltaic silicon can be done only if a solid experimental database concerning the properties of the material is established. Our



measurements showed that diffusion length in commercially available photovoltaic poly-silicon material covers a range from of 10  $\mu\text{m}$  to 200  $\mu\text{m}$ . Both Fe and Cr concentrations (in the dissolved state) can be as high as  $10^{14} \text{ cm}^{-3}$ . A proper evaluation of gettering efficiency can only take place if its effects are evaluated for the full range of available poly-silicon material properties. The first results of chlorine gettering are very encouraging since they showed a substantial improvement of diffusion length in photovoltaic silicon.

## References

1. D. Huber, A. Bachmeier, R. Wahlich and H. Herzer, *Semiconductor Silicon 1986*, Proceed. 5th Int. Symp. on Silicon Mat. Science and Technology, Proceed. Vol 86-4, Electrochem. Soc., edited by H. Huff, T. Abe and B. Kolbeseu, p. 1022.
2. L. Jastrzebski, O. Milic, M. Dexter, J. Lagowski, D. DeBusk, K. Nauka, R. Witowski, M. Gordon and E. Persson, *Cleaning Technology in Semiconductor Device Manufacturing*, Proceed. of 2nd Int. Symp., Proceed. Vol 92-12, Electrochem. Soc., edited by J. Ruzyllo and R. Novak, p. 294.
3. K. Mishra, presented during 2nd NREL Workshop, August 1992, Breckenridge, Colorado and to be published in Conf. Proceedings.
4. Recombination on the grain boundaries is analogous to recombination on the surface of silicon wafer. This effect was discussed by J. Lagowski during 2nd NREL Workshop, August 1992, Breckenridge, Colorado (see proceedings).
5. L. Jastrzebski, 2nd NREL Workshop, August 1992, Breckenridge, Colorado, Conf. Proceed. in press.

**Table 1.**  
Eutectic Temperatures for Various Heavy Metals[5]

	<u>Cu</u>	<u>Ni</u>	<u>Fe</u>	<u>Mu</u>	<u>Cr</u>	<u>Ti</u>
Temperature ( $^{\circ}\text{C}$ )	700	990	1210	1145	1340	1340

**Table 2.**  
Values of Diffusion Length, Fe Contamination, and Cr Contamination  
for Poly-Crystalline Samples Grown by Various Methods

Wafer	Method	$L_{max}$ ( $\mu\text{m}$ )	$L_{min}$ ( $\mu\text{m}$ )	$L_{avg}$ ( $\mu\text{m}$ )	$Fe_{max}$ ( $\text{cm}^{-3}$ )	$Fe_{avg}$ ( $\text{cm}^{-3}$ )	$Cr_{max}$ ( $\text{cm}^{-3}$ )	$Cr_{avg}$ ( $\text{cm}^{-3}$ )
1	(A)-1	78	41	60	$3 \times 10^{14}$	$1.4 \times 10^{14}$	$7 \times 10^{13}$	$5 \times 10^{13}$
2	(A)-1	56	30	42	$1.1 \times 10^{13}$	$5 \times 10^{11}$	$6 \times 10^{12}$	$1 \times 10^{11}$
3	(C)	77	12	47	$1.4 \times 10^{14}$	$1.6 \times 10^{13}$	$1.3 \times 10^{14}$	$1.6 \times 10^{13}$
4	(C)	150	12	46	$2 \times 10^{12}$	$7 \times 10^{11}$	$1.1 \times 10^{13}$	$2.5 \times 10^{12}$
5	(B)-1	100	50	65	$2 \times 10^{12}$	$4 \times 10^{11}$	$1 \times 10^{12}$	$8 \times 10^{11}$
6	(B)-1	155	75	100	$4 \times 10^{11}$	$> 2 \times 10^{11}$	$2 \times 10^{11}$	$2 \times 10^{11}$
7	(B)-1	49	26	35	$5 \times 10^{11}$	$4 \times 10^{11}$	$2 \times 10^{11}$	$2 \times 10^{11}$
8	(A)-2	50	40	45	$2 \times 10^{12}$	$5 \times 10^{11}$	$5 \times 10^{11}$	$4 \times 10^{11}$
9	(B)-2	200	95	145	$5 \times 10^{11}$	$4 \times 10^{11}$	$3 \times 10^{11}$	$2 \times 10^{11}$
10	(B)-2	150	110	120	$4 \times 10^{11}$	$3 \times 10^{11}$	$2 \times 10^{11}$	$1.5 \times 10^{11}$
11	(B)-2	200	70	95	$3 \times 10^{11}$	$2 \times 10^{11}$	$2 \times 10^{11}$	$1.5 \times 10^{11}$
12	(B)-3	70	45	48	$4 \times 10^{12}$	$2 \times 10^{12}$	$2 \times 10^{12}$	$2 \times 10^{12}$
13	(A)-2	142	12	42	$2 \times 10^{11}$	$> 3 \times 10^{10}$	$1.6 \times 10^{12}$	$1.4 \times 10^{12}$

**Table 3.**  
Change in the Amount of Recombination Centers in  
Mono-Crystalline Silicon and Poly-Silicon Samples (method (A)) for  
Various Processes: TCA Gettering, O<sub>2</sub> and N<sub>2</sub> Annealing

	<u>Diffusion Length (<math>\mu\text{m}</math>)</u>		<u>Concentration of Recombination Centers (a.u.)<sup>(*)</sup></u>		<u>Change in Recombination Center Concentration<sup>(**)</sup></u>
	(Before Process)	(After Process)	Before Process)	After Process)	
Poly TCA	45	65	$5 \times 10^{13}$	$2.4 \times 10^{13}$	(-) $2.6 \times 10^{13}$
Control TCA	270	310	$1.4 \times 10^{12}$	$1.1 \times 10^{12}$	(-) $0.3 \times 10^{13}$
Poly O <sub>2</sub>	72	55	$2 \times 10^{13}$	$3.3 \times 10^{13}$	(+) $1.3 \times 10^{13}$
Control O <sub>2</sub>	260	175	$1.3 \times 10^{12}$	$3.2 \times 10^{12}$	(+) $1.9 \times 10^{12}$
Poly N <sub>2</sub>	42	32	$5.5 \times 10^{13}$	$1 \times 10^{14}$	(+) $4.5 \times 10^{13}$
Control N <sub>2</sub>	265	49	$1.3 \times 10^{12}$	$4.2 \times 10^{13}$	(+) $4.1 \times 10^{13}$

(\*) Estimated assuming capture cross-section similar to that for Fe-B pairs. These figures are in arbitrary units (a.u.).

(\*\*) The minus sign (-) corresponds to a reduction and the plus sign (+) to an increase in the amount of recombination centers during processing.

Comparison of Diffusion Length for Various Processes

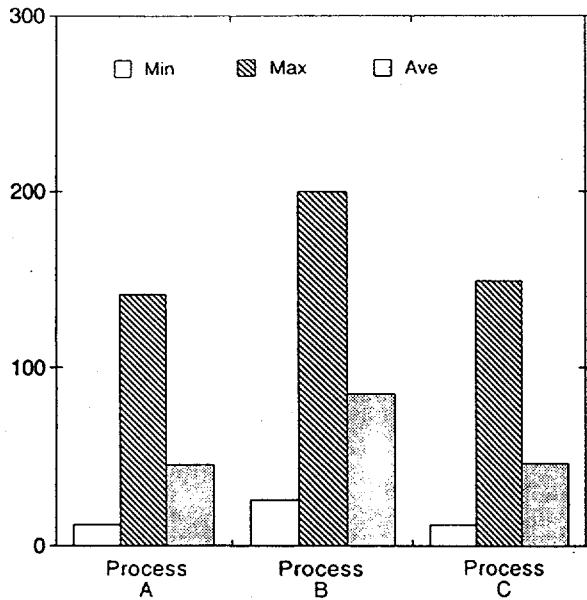


Figure 1. Maximum, minimum and average values of diffusion length for samples grown by various methods.

Comparison of Fe/Cr Contamination for Various Poly Growth Processes

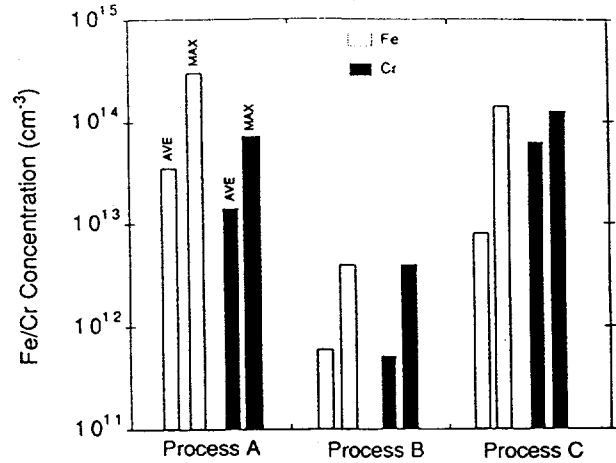


Figure 2. Maximum and average values Cr and Fe concentration observed in poly-silicon samples grown by various methods.

Title: Electronic Processes in Thin Film PV Materials

Organization: Department of Physics, University of Utah, Salt Lake City, Utah

Contributors: P.C. Taylor, principal investigator; G.A. Williams, W.D. Ohlsen, S.Q. Gu, J.M. Viner, K. Gaughan, S. Hershgold, D. Chen, P. Hari

The major objectives of this subcontract are (1) to grow and characterize high quality a-Si:H and related alloys and multilayers using the glow discharge technique, (2) to characterize by optical and magnetic resonance techniques the roles of defects and impurities in amorphous tetrahedrally-coordinated thin films, (3) to determine the quality of the interfaces and junctions which occur in PV devices by employing surface-sensitive optical and magnetic resonance techniques, and (4) to understand the recombination-induced metastabilities (Staebler-Wronski effect) and the frozen-in departures from equilibrium (as mediated by hydrogen diffusion or defect motion) in amorphous tetrahedrally-coordinated thin films. A recent review is available elsewhere.<sup>1</sup>

### Approaches

Several techniques have been employed to accomplish these objectives. Samples are grown in a state-of-the-art glow discharge deposition system and characterized using infrared and Raman spectroscopy, electrical conductivity, electron microprobe, and photothermal deflection spectroscopy (PDS). Other important experimental techniques include nuclear magnetic resonance (NMR), electron spin resonance (ESR), various optical spectroscopies, and double spectroscopies such as optically detected magnetic resonance (ODMR).

### Research Results

The subcontract is divided into several tasks. One task is the growth and characterization of doped and undoped a-Si:H and related alloys. Tertiarybutylphosphine (TBP) and ditertiarybutylsilane (DTBS) have been employed in a standard rf plasma reactor to produce pure and doped a-Si:H and a-Si<sub>x</sub>C<sub>1-x</sub>:H alloys.<sup>2</sup> Because they are less toxic and less pyrophoric, many of these liquid organic sources may be preferable to the usual gases employed in film growth. Samples have been characterized using dark conductivity, infrared vibrational spectroscopy and photothermal deflection spectroscopy (PDS). Ditertiarybutylsilane has been added to silane to vary the bandgap of a-Si<sub>x</sub>C<sub>1-x</sub>:H alloys from E<sub>04</sub> of about 1.9 to about 3 eV. Room temperature dark conductivities as high as  $3 \times 10^{-6} \Omega^{-1} \text{cm}^{-1}$  have been achieved by adding 10% DTBS (E<sub>04</sub> = 2.2 eV) and 1% TBP to silane.

A second task concerns non-equilibrium phenomena in a-Si:H and related alloys. We have initiated studies of local diffusion of hydrogen in a-Si:H using NMR techniques<sup>3</sup>. The dipolar interaction of hydrogen (~ 10 at. %) in boron-doped amorphous silicon has been studied using the Jeener-Broekaert pulse sequence. The sample was prepared on an Al foil substrate at a

temperature of 230°C using a standard glow discharge system (operating at 1 W rf power). The diborane/silane ration was  $10^{-4}$ . The same sample was removed from the Al substrate using dilute hydrochloric acid. The Jeener-Broekaert pulse sequence consists of three pulses:  $\pi/2|_{x'} - \tau_1 - \pi/4|_{y'} - \tau_2 - \pi/4|_{y'} - \text{echo}$ . We measured  $T_{1D}$ , the dipolar spin lattice relaxation time, for  $\tau_1 = 82 \mu\text{s}$ ,  $\tau_1 = 100 \mu\text{s}$  and  $\tau_1 = 50 \mu\text{s}$  at 299°K. The value of  $T_{1D}$  was found to be independent of  $\tau_1$ . At 335°K we found  $T_{1D}$  to be much longer than at room temperature. The values of  $T_{1D}$  at 299 K, 314 K and 335 K are, respectively, 0.7 ms, 1.2 ms and 1.8 ms (see Fig. 1). From the data we estimate an activation energy for microscopic motion to be  $\sim 0.2 \text{ eV}$ .

A third task involves the study of recombination-induced metastabilities in a-Si:H and related alloys. The measurement of photoluminescence (PL) from nitrogen-rich hydrogenated amorphous silicon nitride (a-SiN<sub>1.6</sub>:H) films<sup>4,5</sup> provides a probe of optically-induced metastabilities in these films. Excitation at 4.8 eV gives a PL spectrum of approximately Gaussian lineshape centered at 2.9 eV with a full width at half maximum of 1.4 eV. The PL intensity at 2.9 eV fatigues under continuous 4.8 eV excitation, but may be restored by thermal annealing or photobleaching with light of energy  $\geq 2 \text{ eV}$ . For emission at 2.9 eV, the PL excitation spectrum in the range 3.0 to 5.2 eV follows the a-SiN<sub>1.6</sub>:H film optical absorption edge at low energy and then decreases with a maximum at approximately 5.4 eV.

We have also employed both light-induced electron spin resonance (LESR) and PL after light soaking in a-Si:H to probe metastabilities<sup>6</sup>. Different dependences on the light soaking temperature for the ESR spin density and the PL peak intensity at  $\sim 1.3 \text{ eV}$  suggest that a non-radiative process, that does not directly involve neutral dangling bonds, influences the photoluminescence at the peak. After light soaking no clear increase of the peak in the low energy luminescence region ( $\sim 0.8 \text{ eV}$ ) was observed even at higher temperatures ( $> 200 \text{ K}$ ), where the low energy luminescence band is relatively more important.

An additional task concerns investigations of defects and impurities in a-Si:H and related alloys. We have been using excitation spectroscopy of PL (PLE) and time resolved PL to probe defects which produce absorption below the gap in a-Si:H.<sup>7,8,9</sup> Photoluminescence in a-Si:H has been investigated using optical excitation energies  $E_x$  varying from 1.27 to 2.0 eV. At low temperatures ( $T < 100 \text{ K}$ ) a strong dependence of both the radiative quantum efficiency and the energy distributions of photoexcited carriers on  $E_x$  has been observed for  $E_x < 1.65 \text{ eV}$  (see Fig. 2). At higher temperatures ( $T > 200 \text{ K}$ ), the dependence of the energy distribution of carriers on  $E_x$  disappears within a narrow interval of temperature. A model of phonon-assisted absorption has been proposed to account for the experimental results.<sup>7</sup>

A final task is the training of graduate students and postdoctoral research associates. Three students are currently being trained under partial support of this subcontract. In addition, two postdoctoral research associates are benefiting from training received under this program. We currently have active collaborative efforts with several universities and corporations. All of these institutions have provided well characterized samples to use for various research purposes.

Although they do not fall directly under any of the tasks of the present subcontract, we have measured the optical bistability in a-Si:H because of the potential of this material as a bistable optical switch.<sup>10,11</sup>

## Conclusions

Major accomplishments of the previous year include (1) the characterization of  $a\text{-Si}_x\text{C}_{1-x}\text{:H}$  alloys which have been grown using liquid organic sources mixed with silane, (2) measurements of local diffusion of hydrogen in B-doped and intrinsic a-Si:H using NMR techniques, (3) the extension of PLE and time-resolved PL spectra in a-Si:H down to 1.1 eV, (4) the measurement of PL fatigue in  $a\text{-Si}_x\text{N}_{1-x}\text{:H}$  alloys, and (5) an investigation of the temperature dependences of both the light-induced PL decay and ESR increase in a-Si:H. Future directions for the research include (1) growth of a-Si:H and related alloys using other less toxic sources, (2) continuation of below-gap spectroscopy of a-Si:H using PLE and time resolved PL, (3) continuation of the measurements of local hydrogen diffusion in boron-doped, phosphorus-doped and intrinsic a-Si:H using NMR techniques, (4) investigations of the optical properties of  $a\text{-Si}_x\text{Ge}_{1-x}\text{:H}$  and  $a\text{-Si}_x\text{N}_{1-x}\text{:H}$  alloys, and (5) an examination of the correlations between optically induced metastabilities observed in PL, ESR and optical absorption experiments in a-Si:H and related alloys.

## References

1. "Amorphous Semiconductors" (A. Madan and P.C. Taylor), in Encyclopedia of Physical Science and Technology (Academic Press, Inc., San Diego, CA, 1993), in press.
2. "Growth of a-Si:H and Related Alloys using Liquid Organic Sources" (K. Gaughan, S. Hershgold, J.M. Viner and P.C. Taylor), *J. of Non-Crystalline Solids*, **137&138**, 709 (1991).
3. "Dipolar Measurements of Hydrogen in Amorphous Silicon" (P. Hari, P.C. Taylor and R.A. Street), in Amorphous Silicon Technology - 1992, edited by A. Madan, Y. Hamakawa, M.J. Thompson, E.A. Schiff and P.G. LeComber (Materials Research Society, Pittsburgh, 1992), Vol. 258, p.293.
4. "Photoluminescence in Nitrogen-rich  $a\text{-SiN}_x\text{:H}$ " (D. Chen, J.M. Viner, P.C. Taylor and J. Kanicki), in Amorphous Silicon Technology - 1992, edited by A. Madan, Y. Hamakawa, M.J. Thompson, E.A. Schiff and P.G. LeComber (Materials Research Society, Pittsburgh, 1992), Vol. 258, p. 661.
5. "Photoluminescence in a-Si:H and  $a\text{-Si}_{1-x}\text{N}_x\text{:H}$ " (S.Q. Gu, D. Chen, J.M. Viner, M.E. Raikh and P.C. Taylor), PVAR&D meeting, 1992, in press.
6. "Correlations of Changes in ESR and PL with Light Soaking in a-Si:H" (M. Yoshida and P.C. Taylor), in Amorphous Silicon Technology - 1992, edited by A. Madan, Y. Hamakawa, M.J. Thompson, E.A. Schiff and P.G. LeComber (Materials Research Society, Pittsburgh, 1992), Vol. 258, p. 347.
7. "Photoluminescence Excitation Spectroscopy in a-Si:H: Evidence for Phonon Assisted Absorption" (S.G. Gu, M. Raikh and P.C. Taylor), *Phys. Rev. Lett.* **69**, 2697 (1992).
8. "Subband Recombination in a-Si:H" (S.Q. Gu and P.C. Taylor), in Amorphous Silicon Technology - 1992, edited by A. Madan, Y. Hamakawa, M.J. Thompson, E.A. Schiff and P.G. LeComber, (Materials Research Society, Pittsburgh, 1992), Vol. 258, p. 771.

9. "Subband Optical Excitation and Recombination in a-Si:H" (S.Q. Gu and P.C. Taylor), J. of Non-Crystalline Solids, 137&138, 591 (1991).
10. "Temperature Switch Based on Optical Bistability" (Z.Y. Xu, J. Tann, M. Gal and P.C. Taylor), Opt. Quantum Electron. 24, 587 (1992).
11. "Optical Bistability in an Hydrogenated Amorphous Silicon Fabry-Perot Etalon" (Z.Y. Xu, J. Tann, M. Gal, K. Gaughan, I. Viohl and P.C. Taylor), Int. J. of Optoelectronics 6, 29 (1991).

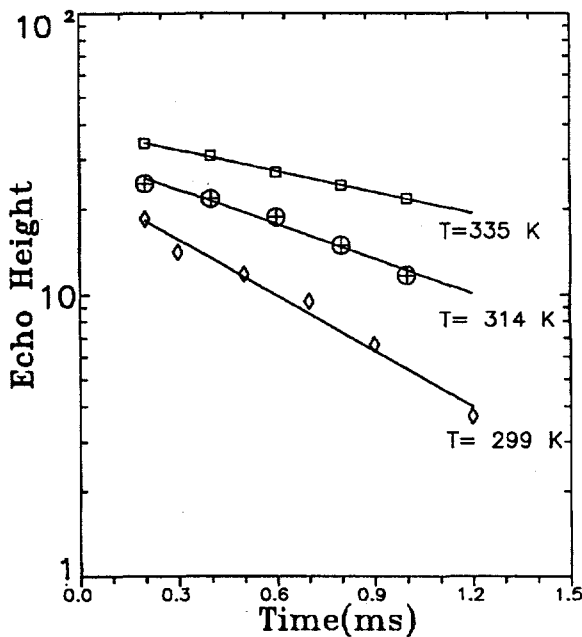


Fig. 1.  $T_{1D}$  as a function of temperature. The  $T_{1D}$  at 299 K, 314 K and 335 K are, respectively, 0.7 ms, 1.2 ms and 1.8 ms.  $T_{1D}$  was obtained by a least squares fit to the data. From these data we estimate the activation energy to be 0.2 eV.

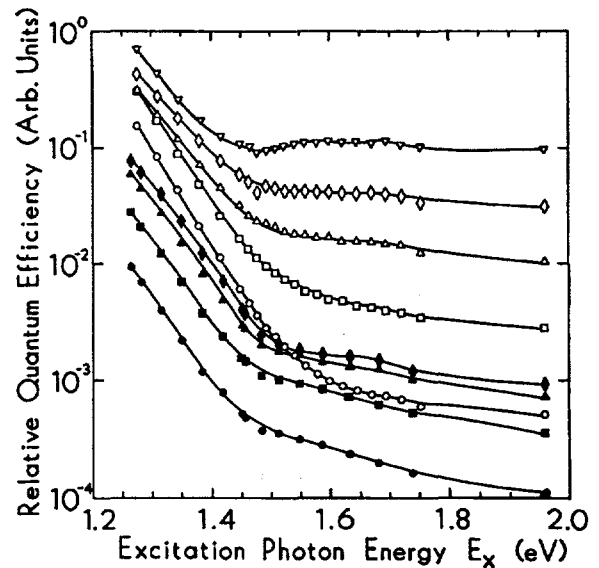


Fig. 2. The relative quantum efficiency as a function of  $E_x$  at 77 K (open symbols) and 220 K (solid symbols) for PL measured at 0.8 eV ( $\circ$ ), 0.9 eV ( $\square$ ), 1.0 eV ( $\Delta$ ), 1.1 eV ( $\diamond$ ) and 1.2 eV ( $\nabla$ ).

## 2.0 POLYCRYSTALLINE THIN FILMS

Kenneth Zweibel (Manager)

The objective of the Polycrystalline Thin Film Project is to develop thin-film, flat-plate modules that meet DOE's long-term goals of reasonable efficiencies (15%-20%), very low cost (near \$50 m<sup>2</sup>), and long-term reliability (30 years). The approach relies on developing PV devices based on highly light-absorbing compound semiconductors such as CuInSe<sub>2</sub> and CdTe, as well as thin-film crystalline silicon. These semiconductors are fabricated as thin films with minimal material and processing costs.

The project concentrates on those materials that are effective as polycrystalline films: CuInSe<sub>2</sub> (CIS), CdTe, and film-Si Polycrystalline thin film CuInSe<sub>2</sub> and CdTe cells have each achieved about 15% active area efficiency on cells measured at NREL (14.8% CIS; 15.8% CdTe). For both materials, active-area efficiencies in the 10%-14% range have been reported by more than 20 laboratories (for CIS: NREL, ARCO Solar, Boeing Aerospace, ISET, EuroCIS Consortium, University of Stuttgart; for CdTe: NREL, Monosolar, Kodak, IEC, Ametek, University of South Florida, Georgia Institute of Technology, Matsushita Battery, SOHIO, BP Solar, Photon Energy, Microchemistry, Korea Advanced Institute of Science and Technology, Battelle Europe, and University of Queensland). Meanwhile, CIS submodules have achieved 11.1% (1000 cm<sup>2</sup>) and 9.7% (3900 cm<sup>2</sup>) aperture-area efficiencies. CdTe has achieved 10% (710 cm<sup>2</sup>) and 6.5% for very large modules (7000 cm<sup>2</sup>). CIS and CdTe modules have been tested outdoors at NREL for substantial periods (up to 4 years) with little or no change from their initial efficiencies.

Because CIS and CdTe are successful at the cell and submodule levels in terms of efficiency and intrinsic stability, the next step is to assist them in becoming successful at the product level, i.e., in terms of reaching practical, low-cost manufacture of stable, 10%-efficient (or more) power modules. At manufacturing costs of under \$100/m<sup>2</sup>, such power modules would cost less than \$1/W. This kind of achievement is within the range of existing CIS and CdTe cell/submodule technology, but depends critically on addressing manufacturability and reliability issues.

Major progress during 1992 occurred in the CdTe technology. During the year (see Table 1-3), records were repeatedly set for laboratory cell efficiency. These records, which reached 15.8% by the end of the year (up from 12.7%) were the highest for any non-single-crystal thin-film cell of any sort (any material, any structure, including multijunctions). This was achieved using simple, single-junction cells made by a method that has already been adopted by industry (Solar Cells Inc.) for commercial development.

In parallel with these cell results, major progress occurred in CdTe module development. Early in the year, Photon Energy (now Golden Photon, see below) made their first 4-square-foot CdTe modules, reaching 21 W (then the most for any CdTe module). Researchers subsequently focused on shakedown tests of their pilot production at these sizes. In a more spectacular development, researchers at Solar Cells Inc. began CdTe module development at the 8-square-foot size, and within 6 months of making their first films made a module with a reported efficiency of 6.5% (47 W). This is the highest efficiency thin-film module of any kind at that size.



Finally, the CdTe industrial infrastructure was bolstered by the entry of Coors (through its subsidiary, Golden Technologies). Coors purchased Photon Energy for the purpose of commercializing Photon Energy's CdTe technology in September 1992. The new company, Golden, Photon, is headquartered in Golden, Colorado.

CIS progress was mixed. Siemens Solar, the technology leader, faltered in its progress toward commercial module production. Although some module efficiencies near 10% were achieved, yields peaked at about 8%. Several manufacturing issues were identified as causing this shortfall. Meanwhile, however, efficiencies at the cell level rose almost as spectacularly as those for CdTe (Table 1-3), with a non-NREL-funded group (EuroCIS) reaching 14.8% active-area efficiency. Boeing made the highest total-area efficiency, 13.7%, using a Ga-alloyed cell, and EuroCIS reported 14.6% (active area) cells with S-Se alloys. These cell results in CIS alloys with Ga and S were important technical achievements.

ISSET reached 11% (active area) efficiency using a nonvacuum method of depositing Cu-In. This replacement of a relatively expensive sputtering step with an inexpensive nonvacuum step could turn out to be one of the seminal technical achievements of the year if it is followed up with module development and manufacturing.

**Title:** Development of Large-Area Monolithically Integrated Silicon-Film Photovoltaic Modules

**Organization:** AstroPower, Inc.  
Solar Park  
Newark, DE 19716-2000

**Contributors:** J.A. Rand, Principal Investigator, J. E. Cotter, A.E. Ingram,  
T.H. Lampros, T.R. Ruffins, V.C. Turner, R.B. Hall, A.M. Barnett

### Objective

The objective of this program is to develop Silicon-Film™ Product III into a low cost, stable solar cell for large scale terrestrial power applications. The Product III structure is a thin (<100 μm) polycrystalline layer of silicon on a durable, insulating, ceramic substrate. The insulating substrate allows the silicon layer to be isolated and metallized to form a monolithically interconnected array of solar cells (see Figure 1). High efficiency is achievable with the use of light trapping and a passivated back surface. The long term goal for the product is a 1200 cm<sup>2</sup>, 18% efficient monolithic array. The short term objectives are improving material quality and fabricating 100 cm<sup>2</sup> monolithically interconnected solar cell arrays. Recent improvements in material quality (through reduced impurity contamination) have resulted in minority carrier diffusion lengths over 20 μm. A solder dipped interconnection process has been developed that will allow low-cost production processing. Test data for a 4 cell device has indicated a V<sub>OC</sub> of 2.0 V and low shunt conductance (< 0.1 mS/cm<sup>2</sup>) due to limited conduction through the ceramic and no process related metallization shunts.

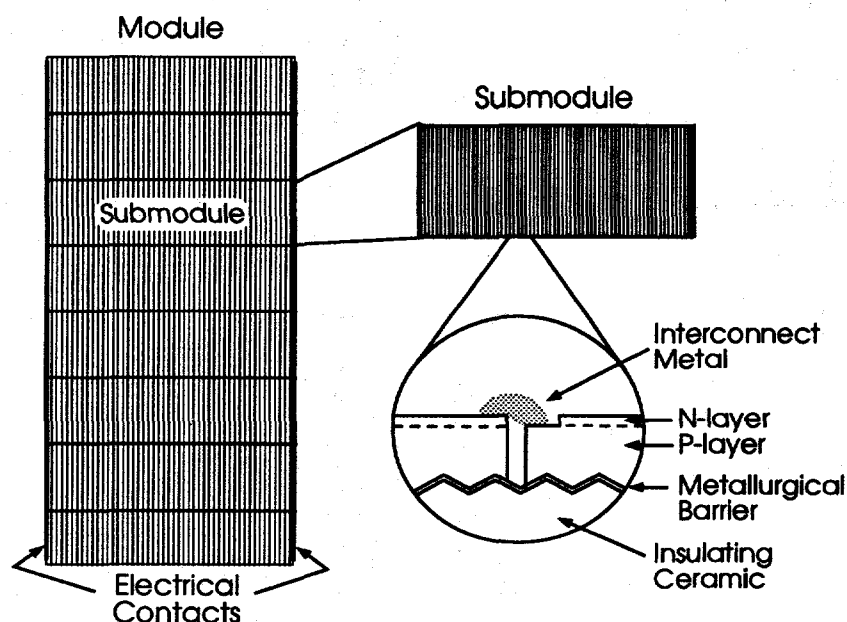


Figure 1. Silicon-Film™ Product III

## Technical Approach

Material quality has been the key issue in the development of Product III over the past year. Thin, large-grain polysilicon layers can be grown routinely on ceramic substrates using the Silicon-Film process. Minority carrier diffusion lengths, however, had been limited to less than 10  $\mu\text{m}$ . Metallic impurities and dislocations are two potential causes being investigated in detail. Isolating impurity sources has resulted in recent improvements in  $L_n$ . Issues for the monolithic integration process are 1) developing a mechanically durable, high-resistivity ceramic substrate that does not contaminate the silicon layer, and 2) developing low-cost metallization and array interconnection techniques. Significant progress has been made in each area.

## Materials Results

In order to track impurity contamination effects, silicon feedstock and finished products have been evaluated by inductively coupled plasma - mass spectroscopy (ICP-MS). Using this chemical analysis technique a number of contamination sources in the process sequence were identified. The silicon feedstock contains on the order of 4 ppm iron, introduced through classification procedures. The silicon deposition process has added aluminum, chromium, copper, and tungsten at the ppm level. All of the transition metals are known to have large segregation coefficients. After impurity segregation effects, all impurities except aluminum are below ICP-MS detection limits (typically 1 ppm). However, impurities such as tungsten could continue to have a significant adverse effect on  $L_n$  at such levels. Silicon-Film layers produced in this manner are approximately 100  $\mu\text{m}$  thick with aspect ratios (grain width to height) on the order of 10 to 1. With these impurities present, diffusion lengths have been limited to 5 to 8  $\mu\text{m}$ , and gettering processes have had no appreciable effect.

Impurities such as tungsten are known to be immobile in silicon and are unaffected by gettering. To evaluate the impurity impact, a second experimental silicon deposition process, known to be free of tungsten, was developed. Diffusion length data taken on the higher purity material are shown in Figure 2. The material starts at an average  $L_n$  of 12.5  $\mu\text{m}$  and increases to an average of 18.6  $\mu\text{m}$  with gettering. The control set of devices (with impurities present) has an average  $L_n = 6.3 \mu\text{m}$  and decreases to 5.6  $\mu\text{m}$  with gettering.

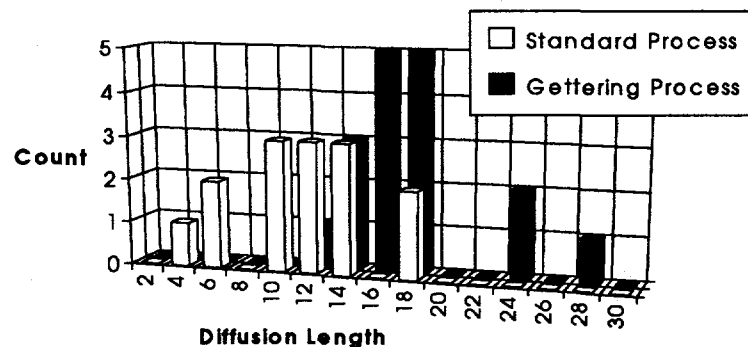
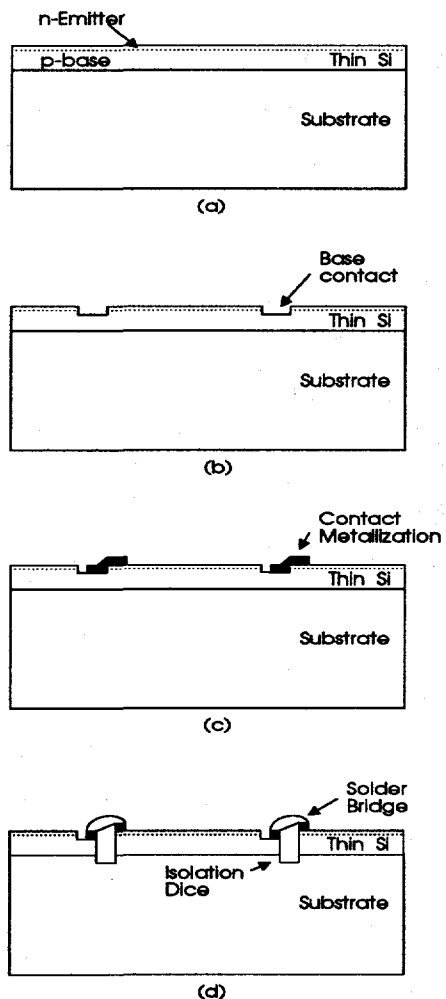


Figure 2. Effects of gettering on silicon layers known to be free of tungsten.

## Device Results

The current Product III device process is illustrated in **Figure 3**. A thin film of p-type silicon, which may or may not include a metallurgical barrier, is diffused from a  $\text{POCl}_3$  source to form the n-type emitter (a). Photolithography is used to define the base contact area on the top surface, which is exposed by plasma etching through the emitter (b). Photolithography and metal liftoff are used to define the contact metallization area, which overlaps part of the exposed base and part of the adjacent emitter (c). A single metal evaporation is needed to form both emitter and base contact. An isolation trench is then formed by dicing down the middle of the evaporated metallization to isolate the individual solar cell elements. Saw damage from the dicing step is removed, and the final, low-temperature interconnect metallization is added (d). A similar process, based on plated electrical contacts is described elsewhere [1]. The evaporated metal process is presently being used on laboratory scale devices.



**Figure 3.** Process sequence for monolithic interconnection of Silicon-Film on ceramic.

Resistivity, flatness, and mechanical strength of the ceramic substrate are critical issues for the monolithic integration process. Ceramic resistivities have been measured over  $15 \text{ k}\Omega\text{cm}$ , resulting in a base-to-base shunt resistance through the ceramic of over  $10 \text{ k}\Omega$ . Flatness is required for the photolithography and dicing in the present laboratory scale process. Mechanical strength of the ceramic is important to assure the durability of the finished array. All properties have been achieved by varying the thickness and composition of the ceramic.

Two low-temperature interconnection metallization techniques have shown promise. The first employs conductive epoxy squeegeed into the isolation dice, the second is based on conventional solder-dipping technologies. **Figure 4** is an SEM photomicrograph of a solder-dipped interconnection presently being used on the laboratory scale devices.

To demonstrate the feasibility of the process, complete integrated arrays are being fabricated on ceramic substrates. Arrays of 15 elements are formed on  $50 \text{ cm}^2$  substrates. The process sequence is that shown in **Figures 3 and 4**. Initial device data indicates that open circuit voltages of  $500 \text{ mV}$  per element have been measured on complete arrays (without anti-reflection coating (ARC) or surface

passivation). Early devices were shunted due to excessive ceramic conduction and metallization shunts. Both problems have been solved and shunt conductances of less than  $0.1 \text{ mS/cm}^2$  have been measured. Short circuit currents of  $13.3 \text{ mA/cm}^2$  (no ARC) have been measured on devices with over 10 elements. The low currents are due to poor blue response due to a deep emitter formation. An etch back and passivation process has been developed, but not yet implemented on these samples. As reviewed in the "Materials Results" section, diffusion lengths have been recently improved, and currents of  $24\text{-}26 \text{ mA/cm}^2$  (with ARC) are expected with the etch back/passivation processing. Fill factors have been very low (0.5 -0.6) due to high series resistance. The resistivity of the base layer is  $1 \text{ }\Omega\text{cm}$  with the present processing sequence. Lowering that resistivity, as well as narrowing the present element width (presently  $0.5 \text{ cm}$ ) will improve fill factors in the short term. Although monolithic multi-element arrays are being formed, no process steps have been optimized. The data to date indicates that all device and processing issues can be optimized in the short term.

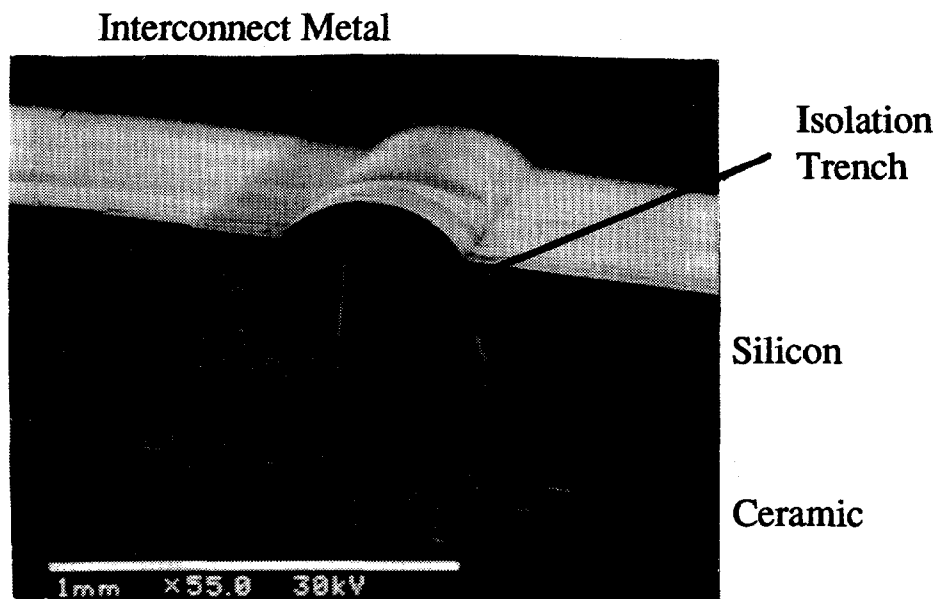


Figure 4. SEM photomicrograph of a solder-dipped interconnection

### Conclusions

Significant improvements have been made in the material quality of Silicon-Film layers on ceramic substrates. Thin, large-grain polysilicon layers can be grown routinely on ceramic substrates. Minority carrier diffusion lengths, however, had been limited to less than  $10 \text{ }\mu\text{m}$ . Recent success identifying and controlling contamination sources has led to lifetime improvements and the development of a successful gettering process. Prototype arrays are now being fabricated with improved material. Optimizations in device processing are expected to generate monolithic arrays with efficiencies over 8% in the short term.

### References

[1] Annual Subcontract Report, (July 1992), NREL/TP-41113-4996, 28 pp. Available NTIS: Order No. DE92010600.

**Title:** Research on Polycrystalline Thin Film CuInGaSe<sub>2</sub> Solar Cells

**Organization:** Boeing Defense & Space Group, Seattle, WA

**Contributors:** B. J. Stanbery, program manager; W. S. Chen and J. M. Stewart, co-principal investigators; W. E. Devaney and R. A. Murray

## Objectives

The objectives of this research effort are to fabricate high efficiency CdZnS/CuInGaSe<sub>2</sub> thin film solar cells, and to develop improved transparent conductor window layers such as ZnO.

## Approach/Background

ZnO/CdZnS/CuGaInSe<sub>2</sub> thin film solar cells have been fabricated by elemental co-evaporation of the CIGS film, aqueous chemical deposition of thin (<0.05 μm) CdZnS films, and reactive sputtering of ZnO:Al. Various combinations of gallium and zinc alloy compositions as well as different temperature and I/III gradient profiles have been studied.

As a practical matter, significant corollary effort is necessary to redesign and modify the equipment, particularly the CIGS deposition system, since it is highly customized for this application. Early in this fiscal year, for example, we redesigned and built a new substrate heater to eliminate problems encountered with arcing in the original design under normal deposition conditions. The resulting increase in system uptime significantly improved our throughput, enabling rapid progress that led to efficiencies in excess of 13%.

## Status/Accomplishments

We have made significant improvements in the performance of ZnO/CdZnS/CuInGaSe<sub>2</sub> cells in the course of our contract efforts during the 1992 fiscal year, achieving all of the technical performance milestones. We fabricated during FY 1992, a ZnO/Cd<sub>1-y</sub>Zn<sub>y</sub>S/CuIn<sub>1-x</sub>Ga<sub>x</sub>Se<sub>2</sub> thin film solar cell with Y=0.20 and X=0.26 which NREL measured at **13.7% total area efficiency** (figure 1). This is *the highest reported total area efficiency for a CIS thin film solar cell* and exceeds our key technical milestone for Phase 2 of this contract. It is strong evidence of our expertise in materials and device processing, and device and equipment design. These results also clearly demonstrate the value to NREL of the synergy between this contract and Boeing's related IR&D activities.

This particular result is a consequence of certain specific improvements in various aspects of materials deposition. First, detailed device analysis of this and other recent cells showed that substantial reduction in the series resistance of a lumped parameter equivalent circuit model has been achieved. We believe that this is a bulk selenide effect resulting from slightly modified temperature and elemental group I/III ratio profiles during CIGS deposition. Second, improvements in our CdZnS aqueous chemical deposition process increased both yields and performance by

reducing leakage currents, presumably at the heterojunction. Together, these first two effects resulted in significantly higher fill factors for our more recent devices, particularly for  $\text{CuIn}_{1-x}\text{Ga}_x\text{Se}_2$  compositions where  $x \geq 0.20$ . Alone, this second effect enabled some reduction in short-wavelength above-gap absorption losses by permitting the use of optically thinner CdZnS layers without adverse yield consequences. Third, improved process parameters for the deposition of ZnO:Al by reactive RF magnetron sputtering from sintered, hot-pressed  $\text{ZnO}+\text{Al}_2\text{O}_3$  targets effectively reduced parasitic optical losses due to both absorption and diffuse scattering, reducing both IR and broad-band losses. These last two factors reducing absorption losses effectively increased device short-circuit current densities.

### **FY 1993 Milestones**

Boeing capital funds have been used to procure and install a new dual rotating cathode sputtering source which will be used to investigate lower-cost, higher rate processes for the deposition of device quality ZnO. New process parameters for CIGS deposition will be studied in an effort to improve overall cell performance. We do not believe that temperature and elemental group I/III ratio profiles during CIGS deposition have yet been globally optimized. We anticipate the result of such optimization to be total area cell efficiencies exceeding 14%, our Phase 3 key technical milestone.

### **Major Project Reports**

W. E. Devaney, W. S. Chen, J. M. Stewart and B. J. Stanbery, "Analysis of High Efficiency  $\text{CuInGaSe}_2$  Based Solar Cells".

B. J. Stanbery, W. S. Chen, W. E. Devaney and J. M. Stewart, "Research on Polycrystalline Thin Film  $\text{CuGaInSe}_2$  Solar Cells".

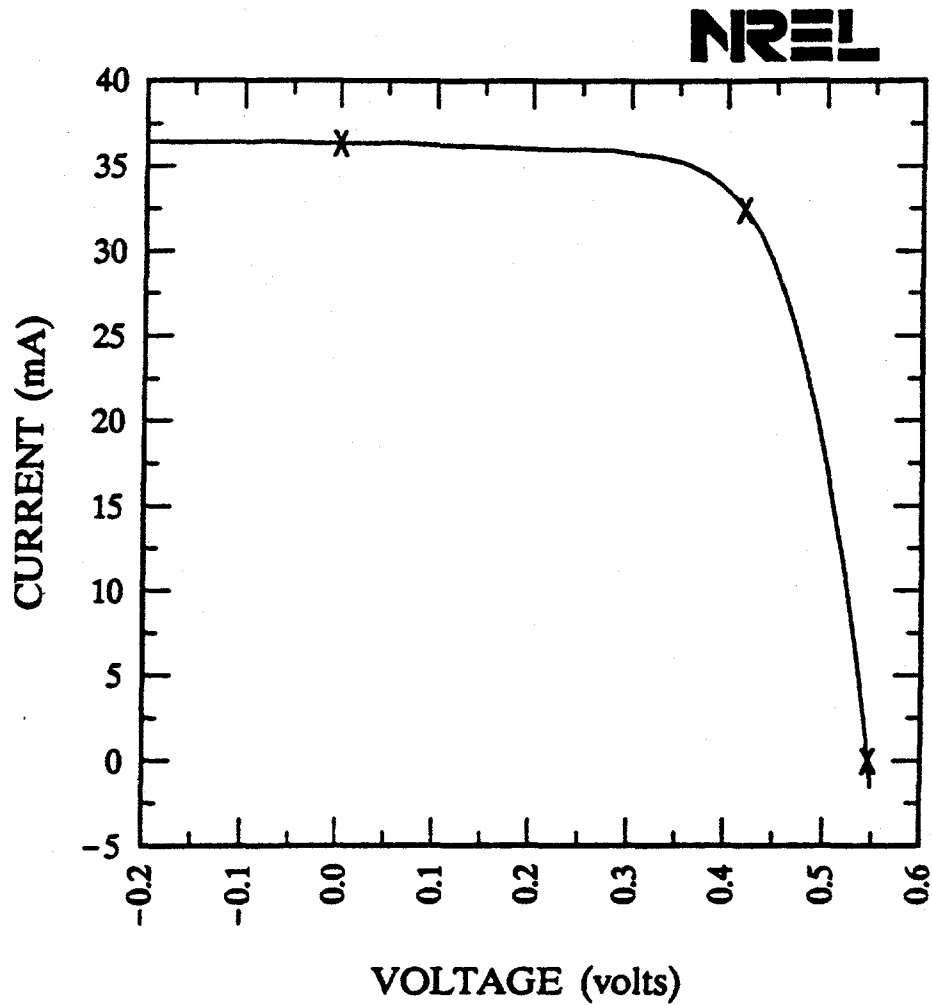
# Boeing, ZnO/CdZnS/CIGS/Mo/Al Global

Sample: 1516BD

Temperature = 25.0°C

Jul. 1, 1992 10:56 am

Area = 0.9895 cm<sup>2</sup>



$V_{oc} = 0.5458$  volts

$I_{sc} = 36.34$  mA

$J_{sc} = 36.71$  mA/cm<sup>2</sup>

$P_{max} = 13.56$  mW

Fill factor = 68.38 %

$I_{max} = 32.44$  mA

Efficiency = 13.7 %

$V_{max} = 0.4181$  V

Figure 1: NREL measurement of the best CIGS cell fabricated in FY 1992 under this contract.



**Title:** Polycrystalline Thin Film Cadmium Telluride Solar Cells Fabricated by Electrodeposition

**Organization:** Department of Physics, Colorado School of Mines, Golden, Colorado

**Contributors:** J.U. Trefny, T.E. Furtak, N. Wada and D.L. Williamson, co-principal investigators; D. Kim, research associate; D. Du, Y. Qu and S. Pozder

## Objective

The main objective throughout all phases of this project, which began on March 20, 1992, is the development of techniques for the growth of high-quality thin films and devices. The research builds upon work performed at Ametek corporation until about 1990 when the laboratory know-how and equipment were transferred to Colorado School of Mines. The intent at CSM is to build upon the Ametek experience and expertise regarding polycrystalline, thin-film, CdTe n-i-p solar cells to improve certain processing steps and the potential for economic, large-scale production.

## Sample Preparation

Commercial SnO<sub>2</sub>-coated glass substrates were coated with CdS by a dip-coating process. These were then annealed at 450°C for 50 min in N<sub>2</sub> after a CdCl<sub>2</sub> treatment. CdTe films were deposited on the CdS/SnO<sub>2</sub>/glass substrates by an electrochemical method. Samples were treated with CdCl<sub>2</sub> before annealing at 410°C for 30 min in air. An etching in Br-MeOH solution was followed by the deposition of Au back contacts (0.03 cm<sup>2</sup>) by vacuum evaporation.

## Materials and Device Characterization

X-ray diffraction (XRD), small-angle x-ray scattering (SAXS), Raman scattering, and optical transmission measurements were made for both as-deposited and annealed CdS layers. XRD data were taken for both as-deposited and annealed CdTe layers. Current-voltage (J-V) measurements under light were made to evaluate the dot cell performances.

## Results and Discussion

As-deposited CdS consists of a small grain-size hexagonal (h) or cubic (c) structure with a strong preferred orientation of the (002) [h] or (111) (c) grains parallel to the film surface. After annealing, the CdS layers had a hexagonal structure with a near-random orientation. Annealing also resulted in both larger grains and better crystallinity judging from XRD and Raman scattering data.

Figure 1 shows Raman scattering data from various CdS films: (A) annealed at 450°C for 50 min in N<sub>2</sub>, (B) annealed under the same condition as (A) after CdCl<sub>2</sub> treatment, and (C) as-deposited. Single crystal CdS exhibits an LO mode at  $\approx 301$  cm<sup>-1</sup>. It is known that as the crystalline size becomes smaller, the LO peak position down-shifts and its width becomes broader. Raman scattering is thus a useful tool to probe the grain size and the crystallinity of thin films.

The LO-phonon Raman peak for as-deposited CdS (C) is broad and the peak position is not well-defined, suggesting a poor crystallinity and small grain size in the film. The sample annealed without CdCl<sub>2</sub> treatment (A) shows a large decrease in the peak width, and the peak position is at 298 cm<sup>-1</sup>. The CdCl<sub>2</sub> treated CdS exhibits the LO peak at 299 cm<sup>-1</sup>, which means a larger grain size than sample (B). This result agrees well with the results of other researchers regarding the beneficial effect of CdCl<sub>2</sub> on grain growth.

We have obtained a first set of SAXS results from a CdS film deposited on ZnO-coated c-Si. Figure 2 compares the as-deposited CdS with the ZnO/Si substrate and demonstrates a relatively strong SAXS signal due to some type of electron density fluctuation. The predominant size of the scattering centers is about 1.3 nm; if we assume they are microvoids, then a volume fraction of about 6% is obtained. If the scatterers are some other type of defect with a density greater than zero, then an even larger volume fraction must be present since the SAXS is proportional to the electron density contrast with the CdS material. Further experiments are underway to examine the effect of annealing and CdCl<sub>2</sub> treatment on the observed microstructure. We note that SAXS provides a means of characterizing the bulk microstructure on a scale comparable to that of the scanning tunneling microscope (STM) which characterizes the surface structure.

As-deposited CdTe showed a strong preferred orientation of (111) parallel to the film surface. A transition to a near-random texture occurred upon annealing. Annealing also resulted in a better crystallinity judging from the XRD data. Comparison between XRD patterns obtained from our CdTe and CdTe films previously made by Ametek by a comparable process showed a remarkable similarity. This suggests that our CdTe layers are comparable to those of Ametek's in terms of crystallinity and microstructure.

Table 1 shows a comparison between cells made using our CdTe (S-11) and those using Ametek's CdTe (A-40). Although the J<sub>sc</sub> are the same for both cells, S-11 shows a significantly lower V<sub>oc</sub> and FF, probably due to a low shunt resistance. An STM image of a CdS layer which had a nominal thickness of 1000 Å showed that there was a thickness variation of several hundred angstroms. It is likely that the CdS layers have pinholes which deteriorate the junction performance. An investigation on this issue is currently underway.

## Conclusions

During the first months of the project we have made substantial progress on several aspects of the CdTe solar cell process. Dip coating has been established as a viable technique for the CdS layer and CdTe layers of steadily improving quality are now being deposited by electrochemical methods in our laboratory. A number of characterization techniques are being employed to assess the cell materials as well as complete devices. Notable among these are Raman spectroscopy and SAXS as discussed above.

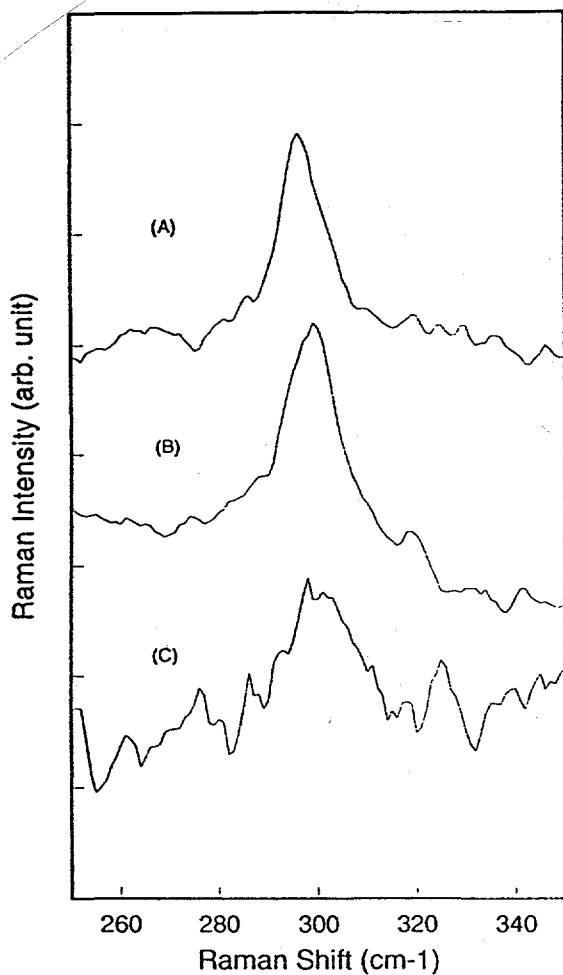


Figure 1. Raman spectra taken from CdS deposited on SnO<sub>2</sub> coated glass substrates: (A) annealed at 450°C for 50 min in N<sub>2</sub> without CdCl<sub>2</sub> treatment, (B) annealed same as (A) after CdCl<sub>2</sub> treatment, and (C) as-deposited.

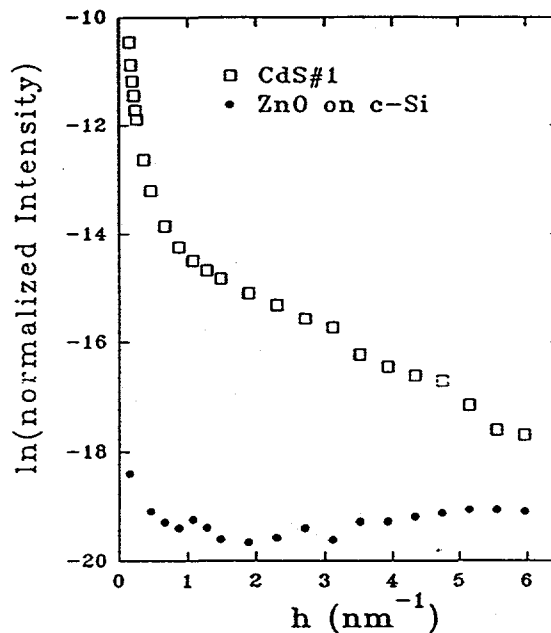


Figure 2. Small-angle x-ray scattering (SAXS) data for an as-deposited CdS film on ZnO-coated crystalline silicon. The parameter  $h = (4\pi/\lambda) \sin \theta$ , where  $2\theta$  is the scattering angle and  $\lambda$  is the x-ray wavelength (0.154 nm).

Table 1. Comparison of CdS/CdTe/Au dot cells made of CdTe layers deposited either by CSM (S-11) or by Ametek (A-40)

	V <sub>ocs</sub> V	J <sub>scs</sub> mA/cm <sup>2</sup>	FF,%	η,%
S-11	0.63	21	43	5.7
A-40	0.73	21	56	8.8

**Title:** Role of Polycrystallinity in CdTe and CuInSe<sub>2</sub> Photovoltaics

**Organization:** Department of Physics, Colorado State University, Fort Collins, Colorado

**Contributors:** J. R. Sites, principal investigator; R. A. Sasala, X. X. Liu, and I. L. Eisgruber

### Objectives

The objectives of this program are quantitative separation of individual loss mechanisms and characterization of extraneous electron states responsible for excessive forward recombination current in polycrystalline thin-film cells.

### Transient Voltage Effects

The open-circuit voltage of most polycrystalline thin-film solar cells is a function of how long the cell has been exposed to illumination [1-4], or equivalently how long the cell has been voltage biased. The voltage is larger when the time spent near  $V_{OC}$ , either due to illumination or external bias, is greater. The effect is reversible and is roughly logarithmic over several decades of time. Fig. 1 shows the experimental apparatus which is designed to switch illumination, load, or external bias in less than a millisecond and record the subsequent photovoltage as a function of time. Temperature is sufficiently well controlled that its effect on photovoltage is less than 2 mV.

Fig. 2 shows the effect for four CuInSe<sub>2</sub> cells fabricated by different processes. Most CuInSe<sub>2</sub> cells and alloy cells with enhanced bandgap show a difference in  $V_{OC}$  of about 20 mV between 1 ms and 2000 s. An exception is pure-CuInSe<sub>2</sub> cells made at Siemens where the effect is 3-6 mV. CdTe cells show a  $V_{OC}$  effect closer to 40 mV. To a first approximation, the entire current-voltage curve is shifted in the voltage direction by the same amount as  $V_{OC}$ . The magnitude of the voltage effect is roughly the same at temperatures between 250 and 350 K, but the voltage appears to saturate more quickly at higher temperatures. In general the recovery time is similar to the saturation time.

The cause of the transient voltage effect is most likely trapping states in the depletion region which have a wide range of fairly long time constants. The consequences of the effect are two fold: (1) a possible error in voltage measurements of 5% and (2) additional pitfalls in I-V analysis. There may also be other related effects that have not yet been documented. In practical terms, the I-V curve after kilosecond exposure would seem to be a more logical standard than that after a few milliseconds, or even a few seconds. It is suggested, therefore, that when a pulse simulator is used, the cell should be forward biased near  $V_{OC}$  for a few minutes prior to illumination, and that the voltage sweep for an I-V curve go from highest to lowest voltages.

### CdTe Cells

During the past two years, a large number of laboratories using a variety of techniques have fabricated CdTe cells with efficiencies well above 10%.

Furthermore, there are significant variations in which loss mechanisms are most dominant [3,5], which suggests the possibility of still higher efficiencies by combining the loss reductions achieved in the different laboratories.

Several high-efficiency CdTe cells fabricated at the University of South Florida (USF) have been measured and analyzed at Colorado State. These cells have efficiencies slightly above or below 15%. The improved values result primarily from  $V_{OC}$  being as high as 860 mV and  $V_{MP}$  as high as 710 mV. The latter corresponds to a fill factor of 0.755, where the values of quality factor, series resistance, and shunt resistance under illumination are 2.0,  $0.4 \Omega\text{-cm}^2$  and  $2.5 \text{K}\Omega\text{-cm}^2$  respectively. Perhaps, more importantly, all the individual parameters were constant over a period of 100 days. In contrast (see Fig. 3), the highest-efficiency cell from a year earlier showed a marked increase in series resistance and corresponding decreases in fill factor and efficiency over a similar time period.

The photocurrent of the cell described above is slightly low due to significant losses below 600 nm. Other USF cells have had lower losses in the window-bandgap region resulting in currents 1-2  $\text{mA/cm}^2$  higher, and Photon Energy (PE) has had a still higher photocurrent. If the highest PE photocurrent could be applied to the USF cell in Fig. 3, the efficiency would be 17%.

#### References

1. Ruberto, M. N., and A. Rothwarf, J. Appl. Phys. 61, 4662 (1987).
2. Albright, S. P., B. Ackerman, and R. R. Chamberlain, Photon Energy Annual Report to NREL (1991).
3. Sites, J. R., Colorado State University Annual Report to NREL (1992).
4. Sasala, R. A., and J. R. Sites, Am. Inst. Phys. Conf. Series, in press.
5. Sasala, R. A., X. X. Liu, and J. R. Sites, Int. J. Solar Energy, in press.

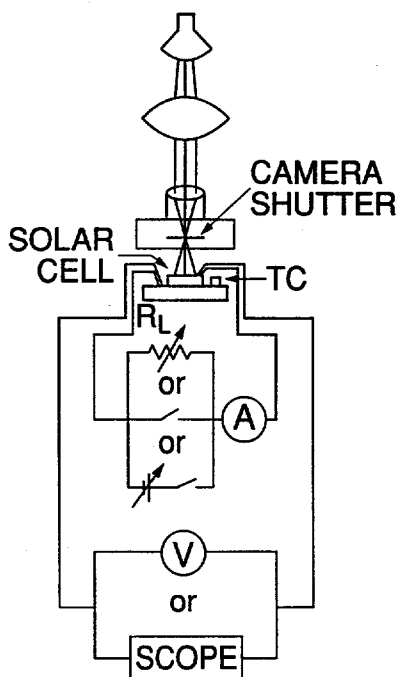


Fig. 1. Apparatus for transient voltage measurement.

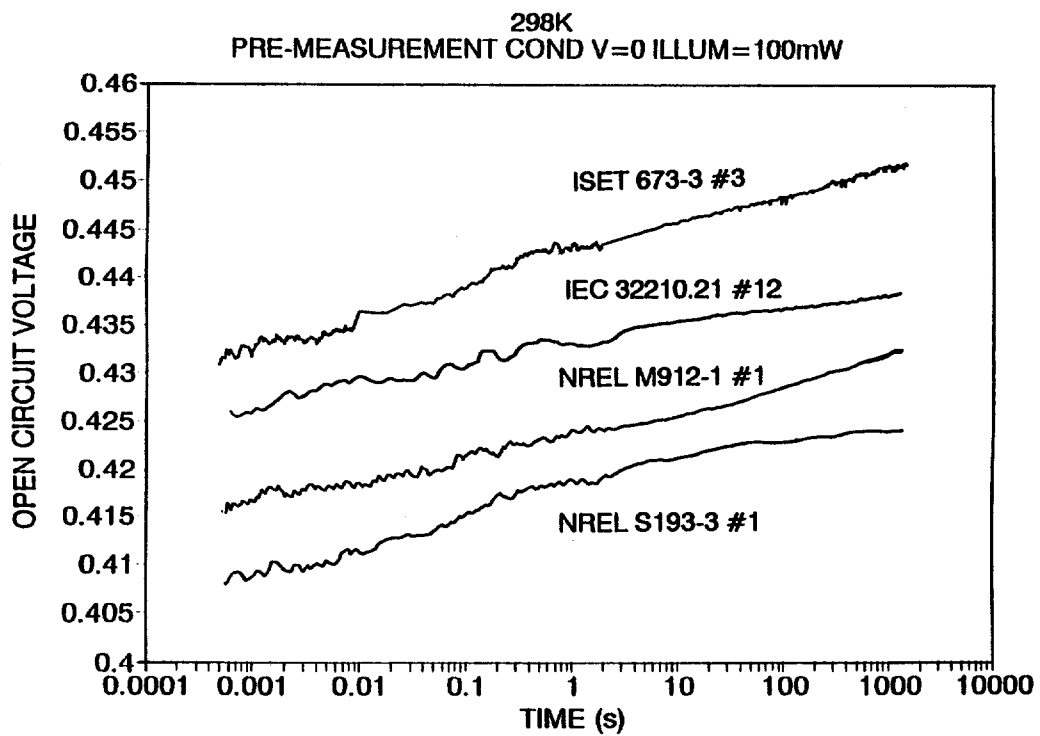


Fig. 2.  $V_{OC}$  transients for four cells after switching from  $J_{SC}$  to  $V_{OC}$ .

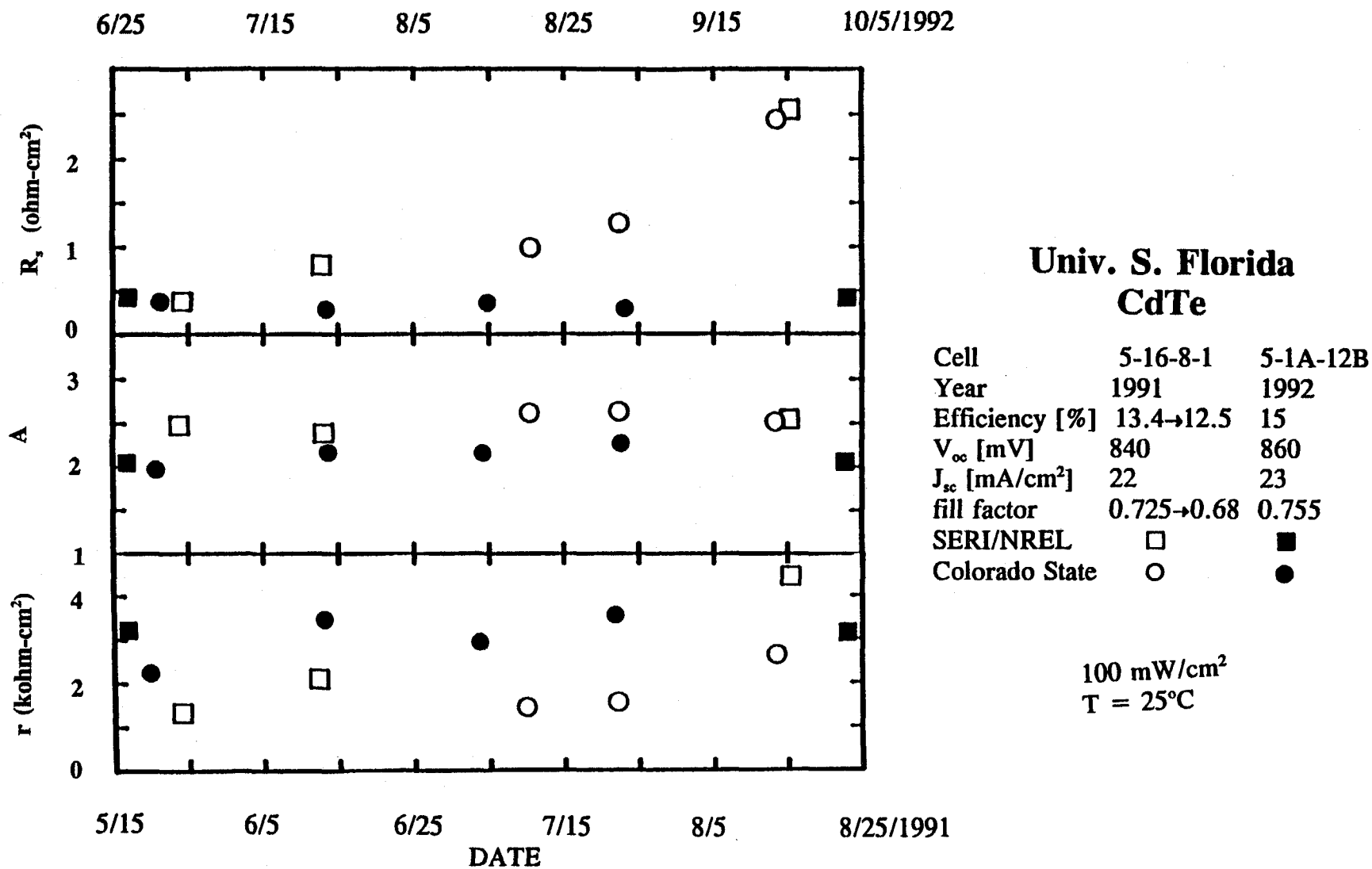


Fig. 3. Fill-factor parameter tracking in 1991 and 1992 highest efficiency CdTe cells.

**Title:** Non-H<sub>2</sub>Se, Ultra-Thin CIS Devices

**Organization:** Energy Photovoltaics (EPV), Inc.  
Princeton, New Jersey

**Contributors:** Z. Kiss, program manager, A.E. Delahoy,  
principal investigator; J. Britt,  
G. Butler, F. Faras, A. Sizemore, F.  
Ziobro.

## **BACKGROUND**

First generation thin film PV modules based on amorphous silicon have been in the marketplace for several years, and second generation, higher efficiency thin film modules based on polycrystalline compound semiconductors such as copper indium diselenide or cadmium telluride are now under intensive development. CIS modules having a power density of 100 W/m<sup>2</sup> have been reported but appear to have been fabricated using the highly poisonous gas hydrogen selenide.

## **OBJECTIVES**

The overall objective of this subcontract is to develop technology capable of producing efficient, large area CIS-based PV modules. The various processes should be compatible with the demands of manufacturing and should therefore be capable of good control, high material utilization and safe operation. A particular objective is the production of a 50W CIS module via processes exhibiting the above features.

## **APPROACH**

EPV has chosen an all-vacuum approach for material deposition. This approach offers the required levels of control, purity, throughput, and safe containment of materials. The formation of CIS is accomplished by selenization of copper and indium containing precursor layers prepared by magnetron sputtering. The selenization is conducted using elemental selenium and not hydrogen selenide [1].

## **RESULTS**

At the end of Phase I (duration 8 months) EPV delivered to NREL a 1.47 cm<sup>2</sup> CIS cell with an active area efficiency of 10.5% [2].

The CIS was prepared by elemental selenization of an annealed stack of Cu-In layers according to a specific Se flux versus time profile which in turn depends on the chosen substrate temperature versus time profile. This process, developed by EPV, is self-stabilizing, and results in automatic convergence of valence stoichiometry.



The Cu-In layers were deposited in a load-locked magnetron sputtering system onto Mo-coated, 929 cm<sup>2</sup> (1 ft<sup>2</sup>) soda lime glass substrates. In order to obtain good devices, it was found that the Cu-In precursors must be annealed. X-ray diffraction showed that the annealing step changed the dominant intermetallic compound in the precursor from CuIn<sub>2</sub> to Cu<sub>11</sub>In<sub>9</sub>. After selenization, single phase, polycrystalline CuInSe<sub>2</sub> was normally obtained, with the ordered chalcopyrite structure being observed. Film compositions were determined by electron microprobe and found to be of the form Cu<sub>1-δ</sub>In<sub>1+δ</sub>Se<sub>2+δ</sub> with δ ranging from 0.02 to 0.16.

The following device structure was adopted: soda lime glass/Mo/CIS/CdS/ZnO:Al. The use of doped ZnO to reduce the surface resistance allows a reduction in CdS thickness from 2 μm to less than 0.05 μm, thereby improving short wavelength response and reducing the (already small) cadmium level in the device.

At the present stage of development, the CdS window layer is deposited by chemical bath deposition from acetate salts, resulting in cells with better junction uniformity and higher short-circuit current densities than cells using vacuum evaporated CdS.

A careful study of the effect of Cu/In ratio in both precursors and CIS films on device performance was completed. This showed an approximate plateau in conversion efficiency for CIS Cu/In ratios in the range 0.89-0.83, with a very strong decline in the range 0.83-0.74. In the plateau region a ±6% variation in precursor Cu/In ratio resulted in a ±3% variation in cell efficiency, supporting the claim that the selenization process is self-stabilizing.

Optimization of the selenization rate/temperature/time profile and CBD CdS layer, together with careful device engineering, resulted in 10.5% active area efficiency CIS solar cells. The parameters of these cells are summarized in Table 1. The quantum efficiency of an EPV CIS cell is shown in Figure 1, together with that of an NREL cell for comparison purposes.

Scale-up of the CBD CdS and sputtered ZnO was accomplished, thereby allowing fabrication of 30.5 x 30.5 cm<sup>2</sup> (1 ft<sup>2</sup>) modules. Patterning of the Mo was successfully performed using both chemical etching and laser techniques. Mechanical scribing was employed for the CIS and ZnO isolation scribes. The 1 ft<sup>2</sup> modules consist of 55 serially-interconnected cells, 0.5 cm in width.

In smaller diagnostic modules, V<sub>oc</sub> maps showed good uniformity of response for all cells (see Figure 2) but fill factor limitations due to interconnect resistance were observed.

## CONCLUSIONS AND FUTURE DIRECTIONS

Substantial progress in CIS technology was made during the first phase of this subcontract. Using unalloyed CIS, active area cell efficiencies in excess of 10% were achieved, and a better understanding was acquired of the parameters that need to be controlled during precursor formation and selenization. The CdS and ZnO processing steps to convert CIS to finished devices are now routinely and reliably accomplished. In the module area, however, diagnostics indicate the presence of substantial ZnO/Mo interconnect resistance in some modules, and work is required to eliminate these occurrences.

The next phase of this work will focus on the following areas: a) further improvement of CIS material quality b) exploration of alloys and modified cell structures c) production of well-engineered 1 ft<sup>2</sup> modules d) research to duplicate the superior junction properties of CBD CdS using vacuum deposited CdS and e) equipment scale up for CIS coating on 0.5 x 1.25 m<sup>2</sup> substrates.

## REFERENCES

1. "A New Self-Stabilizing Selenization Process for the Formation of CuInSe<sub>2</sub> Solar Cells", A.E. Delahoy, F. Faras, A. Sizemore, F. Ziobro and Z. Kiss, NREL PV AR&D 11th Review Meeting, Denver, CO, May 13-15, 1992; AIP Conf. Proc. Vol. 268, 1992, pp. 170-176.
2. "Non-H<sub>2</sub>Se, Ultra-Thin CIS Devices", A.E. Delahoy, J. Britt, and Z. Kiss, Annual Subcontract Report for the period 10 March 1992 - 9 November 1992, Contract No. XG-2-12051-1, Report No. NREL/TP-413-5334; DE93000078.

Table 1 Parameters for CIS cell delivered to NREL

Cell #	V <sub>oc</sub> (mV)	I <sub>sc</sub> (mA)	FF (%)	Active area (cm <sup>2</sup> )	Active area efficiency (%)
11-11-1-6-3C	441	39.6	66.0	1.10	10.5

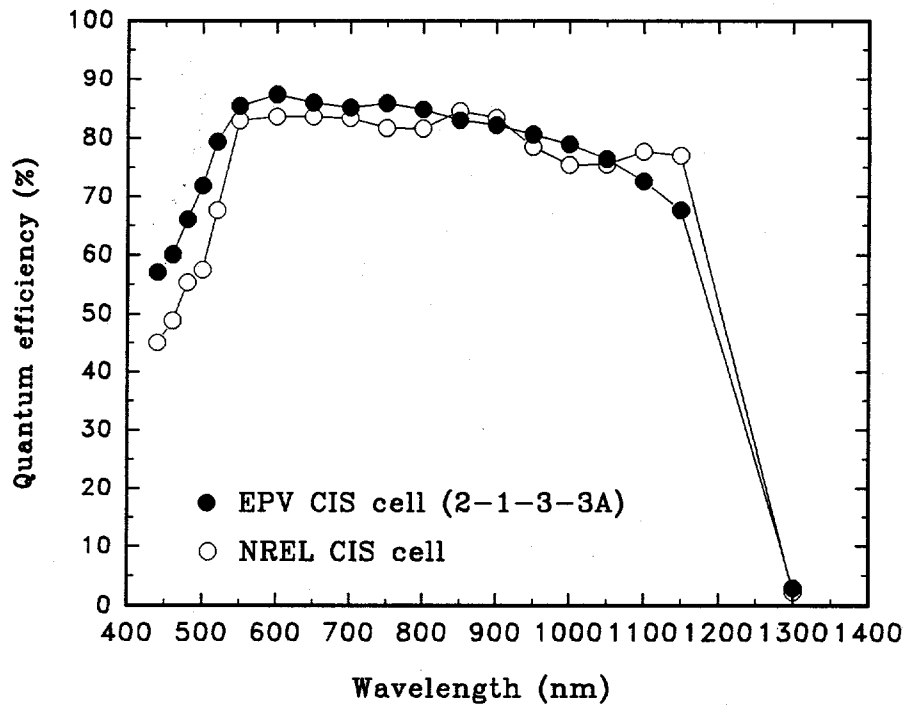


Figure 1. External quantum efficiency versus wavelength for an EPV CIS cell

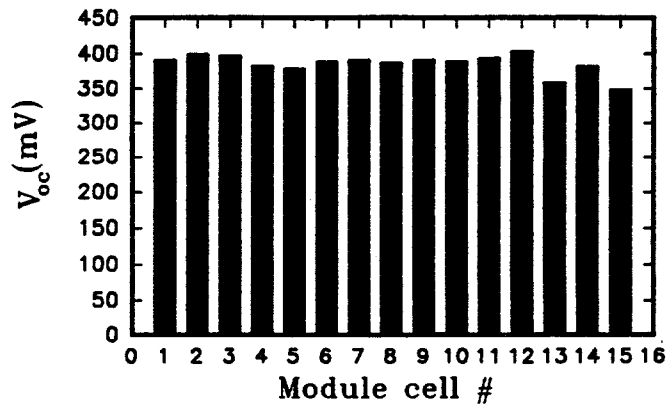


Figure 2.  $V_{oc}$  map at 1 sun illumination for a diagnostic module with 15 subcells

**Title:** Polycrystalline CuInSe<sub>2</sub> & CdTe PV Solar Cells

**Organization:** Florida Solar Energy Center  
University of Central Florida  
Cape Canaveral, Florida

**Contributors:** Neelkanth G. Dhere, Principal Investigator;  
James V. Santiago, Shanker Kuttath, Debbie L. Waterhouse\*, Mark Wollam, Isaiah O. Oladeji.

## Objectives

The major thrust areas of the project are to develop scalable processes for the fabrication of CuInSe<sub>2</sub> and CdTe solar cells, to avoid the use of extremely toxic H<sub>2</sub>Se in the fabrication of CuInSe<sub>2</sub> thin-film solar cells; to optimize selenization parameters to improve adhesion; to improve the metallic back-contact; to reduce the thickness of active CdTe layer and the process temperature; to optimize the solution growth of CdS and (CdZn)S heterojunction partner layers; and to improve the conversion efficiency of CuInSe<sub>2</sub> and CdTe solar cells.

## Technical Approach

The project was initiated in April 1992. Sputtering was chosen as a scalable technique for the fabrication of thin-film solar cells. A multichamber vacuum coating unit was fabricated and installed. Investigations were carried out for DC magnetron-sputter-deposition of individual Mo, Cu, and In thin films for CuInSe<sub>2</sub> solar cells, and RF magnetron-sputter-deposition of Te and DC magnetron-sputter-deposition of Cd thin films for CdTe solar cells.

Solution growth of CdS was investigated for use as heterojunction partner in CuInSe<sub>2</sub> and CdTe polycrystalline-thin-film solar cells. Growth from aqueous solutions is an inexpensive, highly reproducible, and easily controllable technique which can yield conformal CdS layers with excellent optoelectronic properties. The solubility product helps in maintaining constant stoichiometry for any ratio of cations and anions, because of the deposition taking place from ions which are being generated slowly.

Recently a new setup has been installed for the heat treatment of the multilayer thin films for the formation of compound layers, their recrystallization, and the fabrication of complete cells. The deposited thin films were analyzed by various material characterization techniques.

## Results

### Solution Grown CdS Layers

Comparative studies were carried out on the solution-growth of CdS films on plain- and SnO<sub>2</sub>:F-coated soda-lime glass substrates using either cadmium chloride or cadmium acetate as the source of cadmium ions. Thiourea was employed as the source of sulphur ions. The complexing agent was ammonium hydroxide. Films were grown with or without the use of a buffer solution.

Ammonium chloride or ammonium acetate were used as buffer solutions depending on whether cadmium chloride or cadmium acetate was employed as a Cd source. Because of the weak bonding of the cadmium cation with the acetate anion, cadmium acetate resulted in higher quality CdS thin films in comparison to cadmium chloride which tends to decompose less readily. The primary parameters that control the reaction rates both in cadmium acetate and cadmium chloride processes viz. concentrations, temperature, pH and reaction time were varied to determine optimum conditions for the growth of good quality CdS layers. In the conventional method where no buffer solution is used, larger fraction of the available ammonia is hydrolyzed to form ammonium and hydroxyl radicals. The hydroxyl radicals react readily with cadmium ions to form cadmium hydroxide. It also hydrolyses thiourea giving out sulphur ions. The overall effect is a faster reaction between cadmium and sulphur ions increasing the rate of CdS formation. At high reaction rates, the homogeneous reaction in the solution was found to result in particulate formation leading to inferior films. Growth with the buffer solutions proved effective in limiting the homogeneous reaction by slowing down the release of cadmium ions into the solution and thus favoring the heterogeneous ion-by-ion growth of smooth CdS layers. Figure 1a compares the optical properties of CdS films grown with and without the buffer solution. Heterogeneous growth was found to depend critically on the availability of nucleation sites on the substrate. Thus growth on plain glass substrates was extremely slow and patchy whereas the growth was steady and uniform on a SnO<sub>2</sub>:F coated glass or Si/SiO<sub>2</sub> substrates. Conformal CdS layers with good optoelectronic properties were obtained on SnO<sub>2</sub>:F coated glass substrates at slow rates of deposition. Very thin (~500 Å) CdS layers are preferred in CuInSe<sub>2</sub> solar cells while somewhat thicker (2,500 Å) layers are more suitable in CdTe solar cells. Films in the required ranges of thicknesses with excellent optical properties were obtained by varying the growth parameters, e.g. deposition time (Fig. 1b). This work resulted in a M.S. thesis of a UCF student.

### **Fabrication of Multichamber Coating Unit**

A multichamber vacuum coating system was fabricated. It has a 6" six-way cross chamber pumped by a corrosion resistant, hybrid turbomolecular pump with a molecular drag stage; and another 18" diameter chamber pumped with a cryopump having a large argon-pumping capacity for sputtering applications. A third six-way cross has been provided for post-deposition annealing in the presence of plasma. The six-way crosses with ultra-high vacuum type oxygen-free-high conductivity copper gaskets were chosen for obtaining clean hydrocarbon-vapor-free conditions and easy access from all sides for installation of sputter-guns, gas lines, pumps, gauges, substrate heating and biasing. The larger 18" diameter chamber has been provided with three sputtering targets of Mo, Cu, and In, and an evaporation source. The volumes of the chambers dictated the pumping speeds of fluoro-carbon lubricated mechanical pumps and roughing lines utilized for obtaining vacuum of  $<4 \times 10^{-2}$  Torr in 3-4 minutes. The effective pumping speeds of high vacuum pumps were chosen for obtaining base pressure  $<10^{-6}$  Torr utilizing the surface areas and instantaneous degassing rates of chamber walls and components. A liquid nitrogen baffle was fabricated and installed in the 6" six-way cross chamber so as to provide partial protection to the gate valve and the vacuum pumps from high vapor pressure materials viz. Cd and Te.

### **CuInSe<sub>2</sub> Thin Films**

Thin films of Mo, Cu, and In were deposited on clean soda-lime glass substrates by DC

magnetron-sputter deposition. Sputtering gas pressure and plasma parameters were optimized to obtain requisite thicknesses of Cu and In in a reproducible manner. Investigations are continuing on the deposition of Mo back-contact layers. Arrangements have been made in the 18" diameter for sequential sputter-depositions of Mo, Cu, and In thin films without breaking vacuum.

### **CdTe Thin Films**

Experimental parameters have been optimized for the RF magnetron-sputter-deposition of Te thin films and DC magnetron-sputter-deposition of Cd thin films. A set-up for sequential sputter-deposition of Cd and Te layers has been installed in the six-way-cross chamber.

### **Materials Analysis**

Thicknesses of thin films and multilayers were measured by profilometry at UCF. Composition of the films and interdiffusion between layers were analyzed by energy dispersive x-ray spectroscopy and Auger electron spectroscopy at UCF, x-ray photoelectron spectroscopy at the Kennedy Space Center (KSC), and Rutherford backscattering at the University of North Carolina. Structure and morphology were studied by x-ray diffraction at KSC, and scanning electron microscopy at FSEC. Optical absorption spectroscopy was carried out at UCF and NREL. The electrical conductivities in the dark and under illumination were measured at UCF.

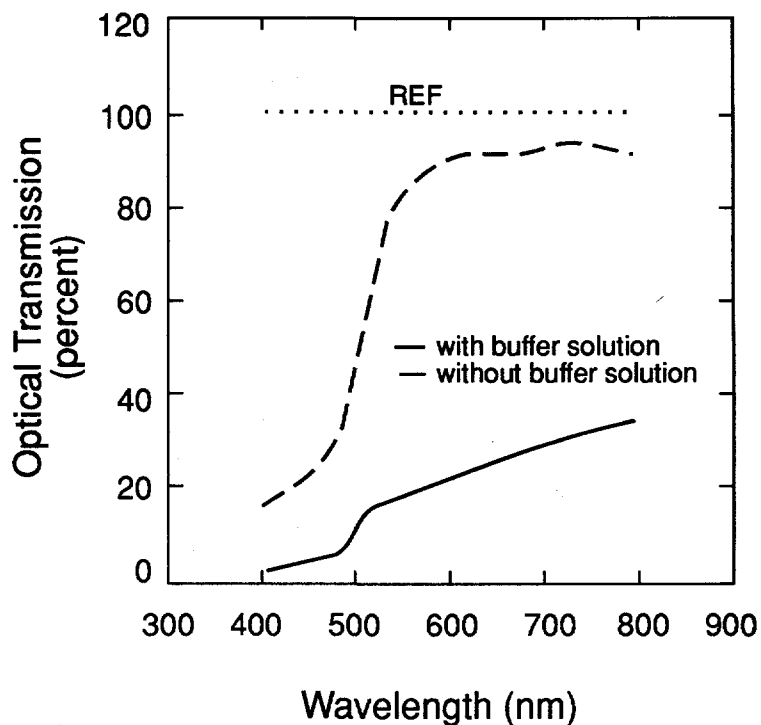
### **Device Fabrication**

During the initial phase, solar cells are being prepared based on the structures: CdS/CuInSe<sub>2</sub>/Mo/Glass, ZnO/thin CdS/CuInSe<sub>2</sub>/Mo/Glass, and Glass/SnO<sub>2</sub>/CdS/CdTe/Graphite:Cu. The photolithography is being carrying out at UCF.

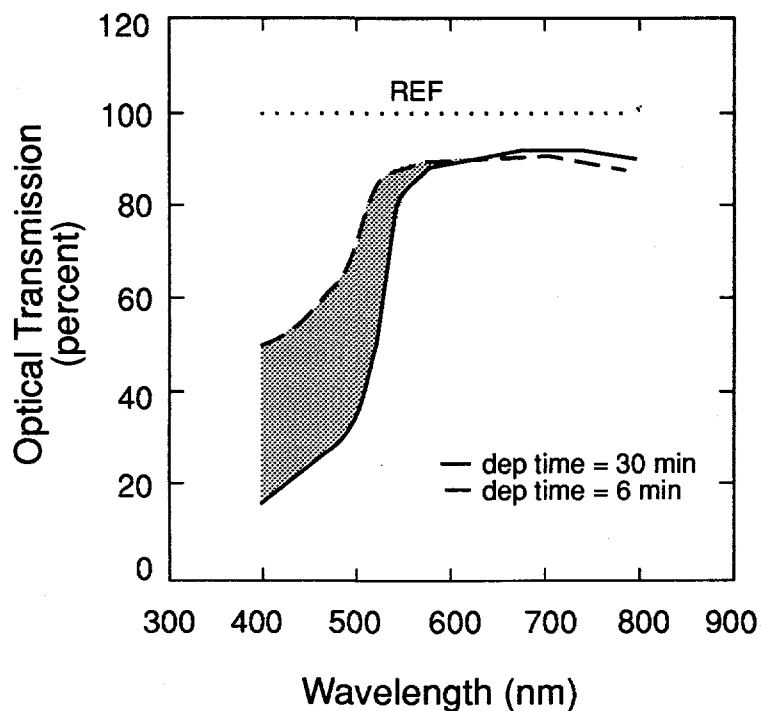
### **References**

\*Present address: Walt Disney Design and Engineering, Kissimmee, Florida.

1. N. G. Dhere, "Vacuum System Design of a Multichamber Metalorganic Magnetron Sputtering Unit", presented at the 21st Ann. Symp. Applied Vac. Sci. and Technol., Clearwater Beach, FL, Feb. 1992.
2. J. V. Santiago and N. G. Dhere, Design and Construction of Metalorganic Magnetron Sputtering System", presented at the 21st Ann. Symp. Applied Vac. Sci. and Technol., Clearwater Beach, FL, Feb. 1992.
3. D. L. Waterhouse and N. G. Dhere, "Solution-Grown CdS Layers for Polycrystalline-Thin-Film Solar Cells", presented at the Ann. Conf. of Am. Solar Energy Soc., Solar 92, Cocoa Beach, FL, June 1992.
4. J. V. Santiago and N. G. Dhere, "Plasma-Assisted Selenization of CuInSe<sub>2</sub> for Polycrystalline-Thin-Film Solar Cells", presented at the Ann. Conf. of Am. Solar Energy Soc., Solar 92, Cocoa Beach, FL, June 1992.
5. N. G. Dhere, "CuInSe<sub>2</sub> Polycrystalline-Thin-Film Solar Cells Prepared by Plasma-Assisted Selenization Without the Use of Toxic H<sub>2</sub>Se Gas", presented at the Ann. Conf. of Am. Solar Energy Soc., Solar 92, Cocoa Beach, FL, June 1992.



(a)



(b)

Figure 1. (a) Comparison of optical transmission spectra of CdS films grown with and without the buffer solution; (b) Optical transmission spectra of very thin and somewhat thicker solution grown CdS layers grown respectively in 6 min and 30 min.

**Title:** Development of High efficiency CdTe Solar Cells

**Organization:** School of Electrical Engineering, Georgia Institute of Technology, Atlanta, Georgia.

**Contributors:** A. Rohatgi, H.C. Chou, A.K. Bhat, S. Kamra

**Objective:**

The objective of this program is to improve the basic understanding of efficiency limiting mechanisms in polycrystalline CdTe cells, fabricate high efficiency CdTe cells, and provide guidelines for achieving CdTe cell efficiency above 15%.

**Film growth:**

CdTe films were grown by MOCVD at 400°C on CdS/SnO<sub>2</sub>/glass substrates supplied by Solarex Corporation. The Cd/Te ratio in the growth ambient was varied from 0.02 to 6 by controlling carrier gas flow rates and the temperatures of the bottles that contain the metallorganic precursors dimethylcadmium and diisopropyltellurium.

The CdS films on SnO<sub>2</sub>/glass substrates were grown using the solution growth technique starting with cadmium chloride, ammonium chloride and thiourea. We have recently started growing the CdS films at Georgia Tech. Process optimization is being done to increase uniformity and improve film quality.

**Cell fabrication:**

P-n CdTe cells were fabricated by treating the CdTe films with a CdCl<sub>2</sub>-methanol solution followed by an air anneal at 400°C for 30 minutes. Contact to p-CdTe was made by a sequential evaporation of 100 Å Cu and 400 Å Au followed by an anneal at 150°C in argon atmosphere for 90 minutes. Finally, bromine-methanol etch was performed on the entire structure to etch off any residual Cd and Te oxides. In selected instances the conventional 400°C furnace anneal for 30 minutes was replaced by rapid thermal processing at temperatures up to 700°C in controlled O<sub>2</sub>-N<sub>2</sub> ambient.

**Material and device characterization:**

Auger spectroscopy, spectral quantum efficiency, and photoluminescence measurements were made to characterize the devices.

**Results and discussion:**

The objective of doing Auger spectroscopy was to examine the atomic inter-diffusion at the CdS-CdTe interface. As can be seen in Figure 1, atomic inter-diffusion at the interface was maximum when the CdTe film was grown under Te-rich conditions. Cell efficiencies with Te-rich ambient were higher (10%-12%) in comparison with those for Cd-rich ambient conditions (7%-8%). The higher V<sub>oc</sub> under Te-rich conditions is possibly due to a reduction in the interface states. It was also found that the post-growth 400°C furnace anneal had no detectable effect on the atomic composition at the interface. As suggested in the literature [1], some inter-diffusion and the formation of solid solutions of CdS<sub>1-x</sub>Te<sub>x</sub> during annealing are possible. However, our results suggest that the compositional differences in the MOCVD grown films primarily stem from the



differences in the growth ambient.

Spectral quantum efficiency (SQE) data were collected from cells with CdTe films grown under different ambient conditions. Figure 2 shows the SQE data from cells in which the CdTe films were not treated with CdCl<sub>2</sub>-methanol solution. The data indicate that the effect of Te-rich ambient is to create p-type CdTe and a p-n junction at the CdTe-CdS interface. It appears that the absence of excess Te in the growth ambient creates a homojunction in the CdTe films which results in low SQE values at short wavelengths. SQE data of cells with CdCl<sub>2</sub> treated CdTe films indicate high collection efficiency for cells grown in Te-rich (Te/Cd mole ratio  $\approx$  6.0) and extremely Cd-rich (Te/Cd  $\approx$  0.02) conditions, but lower SQE for cells that were grown under an intermediate Te/Cd mole ratio of about 0.1 (See Figure 3a.). Moreover, under forward bias SQE drops less rapidly for the "Te-rich" CdTe cells as compared to that for the "Cd-rich" CdTe cells (Figure 3b). This is possibly due to fewer interface states at the CdS-CdTe interface resulting from the enhanced inter-diffusion at the interface in films grown in Te-rich ambient.

Some of the CdTe films fabricated under different Te/Cd mole ratios were studied using photoluminescence lifetime measurements in collaboration with Dr. Richard Ahrenkiel at the NREL laboratories. The PL measurements were performed at 295 K using 600 nm radiation from a pulsed laser. Table 1 contains the measured lifetimes from films grown under different conditions. The PL data show that the post-growth CdCl<sub>2</sub> treatment increases carrier lifetime. Additionally, Te-rich growth ambient gives higher lifetimes. These results clearly indicate that a Te-rich growth not only improves the interface quality and produces p-type CdTe, but also reduces bulk defects.

Treatment with CdCl<sub>2</sub>-methanol solution followed by a 30 minute anneal at 400°C in air has been routinely used by several groups to produce CdTe solar cells with efficiencies exceeding 10% [1,2,3]. Although this post-growth treatment is known to enhance grain regrowth and significantly improve cell performance, it is suspected that the presence of an excessive amount of CdCl<sub>2</sub> gives rise to chlorine related defect states that ultimately limit the cell efficiency [3]. By using Rapid Thermal Processing (RTP) instead of the conventional furnace annealing, it is possible to anneal the CdS-CdTe films at temperatures up to 700°C for short durations. We believe that the higher temperatures achieved will allow grain regrowth in the presence of lower concentration of CdCl<sub>2</sub>, and thus reduce the chlorine related defects. So far we have set-up the RTP system for CdTe solar cells and have made limited progress with cell efficiencies of about 8.2%. Process optimization with different RTP conditions is in progress.

Finally, using the in-house growth of CdS films on textured SnO<sub>2</sub>/glass substrates supplied by Solarex, we have recently achieved 11.5% to 12.0% efficient CdTe cells (Table 2). In-house CdS growth and optimization has not only improved the cell efficiencies, but also the yield.

#### **Conclusions:**

We have made an attempt to identify and understand some of the factors that affect the CdS-CdTe interface and the CdTe films in order to improve solar cell performance. It was shown that a Te-rich growth ambient allows more inter-diffusion at the CdS-CdTe interface, and increases carrier lifetimes in CdTe films. SQE and cell efficiency are also higher when a Te-rich ambient is used. More experimentation with different RTP conditions are required to find out whether the interface and bulk properties of the CdS-CdTe cells can be suitably modified to further improve the cell efficiencies.

**References:**

1. B.N. Baron, R.W. Birkmire, J.E. Phillips, W.N. Shafarman, S.S. Hegedus, B.E. McCandless, University of Delaware, Polycrystalline Thin Film Materials and Devices, annual report to SERI, March 1991.
2. T.L. Chu, University of South Florida, Final technical report to NREL, December 1991.
3. S.A. Ringel, A.W. Smith, M.H. MacDougal, and A. Rohatgi, J. Appl. Phys., 70 (1991) 881.

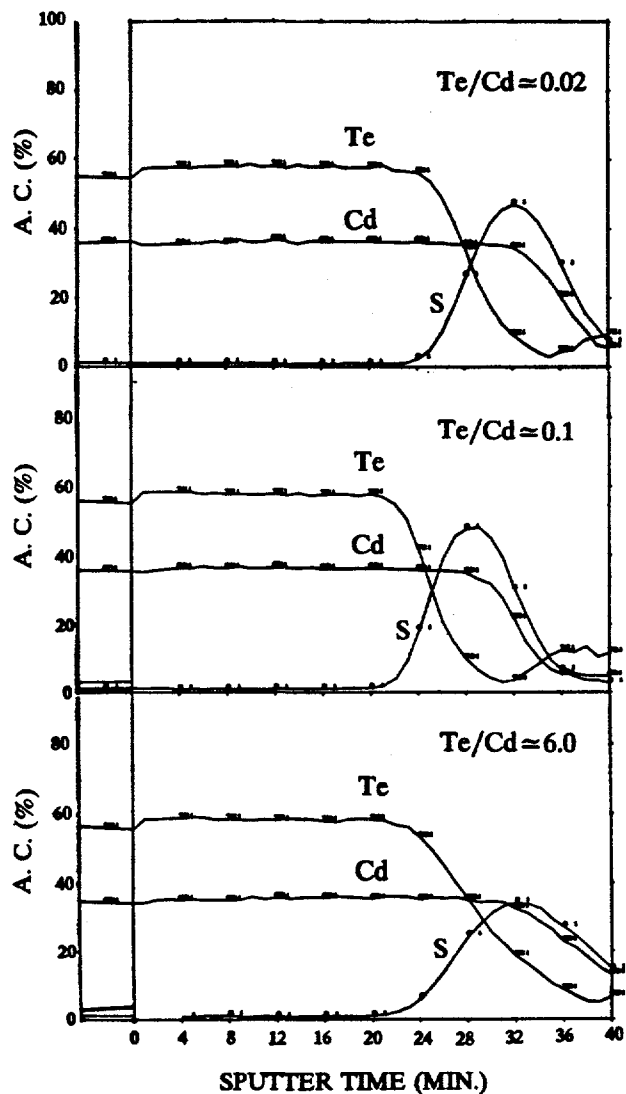


**Figure 1:** Auger data showing that inter-diffusion at the CdS-CdTe interface is maximum when the MOCVD growth is done in Te-rich ambient.

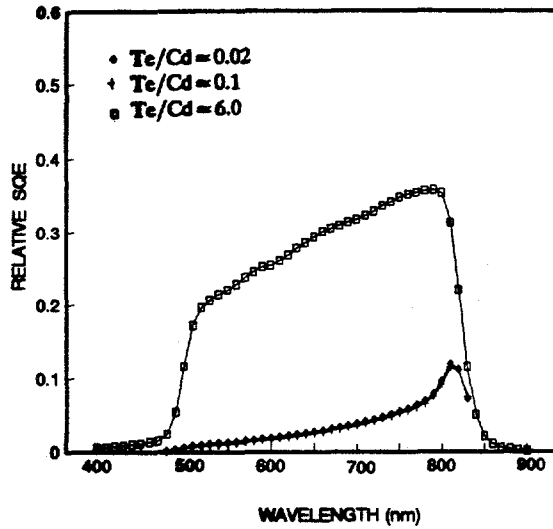


Figure 2: Relative SQE of cells in which the CdTe films were not treated with CdCl<sub>2</sub>-methanol solution.

Table 1: Photoluminescence lifetimes

Te/Cd mole ratio	CdCl <sub>2</sub> treatment	Lifetime (nsec)
0.02	No	0.116
0.1	No	0.121
6.0	No	0.153
0.02	Yes	0.201
0.1	Yes	0.210
6.0	Yes	0.236

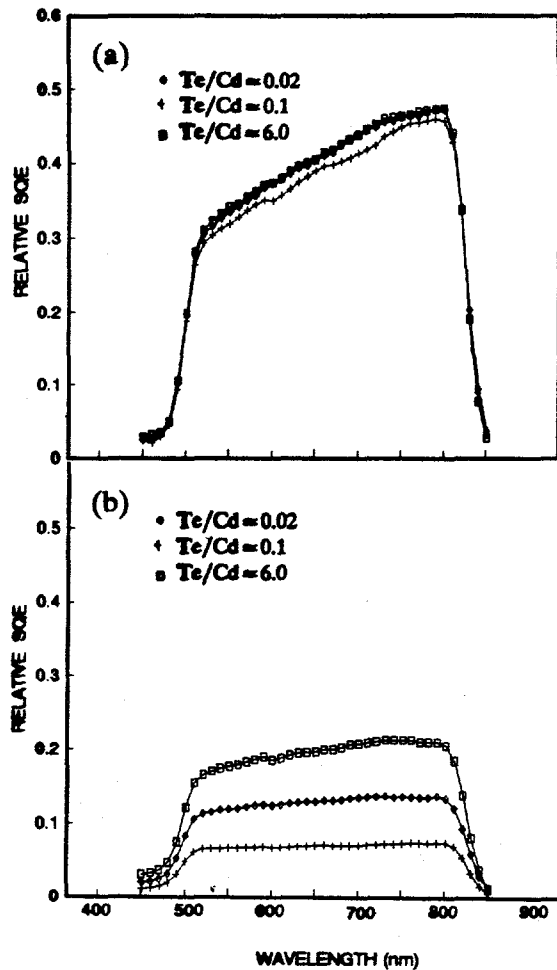


Figure 3: Relative SQE of cells with (a) zero voltage bias, (b) forward voltage bias of 0.6 V.

Table 2: CdTe cells tested at Georgia Tech

Cell ID#	V <sub>oc</sub> (volts)	J <sub>m</sub> (mA/cm <sup>2</sup> )	FF	η
A13-3-7	0.76	24.6	0.64	11.9%
A27-4-2	0.75	24.5	0.66	12.0%
A27-4-4	0.75	24.0	0.65	11.7%

**Title:** High-Efficiency, Large-Area CdTe Panels

**Organization:** Golden Photon, Inc., El Paso, Texas

**Contributors:** S.P. Albright, principal investigator; R.R. Chamberlin, and J.F. Jordan

### **Introduction and Objectives**

Golden Photon, Inc. is committed to the accelerated development of CdS/CdTe low-cost, high performance, saleable photovoltaic modules. Insuring state-of-the-art performance utilizing low-cost, large-scale manufacturing techniques for CdTe modules are the objectives of the primary efforts at Golden Photon, Inc.

### **Specific Goals For The Present Subcontract**

The specific objectives of this three year program are:

- \* To achieve active area efficiencies of greater than 14% on small cells,
- \* To achieve aperture area efficiencies of greater than 13% on 1 ft<sup>2</sup> modules,
- \* To achieve aperture area efficiencies of greater than 12.5% on 4 ft<sup>2</sup> modules,
- \* To achieve greater than 20-year module life (based on life testing extrapolations) with no greater than 10% efficiency degradation.

### **Experimental**

In order to meet the goals and milestones within this project at least five(5) basic tasks have been specified. They include:

- \* Windows, Contacts and Substrates (external device optimization)  
This task includes improvements to the CdS window layers, improvements in electroding, and improvements in module division and interconnection.
- \* Absorber Material (Internal device optimization)  
This task includes primarily the characterization, evaluation, and improvement of morphology effects of the CdTe,
- \* Optimization of Device Structure  
This task includes the electronic characterization and modeling of the device, and the development of improved device structures where applicable.
- \* Encapsulation  
This task includes the analysis and optimization of present methods, as well as the development of improved methods.
- \* Process Optimization  
This task includes optimization toward improved understanding and control of process parameters.
- \* Employee Safety Evaluation and Improvement  
This task includes the evaluation and improvement (where necessary) of monitoring program for Cd in the workplace, as well as evaluation and improvement (where necessary) of policies and practices affecting worker safety in the workplace,

## Results and Projections

A summary of the status of the development of CdTe/CdS devices and modules at Golden Photon, Inc. includes attained milestones such as the following:

- \* Efficiencies of 12.7% have been achieved on small area devices.
- \* Modules with areas of 929 cm<sup>2</sup> have been achieved with over 8% aperture area efficiency (active area up to approximately 9.5-9.9% efficiency)
- \* Modules with areas of 3716 cm<sup>2</sup> have been achieved with up to 21.3 watts, normalized via a pyranometer.
- \* Life testing at NREL (and GPI) shows that a percentage of modules are stable within measurement error. Optimization and design improvement continues.
- \* Irregularities have been observed to affect the accuracy of the measurements of cells and especially modules. They result from an inability to instantaneously equilibrate to an existing or changing bias condition.

### One Square Foot and Four Square Foot Module Efficiencies

Two 30.5 cm x 30.5 cm modules (929 cm<sup>2</sup>) were sent to NREL in September 1991. [1] They represent some of the highest active-area efficiency CdS/CdTe modules yet developed at GPI. It was concluded that GPI has attained aperture area efficiencies on modules between 7.6% and 8.3% on 929 cm<sup>2</sup> modules. Due to some questions regarding measurement issues, a range is reported. Active area efficiencies are rather high, due to poor utilization of module area (non-optimized interconnection losses). Active area efficiencies on similar 929 cm<sup>2</sup> modules have been observed at GPI with up to 9.4-9.9%. Interconnection optimization, uniformity across the modules and improvement of the fill factor should result in significant improvements in module output in the relatively near term.

A 61 cm x 61 cm module (3716 cm<sup>2</sup>) was tested at NREL in November, 1991, with a corrected output (to 1000 watts/m<sup>2</sup> using a pyranometer reading) of 21.3 W. Present efforts at GPI are directed toward achievement of improved module outputs on this size (61 cm x 61 cm) substrate.

### Reliability Status

Figures 1 and 2 shows life testing data from the group of submodules delivered to NREL and life tested for the longest over the past several years. [2] Due to both sample variations and the size of the measurement error bars, the life testing results have not been homogeneous. Over different sets, some have appeared to degrade somewhat; several have shown no signs of degradation within the estimated measurement error limits. However, without smaller error bars, conclusions are difficult to draw. Lot-to-lot and module-to-module variabilities have been traced primarily to quality assurance issues.

The fact that a number of modules have shown no significant degradation indicates that there is no inherent degradation problem associated with the GPI CdTe modules. As further improvements to the encapsulation design and methods as well as module measurement techniques are made, reliable module lifetimes are expected to become more homogeneous and are expected to show excellent continuing reliability on both real time and accelerated life tests.

### Performance Measurement Issues

A quite visual demonstration of a pre-bias sensitivity observed during measurements of these devices and modules is provided by some experimental work by K.Emery as shown in Fig. 3.[3] Notice the slowness of the response re-equilibration after each change in pre-biasing condition. Also notice the reversibility of this effect. With relaxation times such as this it is no surprise that difficulty has been encountered in accurately measuring such modules. It appears quite necessary to incorporate a maximum power point tracking algorithm and/or maintain the voltage bias on the modules near the maximum power point voltage in order to insure that sufficient voltage bias equilibration is attained prior to actually taking a current-voltage performance curve. This and other issues affecting measurement accuracy (i.e. spectral and temperature issues) continue to be addressed.

The performance testing procedure for CdS/CdTe modules has been suggested to include at least the following:

- \* Insure that pre-bias at the maximum power point is adequate
- \* Scan from + to - during voltage ramp
- \* Control the module (and reference) temperature during testing  
(Once accurate module temperatures are able to be measured and once accurate temperature coefficients are determined, then a measurement and correction procedure will allow more practicality)
- \* Use a CdTe submodule (Standardized at NREL) as outdoor insolation reference in order to avoid spectral issues.
- \* Recalibrate reference on a regular basis.

### **CONCLUSIONS AND FUTURE PLANS**

Progress has been made, and advancement is expected to proceed in an accelerated fashion through Phase 3 of this subcontract and beyond. The results should approach or exceed the proposed milestones.

The most important areas under the next phases of this subcontract are:

- \* Continued development of efficiencies on small devices.
- \* Continued efficiency improvements (both active area and aperture area) on 929 cm<sup>2</sup> and 3716 cm<sup>2</sup> modules.
- \* Continued efforts in encapsulation design and the quality control steps of the encapsulation assembly sequence.
- \* Continued and expanded life testing at both NREL and GPI to insure quality and longevity.
- \* Continued efforts towards low-cost manufacturing of modules

### **REFERENCES**

1. Report # 9203, NREL Advanced Systems Outdoor P.V. Test Facility, November 3, 1991.
2. D.Waddington, Personal Communication, 9/11/92.
3. K.Emery, NREL, Personal Communication, 8/19/91.

## Life Test Data For 6711-3, 6711-6, 8905-5

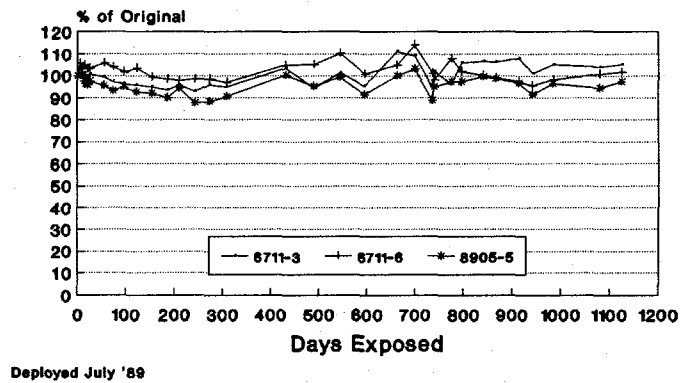


Fig. 1

## Life Testing of #178, #200, #AA961 From NREL

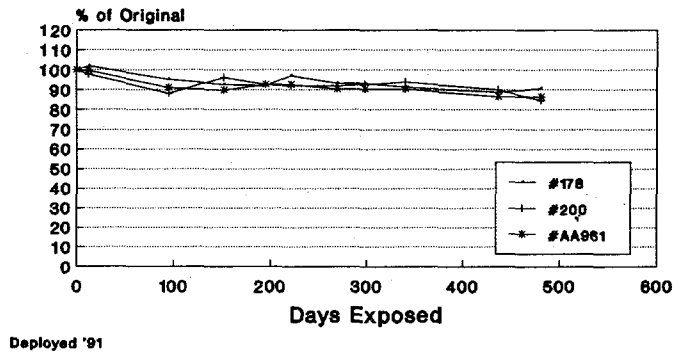


Fig. 2

## RELAXATION CURVES For Pre-Biased Conditions

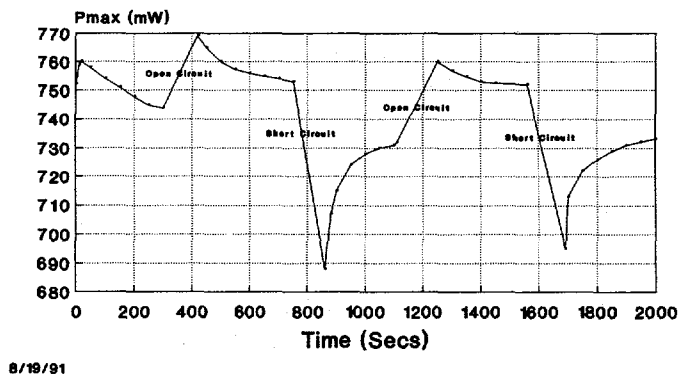


Fig. 3

**Title: Low-cost CuInSe<sub>2</sub>, Submodule Development**

**Organization: International Solar Electric Technology (ISET),  
8635 Aviation Blvd., Inglewood, CA 90301**

**Contributors: V.K. Kapur, program manager; B.M. Basol, principal investigator;  
A. Halani, C.R. Leidholm and A.J. Minnick**

The objectives of this program are the fabrication of 0.09 m<sup>2</sup> (1 ft<sup>2</sup>) area CuInSe<sub>2</sub> (CIS) submodules using the selenization technique and development of novel, non-vacuum processes for CIS thin-film deposition. In our FY 1991 report, we had described a novel approach to Cu-In precursor preparation that after selenization, yielded highly uniform CIS films and 12.4%-efficient devices. In that work we utilized an E-beam evaporation/selenization approach to process small-area samples. During this period, we activated our 0.09 m<sup>2</sup> (1 ft<sup>2</sup>) processing facility and obtained large-area, monolithically integrated submodules.

### **Large-Area Processing**

Details of the selenization technique used in this work and the device fabrication steps have been previously described and will not be repeated here [1,2]. In summary, the Cu-In precursors were sputter-deposited onto Mo-coated soda-lime glass substrates. Selenization was carried out at around 400°C in a H<sub>2</sub>Se atmosphere. After the selenization step, CIS films were coated with a thin (1000-2000-Å) CdS layer using the solution-growth technique. This step was then followed by the deposition of a ZnO window layer using the MOCVD method. For some devices, an Al grid was evaporated onto the ZnO window to form the top contact. No fingers were employed in the monolithically integrated module structures.

Modules with areas measuring up to 0.09 m<sup>2</sup> (1 ft<sup>2</sup>) were fabricated on soda-lime glass substrates. The first step in fabrication process was the formation of the back electrical contact. This was accomplished by sputtering a 1-2-µm-thick Mo layer on a glass sheet. The Mo layer was then laser-scribed to produce 52 electrically isolated segments measuring approximately 0.5 cm x 30 cm. After cleaning the surface of the substrate, a 100-200-Å-thick Te film was deposited on the MO layer. This was then followed by the deposition of an In and a Cu film using the D.C. magnetron sputtering technique. Selenization was carried out in a reactor that could accommodate multiple 0.09 m<sup>2</sup> (1-ft<sup>2</sup>) substrates. Cell integration was accomplished by a series of film depositions and mechanical scribes as described below.

First, a 1000-2000-Å-thick layer of CdS was deposited on the CIS layer using the dip coating method. A 2-3-mil-wide channel was then scribed in the composite film to expose the Mo contact along the edges of the Mo segments. A layer of doped ZnO was then applied by MOCVD to form the top electrode and to make the electrical connection, through the scribes, with the lower Mo contacts. Module integration was completed by making a final isolation scribe through ZnO/CdS/CIS layers. Both of the latter scribes were made using a mechanical scriber.



It should be noted that these modules represent our first attempt to process large-area devices using the sputtering technique. During the last 6 months, we have fabricated several modules with aperture areas close to  $0.09 \text{ m}^2$  (1-ft<sup>2</sup>) and power outputs of about 3 W. These early devices generally suffered from a poor fill factor, which was typically around 40%-45%. Analysis of small-area devices cut from the  $0.09 \text{ m}^2$  (1-ft<sup>2</sup>) samples indicated that there was a non-uniform distribution of stoichiometry over the substrate. In our process, the CIS layer is formed by selenizing a Cu-In alloy. Use of the Te/In/Cu deposition sequence and the high energy sputtering process produces a well-alloyed Cu-In precursor. However, stoichiometric uniformity is a strong function of the thickness distributions of the individual Cu and In deposits over the  $0.09 \text{ m}^2$  (1-ft<sup>2</sup>) substrate. We have carried out some experiments to determine stoichiometric uniformity of the Cu-In precursors before they were selenized. In these experiments, large-area substrates were cut into small pieces, and the Cu-to-In ratios of each piece were determined using Atomic Absorption Spectroscopy. Figure 1 shows the distribution of Cu/In molar ratios across a  $0.09 \text{ m}^2$  (1-ft<sup>2</sup>) area. From this figure, it is clear that, after selenization, certain portions of the module fabricated on such a precursor would have stoichiometric ratios very close to or larger than 1.00, and this would limit the performance of the overall module. It should be noted that the intended Cu-to-In ratio range for this specific sample was 0.9-0.96. This, we believe, is an equipment related issue that we will correct. Variations in the magnetron cathode deposition rates along the length of the target causes the observed stoichiometric variations. We have fabricated small-area (about 40-cm<sup>2</sup>) submodules of better uniformity with about 7.5% efficiency.

### Non-vacuum Processing

CIS is a very promising photovoltaic material. However, processing techniques available to deposit thin films of this compound for solar cell applications are rather limited. Although many of the deposition approaches that proved successful for CdTe solar cell processing (such as spraying, screen printing, and electrodeposition) have also been tried for CIS, they have not yet been successful. This, to a large extent, is due to the formation of secondary phases in the deposited CIS film. The two techniques that yielded high-efficiency CIS solar cells are the selenization technique and vacuum evaporation. Both of these approaches involve vacuum processing. Therefore, the aim of our study was to demonstrate the feasibility of CIS processing via a low-cost, non-vacuum approach. We have achieved this goal and demonstrated, for the first time an over 10%-efficiency solar cell on a CIS film prepared completely by a non-vacuum technique. The illuminated I-V characteristics of this device, as measured by NREL are shown in Fig. 2. Processing details of this technique will be made available after we receive patent protection.

### References

1. V.K. Kapur, B.M. Basol and E.S. Tseng, Solar Cells (1988) 69.
2. B.M. Basol, V.K. Kapur and A. Halani, Proc. 22nd IEEE Photovoltaic Specialists Conf., IEEE, New York (1991) 893.

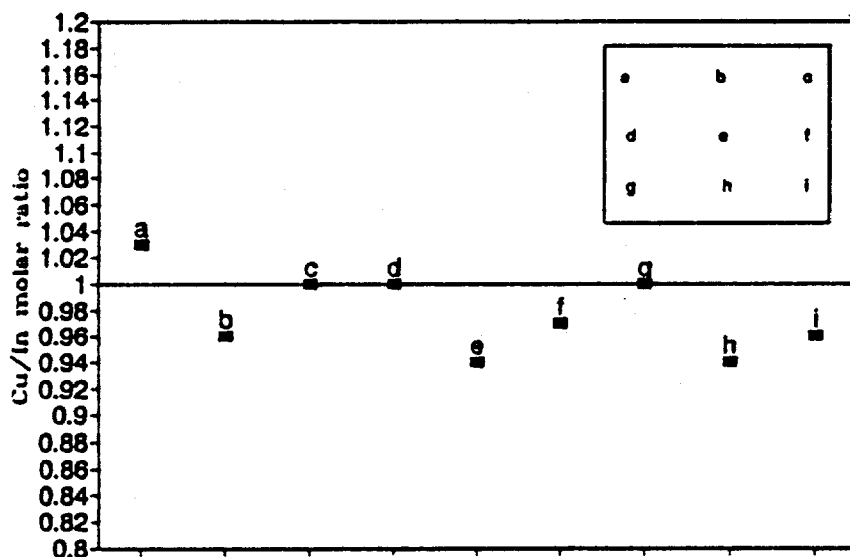


Fig. 1 Cu-to-In molar ratio at various points on a 1 ft<sup>2</sup> substrate.

Sample: R297B-1      Temperature = 25.0°C  
 Aug. 14, 1992 10:20 am      Area = 0.0896 cm<sup>2</sup>

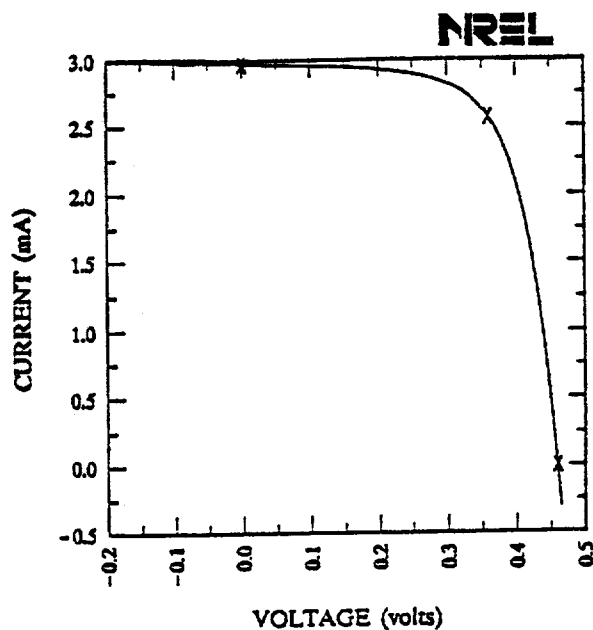


Fig. 2 Illuminated I-V characteristics of a CIS cell made on a film obtained by the non-vacuum technique.

**Title:** Innovative Sputtering Techniques for CIS and CdTe Submodule Fabrication

**Organization:** Martin Marietta Astronautics Group

**Contributors:** J.H. Armstrong, Principal Investigator, B.R. Lanning, W.C. Moshier, E.C. Jelks, J.L. Draper, M.S. Misra

## **OBJECTIVES**

This project, Innovative Sputtering Techniques for CIS and CdTe Submodule Fabrication, consists of two sequential 12-month phases. Objectives of this project are the following:

- (1) To develop large-area deposition technology using rotating cylindrical magnetron sputtering for polycrystalline thin-film CdTe and CIS photovoltaics, and
- (2) To produce CIS modules up to 930 cm<sup>2</sup> (1 ft<sup>2</sup>) using state-of-the-art deposition and cell definition technologies with potential for production scaleup and low-cost fabrication.

## **APPROACH**

This project, initiated in September of 1991, utilizes a dual rotating cylindrical magnetron (C-Mag™) from AIRCO, Inc. to sputter thin films to fabricate copper-indium-diselenide (CIS) and cadmium-telluride (CdTe) photovoltaic devices over large areas. Key advantages from the unique geometry of the rotating C-Mag™ include (1) more efficient target utilization and (2) more efficient target cooling [1,2]. These advantages lead to significantly higher deposition rates compared to conventional planar technology. Furthermore, the close proximity of the targets can lead to unique cosputtering processing and reduced equipment cost (a dual C-Mag™ inhabits the same space as a single planar magnetron). Systems handling substrates as large as 3.5 m x 6 m have been built for architectural glass.

Three tasks are identified in this project, namely,

Task 1: Thin-Film Deposition

Task 2: Device Manufacture and Scaleup

Task 3: Monolithic Integration for Submodule Fabrication

Task 1, which began at the beginning of the project, has been completed. Task 2 began six (6) months after authority to proceed (ATP) and continues through the end of Phase 2. Task 3 began at the start of Phase 2 and will continue through the end of the program. Below is a brief description of these tasks.

### **Task 1 — Thin-Film Deposition**

A key issue for the commercialization potential of polycrystalline thin-film photovoltaics is low-cost, large-area deposition techniques with potential for large-volume production. Many deposition techniques produce high-quality devices but do not exhibit high compositional uniformity over large areas. Other techniques can result in large-volume production but has not exhibited high-efficiency devices.

Of the myriad of thin-film technologies available, two appear to be the most promising in terms of deposition efficiency, large-area film uniformity, and potential for high-volume manufacturing. Magnetron sputtering offers proven large-area deposition with good film uniformity. Electrodeposition, the second technique, offers the advantages of very low-cost capital investment, as well as the potential for large-area deposition. Furthermore, electrodeposition can produce films of uniform thickness and composition and lends itself easily to *in situ* intelligent processing technologies. In this task, a custom-design sputtering chamber was fabricated to accommodate the Model 940 Dual C-Mag™ and electrodeposition was used to supplement sputtering for manufacturing CdTe devices.

In all cases, films are subjected to extensive material testing to quantify and correlate fabrication and performance parameters. Material testing such as glancing incidence diffractometry (GID), fast Fourier transform infrared spectrometry (FTIR), atomic absorption (AA), Auger electron spectroscopy (AES), scanning electron microscopy/energy dispersive X-ray spectroscopy (SEM/EDX), spectrophotometry, and reflection measurements shall be performed. Adhesion and electrical conductivity measurements will also be conducted to optimize performance of these films.

**C-Mag™ Magnetron Sputtering** — A unique solution to the problems of inefficient target material utilization and difficulty in deposition materials with low melting temperature is to make the target move with respect to the magnet assemblies. Such a solution is the rotating cylindrical magnetron as shown schematically in Figure 1. In this geometry, the targets are cylindrical and hollow to accommodate both cooling water and magnets. High-temperature seals at both ends of the target allow it to be rotated about its primary axis by a DC drive motor. High-strength iron-neodinium-boron (Fe-Nd-B) permanent magnets, which are used to define the race-track, are held in place near the surface of the target parallel the target's primary axis.

**Electrodeposition** — Electrodeposition is another thin-film deposition technique with promise of large-area, large volume production. Some work has been done on electrodeposition of thin films for PV [3]. In principal, the codeposition of two metals is the same as the deposition of a single metal, whereby the passage of a high current density in a bath of the mixed metallic salts will result in a deposit of the two metals. Unfortunately, deposits obtained under high current density are porous, nonadherent, and in most cases compositionally inhomogeneous. To codeposit two metals effectively, conditions must be optimized for depositing the less-noble metal without employing an excessive current density.

**Chemical Immersion Deposition of CdS** — Cadmium sulfide (CdS) is used in both the CIS and CdTe cell configuration as the n-type window layer. Thin films of CdS are commonly prepared by vacuum evaporation, sputtering, and spray pyrolysis although another inexpensive method for preparing thin films of CdS is by a chemical solution growth technique. In this method, CdS can be prepared by decomposition of thiourea (or thioacetamide) in an alkaline solution of cadmium salts where the salt can be CdSO<sub>4</sub>, Cd(NO<sub>3</sub>)<sub>2</sub>, or CdCl<sub>2</sub>. Substrates are immersed in a pH-adjusted salt solution at temperatures less than 90°C, and upon the addition of thiourea, CdS indiscriminately deposits on properly activated surfaces.

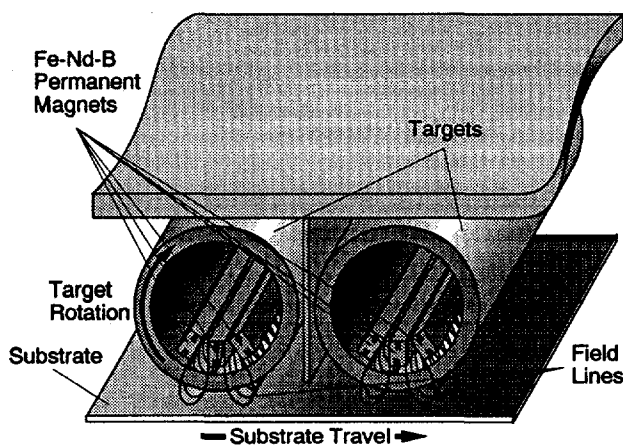


Figure 1 — Schematic of Dual Rotating Cylindrical Magnetron.

## Task 2 — Cell Fabrication and Scaleup

Task 2 utilizes techniques developed in Task 1 to produce CIS and CdTe devices and to scaleup deposition for implementation in submodule fabrication. Basic cell structure is TCO/CdS/CIS/Mo/glass and glass/TCO/CdS/CdTe/back contact for CIS and CdTe respectively. Initial cells are 1 mm<sup>2</sup> to develop fabrication techniques with scaleup to 1 cm<sup>2</sup>. Although the bulk of devices manufactured in this task will be made with two-step CIS processing from ISET [4], other innovative selenization [5] and cosputtering techniques will be used when appropriate. Material characterization of these devices will follow those outlined in Task 1. In addition, devices are to be characterized by light/dark I-V response, capacitance, thermal response and spectral response. From these data, devices will be optimized.

## Task 3 — Monolithic Integration for Submodule Fabrication

Data obtained in Tasks 1 and 2 will be combined with monolithic integration techniques developed by Martin Marietta IR&D project D-17R, Photovoltaic Technologies, to produce monolithically-integrated submodules from either CIS or CdTe. Both photolithography and laser scribing will be investigated for scribing the back contact, p-n stack, and the TCO for device definition. Cells will be nominally 0.5 cm wide and will run the length of the substrate. Early demonstrations of monolithic integration will be performed on small-area devices (5 cm x 5 cm) and scaleup of all processes will lead to a 930 cm<sup>2</sup> submodule. Particular care will be taken in testing and evaluation of the interconnect region. Submodules of 15 cm x 15 cm or less will be tested with an X-25 light source in AM1.5 insolation, while tests on larger modules will be conducted at NREL.

## RESULTS

**C-Mag Sputtering** — A photograph of the Martin Marietta C-Mag<sup>TM</sup> sputtering system used in this investigation is shown in Figure 2. Cathodes powered by 10 kW DC power supplies are mounted onto a swinging door which facilitates easy access for cleaning and maintenance. A mechanical pump serves to rough out the chamber, while a turbo pump was selected for clean high vacuum down to 10<sup>-7</sup> Torr. A liquid nitrogen Meissner trap is installed to minimize contamination of the turbopump by heavy metal vapor (Cd, Se) which could be potential hazardous. Constant substrate speed is maintained by a high-speed stepper motor with gear reduction. All aspects of the sputtering operation are controlled by microcomputer.

Several types of C-Mag targets were studied to reduce material costs. Preliminary tests with target material plasma-sprayed onto stainless steel backing tubes indicated that purity and density would be an issue. Consequently, cast targets were selected. In the case of materials whose structural integrity would be insufficient to withstand the operational parameters of the C-Mag, such as indium and selenium,

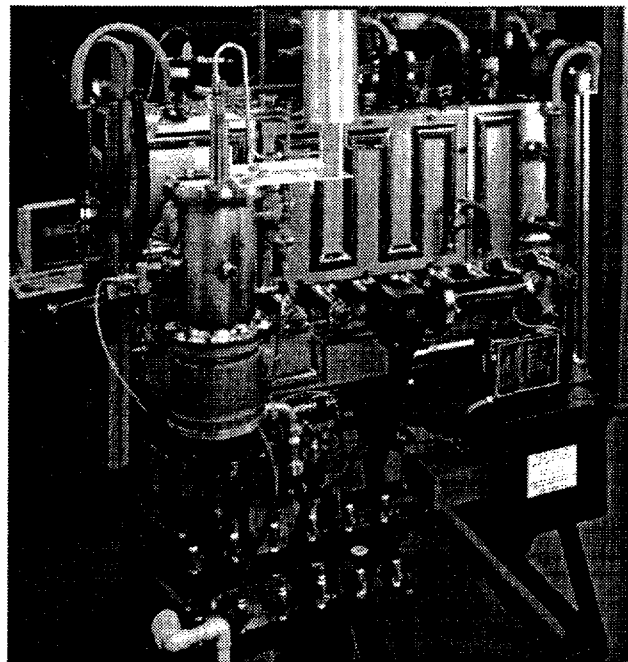


Figure 2 — Photograph of Martin Marietta C-Mag Sputtering System.

targets were cast around a stainless steel backing tube which contained the mounting threads, seal mating surfaces, and the virtual leak bleed slots of a target. In each case, target material purity was a minimum of 99.99%. Targets of 99.95% molybdenum and 99.99% copper were cast into a solid billet and machined to tolerances cited by AIRCO for their targets.

**Film Uniformity of C-Mag Sputtered Films**— Film uniformity with the C-Mag sputtering system over a 30.5 cm x 30.5 cm (12 in. x 12 in.) was studied by depositing 400 Å of copper which corresponded to an optical density of 1.0. Variations of the optical density over the surface is shown in Figure 3. Maximum variation in the optical density was 3.6% which was due to nonuniformity of substrate plate speed. Subsequent tests conducted at Martin Marietta under another program identified plate weight as a key issue with substrate speed variations and a titanium plate is being fabricated to eliminate this issue.

Prepared substrates were heated to a minimum of 120°C, and to ensure a clean target surface, Operating pressure for the Mo deposition was set at 7.5 millitorr by adjusting the throttle valve on the turbopump to control vacuum conductance. The combination of substrate preheating resulted in significantly higher film adhesion. Tape tests using Kapton tape burnished onto the film resulted in the removal of adhesive from the tape. No pinholes on the surface of the film were observed from transmission optical microscope studies. Also, the higher purity of the cast Mo target (99.95%) resulted in a much lower resistivity film (30 mΩ — 40 mΩ).

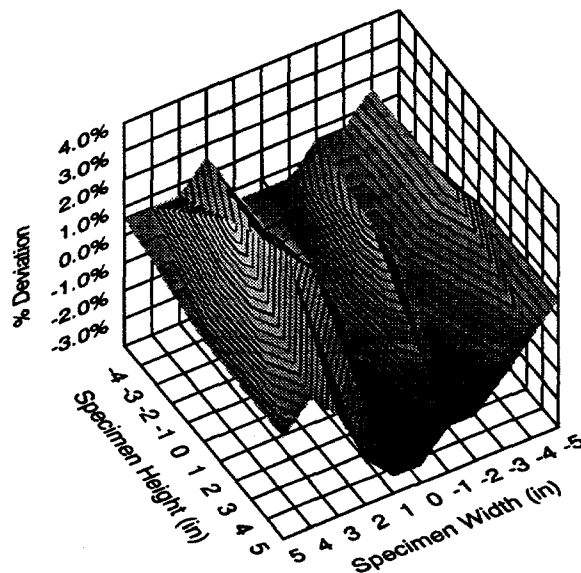


Figure 3 — Optical Uniformity of C-Mag Sputtered Cu Film Over 12 in. x 12 in. Area.

Cu and In films were also deposited onto the highly-adhesive Mo-coated glass. Cu films were deposited at 8.2 mT to 8.6 mT operating pressure at different substrate speeds. Depositing indium films by the Martin Marietta C-Mag system was far more difficult, however. Original tests conducted at 2 kW appeared to deposit material at a significant rate, but an apparent flaw at the In/backing tube interface caused a momentary separation of the In after several thermal cycles which resulted in localized melting. A new vendor-supplied In target resolved interfacial issues, resulting in significant increases in deposition rate. A three order of magnitude increase in deposition rate of In was observed for C-Mag sputtering compared to in-house planar tests.

Once compositional variations due to In target/film density were identified and addressed, glass/Mo/Cu/In stacks were selenized at ISET by the two-stage process which involved a 400°C, 30 minute heat treatment in a H<sub>2</sub>Se atmosphere. Once again, films appear to be Cu-rich, although the films themselves were measured to be In rich. A variation of the stack geometry involved glass/Mo/In/CuIn where the CuIn cosputtered stack was used to guard against In loss which would result in a Cu-rich film. These films exhibited good resistivity and were subsequently identified for further fabrication of devices.

In order to assess the effects of H<sub>2</sub>Se upon the interfacial integrity of the CIS devices, some films were selenized using the Se-vapor selenization techniques developed by NREL [5]. A variety of configurations were tested, including glass/Mo/Cu/In, glass/Mo/In/Cu,

glass/Mo/In/Cu/In/Cu, and glass/Mo/In/CuIn. As was the case in the H<sub>2</sub>Se case, In loss was evident. Consequently, the best results were obtained when glass/Mo/Cu/In stacks were annealed in an Ar atmosphere at 130°C for 30 minutes to promote alloying of the Cu and In. Cu/In sandwiches tried later in the evaluation appeared to be extremely copper lean, making it extremely difficult to manufacture devices with sufficient adhesion for analysis. However, films with adequate adhesion and reasonable film conductivity were also used in device fabrication.

Poor adhesion at the Mo-CIS interface and discoloration of the Mo films exposed by removal of CIS layer was quantified by X-ray diffraction on specimen C-147. As shown in Figure 4, selenization of the underlying Mo films was observed by the appearance of Mo<sub>3</sub>Se<sub>4</sub> and Mo<sub>15</sub>Se<sub>19</sub> phases. In addition, a Mo<sub>4</sub>Se<sub>5.33</sub> high-temperature phase was observed as well, but it is not yet known if this phase is present at the surface or in the bulk of the film. Glancing incidence diffractometry will be used in subsequent investigations to identify the nature of this film, as well as stress analysis of the Mo films.

**CIS Device Fabrication** — Films from H<sub>2</sub>Se selenization with sufficient adhesion and low electrical conductivity (Cu-lean) were used in device fabrication. Results from the H<sub>2</sub>Se selenized films provided the best response with an efficiency of 8.4% total area (Fig. 5). These devices displayed a respectable 66.57% fill factor and a 29.18 mA/cm<sup>2</sup> current density. V<sub>oc</sub> of this device was low at 0.4317V. Other devices on the same substrate were also tested, with the lowest efficiency of the batch at 7.7%, indicating a good uniformity across the substrate.

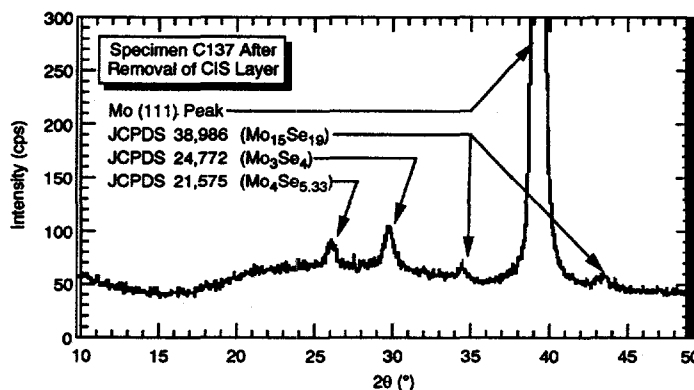


Figure 4 — X-Ray Analysis of Mo Film Beneath Poorly-Adhering CIS Layer Indicating Selenization of Mo Back Contact.

Sample: MM/ISET-1      Temperature = 25.0°C  
 Aug. 26, 1992 12:18 pm      Area = 0.0887 cm<sup>2</sup>

Fill Factor	=	66.57%
Efficiency	=	8.4% (total area)
V <sub>oc</sub>	=	0.4317 V
I <sub>sc</sub>	=	2.590 mA
J <sub>sc</sub>	=	29.18 mA/cm <sup>2</sup>
P <sub>max</sub>	=	0.744 mW
I <sub>max</sub>	=	2.277 mA
V <sub>max</sub>	=	0.3269 V

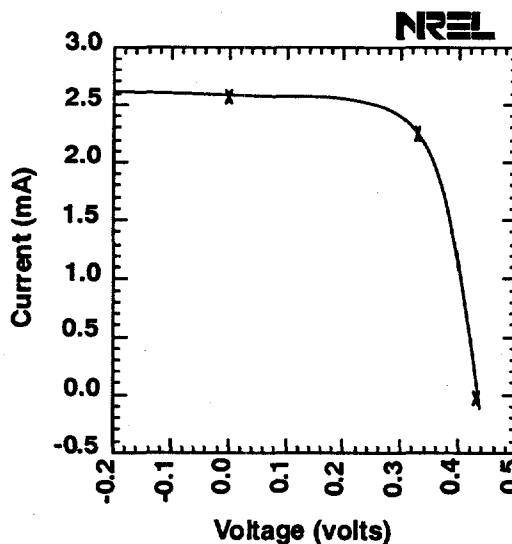


Figure 5 — Performance of CIS Device Manufactured by ISET Two-Step Process from C-Mag Sputtered Films.

Other CIS devices were manufactured from the Se-vapor selenized films. Se-vapor devices posted a respectable 7.45% efficiency with a fill factor of 64.9%. In both the  $H_2Se$  and Se-vapor selenization, processing parameters were not optimized for the CIS films. Consequently, the processing parameters are being optimized during the second phase of the contract.

**CdTe Films** — Since the development of each film and its interaction with the over and underlying film(s) constituted a research task in itself, the results from this development effort will be presented in terms of each of the constitutive elements or films in the cell. For the superstrate configuration, this involved the following stacked sequence: 1) rigid glass substrate 2) transparent conductive oxide, 3) CdS window layer, 4) CdTe absorber layer, and 5) back contact (i.e. back surface field). TCO-coated glass substrates were supplied and therefore results from the first task was divided into just the CdS window layer and CdTe absorber layer development tasks.

**Solution-Grown CdS** — Based on preliminary results from work completed under IR&D (D-17R), i.e. development of stability/distribution diagrams which defined CdS precipitation equilibria as a function of cadmium and complexing ion (ammonia) concentration, solution-grown CdS films were deposited onto ITO-coated glass substrates. Films, with uniform thicknesses ranging from 200 to 3800 Å, were deposited onto substrates with areas up to 930 cm<sup>2</sup> (1 ft<sup>2</sup>). Coating thicknesses across a 930 cm<sup>2</sup> (1 ft<sup>2</sup>) area were measured using surface profilometry and variations in the thickness were less than 5%.

By varying the specific solution chemistry and concentrations in the deposition bath, CdS films could be produced at rates between 500-4000 Å/hr, with specific crystallographic structures and orientations, and with little or no homogeneous precipitation in the bulk solution. Optical transmission, Auger Electron Spectroscopy (AES), and X-ray Diffraction (XRD) were used to evaluate the quality of the CdS films prepared in this manner.

Optical transmission was used to evaluate not only the light transmitting characteristics of the CdS, but the quality/integrity of the film. For example, in the presence of pinholes in the coating, the optical transmission at wavelengths below the 520 nm absorption edge increases above the low, flat response of a coherent, uniform film. This behavior is shown in the transmission spectrum presented in Figure 6. A typical spectrum for a uniform, continuous 1600 Å-CdS coating is given by curve (a) where the transmission decreases sharply to less than 10% for wavelengths less than 520 nm (transmission is through a glass/ITO/CdS substrate). The sharp increase in the transmission at 520 nm corresponds to the absorption edge for CdS. As the pinhole density increases and the film thickness remains constant, percent transmission will increase in the 300-520 nm range of the spectrum; this is shown by curve (b) where the observable pinhole density was much greater than the film of curve (a).

In addition to the pinholes, the optical transmission curve was used to qualitatively evaluate the impurity content of the film. Above 520 nm, there is usually an observable maximum in the spectral response of the CdS. Shifts in this maximum to longer wavelengths is indicative of extraneous interface states in

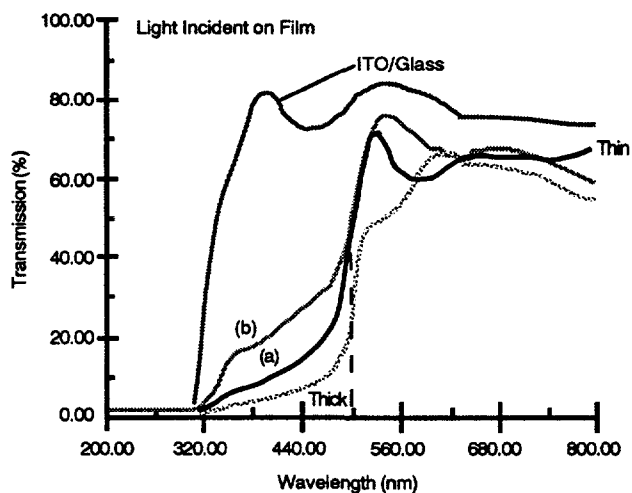


Figure 6 — Transmission Spectrum for Solution-Grown, 1600Å Thick CdS Films on Glass/ITO Substrates (Also Shown are Spectrum for an Uncoated Glass/ITO Substrate and 3500Å Coating).



the bandgap (formation of lower bandgap window or impurities/defects in the coating. Shifts in the maximum were observed although the correlation between peak shifts and device performance is still in progress.

As-deposited, solution-grown CdS films were analyzed with X-ray diffraction and the results are shown in Figure 7. These films are hexagonal with measured lattice parameters of  $a = 4.07 \text{ \AA} - 4.1 \text{ \AA}$  and  $c = 6.653 \text{ \AA} - 6.654 \text{ \AA}$ . In the as-deposited condition, the films are highly oriented with preferred growth directions of (002). When heat treated at  $450^\circ\text{C}$  for 30 minutes in  $\text{H}_2/\text{Ar}$ , the structure of the film does not change; the films remain highly oriented. When sandwiched between the TCO and an electrodeposited CdTe film, however, the CdS structure is not thermally stable.

**Electrodeposited CdTe** — CdTe was electrodeposited onto CdS/ITO/glass substrates using both constant potential and constant current control. Films deposited under potential control were fine-grained, adherent, and uniform and were reproducibly deposited at thicknesses between 1.5  $\mu\text{m}$  – 2.0  $\mu\text{m}$ . TEM bright field and XRD were used to characterize the as-deposited and heat treated CdTe films. Results from these analysis indicated the films were microcrystalline with grain sizes in the range of  $500 \text{ \AA} - 1000 \text{ \AA}$ . With heat treatments for 20 minutes at  $400^\circ\text{C}$ , grain sizes increased to 0.5  $\mu\text{m}$  although the grains were heavily faulted and exhibited a high density of dislocations. An example of a heat treated CdTe grain is presented in the bright field TEM micrograph of Figure 8.

The structure of as-deposited CdTe films is cubic (zincblende) with a measured lattice parameter of  $\sim 6.51 \text{ \AA}$ . These films are partially amorphous with a preferred growth direction of (111). When heat treated at  $350\text{--}400^\circ\text{C}$  for 20-30 minutes in air (in the presence of  $\text{CdCl}_2$ ), the lattice parameter contracts from  $6.51$  to  $6.487 \text{ \AA}$  as the grain size increases and the film becomes more crystalline (polycrystalline). This shift in lattice parameter can be seen in the peak shifts in the XRD spectra shown in Figure 9. With the heat treatment, the peak height increases and width decreases as the peak maximum shifts to higher angles (smaller d-spacings). Birkmire [6] has attributed this peak shift to the formation of a solid solution phase between the diffusing sulfur and CdTe (i.e. the phase  $\text{CdTe}_{(1-x)}\text{S}_{(x)}$ ).

In addition to constant potential/current electrodeposition of CdTe, pulsed electroplating of CdTe has also been used with limited success to produce rapidly deposited, adherent, CdTe films.

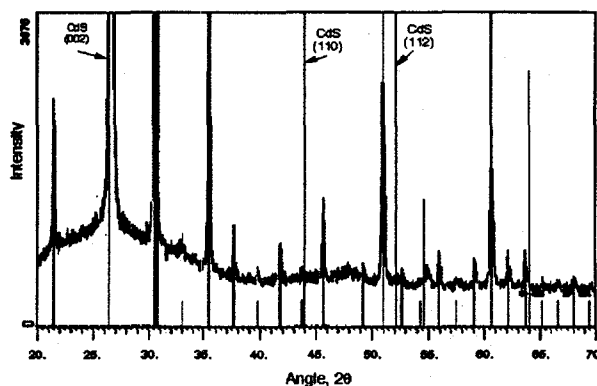


Figure 7 — X-Ray Diffraction of As-Deposited, Solution-Grown CdS Film on Glass/ITO Substrate (Unlabeled Peaks Due to Indium-Tin-Oxide).



Figure 8 — TEM Bright Field Examination of Heat-Treated CdTe Film.

Using this technique in dilute solutions, deposition rates were increased an order of magnitude over conventional constant DC plating rates. However, in order to optimize device performance, this technique was temporarily discontinued in favor of the more conventional, proven approaches.

**CdTe Film Optimization** — Earlier, CdTe growth behavior was found to be intimately related to the morphology and chemical stability of the underlying substrate. Since device performance is dependent on the grain size and orientation of the CdTe film, which is in turn dependent on the underlying substrate, variations in each film had a marked effect on the overall performance of the device. In general, deposits of CdTe were fine-grained because the underlying CdS deposit was fine-grained. For coherent/adhesive coatings, the electrodeposited CdTe should be fine-grained. As a highly efficient absorber layer in a thin-film 'polycrystalline' solar cell, the CdTe film should be large-grained; preferably columnar grains oriented perpendicular to the substrate surface. In the formation of thin-film polycrystalline CdTe deposits, there is therefore a trade-off between fine-grained deposits which are adherent and course-grained deposits which are good p-type layers but loosely adherent.

In the electrodeposition process, the grain size is controlled by 1) current density, 2) temperature, and 3) concentration. High current density and elevated temperature favor course-grained, loose deposits. The current density in CdTe deposition, however, is limited by the requirement to control the deposition potential; since the applied potential controls the Cd/Te ratio in the deposit, CdTe stoichiometry (and current density) are set by the deposition potential (under current control, more CdTe can be deposited, but the deposits become more cadmium-rich as the current density is increased). Therefore, the requirement to control CdTe stoichiometry with a potentially controlled system places a limit on the maximum current density for the process.

**CdTe Device Characterization** — Two primary new efforts were started in phase II of this activity to characterize the electrical behavior of the CdTe devices: (1) computer modeling and (2) I-V curve measurement and analysis. These efforts proved to be very useful in guiding this second phase of CdTe process development and should help define the direction for achieving device efficiencies over 10 % in the future.

The starting point for solar cell model development was the conventional five parameter equivalent circuit consisting of a diode with saturation current  $I_{sat}$  and diode ideality factor  $A$ ; a parallel current source  $I_L$  to represent generation of current with light flux; a parallel resistance  $R_p$  to represent leakage around the junction; and a series resistance  $R_s$ . The I-V curve solution for this equivalent circuit was computed using Newton's method.

Measurement and analysis of initial CdTe devices showed that at least two problems needed to be addressed, namely (1) increasing the carrier concentration and quality of the p-type CdTe and (2) eliminating the back Schottky contact. Since early CdTe films were mainly grown directly as p-type films, it was decided to concentrate on using a process in which type-conversion of n-type CdTe was obtained by a 350°C to 400°C post anneal. Earlier work by Basol indicates that superior p-type material can be grown by this approach. To improve the back contact, careful

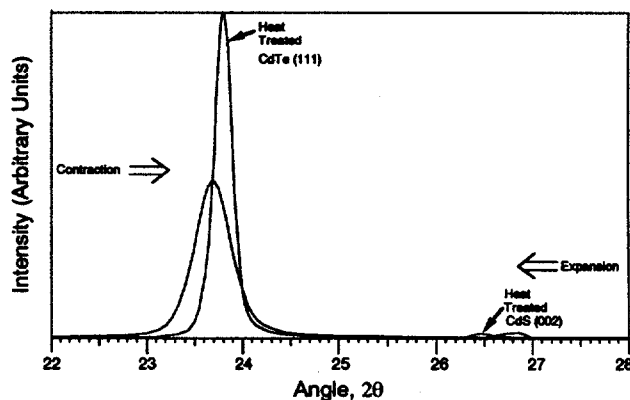


Figure 9 — X-Ray Diffraction of Heat-Treated and As-Deposited Glass/ITO/CdS/CdTe Stacks Revealing the Formation of Solid Solutions Across Heterojunction.

attention was given to the etching of the CdTe just prior to contacting, so that a Te-rich surface could be obtained. Electrical contact for I-V measurements was done through wire probes to the Au-CdTe and through indium-soldered contacts to the Au-TCO.

Electrical characteristics of a CdTe device with 6.3 % efficiency, fabricated with this process, are shown in Figure 10. The equivalent circuit parameters for this device are: device area = 0.0764 cm<sup>2</sup>, I<sub>sat</sub> = 2.494 x10<sup>-4</sup> mA, R<sub>s</sub> = 103.9 Ω, I<sub>L</sub> = 1.22 ma, R<sub>p</sub> = 7143 Ω, and A = 3.5.

Sample: 820-A1-2      Temperature = 25.0° C  
 Sep. 2, 1992 2:49 pm      Area = 0.0764 cm<sup>2</sup>

Fill Factor = 53.69%  
 Efficiency = 6.3% (total area)  
 V<sub>oc</sub> = 0.7372 V  
 I<sub>sc</sub> = 1.220 mA  
 J<sub>sc</sub> = 15.98 mA/cm<sup>2</sup>  
 P<sub>max</sub> = 0.483 mW  
 I<sub>max</sub> = 0.958 mA  
 V<sub>max</sub> = 0.5042 V

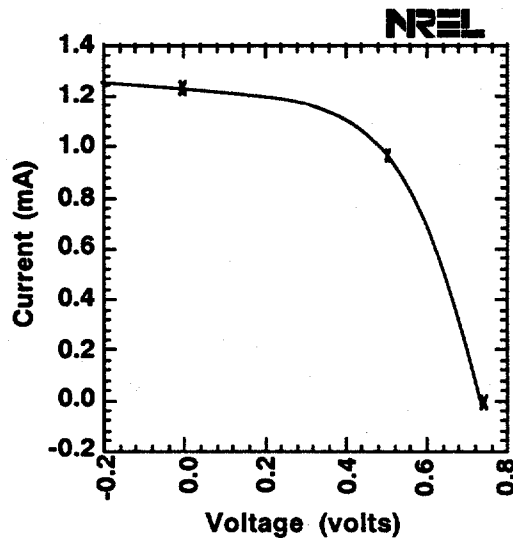


Figure 10 — Electrical Properties of Electrodeposited CdTe Device.

The high series resistance is primarily due to the poor TCO used, which had a resistance of about 56 Ω/square. Figure 11 shows a simulation of this device, first with the measured series resistance, and second with a simulated series resistance of 10 ohms. As can be seen in the figure, the poor quality TCO causes the device efficiency to be degraded from 7.4 % to the 6.3 % measured.

Another technical issue raised by these measured device parameters is the high diode ideality factor A. The device likely is dominated by recombination effects, possibly at the grain boundaries. Future work will address this issue.

**Monolithic Integration** — Mo films 1μm thick were deposited by C-Mag onto a large 930 cm<sup>2</sup> substrate. In-house laser scribing with 48 in. x 96 in. substrate capability was used to scribe the Mo back contact on a 5 cm x 5 cm substrate as shown in Figure 12. At present, CuIn/Mo precursor stacks are being scribed and small 5 cm x 5 cm minimodules are in progress to demonstrate monolithic integration.

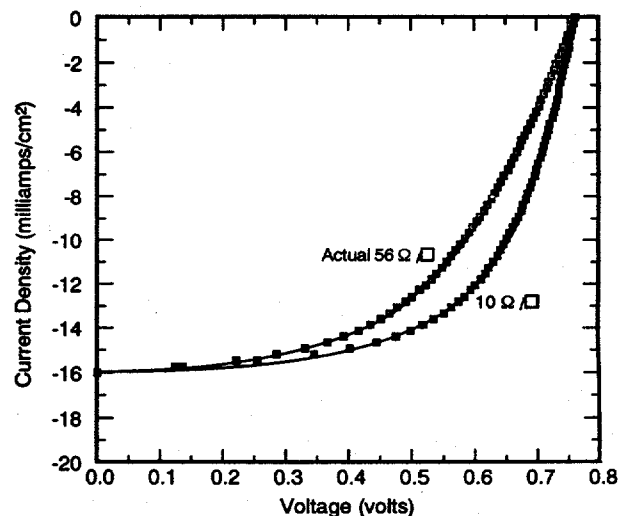


Figure 11 — Modeling of a CdTe Device with Low and High-Resistance TCO.

## SUMMARY

CIS devices were manufactured from films deposited by the dual rotating cylindrical magnetron sputtering system. Devices made by the ISET two-step selenization process demonstrated 8.4% efficiency (active area, AM1.5). Deposition rates far in excess of conventional sputtering systems were observed, indicating that the C-Mag could be used in a production environment to reduce cost of fabricating submodules. Electrodeposition was used for CdTe devices with AM1.5 active area efficiency of 6.3%. Monolithic integration techniques will be used in the next phase of this investigation to produce large-area (930 cm<sup>2</sup>) submodules.

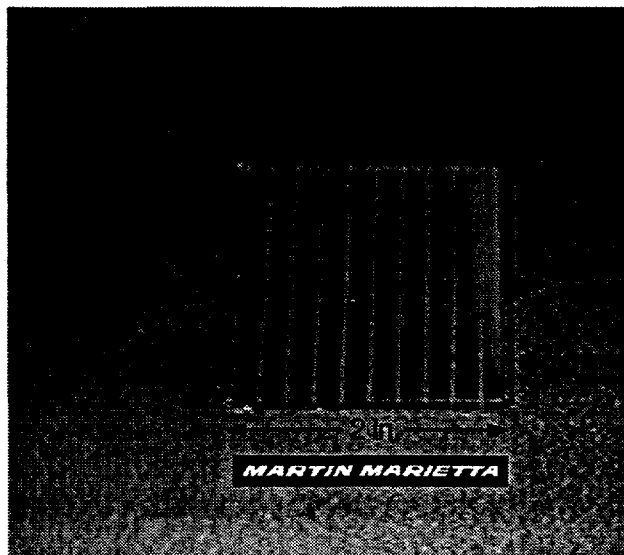


Figure 12 — Photograph of Laser-Scribed Mo Film on 930 cm<sup>2</sup> Substrate.

## ACKNOWLEDGEMENTS

International Solar Electric Technologies, Inc. (ISET) is a major subcontractor in this effort.

## REFERENCES

1. D. Griffin: "The New C-Mag™ Dual Rotatable Sputtering Cathode: Present Status and Future Considerations," proceedings of the Third International Conference on Vacuum Web Coating, San Antonio, TX, 12-14 November, 1989.
2. C. Boehmler: "Film Properties of Coatings Deposited by C-Mag™ Rotatable Sputtering Cathode," AIRCO Technical Report, AIRCO Coating Technology, Concordia, CA.
3. B. Basol, "Electrodeposited CdTe and HgCdTe Solar Cells, *Solar Cells*, 23 (1988) p. 69.
4. B.M. Basol and V.K. Kapur: "CuInSe<sub>2</sub> Thin-Films and High-Efficiency Solar Cells Obtained by Selenization," *Proc. 21th IEEE Photovoltaic Specialists Conf.*, IEEE, New York, 1990, p. 458
5. D. Albin, J. Carapella, A. Gabor, A. Tennant, J. Tuttle, A. Duda, R. Matson, A. Mason, M. Contreras, and R. Noufi, "Fundamental Thermodynamics and Experiments in Fabricating High Efficiency CuInSe<sub>2</sub> Solar Cells by Selenization Without the Use of H<sub>2</sub>S," AIP Conference Proceedings from Photovoltaic Advanced Research and Development 11<sup>th</sup> Review Meeting, Denver, CO 1992 (in press).
6. R.W. Birkmire, B.E. McCandless, and S.S. Hegedus, "Effect of Processing on CdTe/CdS Materials and Devices," Proc 12th PV AR&D Project Review Meeting, May 13-15, 1992 (in press).

**Title:** Research on High Efficiency, Large Area CuInSe<sub>2</sub>-Based Thin Film Modules

**Organization:** Siemens Solar Industries  
Camarillo, California

**Contributors:** C. Eberspacher, Program Manager; K. Mitchell and R. Gay, Principal Investigators; M. Dietrich, J. Ermer, C. Fredric, C. Jensen, K. Knapp, D. Tarrant, D. Willett

### **Introduction**

Siemens Solar Industries (SSI) began a 3-year, 3-phase cost-shared contract on May 1, 1991 to demonstrate 12.5% aperture-area efficiency on large area (3900 cm<sup>2</sup>) encapsulated thin film CuInSe<sub>2</sub> (CIS) modules. Prior to the contract, SSI had demonstrated a 14.1% active-area efficiency on a 3.4 cm<sup>2</sup> ZnO/thin CdS/CIS/Mo/glass cell and had fabricated monolithic integrated submodules with unencapsulated aperture-area efficiencies of 11.2% on 940 cm<sup>2</sup> and 9.1% on 3900 cm<sup>2</sup> [1]. The best encapsulated large area CIS module power output prior to the contract was a 33.7 W, 8.7% aperture-area efficiency (verified at NREL) over a 3883 cm<sup>2</sup> area [2].

### **Objective**

Demonstrate large-area, stable 12.5% aperture efficiency CuInSe<sub>2</sub> modules using processes than can be transferred to manufacturing. Success in this effort will be a significant contribution to the DOE Five Year Plan to achieve stable submodules with efficiencies of 15% or more made by scalable, low-cost techniques on inexpensive substrates.

### **Approach**

The module design consists of 53 series-connected ZnO/CdS/CIS/Mo/glass cells fabricated on a 4141 cm<sup>2</sup> (128.6 x 32.2 cm) glass substrate with a nominal aperture area of 3895 cm<sup>2</sup> (127.3 x 30.6 cm). Module performance strongly depends on the spatial uniformity of cell and interconnect quality, which in turn depend on the properties of the constituent layers. Initial contract emphasis has been on module diagnostics using improved techniques to characterize the cells and interconnects, such as Voc mapping to evaluate the uniformity of the junction performance and measurements of the voltage drop across interconnects at a fixed forward bias current to evaluate resistance losses due to individual interconnects. The physical nature of defects can be correlated using optical beam induced current (OBIC), electron beam induced current (EBIC), scanning electron microscopy (SEM), and other techniques such as tape adhesion testing. The results of the first year of this research have been published previously [3].

### **Results (FY 1992: 10/91 - 9/92)**

A new champion module with a power of 40.8 watts (10.5% aperture-area efficiency) was demonstrated for an unencapsulated CIS circuit this year. The module parameters were: Voc = 24.5 V (462 mV/cell), Isc = 2.55 A (Jsc = 34.7 mA/cm<sup>2</sup>), with a fill factor of 0.654. The aperture area of this module was 3890 cm<sup>2</sup>.

The importance of the substrate in determining the ultimate performance of the thin-film devices was a recurrent theme over this fiscal year. Imperfections in the as-purchased quality of the surface of the glass can be imaged by a variety of techniques and are apparent as cosmetic defects in the CIS semiconductor films. In addition to these cosmetic issues, some of these imperfections ultimately manifest themselves as areas of poor adhesion while others clearly lead to shunt paths.

Figure 1 shows a fissure in the molybdenum base electrode which has been caused by a scratch in the surface of the glass. Figure 2 shows the impact of this type of defect on the completed device, while Figure 3 shows that the presence of this defect can inhibit the growth of the CIS in the area immediately around the fissure in the molybdenum. The subsequent deposition of the ZnO then leads to a shorted device. Additional details regarding this and other defects has been presented elsewhere [4].

During the formation of the CIS layer, reaction of selenium with the glass substrate has been observed to form sodium selenide, a water-soluble orange-red compound. This may affect the adhesion of the films in the regions near the interconnects, where cuts in the base electrode (for the isolation scribe) allow this reaction to occur. When the CdS layer is not deposited on the CIS, unusual growth of the ZnO occurs to create features (Figure 4) which decorate these cuts in the molybdenum. While the mechanism of this growth is not understood, the decoration is a useful diagnostic for imaging shunt paths in the circuit.

#### **Areas for Future Research.**

Research is focussing on developing an understanding of the role of the substrate on device performance and uniformity, in order to obtain a specification of the requirements for this important component of the circuit. Efforts will continue to address understanding of the mechanisms which control CIS module performance, defining improvements in module design and processing leading to CIS module aperture efficiencies of 12.5%.

#### **References.**

1. K. Mitchell, C. Eberspacher, J. Ermer, K. Pauls, D. Pier, D. Tanner, *Proc. 4th International PV Science and Engineering Conf., Sydney, Australia, Feb. 14-17*, pp. 889-896, (1989).
2. K. W. Mitchell, W. Chesarek, D. R. Willett, C. Eberspacher, J. H. Ermer, R. R. Gay, *Solar Cells 30*, pp 131-136 (1991).
3. K. Mitchell, C. Eberspacher, "Research on High Efficiency, Large Area CuInSe<sub>2</sub>-Based Thin Film Modules, Phase 1: Annual Technical Progress Report For the Period May 1, 1991 to April 30, 1992" (1992).
4. R. Gay, W. Chesarek, C. Fredric, K. Knapp, D. Pier, D. Tarrant, D. Willett, *NREL Photovoltaic Performance and Reliability Workshop, Golden, Colorado, SERI/CP-411-5184, DE93000017*, pp 197-228 (1992).

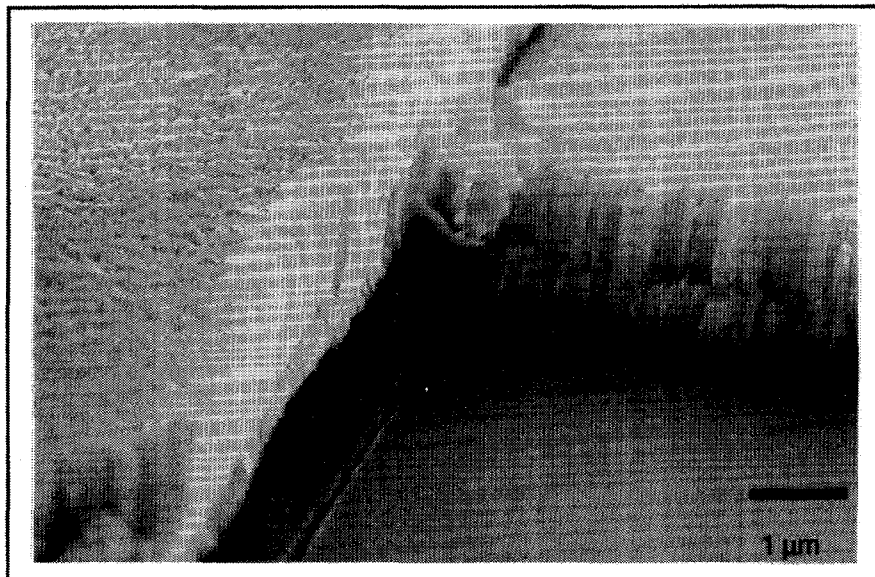


**Figure 1.** SEM image of the molybdenum base electrode grown over a scratch in the glass substrate.

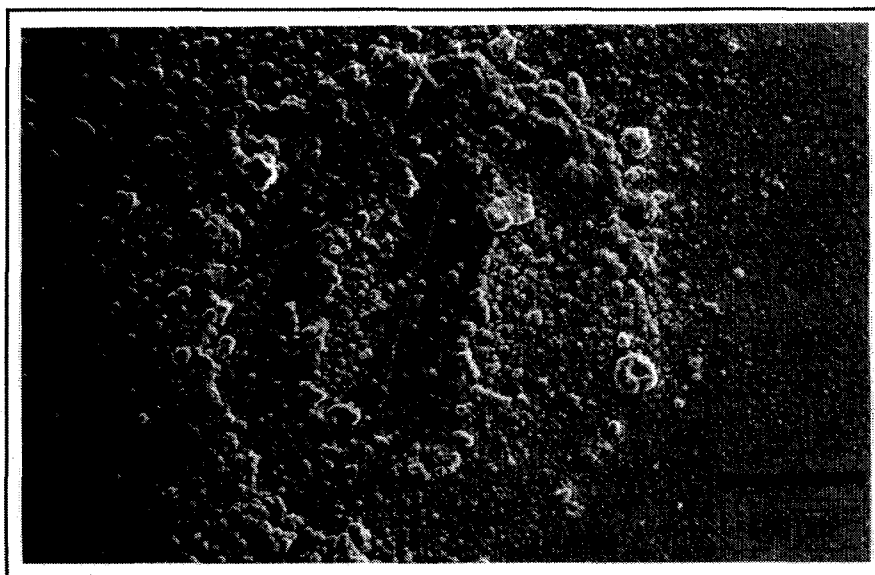


**Figure 2.** SEM image of a completed device grown over a scratch in the glass substrate.

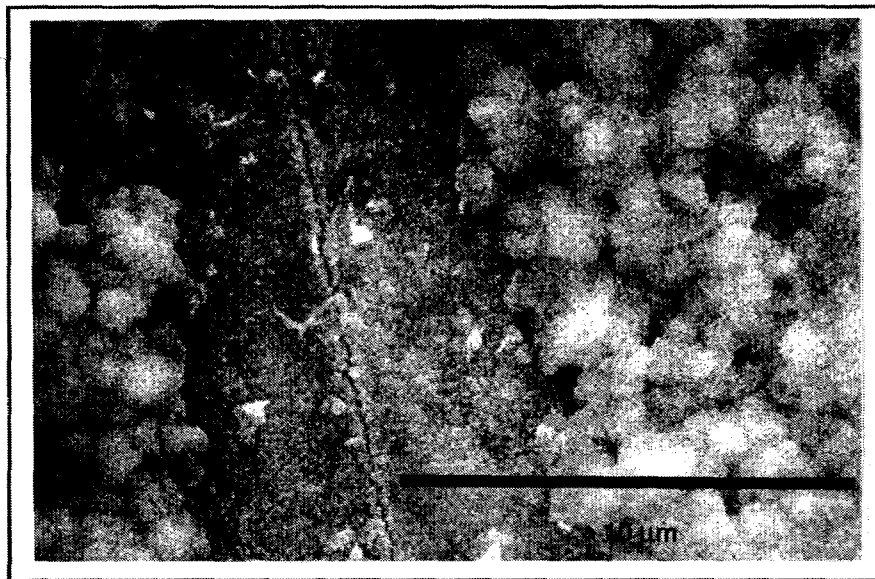


**Figure 3.** SEM image of the of the center of a scratch defect after removing the ZnO, showing the suppression of the growth of the CIS around the fissure in the molybdenum.

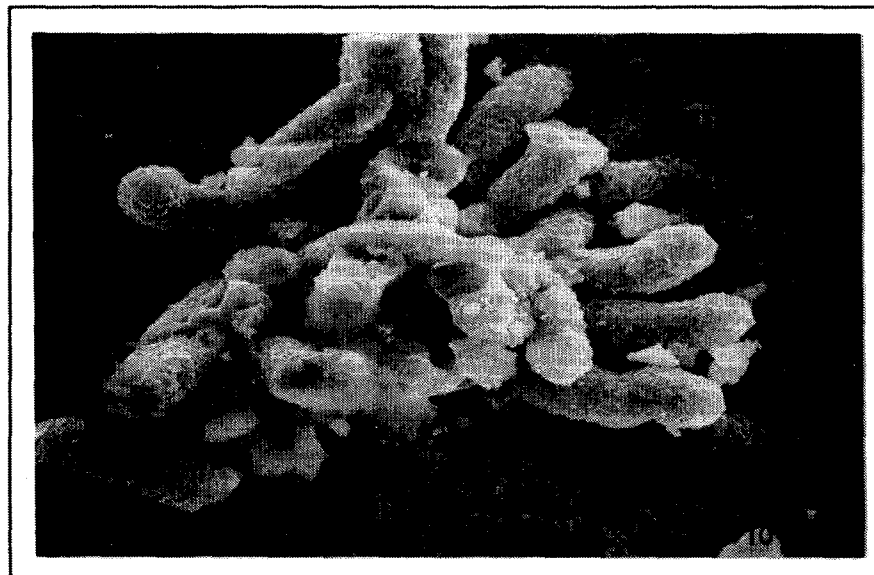


**Figure 4.** SEM image of the unusual growth of the ZnO around defects when CdS is not deposited on the CIS.



**Title:** Development and Application of a  
Computer Model for CdTe and CuInSe<sub>2</sub>  
Based Solar Cells

**Organization:** School of Electrical Engineering  
Purdue University  
West Lafayette, IN 47907

**Contributors:** R. J. Schwartz and J. L. Gray, principal invest-  
igators; Y. J. Lee and J. C. Kim, graduate students

### Objective

The purpose of this research program is to develop an accurate numerical model for CuInSe<sub>2</sub> (CIS) and CdTe based solar cells which can be run on IBM compatibles and Unix-based Sun workstations. Other computing platforms, such as the Macintosh, may also be supported. The model, ADEPT (A Device Emulation Program and Tool), is used to analyze and aid in the design of CIS and CdTe based solar cells and is being released to the photovoltaic community.

### Approach

An accurate numerical model depends on precise knowledge of a variety of material and device parameters, not only for CIS and CdTe, but for window layer materials such as ZnO and CdS, as well. This information is used for the development and verification of the model. Collection of material and device parameters in an ongoing process, since these materials are not well characterized and there is a wide variation in measured material parameters and device performance.

Verification of the models requires a broad base of experimental measurements. A good model will be able to predict all known measurements with the same set of model parameters. Such measurements include, but are not limited to, the illuminated current-voltage characteristic, quantum efficiency, dark current-voltage characteristic, and temperature dependent photoconductivity.

While many device issues can be addressed adequately with a one-dimensional model, some cannot. For example, grain boundary effects can only be modeled realistically with a 2D or 3D model. ADEPT has the ability to handle both 2D and 3D structures, but only at a large computational cost. However, it is expected that 2D simulations will be possible on an IBM 386/7 or higher platform.

## Results

A 1D version of ADEPT for IBM compatibles has been released and is briefly described in [1].

As an example of the use of ADEPT, results of the simulation of a good CIS solar cell [2,3] are shown in Figures 2 and 3. The assumed device structure is shown in Figure 1. A good fit to experiment was obtained for a CIS lifetime of 4.4 ns, a Cu-poor layer thickness of 0.5  $\mu\text{m}$ , and a series resistance,  $R_S$ , of 0.27  $\Omega\text{-cm}^2$  (consistent with measured values [3]). The simulated I-V is nearly identical to the measured characteristic [3] (the only difference is that the short-circuit current was measured at 41  $\text{mA/cm}^2$ ). The simulated quantum efficiency is also in excellent agreement.

## Conclusions

Numerical simulation has already proved its usefulness in analyzing and designing a variety of semiconductor devices, including solar cells. Initial modeling of CIS cells has already improved the understanding of the performance of these cells. As the specific models relevant to absorption, recombination, transport, etc. are improved, the ability of the code to analyze and help design CIS and CdTe based solar cells is expected to become a valuable tool for PV researchers.

## References

1. J. L. Gray, R. J. Schwartz, and Y. J. Lee, "Development of a Computer Model for Polycrystalline Thin-Film  $\text{CuInSe}_2$  and CdTe Based Solar Cells," Purdue University Technical Report TR-EE-92-36, West Lafayette, Indiana, September, 1992.
2. K. W. Mitchell, C. Eberspacher, J. Ermer, and D. Pier, Proceedings of the 20th IEEE Photovoltaic Specialists Conference, (Las Vegas, Nevada 1988), p. 1384.
3. K. W. Mitchell and H. I. Liu, Proceedings of the 20th IEEE Photovoltaic Specialists Conference, (Las Vegas, Nevada 1988), p. 1461.

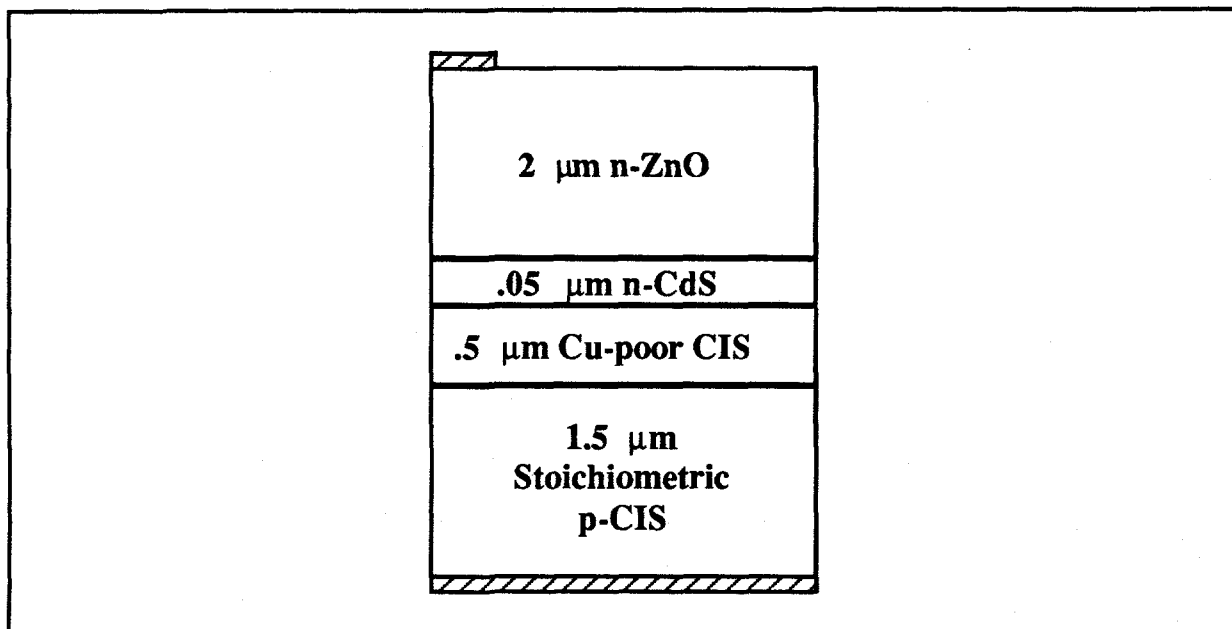


Figure 1. Schematic of modeled ZnO/CdS/CIS Solar Cell.

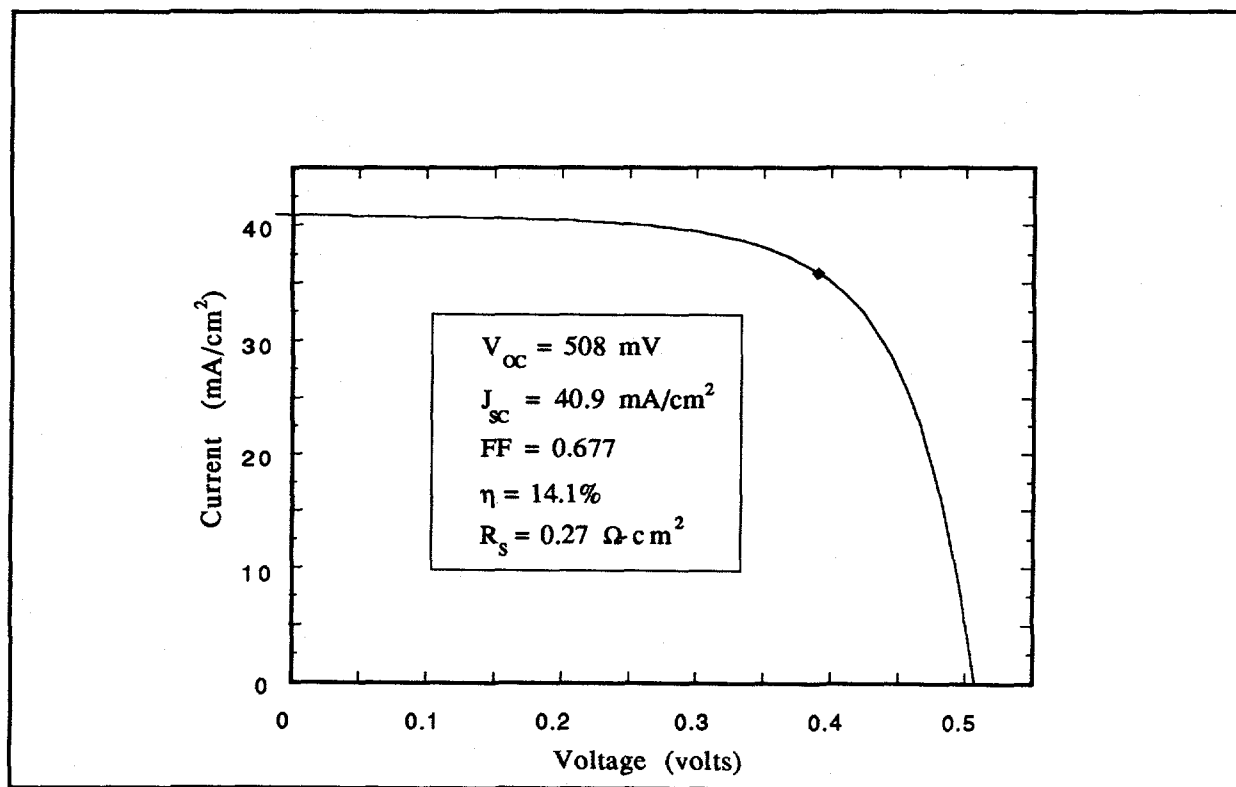


Figure 2. Simulated I-V under  $100 \text{ mW/cm}^2$  AM1.5 conditions.

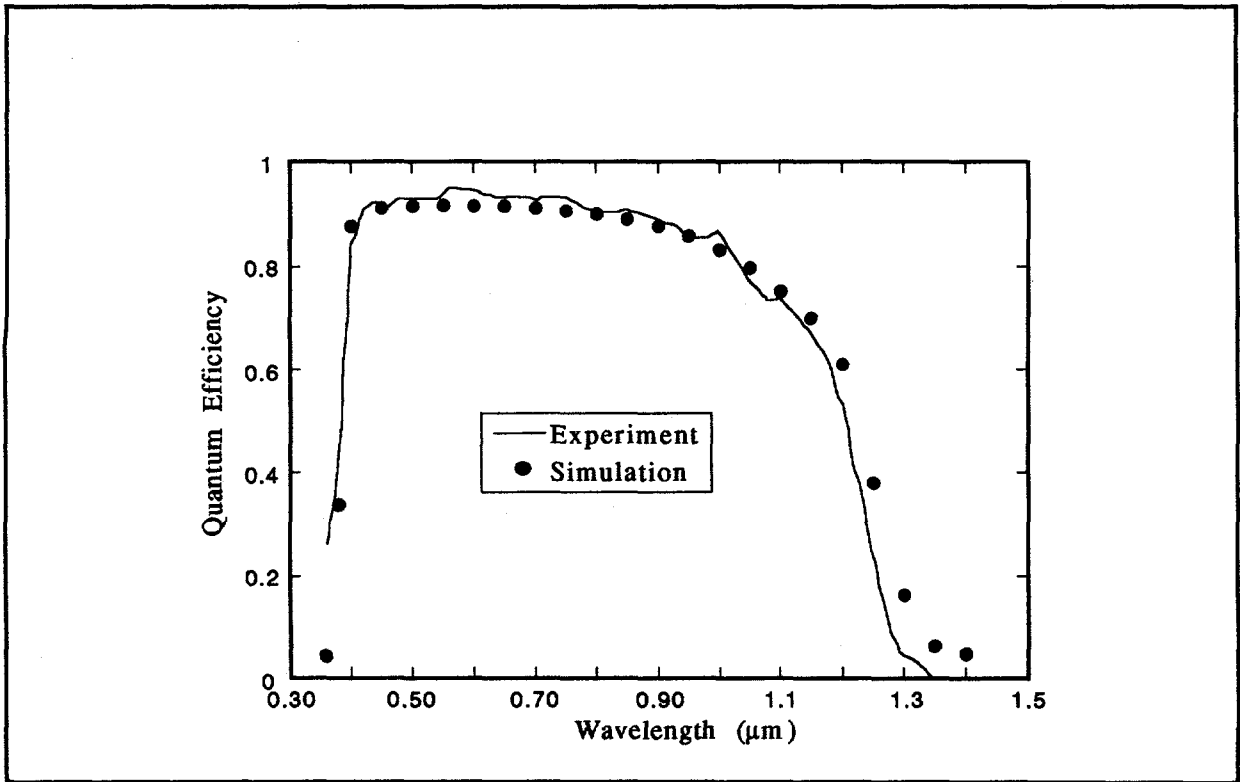


Figure 3. Measured and simulated quantum efficiency of modeled ZnO/CdS/CIS cell.

**Title:** Fabrication of Stable Large Area Thin Film Cadmium Telluride Photovoltaic Modules

**Organization:** Solar Cells, Inc., Toledo, Ohio

**Contributors:** J.F. Nolan, Program Manager; P.V. Meyers, Principal Investigator; T. Zhou, S. Kaake, R. Powell, N. Reiter, J. Foote, R. Harju

## **Objective**

The overall objective is the demonstration of large area thin film CdTe photovoltaic modules fabricated using methods consistent with high throughput manufacturing. Specific goals for the three year program include producing 15% efficient 1 cm<sup>2</sup> solar cells, 12% efficient 8 cm x 8 cm submodules, and 10% efficient 60 cm x 120 cm modules.

## **Approaches Taken**

SCI utilizes deposition onto hot superstrates from elemental vapors as the method for deposition of the thin films. The vapors are produced by sublimation of heated powders of the compounds-CdS and CdTe. SCI chose this method of fabrication based on its suitability for high speed manufacturing. Films can be deposited at rates in excess of 4  $\mu$ m per minute. Furthermore, although the precise methods used at SCI are unique - see Figure 1, the procedure is similar to Close Spaced Sublimation, a process which has produced 15+% CdTe cells in other laboratories. Further studies involve vapor produced from elemental sources and transported by inert carrier gasses.

## **Results**

In order to produce these devices, SCI had to first design and build deposition chambers for the semiconductor and metal films, develop laser scribing techniques, design and build equipment for encapsulation, as well as to assemble or construct various equipment - from glass washers to PV module efficiency measurement apparatus - necessary to process a sheet of SnO<sub>2</sub> coated glass into an encapsulated module. These tasks have been largely completed during the past year.

During this fiscal year SCI has demonstrated the ability to produce uniform films of CdS and CdTe over 60 cm x 120 cm superstrates - a size suitable for manufacturing. Semiconductor deposition time is less than one minute. Small area devices produced on these superstrates have exceeded 9% efficiency. SCI has also produced modules with an (unconfirmed) output of 50 watts (89.7 V Voc, 0.96 A Isc, 63.3 V Vmp, and 0.79 A Imp). See Figure 2. This is equivalent to a total area efficiency of 6.9%. These modules have been encapsulated without loss of efficiency.

Early work on encapsulation suggests that EVA lamination with glass or Tedlar is feasible. Trials suggest that encapsulated modules are capable of passing each of NREL's Interim

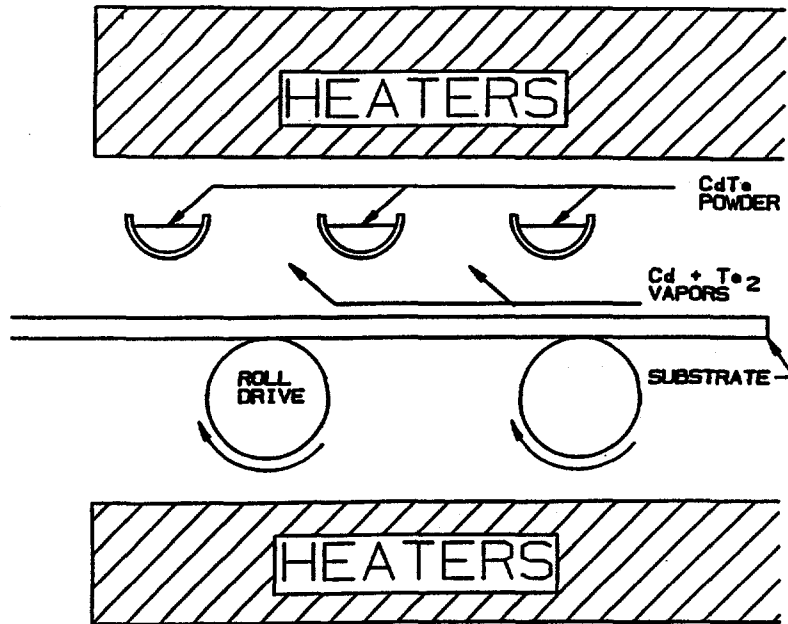
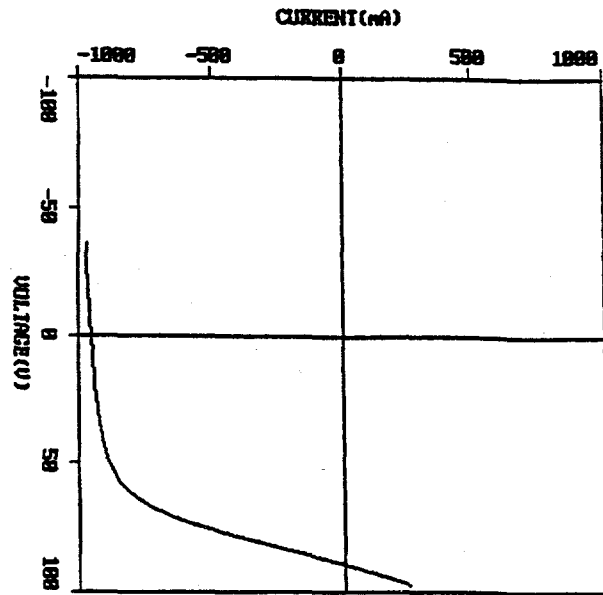


Figure 1. Schematic of SCI semiconductor deposition apparatus. The source powders are heated from above to a temperature - e.g.  $\sim 700^{\circ}\text{C}$  for CdTe - at which the vapor pressure is  $\sim .5$  torr. The elemental vapors then condense onto the relatively cool -  $\sim 600^{\circ}\text{C}$  - substrate as it passes through the deposition zone carried on rollers.



SAMPLE: L505  
 TEMPERATURE: 33.0 Celsius  
 NOTES: ED/LAM TED/LAM  
 TOTAL AREA EFFICIENCY: 6.952  
 CELLS IN SERIES: 11A  
 Vmax: 45.263 V  
 Imax: -790.99 mA  
 Pmax: 50.0 W  
 Rseries: 28.3 Ohms  
 APERTURE AREA EFFICIENCY: 7.315  
 ACTIVE AREA EFFICIENCY: 8.085  
 ACTIVE AREA PER CELL: 53.40 cm<sup>2</sup>  
 Jmax: -14.81 mA/cm<sup>2</sup>  
 Rsh: 13.0 Ohm-cm<sup>2</sup>

DATE: 11-20-1992  
 TIME: 17:02:57  
 TOTAL AREA: 7200.00 cm<sup>2</sup>  
 Vdc PER CELL: 0.774 V  
 Vdc: 89.731 V  
 Isc: -935.88 mA  
 FF: 0.583  
 Rshunt: 1468.8 Ohms  
 APERTURE AREA: 6846.00 cm<sup>2</sup>  
 TOTAL ACTIVE AREA: 6194.40 cm<sup>2</sup>  
 Jsc: -17.90 mA/cm<sup>2</sup>  
 Rsh: 676.1 Ohm-cm<sup>2</sup>

Figure 2. I-V characteristics of a 7200 cm<sup>2</sup> CdTe module. 144

Qualification Tests, but as of this date we have not completed the Initial Tests and Inspections series on a batch of modules.

As part of our R & D effort, one cm<sup>2</sup> devices and 8 x 8 cm<sup>2</sup> 8 cell minimodules are produced on 100 cm<sup>2</sup> superstrates. Confirmed efficiencies on these devices are 10.3% (20.0 mA/cm<sup>2</sup> Jsc, 0.78V Voc, and 0.66 FF) and 6.1% (117.0 mA Jsc, 6.32 V Voc, and 0.54 FF), respectively.

In additional work, CdTe films were deposited from elemental vapors transported by nitrogen gas. These studies are motivated by the hope of achieving improved control over the stoichiometry and transport of the source vapors and by the potential for deposition at atmospheric pressure. Experiments to date have demonstrated the viability of this approach for depositions over the pressure range from 60 to 600 torr.

Also, during this year significant enhancements were made to SCI's analytical capabilities. An analytical system capable of making dark I-V and spectral response measurements is now on line.

### **Conclusions and Future Work**

At this point we foresee no fundamental obstacles which will prevent high throughput manufacturing of large area polycrystalline thin film CdTe photovoltaic modules. Deposition rate, film uniformity, device efficiency, and compatibility with encapsulation procedures seem adequate to justify continuation of the project. During the coming year we will refine and improve these processes in order to improve module efficiency, production yield, and conformity to the Interim Qualification Test standards. Additional studies will address module stability, improved remote vapor transport control, and improved analysis of device operation and limitations.

### **References**

1. Annual Report, Fabrication of Stable, Large-Area, Thin Film CdTe Photovoltaic Modules (May 1992). NREL/TP-413-5011, 16pp. Available NTIS: Order No. DE92016445

**Title:**                    **Research on Polycrystalline Thin Film Submodule Based on CuInSe<sub>2</sub> Materials**

**Organization:**        Solarex Corporation, Thin Film Division  
826 Newtown-Yardley Road, Newtown, PA 18940

**Contributors:**        R.R. Arya, Program Manager and Principal Investigator;  
T. Lommasson, S. Weideman, L. Russell, R. Podlesny,  
S. Skibo and J. Fogleboch

## **Introduction**

The objective of the three year cost-shared research program at Solarex is to develop all pertinent processes and technologies required for low cost, high performance copper-indium-diselenide (CIS) modules. In order to achieve the goal of 12% CIS module (FY 1993), we have focused our efforts on four tasks: (I) Window Layers, Contacts, Substrate, (II) CIS Absorber Layer, (III) Device Structure and (IV) Submodule Design and Encapsulation. In each task we have concurrently addressed (a) basic material improvements, (b) fabrication and characterization of CIS solar cells and (c) scale-up of processes to large area substrates.

Major accomplishments within these tasks are:

- Development of a novel method for CIS preparation called Elemental Deposition and Compound Formation (EDCF). The method comprises of deposition of Cu, In and Se at room temperature followed by heat-treatment in an inert atmosphere.
- Demonstration of 10.2% efficient (active area) CIS solar cell on material prepared by EDCF.
- Scale-up of all processes for contacts, window layers and CIS to 8" x 8" substrate.
- Development of laser/mechanical scribing of CIS submodules - first 8" x 8" submodule fabricated with all Solarex processes.
- Scale-up contacts and window layers to 12" x 13" substrates.
- Completion of design of large area CIS machine - assembly is in progress.

The following sections describe the progress made in each task.

### **Task I: Windows Layers, Contacts, Substrate**

The window layers consists of two thin film layers, CdS and ZnO. The CdS layer is deposited by chemical solution growth and the ZnO layer is deposited by either low pressure chemical vapor deposition (LPCVD) or by sputtering from an Al-doped ZnO target.

The thickness of the CdS layer affects the transmission between 400-500 nm and has been optimized. Figure 1 shows the quantum efficiency versus wavelength measurements of three CIS solar cells with identical CIS and ZnO layers. Short-circuit current densities above 40 mA/cm<sup>2</sup>



have been achieved with < 400 Å thick CdS layer. The CdS process has been scaled-up to 12" x 13" substrates. The long wavelength transmission of LPCVD deposited ZnO layer is found to be a strong function of diborane dopant concentration. Figure 2 shows the quantum efficiency versus wavelength measurements of two devices with identical CIS prepared by EDCF but different window layers. Reduction of diborane dopant gas in ZnO deposition resulted in an increase in short-circuit current density from 35.8 mA/cm<sup>2</sup> to 39.1 mA/cm<sup>2</sup>, mostly due to reduction in long wavelength losses. This process has been scaled-up to 6" x 6" substrates. Sputtered ZnO films have been scaled-up to 12" x 13" substrates. These films have sheet resistance of about 13 ohms/sq. but have higher absorption losses than LPCVD deposited ZnO films of similar thickness.

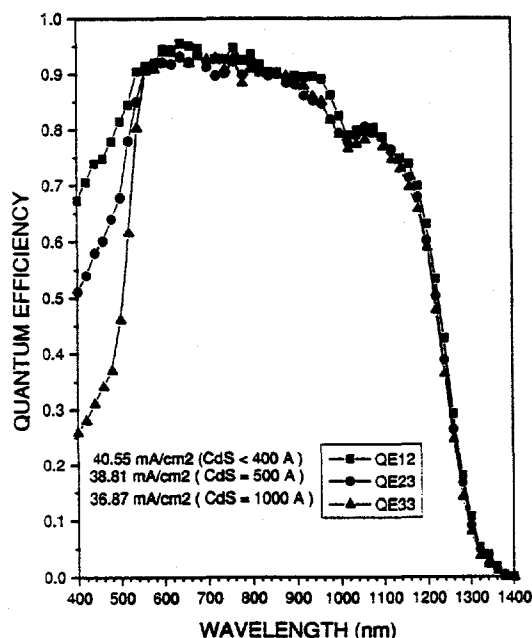


Figure 1 Effect of CdS thickness on CIS Solar Cells

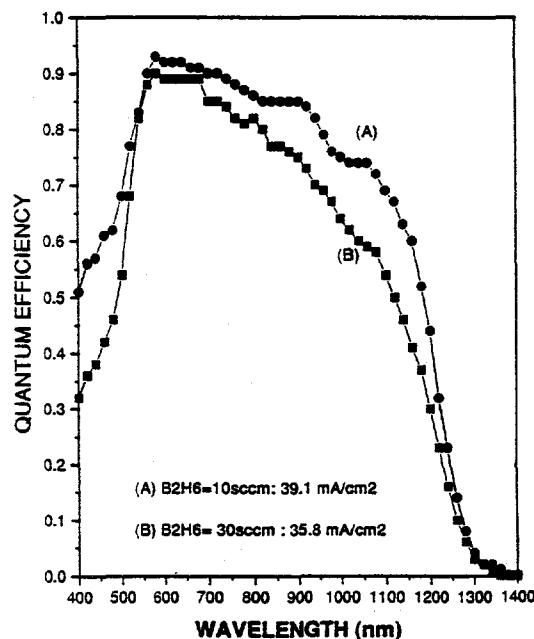


Figure 2 Effect of dopant concentration on long wavelength response of CIS devices

## Task II: CIS Absorber Layer

We have developed a novel process called Elemental Deposition and Compound Formation (EDCF) to prepare CIS thin films. The process constitutes of deposition of Cu, In and Se layers at room temperature followed by heat-treatment in an inert atmosphere. CIS films have been prepared which have proper stoichiometry and p-type conductivity. Table I shows the composition of several CIS films prepared by EDCF process. The process has been scaled-up to 8" x 8" substrates and the spatial compositional uniformity has been mapped-out. Figure 3 shows the Cu/In ratio and the (Cu+In)/Se ratio of CIS films of 1 cm<sup>2</sup>, > 50 cm<sup>2</sup> and > 400 cm<sup>2</sup> substrates. Scale-up from 1 cm<sup>2</sup> to > 50 cm<sup>2</sup> shows excellent uniformity whereas further scale-up to > 400 cm<sup>2</sup> shows some variation in film composition. We attribute the variation on 8" x 8" substrate (> 400 cm<sup>2</sup>) to variations in uniformity of temperature during the compound formation step. Auger depth profile these films indicate compositional uniformity in thickness. X-ray analysis shows strong (112) peak intensity and lacks any extraneous peaks indicating highly oriented chalcopyrite grains devoid of Cu<sub>x</sub>Se and 1:2:3.5 phases.

Sample #	Cu/In	% Cu	% In	% Se
260-7-1	0.91	22.24	24.49	53.27
261-3-1	0.94	22.43	23.97	53.60
261-6-1	0.93	21.97	23.62	54.41
261-2-3	0.96	23.07	23.99	52.94
261-1-4	0.95	22.61	23.92	53.94
261-1-3	0.96	22.59	23.59	53.82
261-2-2	0.95	23.04	24.14	52.82
261-2-1	0.94	22.81	24.29	52.90
262-4-1	0.97	22.08	22.85	55.07
262-2-1	0.99	23.41	23.70	52.89

Table I Composition of CIS Films

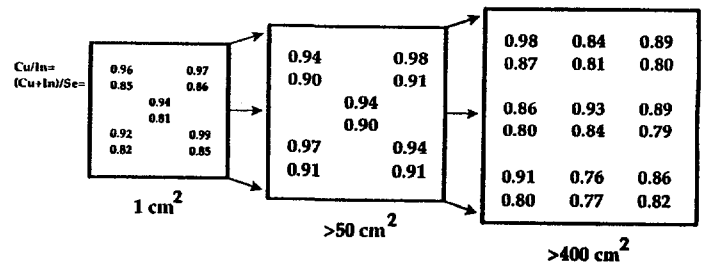


Figure 3 Spatial Uniformity of CIS films

### Task III: Device Structure

Solar cells have been fabricated on EDCF prepared CIS films with the following device structure:

Light => metal grid/ZnO/CdS/CIS/Mo/glass

A comparison of photovoltaic parameters of some good solar cells measured at Solarex and at NREL are tabulated in Table II. The best solar cell had an active area conversion efficiency of 10.2% with the following parameters:

$$V_{oc} = 0.427V, J_{sc} = 37.41 \text{ mA/cm}^2 \text{ and } F.F = 0.641$$

Cell #	$V_{oc}$ (mV)	$I_{sc}$ (mA)	$J_{sc}$ (mA/cm <sup>2</sup> )	FF	Efficiency (Active Area)	Total Area (cm <sup>2</sup> )	Active Area (cm <sup>2</sup> )	Measured At
261-6-1-H2	427	6.734	37.41	0.641	10.23	0.243		NREL
	430	6.168	34.30	0.629	9.30	0.245	0.18	SOLAREX
261-6-1-H1	410	9.260	38.10	0.624	9.75	0.312		NREL
	411	9.065	37.30	0.609	9.30	0.308	0.243	SOLAREX
261-6-1-L3	419	5.856	33.84	0.644	9.13	0.185		NREL
	418	5.655	32.70	0.635	8.70	0.191	0.173	SOLAREX
261-4-3-S3	416	7.090	35.47	0.610	9.00			NREL
	407	7.250	36.20	0.620	9.20	0.250	0.200	SOLAREX
261-4-2-S2	410	12.650	36.14	0.590	8.74	0.410	0.350	NREL
	400	12.500	35.70	0.590	8.47			SOLAREX
261-4-4-S4	422	11.800	34.70	0.580	8.49	0.410	0.340	NREL
	422	12.000	35.30	0.600	9.00			SOLAREX

Table II Comparison of solar cell measurements made at Solarex and at NREL

## Task IV: Submodule Design and Encapsulation

The CIS submodule interconnect scheme is shown in Figure 4. We have developed laser scribing of the Mo film. Laser scribing of glass/Mo substrates yields poor results due to extensive cracking, flaking and burning along the scribe edges. An interlayer of specular tin oxide between glass and Mo improves the laser scribing. The interaction of the laser beam and the glass/tin oxide/Mo composite is more favorable in terms of optical, mechanical and thermal aspects resulting in a clean ablation. This is shown in Figure 5 where the laser scribing on these two types of substrates is shown. The process has been scaled-up to 12" x 13". The other two scribes, namely, the CIS scribe and the ZnO scribe are accomplished with a mechanical scribe. All three scribes have been demonstrated on 8" x 8" substrate. Small area submodules (area ~ 25 cm<sup>2</sup>) with active area efficiency of 7.3% have been fabricated on CIS material deposited at the Institute of Energy Conversion with all other layers and all scribing done at Solarex. Table III shows the photovoltaic parameters of four such submodules.

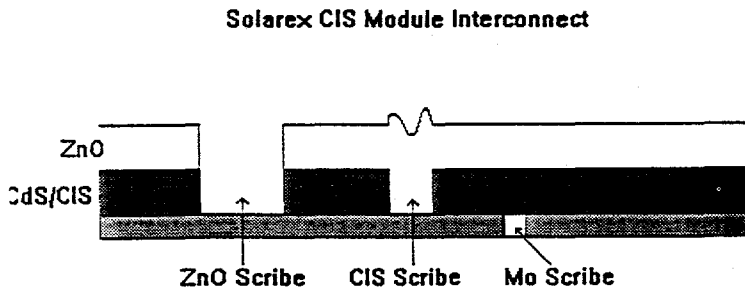


**Figure 4** Diagram of segment interconnect scheme used at Solarex for CIS modules (not to scale)

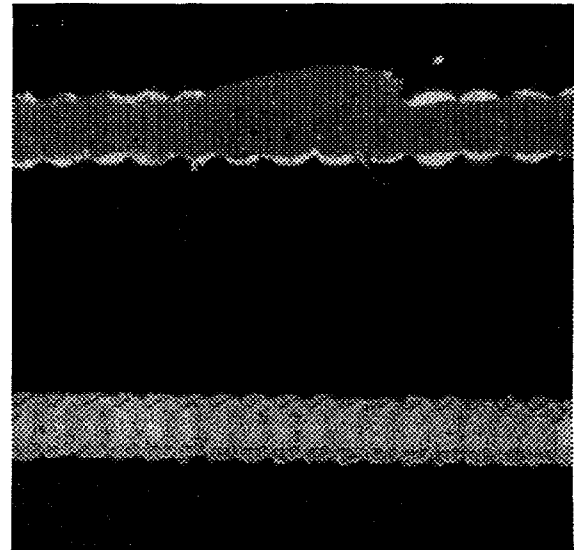


**Figure 5** Laser scribe of glass/Mo (upper) shows cracking, burning and flaking compared to laser scribe of glass/CTO/Mo (lower)

Module ID	Voc (V)	Voc/seg (V)	Fill Factor (%)	Jsc (aperture) (mA/cm <sup>2</sup> )	Jsc (active) (mA/cm <sup>2</sup> )	Efficiency (aperture) (%)	Efficiency (active) (%)
32296	2.849	0.356	38.4	30.7	34.1	4.2	4.7
32297	2.244	0.374	49.2	28.8	32.0	5.3	5.9
32298	2.941	0.368	53.6	29.3	37.2	5.5	7.3
32299	0.345	0.345	45.1	30.7	33.7	4.8	5.3

**Table III** Tabular results for CIS submodules made at Solarex using CIS supplied by the Institute of Energy Conversion

**Title:** Novel Thin-Film CuInSe<sub>2</sub> Fabrication

**Organization:** University of Colorado, Boulder

**Contributors:** A. M. Gabor, A. M. Hermann (principal investigator)

### **Objectives**

The major objective of this project is to produce high quality, thin films of CuInSe<sub>2</sub> (CIS) through rapid annealing of precursor films containing copper, indium, and selenium. The parameter space for the precursor deposition and for the post-deposition anneal must be explored not just for good crystal quality, but for good adhesion and coverage as well.

### **Technical approach**

Prior to this year, we demonstrated the formation of CIS thin films obtained by the rapid annealing of precursor films which were coevaporated onto molybdenum-coated alumina, mainly at substrate temperatures  $\leq 225$  °C [1]. These precursors were meant to be typical of a mixture of copper, indium, and selenium (and binary and ternary compounds of these elements) that could be deposited using a variety of cheap deposition methods. The maximum soak temperature explored during annealing was 700 °C. Albin et. al. [2] had also shown that rapid thermal annealing at higher temperatures was capable of forming large grains ( $>100$   $\mu\text{m}$  wide) of CIS albeit with poor substrate coverage. The precursors for those experiments were thin films of copper-rich CIS with small grains. For FY 1992 we chose to explore higher anneal temperatures for precursors deposited at different substrate temperatures, and with different compositions. Albin had found significant oxygen incorporation in his films, and so we built a vacuum system for the rapid thermal processor to allow pump and purge cycles with argon to remove oxygen from the processing chamber. In addition, we continued to explore soak temperatures  $\leq 550$  °C [3] since in this temperature regime, no warping problems should be experienced with a soda-lime glass substrate which is the substrate of choice for cost reasons. Primary characterization techniques included scanning electron microscopy (SEM) to investigate the film microstructure, electron probe micro-analysis (EPMA) to determine composition, and xray diffraction spectroscopy to determine crystal type and orientation.

### **Results for FY 92**

#### **CIS formation from low temperature anneals ( $T \leq 550$ °C)**

Precursor films of 2-3  $\mu\text{m}$  thickness were coevaporated onto unheated substrates using three elemental sources. They were then placed in the rapid thermal processor and heated to around 500 °C using varying ramp rates. Better adhesion was achieved using molybdenum-coated alumina substrates than molybdenum coated glass. Since alumina and soda-lime glass have very similar coefficients of thermal expansion, the better adhesion with the alumina was probably due to its larger surface roughness. Copper-rich or near stoichiometric films often blistered during the anneal with blister sizes around 10-20  $\mu\text{m}$ . The amount of blistering increased with the ramp rate. The best device was made with a film having  $[\text{Cu}]/[\text{In}] = 0.87$  as measured after an anneal with a ramp rate of 100 to 500 °C and a soak time of two minutes. The device parameters were  $V_{\text{oc}}=0.336$  V,  $J_{\text{sc}}=-19.46$  mA/cm<sup>2</sup>,  $\text{FF}=53.38$ ,  $\eta$  (active area) =3.5%.

Although the films were deposited with a constant copper-to-indium flux ratio throughout the duration of the deposition, the precursors were found to be non-uniform in composition as a function of depth through the films. More copper was found in the back than in the front of the

precursor, but upon annealing, the composition became more uniform as can be seen in Figure 1. This segregation was also found in precursors deposited at substrate temperatures of 170 °C.

### **CIS formation from high temperature anneals ( $T \leq 850$ °C)**

We found improved adhesion for precursors deposited on heated substrates, and the majority of the samples annealed were deposited at a substrate temperature of 170 °C. The films were found to undergo a progression in terms of morphology and grain size as a function of the soak temperature. Normal grain growth occurred between 350 and 650 °C with the grain width at most around the thickness of the film. Between 700 and 850 °C, enhanced growth was seen with grain sizes as large as 100's of  $\mu\text{m}$  observed (see Figure 2). We achieved the enhanced grain growth not just with copper-rich samples, but also with the copper-poor compositions which are necessary for device fabrication. Above 850 °C, agglomeration occurred unless the soak time was only a few seconds. The CIS beaded up on the substrate, resulting in very poor coverage. In general for these high temperature anneals, the longer the soak time, the larger the amount of indium and selenium that was lost from the film due to evaporation. Thus, short soak times may be desired. Alternatively, indium loss could be compensated for in the precursor, a post-anneal selenization could be performed, one could attempt to physically confine the selenium near the surface [4], or one could anneal under higher gas pressure as has been done with nitrogen [5].

The exact temperature at which a morphology or grain-size change occurs depends on the soak time and the composition, with the changes generally occurring at lower temperatures for films with higher copper contents. This is most likely due to the larger presence of a low melting-point  $\text{Cu}_x\text{Se}$  phase in films which are more copper-rich. Upon annealing, copper-rich samples become more copper-rich toward the surface, which may be related to segregation of the  $\text{Cu}_x\text{Se}$  phase.

Most of the annealed films exhibited cracks or voids, and the all the devices made were shorted, presumably due to the CdS window layer touching the molybdenum back contact through the holes. The incomplete coverage of the annealed films may be due to poor wetting of the substrate by any liquid phase, and to differential thermal expansion stress. Also important are volume changes in the film due to phase changes the precursor undergoes on the pathway to CIS, density differences between the solid and liquid phases, mass loss through evaporation, and changes in the porosity of the film.

### **Conclusions and Future Research**

We have shown that enhanced-grain thin films of CIS may be formed by rapid annealing precursors codeposited at room temperature, 170, and 350 °C, although complete substrate coverage is a problem. We plan to continue to explore the parameter space for deposition and annealing to achieve continuous coverage of the enhanced grain films. We will make more devices from the current films by using them as seed layers for further deposition which should plug the holes. We also plan to investigate the effects of grain size on the electrical and optical properties of the films.

## References

1. G. D. Mooney, A. M. Hermann, J.R. Tuttle, D.S. Albin, and R. Noufi, "The Formation of CuInSe<sub>2</sub> Thin Films by Rapid Thermal Processing", *Solar Cells* **30**, 69 (1991).
2. D. S. Albin, G. D. Mooney, A. Duda, J. Tuttle, R. Matson, and R. Noufi, "Enhanced Grain Growth in Polycrystalline CuInSe<sub>2</sub> Using Rapid Thermal Processing", *Solar Cells* **30**, 47 (1991).
3. A. M. Gabor, A. M. Hermann, J. R. Tuttle, A. Swartzlander, D. S. Albin, and R. Noufi, "CuInSe<sub>2</sub> Thin Film Formation by Rapid Annealing of the Elemental Precursor", Conference Record of the NREL 11th Photovoltaic Advanced Research and Development Review Meeting, Denver, Colorado (APS, 1992).
4. S. Yamanaka, M. Tanda, K. Horino, K. Ito, A. Yamada, M. Konagai, and K. Takahashi, "Raman Scattering Study of CuInSe<sub>2</sub> Films Prepared by Three-Source RF-Sputtering and by Selenization of Cu/In/Se Stacked Layers", Conference Record of the 21st IEEE Photovoltaic Specialists Conference, Kissimmee, Florida (IEEE, New York, 1990), p. 758.
5. T. Yamaguchi, Y. Baba, M. Nishimura, J. Matsufusa, and A. Yoshida, "Thermal Crystallization of Copper Indium Diselenide Films in Flowing or Pressurized Atmosphere", *Phys. Stat. Sol. (a)* **128**, 455 (1991).

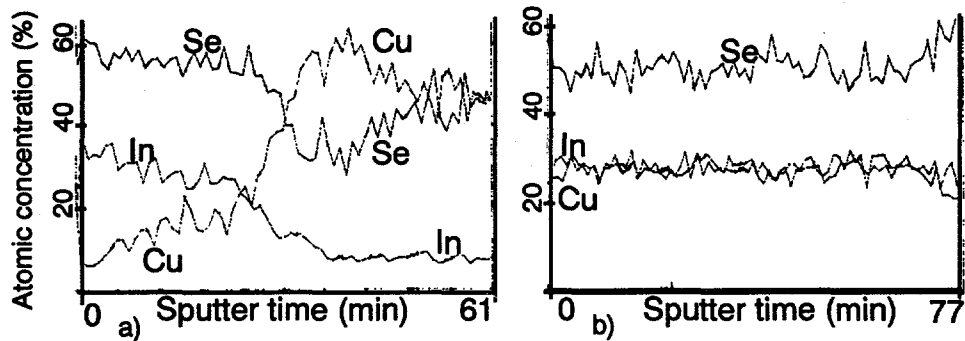


Figure 1. Auger depth profiles of a Cu-poor (a) precursor and (b) annealed sample. The horizontal axis is sputter time or, equivalently, depth in the film. The vertical scale is approximate atomic concentration.

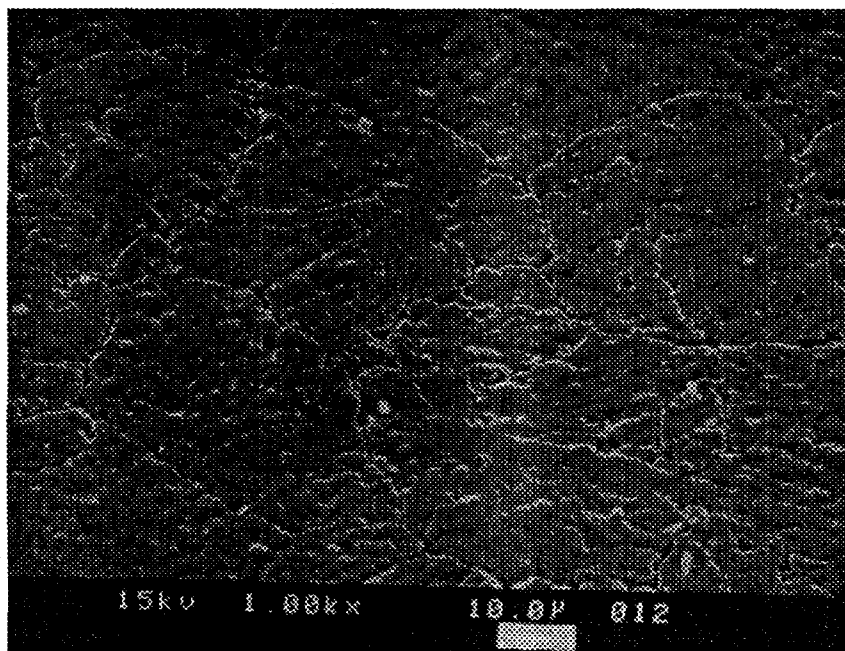


Figure 2. SEM micrograph of a film annealed at 775 °C for 10 s.

**Title:** Polycrystalline Thin-Film Materials and Devices

**Organization:** Institute of Energy Conversion  
University of Delaware  
United States Department of Energy  
University Center of Excellence  
Newark, Delaware 19716-3820

**Contributors:** R.W. Birkmire and J.E. Phillips, principal investigators; S.S. Hegedus, B.E. McCandless and W.N. Shafarman

### Objectives

The objectives of this research are to obtain the understanding of the materials processing, properties and performance of polycrystalline  $\text{CuInSe}_2$  and  $\text{CdTe}$  thin-film solar cells needed to achieve the goals for efficiency, reliability and cost for flat plate thin-film photovoltaic systems set by DOE for the National Photovoltaics Program. A further objective of this program is to support the development of a competitive U.S. photovoltaic industry through collaboration with other research groups and the training of photovoltaic engineers and scientists.

### Technical Approach

Issues for  $\text{CuInSe}_2$  addressed in this work are development of a process for forming  $\text{CuInSe}_2$  films by the selenization of Cu and In layers with Se and understanding the mechanisms that limit  $V_{oc}$  in  $\text{CuInSe}_2/\text{CdS}$  solar cells. Research on  $\text{CdTe}$  is concerned with processing used to fabricate high efficiency  $\text{CdTe}/\text{CdS}$  solar cells with evaporated  $\text{CdTe}$ .

### Results

This is a report on Phase II of a three year phased research program of integrated investigations of processing, properties, and performance of polycrystalline thin film  $\text{CuInSe}_2$  and  $\text{CdTe}$  based heterojunction solar cells.

### CuInSe<sub>2</sub> Processing

$\text{CuInSe}_2$  films were grown by three source elemental evaporation and selenization using both  $\text{H}_2\text{Se}$  and elemental Se. High quality  $\text{CuInSe}_2$  films were made by all three methods leading to high efficiency cells.

Copper-indium bilayers were selenized in 1) a tubular reactor with flowing  $\text{H}_2\text{Se}$  at atmospheric pressure, and 2) an evaporator using a Se source. In both systems, the selenizations were carried out at temperatures ranging from  $150^\circ\text{C}$  to  $400^\circ\text{C}$  for 60 minutes. Additionally, in the tubular reactor, copper-indium bilayers were selenized at  $400^\circ\text{C}$  for 1-45 minutes. The operating conditions in the tubular reactor were selected to ensure that the decomposition of  $\text{H}_2\text{Se}$  to  $\text{Se}_x$  species was less than 1%. The reaction pathways to  $\text{CuInSe}_2$  formation using either  $\text{H}_2\text{Se}$  or Se proceed through the formation of a  $\text{Cu}_{11}\text{In}_9$  alloy and the indium selenide phases ( $\text{In}_2\text{Se}$  and  $\text{InSe}$ )(see Table 1). The only different precursors between the two reacting systems are the copper selenide phases which were



observed with selenization in the evaporator. The reaction with Se proceeds faster than the reaction with  $H_2Se$ .

$CuInSe_2$  superstrate devices were fabricated under various growth conditions using different thicknesses of both In-doped and undoped evaporated CdS as a substrate. Good ohmic contact to the  $CuInSe_2$  was made by both Pt and Ni. Reasonable devices could be made only with  $CuInSe_2$  films having a Cu/In ratio between 0.5 and 0.7 where a  $CuIn_2Se_{3.5}$  phase, in addition to the  $CuInSe_2$  phase, was detected. With Cu/In ratios greater than 0.9, interdiffusion and alloy formation dominate the film. Devices made from selenized films had the best open circuit voltages although all of the devices had low  $V_{oc}$ . All of the devices had a strong light-to-dark crossover in the I-V characteristics. This is attributed to highly resistive and photoconductive CdS which could be caused by Cu diffusion.

### CdTe Processing

By analyzing CdTe/CdS devices fabricated by vacuum evaporation, a self consistent picture of the effects of processing on the evolution of CdTe cells was developed which can be applied to other fabrication methods. In fabricating CdTe/CdS solar cells by evaporation, a 400°C  $CdCl_2$  heat treatment is used which recrystallizes the CdTe and interdiffuses the CdS and CdTe layers. The interdiffusion can change the bandgap of both the CdTe and CdS which modifies the spectral response of the solar cell. After this heat treatment a contacting/doping procedure is used which converts the CdTe conductivity to p-type by diffusion of Cu from the contact. Finally, the cell is treated with  $Br_2CH_3OH$  which improves both  $V_{oc}$  and FF. Analogous process steps are used in most fabrication processes for CdTe/CdS solar cells.

### Device Operation

Research on the mode(s) of operation of these devices has given the following indications.

The effect of interface recombination on the light generated current in a thin film heterojunction solar cell can be reduced by making sure that most of the junction built-in voltage (or diffusion voltage) is across the absorber layer at the interface.

The loss of minority carriers to grain boundary recombination in the polycrystalline absorber can be reduced if the grain boundary edges are more heavily doped than the bulk.

Because of the two dimensional problem created by the grain boundaries, simple one dimensional modeling will only give "averaged" values for the electronic properties of the absorber.

From current-voltage measurements, it appears that recombination in the space charge region of the absorber controls the diode current during solar cell operation.

Analysis of the J-V characteristics as a function of temperature has shown that the  $\text{CuInSe}_2$  cells are controlled by a single current mechanism, SRH recombination. There is no evidence of a transition to a lower A factor at forward bias as had been predicted by a standard interface recombination model. And the diode behavior at a given intensity is described by the standard temperature dependence with no evidence of tunnelling or other mechanisms with different temperature dependence.

In the case of CdTe, if the voltage dependent current collection ( $J_L(V)$ ) as shown by spectral response measurements is included in the diode analysis of current-voltage measurements made under illumination, then both the dark and light analysis give a barrier height ( $\phi$ ) near 1.3 eV with a diode quality factor (A) of about 1.8 (see figures 1 and 2). These are indications that the CdTe/CdS solar cell operates as a p-n heterojunction and has a current transport mechanism dominated by Shockley-Read-Hall recombination in the space charge region of the CdTe.

Table 1a Results summary for the selenization of the Cu-In bilayers in the tubular reactor using the  $\text{H}_2\text{Se}$  gas source

Temperature (°C)	Time (min.)	Cu-In Pre-Treatment	$\text{H}_2\text{Se}$ gas concn (mole%)	Phases Observed			$^1\text{CuInSe}_2(112)$ $^1\text{Cu}_{11}\text{In}_9(313)$
				metals	binary selenides	ternary selenides	
150	60	Yes	1.7	$\text{Cu}_{11}\text{In}_9, \text{In}$	$\text{In}_2\text{Se}$		0
250	60	Yes	1.7	$\text{Cu}_{11}\text{In}_9$	$\text{In}_2\text{Se}$	$\text{CuInSe}_2$	0.08
350	60	Yes	1.7	$\text{Cu}_{11}\text{In}_9$	$\text{In}_2\text{Se}, \text{InSe}$	$\text{CuInSe}_2$	16.4
400	1	No	3.4	$\text{Cu}_{11}\text{In}_9, \text{In}$	$\text{In}_2\text{Se}$		0
400	2	No	3.4	$\text{Cu}_{11}\text{In}_9$	$\text{In}_2\text{Se}, \text{InSe}$	$\text{CuInSe}_2$	1.4
400	5	No	3.4	$\text{Cu}_{11}\text{In}_9$	$\text{In}_2\text{Se}, \text{InSe}$	$\text{CuInSe}_2$	4.2
400	10	No	3.4		$\text{InSe}, \text{In}_2\text{Se}_3$	$\text{CuInSe}_2$	-
400	15	No	3.4		$\text{InSe}, \text{In}_2\text{Se}_3$	$\text{CuInSe}_2$	-
400	30	No	3.4		$\text{InSe}, \text{In}_2\text{Se}_3$	$\text{CuInSe}_2$	-
400	45	No	3.4		$\text{InSe}$	$\text{CuInSe}_2$	-
400	45	No	3.4			$\text{CuInSe}_2$	-

Table 1b Results summary for the selenization of the Cu-In bilayers in the FVD reactor using the elemental Se source

Temperature (°C)	Time (min.)	Phases Observed			$^1\text{CuInSe}_2(112)$ $^1\text{Cu}_{11}\text{In}_9(313)$
		metals	binary selenides	ternary selenides	
150	60	$\text{Cu}_{11}\text{In}_9, \text{In}$	$\text{In}_2\text{Se}$		0
200	60	$\text{Cu}_{11}\text{In}_9$	$\text{In}_2\text{Se}, \text{InSe}, \text{CuSe}$		0
250	60	$\text{Cu}_{11}\text{In}_9$	$\text{In}_2\text{Se}, \text{InSe}, \text{CuSe}, \text{Cu}_7\text{Se}_4$	$\text{CuInSe}_2$	4.0
300	60	$\text{Cu}_{11}\text{In}_9$	$\text{InSe}$	$\text{CuInSe}_2$	37.5
400	60			$\text{CuInSe}_2$	-

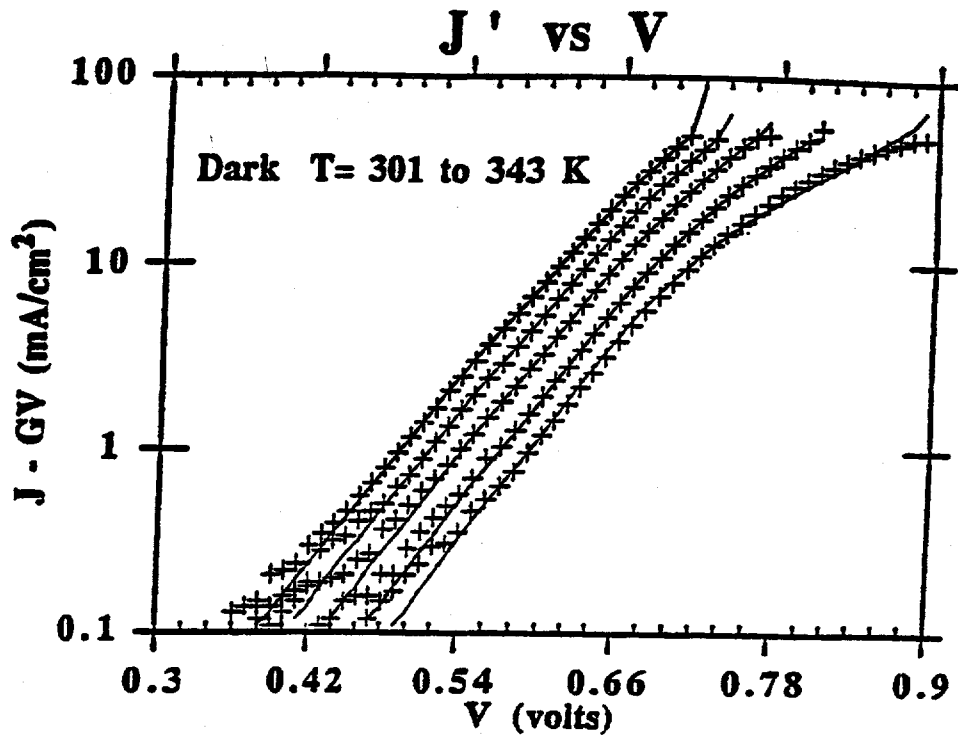


Figure 1.  $J'$  (corrected for shunt conductance vs.  $V$  (Line is for  $A=1.7$ )).

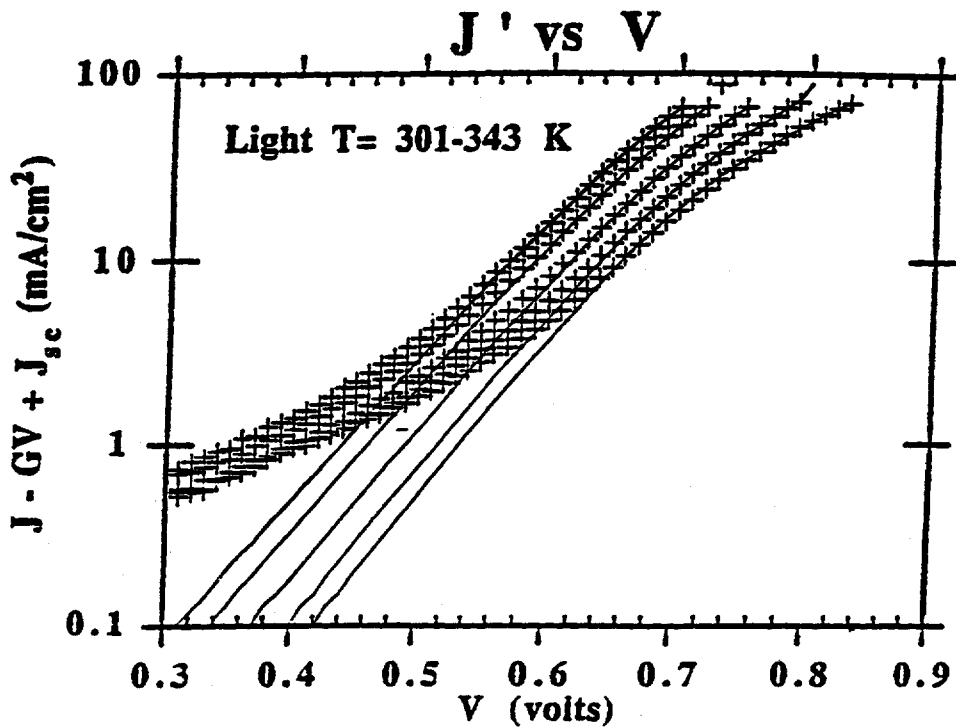


Figure 2.  $J'$  (corrected for shunt conductance and short circuit current) vs.  $V$ . (Line is for  $A=1.9$ ).

**Title:**                    **Advanced Processing Technology for High Efficiency CuInSe<sub>2</sub> Solar Cells**

**Organization:**        Department of Electrical Engineering  
University of South Florida  
Tampa, Florida

**Contributors:**        D. L. Morel, Principal Investigator, G. Attar, S. Karthikeyan,  
A. Muthiah, A. Zafar

### **Objective**

The objective of this project is to develop novel deposition technologies for CuInSe<sub>2</sub>(CIS) which do not use H<sub>2</sub>Se and to develop accompanying junction formation techniques which will result in state-of-the-art device performance.

### **Approach**

CIS solar cells are presently made by one of two techniques: coevaporation of the elements, or deposition of Cu and In followed by annealing in a H<sub>2</sub>Se environment. The coevaporation technique is difficult to scale up because of the precise control that would be required over large areas. While the second process has been scaled up by Siemens<sup>1</sup>, the use of large quantities of H<sub>2</sub>Se in a production environment adds risk and cost to the manufacturing process. An alternative is to use a similar process of metal deposition followed by an anneal step in which the selenium is supplied by a vapor of elemental selenium. There are several laboratories which are reporting progress on this approach and two have reported efficiencies in excess of 10%<sup>2</sup>. This provides an existence proof for the concept, but there are additional factors to be worked. In particular, there is evidence<sup>2</sup> that the conditions for selenium deposition used in these studies may require control measures that add considerably to manufacturing cost.

In recognition of the stringent requirements for manufacturing costs we have chosen two approaches which we feel would honor those requirements. The challenge is to demonstrate that they can produce quality material as have the techniques mentioned above. The first of these techniques, which we call "coat and cook", is a two-step process in which the three elements are first deposited under nominal conditions and at high rates and are then annealed. During the anneal step there is incidental selenium flux present which allows the surface to form properly. The second process is also a two-step process in which the metals are deposited first, and then during the anneal step the selenium is supplied by a "generic flux" from a large area selenium source as in close-space sublimation. Both techniques are run at low to moderate vacuum levels and require little to no control over the selenium flux. Using these techniques we deposited electronic quality CIS from which we made the first CIS thin-film transistors(TFT)<sup>3</sup>. However, TFT's require very thin layers of only a few hundred angstroms, while solar cells require an order of magnitude more thickness. Thus we have had to make significant changes in our film formation procedures.

Our hope is that one or both processes will produce CIS films with good surface as well as

bulk properties. Our expectations are that the surface may not be defect free for the as-made films. Consequently as a parallel effort to CIS development we are focusing resources on surface treatment and junction formation. Although the best devices to date are made with solution deposited CdS, we suspect that the primary role of the solution is to reduce surface defects. It may be that we are forming a shallow homojunction and the CdS per se is incidental. In keeping with this hypothesis we are pursuing various types of surface treatments and deposition techniques for transparent conductors.

## **Results and Discussion**

### Structural Properties

The first six months of this project have focused upon development of representative properties for CIS films. As indicated above, we had previously deposited electronic quality CIS but only in thicknesses of a few hundred angstroms. Our initial concern was to modify our process so that homogeneous films could be made in thicknesses of a micron or more. After having tried a number of process variations we have determined that it is relatively straightforward to achieve good bulk stoichiometry, grain size and homogeneity. Results in Table I below are representative of our findings. The sample was made by the "coat and cook" process in which the metal layers were deposited first followed by a selenium which was 20% thicker than required for stoichiometry. Total film thickness was about 2  $\mu\text{m}$ . The compositions were determined by EDS measurements using an NREL supplied reference of comparable composition<sup>4</sup>.

These results are for a sample which peeled from the substrate. As can be seen the stoichiometry of the top and bottom of the peeled film are equivalent indicating good homogeneity. The third column is the composition of the Mo surface from which the film peeled. The significant quantity of Se, probably in the form of  $\text{MoSe}_2$ , is indicative of its ability to successfully penetrate the metal sublayers during the anneal. The absence of Cu on this surface is also indicative of its diffusion prowess.

Achieving grain size of order one micron has also not been a problem. However, we suspect that there is substructure in what we perceive as grains which is a variable for a given nominal grain size. We believe that such structural issues play a significant role in film adhesion. We have observed that in general large grain size produces poor adhesion. However, we have also been able to achieve good adhesion with large grain size by manipulating our process. This has suggested to us that while large grain size may inhibit adhesion, there are substructural phenomena that can be accessed which override this tendency.

### Electronic Properties

This project has efficiency goals and objectives and will ultimately be judged on that basis. However, in this early stage of process development we have fabricated only diagnostic devices to evaluate our CIS film properties. These devices consist of only a plain vanilla ZnO heterojunction contact in which the ZnO is deposited by sputtering. Since we expect

our films to be dominated by surface states, this junction formation process provides a minimum of disturbance to the surface allowing us to track the effect of film processing on surface as well as bulk properties. To first order we evaluate film bulk properties through  $J_{sc}$  and surface properties through  $V_{oc}$ . These are backed up with other measurements such as spectral response and CV to verify that they are providing proper guidance to our processing efforts.

In addition to pursuing high efficiency we are also concerned with determining the sensitivity of our process to small changes in process parameters, as this is a key issue in manufacturability. An example of this sensitivity for our "coat and cook" process is shown in Fig. 1. The parameter of interest is the thickness of Se. Noting that the stoichiometric thickness in this case is about  $.95 \mu\text{m}$ , we observe that some excess Se is required for good performance, but the performance drops off again as the Se is increased further. To calibrate the results we note that 200 mV is typical for plain vanilla ZnO contacts, and the peak current of 1 mA corresponds to  $20 - 30 \text{ mA/cm}^2$  (these are small area devices with the usual uncertainties). This is recent data which represents work in progress. As we fill in the curve with additional points we will be better able to delineate the sensitivity factor of interest. We also note that this curve is for one particular rendition of our anneal profile. Preliminary results from variations in the profile indicate that the peak values as well as sensitivities are strongly influenced by the profile.

Our results to date suggest that we are able to achieve good bulk properties over a reasonable range of processing space. The challenge now is to control the surface to pursue efficiency optimization. As we have tuned our process toward the optimization of bulk properties we have observed a steadily increasing  $V_{oc}$  as well. We were stuck for some time at 120 mV which suggested that interface states were dominating junction formation. This was corroborated by fabrication of solution deposited CdS junctions which produced identical voltages. In Fig. 2 the presence of the interface states for one of these devices is indicated by the bending up of the CV curve under forward bias. The bulk "acceptor density" for this film is  $9.5 \times 10^{15}/\text{cm}^3$ . We interpret the departure from the linear range as an increase in defects as the surface is approached.

Recently we have seen our  $V_{oc}$ 's for ZnO creep up to and beyond 200 mV. We also observe higher  $V_{oc}$ 's for CdS junctions in these same devices indicating that the interface states are diminishing. In fact, we are now seeing evidence of performance being limited by series and shunt resistance, that is, "device level" rather than material level problems. We take this as a measure of success for our materials development efforts and also as a mandate to now devote necessary attention to device development.

## Conclusions

We have developed a novel, manufacturing compatible process for the deposition of  $\text{CuInSe}_2$  which uses elemental selenium as the source of selenium rather than  $\text{H}_2\text{Se}$ . Bulk properties exhibit good stoichiometry, grain size and  $J_{sc}$ . Surface properties have also been improving as evidenced by steadily increasing  $V_{oc}$ 's for ZnO analytical junctions. Efforts will now be directed toward forming state-of-the-art junctions to optimize efficiencies.

## References

1. J. Ermer, C. Fredric, J. Hummel, C. Jensen, D. Pier, D. Tarrant, and K. Mitchell, Proceedings of the 21st IEEE PV Specialists Conference, Kissimmee, FL, May 21-25, 1990, p. 595.
2. See "Fundamental Thermodynamics and Experiments in Fabricating High Efficiency CuInSe<sub>2</sub> Solar Cells by Selenization Without the Use of H<sub>2</sub>Se", by D. Albin, J. Carapella, A. Gabor, A. Tennant, J. Tuttle, A. Duda, R. Matson, A. Mason, M. Contreras, and Rommel Noufi, to be published in AIP Conference Proceedings, Photovoltaic Advanced Research and Development 11th Review Meeting, Denver, CO, 1992.
3. J. Lai, L. Cai, D. L. Morel, Appl. Phys. Lett. **59**(16), 1991, 1990.
4. We wish to thank Rommel Noufi of NREL for supplying the EDS reference.

TABLE I

ATOMIC PERCENT COMPOSITION			
	PEELED SAMPLE		MO SURFACE
	TOP	BOTTOM	
CU	24.5	23.3	0
IN	27.0	27.6	03.2
SE	48.5	49.1	20.0
MO	0	0	76.8

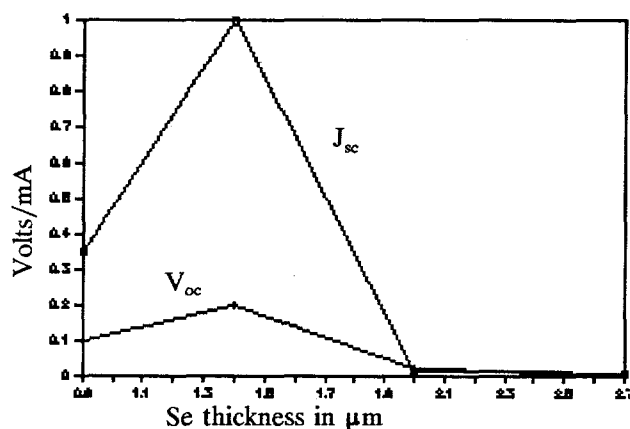


Figure 1.  $J_{sc}$  and  $V_{oc}$  vs. Se thickness.

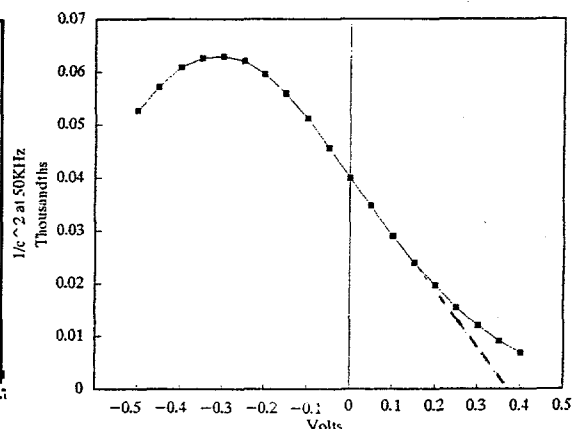


Figure 2.  $1/C^2$  vs. bias.

**Title: Thin Film Cadmium Telluride Photovoltaic Cells**

**Organization:** Department of Physics and Astronomy  
The University of Toledo  
Toledo, OH 43606

**Contributors:** Alvin D. Compaan, principal investigator; Randy G. Bohn, co-investigator; Charles N. Tabory, Meilun Shao, Yuxin Li, Zhirong Feng, Andreas Fischer, and Li-Hua Tsien.

### **Objectives**

In the second year of support from the Polycrystalline Thin Films Program, our principal objective has been improved performance of small-area CdTe solar cells grown by the techniques of radio-frequency (rf) magnetron sputtering and laser-driven physical vapor deposition (LDPVD). Although some fundamental studies of the LDPVD process continued, much of the LDPVD effort focussed on exploring issues such as doping, optimizing of layer thickness, and optimizing contacting procedures, which would be relevant to the rf sputtering process. As of October 1992, the all-LDPVD process has produced a 10.5% solar cell and the rf sputtering process (used for both CdS and CdTe) has yielded a 10.4% (AM1.5) cell.

### **Technical Approaches**

At the University of Toledo, we have been pursuing in parallel the two vacuum-based techniques described above.<sup>1,2,3</sup> Over the past year more effort has shifted to rf sputtering as a technique more easily scalable to large areas and one with which the glass industry already has significant experience for coatings. Most of this effort has addressed the sputtering of CdTe but some effort has been given to CdS films as well.

The laser deposition work has included pure CdS, CdTe and ZnTe thin film depositions and some effort has been given toward examining doping effects in these materials. Although there are some significant differences between sputtering and LDPVD, especially in the kinetic energy of the atomic species (~20 eV for LDPVD and hundreds of eV for sputtering), much of the deposition physics is similar.<sup>4</sup> Thus we have often used LDPVD to help optimize parameters for sputtering. These include deposition temperatures, film thicknesses, substrate preparation, post-deposition treatments, and contacting. Our system for LDPVD has the advantage of permitting rapid target preparation since we cold press the targets ourselves. Also, three or four sequential depositions from different solid targets can be done onto a single substrate without exposure to air.

During the second year, Solar Cells Inc has no longer been a lower-tier subcontractor in this project; however, there have been continuing collaborations between the UT group and SCI. This has included some preliminary work on rf sputtering of ZnTe.



In addition to the film growth, device fabrication, and device characterization measurements such as IV and spectral quantum efficiency, we have pursued fundamental studies on the nature of the laser ablation plume and detailed characterization studies of the as-deposited and post-deposition-treated films. Our transient optical studies of atomic emission lines in the laser ablation plume have yielded measurements of the translational kinetic energies ( $\leq 25$  eV) and internal excitation energies ( $\geq 6$  eV for some of the atomic species).<sup>2,5,6</sup> To examine the materials properties of the films, we have actively pursued Raman scattering and photoluminescence, SEM and EDS studies, as well as electrical conductivity and Hall effect measurements.<sup>7</sup>

### **Studies of Doping of CdS, CdTe, and ZnTe**

With the LDPVD process, dopants have been incorporated into the films simply by mixing the dopant powders into the pure semiconductor powder before pressing into the final target receptacle and performing the laser deposition in the usual way. This works very well for CdS:In and ZnTe:Cu but only low electrical activities have been observed for various dopants in CdTe (Sb, As, P). Results obtained for ZnTe:Cu are described below.

A series of laser-deposited films of ZnTe:Cu were grown on Corning 7059 glass at 300 °C. The film resistivities, measured in a parallel stripe configuration, are shown in Figure 1 as a function of the amount of copper included in the target as elemental Cu powder mixed with the pure ZnTe powder before target pressing. Little change in resistivity occurs until the copper concentration in the target rises above 0.3 atomic percent. However, above this amount the resistivity falls dramatically over more than six orders of magnitude with a factor of three increase in Cu density. SEM/EDS measurements have shown the presence of Cu in the most heavily doped films at approximately the same concentration as the elemental Cu added to the target. In collaboration with Solar Cells Inc we have recently prepared Cu-doped ZnTe by rf sputtering and observed doping effects roughly similar to those described here for LDPVD films.

### **Results Obtained with the LDPVD Process**

During the past year steady progress has been made in improving the performance of cells grown by LDPVD--with efficiencies rising from 8.7% to 10.5%. We have determined that for this process the optimum CdS thickness is  $\sim 1000\text{\AA}$  with  $V_{OC}$  dropping for thinner CdS layers. The minimum CdTe thickness consistent with optimum efficiency is about 1.3  $\mu\text{m}$  but we have found greater than 10% efficiencies with CdTe thicknesses from 1.0 to 1.8  $\mu\text{m}$ . The best cell tested at NREL yielded  $J_{SC} = 20.69$  mA/cm<sup>2</sup>,  $V_{OC} = 0.7644$  V, FF = 66.64%, and efficiency = 10.5%. See Fig. 2. This cell was prepared on 10  $\Omega/\text{square}$  SnO<sub>2</sub>-coated soda-lime glass from LOF. The CdS and CdTe films were grown by laser deposition at 325 °C. About 0.2  $\mu\text{m}$  of CdCl<sub>2</sub> was then laser deposited at  $\sim 100$  °C followed by a 400 °C anneal in air. The contacts were evaporated Cu/Au.

### **Results Obtained with RF Sputtering**

Since our first rf sputtered film of CdTe was grown last year, we have continued to improve the film quality as measured by as-deposited grain size and photoluminescence. Photoluminescence of CdTe films deposited at different substrate temperatures is shown in Fig 3. In addition, during

the past year we have begun sputter deposition of CdS layers as well. Relying on experience gained from the LDPVD growth process, the photovoltaic performance of the all-sputtered cells has improved rapidly. NREL tests on one small cell have yielded an efficiency of 10.4% with  $V_{OC} = 0.8146$  V,  $J_{SC} = 17.61$  mA/cm<sup>2</sup>, and FF = 72.8%. See Fig. 4. Other than the sputtering, most of the processing steps were similar to those used for the LDPVD cells. Abou-Elfotouh, et al,<sup>8</sup> have recently reported the fabrication of a 6.7% efficient cell in which the CdTe was grown by rf sputtering and the CdS layer by evaporation. To our knowledge, ours is the first reported CdS/CdTe cell in which both layers were prepared by sputtering. Efforts are underway to reduce the CdS thickness to improve the short-circuit current. The excellent open circuit voltage and high fill factor suggest considerable promise for rf magnetron sputtering as a commercializable technology for large-area thin-film photovoltaics.

### Issues presently being addressed

In order better to simulate the effects of large area depositions and to be able to continue to evaluate new materials and dopants for possible use with other deposition methods including sputtering, we are modifying our LDPVD system to incorporate full x-y rastering over larger target areas. In addition, we will use larger polycrystalline sintered targets similar to those used in our sputtering system. Efforts are being put into finding contacting procedures and materials other than the presently used Cu and Au. We are also addressing further optimization of the layer thicknesses in the sputtered films and examining the relationship between film morphology and deposition conditions.

### References

1. A. Compaan, R.G. Bohn, A. Aydinli, A. Bhat, L. Tsien, S. Liu, Z. Chen, and C.N. Tabory, Annual Report, Photovoltaic Program, FY 1990. (March 1991). SERI/TP-211-3643. Available NTIS: Order NO. DE 90000318.
2. A. Compaan, R.G. Bohn, A. Aydinli, C. N. Tabory, L. Tsien, S. Liu, M. Shao, M.E. Savage, and Y. Li, Annual Report, Photovoltaic Program, FY 1990. (March 1992). NREL/TP-410-4724. 306 pp. Available NTIS: Order No. DE92001248.
3. A. Compaan, A. Bhat, C. Tabory, S. Liu, M. Nguyen, A. Aydinli, L-H. Tsien, and R.G. Bohn, Solar Cells **30**, -79 (1991).
4. A. Compaan, A. Bhat, C. Tabory, S. Liu, Y. Li, M.E. Savage, M. Shao, L. Tsien, and R.G. Bohn, Proc. 22nd IEEE Photovoltaic Specialists Conference-1991, 957 (1992).
5. A. Compaan, G.G. Bohn, A. Bhat, C. Tabory, M. Shao, Y. Li, M.E. Savage, and L. Tsien, NREL 11th Photovoltaic Advanced Research and Development Review Meeting (Denver May 13-15, 1992) AIP Conference Proceedings (to be published)
6. A. Bhat, Ph.D. Dissertation, U. of Toledo (1991), unpublished.
7. A. Compaan and A. Bhat, Int. J. Solar Energy, in press 1992
8. F. Abou-Elfotouh, M. Soliman, A.E. Riad, M. Al-Jassim, & T.J. Coutts, Proc. 22nd IEEE Photovoltaic Specialists Conference-1991, 1109 (1992).

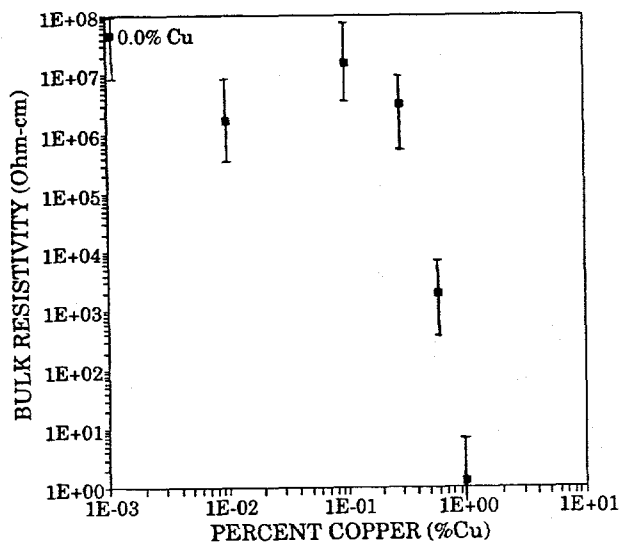


Fig. 1 Resistivity of ZnTe:Cu vs. atomic percent Cu in the target.

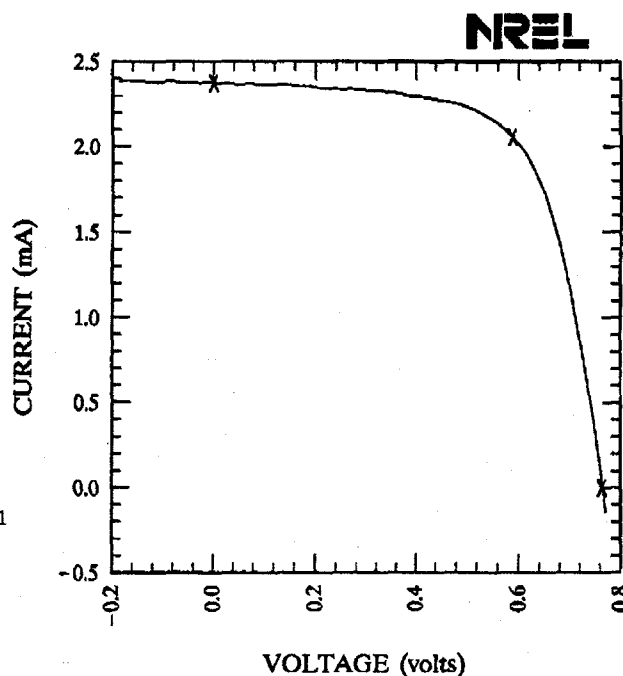


Fig. 2 I-V characteristics of LDPVD-grown CdS/CdTe cell (SC299-8).  $V_{oc}=0.764$  V,  $J_{sc}=20.7$  mA/cm<sup>2</sup>, FF=66.64%, and  $\eta=10.5\%$ . Cell area = 0.115 cm<sup>2</sup>.

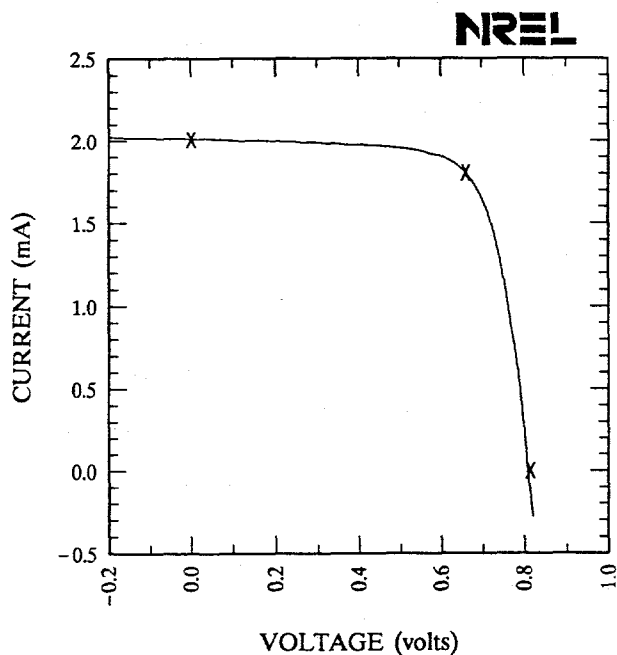


Fig. 4 I-V characteristics of an all-sputtered CdS/CdTe cell (SSC-4-29).  $V_{oc}=0.815$  V,  $J_{sc}=17.61$  mA/cm<sup>2</sup>, FF=72.8%, &  $\eta=10.4\%$ . Cell area = 0.114 cm<sup>2</sup>.

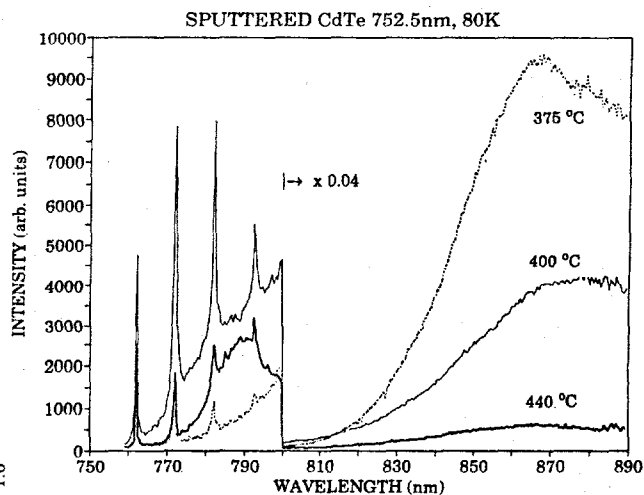


Fig. 3 PL spectra from sputtered CdTe films grown at substrate temperatures of 375, 400, and 440 °C.  $\lambda=752.5$  nm;  $T\cong 80$  K. Spectra have been corrected for spectrometer and detector response.

**Title:** Investigation Of Polycrystalline Thin Film CuInSe<sub>2</sub>  
Solar Cells Based On ZnSe Windows

**Organization:** Electronic Materials Laboratory  
Washington State University / Tri-Cities  
Richland, Washington

**Contributors:** Larry C. Olsen, principal Investigator;  
F.W. Addis, D.H. Huber, D. M. Greer.

### **Objectives /Approach**

The purpose of this program is to improve the performance of CIS-based and CIGS-based solar cells by developing and testing the use of ZnSe window layers. The use of ZnSe window layers is expected to lead to a ZnSe/CIS solar cell structure which exhibits a conversion efficiency > 14 %, and possibly higher efficiencies for ZnSe/CIGS cells, since ZnSe provides an improved lattice match with CIGS compared to CdS. The program is structured into three tasks: (1) CIS and CIGS cells with ZnSe windows; (2) Material and device characterization; and, (3) Device modeling. Task 1 comprises the major thrust of the program. This task involves acquisition and characterization of CIS substrates, MOCVD growth of ZnSe and ZnO and fabrication of ZnO/ZnSe/CIS solar cells. Task 2 includes T-I-V and photoresponse analyses of completed cells and Al/Schottky barriers. Finally, Task 3 concentrates on device modeling to support experimental studies. In particular, the utility of PC-1D software for analysis of CIS solar cell performance will be evaluated.

### **CIS and CIGS Cells with ZnSe Windows**

*Substrate Characterization* -- CIS substrates have been acquired from Siemens and ISET. Most of the work to date has been carried out with Siemens material. These CIS substrates consist of a CIS layer deposited onto Mo coated glass. The Siemens 10 cm square substrates are diced into nominally 2 cm x 2 cm die for various studies discussed below. Al/CIS Schottky barriers have been utilized extensively in this program for diagnostic purposes. For example, Al/CIS barriers were utilized for determining an approach to surface treatment prior to ZnSe deposition to form a heterojunction. It was determined that etching the CIS substrate with either KBr, Br or KCN aqueous solutions prior to Al deposition leads to consistent Al/CIS Schottky barrier properties.

*ZnSe/CIS and ZnSe/CIGS Heterojunctions* -- ZnSe/CIS heterojunctions are fabricated by MOCVD growth of ZnSe films on CIS substrates. MOCVD growth of ZnSe is accomplished in a SPIRE 500XT reactor housed in the Electronic Materials Laboratory by reacting a zinc adduct with H<sub>2</sub>Se. Work on this program (beginning 2/15/92) has led to procedures for growing n-type ZnSe with iodine as a dopant.

Ethyl iodide was mixed with helium and installed on one of the gas lines to the system. It is straight forward to grow ZnSe with a resistivity on the order of .05 ohm-cm on single crystal surfaces at 250°C. Iodine-doped ZnSe films grown on CIS have a much higher resistivity, but it is sufficiently low for heterojunction growth. ZnSe films have been grown on CIS substrates at 200°C to 250°C. Figure 1 gives X-ray diffraction results for a ZnSe film grown by MOCVD on a Siemens substrate at 200°C. Note the strong ZnSe (111) line intensity along with the CIS (112) line intensity. ZnSe/CIS heterojunctions were studied by growing n-ZnSe films onto 2 cm x 2 cm CIS substrates and then depositing an array of aluminum circular areas 2.8 mm in diameter on top of the ZnSe to serve as a contacts. Al films are deposited with a thickness of 80 to 100 Å so that light can pass through the film. Figure 2A gives I-V characteristics for a diagnostic device illuminated by an ELH bulb simulator with the intensity adjusted to approximately compensate for the 20 to 25 % transmittance of the Al film. Figure 2B depicts the device structure. Clearly, the efficiency value is an extrapolated result. It is significant, however, that under conditions for which the photon flux entering the ZnSe/CIS structure is similar to that for AM1 illumination, the open-circuit voltage is 512 mV and the fill factor is 0.617.

*ZnO Deposition* -- Modification of the WSU SPIRE 500XT reactor for ZnO growth has been accomplished. Tetrahydrofuran (THF) is reacted with a zinc adduct to grow ZnO. Three runs have been carried out to grow ZnO on substrates at 350°C. The ZnO films were not intentionally doped, but exhibited resistivities from .02 to 6 ohm-cm. Future work will involve further characterization of the system for growth of undoped and doped ZnO.

*Solar Cell Fabrication* -- A complete cell has not yet been fabricated. Recently, however, diagnostic devices were fabricated and have given encouraging results. Figure 3A gives illuminated characteristics for a device described in Figure 3B. Again, the light intensity was adjusted to compensate for the 20 to 25 % transmittance of the Al film. The ZnO film was approximately 0.3 µm thick and had a resistivity of 6 ohm-cm. Measurement of I-V characteristics between two Al circular areas indicates that a barrier exists between Al and ZnO. Thus, the illuminated I-V characteristics shown in Figure 3A are affected by contact resistance between Al and ZnO. We have verified that Al will make a low resistance contact with low resistance ZnO. Cell structures on the order of 1 cm<sup>2</sup> will be fabricated in the near future. These devices will involve a thin layer of high resistance ZnO and a thick layer of low resistance ZnO. It should be noted that the device described in Figure 3B involved MOCVD growth of ZnO onto a ZnSe/CIS heterojunction at 350°C for one hour. Thus, it appears that the ZnSe/CIS interface is rather stable.

### **Device Characterization and Device Modeling**

Device characterization has primarily involved dark and illuminated I-V analyses at room temperature. The approach utilized for the analyses is basically the same as previously described in Reference 1. Table 1 list results for a typical Al/CIS Schottky

barrier, and a typical ZnSe/CIS heterojunction. The I-V characteristics have been interpreted in terms of two loss mechanisms, one dominant at low voltages, .15 to .35 Volts, say, and one at higher voltages, .35 to .60 Volts, say. The low voltage mechanism is probably due to multiple step tunnelling while the upper mechanism is undoubtedly due to depletion region recombination. It appears that the I-V properties usually improve under illumination. Device modeling involve a low level effort to evaluate the utility of PC-1D for modeling of CIS-based solar cells.

### Conclusions

Based on characteristics of small area ZnSe/CIS and ZnO/ZnSe/CIS diagnostic devices, it appears that efficient ZnSe/CIS solar cells can be fabricated. Since ZnSe lattice matches CIGS with 70 % Ga, prospects for high efficiency ZnSe/CIGS cells also appear very likely. Finally, the key capabilities for fabrication of reasonable size ZnSe/CIS solar cells are now in place.

### References

1. Larry C. Olsen, et al., Proc. 18th IEEE Photovoltaic Specialists Conf.(1985).

TABLE 1 -- I-V PARAMETERS

Device	Rs • Area (Ohm • cm <sup>2</sup> )	Low Voltage Mechanism		High Voltage Mechanism	
		J <sub>0</sub> (A/cm <sup>2</sup> )	A	J <sub>0</sub> (A/cm <sup>2</sup> )	A
Al/CIS(Dark)	0.3	6.2 x 10 <sup>-4</sup>	14.4	1.0 x 10 <sup>-5</sup>	1.8
ZnSe/CIS 453-H(Light)	.048	1.56 x 10 <sup>-3</sup>	9.4	1.2 x 10 <sup>-7</sup>	1.6

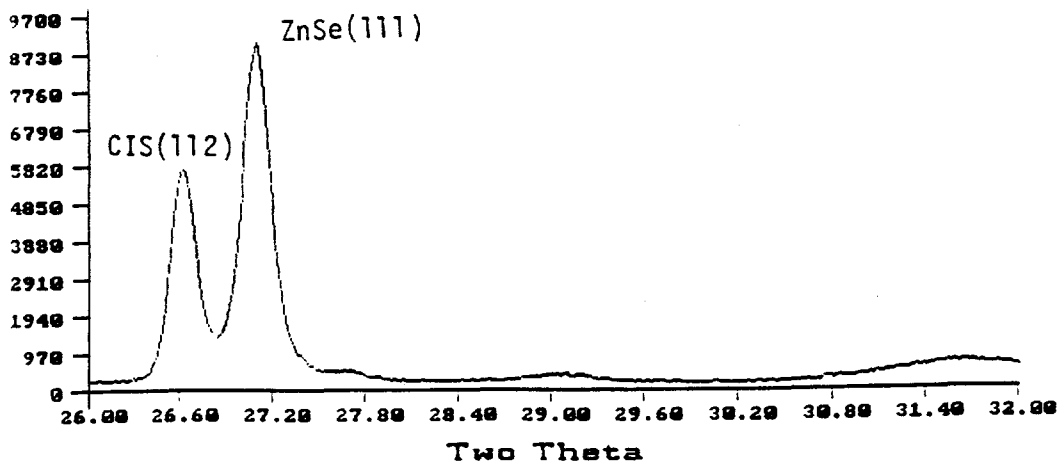
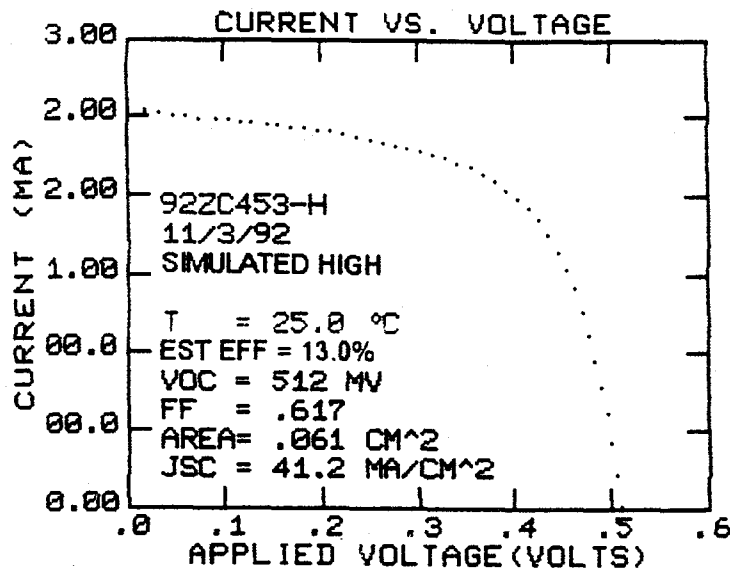


Figure 1. XRD Results for a 1 μm ZnSe Film Grown on a CIS Substrate.

(A)



(B)

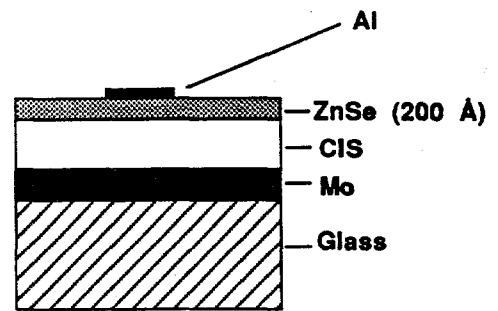
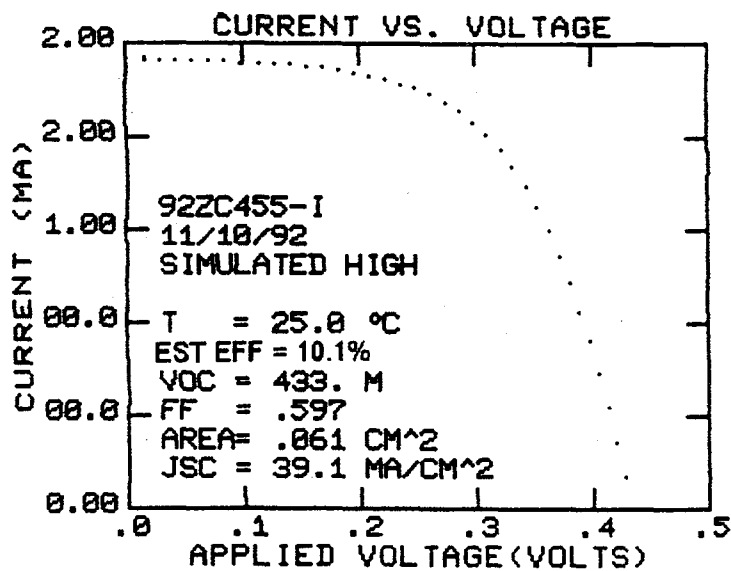


Figure 2. (A) I-V Characteristics For A .06 cm<sup>2</sup> ZnSe/CIS Heterojunction Under Approximate AM1 Illumination Taking Into Account Absorption in Top Al Film; (B) Cross Section Of Device (Not to Scale).

(A)



(B)

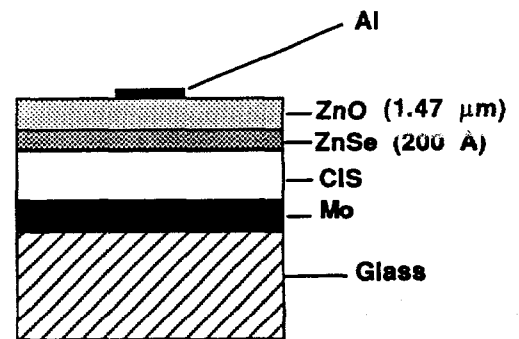


Figure 3. (A) I-V Characteristics For A .06 cm<sup>2</sup> ZnO/ZnSe/CIS Device Under Approximate AM1 Illumination Taking Into Account Absorption in Top Al Film; (B) Cross Section Of Device (Not to Scale).





## 4.0 AMORPHOUS SILICON RESEARCH PROJECT

Werner Luft (Manager)

Amorphous silicon photovoltaic commercial products had a 25% share of the worldwide photovoltaics market in 1991. The product is reliable, as exemplified by 10-year warranties of commercial power modules. The potential for low costs is the same as for any other thin-film photovoltaic technology, namely \$1-2/W. Gradual efficiency improvements are constantly being demonstrated. The best prototype module stable efficiencies are now 8.9%.

The near-term objective of the Amorphous Silicon Research Project is to achieve 12% stable prototype module efficiency by 1994 in accordance with the goals in DOE's *Photovoltaics Program Plan FY 1991-FY 1995* through better understanding and improvement of the optoelectronic properties of amorphous-silicon-based alloy materials. Additional near-term objectives are to gain an understanding of the metastability in amorphous silicon, reduce the costs to \$1/Wp, and to foster a viable amorphous silicon photovoltaic industry in the United States. A transition in emphasis did occur in FY 1990 from single-junction amorphous silicon cell and submodule research to multijunction module research, and from initial efficiency to stabilized efficiency. NREL implemented the transition in FY 1991 to focus industrial subcontractors and university subcontractors on *stabilized* efficiencies, rather than to focus on maximizing initial performance and minimizing degradation. The focus on stabilized efficiency continued in 1992.

Long-term objectives (year 2005) are to achieve commercial amorphous silicon module stable efficiencies of over 12%, elimination of the Staebler-Wronski effect, reduction of module costs for electric power utility applications to \$0.50/Wp corresponding to 6 cents/kWh.

The Amorphous Silicon Research Project (ASRP) consists of three tasks: 1) subcontracted research, 2) NREL a-Si research, and 3) surface and interface analysis. Within the subcontracted research there are two principal activities: subcontracted multidisciplinary research activities, and subcontracted fundamental research activities. The subcontracted multi-disciplinary research activities are performed under cost-shared programs between government and industry by broad-based research teams located at the individual industrial facilities that perform focused research ranging from feedstock materials through to the development of modules. The subcontracted fundamental research activities involve basic and supporting research done by academia and research laboratories to aid the industry groups' advances of the technology base. The cost-shared subcontracted multidisciplinary research programs address issues related to all aspects of 2-terminal amorphous silicon multijunction cells and modules using same-bandgap or different-bandgap device structures. Research was performed to advance the stabilized conversion efficiency of multijunction modules having areas of at least 900 cm<sup>2</sup>, using glow discharge deposition as the primary method of fabricating the amorphous silicon films. The stability of these devices was examined for fundamental changes in the bulk material properties, for temperature effects such as diffusion, for fabrication and area-related defects (interfaces), and for extrinsic degradation related to module encapsulation and framing issues. Transparent conductors were studied to improve the electrical conductivity while achieving optical transmissions greater than 85%. The quality and controlled texturing of ZnO transparent conductors based on low-cost processes was emphasized. The opto-electronic properties of a-SiGe:H and a-SiC:H alloy materials were investigated to determine the limits of these materials with regard to their use in practical multijunction devices. The interconnection of cells in a series-connected module

configuration was a major issue studied, since it affects conversion efficiency through the inactive area losses, influences stability through changes over time in the contact resistance, and influences cost through its impact on yield and on the number and types of processing steps.

Subcontracted research, cost-shared with industry, was initiated in FY 1990 to transfer the small-area technology developed under previous government/industry initiatives to large-area multijunction modules that are stable, reliable, reproducible, and have low cost. For this purpose, a new government/industry program with 3-year subcontracts was started in FY 1990. Four subcontracts were awarded (Solarex, Glasstech Solar Inc., United Solar Systems Corporation, and Advanced Photovoltaic Systems). One of these (GSI) was subsequently terminated after 6 months of work. The principal objectives of this research are: 1) to conduct research on semiconductor materials and non-semiconductor materials to enhance two-terminal, multijunction, thin-film, large-area, all-amorphous-silicon-alloy device performance; 2) to develop high-efficiency, *stable*, *reproducible*, and *low-cost* multijunction photovoltaic modules based on all-amorphous materials; 3) to demonstrate in stable 12% (AM 1.5) aperture area solar conversion efficiency for different-bandgap modules; and 4) to demonstrate in stable 10% (AM 1.5) aperture-area solar conversion efficiency for same-bandgap modules. The modules will be at least 900 cm<sup>2</sup> in area and consist of at least two integrally stacked devices using all-amorphous-silicon alloy materials. The government/industry program has been highly successful and significant advances have been made in cell/module performance.

The total subcontracted fundamental research program (with the exception of ZnO transparent electrode development) was re-competed in FY 1990. Ten 3-year awards were made in FY 1991 under the competitive procurement to Colorado School of Mines, Institute of Energy Conversion, Iowa State University, North Carolina State University, Pennsylvania State University, Syracuse University, University of Illinois, University of North Carolina, University of Oregon, and Xerox. Two additional non-competitive awards were made to the National Institute of Standards and Technology and the Jet Propulsion Laboratory. The subcontract with the Jet Propulsion Laboratory was terminated in FY 1992 because the research did not reach the milestones. The following general areas are being addressed in support of the multidisciplinary activities: light-induced stability, alternative material deposition approaches, amorphous silicon alloy materials, and material characterization. Several models have been proposed to explain metastable effects observed in amorphous silicon films. More research was done to differentiate between the often subtle aspects and predictions of the models. More importantly, research was done on photovoltaic devices to correlate light-induced changes in the films with light-induced changes in the device performance. Continued research was done on both high and low bandgap alloys to determine the relationship of observed structural inhomogeneities to electrical transport properties. Research was done on high and low bandgap alloys in device structures and under measurement conditions that simulate the intended end-use environment of the materials. Alternative deposition methods are explored to improve or develop discrete component layers such as wide bandgap, high conductivity doped layers, or alloy films. As the amorphous silicon technology matures, more sophisticated measurement and characterization techniques are needed for studies from the atomic level to characterization of materials in efficient photovoltaic devices. Collaborations between the fundamental research groups, government/industry research groups, and the NREL internal research groups was maintained through sample exchanges, workshops, and co-publications.

The objective of NREL in-house amorphous silicon research is to provide technical leadership and innovation, provide linkage between industry and universities, ensure effective scientific collaboration, provide continuity for research in the United States, and ensure validity of external research results.

During FY 1992, the NREL in-house research by the amorphous silicon group covered four investigations: 1) hot wire (HW) film deposition, 2) improved hot wire solar cells, 3) intrinsic layer/p-i-n cell degradation study, and 4) experimental investigation of metastability. The first investigation was to better understand the hot-wire deposition technique for a-Si:H materials suitable for stable high-efficiency solar cells. The investigation will fully characterize the electronic properties of hot-wire films. The second investigation built on the results of the first to make solar cells with better stabilized performance using HW deposition for some of the semiconductor layers. The third investigation determined whether the degradation caused by light-soaking of intrinsic a-Si:H layers correlates with the degradation of solar cells using such intrinsic layers; and under what conditions. Finally, the last project was to experimentally determine which of two models of the Staebler-Wronski effect is valid, and to what extent. The deposition of a-Si:H using concentrated silane was stopped at the beginning of May 1991 for safety reasons in the existing laboratories in Building 16 of NREL. To restart deposition from concentrated silane, the activity was moved to the Joyce Street leased facility. A Safety Analysis Review was prepared for the Joyce Street facility. Facility modifications as well as deposition equipment modifications were required and implemented to meet safety demands. Shake-down of the modified facility and equipment was expected to be completed by November 1992.

Surface analysis techniques, including scanning Auger microscopy, x-ray photoelectron spectroscopy, secondary ion mass spectrometry, electron energy loss spectroscopy, and scanning tunneling microscopy was used to support the chemical and compositional properties and the electronic structure of amorphous silicon materials and devices.



**Title: Research on Amorphous-Silicon-Based Thin Film Photovoltaic Devices**

**Organization: Solarex Corporation, Thin Film Division  
826 Newtown-Yardley Road, Newtown, PA 18940**

**Contributors: R.R. Arya, Program Manager; L. Yang, Task I Project Leader; R.V. D'Aiello, Task II Project Leader; J. Newton, Task III Project Leader; M. Bennett, L. Chen, B. Fieselmann, Y.-M. Li, R. Podlesney, C. Poplawski, K. Rajan, S. Wiedeman, G. Wood**

### **Introduction**

Amorphous silicon based triple junction devices offer the potential for achieving low-cost and high performance modules. In the triple junction approach, the bandgap and thickness of the i-layer's of each component cell can be optimized to respond to different parts of the solar spectrum resulting in thinner component cells and better stability. The objective of this three year cost-shared program is to demonstrate a 12% efficient (FY 1993) stable\* module. Towards this goal we have been addressing the important technological issues under three separate tasks. These tasks are: (I) semiconductor materials research, (II) non-semiconductor materials, and (III) module research.

Major accomplishments within these tasks are:

- Improvements in a-Si:H material properties which have led to the demonstration of high  $V_{oc}$  and definite stabilization in single junction devices.
- The demonstration of high open-circuit voltage ( $V_{oc} \sim 1V$ ) in a-SiC:H i-layer single junction devices prepared from novel feedstocks.
- Development of textured ZnO front contact which has led to the demonstration of about 23 mA/cm<sup>2</sup> total current in a triple junction solar cell.
- The demonstration of only 14% degradation in a-Si/a-Si/a-SiGe triple junction modules.
- The demonstration of 8.25% efficiency in a-Si/a-Si/a-SiGe triple junction module after 600 hours of light soaking.

### **Task I: Semiconductor Material Research**

Amorphous silicon films prepared by d.c glow-discharge of silane + hydrogen are found to be superior to those prepared with pure silane. At lower than normal deposition temperatures, the effect of increased H-dilution reduces the total H-content and the IR peak at 640 cm<sup>-1</sup> associated with dihydride bonds. The initial photovoltaic parameters of two single junction devices prepared with H-dilution of the i-layer are shown in Table I.

---

\* 600 hrs., AM1.5 exposure, 50°C; area  $\geq 900$  cm<sup>2</sup>

Cell #	$V_{oc}$ (V)	$J_{sc}$ (mA/cm <sup>2</sup> )	FF	Efficiency (%)	i-layer (Angstrom)
287-3	0.910	12.2	0.725	8.05	1500
287-2	0.917	13.4	0.718	8.82	3500

The improvement in stability of a-Si:H single junction devices is shown in Figure 1 where a comparison of normalized efficiency of similar devices (same i-layer thickness) prepared with and without H-dilution are shown. Devices prepared with H-dilution clearly show definite stabilization after about 100 hours of light-soaking.

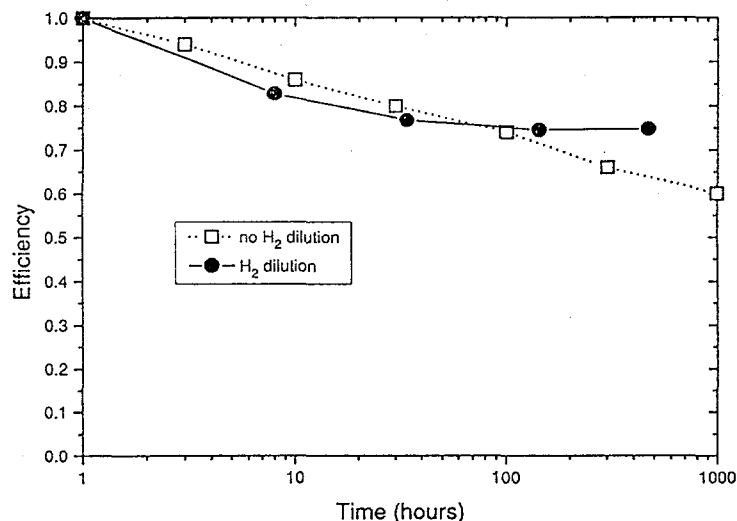


**Figure 1** - Normalized efficiency as a function of light-soaking time for single junction a-Si:H solar cell prepared with and without H-dilution

In order to increase the open-circuit voltage of the present triple junction devices we have been developing a-SiC:H intrinsic alloys. The most promising results have been obtained with a-SiC:H prepared from either trisilylmethane (TSM) or from CH<sub>4</sub>+H<sub>2</sub> feedstock. In both cases p-i-n devices have resulted in high  $V_{oc}$ , as high as 0.991V. The photovoltaic parameters of some a-SiC:H devices are summarized in Table II.

i-layer feedstock	i-layer thickness	$V_{oc}$ (mV)	$J_{sc}$ (mA/cm <sup>2</sup> )	FF	Efficiency (%)
CH <sub>4</sub> +H <sub>4</sub>	2000	967	9.11	0.669	5.9
CH <sub>4</sub> +H <sub>4</sub>	2000	981	8.04	0.636	5.0
TSM	700	941	7.29	0.721	5.0
TSM	1000	991	7.6	0.619	4.7

The light-induced degradation in these devices is only marginally more than a-Si:H devices.

## Task II: Non-Semiconductor Research

The present absorption in the textured tin oxide front contact results in current loss of about 4 mA/cm<sup>2</sup>. We have been developing textured zinc oxide by atmospheric pressure chemical vapor deposition (APCVD) to minimize this loss. ZnO films with conductivity on the order of 5X10<sup>-4</sup> (ohm-cm)<sup>-1</sup> and film texture between 5-50% have been prepared. The ZnO films have significantly lower absorption than SnO<sub>2</sub> films of comparable texture and sheet resistance. The higher optical transmission in ZnO films translates to higher currents in both single and triple junction devices. Figure 2 shows the quantum efficiency versus wavelength measurements of the best triple junction device made on ZnO front contact. The total current collected from the three component cells is more than 23 mA/cm<sup>2</sup>. A comparison of the photovoltaic parameters of this device to a typical device prepared on tin oxide front contact is tabulated in Table III.

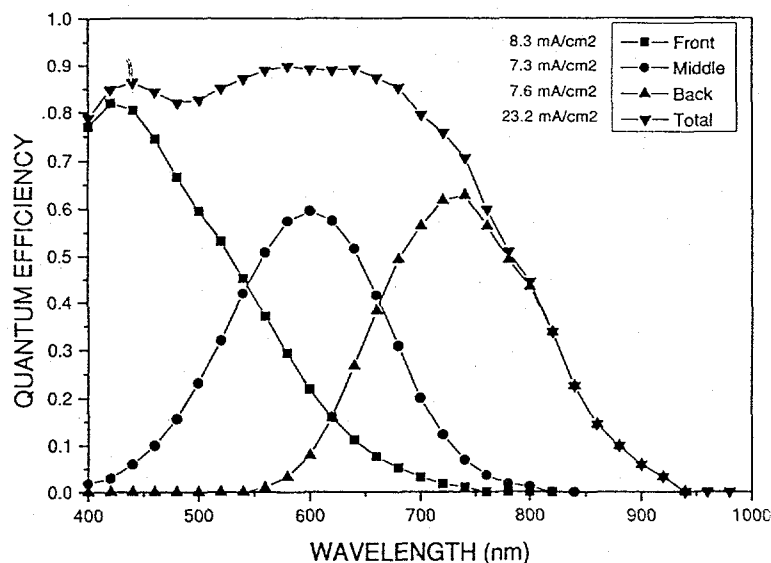


Figure 2 - Quantum efficiency versus wavelength measurement of a-Si/a-Si/a-SiGe triple junction device on ZnO front contact

Front Contact	V <sub>oc</sub> (V)	J <sub>sc</sub> (mA/cm <sup>2</sup> )	FF	Efficiency
Tin Oxide	2.39	6.4	0.669	10.2
Zinc Oxide	2.23	7.4	0.618	10.2

Despite substantial improvement in J<sub>sc</sub>, from 6.4 mA/cm<sup>2</sup> to 7.4 mA/cm<sup>2</sup>, the conversion efficiency is similar. This is due to lower V<sub>oc</sub> and FF caused by high contact resistance at the ZnO/p interface which we are presently investigating.

### Task III: Submodule Research

Triple junction a-Si/a-Si/a-SiGe large area modules have been made in which the i-layers of the front two junctions are deposited with H-dilution. Initial aperture area efficiency of these modules have ranged from 9.6% to 10%. The photovoltaic parameters of four modules measured at Solarex and at NREL are summarized in Table IV.

Module #	V <sub>oc</sub> (V)	I <sub>sc</sub> (mA)	FF	Solarex Efficiency	NREL Efficiency
D2280.1	61.1	189.7	0.663	9.74	9.80
D2297.1	61.48	191.2	0.652	9.70	8.84
D2297.2	61.18	187.0	0.665	9.63	9.61
D2300.1	60.78	189.4	0.682	9.95	10.01

Significant improvements have also been achieved in the stability of these modules compared to those prepared with no H-dilution in the front two components. The best stability data was obtained on a module with initial efficiency of 9.6%. This module had an efficiency of 8.25% after 600 hours of light soaking. Figure 3 shows a comparison of the normalized efficiency of the best no H-dilution module with that of the best H-dilution module. With no H-dilution the module had degraded 12.5% after 100 hours and 19% after 600 hours where as with H-dilution the module degraded 11% after 100 hours and only 14% after 600 hours, showing the stabilization in light-induced degradation.

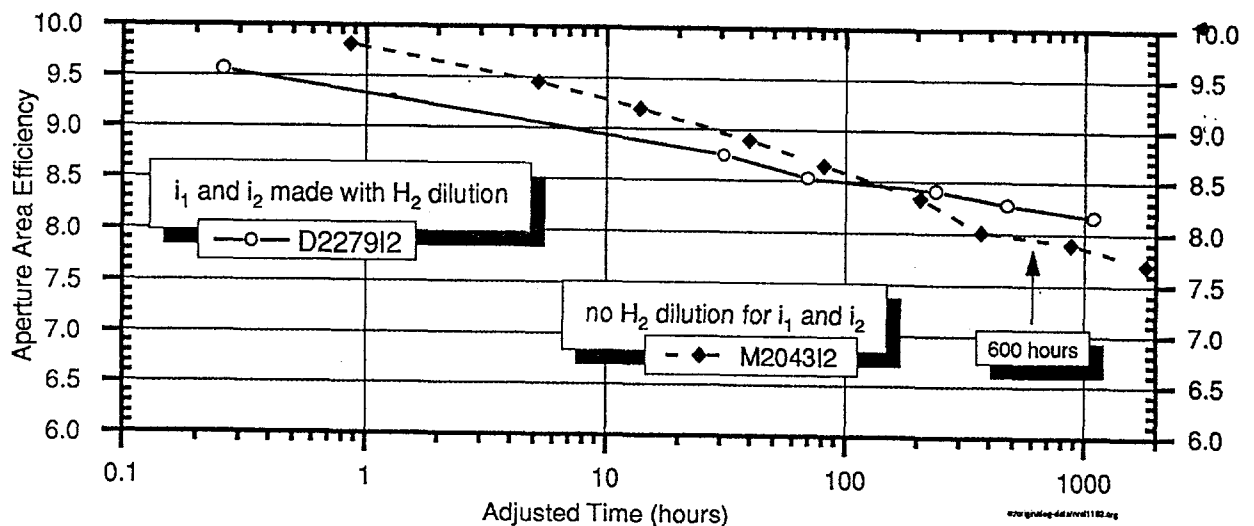


Figure 3 - Best Modules with and without H-Dilution - degraded on Na Vapor Lamps at 50°C



**Title:** Research on Stable, High-Efficiency Amorphous Silicon Multijunction Modules

**Organization:** United Solar Systems Corp.  
Troy, Michigan

**Contributors:** S. Guha, principal investigator, A. Banerjee, E. Chen, R. Clough, T. Glatfelter, G. Hammond, K. Hoffman, M. Hopson, N. Jackett, M. Lycette, J. Noch, T. Palmer, K. Parker, I. Rosenstein, D. Wolf, X. Xu, J. Yang and K. Younan.

### **Objective**

The principal objective of the program is to conduct research on semiconductor materials and non-semiconductor materials to enhance the performance of multi-bandgap, multijunction, large-area amorphous silicon-based alloy modules. The goal is to demonstrate stabilized module efficiency of 10% for multijunction panel of area greater than 900 cm<sup>2</sup> by December, 1992.

### **Approach**

Double-junction and triple-junction cells are made on Ag/ZnO<sub>x</sub> back reflector deposited on stainless steel substrates. a-SiGe alloy is used for the *i*-layer in the bottom cell; the other cells use a-Si alloy. After evaporation of antireflection coating, silver grids and bus bars are put on the top surface, and the panel is encapsulated in a EVA/Tefzel structure to make a one-square-foot monolithic module.

### **Status/Accomplishments**

#### **Effects of microvoids on cell performance**

Using a combination of infrared absorption and small-angle X-ray scattering (SAXS) on hydrogenated amorphous silicon alloy films and efficiency measurements of solar cells with intrinsic layers prepared under nominally identical conditions to those of the films, we have investigated [1] the effect of change in microvoid density in the intrinsic layer on solar cell performance. The microvoid density is changed by altering the deposition rate. The results are shown in Table I. With increasing microvoid density, both the initial and light-degraded performance of solar cells are found to deteriorate.

The annealing kinetics of the metastable defects are also found to depend on the density of microvoids. With increasing microvoid density, some light-induced defects are created which are harder to anneal out.

### Correlation between film property and cell performance

In order to determine the degree of correlation that exists between material properties and solar cell performance, we have studied [2] the material properties of amorphous silicon-germanium alloy films with different germanium contents and also the performance of solar cells with the intrinsic layers deposited under nominally identical conditions. In Table II, we show the film properties as a function of Ge-content in both the initial and the light-degraded states. Surprisingly, we find negligible change in the defect density as measured by constant photocurrent method (CPM). The efficiencies of the corresponding cells, however, decrease by a large amount (Table III). There must, therefore, be other changes taking place after light-soaking which affect the solar cell performance, but cannot be detected by CPM. New states may be created above the Fermi level; the capture cross-section of the light-induced states could also be different. CPM would be insensitive to these changes.

### Stability study on double-junction cells

We have studied the effect of bandgap variation of the bottom cell and the current mismatch between the component cells on the light-induced degradation of double-junction, dual-bandgap cells [3]. The best performance was obtained by incorporating a profiled bandgap in the bottom cell having a bandgap of 1.41 eV at the narrowmost region. A stabilized active-area efficiency of 11.16% was observed after 600 hours of one-sun illumination at 50°C. **This is believed to be the highest stabilized value reported to date on amorphous silicon-based multijunction solar cells.** Efforts are under way to translate these small-area results into 10% one-square-foot stabilized panel efficiency.

### Module results

A large number of double- and triple-junction modules of area  $> 900 \text{ cm}^2$  was fabricated [4]. A summary of some double-junction module results measured at USSC and NREL is shown in Table IV. The highest initial aperture-area efficiency measured indoors at NREL on our modules is 9.3%. **This is the highest initial aperture-area efficiency measured by NREL on multi-bandgap, multijunction panels with area larger than  $900 \text{ cm}^2$ .** The same module measured 9.6% under the USSC Spire simulator. Light-soaking measurements carried out both at USSC and NREL on our modules show typically 15% degradation after 1000 h of one-sun light-soaking at 50°C.

### References

1. S Guha, J. Yang, S. J. Jones, Y. Chen and D. L. Williamson, Appl. Phys. Lett. 61, 1444, 1992.
2. X. Xu, J. Yang and S. Guha, Appl. Phys. Lett. (to appear).
3. J. Yang and S. Guha, Appl. Phys. Lett., Dec. 14, 1992.
4. S. Guha, J. Yang, A. Banerjee, T. Glatfelter and X. Xu, NREL PV AR&D Meeting, Denver, May 1992.

**Table I. Material Properties and Cell Performance for Samples Prepared at Two Different Deposition Rates**

Deposition rate	0.14 nm/sec	1.35 nm/sec
Void fraction	1%	4%
Predominant void diameter	-	0.9 nm
Hydrogen content	8%	12%
Microstructure fraction (R)	8.4%	18.4%
$C_H$ (2000)	6.4%	6.3%
Initial efficiency	7.85%	6.31%
Degraded efficiency	6.53%	3.5%
Initial red fill factor	0.67	0.52
Degraded red fill factor	0.52	0.43
Initial blue fill factor	0.73	0.67
Degraded blue fill factor	0.67	0.40

**Table II. Properties of a-SiGe Alloys with Different Ge-content**

Sample	Ge-Content (%)	Optical Gap (eV)	Eu (meV)	$\mu\tau$ ( $\text{cm}^2\text{V}^{-1}\text{S}^{-1}$ )		Defect Density ( $\text{cm}^{-3}$ )	
				Init.	Degraded	Init.	Degraded
4827	19	1.55	51	$8 \times 10^{-7}$	$2.7 \times 10^{-7}$	$5.1 \times 10^{15}$	$1.2 \times 10^{16}$
4830	30	1.50	52	$3 \times 10^{-7}$	$1.5 \times 10^{-7}$	$3.1 \times 10^{15}$	$6.6 \times 10^{15}$
4829	41	1.41	49	$1 \times 10^{-7}$	$4.0 \times 10^{-8}$	$5.6 \times 10^{15}$	$6.5 \times 10^{15}$

**Table III. Performance of Single-junction a-SiGe Alloy Solar Cells before and after Light Soaking for 600 Hours under One-sun Illumination at 50°C**

<i>i</i> -layer Bandgap	State	AM1.5 Performance				Fill Factor	
		$J_{sc}$ (mA/cm <sup>2</sup> )	$V_{oc}$ (V)	FF	$\eta$ (%)	Blue	Red
1.55 eV	Initial	18.50	0.80	0.62	9.18	0.60	0.59
	Degraded	17.21	0.76	0.50	6.54	0.59	0.54
1.50 eV	Initial	20.93	0.70	0.55	8.06	0.58	0.60
	Degraded	17.81	0.66	0.43	5.05	0.48	0.46
1.41.eV	Initial	22.39	0.61	0.52	7.10	0.60	0.59
	Degraded	19.92	0.57	0.40	4.54	0.49	0.48

**Table IV. A Summary of Module Results Measured at USSC and NREL**

Module #	Location	$I_{sc}$ (A)	$J_{sc}$ (mA/cm <sup>2</sup> )	FF	$V_{oc}$ (V)	$P_{max}$ (W)	Area (cm <sup>2</sup> )	Eff (%)
1077	USSC	1.27	8.4	0.67	9.97	8.4	909	9.3
	NREL	1.36	9.0	0.60	9.94	8.3	912	9.1
1078	USSC	7.9	8.6	0.65	1.67	8.5	923	9.2
	NREL	8.4	9.1	0.60	1.66	8.3	924	9.0
1103	USSC	7.9	8.8	0.64	1.66	8.4	901	9.3
	NREL	8.3	9.2	0.59	1.67	8.3	903	9.1
1118	USSC	8.0	8.9	0.65	1.65	8.6	902	9.6
	NREL	8.6	9.5	0.59	1.65	8.4	903	9.3

# Research on Stable, High-Efficiency Amorphous Silicon Multijunction Modules Phase I

Advanced Photovoltaic Systems  
Princeton, New Jersey

F. J. Kampas, program manager,  
J. Del Cueto, M. Ghosh, R. Romero, and J. Xi, principal investigators

## Objectives

The overall goal of this research program is the demonstration of a stable, aperture area efficiency of 10% for two-terminal, similar-bandgap, multijunction all-amorphous-silicon-alloy modules having an aperture area of at least 900 cm<sup>2</sup>. The major milestones for Phase I of the program are demonstration of an amorphous silicon, similar-bandgap multijunction module with a stable aperture-area efficiency greater than 7% and a 1 cm<sup>2</sup> multijunction cell with a stable efficiency greater than 8.5%.

## Approach

The project was divided into three tasks: semiconductor materials research, non-semiconductor materials research, and module research. The semiconductor materials task concentrated on finding feed stock materials and deposition conditions which produced uniform, high-quality intrinsic and doped films over areas of 900 cm<sup>2</sup>. The fabrication of the 8.5% stable 1 cm<sup>2</sup> device was also included in this task. The non-semiconductor materials task was aimed toward low-resistivity, high-transmittance and high haze transparent conducting oxides (TCOs) for front contacts and high-reflectivity back contacts. The goal of the module research task was the achievement of the 7% stable one-square foot tandem module.

## Semiconductor Materials Results

The goals for individual layers in the semiconductor materials research were achieved or approached very closely. Intrinsic amorphous silicon films were produced with a hole diffusion length of 420 nm and a photosensitivity of  $2.8 \times 10^5$ , exceeding the requirement by a factor of 3 for both parameters. Amorphous p-layers with a conductivity of  $1 \times 10^{-3}$  Siemens/cm and bandgap of 1.95 eV were fabricated. This was close to the goal, which was for a conductivity a factor of two higher at that bandgap. Amorphous n-layers with a conductivity of  $3 \times 10^{-3}$  Siemens/cm with a bandgap of 1.84 eV were fabricated. In that case, the goal was  $1 \times 10^{-3}$  Siemen/cm for a film with a bandgap of 1.85 eV. Microcrystalline n-layers were deposited with conductivity ranging from 7-10 Siemen/cm on a one square foot substrate, the goal in the contract being 1 Siemen/cm. The goals in the contract on the uniformity of films were all met.

## Non-Semiconductor Materials Results

The non-semiconductor materials research was conducted on tin oxide and zinc oxide TCOs, non-semiconductor contact (recombination) layers, and on zinc oxide back reflectors and buffer layers.

Most of the TCO research was performed on the following system: soda-lime glass/SiO<sub>2</sub>/SnO<sub>x</sub>:F deposited using APCVD (Atmospheric Chemical Vapor Deposition). The goals were the following: sheet resistance < 7 ohms/square; integrated transmittance > 82%; and non-uniformity (2 sigma) < 10% over the square foot substrate. The goals were nearly achieved. One sample has a transmittance of 80.5% and a sheet resistance of 7.3 ohms/square; another had

a transmittance of 84% with a sheet resistance of 8.4 ohms/square. Non-uniformity of sheet resistance was found to be below 10% for all samples. However, we were not successful in obtaining good uniformity of deposition of zinc oxide using LPCVD (Low Pressure Chemical Vapor Deposition), the technique originally chosen.

Sputtered zinc oxide was investigated as a buffer layer between the TCO and the p-layer of devices. It was found that use of the buffer layer enabled a wider range of silicon deposition conditions to be used without damage to the TCO.

Two non-semiconductor materials,  $\text{Nb}_2\text{O}_5$  and  $\text{TiO}_2$ , were tried as contact layers between the two stacks of the tandem devices. Sputtered  $\text{Nb}_2\text{O}_5$  was found to be too resistive. Better results were obtained from resistive evaporation of the two materials. However, the results were not very reproducible, presumably due to variations in stoichiometry. The best results were obtained without non-semiconductor contact layers.

The use of sputtered zinc oxide to improve the reflectivity of the back contact was extensively investigated. The contract's goal in the area of back reflectors was a quantum efficiency greater than 0.4 at 700 nm from a single-junction device with an i-layer thickness of 450 nm or less. This best result achieved was a quantum efficiency of 0.4 from a single-junction device with an i-layer thickness of 480 nm. Short-circuit current density enhancements of 1.0-1.3 mA/cm<sup>2</sup> were typically seen on tandem-junction devices. However, loss of fill factor resulting from the use of zinc oxide as a back reflector was a problem that required a great deal of attention. It was eventually discovered that the n-layer deposition conditions as well as the zinc oxide deposition conditions required optimization.

### **Tandem-Junction Device Results**

One of the major milestones of Phase I of the contract was the demonstration of a 1 cm<sup>2</sup> tandem-junction devices with a stabilized efficiency of 8.5%. As usual, stabilized efficiency was defined as the efficiency after 600 hours of light soaking with 1000 W/m<sup>2</sup> of AM1 spectrum light, with the cell held at 50 C. We did not achieve that result; the highest stabilized efficiency measured for a device was 6.73% (after 690 hours of light soaking). The primary problem was our lack of a good contact layer between the two stacks of the device. As described earlier, non-semiconductor "recombination" layers were tried, without good results. Another approach tried was the use of a p<sup>+</sup> layer (without carbon) between the two stacks (between n1 and p2), as described in the literature[1]. This gave a good contact but had unacceptably high light absorption. The result was a low current from the second stack, as shown by quantum efficiency measurements. Consequently, the device with the best stabilized efficiency had the structure Asahi SnO<sub>2</sub>/ZnO/p-i-n-p-i-n/ZnO/Ag/Al. The initial I-V curve of the device showed a problem with contact between the stacks. This problem was exacerbated by light soaking.

During the next phase of the contract, we will be fabricating tandem devices (and modules) with microcrystalline n1 layers. It is expected that this will solve the problem of the contact between the two stacks.

### **Tandem-Junction Module Results**

The second major milestone of Phase I was the demonstration of a one-square foot tandem module with a stabilized efficiency of 7%. The amorphous silicon deposition system intended for use in fabricating one-square foot tandem modules had recently been put into operation at the beginning of the contract. It was found to have a problem with cross-contamination which eventually necessitated a major redesign. Consequently, all tandem modules were deposited on 31" x 61" substrates in APS' manufacturing facility. One square foot modules were cut from these. Since the manufacturing silicon deposition systems deposits on 48 substrates

simultaneously using multiple driven electrodes, it was possible to deposit modules with a number of combinations of layer thicknesses in one deposition run. Thus optimization proceeded more rapidly than it might have otherwise.

Initially, commercial tin oxide TCO was used. Later on APS tin oxide was used, as the higher haze gave increased current densities. The overall structure of the tandem modules which gave the best results was APS SnO<sub>2</sub>/p-i-n-p-i-n/ZnO/Al. As for devices, the lack of a good contact layer between the stacks limited results.

A plot of aperture area efficiency vs log(light soaking time) for several square-foot tandem modules is shown in Fig. 1. Identical layer deposition times were used for the module using commercial tin oxide and the module using APS tin oxide and a zinc oxide back reflector. Quantum efficiency measurements on diagnostic devices patterned from other substrates deposited using the same conditions were made. These revealed that the module made on commercial tin oxide was bottom cell limited. The module made on APS tin oxide and using a zinc oxide back reflector was top cell limited. This is due to the improved red response resulting from the hazier tin oxide and the improved back reflector. The smaller degradation of the module using the APS tin oxide and the zinc oxide back reflector presumably results from the fact that it was initially top cell limited, as the bottom cell degrades more on light soaking.

The module with the highest initial efficiency, which used APS tin oxide but no zinc oxide back reflector, was deposited with different layer thicknesses than the other two. It initially was current matched. These results demonstrate the importance of optimizing the layer thicknesses for the light-soaked state. The best result obtained was an aperture area efficiency of 5.48% measured after 888 hours of light soaking. Two 31" x 61" tandem modules, using commercial tin oxide, had initial aperture area efficiencies of around 5.8%. These were encapsulated and sent to NREL for long term outdoor testing.

In the second phase of the contract, we expect to fabricate tandem modules using our one-square foot amorphous silicon deposition system. These modules will have microcrystalline n-layers and should give substantially improved results.

## References

1. S. Wiedemann, J. Morris, and L. Yang, Proceedings of the 21st IEEE Photovoltaics Specialist Conference, Kissimmee, Florida, p. 1529.

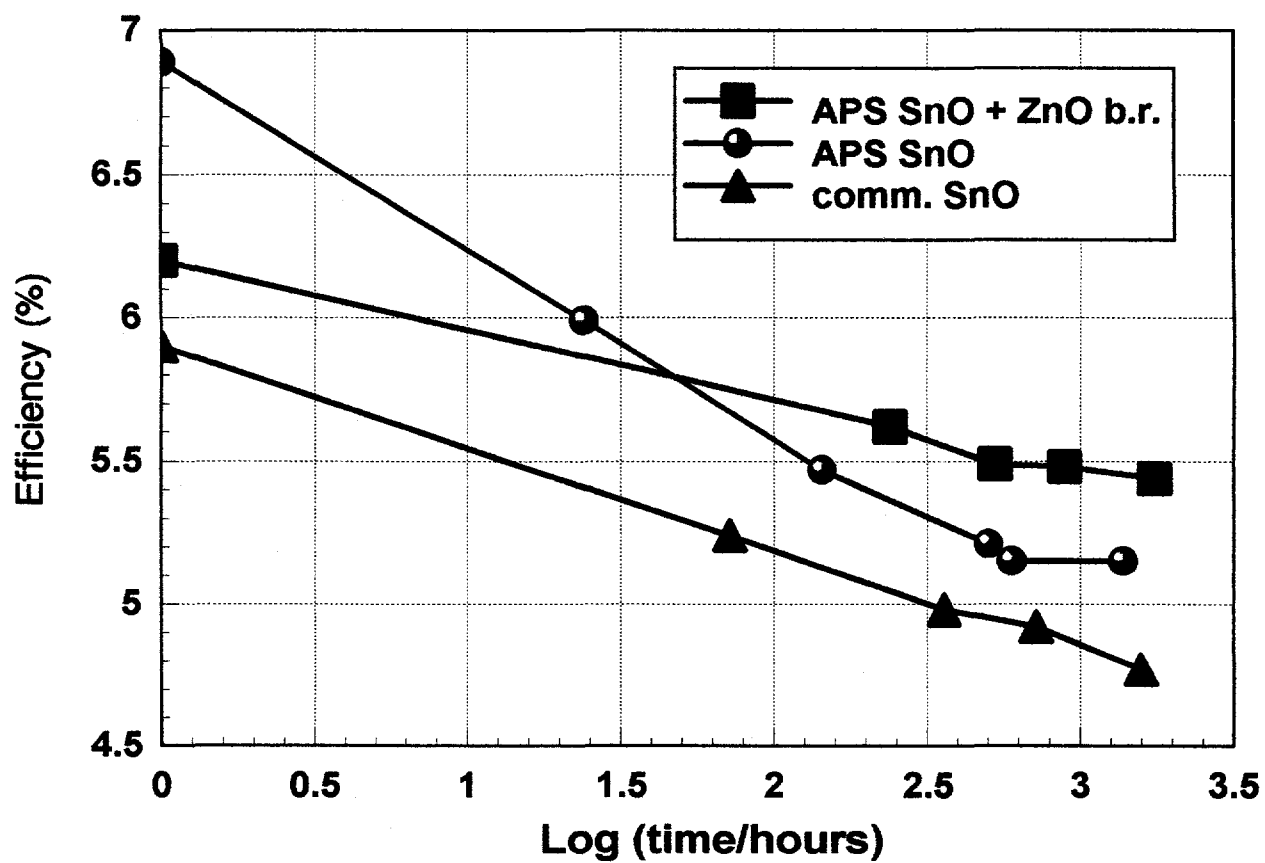


Figure 1. Aperture area efficiencies of tandem modules as a function of light-soaking time. Leftmost points are initial efficiencies.



## Title: Small Angle X-ray Scattering of Amorphous Silicon-Based Semiconductors

Organization: Department of Physics, Colorado School of Mines, Golden, Colorado

Contributors: D.L. Williamson, principal investigator; S.J. Jones and Y. Chen

### Objectives

The objectives of this research are to determine whether the presence of microstructure as detected by small angle x-ray scattering (SAXS) 1) limits the photovoltaic properties of current device-quality a-Si:H, 2) plays any role in determining the photo-stability of a-Si:H and its alloys, and 3) is responsible for the reduced photovoltaic performance upon alloying a-Si:H with Ge or C. In addition, efforts are ongoing to improve the SAXS measurement and analysis capabilities as applied to these types of materials.

### Approach

The approach is to focus on the microstructural characterization of relevant materials using an unusual technique that is sensitive to structural features on a size scale from about 1 to 30 nm and to work closely with groups that can supply systematic sets of samples and the associated opto-electronic data to help address the above objectives. Good quality substrates suitable for the SAXS studies are supplied by us to the film makers along with detailed instructions on sample requirements. This approach of using a single measurement system to examine materials prepared in different deposition systems and by different methods from many groups has the added advantage of providing reliable comparisons. The SAXS measurements are supplemented by in-house flotation density, Raman, infrared absorption, x-ray diffraction and annealing studies of the same films used for the SAXS. Access to SAXS beamlines at the National Synchrotron Light Source at Brookhaven National Laboratory provides data complementary to those from the in-house facility.

### Results

In FY 1992, SAXS measurements were made on a large number of samples from the following groups: USSC (S. Guha), Solarex (Y.-M. Li), JPL (Y. Shing), Xerox (N. Johnson), NREL (H. Mahan/R. Crandall), U. Illinois (J. Abelson), Harvard U. (W. Paul), Princeton U. (S. Wagner), Iowa State U. (J. Shinar), Utrecht U. (M. Van den Boogaard), U. Neuchatel (U. Kroll), Stuttgart U. (G. Bauer), Ecole Polytechnique-Paris (P. Cabarrocas), and IACS-India (R.O. Dusane/R. Crandall). Results of some of this work have been published [1-4] and will be briefly summarized here. Other new results will also be summarized.

A correlation between the microstructure of a-Si:H as detected by SAXS and solar cell properties has been measured for the first time [1]. This was done by depositing i-layer films for SAXS with the same system and same conditions used to prepare the i-layer in p-i-n solar cells at USSC. The microstructure was systematically varied by increasing the deposition rate from 0.14 nm/s to 1.35 nm/s. SAXS data are shown in Fig. 1 in comparison to data from crystalline Si. It was shown that as the volume fraction of microvoids increased from about 1% or less for the smallest deposition rate to about 4% for the highest, the initial efficiency decreased by 20% and the light-degraded efficiency (600 hours illumination) decreased by 46%. Thus, solar cells with more microvoids in the i-layer clearly have poorer photovoltaic performance and show less photo-stability.

Measurements have now been done for a large number of a-SiGe:H alloys with Ge contents from 6% to 100%, all prepared by the glow-discharge technique. Figure 2 shows the results of flotation density measurements up to 60% Ge, the upper limit on density of suitable flotation liquids. This method was applied to Si-Ge alloy thin films for the first time to our knowledge [2]. There is a clear trend of an increasing density deficit upon increased alloying and this supports the interpretation of the SAXS as originating from low density regions such as microvoids. A systematic set of alloys with less than 40% Ge has revealed a striking correlation between the integrated SAXS signals, the defect density, and the photo/dark conductivity ratio as shown in Figs. 3a and 3b. It is interesting that although there is a sharp rise in the SAXS signals above 20% Ge, Fig. 2 shows no correlated sharp change in the film density as determined by flotation measurements. SAXS studies do show a change to oriented microstructure suggestive of columnar growth above 20% Ge. The high sensitivity of the SAXS technique has been demonstrated by the detection of oriented microstructure in a-Ge:H films that were homogeneous according to TEM studies.

A carefully correlated SAXS and IR study of a-Si:H deposited by rf sputtering and annealed at temperatures from 250 to 400 °C showed that the SAXS signals begin to increase and bonded H begins to decrease at the same temperature of 350 °C [3]. Further studies are underway with anneals up to the crystallization of the films.

Comparison of SAXS from device-quality a-Si:H prepared by reactive magnetron sputtering with that from the standard glow-discharge device-quality a-Si:H revealed significant differences [4]. More and larger voids were found in the sputtered films in addition to oriented microstructure consistent with columnar-type structure. Alloying with C by the sputtering method produced enhanced SAXS signals and evidence for columnar microstructure [4].

Several additional sets of samples have established differences in microstructure caused by alternate deposition methods and conditions. Methods which utilize electron cyclotron resonance (ECR) and a hot wire filament to decompose silane (HW), both produced more SAXS-determined microstructure than the standard glow discharge (GD) method. We should note that HW samples with the very low H contents that suggested better photo-stability have not yet been produced for SAXS studies. The remote hydrogen plasma method (RHP) and the very-high frequency GD technique, both produced films which yielded the weak SAXS typical of that from the GD method. In addition, plasma conditions which use higher powers or include the inert gases He or Ar all induced more SAXS-detected microstructure that is very likely related to enhanced void formation. Dilution with hydrogen gas, however, reduced the SAXS signals compared to undiluted deposition. In spite of the significantly larger SAXS from many of these materials, relatively high photo/dark conductivity ratios have been observed. It will be of particular importance to establish whether any of these alternate deposition methods or conditions can yield solar cell efficiencies and stabilities comparable to or better than those known from the GD process.

Since the SAXS from the device-quality GD a-Si:H is quite weak, it is important to establish the relative strengths of other scattering mechanisms compared to that from microvoids in order to determine whether the voids are part of the residual microstructure in this material. Thus we have been examining the contributions in our small angle range from thermal diffuse scattering, Compton scattering, and random alloy scattering (also known as Laue monotonic scattering). We now have data and calculations demonstrating all three of these contributions and although they are small, they are not negligible, particularly the Laue monotonic scattering. Correction for the latter is straightforward since it is nearly angle independent over our range of angles.

Corrections for the other two mechanisms also appear feasible. Modeling of the observed tilting effects is continuing on the basis of ellipsoidal voids with preferred orientations.

The possible interdiffusion of Si or Ge and Al at the a:Si:H/Al foil and a-Ge:H/Al foil interfaces was examined in order to establish whether this could be a problem in producing the SAXS samples. Systematic anneals followed by AES depth profiling through the interfaces showed essentially no interdiffusion until 500 °C for the Si and 450 °C for the Ge. The presence of a 10 nm oxide layer, as detected by AES, on the SAXS Al foil probably serves as an effective diffusion barrier.

## References

1. S. Guha, J. Yang, S.J. Jones, Y. Chen and D.L. Williamson, *Appl. Phys. Lett.* **61** (1992) 1444.
2. S.J. Jones, Y. Chen, D.L. Williamson and G.D. Mooney, *Mat. Res. Soc. Symp. Proc.* **258** (1992) 229.
3. H. Jia, J. Shinar, Y. Chen and D.L. Williamson, *Mat. Res. Soc. Symp. Proc.* **258** (1992) 281.
4. Y. Chen, S.J. Jones, D.L. Williamson, S. Yang, N. Maley and J.R. Abelson, *Mat. Res. Soc. Symp. Proc.* **258** (1992) 311.
5. D.L. Williamson, A.H. Mahan, B.P. Nelson and R.S. Crandall, *Appl. Phys. Lett.* **55** (1989) 783.

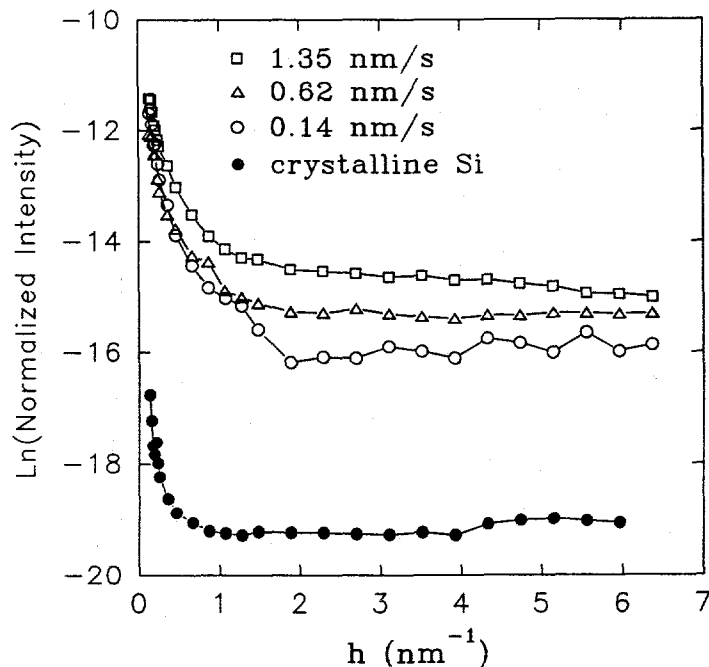


Figure 1. SAXS data from a-Si:H films produced by USSC at the deposition rates indicated and compared to data from a crystalline Si wafer. The intensity has been normalized and corrected for substrate effects according to the procedure in ref. 5.  $h=4\pi\sin\theta/\lambda$ , where  $\lambda=0.154$  nm and  $2\theta$  is the scattering angle.

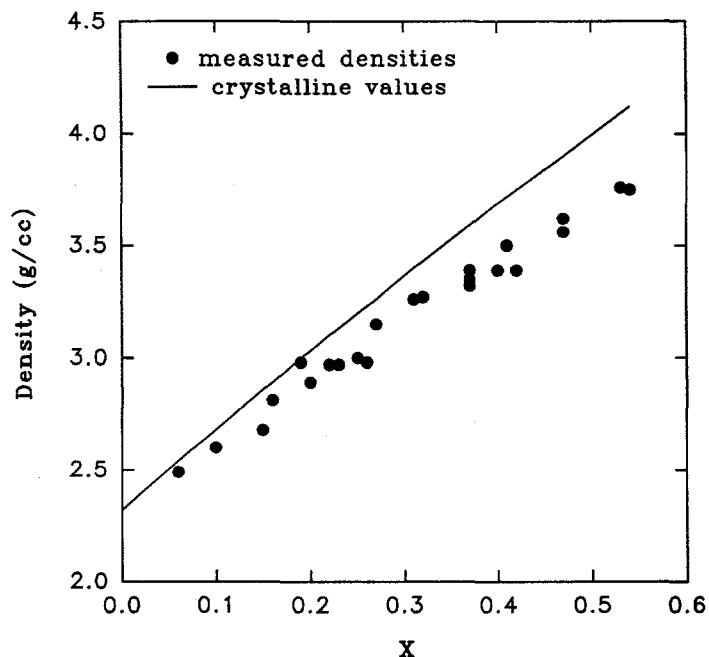


Figure 2. Mass density of  $a\text{-Si}_{1-x}\text{Ge}_x\text{:H}$  alloys determined by the flotation method [2].

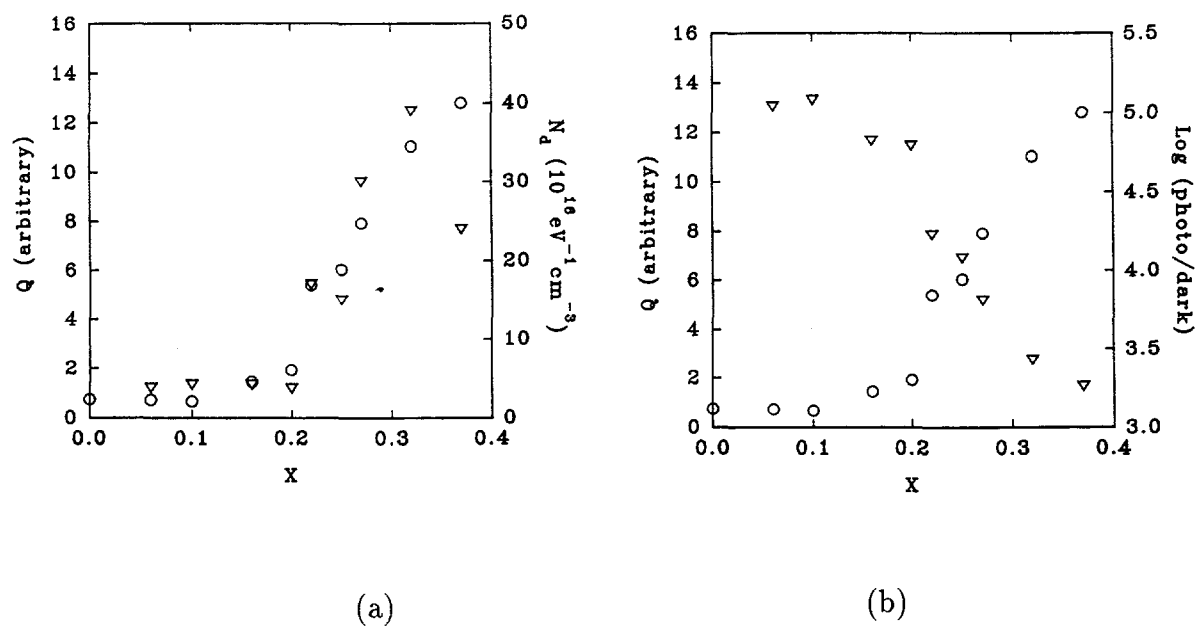


Figure 3. Correlation of the integrated SAXS intensity,  $Q = \int I dh$  (circles), and (a) the defect density (triangles) as determined by photothermal deflection spectroscopy and (b) the photo/dark conductivity ratio (triangles) versus Ge content,  $X$ .

**Title:** Optimization of Transparent and Reflecting Electrodes for Amorphous Silicon Solar Cells

**Organization:** Department of Chemistry,  
Harvard University, Cambridge, MA.

**Contributors:** R. G. Gordon, Principal Investigator;  
J. Hu; J. Musher; H. Hummel; D. Lacks

## SUMMARY

### OBJECTIVES

Transparent conducting materials are essential components of many kinds of solar cells, in which they serve as front-surface electrodes. In tandem cells, back surface electrodes also need to be transparent. Finally, some designs for highly reflective back contacts also call for a transparent conducting layer. The compositions of these transparent conducting layers are usually based on oxides of tin, indium and/or zinc, and are hence referred to as transparent conducting oxides (TCO). In addition to having low electrical resistance and low optical absorption, the structure of a TCO must minimize reflection losses. The TCO must also resist degradation during cell fabrication and use. Finally, the method for making the TCO must be inexpensive and safe.

Our general objectives are to improve the performance of TCO materials and the methods for their production. We aim to reduce their electrical resistance, optical absorption and reflection losses, and to lower the deposition temperature to avoid thermal degradation of other cell components. For the production method, the prime consideration is to deposit the TCO layers at a high rate with relatively simple apparatus. The method chosen is chemical vapor deposition at atmospheric pressure (APCVD), since it has been demonstrated in the glass-coating industry to be the most cost-effective method for making large areas of TCO coatings.

### RESULTS

#### Preparation and Characterization of Textured Zinc Oxide Films

Zinc oxide is a promising material for forming less expensive TCO layers, since zinc metal is much less expensive than tin or indium. Also, zinc is much more abundant in the earth's crust, than is tin or indium, so that even large-scale use of solar cells would not lead to any shortage of zinc. Also, zinc is widely distributed on earth, and is mined in many countries, so continuity of supply is assured in any kind of political situation. In contrast, tin is mined in large quantities in only a few countries.

We discovered that fluorine can be used to dope zinc oxide to very high electron mobility, and therefore very high transparency. The absorption loss in fluorine-doped zinc oxide is less than half of the loss in fluorine-doped tin oxide having the same sheet resistance.[1,2] Fluorine is also a preferred dopant for zinc oxide, since it is known to be electrically inactive, or even beneficial, in hydrogenated amorphous silicon.

The fluorine-doped zinc oxide is produced by CVD from diethyl zinc, ethanol and hexafluoropropene at atmospheric pressure, in the temperature range 375 to 450 C. Films deposited under these conditions show good adhesion to the glass substrates (Scotch tape test). The highest electrical conductivity and light transmission are found for films deposited at the highest temperatures (450 C), and containing about 0.5 atomic percent fluorine. With this material, we could produce a TCO with a sheet resistance of 5 ohms per square and a visible absorption loss of only about 3%, at growth rates up to 250 nm/minute.

We discovered that the amount of texture (roughness) of the zinc oxide films depends dramatically on the amount of water vapor in the growth atmosphere. Small amounts of water vapor (about 1% of the ethanol concentration) produce smooth films, but decreasing the water content to less than 0.25% of the ethanol content produces textured (rough) zinc oxide films suitable for efficient light-trapping in solar cells. Eliminating the water entirely, however, almost completely eliminates film growth, so a small, controlled source of water vapor is essential to control of film texture[1].

Depositions of zinc oxide films were carried out using boron[3], aluminum[4] or gallium[5] as dopants instead of fluorine. Detailed optical, electrical and structural characterization of these films was done. The electrical conductivities achieved were comparable to those we found using fluorine as a dopant. The highest electron concentrations were achieved with gallium, but the mobilities were lower than with fluorine. The higher electron concentrations might be helpful in producing lower contact resistances between the zinc oxide and other layers in a solar cell. The lower mobility of the boron, aluminum or gallium-doped layers, however, also results in higher optical absorption and lower transparency than with fluorine. Therefore, an optimum transparent conductor for solar cells might consist mainly of fluorine-doped zinc oxide, covered by a thin surface layer of gallium-doped zinc oxide. Such a multilayer coating can be produced practically in a multi-chamber CVD furnace.

### **Solar Cell Deposition on Zinc Oxide Films**

Samples of fluorine-doped zinc oxide films were sent to Solarex Corporation, where amorphous silicon solar cells were grown on them. The cells showed extremely high 700 nm quantum efficiencies, up to 65%, compared to the lower values of 47% for control cells made on standard fluorine-doped tin oxide. These measurements confirm that the optical absorption in the fluorine-doped zinc oxide is remarkably smaller than in other TCO materials.

The cells grown on zinc oxide, however, also have lower open circuit voltages and fill factors than the ones grown on tin oxide. A higher contact resistance seems to develop at the interface between the zinc oxide and the amorphous silicon. Studies are underway to determine the origin of this contact resistance, and to find ways to eliminate it.

### **Zinc Oxide Deposition for Applications as Final Contact for Solar Cells.**

The reaction of diethylzinc and ethyl alcohol is too slow to deposit zinc oxide at temperatures below 300 C. However, by switching to tertiary-butyl alcohol, we found that zinc oxide films could be deposited at these low temperatures. However, neither the boron, aluminum or the fluorine dopants were found to be electrically active when the deposition temperature was below 300 C. Therefore, these low-temperature films had very low electrical conductivity.

Gallium-doped zinc oxide films were produced by the CVD reaction of diethyl zinc, water and triethyl gallium at substrate temperatures as low as 150 C. The conductivity of films made at 150 C is very low, but rises to about  $200 \text{ ohm}^{-1}\text{cm}^{-1}$  at 260 C,  $500 \text{ ohm}^{-1}\text{cm}^{-1}$  at 300 C, and  $4000 \text{ ohm}^{-1}\text{cm}^{-1}$  at 470 C. Improvement of the conductivity of the low-temperature films is still desirable for applications as final contacts to solar cells.

### **Development of Zinc Oxide Layers which are Compatible with New Amorphous Silicon Processing Requirements**

In order to provide zinc oxide films with more uniform thickness as substrates for growth of solar cells, a new deposition apparatus was constructed. It consists of a long furnace with a moving platform, constructed by BTU Engineering, and a CVD nozzle built by the Watkins Johnson Company. The gas-handling system was designed and built at Harvard. Initial tests have made films with thickness uniformity of  $\pm 10\%$  over an area of 10 cm by 10 cm. Optimizations of process conditions and film properties are now in progress.

### **Growth and Bonding Theory**

Our density functional theory of chemical bonding has been developed further, and programs written to carry it out. The theoretical energy and structure are in good agreement with experiments on  $\alpha$ -quartz and  $\alpha$ -cristobalite. The new bonding theory has also been applied to two other phases of silicon dioxide which are stable at high pressures. The structure and energy of these phases are in good agreement with the calculations, and the pressures of the phase transitions are also in general agreement with experiment. The calculations will be extended to zinc oxide and tin oxide.

### **CONCLUSIONS**

- Textured fluorine-doped tin oxide films with high electrical conductivity (5 ohms/square) and low optical absorption (3%) were produced by chemical vapor deposition at atmospheric pressure (APCVD) on glass substrates at about 450 C, at moderate deposition rates (up to 250 nm per minute).
- Amorphous silicon solar cells grown on these textured films show very high quantum efficiencies, which demonstrates the high light-trapping ability of this texture, and the high transparency of the zinc oxide film.
- Transparent, highly conductive gallium-doped zinc oxide films were grown by APCVD at temperatures above 300 C. The electron concentrations are higher than for fluorine-doped films, but their transparency is lower. These layers may be suitable for low-resistance contact to p-type amorphous silicon on the front surface of a solar cell.
- Conductive gallium-doped zinc oxide films were grown at temperatures below 300 C, but they have much lower conductivities than the films grown at higher temperatures.
- An apparatus was designed and built to deposit transparent conductive films with uniform thicknesses over an area of 10 cm by 10 cm.

## References

1. Jianhua Hu and Roy G. Gordon, *Solar Cells* **30**, 437 (1991).
2. Jianhua Hu and Roy G. Gordon, *Materials Research Society Symp. Proc.* **202**, 457 (1991).
3. Jianhua Hu and Roy G. Gordon, *J. Electrochem. Soc.* **139**, 2014 (1992)
4. Jianhua Hu and Roy G. Gordon, *J. Appl. Phys.* **71**, 880 (1992)
5. Jianhua Hu and Roy G. Gordon, *J. Appl. Phys.* **72**, (1 December, 1992)



**Title:** Comprehensive Research on Stability and Electronic Properties of Amorphous Silicon Alloys and Devices

**Organization:** Iowa State University, Microelectronics Research Center, Ames, Iowa

**Contributors:** Vikram L. Dalal, Principal Investigator  
Ralph Knox, Kay Han, J. K. Lee, P. Garikepati,  
N. Kandalajt, G. Baldwin, E. X. Ping

### Text

#### **I. Objective**

The objective of the program is to improve the stability and electronic properties of a-Si:H and a-(Si,Ge):H materials and devices.

#### **II. Research Approach**

The basic research approach is to carefully control the deposition of amorphous semiconductors, using alternative deposition techniques. In particular, we want to control the microstructure of a-Si:H and a-(Si,Ge):H alloys, and also control the nature of bonded H. This approach is suggested by the fact that amorphous materials are not homogeneous; rather, they have localized defects such as microvoids, columnar structures and associated with such defects, a multiplicity of H bonds. Much of the instability comes from poorly bonded Si atoms, or Si-H bonds, at such localized defects. Therefore, to improve the stability, and electronic properties, one must strive to reduce such localized defects, and improve the overall structure of the material, making it as homogeneous as possible, while still retaining the useful optical properties of the amorphous state.

To control the microstructure and localized bonding, we use a plasma deposition technique which allows control of growth using localized surface chemical reactions.

#### **III. Growth Technique**

The basic growth technique is called reactive plasma beam deposition. It uses an energetic beam of H atoms to react with the surface during growth of the film. The beam of H atoms is generated by a remote electron-cyclotron-resonance (ECR) source, and it reacts with SiH<sub>4</sub> which is introduced near the surface to produce the film. Fig. 1 shows the schematic diagram of the apparatus. The flux of H atoms is controlled by controlling the pressure in the chamber. At lower pressures, there are more H atoms to react with the growing film.

We find that by controlling the H atom flux, we can smoothly change the morphology of the film from amorphous to poly-crystalline. We find that the atomic H flux is important in allowing us to grow

high quality a-Si:H films at much higher temperatures(350-400C) than is the case for glow-discharge deposited films. The stability of these films is better than comparable glow discharge films by a factor of 2-3.

#### **IV. Devices**

We have started to make proof-of-concept devices using this new technique. We have successfully grown doped p and n layers using this new technique, and have made devices of approximately 6.5% efficiency using this new technique.

We have also been experimenting with a new type of device, **graded bandgap solar cell**, in a-Si:H. We have discovered that grading of bandgap allows one to introduce extra electric field in the device which allows for more stable devices to be made. The graded bandgap structures were made in a RF triode glow discharge system by using combinations of high temperatures and high H dilution. We have made devices of over 8.5% efficiency p-i-n devices with graded gaps, and the stability of these devices is significantly better than for standard devices.

#### **V. Future work**

The future work will focus on the following areas:

1. Improving the material properties, and device performance, of a-Si:H cells made with reactive plasma beam deposition.
2. Making improved a-(Si,Ge):H films and devices using reactive plasma beam techniques.
3. Combining the chemical growth technique with the improved device design so as to produce high performance, stable cells in both a-Si:H and a-(Si,Ge):H alloys.

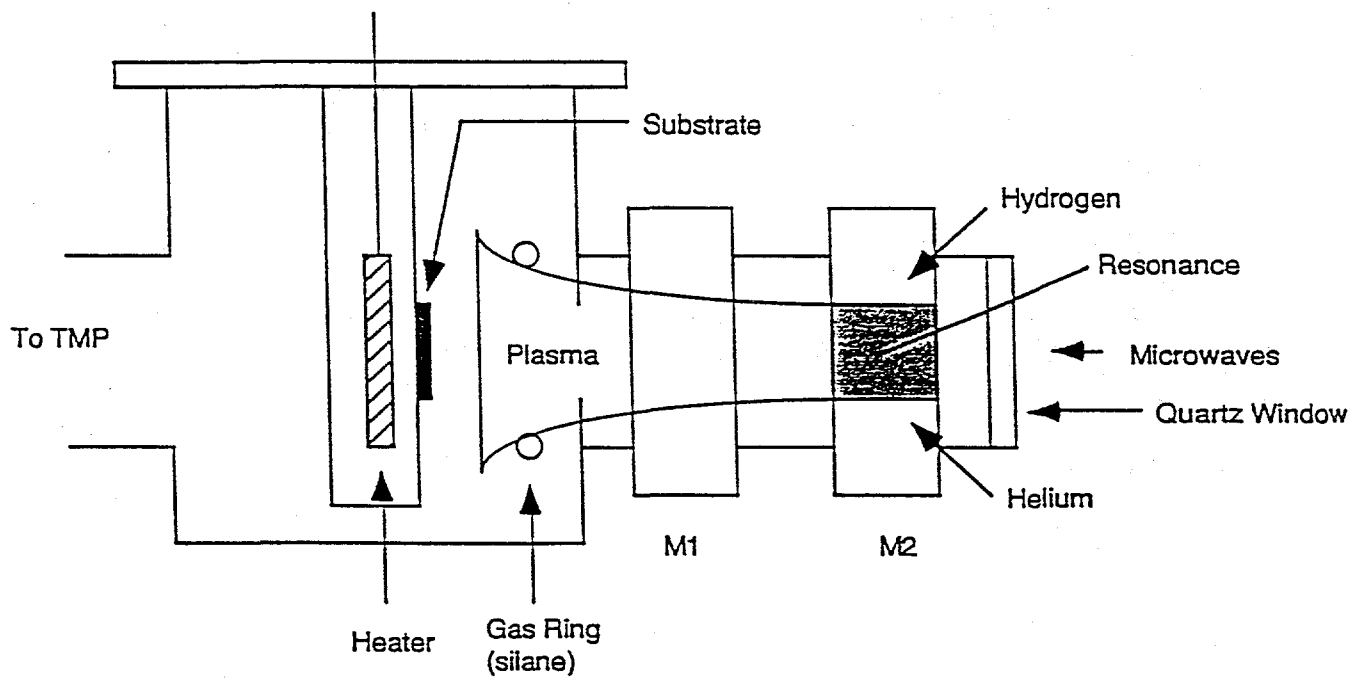


Figure 1 : Schematic Diagram of Reactive Plasma Beam Deposition System

**Title:** Growth Mechanisms and Characterization  
of Hydrogenated Amorphous Silicon Alloy  
Films

**Organization:** National Institute of Standards and Technology (NIST)  
Boulder, Colorado

**Contributors:** A. Gallagher, G. Stutzin, R. Ostrom, D. Tanenbaum

## **Objective**

The overall objective of this work is to establish the atomic scale morphology of glow-discharge produced a-Si:H, a-Ge:H and a-Si:Ge:H film and its dependence on deposition discharge conditions. From this we hope to establish a definitive, in situ diagnostic of film quality and to use this to discover deposition methods that lead to superior photovoltaic behavior. The approach taken is to measure the morphology and atomic species of the as-grown film surface with atomic scale resolution using a scanning tunneling microscope (STM). Many of the limitations of a-Si:H based photovoltaics can be attributed to micro voids, boundary defects, and microparticulate incorporation; these can be detected at the growing surface with the STM.

## **Technical Approach**

We are initially studying a-Si:H and alloy film deposition onto oriented, atomically smooth and clean surfaces of crystal Si and GaAs. This requires ultra high vacuum (UHV) operation of the STM and other surface diagnostic equipment, and exacting sample preparation. The film deposition is done in an attached, turbomolecular pumped chamber. The film-coated substrates are transferred into the UHV chamber after termination of the glow discharge and deposition-gas flows. Repeated and varied depositions on a single sample are studied in this experimental arrangement, without exposure to air.

Morphology of a-Si:H film surfaces.

We present here a few examples of the surface morphology of intrinsic a-Si:H film growth on crystal Si and GaAs. The film is deposited at  $T_s = 25 - 250^\circ\text{C}$  on the grounded electrode of an rf silane discharge. The electrodes are 5 cm square with 1.6 cm gap, placed in a 5.5 cm diameter stainless steel tube. The gas flow is 10-20 sccm and the entire tube and electrodes are heated. The silane pressure, at  $250^\circ\text{C}$ , is typically 0.5 Torr and the film deposition rate on the substrate is  $\sim 2 \text{ \AA/s}$ .

The atomic-scale morphology of the surface of a 100  $\text{\AA}$  thick layer of a-Si:H film on an atomically flat GaAs crystal is shown in Fig. 1. This is typical of many different regions of the surface. In essence, most 100  $\text{\AA}$  square regions of the surface are flat within one atomic layer (2-5  $\text{\AA}$ ) and 1000  $\text{\AA}$  squares are flat within several layers (10  $\text{\AA}$ ). The surface undulations occur at shallow ( $< 20^\circ$ ) angles to horizontal, and no incipient voids or nanoparticulates are seen. The very smooth films obtained at this early stage in the growth are indicative of excellent surface diffusion and valley filling by film precursors ( $\text{SiH}_3$ ).

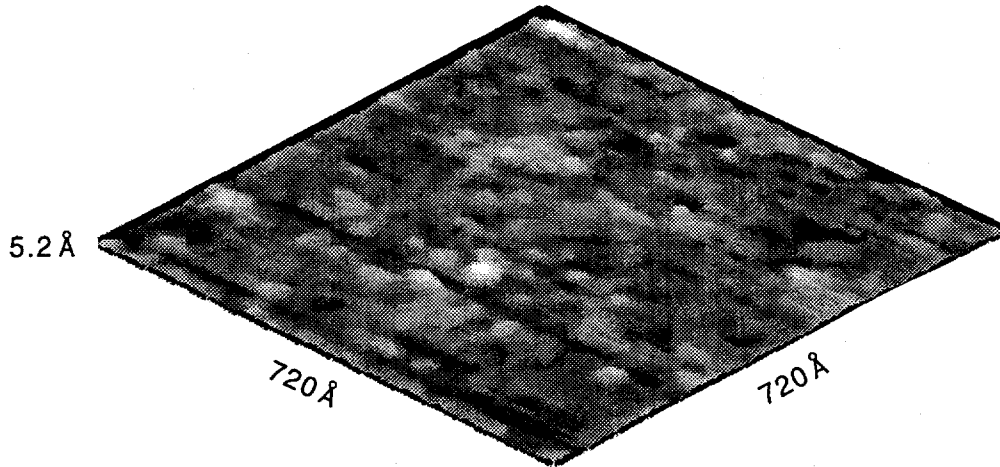


Fig. 1 A surface region of a 100 Å thick intrinsic a-Si:H film deposited on GaAs.

Figures 2-4 show different regions of the surface of 1000 or 4000 Å thick intrinsic a-Si:H film, deposited at 250°C. The hilly surfaces in Fig. 2 have height variations of several hundred Å, and a range of width scales. We show examples with ~200, 500, and 2000 Å wide hills in the figure. In Fig. 3 we show a portion of a narrow trench that traverses another region of the surface. This trench is too narrow and steep-sided to be fully penetrated by the STM probe tip; it clearly implies a growing void surface. The very rough surface regions in Figs. 2 and 3 are examples of the majority of all regions surveyed on 1000-4000 Å thick films. However, we have also found some very smooth areas on these same film surfaces; some of these are almost as smooth as that in Fig. 1. Figure 4 shows a particularly interesting example of this enormous variation in surface morphology. There the left, front quadrant contains many steep hills of ~40 Å height, while the remainder is flat within 5 Å. A high resolution scan of the 100 Å square at the front corner of Fig. 4 is flat within 2 Å.

The very large range of surface morphologies, illustrated in the figures implies a similarly large variation throughout the film in morphology and void structure. This amazing inhomogeneity in the morphology of device-quality a-Si:H is startling and unexpected. That it is seen primarily beyond 1000 Å thickness implies a growing instability, yet the fact that very smooth regions of ~2000 Å size are also seen on 4000 Å thick films implies that it should be possible to grow dense, homogeneous films. At this time all proposed causes and methods for elimination of the voids and irregular regions are conjectural. Studies of different deposition conditions, and their effect on film morphology, are under way.

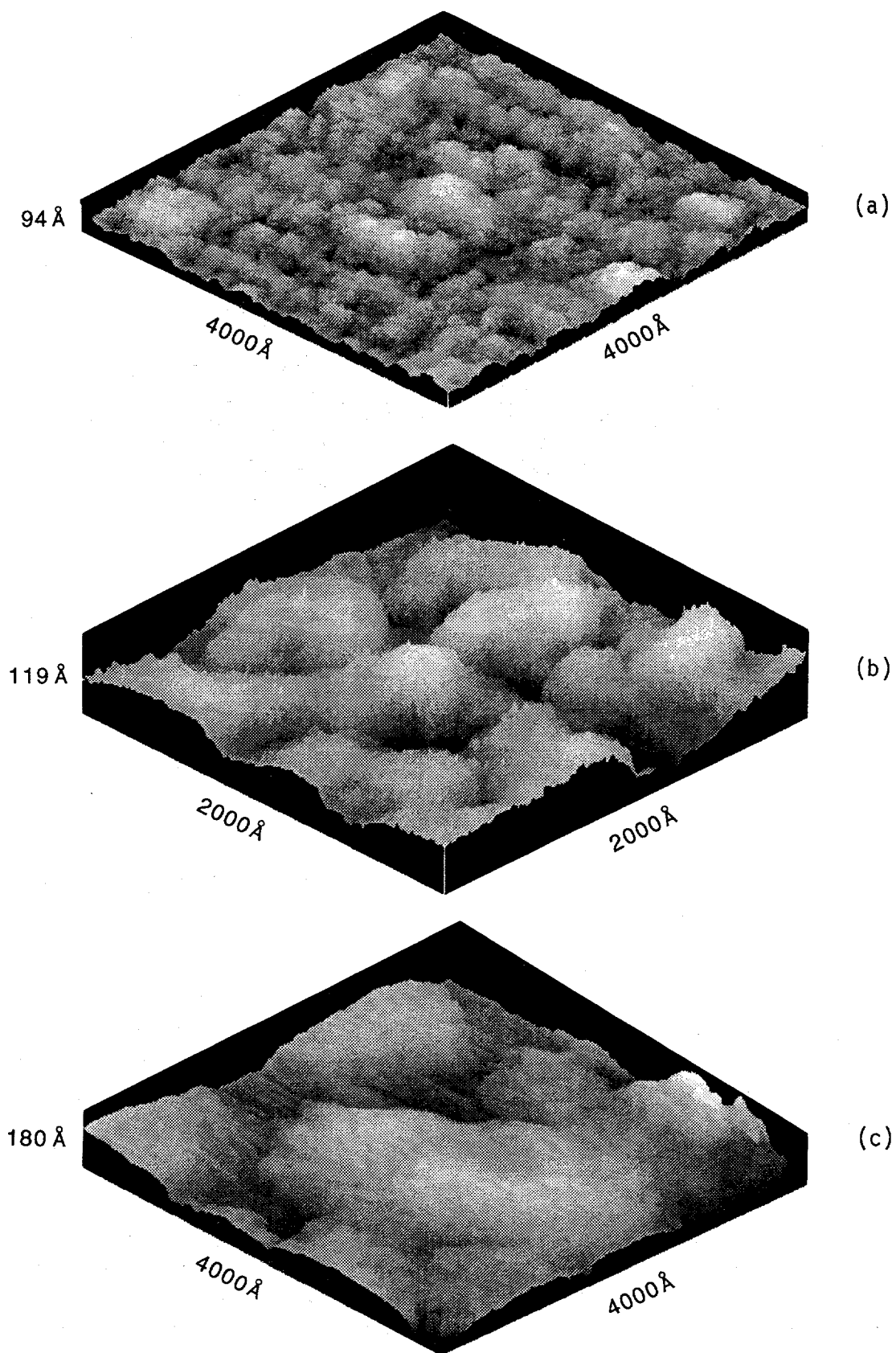


Fig. 2 Three examples of hilly surface regions, with varying hill size: (a) and (c) are from 4000 Å thick films, and (b) is from a 1000 Å thick film. Data points were taken at 10 Å intervals.

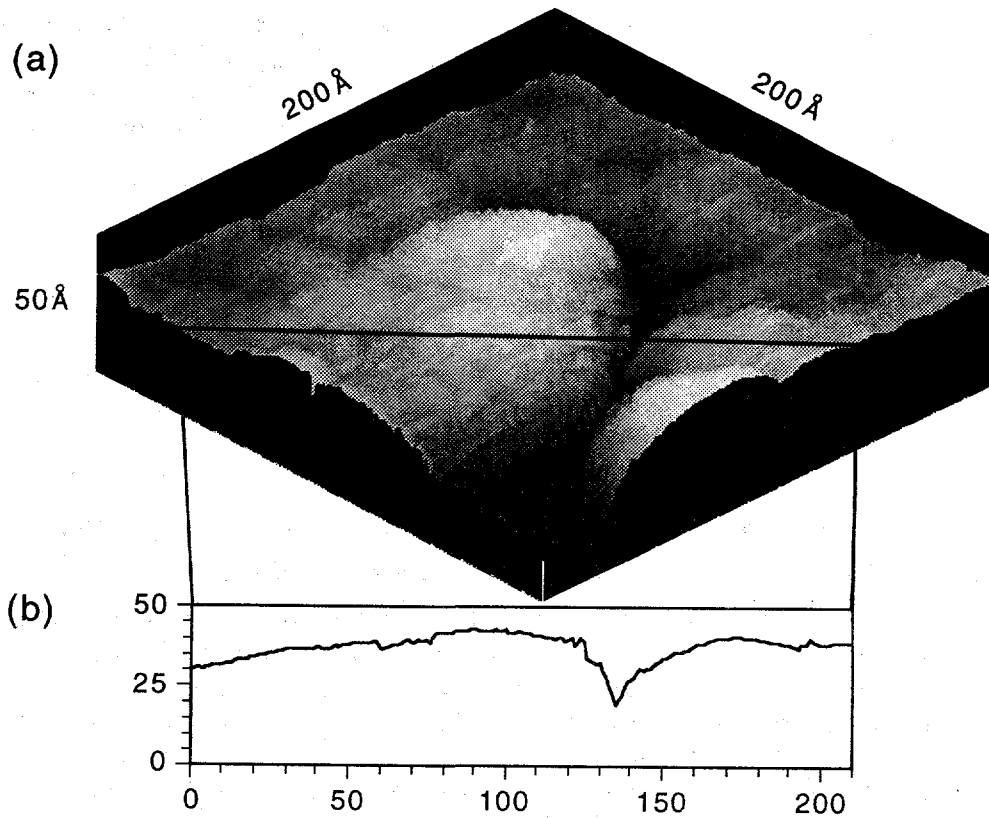


Fig. 3 Shaded view and cross section of a surface region of a 4000 Å thick a-Si:H film, showing a steep, narrow canyon.

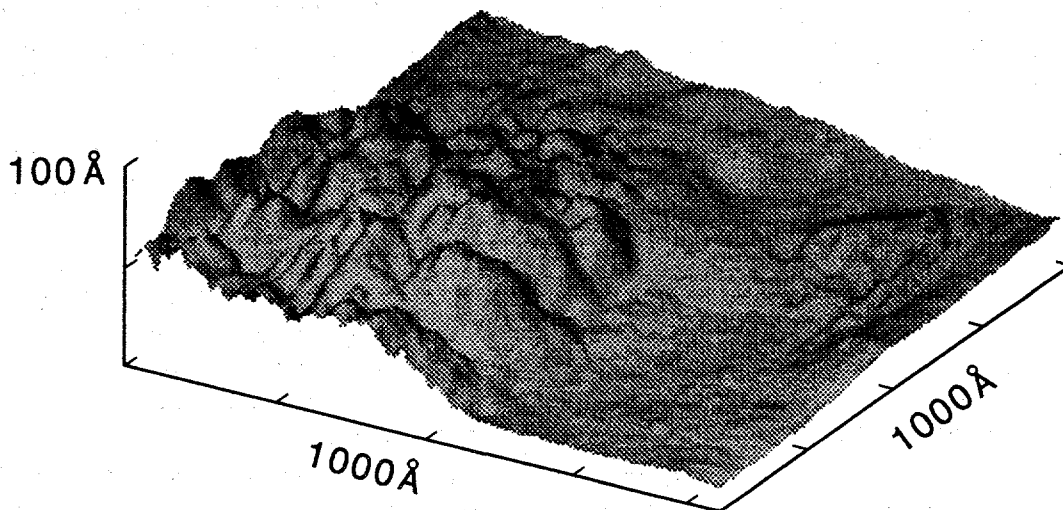


Fig. 4 Topology of a surface region on a 4000 Å thick a-Si:H film, demonstrating smooth and lumpy regions.

**Title:** **Fundamental Studies of Defect Generation in Amorphous Silicon Alloys<sup>a</sup>, and Transport in Microcrystalline Si<sup>b</sup>, both Grown by Remote Plasma-Enhanced Chemical-Vapor Deposition**

**Organization:** Departments of Physics, and Materials Science and Engineering,  
North Carolina State University  
Raleigh, North Carolina 27695-8202

**Contributors:** Professor G. Lucovsky: Principal Investigator;  
Professors. J. Berhnolc and R.J. Nemanich, Collaborators  
B.N Davidson, M.J. Williams, S.S. He  
S.M. Cho, D.J. Stephens  
W.A. Turner and Zi Jing: Post Doctoral Fellows

Research performed under two NREL sub-contracts, a) XM-9-18141-2 and b) XG-1-10063-1.

### **1. Deposition of Doped $\mu\text{-Si}$ by Reactive Magnetron Sputtering**

We have had considerable difficulty in reproducing our original results on B-compensated  $\mu\text{-Si}$ , primarily due to chamber cleanliness issues in our remote PECVD system. This prompted us to switch our effort on B-compensated  $\mu\text{-Si}$  to the dual magnetron sputtering system. Reactive magnetron sputtering (RMS) is chemically cleaner than Remote PECVD when used to prepare  $\mu\text{-Si:B}$  because the dopant is introduced in the solid phase rather than as a gas so that the problem of gas adsorption and release during subsequent depositions is eliminated. Three new targets were purchased, one 99.9999 purity undoped silicon, and two doped with boron to resistivities of 0.005-0.020  $\Omega\text{-cm}$ , and  $\sim 0.1 \Omega\text{-cm}$ , respectively.

Three samples were first prepared using combinations of the undoped and the more lightly B-doped targets. The conductivity activation energy for these ranged from 0.26 (undoped target) to 0.56 eV (doped target), and a conductivity activation energy of 0.43 eV was obtained by simultaneously depositing from the two targets. This demonstrates not only the ability to deposit doped  $\mu\text{-Si:H}$  using RMS, but also the viability of varying the B-atom concentration. The microcrystallinity of the deposited films was established by Raman scattering measurements.

The lightly B-doped target was then replaced with the more heavily B-doped target and the process described above was repeated. While the system was open, a previously identified vacuum leak in the Ar feed gas line was repaired, reducing the base vacuum from the mid  $10^{-7}$  torr range to approximately  $10^{-8}$  torr. A small indication of Si-O bonding in the infrared, IR, spectrum, present to this point, disappeared, however, microcrystalline samples prepared from this point on, showed a pronounced incorporation of bonded oxygen upon post-deposition exposure to the atmosphere.

A series of samples was prepared by systematically varying the hydrogen partial pressure while keeping all other parameters constant;  $P_{\text{Ar}} = 2.0$  mtorr,  $T_s = 200$  °C and a power of 100 W applied to the undoped c-Si target. Samples prepared using  $P_{\text{H}_2}$  of 1.0 mtorr and below were amorphous, while samples prepared at 1.25 mtorr and above were microcrystalline. A  $\mu\text{-Si}$  sample in which post deposition oxidation does not occur was prepared using 1.25 mtorr of  $\text{H}_2$ . A  $\mu\text{-Si}$  sample prepared at 1.50 mtorr displays post-deposition oxidation.

When attempts were made to incorporate B into a microcrystalline film prepared under these conditions, the incorporation of the B was correlated with post-deposition oxidation. We must determine whether B-atom incorporation by itself, or changes in the deposition rates and film morphology, generate a material that has a microstructure that promotes post-deposition oxidation. To study the opto-electronic properties of B-doped, microcrystalline materials, a series of samples,



capped with a very thin layer of high-quality a-Si:H is being prepared. The cap should reduce, if not eliminate, atmospheric instability.

## 2. Photoluminescence and PDS in $\mu\text{c-Si:B}$ (Collaboration with University of Utah)

The photoluminescence, PL, spectra of samples of  $\mu\text{c-Si:B}$ , prepared by remote PECVD, were studied (at 4K and 77K) in a collaborative effort with Professor P.C. Taylor's group at the University of Utah. The films for these studies had different amounts of B-incorporation, and covered a B-concentration range that corresponded to: i) n-type materials in which the active B-atom concentration was too small to compensate donor-like native bonding defects; ii) *quasi-intrinsic*  $\mu\text{c-Si:B}$  in which, the active B-atom concentration compensated the native bonding defects; and iii) p-type material in which the active B-concentration exceeded the density of native bonding defects.

For heavily doped  $\mu\text{c-Si}$  (both n-type and p-type) with high conductivities,  $\sim 6$  S/cm for p-type and 40 S/cm for n-type, the photoluminescence is weak, and the PDS spectra indicates a relatively high density of mid-gap defect states characterized by sub-bandgap absorption constants in excess of 2-300  $\text{cm}^{-1}$  at  $\sim 0.8$  eV. These results are essentially the same as those obtained for doped a-Si:H. For B-compensated samples with low dark conductivities,  $\sim 10^{-7}$  to  $10^{-5}$  S/cm, there are two strong PL features: i) at 0.8 to 0.9 eV and associated with band-tail to defect state transitions; and ii) at  $\sim 1.2$ -1.3 eV and associated with band-tail to band-tail transitions. These samples display sub-bandgap absorption constants below about  $100 \text{ cm}^{-1}$ , so that there is a correlation between stronger PL and lower sub-bandgap absorption.

## 3. Transport Mechanisms in Si and Si,C Amorphous and Microcrystalline Films

Systematic variations of room-temperature dark conductivities and dark conductivity activation energies for n-type and p-type  $\mu\text{c-Si}$  and  $\mu\text{c-Si,C}$  thin films with optical band-gaps between 1.9 and 2.2 eV and deposited by remote PECVD are interpreted in terms of a band alignment model. This leads to a conclusion that the maximum attainable dark conductivities of these microcrystalline thin films are limited by either thermally-assisted transport *through, or over* interfacial potential barriers between Si crystallites, c-Si, and the encapsulating *amorphous* materials: a-Si:H and a-Si,C:H, respectively. The dark conductivity of these films is thermally activated,  $\sigma = \sigma_0^* \exp(-E_{\sigma}^*/kT)$ , where  $\sigma_0^*$  is an *effective* conductivity prefactor, and  $E_{\sigma}^*$  is an *effective* activation energy. The conductivity prefactors follow a common Meyer-Neldel rule,  $\sigma_0^* = C \exp(E_{\sigma}^*/E_0)$ , for all of the a-Si:H, a-Si,C:H and  $\mu\text{c-Si,C}$  films, as well as  $\mu\text{c-Si}$  films with  $E_{\sigma}^* > 0.2$  eV, with  $E_0 \approx 0.11 \pm 0.02$  eV, and  $C \approx 5 \pm 1$  (S/cm).  $\mu\text{c-Si}$  films with  $E_{\sigma}^* < 0.2$  eV also follow a Meyer-Neldel rule, but with  $E_0 \approx -0.02 \pm 0.005$  eV, and  $C \approx 265 \pm 10$  (S/cm). In addition, for *similarly doped* a- or  $\mu\text{c-Si}$ , and a- or  $\mu\text{c-Si,C}$  alloys grown from a ratio of  $\text{CH}_4$  to  $\text{SiH}_4 = 0.5$ ,  $E_{\sigma}^*(\text{Si,C}) \approx E_{\sigma}^*(\text{Si}) + 0.18 (\pm 0.02)$  eV. These data are explained by a model in which transport in the  $\mu\text{c}$ -materials is determined by: i) the free carrier density in the doped Si crystallites; ii) internal potential barriers, associated with intrinsic band offsets and heterojunction formation, between the crystallites and the encapsulating amorphous phases; and iii) the transport path through the amorphous phase. For  $\mu\text{c}$ -films with  $E_{\sigma}^* > 0.2$  eV, transport across the internal potential barriers is by thermionic emission, whilst for films with  $E_{\sigma}^* < 0.2$  eV, the transport is by thermally-assisted direct tunneling from band states of the Si crystallites into band-tail states of the intervening amorphous phase.

## 4. Formation of Device Structures using Doped a-Si:H and $\mu\text{c-Si}$

We have studied the properties of a-Si:H and  $\mu\text{c-Si}$  in metal-insulator-semiconductor, MIS, capacitors, and in thin-film transistor, TFT, devices. We have used inverted structures with a two-component dielectric layer: an stoichiometric  $\text{SiO}_2$ , prepared by remote PECVD and in contact with the metal electrode (deposited onto the glass substrate), and a silicon nitride film, onto which the a-Si and/or  $\mu\text{c-Si}$  layers are deposited. The performance of MIS device structures is critically

dependent on the nitride material. Remote PECVD nitrides typically have both N-H and Si-H bonding, so that the demarcation point between hydrogenated *quasi-stoichiometric* nitrides and sub-nitrides ( $\text{SiN}_x$ ,  $x < 4/3$ ) cannot be established by the bonded-H alone. We have varied the ratio of the N-atom to Si-atom sources gases,  $\text{NH}_3$  and  $\text{SiH}_4$ , and deposited films that span a concentration range from hydrogenated sub-nitrides to nitrides.

TFTs, have integrated oxide/nitride dielectrics into an inverted gate structure in which the oxide is in contact with the W-gate, and the nitride is contact with the undoped a-Si:H channel.  $n^+$  a-Si:H has been used for the source and drain contacts. The oxide, nitride, undoped a-Si:H, and  $n^+$  a-Si:H layers are deposited sequentially by remote PECVD at 250°C, and the device structure is then defined by lithographic techniques. The deposition variables have been adjusted to yield stoichiometric  $\text{SiO}_2$  layers with bonded-H below the level of IR detection. We have systematically varied the source gas ratio,  $R = \text{NH}_3$  to  $\text{SiH}_4$ , between 2.5 and 12.5. Using on-line AES, Si-Si bonds are present for  $R$  less than 9, but not for source gas ratios of 10 or more. The electrical characteristics of the TFT's improve significantly as the gas phase ratio  $R$  is increased from 2.5 to approximately 10, and then decrease as  $R$  is further increased to 12.5. Additional improvements in the electrical performance of the TFTs have been made by: (i) a pre-deposition nitridation of the a-Si:H surface for the bottom-gate devices, and (ii) a post-deposition oxidation of the back-side of the channel for the top-gate structures that is performed after the patterning. The back surface oxidation of the channel reduces carrier scattering and/or recombination processes at that surface, and increases the channel mobility. The performance of the TFTs peak for a source gas ratio of  $\sim 10$ , where the channel mobility is  $\sim 1.6 \text{ cm}^2/\text{V-s}$ , the threshold voltage is 2.3 V; and the ratio of  $I_{\text{on}}$  to  $I_{\text{off}}$  is in excess of  $10^5$ . Preliminary measurements of TFT's using P-doped  $\mu\text{-Si}$  source and drains, and undoped channels have yielded channel mobilities of the order of  $0.5 \text{ cm}^2/\text{V-s}$ , and a ratio of  $I_{\text{on}}$  to  $I_{\text{off}}$  of the order of  $10^3$ . We anticipate improvements in these device properties using the higher resistivity B-compensated  $\mu\text{-Si}$  materials as a channel material.

### 5. Transport and Defect States in a-Si:H by Femto-Second Spectroscopies

We have collaborated with Professor Heinz Kurz's group at RWTH in Aachen, Germany, and have studied the properties of a-Si:H on a Femto-second time scale. In one set of experiments, we have studied the spectral- and time-resolved reflectivity and transmission of hydrogenated amorphous silicon, a-Si:H, with 50 fs time resolution. Electron-hole pairs are photo-excited into the extended states of a-Si:H by an ultrashort pump pulse at a photon energy of 2 eV. The spectral dependence of the optical response has analyzed in terms of a hopping model for the transport of the photogenerated carriers in the extended states of a-Si:H, and a hopping distance of 2.3 Å has been obtained.

In a second set of experiments, the temporal evolution of the photo-induced optical response is studied for a broad range of excitation densities from  $10^{18}$  up to  $10^{20} \text{ cm}^{-3}$ , and on a time scale of up to 200 picoseconds, ps. The optical response has been analyzed in terms of recombination and trapping mechanisms for carriers in the extended states of a-Si:H. Non-radiative quadratic recombination has been identified as the dominant relaxation mechanism for photo-induced carriers in the extended states of photovoltaic grade a-Si:H with mid-gap defect state densities of the order of, or less than about  $10^{16} \text{ cm}^{-3}$ . For photo-generated carrier densities between  $10^{18} \text{ cm}^{-3}$  and  $10^{20} \text{ cm}^{-3}$ , and for time delays up to 200 ps, the experimental data do not show any indication for trapping of photo-excited free carriers into localized bandtail states, consistent with recent time-of-flight transport measurements.

### 6. Modeling of Bond-Angle Disorder Effects in a-Si:H and a-Si,Ge:H

These model calculations have demonstrated that bond-angle distortions, present in a-Si:H, and a-Si,Ge:H, play a significant role in determining the energies of localized states. For the a-Si:H system, bond-angle distortions can shift the energy of the Si-H anti-bonding state out of the

conduction band, and thereby generate a localized state that has all of the attributes of the floating bond state first described by Pantelides. Since relatively large bond-angle distortions,  $\sim 16^\circ$  or more, are required to move these states into the bandgap, their numbers will be small with respect to the density of bonded H-atoms, but is none-the-less sufficiently large, at least of the order of  $10^{16}$  to  $10^{18}$   $\text{cm}^{-3}$ , to have an effect on the electronic properties.

Bond-angle disorder also produces an energy spread in the Si-atom and Ge-atom dangling bonds in a-Si,Ge:H alloys. The separation between these dangling bond states in idealized tetrahedral networks is  $\sim 0.13 \pm 0.02$  eV. Energy level broadening of  $\sim 0.3$  eV or more will occur for bond-angle deviations of the order of  $6^\circ$ - $8^\circ$  which is characteristic of fully relaxed amorphous networks and thereby induce the spectral overlap of the Si and Ge-atom dangling bonds.

## 7. Studies of N-doped a-Si:H

We have studied the properties a-Si:H:N alloys over a N-alloy range in which the  $E_{04}$  band-gap shifts from 1.9 eV for a-Si:H, to approximately 2.4 eV. We have studied: i) the photoconductive response at high light-levels, the decay of the photoconductivity under 100  $\text{mW}\cdot\text{cm}^{-2}$  illumination, and the IR transmission as a function of the silane to molecular  $\text{N}_2$  flow rates. Film thicknesses for this study were in the range of  $1\mu\text{m}$ . The ratio of photoconductivity to dark conductivity did not change in any significant way with the addition of N to the a-Si:H films, and is typically of the order of  $3\text{-}5 \times 10^4$ . This supports our previously reported results. Films were light-soaked for periods of time up to about 90 hours. In general the decrease of the photoconductivity reached its steady-state value for 1000 minutes of light-soaking. The ratio of the initial photoconductivity to the steady-state, light-soaked photoconductivity was typically between 10 and 15. Photodegradation curves were analyzed in terms of a stretched exponential. We have previously shown that the time constant for this function can be determined by fitting the decay curve to a power law function, and finding the time at which the derivative of that fitted function goes through its maximum value. Analysis of the photodegradation by this technique yields characteristic times of the order of 3 to 5 minutes. The corresponding values of the light to dark ratio of currents, the ratio of initial to steady-state, light-soaked photoconductivities and degradation times are:  $7 \times 10^4$ , 15, and 6 minutes, respectively, so that the addition of bonded N-atoms does not change the properties of these alloys with respect to a-Si:H, to the same degree that the addition of C-atom concentrations that change the  $E_{04}$  band-gap by a similar amounts. Attempts were made to obtain minority carrier transport properties of these a-Si:H:N alloys by the steady state photocarrier grating technique described below. To date these efforts have not been successful.

## 8. Studies of Minority Carrier Transport in a-Si and $\mu\text{c-Si}$

We have used the steady state photocarrier grating technique (SSPG) to study minority carrier transport in a-Si:H and  $\mu\text{c-Si}$ . To test our apparatus, we used a previously measured sample by supplied by Dr. W. Paul of Harvard. His group obtained a value of  $1356 \pm 100 \text{ \AA}$  for the ambipolar diffusion length,  $L$ , using an illumination level,  $I = 1$  mW of laser power. We obtained a value of  $L = 1150 \pm 100 \text{ \AA}$  at a power level of 4 mW.  $L$  was found to exponentially decrease as the laser intensity increased, and using our data, we have found that  $L = 1368.6 * e^{-0.045 * I}$ . For an illumination of 1 mW power, this yields  $L = 1308 \pm 100 \text{ \AA}$ , a value close to that determined by Professor Paul's group. We also studied B-compensated  $\mu\text{c-Si}$ ,  $\mu\text{c-Si:B}$ , prepared by Remote PECVD using 10 sccm of 10 % silane in helium, and 10 sccm of 1ppm diborane in helium. At an illumination of level 10 mW, and under the application of 100 volts, the  $\mu\text{c-Si:B}$  photoconductivity is  $\sim 10^{-2} (\Omega\cdot\text{cm})^{-1}$ . For the same illumination and an electric field of  $E = 243 \text{ volt}\cdot\text{cm}^{-1}$ , and assuming zero surface recombination velocity, we have obtained  $L = 403 \pm 50 \text{ \AA}$ . If we assume a similar dependence between  $L$  and  $I$  as for a-Si:H, this corresponds to a value of  $L \approx 600 \text{ \AA}$  for  $I \approx 1$  mW.

**Title: In Situ Characterization of Growth and Interfaces in a-Si:H Devices**

**Organization: Materials Research Laboratory, Department of Physics, and Department of Electrical and Computer Engineering, The Pennsylvania State University, University Park, PA.**

**Contributors: R.W. Collins and C.R. Wronski, Principal Investigators, I. An, Y.M. Li Research Associates, Y. Lu, Graduate Assistant.**

## **Objective and Approach**

Because of the stringent demands placed on amorphous silicon-based devices, techniques for real time monitoring of film growth and interface formation are important. Optical probes are among the few techniques that can be applied to monitor plasma-enhanced chemical vapor deposition (PECVD). Ellipsometry is the most powerful such probe because it provides measures of the amplitude and phase changes that polarized light undergoes upon reflection from a surface.

Real time ellipsometry can be applied to understand film growth through the characterization of process-property relationships on a monolayer scale. It can also be used to troubleshoot, assess reproducibility, and solve problems. Ultimately, if data analysis can be performed in real time, then feedback can be applied to adjust preparation parameters to obtain desired film properties.

The following has been the focus of research in FY 1992: (1) assessment of in situ H treatments to modify the properties of a-Si:H films and interfaces, (2) characterization of the microstructural development of amorphous silicon-carbon (a-SiC:H) alloys, including optimization of the material and (3) characterization of the interactions between a-SiC:H and transparent conducting oxides.

## **Research Results and Conclusions**

### **H Modification of Thin Films**

Optimum PECVD a-Si:H films modified in situ by atomic H exposure have been studied [1]. The goal of this work is two-fold: (i) to improve the stability of films and device interfaces by relaxing the Si-Si bond structure, and (ii) to understand the kinetic role of atomic H in equilibrating the near-surface of the film during growth. The hydrogenation process we have developed employs a heated filament and is easily adapted to existing PECVD facilities.

\* We have found that alternating growth and atomic H-treatments, which typically result in the controlled incorporation of up to 5 at.% additional H in monohydride configurations, can make minor improvements in the subgap absorption and stability compared to control films prepared without the treatments [2]. Overall, the improvements reduce the run-to-run variability in film quality that exists for control samples, however the routine H-treated films exhibit very similar electronic characteristics to the best control films. This suggests that the excess H can in fact passivate the defects and impurities that exist under less than optimum growth or vacuum conditions, otherwise the H is paired in configurations that are stable and inert.

\* For optimum PECVD a-Si:H, atomic H interacts more readily with the near-surface material than might be expected based on the H diffusion coefficient obtained on multilayers [2,3]. Real time ellipsometry suggest that H incorporation is reaction-limited in the top >200 Å of the film, implying a diffusion coefficient >2x10<sup>-15</sup> cm<sup>2</sup>/s, possibly larger. In general, the results provide a full picture of H-trapping and release in the near-surface of a-Si:H in the growth environment.

### **Nucleation and Microstructural Development in a-SiC:H**

We have studied the effect of H-dilution on the nucleation and growth of a-SiC:H on smooth c-Si

wafers [4]. In these depositions, the substrate temperature was 250°C and the reactive gas partial pressure was 75 mTorr. The SiH<sub>4</sub>:CH<sub>4</sub> flow ratio was set at 3:2, leading to a gap ~0.2 eV wider than a-Si:H. The purpose of this work is to develop optimum conditions for high quality a-SiC:H that can be applied as the p-layer of mid- or wide-gap cells or the i-layer of wide-gap cells.

\* The film thickness  $d_s^*$  at which nuclei make contact to form a bulk-like film, which is related to the nucleation density  $N_d$  via  $N_d \sim [2d_s^*]^{-2}$ , increases from 14 Å without dilution to 25 Å at a dilution level, H<sub>2</sub>:(SiH<sub>4</sub>+CH<sub>4</sub>), of 25:1. Thus,  $N_d$  decreases by 3X with increasing dilution.

\* After nuclei make contact, long term smoothing of nucleation-induced surface roughness is observed under high dilution conditions. For lowest dilution, however, only a weak initial smoothing effect is observed followed by long term roughening. See Fig. 1.

\* The final void density of bulk films prepared without H dilution are 5 vol.% higher than those prepared with 20:1 dilution. A weak increase in void vol.% at the highest dilution levels may be related to H-etching of weaker bonds that connect coalesced nuclei. See Fig. 2.

\* The improved microstructure with H dilution is also accompanied by improved photo-electronic properties as shown in the typical absorption spectra of Fig. 3.

The decrease in nucleation density with H-dilution reveals less sticking and/or a high diffusion length of the precursors on the substrate surface; the enhanced surface smoothing indicates a higher surface diffusion length of the precursors on the a-SiC:H itself. Etching at high H-dilution levels may also contribute to surface smoothing.

#### Deposition of a-SiC:H on TCO's: Chemical Interactions

We have studied the comparative stability of various TCO's, SnO<sub>2</sub>, In<sub>2</sub>O<sub>3</sub>:Sn (ITO), and ZnO, under identical, weak atomic H fluxes. We have then characterized the growth of intrinsic a-SiC:H prepared with 20:1 H<sub>2</sub>:(SiH<sub>4</sub>+CH<sub>4</sub>) flow ratio at T<sub>s</sub>=250°C onto SnO<sub>2</sub> and ZnO. This research are a prelude to more complex studies of the growth of p-type a-SiC:H on the TCO.

\* The TCO's showed variability in the nature and time scale of the interaction with atomic H generated by a remote filament. For a ~500 Å CVD SnO<sub>2</sub> film, complete transformation to a metallic structure occurred over 5 min, whereas for 500 Å sputtered ITO, such a transformation occurred over 20 min. For ~300 Å sputtered ZnO, no reduction at all was observed over 25 min, however H-diffusion into the film was evident, leading to a perceptible increase in the band gap.

\* Analogous features have been observed in the initial stages of growth of a-SiC:H on the SnO<sub>2</sub> and ZnO. However, because the time of TCO exposure to plasma H is shorter, the effects are most likely confined to the near-interface, but with greater damage from direct plasma contact.

\* For SnO<sub>2</sub>, ~70 Å of surface roughness was detected, which led to a modulated TCO/a-SiC:H interface (see the two model structures of Fig. 4), complicating data interpretation. In order to fit the low energy optical absorption behavior of the TCO/a-SiC:H interface (evident in Fig. 4 in the experimental  $\psi$  spectrum), we needed to include 7 vol.% metal [denoted "osc" in structure (a) of Fig. 4] at the modulated interface. However, it is difficult to tell whether the metal is dispersed throughout the near-interface region (70 Å) or localized at the modulated interface (effective 5 Å).

\* For sputtered ZnO the surface was found to be very smooth (roughness <20 Å). The close fit to the  $\psi$  spectrum for a-SiC:H on ZnO in Fig. 5 demonstrates no measurable excess subgap absorption at the interface due to free metal. However, from the real time studies, we have observed a clear shift in the band gap of the ZnO due to H interaction. At this point, the thickness of the affected region is unclear; if we assume that the top 20 Å is affected the shift is ~0.1 eV. Clearly such an effect may increase the resistance at the junction.

## Future Work

- \* H treatments will be applied to interfaces in solar cell structures prepared in a two-chamber system to see if improvements in device performance can be obtained. It is possible that irreproducibilities associated with impurities can be prevented.
- \* Further attempts to improve the microstructure and electronic properties of a-SiC:H will be undertaken. Different substrate temperatures and even higher dilution levels will be explored.
- \* Growth procedures designed to minimize TCO/a-SiC:H interactions will be studied. We will extend our research to the p-type a-SiC:H interface with TCO and with the overlying i layer.
- \* We will assess the ability of real time ellipsometry to control C grading in a-SiC:H i layers.

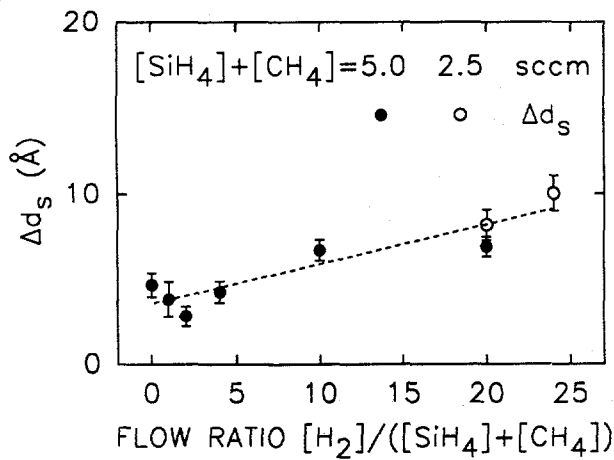


Figure 1 Surface smoothing between the time of nuclei contact and 50 Å bulk film thickness for a series of a-SiC:H films vs. H<sub>2</sub>:(SiH<sub>4</sub>+CH<sub>4</sub>) flow ratio. For the (solid, open) points, the total (SiH<sub>4</sub>+CH<sub>4</sub>) flow was (5, 2.5) sccm, respectively.

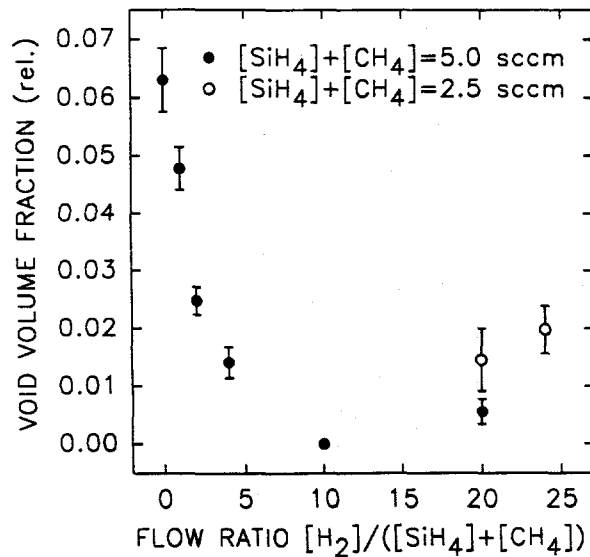


Figure 2 Void fraction for a-SiC:H vs. H<sub>2</sub>:(SiH<sub>4</sub>+CH<sub>4</sub>) flow ratio. For the (solid, open) points, the total (SiH<sub>4</sub>+CH<sub>4</sub>) flow was (5, 2.5) sccm, respectively

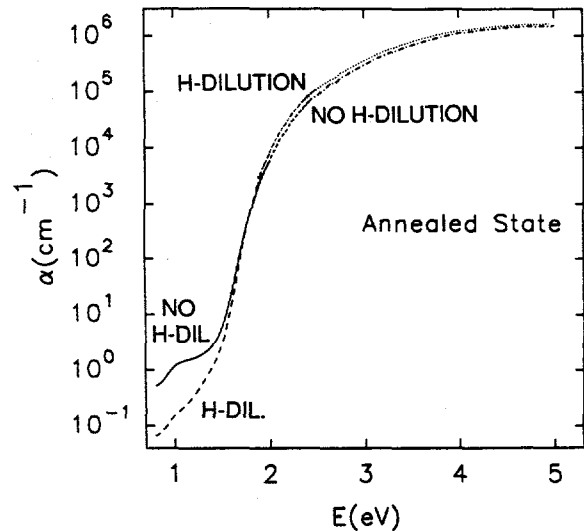


Figure 3 Absorption coefficient from ellipsometry, transmission/reflection, and dual-beam photoconductivity for a-SiC:H films prepared without H-dilution, and with a 20:1 ratio of H<sub>2</sub>:(SiH<sub>4</sub>+CH<sub>4</sub>). [See Ref 5].

## References

- [1] Annual Report, Photovoltaics Program, FY 1991, (March 1992). NREL/TP-410-4724. 55 pp. Available NTIS: Order No. DE92001248.
- [2] Y.M. Li et al., Mater. Res. Soc. Symp. Proc. **258**, 57 (1992); I. An et al. *ibid.*, p. 27.
- [3] Ilsin An, Y.M. Li, C.R. Wronski, and R.W. Collins, Phys. Rev. B, in press (1993).
- [4] R.W. Collins, I. An, H.V. Nguyen, Y. Lu, Thin Solid Films, in press (1993).
- [5] R.M. Dawson, Y.M. Li, M. Gunes, D. Heller, S. Nag, R.W. Collins, and C.R. Wronski, M. Bennett, and Y.M. Li, Mater. Res. Soc. Symp. Proc. **258**, 595 (1992).

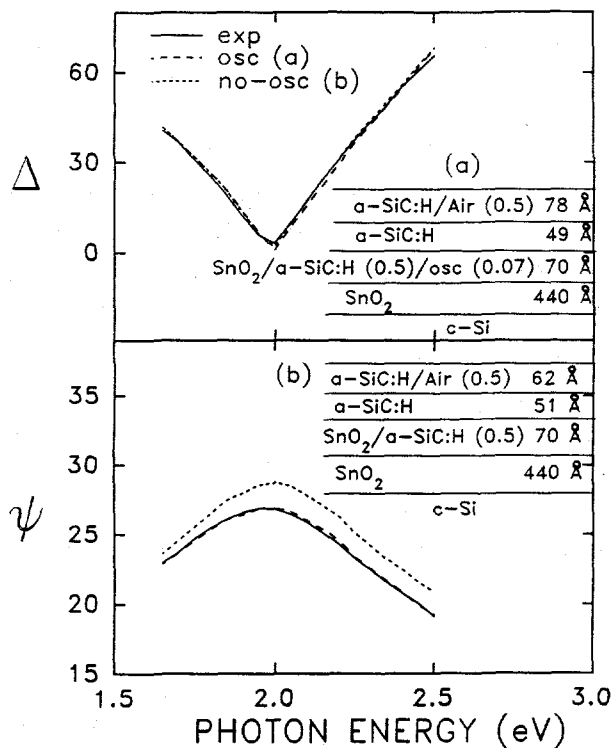


Figure 4 Ellipsometric spectra in the near-gap region for a-SiC:H on SnO<sub>2</sub>, along with optical models that include bulk, surface, and interface roughness layers. Model (a) includes 7 vol.% metal in the interface layer ("osc"; dashes), whereas model (b) includes no metal ("no-osc"; dots). The metal indicating TCO reduction is required to fit the  $\psi$  spectrum at low E.

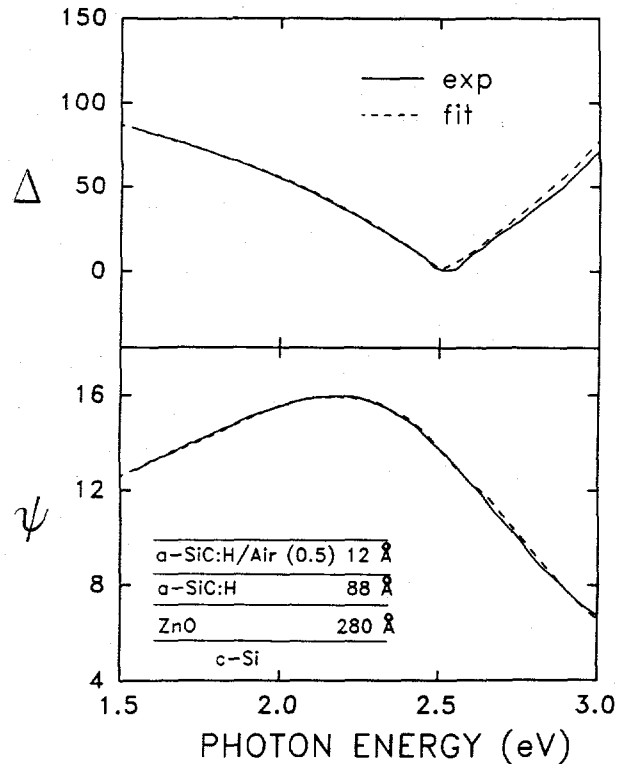


Figure 5 Ellipsometric spectra in the near-gap region for  $\sim 100$  Å a-SiC:H on ZnO along with a fit to an optical model that includes a-SiC:H bulk and surface roughness layers. In this case the TCO is smooth so an interface roughness layer is not needed. Furthermore, no free metal at the interface is required to fit the  $\psi$  spectrum at low E.

**Title:** Research on Defects and Transport in Amorphous Silicon-Based Semiconductors

**Organization:** Department of Physics, Syracuse University, Syracuse, New York 13244-1130

**Contributors:** Eric A. Schiff, principal investigator; Qing Gu and Qi Wang.

Photocurrent transport is the mechanism underlying solar cell operation. Our research in the last year has significantly improved our knowledge of electron transport in *alloys* of a-Si:H (a-Si<sub>1-x</sub>Ge<sub>x</sub>:H and a-Si<sub>1-x</sub>C<sub>x</sub>:H). We have also worked to link this fundamental research to solar cell performance. We studied the correlation of electron transport properties to “blue” fill factors of comparable solar cells, and we discovered evidence for a fundamental deficiency in the nearly universal use of Shockley-Read kinetics in describing trapping and recombination in a-Si:H.

In this report we highlight some results obtained in four areas:

- *Fill Factors and Electron Transport in a-Si<sub>1-x</sub>Ge<sub>x</sub>:H Alloys.* For a-Si<sub>1-x</sub>Ge<sub>x</sub>:H prepared at Energy Conversion Devices, Inc. we found good correlations between the the “blue” fill factor  $FF_B$  in solar cells and both the electron deep-trapping mobility-lifetime product  $\mu\tau_{e,t}$  and the conduction bandtail width  $\epsilon_0$  estimated from the electron mobility [1]; the data are shown in Fig. 1. These data also show the considerable scatter which has frustrated attempts to use “bulk” characterizations to accurately predict solar cell performance. We believe that this difficulty is due to small inhomogeneities in materials which are not quantitatively described by present characterization techniques, and we are planning work to address this difficulty.
- *Electron Mobilities in a-Si<sub>1-x</sub>Ge<sub>x</sub>:H Alloys.* For electrons in a-Si<sub>1-x</sub>Ge<sub>x</sub>:H, we discovered a beautiful trend in the temperature-dependent electron drift mobility by simply interpolating measurements so that they all correspond to a specific ratio of distance  $L$  and measuring field  $E$  [2]. The results are presented as Fig. 2; they include our recent measurements on Energy Conversion Devices, Inc. material as well as earlier work. From the correlation of these results with optical bandgaps for a-Si<sub>1-x</sub>Ge<sub>x</sub>:H, we have proposed that there is a fundamental tradeoff between the gap and electron mobility for a-Si<sub>1-x</sub>Ge<sub>x</sub>:H. This work was in collaboration with Subhendu Guha (United Solar Systems Corp.).
- *Electron Mobilities in a-Si<sub>1-x</sub>C<sub>x</sub>:H Alloys.* We have performed the first electron time-of-flight measurements on a-Si<sub>1-x</sub>C<sub>x</sub>:H [3]. Results for three alloys and for a reference a-Si:H specimen prepared at Solarex, inc. are presented in Fig. 3 using the same  $L/E$  ratio as for Fig. 2. It is clear carbon alloying diminishes the electron drift mobility; we have not yet come to any conclusions regarding the applicability of multiple-trapping or the widths of exponential bandtails. This work was in collaboration with Yuan-Min Li (Solarex).
- *Optical Bias and Electron Drift in a-Si:H.* We showed that optical bias suppresses electron deep trapping in a-Si:H [4]. This result is illustrated in Fig. 4, which



shows the transient behavior of the integrated charge measured in an external bias circuit following absorption of a short laser impulse. The lowest curve was measured without optical bias, and shows a "plateau" after about 1  $\mu$ s which is the signature of deep-trapping. Successively higher curves were measured at successively higher levels of bias, and show the unexpected behavior that bias suppresses the deep-trapping plateau. We believe that this effect is inconsistent with the standard "Shockley-Read" or multiple-trapping view of photoconductivity in a-Si:H, and instead requires consideration of multiple configurations of the defects. This work was in collaboration with Daxing Han and Marvin Silver (University of North Carolina).

In addition to these topics, we have worked on high field electron transport in a-Si:H (collaboration with J. B. Chevrier and B. Equer, Palaiseau) [5], and we have commenced a project on photocarrier grating measurements. We have also published papers summarizing earlier research on:

- (i) Transient photocharge measurements and electron emission from deep levels [6].
- (ii) Delayed field measurements of electron emission from deep levels [7].
- (iii) Effects of high temperature post hydrogenation on a-Si:H [8].
- (iv) Temperature-dependent electron spin resonance (ESR) and the defect correlation energy in a-Si:H [9].
- (v) A short review of the "hydrogen deficit" view of defects in a-Si:H [10].
- (vi) Effects of light-soaking on the electron mobility in a-Si:H [11].

## References

1. Qi Wang, Homer Antoniadis, E. A. Schiff, and S. Guha, in *Amorphous Silicon Technology - 1992*, edited by M. Thompson, *et al* (Materials Research Society, Pittsburgh, 1992), p. 881.
2. Qi Wang, Homer Antoniadis, E. A. Schiff, and S. Guha, unpublished manuscript.
3. Qi Wang, E. A. Schiff, and Y.-M. Li, unpublished research.
4. Daxing Han, E. A. Schiff, and M. Silver, unpublished manuscript.
5. Qing Gu, E. A. Schiff, J. B. Chevrier, and B. Equer, unpublished research.
6. Homer Antoniadis and E. A. Schiff, *Phys. Rev. B* **46**, 9482 (1992).
7. Homer Antoniadis and E. A. Schiff, in *Amorphous Silicon Technology - 1992*, *loc. cit.*, p. 783.
8. J.-K. Lee and E. A. Schiff, in *Amorphous Silicon Technology - 1992*, *loc. cit.*, p. 185.
9. J. K. Lee and E. A. Schiff, *Phys. Rev. Lett.* **68**, 2972 (1992).
10. Sufi Zafar and E. A. Schiff, in *Amorphous Silicon Technology - 1992*, *loc. cit.*, p. 199.
11. Qi Wang, Homer Antoniadis, and E. A. Schiff, *Appl. Phys. Lett.* **60**, 2791 (1992).

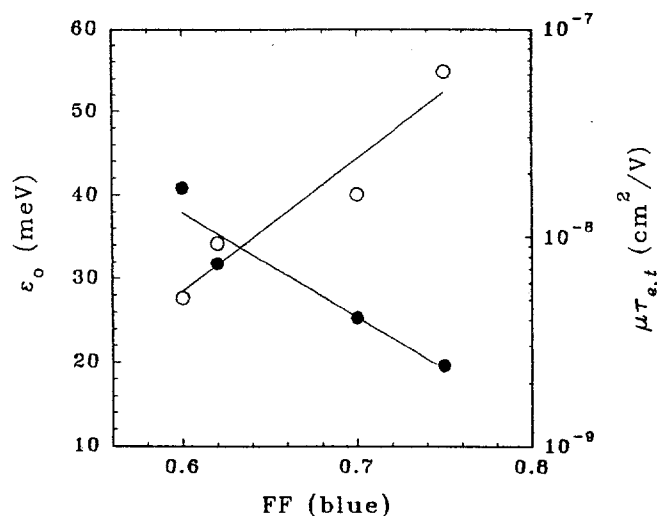


**Fig. 1:** Correlation of the blue fill factor  $FF_B$  measured in  $0.32 \mu\text{m}$  solar cells with electron deep trapping mobility lifetime products ( $\mu\tau_{e,t}$ ) and conduction bandtail widths  $\epsilon_0$  measured on comparable a-Si<sub>1-x</sub>Ge<sub>x</sub>:H materials.

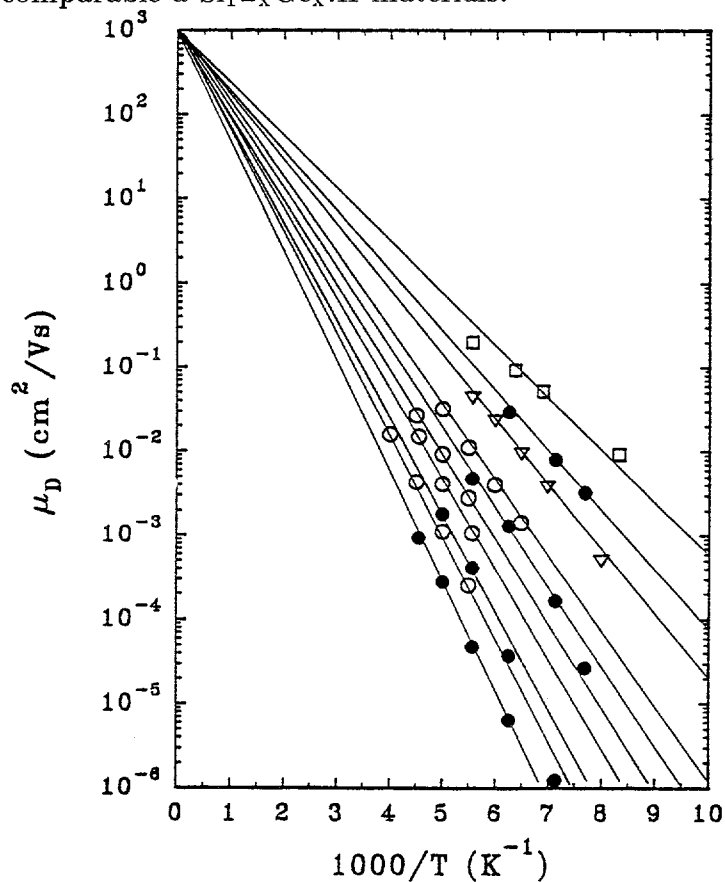


**Fig. 2:** Temperature-dependent electron drift-mobility  $\mu_D$  measured in many specimens of a-Si<sub>1-x</sub>Ge<sub>x</sub>:H from different laboratories; all drift-mobilities correspond to the ratio  $L/E = 2 \times 10^{-9} \text{ cm}^2/\text{Vs}$  of the distance  $L$  and field  $E$  in a time-of-flight measurement. Lower curves correspond to smaller optical gaps.

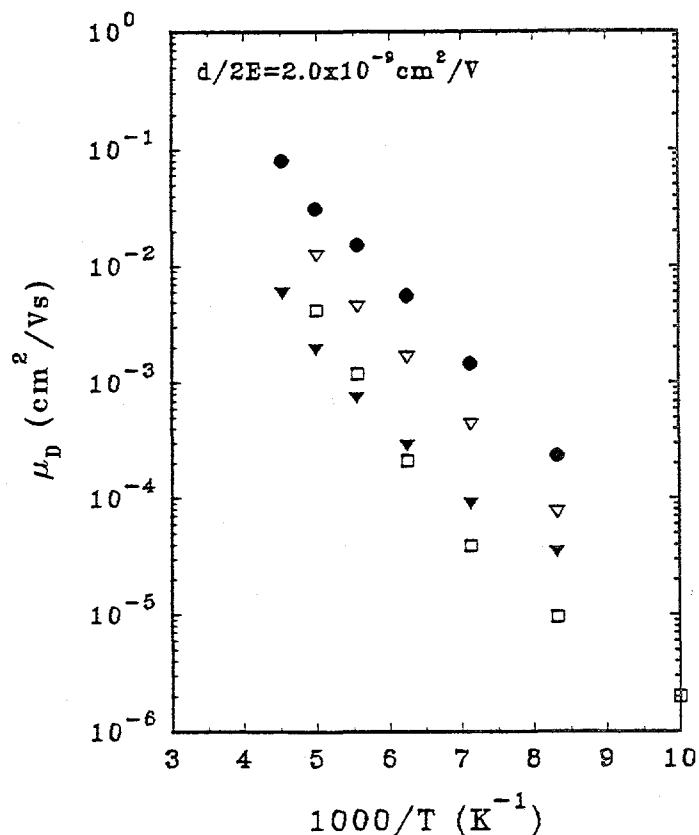


**Fig. 3:** Temperature-dependent electron drift-mobility  $\mu_D$  measured in several specimens of  $a\text{-Si}_{1-x}\text{C}_x\text{:H}$  prepared at Solarex, Inc.. The  $L/E$  ratio is the same as for Fig. 2; the uppermost curve is unalloyed  $a\text{-Si:H}$ , and successively lower curves correspond to *larger* optical gaps.

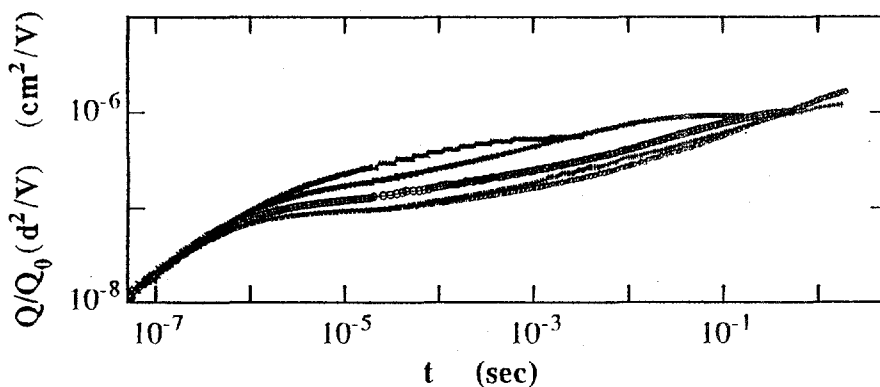


**Fig. 4:** Transient photocharge measurements  $Q(t)d^2/Q_0V$  in an  $a\text{-Si:H}$  specimen under varying levels of optical bias;  $Q_0$  is the photogenerated charge,  $d$  is the interelectrode gap, and  $V$  is the bias voltage. Higher lying curves correspond to higher levels of optical bias.

**Title:** Charge Transport Measurements in Hydrogenated Amorphous Silicon by Photoconductive Frequency Mixing

**Organization:** Department of Physics, University of California at Los Angeles

**Contributors:** R. Braunstein, principal investigator; Yi Tang, I. Shaltout

## Introduction

The charge transport properties of amorphous semiconductors, such as the mobility and lifetime, are influenced by a variety of effects making it difficult to extract microscopic transport parameters from a given experiment. Multiple trapping in localized band-tail states results in a dispersive drift mobility making it difficult to ensure that transit times are obtained in the full charge collection regime in the time-of-flight measurements. Steady state photoconductivity merely yields the mobility-lifetime product. To distinguish between models of mobility involving disorder induced band-tail broadening and long-range potential fluctuations resulting from charge donor and acceptor states, it is necessary to determine drift as well as extended-state mobilities. We have developed the technique of photoconductive frequency mixing that can separately determine drift, extended-state mobility and lifetime [1-3].

This report covers the summer period 7/1/92 to 9/30/92.

## Accomplishments

### 1. a-Si:H and a-SiC:H Photo-degradation

Figures 1a,1b,1c show the photo-degradation of the dc photoconductivity  $\sigma_p$ , recombination time  $\tau_R$ , and the drift mobility  $\mu_d$  in intrinsic a-Si:H (provided by Dr. B. von Roedern of NREL) produced by the glow discharge deposition process as determined by our photoconductive frequency mixing technique. Both mobility and lifetime were found to decrease continuously following the light-soaking process, which indicates the possible existence of long-range potential fluctuations [4] and a change in the recombination processes due to light-soaking. For the first time, evidence is provided that the degradation is accompanied by loss of mobility, a fact that is neglected in all prevailing models for the Staebler-Wronski effect. The details of the experimental work and analyses are reported in [2,3]. Figures 1d, 1e, and 1f show the photo-degradation of a-SiC:H (provided by Dr. Y. M. Li of Solarex) with respect to the dc photoconductivity, recombination time, and drift mobility. It should be noted that although the dc photoconductivity and lifetime are decreasing monotonic function of illumination time, the drift mobility is initially independent then increases and finally decreases as a function of illumination time. These photo-degradation studies utilizing *in situ* our photoconductive frequency mixing technique to deconvolute the mobility  $\mu_d$  and recombination time  $\tau_R$  indicate that in some instances the degradation of both  $\mu_d$  and  $\tau_R$  could be described by stretched exponential functions. However a noticeable difference of the fitting parameters for  $\mu_d$  and  $\tau_R$  was found. Table I indicates the stretched exponential parameters  $\beta$  and  $\tau_0$  are not proper material parameters to characterize uniquely the processes responsible for the photo-degradation process. Our results are consistent with the finding that there are degradation mechanisms that occur on different times scales in solar

cells.

## 2. Drift and Extended State Mobility in Compensated a-Si:H

The mobilities of a series of compensated a-Si:H samples measured earlier by the time-of-flight technique [5] were determined by our photomixing technique. The samples were provided by Dr. R. A. Street of Xerox and were prepared by plasma deposition of SiH<sub>4</sub> with equal volume concentrations of B<sub>2</sub>H<sub>6</sub> and PH<sub>3</sub> [5]. The drift mobility of electrons as a function of temperature is shown in Figure 2a. The drift mobility and the extended state mobility as a function of compensation are shown in Figure 2b. Both the drift and extended mobility decrease as the compensation increases. Modelling these transport processes in the context of our photomixing technique [1-3], it was shown that long-range potential fluctuations can account for the decrease in the extended mobility in compensated samples as well as uncompensated samples.

## 3. Temperature Dependence of the Mobility in CuInSe<sub>2</sub>

Efficiencies >18% can be obtained with CuInSe<sub>2</sub>-based (CIS) solar cells if such devices are operated well below 300 K [6]. We have investigated a device-grade CIS-layer employing our photomixing technique [1-3]. The featureless temperature dependence of the dc photocurrent and the mobility leads us to conclude that the reported maximum in cell efficiency below 200 K is not determined by the transport or recombination phenomena in the bulk of the CIS absorber but may be due surface and interface processes. Figure 3b shows the dc photocurrent I<sub>p</sub>, dark current I<sub>d</sub> and the mixing current I<sub>mix</sub> as a function of dc bias when the co-planar gold contacts were asymmetrically illuminated. As can be seen both the dark current and the photocurrent show ohmic behavior, but the photomixing current shows non-ohmic behavior, since it is non-zero at zero d.c. bias. This indicates the existence of a built-in electric field near the contact which is determined to be 2900V/cm which can be due to grain boundaries and Schottky barriers.

## Conclusions and Future Work

We have demonstrated the power of photoconductive frequency technique [1-3] to separately determine the drift, extended state mobility and lifetime in a range of photo-voltaic materials. By extending these measurements to higher frequencies and combining them with computer simulations further insight can be gained in the microscopic understanding of transport in these materials.

**Table I** Summary of results for light soaking for a-Si:H and a-SiC:H

		$\beta$	$\tau_0$ (min)
a-Si:H	From Photoconductivity	0.648	295
	From Recombination Lifetime	0.642	125
	From Drift Mobility	0.491	163
a-SiC:H	From Photoconductivity	0.874	199
	From Recombination Lifetime	0.925	170

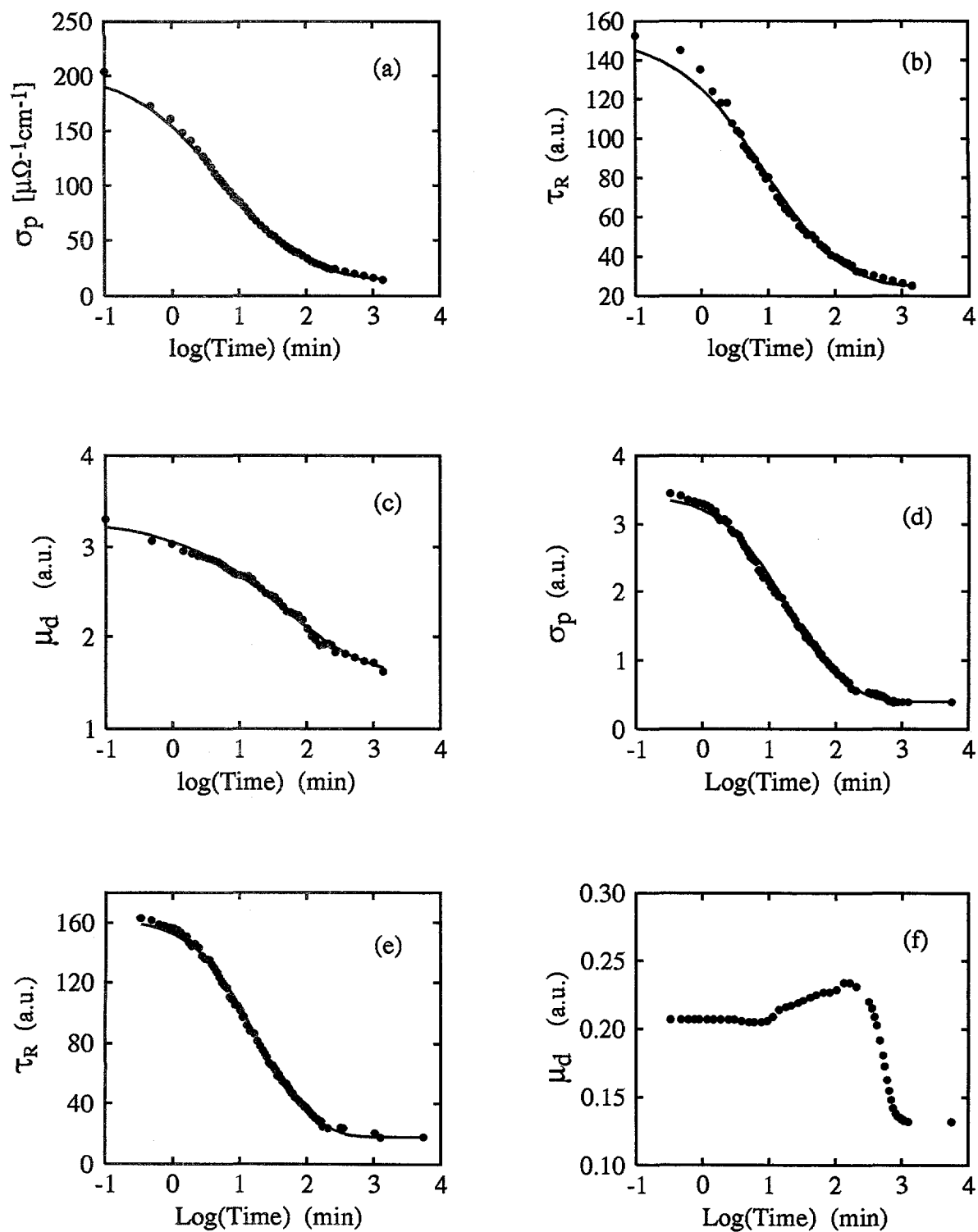


Fig. 1 Light soaking on a-Si:H (a-c) and a-SiC:H (d-f). Solid lines are curve fit to the stretched exponential function. Different stretched exponential parameters were found, which are shown in Table I.

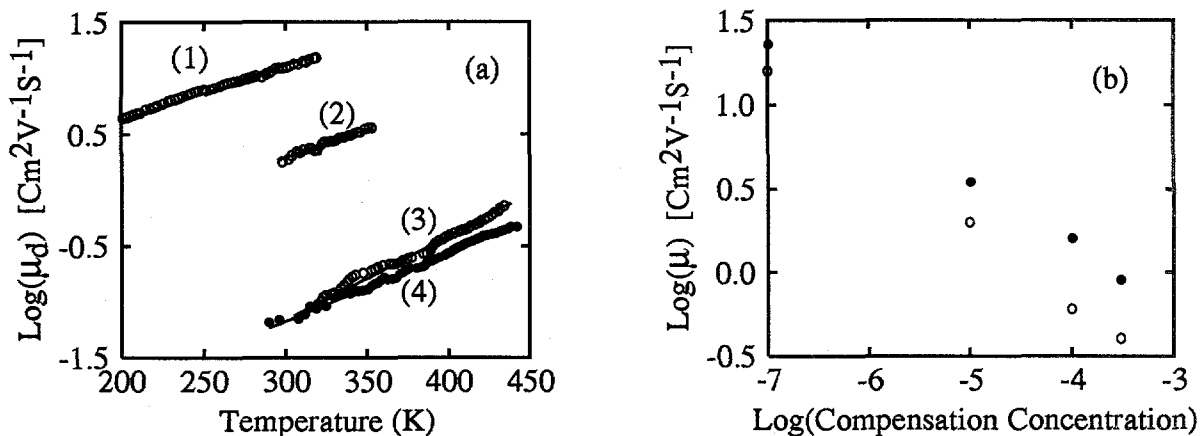


Fig. 2 Mobilities for intrinsic and compensated a-Si:H. In (a), (1), (2), (3) and (4) correspond to intrinsic and compensation levels of  $10^{-5}$ ,  $10^{-4}$ ,  $3 \times 10^{-4}$  respectively. In (b) open and closed circles correspond to the drift and extended state mobilities and -7 for  $\text{Log}(\text{Compensation Concentration})$  corresponds to the intrinsic a-Si:H.

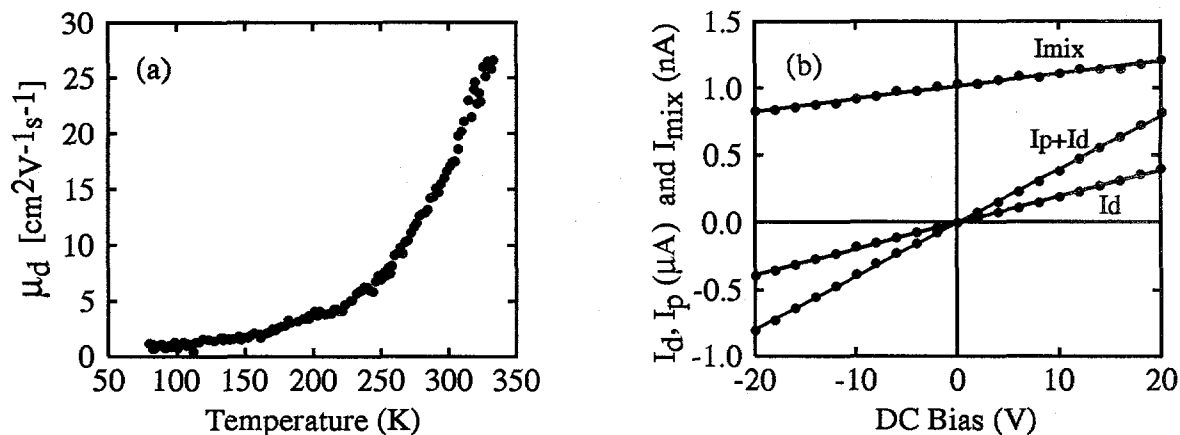


Fig. 3 Drift mobility (a), dark, photo and mixing currents (b) for  $\text{CuInSe}_2$ .

### References

1. E. R. Giessinger, R. Braunstein, S. Dong and B. G. Martin, *J. Appl.* 69, 1469 (1991).
2. Yi Tang, R. Braunstein, and B. von Roedern: "Photomixing determination of mobility and lifetime in intrinsic a-Si:H" Proceedings of the Materials Research Society Spring meeting (April, 1992), San Francisco, California. To be published.
3. R. Braunstein and Yi Tang: "Charge transport measurements in amorphous semiconductors by photoconductive frequency mixing". Proceedings of the 21th International Conference on the Physics of Semiconductors (August, 1992), Beijing, China. To be published.
4. H. M. Branz and M. Silver, *Phys. Rev.* B42, 7420 (1990).
5. J. A. Howard and R. A. Street, *Phys. Rev.* B44 7935 (1991).
6. K. W. Mitchell and H. I. Liu, Proc. 20th IEEE PV Specialists Conference (1988), Las Vegas, 1461.

Title: Stable, High Efficiency Amorphous Silicon Solar Cells with Low Hydrogen Content

Organization: Institute of Energy Conversion  
University of Delaware  
United States Department of Energy  
University Center of Excellence  
Newark, Delaware 19716-3820

Contributors: J.E. Phillips, project director;  
S.S. Hegedus, principal investigator

### Objectives

The current project is phase II of research on the development of amorphous silicon based solar cells that have a stabilized efficiency greater than 12%. The present objectives are to develop the most stable materials, understand the nature of the Staebler-Wronski effect in a-Si:H and the transport phenomena in the Si-Ge alloy system. Results from those studies will provide the materials and design parameters necessary to develop solar cells with greater stabilized efficiency.

### Technical Approach

During this phase of the work, IEC has produced and analyzed both amorphous silicon germanium and amorphous silicon films and solar cells with reduced hydrogen content in order to make progress towards high stabilized efficiency multijunction solar cells. IEC has both a photo CVD and a multichamber plasma CVD system. Materials from both reactors were studied. Single junction solar cells were numerically modeled in order to guide solar cell designs and to determine the relative contributions of interface and bulk properties on solar cell performance. Some of the analysis and measurements of amorphous silicon and silicon-germanium films has been done in collaboration with C. Wronski at Pennsylvania State University, J. D. Cohen at the University of Oregon, P. M. Fauchet at the University of Rochester and the group at the University of Neuchatel.

### Conclusions

Thus far the low hydrogen (<5%) materials prepared by both the plasma and photo-CVD reactor do not offer greatly improved stability as compared to standard amorphous silicon materials (see Table 1). It is, however, clear that stability of low hydrogen materials is comparable to standard materials. Low hydrogen amorphous silicon could be useful for some i-layer applications. For example, the triple stacked solar cell could substitute a thinner more degradation resistant lower band gap low hydrogen i-layer in the middle solar cell.

The performance of a graded a-SiGe:H device (3520-11) having a thin (<0.1  $\mu\text{m}$ ) graded a-SiGe:H i-layer with a minimum  $E_G$  of 1.3 eV was monitored during 265 hours of exposure to 100 mW/cm<sup>2</sup> ELH illumination at -25°C. The performance of the best cell is given in Table 2. The largest loss in FF (~3%) occurs in the first 12 hours of light soaking. Subsequent testing after 265 hours of light exposure showed little change in FF or efficiency.



The current voltage behavior of some of the amorphous silicon germanium solar cells was analyzed to extract the lumped equivalent circuit parameters needed to represent the devices in a multi-junction configuration. Circuit modeling will guide the design and enhance the performance of multijunction solar cells. Issues of current matching and tunnel junctions can be studied. Current voltage characteristics of IEC and Solarex a-Si and graded a-SiGe single junction cells, obtained at current densities expected in tandem devices (8-9 mA/cm<sup>2</sup>), were modelled using the SPICE circuit simulator. Table 3 gives the diode model parameters and Figures 1 and 2 show the measured and modelled JV characteristics.

The silicon germanium alloys do not appear to be markedly less stable than amorphous silicon. Table 4 shows a-SiGe film properties obtained on our photo-CVD material at University of Oregon. The Urbach energy is uniformly low (<60 meV). Film 3481 was deposited under conditions used in our graded a-SiGe solar cells. Note that the defect density increased by 3X and electron transport decreased by 10X after 100 hrs of light exposure.

#### References

"Photochemical Vapor Deposition of Amorphous Silicon Alloy Materials and Devices:", B.N. Baron, C.M. Fortmann, and S.S. Hegedus, Final Report to SERI under Subcontract No. XL-8-18092-1, Mod. 5, 5/1/88 to 2/28/91.

"Stable, High Efficiency Amorphous Silicon Solar Cells with Low Hydrogen Content", C.M. Fortmann and S.S. Hegedus, Annual Report to NREL under Subcontract no. XG-1-10063-4, 3/1/91 to 1/31/92.

Table 1  
Photoconductivity before and after 200 hrs light soaking  
for low hydrogen content amorphous silicon films

Film #	Deposition Method	Substrate Temperature (°C)	Growth Rate (Å/sec)	Hydrogen Content (%)	Photoconductivity (μS/cm)	
					Initial	Final
4061	plasma	350	1.5	2.8	88	7.5
4062	plasma	350	7.3	2.4	21	4.8
4063	plasma	350	2.9	3.6	16	4.7
4064	plasma	350	3.3	4.0	11	4.1
4065	plasma	350	9.4	3.1	20	3.4
4015	plasma	250	1.4	4.0	21	3.5
3098	photo	205	2.0	5.4	18	4.6
3323	photo	205	0.9	6.1	34	6.5

**Table 2**  
**Performance of cell 3520-11-1 (graded a-SiGe) during light exposure at 100 mW/cm<sup>2</sup>, 25°C.**

Condition	V <sub>oc</sub> (V)	J <sub>sc</sub> (mA/cm <sup>2</sup> )	FF (%)	η (%)
init. test	.605	16.85	58.5	6.0
15 min/160°C	.614	16.94	57.0	5.9
12 hrs	.585	16.5	53.9	5.2
100 hrs	.579	16.2	54.1	5.1
169 hrs	.565	16.2	53.0	4.9
265 hrs	.574	16.0	53.4	4.9

**Table 3**  
**Results of fitting illuminated J(V) data to diode circuit model.  
 Samples 3396, 3520 are from IEC, L1324 and L1331 are from Solarex.**

Sample #	i-layer	J <sub>L</sub> (mA/cm <sup>2</sup> )	G (mS/cm <sup>2</sup> )	J <sub>o</sub> (mA/cm <sup>2</sup> )	A	R (Ω-cm <sup>2</sup> )
3396	a-Si:H	9.0	1.6	3.5E-4	3.2	0.1
3520	graded a-SiGe:H	9.0	1.0	2.2E-2	3.7	0.5
L1324	a-Si:H	8.6	0.8	2.1E-3	3.8	1.0
L1331	graded a-SiGe:H	8.6	0.8	1.4E-2	4.1	0.9

**Table 4**  
**Characteristics of a-SiGe:H Photo-CVD Materials Measured at U of Oregon**

Sample#	χ <sub>Ge</sub>	E <sub>g</sub> (eV)	E <sub>u</sub> (meV)	N <sub>D</sub> (A) (*10 <sup>15</sup> cm <sup>-3</sup> )	N <sub>D</sub> (B) (*10 <sup>15</sup> cm <sup>-3</sup> )	(μτ) <sub>n</sub> (A) (*10 <sup>-9</sup> cm <sup>2</sup> -V <sup>-1</sup> ) <sub>n</sub>	(μτ) <sub>n</sub> (B) (*10 <sup>-9</sup> cm <sup>2</sup> -V <sup>-1</sup> ) <sub>n</sub>
a-Si:H	0	1.8	42	3.5	8.6	6	--
3539	0.25	1.6	50	6.0	15.0	1.5	0.4
3512	0.42	1.46	51	8.0	32	2.8	0.6
3511	0.50	1.40	51	15	40	1.1	0.35
3481	0.60	1.35	52	20	60	0.7	0.08
3420	0.60	1.28	57	100	--	0.03	--
3422	1.0	1.0	50	900	--	--	--

(A) Annealed state, (B) degraded @ 100mW/cm<sup>2</sup> for 100 hours

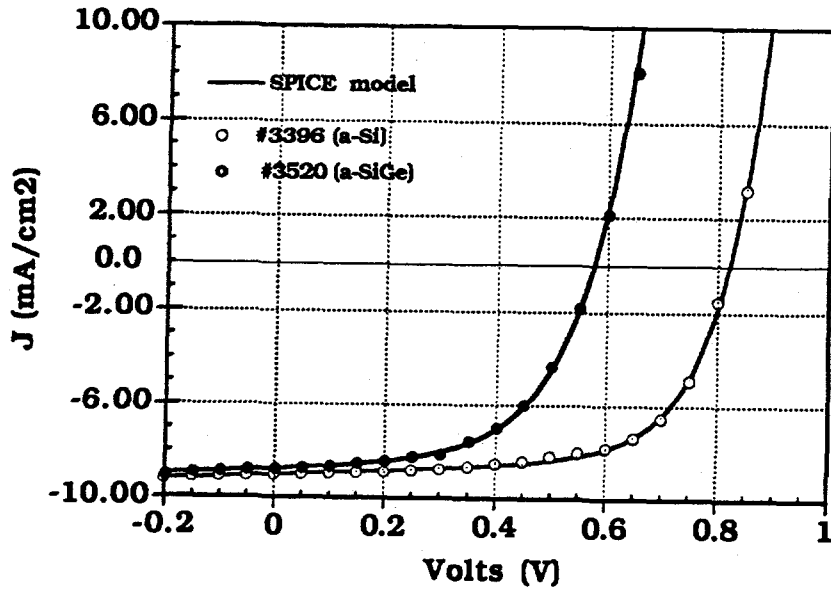


Figure 1. Measured and calculated (SPICE) J-V data for IEC devices #3396 (a-Si) and #3520 (a-SiGe). Calculated values using parameters of Table 3.

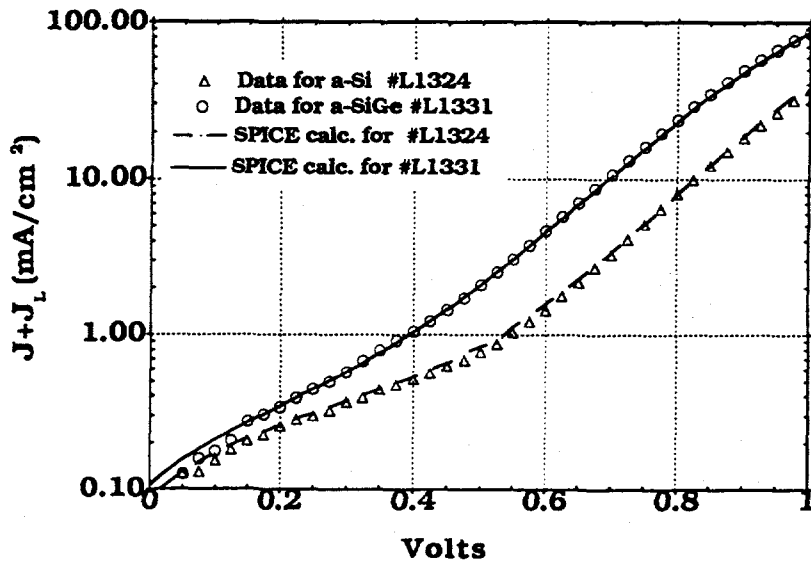


Figure 2. Measured and calculated (SPICE) J-V data for Solarex devices #L1324 (a-Si) and #L1331 (a-SiGe). Calculated values using parameters of Table 3.

**Title:** Research on Silicon-Carbon Alloys and Interfaces

**Organization:** Coordinated Science Laboratory  
University of Illinois  
Urbana, Illinois

**Contributors:** T.J. McMahon, program manager; J.R. Abelson and N. Maley, principal investigators; S.-Y. Yang and Y. Yang

## Objective and Approach

Our objectives are to (i) identify the factors which dominate the electronic properties of the "top junction" of a-Si:H solar cells, i.e., the TCO/p-doped a-SiC:H and p-doped a-SiC:H/undoped a-Si:H interfaces and (ii) modify film growth to improve these interfaces and solar cell performance. We deposit the films by reactive magnetron sputtering (RMS) because the method (i) provides independent control of hydrogen incorporation via the H<sub>2</sub> partial pressure, (ii) has been used in our laboratory to deposit device quality a-Si:H layers, (iii) produces a-SiC:H films with dense microstructure and good electrical properties, and (iv) is an industrially mature process for the mass production of thin film coatings.

We use both in situ and ex situ techniques to analyze the films and interfaces. Si-H and C-H bonding in films  $\geq 5$  Å thick is measured by real time in situ infrared reflectance spectroscopy. Ex situ XPS measurements are used to determine interface reactions for film growth on SnO<sub>2</sub> and ZnO. A Kelvin probe (KP) is being modified for in situ measurements of the electrostatic potential profile across the different layers of the top junction. The combination of IR, XPS, and KP is intended to elucidate the fundamental relationships between deposition conditions, bonding, and electronic performance.

## Results

### a-SiC:H Growth

We have grown hydrogenated amorphous silicon-carbon (a-SiC:H) alloys by dc reactive magnetron sputtering (RMS) using a silicon target and argon, hydrogen and methane as the process gases. Last year we reported that high quality a-SiC:H films can be grown with optical bandgaps from 1.8 to ~2.2 eV, as required for multi-junction solar cells. Furthermore, the H bonding in RMS films is dominated by Si and C monohydrides, rather than the clustered H groups found in typical plasma-assisted chemical vapor deposition (PACVD) layers. Our working hypothesis is that such improvement in the microstructure should be associated with improved electronic stability. Recent work at Solarex using novel feedstocks such as trisilyl methane and disilyl methane in PACVD has shown a correlation between denser microstructure and improved solar cell performance.<sup>1</sup>

This year we installed and investigated an industrially-sized sputtering source, i.e., a 5"x12" Si cathode. Actual solar cell production would use a longer cathode, sized to the width of the substrate glass, but the operating characteristics and results are expected to be very similar. The films grown by the mini and large magnetrons have been characterized using Near IR-Vis optical absorption, FTIR, spectroscopic ellipsometry, thermal evolution, sputtered neutral mass spectroscopy, SAXS, photo conductivity, dark conductivity activation energy, sub-gap absorption, and light soaking. Figure 1 shows the dependence of Tauc gap ( $E_g$ ) on the hydrogen partial pressure ( $P_{H_2}$ ) for a-SiC:H films grown with the two magnetrons and a-Si:H films grown with the mini magnetron. For a given  $P_{H_2}$  we see a large variation, up to 0.5 eV, in  $E_g$  for the a-SiC:H films due to the choice of the other deposition parameters. In general,  $E_g$  increases with the partial pressure of methane ( $P_{CH_4}$ ) and decreases with increasing deposition temperature and

target current. The microvoid content of the RMS a-SiC:H films was investigated by small angle X-ray scattering (SAXS) and found to be higher than for unalloyed a-Si:H, but lower than for PACVD material. Figures 2 and 3 show the similarity in the density of states and Urbach slopes for the a-SiC:H films grown with the two magnetrons. Data for a-Si:H films grown with the mini magnetron are also shown for comparison. For  $E_g \sim 1.9 - 2.0$  eV, as required for the absorber layer in the top cell of a tandem structure, we see that RMS films have  $E_{\text{Urbach}}$  between 60 and 70 meV and DOS between  $2E15$  and  $4E16$   $\text{cm}^{-3}$ . Since the structural, optical, and electrical properties of RMS a-SiC:H alloys are quite sensitive to the deposition parameters, further improvements are quite likely with continued optimization of film growth.

### Studies of the TCO/a-Si:H Interface

The "top contact" in p-i-n solar cells, namely the interface between the SnO<sub>2</sub> transparent conductive oxide (TCO) and a-Si:H or a-SiC:H, strongly influences device performance. This interface is fundamentally complex because it involves the deposition of a hydrogenated compound on top of an oxide! If the SnO<sub>2</sub> is reduced to elemental Sn, then the optical transmission is decreased and the work function of the contact changes.

We studied the reduction of SnO<sub>2</sub> during RMS deposition of a-Si:H using real time ellipsometry and ex-situ X-ray photoelectron spectroscopy (XPS). We deposited very thin ( $\sim 70\text{\AA}$ ) amorphous silicon layers and varied both the hydrogen content and substrate temperature. Both ellipsometry and XPS showed that the reduction of SnO<sub>2</sub> to elemental Sn increases with hydrogen flux and substrate temperature. Conversely, the reduction is almost absent ( $\leq 0.2$  monolayers) during the growth of unhydrogenated a-Si at  $< 200^\circ\text{C}$ . We believe that the interface can be improved by initiating RMS growth without hydrogen to avoid SnO<sub>2</sub> reduction, and then adding hydrogen to post-hydrogenate the a-Si. Other studies in our group show that a H-containing growth flux can effectively penetrate  $\sim 50\text{\AA}$  in a-Si.

To evaluate the electrical potential profile of the contact, we use a Kelvin probe (KP) to measure changes in the sample work function. Our plan is to do in situ measurements of the surface potential as a function of a-Si:H thickness, and then deduce the interface potential through modeling of the measured band bending. To test the KP we have done some ex situ measurements during the deposition of a-Si:H on ZnO substrates. Growth was interrupted periodically to move the sample from the deposition chamber into the KP chamber. Figure 4 shows that for undoped a-Si:H on ZnO, the Schottky barrier height is 0.43 eV and the depletion region width is 40 nm. This depletion width is considerably less than what we expect from the bulk film properties measured by CPM under the same deposition conditions. It may be due to a defective a-Si:H/ZnO interface or a high surface defect density from periodically exposing the sample to atmosphere to perform the measurements. However, Figure 4 clearly shows the capabilities of KP and we expect it to be operational in the in situ mode in the next phase of our research.

### Conclusions and Future Work

The results here clearly demonstrate the potential of (i) reactive magnetron sputtering to improve undoped high gap alloys and (ii) XPS and Kelvin probe to study interface formation. IR reflectance studies of a-SiC:H film growth are in progress. Future work will focus on depositing p-doped films and carrying out in situ studies of TCO/p and p/i interface formation using IR, Kelvin probe, and spectroscopic ellipsometry.

### References

- 1) Y.-M. Li, B. Fieselman, and A. Catalano, Presented at the 22nd IEEE PVSC, Las Vegas, 1991.

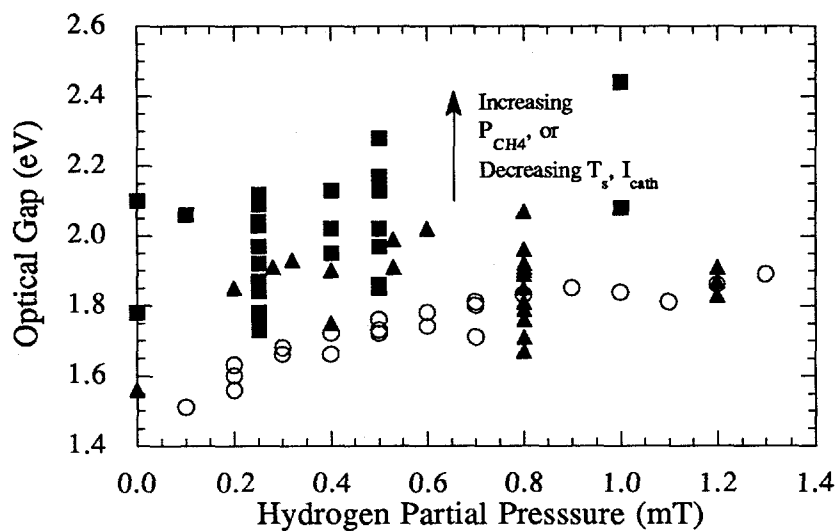


Figure 1: Tauc gap vs  $P_{H_2}$  for a-Si:H (circles) and a-SiC:H (squares: mini magnetron; triangles: large magnetron) films.

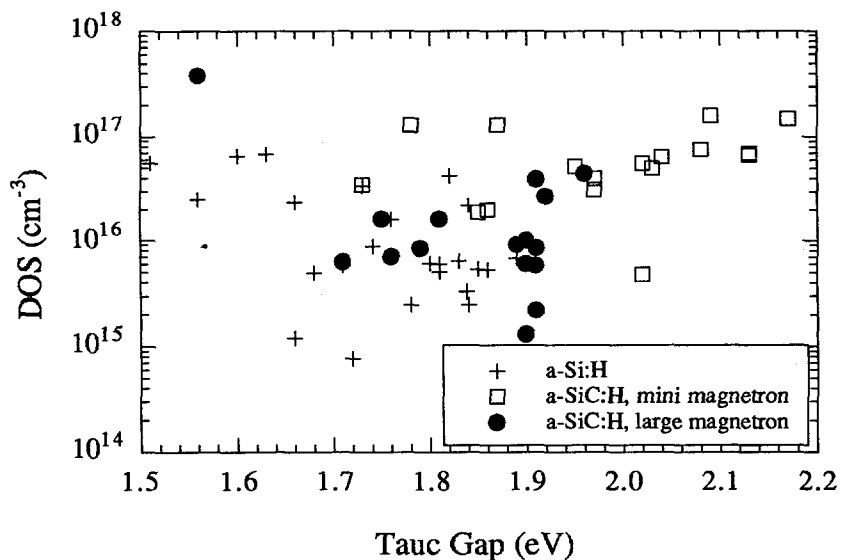


Figure 2: Dual beam photoconductivity density of states vs Tauc gap for RMS a-Si:H and a-SiC:H films.

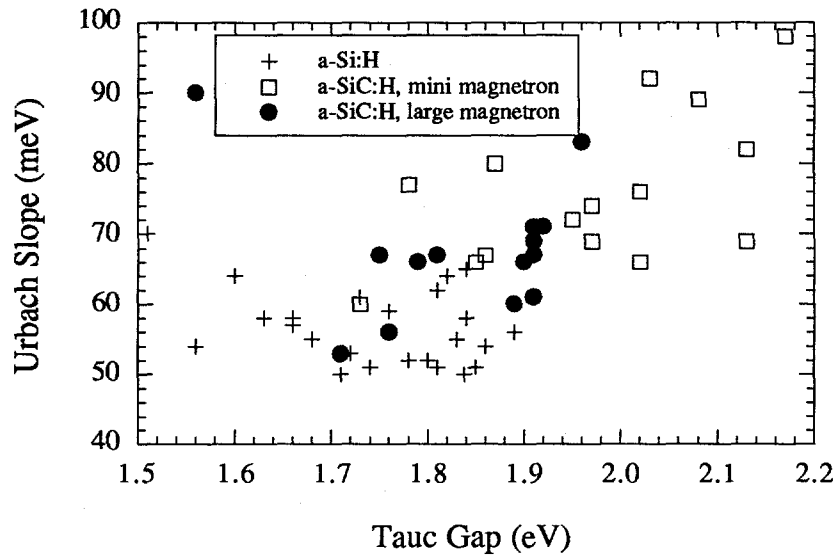


Figure 3: Urbach slope vs Tauc gap for RMS a-Si:H and a-SiC:H films.

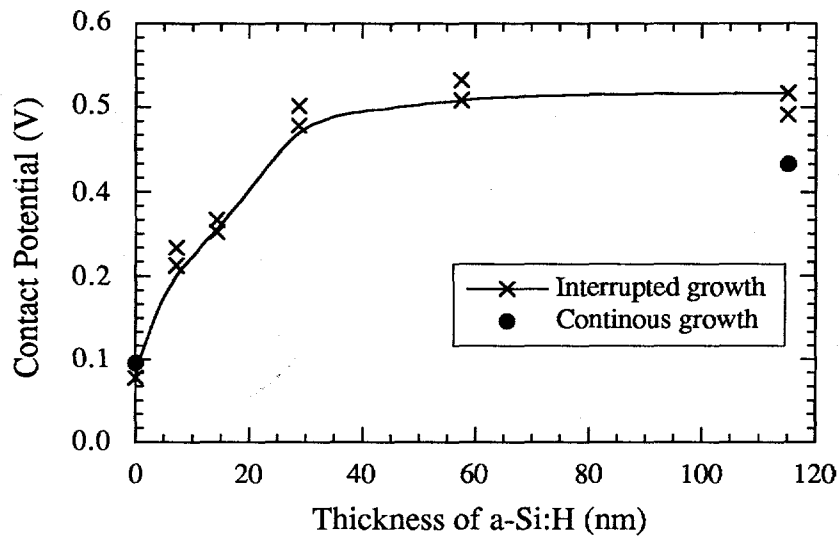


Figure 4: Evolution of contact potential with film growth for a-Si:H on ZnO from ex situ Kelvin probe measurements.

**Title:** RECOMBINATION AND METASTABILITY IN AMORPHOUS SILICON AND SILICON GERMANIUM ALLOYS

**Organization:** Department of Physics and Astronomy  
University of North Carolina  
Chapel Hill, NC 27599-3255

**Contributors:** M. Silver, Daxing Han, Keda Wang and M. Kemp

The objectives of our research were (1) to determine how recombination, trapping and band mobility modifications affecting the electronic properties of amorphous semiconductors can be characterized and described by an appropriate spectrum of defect states, (2) how light induced defects (SWE) in a-Si:H and native defects in a-Si:Ge:H affect the transport properties in these materials.

Experimentally we focused on electroluminescence (EL) and forward bias current studies as a function of device parameters such as thickness of the i-layer and p-i junction properties. Photo degradation studies also continued. The most interesting part of our data relates to the comparison of the energy spectral of EL in thin p-i-n and p-b-i-n cells, where b is the buffer layer between p- and i-layer. As noted last year, thin p-i-n cells (0.4  $\mu\text{m}$ ) show primarily defect band luminescence at elevated temperatures ( $T \geq 200$  K) while buffered p-i junctions show both defect and main band luminescence. However, in both cases the lifetimes are governed by nearest neighbor recombination ( $10^{-6}$  sec).

### Experimental Research

We studied the spectral response of EL verse temperature using Ge detector with a set of interference filters. In figure 1 we show the spectral response of a 0.4 $\mu\text{m}$  p-i-n device at various temperatures. These devices were obtained from Solarex. As one can see, the spectra's peaks at approximately 0.9 eV at room temperature ( $T = 300$  K), which indicated that the photon emission is dominated by the defect band luminescence. As temperature is decreased ( $T = 200$  K) a shoulder appears near 1.1 eV, until 80 K the EL is dominated by the main band luminescence peaked at 1.2 eV. This is similar to that observed in photoluminescence (PL). Similar results were obtained on buffered samples (p-b-i-n) which were also 0.4  $\mu\text{m}$  thick. These results are shown in figure 2. In these samples one observes some semblance of the 1.2 eV band even up 300 K. The 200 K data is most striking in that one sees defect and main band emission of comparable intensity. The line shape of the spectrum for p-b-i-n cell at 200 K is similar as that for p-i-n cell at 140 K. Figure 3 shows the comparison between the p-i-n and p-b-i-n sample at 200 K. The difference in the recombination mechanism is clear.

The results presented above suggest that the luminescence in thin cells is coming from near the p-i junction since the i-n interface is the same for buffered and non-buffered samples. Additional support for this interpretation comes from the comparison between thin (0.4  $\mu\text{m}$ ) and thick (2.0  $\mu\text{m}$ ) p-i-n devices. At near room temperatures, in thick devices the main band emission is still obvious while in thin devices, one sees only defect emission. (These results were presented last year in our annual subcontract report.) The thicker the i-layer the more the recombination takes place away from the p-i interface, e.g., the smaller the effect of the p-i junction on the recombination. If the metastable defects are caused by the tail-to-tail non-radiative recombination (the tail-to-tail radiative recombination gives the main band luminescence), it would appear that thin



p-i-n samples are more stable than thick p-i-n or thin p-b-i-n because the absence of the tail-to-tail recombination, or the defects recombination domination.

Last year we showed that the radiative life time distribution contained two peaks: (1) at  $10^{-6}$  sec that was attributed to nearest neighbor recombination and (2) at  $10^{-4}$  sec that was attributed to transport limited recombination. We have measured the temperature dependence of the lifetime distribution in  $2\mu\text{m}$  samples. We observed that the short lifetime around  $10^{-6}$  sec is independent of temperature but the longer lifetime depends on temperature. The experimental results are in good agreement with our theoretical calculations. The lifetime distribution in thin  $0.4\mu\text{m}$  samples also have been measured. Both p-i-n and p-b-i-n samples showed only one peak at  $10^{-6}$  sec. These results are seen in figure 4. Consequently defect luminescence is also governed by nearest neighbor recombination.

Finally we observed interesting effects in the transient forward bias response depending upon the strength of a reverse bias applied between forward bias pulses. These results are shown in figures 5a and 5b for a  $10\mu\text{m}$  p-i-n sample at annealed state A and light-soaked state B. What should be noted is that the stronger the reverse bias, the larger is the initial space charge limited current and the more delayed the recombination current rise. As shown in Fig. 5b the delay of the recombination current rise is much more pronounced at light-soaked state B. We believe that this result is due to the slow relaxation of positively charged defects in the bulk. Relaxation processes are now considered to be important in the kinetics governing the Staebler-Wronski effect and de-trapping.

#### Publications:

1. "The puzzle surrounding luminescence models", M. Kemp and M. Silver, *J. Non-Cryst. Sol.* **141** (1992) 88.
2. "Reverse Recovery and Decay of Stored Excess Carriers in a-Si:H p-i-n Diode", Daxing Han, Keda Wang and M. Silver, MRS spring meeting, April 27- May 1, 1992, San Francisco, p.837.
3. "Effect of Photo Degradation on Transient and Steady State Forward Bias Characteristics of A a-Si:H p-i-n Diode", R. Amokrane, R. Vanderhagen and M. Silver, MRS spring meeting, April 27- May 1, 1992, San Francisco, p.467.
4. "A Monte Carlo investigation of low-temperature geminate pair recombination dynamics in amorphous semiconductors," M. Kemp and M. Silver, *Phil. Mag. Lett.* **66** (1992) 169.
5. "Time-resolved Transient Electroluminescence in a-Si:H," Keda Wang, Daxing Han, M. Kemp and M. Silver, to be published in *Appl. Phys. Lett.*
6. "Optical Bias Effects in Electron Drift Measurements and Defect Relaxation in a-Si:H," Daxing Han, E. A. Schiff, and M. Silver, submitted to *Phys. Rev. B*.
7. "Electroluminescence and Forward Bias Current in p-i-n and p-b-i-n a-Si:H Solar Cells," Keda Wang, M. Silver, and Daxing Han, submitted to *J. Appl. Phys.*

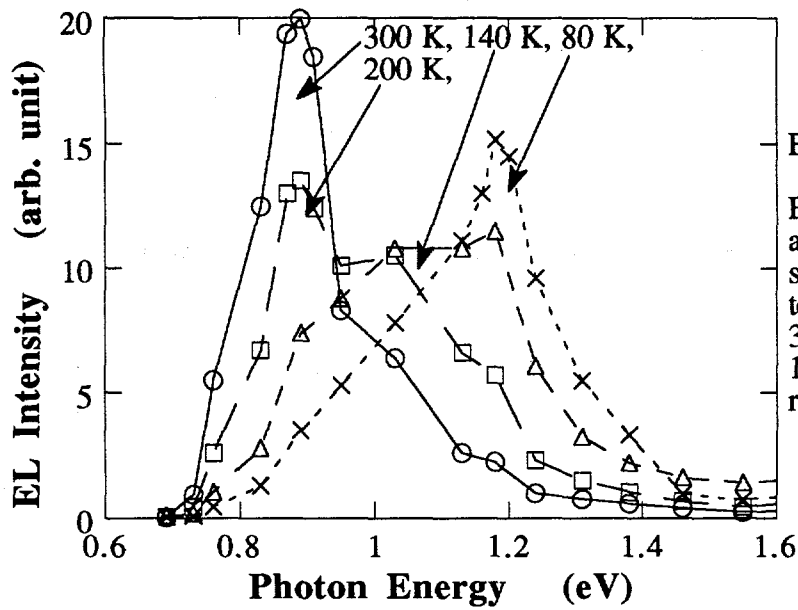


Fig. 1  
EL spectra for a 0.4 μm p-i-n solar cell at temperatures of 300 K, 200 K, 140 K and 80 K, respectively.

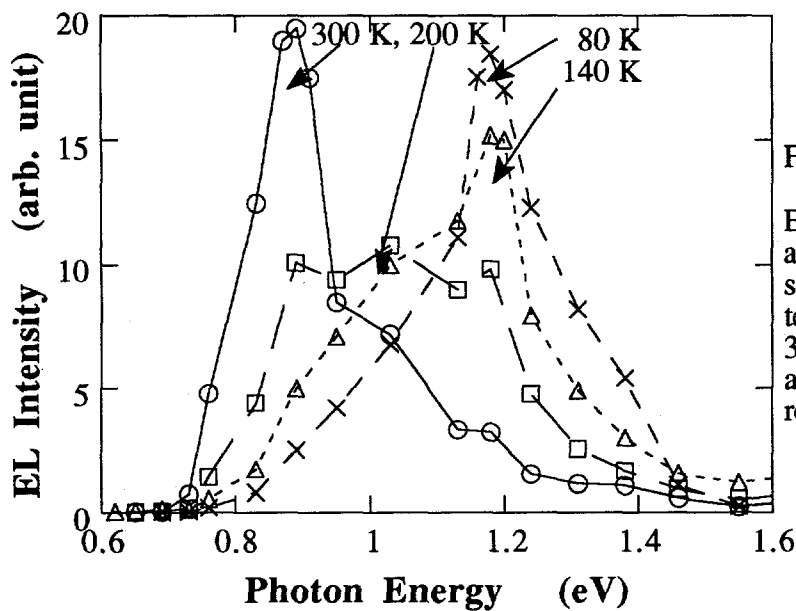


Fig. 2  
EL spectra for a 0.4 μm p-b-i-n solar cell at temperatures of 300, 200, 140, and 80 K, respectively.

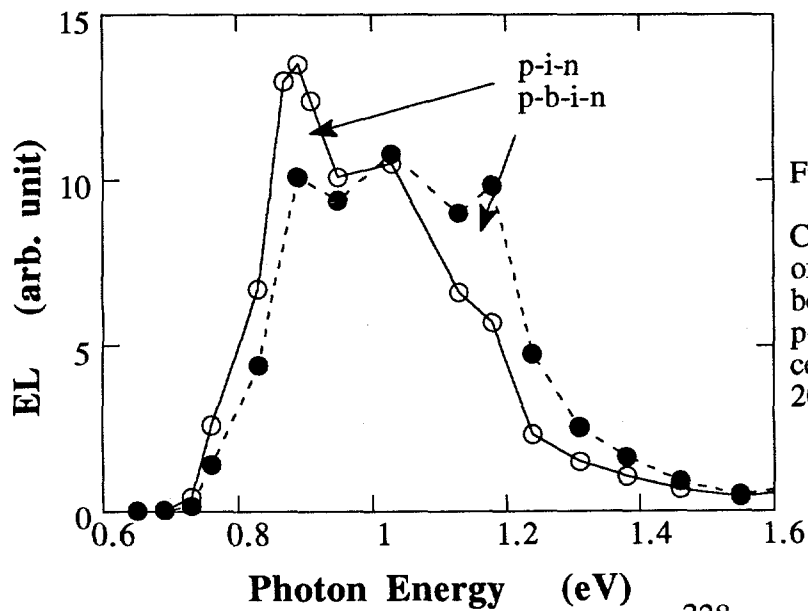


Fig. 3  
Comparison of EL spectra between 0.4 μm p-i-n and p-b-i-n cells at 4V, 200 K.

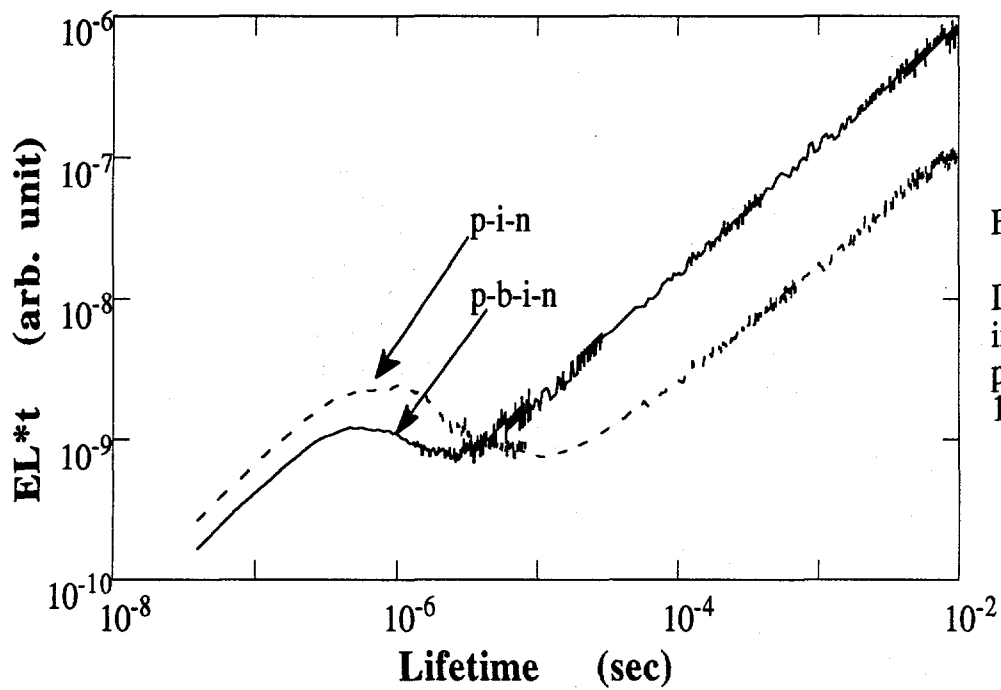


Fig. 4  
Lifetime distribution in  $0.4 \mu\text{m}$  p-i-n and p-b-i-n cells at 4 V, 120 K.

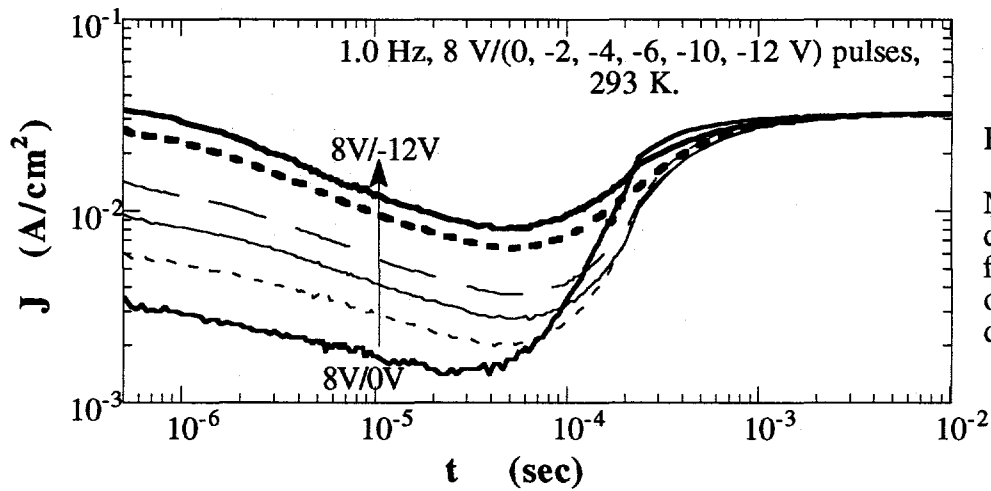


Fig. 5a  
Negative bias dependence of forward current on a  $10\mu\text{m}$  p-i-n diode at State A.

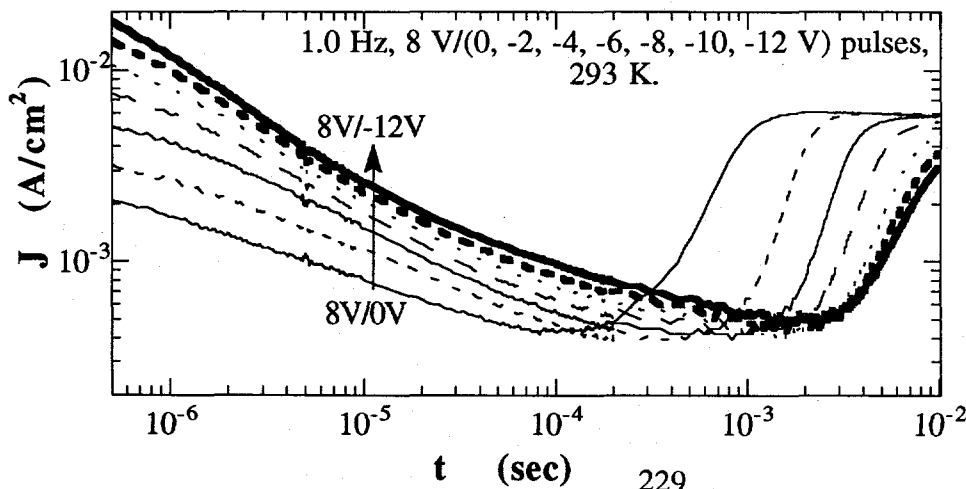


Fig. 5b  
The same sample as in Fig. 5a at State B.

Title: Microscopic Origins of Metastable Effects in a-Si:H and Deep Defect Characterization in a-Si,Ge:H Alloys

Organization: University of Oregon, Eugene, Oregon

Contributors: J. David Cohen, principal investigator; John Hautala and Thomas Unold

The primary research goals of this program are to elucidate the basic mechanisms by which a-Si:H degrades with light exposure, and to study the defect structure in low bandgap a-Si,Ge:H alloys. During the past year we have concentrated our efforts in two types of studies: (1) A study of photo-CVD a-Si,Ge:H samples encompassing a range of Ge concentrations, to determine the deep defect concentrations, the mobility-lifetime ( $\mu\tau$ ) products for holes, and how these quantities are altered by light soaking; and (2) A study of light induced degradation in lightly carbon contaminated a-Si:H samples.

### Approach

A series of a-Si,Ge:H alloy samples of different compositions were obtained through a collaboration with C.M. Fortmann at the University of Delaware. These samples were grown on p<sup>+</sup> c-Si substrates by the photo-CVD growth method, by decomposing a mixture of SiH<sub>4</sub>, GeH<sub>4</sub>, and H<sub>2</sub> with UV radiation from a mercury vapor light source. Semi-transparent palladium contacts served as Schottky barriers for our junction capacitance measurements and a few of these samples were co-deposited on quartz substrates for ESR measurements. Samples for the carbon contamination studies were deposited by the glow discharge growth method using a small reactor at the University of Oregon. A series of 4 samples were grown with different admixtures of CH<sub>4</sub> gas in the chamber to vary the carbon content over the range <0.1at.% to 2at.%.

Techniques employed to characterize the electronic properties of these samples included drive-level capacitance profiling<sup>1</sup> to deduce the midgap deep defect densities, and capacitance vs. temperature and frequency measurements<sup>2</sup> to determine the activation energy of conductivity. For the carbon contamination studies we used ESR to corroborate the defect levels obtained by capacitance profiling and also to attempt to distinguish between charged and uncharged deep defect levels. SIMS analysis, performed by Sally Asher at NREL, was employed to establish actual carbon (and also oxygen and hydrogen) profiles in these samples.

For the low gap alloy studies we employed two sub-band-gap optical spectroscopic methods: transient photocapacitance and junction photocurrent measurements. These methods, like other sub-band-gap optical methods, disclose the energy distribution of deep defects within the mobility gap and also the Urbach energy of the bandtail distribution of states. In addition, by comparing the photocapacitance and photocurrent spectra in detail, we can separate majority and minority carrier processes induced by the optical transitions. Thus we can estimate a value of  $(\mu\tau)_h$  for these samples. The details of our analysis of such data has been given previously.<sup>3</sup>

Light soaking of the a-Si:H samples was carried out using the 1.9eV spectral line of a Kr<sup>+</sup> laser. The light intensity was roughly 7.5W/cm<sup>2</sup> and was applied for times up to 10h to try to observe saturation. To keep the sample surface temperature below 60°C at such light intensities, the samples were immersed in methanol during illumination. Light soaking of the a-Si,Ge:H samples were carried out using both tungsten halogen and Xe arc lamps with suitable filters to ensure uniform absorption in these samples of varying optical gaps. All samples were light soaked at intensities ranging between 200

and  $400\text{mW}/\text{cm}^2$  for at least 50h and fan cooled to reduce annealing effects. For the studies of these low gap alloys, however, we did not attempt to reach saturation for the light induced effects.

### Results of Low Gap a-Si,Ge:H Alloy Studies

In Fig. 1 we display 2 pairs of spectra (photocapacitance and photocurrent) for an a-Si,Ge:H sample with 25at.% Ge before and after light soaking. These spectra clearly reveal that the defect density increases by almost a factor of 3 after light exposure and that this appears to occur in two fairly distinct defect bands. We also observe that the *difference* between the photocapacitance and photocurrent spectra decreases in the band-tail region after light exposure. This indicates a marked decrease in  $(\mu\tau)_h$ .

Figure 2 displays annealed state photocurrent transient spectra across the alloy range. It is interesting to note that the slope of the Urbach tail,  $E_U$ , is surprisingly constant ( $50\text{meV}+2\text{meV}$ ) throughout the entire alloy range. This implies that structural disorder is *not* substantially increased with alloying in these films. We also note that the sample with the lowest Ge content appears to exhibit spectra more similar to a-Si:H; that is, revealing a large defect "shoulder" near  $E_C-0.9\text{eV}$ .

In Table I we summarize the electronic properties found by these studies over the entire range of alloys studied to date. We can make several comments. First, compared to a-Si,Ge:H properties reported in the literature grown by the glow discharge method<sup>4</sup>, these photo-CVD samples exhibit remarkably low defect densities at relatively high Ge content. In a couple cases indicated in the Table, these capacitance derived defect levels have been verified by ESR spectroscopy. Second, we note that films tend to degrade similarly for all compositions to the extent that we observe factors of 2 to 3 increases in the midgap optical signal after 50h light exposure at  $400\text{mW}/\text{cm}^2$ . Finally, it appears the degradation in  $(\mu\tau)_h$  with light soaking becomes larger for larger Ge content, up to a factor of 10 for the 60at.% Ge sample. This fact may support the idea that the mobility in the a-Si,Ge:H alloys is not simply a function of the deep defect density alone.

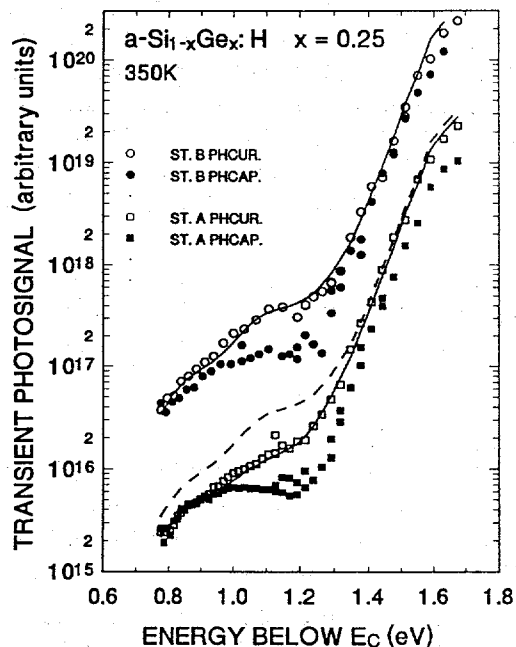


FIG. 1. Comparison of transient photocapacitance and photocurrent in state A and state B.

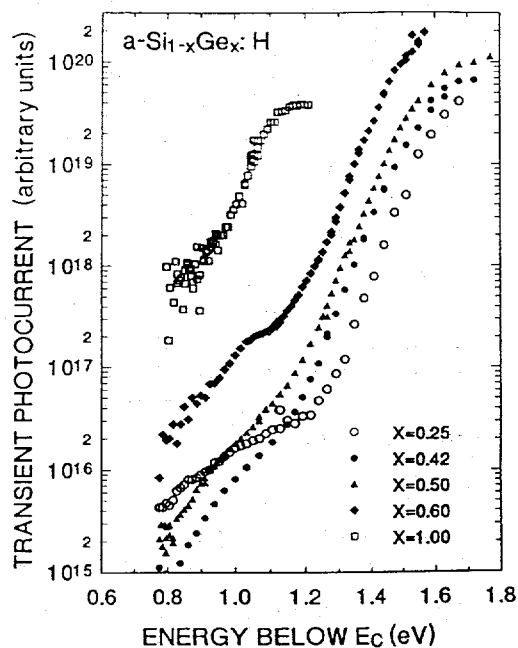


FIG. 2. Comparison of transient photocurrent spectra in state A for various compositions.

TABLE I. Summary of electronic properties of the photo-CVD a-Si,Ge:H samples employed in this study. A glow discharge a-Si:H sample is included for comparison. Defect densities marked with an asterisk (\*) have also been determined by ESR.

Sample a-Si <sub>1-x</sub> Ge <sub>x</sub> :H	X	E <sub>g</sub> /(eV)	E <sub>u</sub> (meV)	E <sub>a</sub> /(eV)	Nd/(cm <sup>-3</sup> ) State A	(μτ) <sub>p</sub> /(cm <sup>2</sup> /V) State A	Nd/(cm <sup>-3</sup> ) State B	(μτ) <sub>p</sub> /(cm <sup>2</sup> /V) State B
a-Si:H	0.00	1.80	42	0.70	3.5x10 <sup>15</sup>	6x10 <sup>-9</sup>	9x10 <sup>15</sup>	—
3539	0.25	1.60	50	0.65	6x10 <sup>15*</sup>	1.5x10 <sup>-9</sup>	1.5x10 <sup>16</sup>	4x10 <sup>-10</sup>
3511	0.42	1.46	51	0.69	7.8x10 <sup>15</sup>	2.8x10 <sup>-9</sup>	3.2x10 <sup>16</sup>	6x10 <sup>-10</sup>
3511	0.50	1.40	51	0.61	1.5x10 <sup>16</sup>	1.1x10 <sup>-9</sup>	4x10 <sup>16</sup>	3.5x10 <sup>-10</sup>
3481	0.62	1.30	52	0.57	2x10 <sup>16</sup>	7x10 <sup>-10</sup>	6x10 <sup>16</sup>	7.8x10 <sup>-11</sup>
3420	0.62	1.30	57	0.52	1x10 <sup>17*</sup>	3x10 <sup>-11</sup>	—	—
3422	1.00	1.05	50	0.45	9x10 <sup>17</sup>	—	—	—

### Light Induced Degradation in Carbon Contaminated a-Si:H

We have begun studies to follow up our previous observation that small levels of carbon impurity contamination (<1.at%) can affect the light induced degradation behavior of a-Si:H films. Our previous studies had utilized samples in which the [C] level was modulated during growth by toggling on and off a small admixture of CH<sub>4</sub> gas. We then probed the defect density using capacitance profiling measurements to correlate the [C] SIMS profiles with the deep defect spatial profiles before and after light exposure. These studies showed a quite strong correlation between light induced defect concentrations and carbon content down to levels of about 0.1at.%.<sup>5</sup> However, other studies employing different measurement methods to measure defect densities (ESR, sub-band-gap absorption) on uniform samples have reported an absence of any such a correlation up to [C] levels of >1at.%.<sup>6,7</sup>

For our current studies we employed samples with uniform [C] profiles and carried out side-by-side measurements using both capacitance profiling and ESR spectroscopy to determine absolute defect densities at various stages of high intensity light soaking. Results for two samples with 0.01at.% and 0.7at.% carbon are shown in Fig. 3. We first note that both measurement methods give defect densities that agree quantitatively to within a factor of 2 over the entire range of exposure times. Differences at early times for the higher carbon sample are almost certainly due to excess light contamination of the ESR sample during loading into the sample probe. The differences in the low carbon sample at long exposure times, on the other hand, are probably real and indicate differences in the relative populations of charged *vs.* neutral defects.

More interesting is the comparison between the low and high carbon containing samples. For the lower [C] sample, we observe clear evidence for saturation after about 10<sup>4</sup> s exposure, at a level of 4 x 10<sup>16</sup>cm<sup>-3</sup> defects. However, for the higher C sample, we have no such evidence for saturation, and the defect density reaches a level twice as high after the longest exposure times.

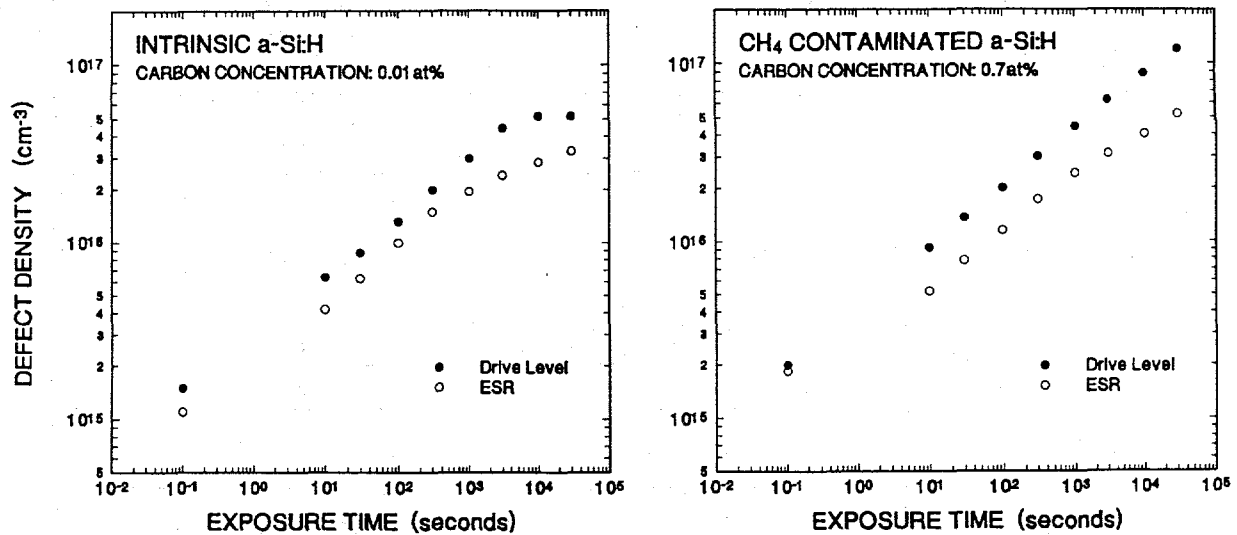


FIG. 3. Defect densities determined by drive-level capacitance profiling and ESR for two samples containing different carbon impurity levels.

### Important Issues for Future Study

Our results for a-Si<sub>x</sub>Ge<sub>1-x</sub>H samples grown by the photo-CVD method indicate lower defect densities at high Ge concentrations than have been reported for glow-discharge samples. We clearly need to test this by carrying out the same measurements reported here on high quality glow-discharge samples, and upon a-Si<sub>x</sub>Ge<sub>1-x</sub>H material grown by various alternative deposition methods. Collaborative arrangements to obtain such samples have already been established. We also wish to test the idea that the  $\mu\tau$  products for holes for the higher Ge samples may also exhibit an anomalously large decrease after light soaking.

The impurity dependence studies for carbon contaminated a-Si:H will be extended to examine other materials properties, especially the effects on the hole  $\mu\tau$  product as carried out for the a-Si<sub>x</sub>Ge<sub>1-x</sub>H alloys. We also plan to extend studies to other impurities, particularly oxygen and hydrogen.

### References

1. Michelson, C.E., Gelatos, A.V., and Cohen, J.D., *Appl. Phys. Lett.* **47**, 397 (1985).
2. J.D. Cohen, in *Hydrogenated Amorphous Silicon*, ed. by J.I. Pankove, Vol. 21C of *Semiconductors and Semimetals*, (Academic Press, New York, 1984), p. 9.
3. J.D. Cohen, T. Unold, A.V. Gelatos, and C.M. Fortmann, *J. Non-Cryst. Solids* **141**, 142 (1992).
4. S. Aljishi, Z.E. Smith, and S. Wagner, in *Amorphous Silicon and Related Materials*, ed. by H. Fritzsche (World Scientific, Singapore, 1989), p. 887.
5. T. Unold and J.D. Cohen, *Appl. Phys. Lett.* **58**, 723 (1991).
6. A. Skumanich and N.M. Amer, *Phys. Rev.* **B37**, 8465 (1988).
7. T. Shimizu, et. al., *J. Non-Cryst. Solids* **137&138**, 391 (1991).

**Title:**            **Stability, Electronic Properties and Structure of a-Si:H and its Alloys**

**Organization:**   Xerox Palo Alto Research Center, Palo Alto, CA 94304

**Contributors:**   W. B. Jackson, N. M. Johnson, C. Nebel, P. Santos, R. A. Street (Principal Investigator), R. Thompson, C. C. Tsai.

The aim of this research project is to improve the performance of a-Si:H-based solar cells through the understanding of metastability, doping and growth.

### **Effects of Bias Voltage on the Hydrogen Diffusion in a-Si:H**

Studies of the effects of bias and illumination on the hydrogen diffusion explore the detailed relationship between the hydrogen diffusion, electronic carriers and the metastability properties of a-Si:H. Illumination enhances the H diffusion, with the effect being most clearly discernible in the temperature range 200-300°C. In contrast, a reverse bias suppresses the diffusion. Figure 1 compares the diffusion with and without a bias, and shows that the excitation rate of hydrogen from Si-H bonds is suppressed when carriers are removed by the field [1]. However, a small fraction of the hydrogen does diffuse and forms an exponential spatial profile exhibiting a mean free path of about 400Å, which is substantially larger than the diffusion distance of hydrogen in the absence of bias. We considered whether the results indicate a drift of charged hydrogen, but two measurements do not support this model. First, the migration of hydrogen occurs in both directions of the field with a similar characteristic lengths. This would require equal concentrations of positive and negative hydrogen with roughly equal drift lengths, which seems an unlikely coincidence. Second, the shape of the hydrogen distribution does not change with field once this exceeds about  $2 \times 10^4$  V/cm, whereas the drift length should increase linearly with applied field.

The data supports an alternative explanation, that the bias suppresses retrapping of hydrogen into deep states, allowing the hydrogen to migrate further in the shallow states. Reduction of the H trapping rate could occur because either the capture cross section or the number of trapping sites is reduced. Rough estimates of the cross section give the number of traps as of order  $10^{16}$  cm<sup>-3</sup>. We suggest that the hydrogen traps may be simply the dangling bond defects. It is known that reverse bias annealing reduces the defect density of a-Si:H below that in the absence of bias, and would therefore account for the increase in the mean free path.

### **Current-induced and Light-induced Defects**

A recent report claims that current induced degradation is not accompanied by an increase in the sub-gap defect absorption band, unlike light-induced degradation. We therefore studied the defect creation by these two processes in n-i-p devices. The defect density was measured by CPM and from the reverse bias current, which arises from thermal generation of electron-hole pairs from mid-gap states and is therefore proportional to the defect density. Both CPM and the reverse bias current were measured on the same sample after different defect creation and annealing processes. Light induced defects were created with filtered light from a xenon or tungsten lamp, and current induced defects were created at various values of the forward bias.



Our primary observation is that defect creation by light or by forward current both increase the subgap absorption. Furthermore, the absorption band has the same shape for the two defect creation processes. The increase of absorption is roughly proportional to the corresponding increase in reverse bias current, showing approximate linearity between the measurements of the defect density. However, we also find that for the same reverse bias current, the subgap absorption tends to be higher for light-induced defects compared with current induced defects, by a factor of 1.5-2. Studies of the reverse current-voltage characteristics suggest that the origin of this small difference is related to a different spatial distribution of defects.

### **Kinetics of Dopant Activation and Passivation in a-Si:H**

The activity of n-type and p-type dopants in a-Si:H is temperature dependent through a mechanism of slow thermal equilibration. The doping efficiency exhibits metastability because the activated relaxation time allows a non-equilibrium frozen state to be induced by fast quenching. The dopant metastability is closely related to the light-induced defect metastability of a-Si:H. Detailed measurements of the equilibration kinetics were performed on phosphorus doped a-Si:H over the temperature range 70°-160° C, to improve understanding of the metastability effects [2]. An asymmetry is found between creation and passivation of active dopants. Both processes are thermally activated with an energy of ~1 eV, but the time constant is a complex function of the initial and final temperature. For example, figure 2 shows that the dopant passivation kinetics (i.e. cooling from higher temperature) follow a stretched exponential time dependence with a temperature dependent exponent while the activation kinetics (i.e. warming from a lower temperature) is a stretched exponential with a constant exponent of 0.85.

### **Transient Double Injection in p-i-n Sensors**

The forward bias current in amorphous silicon p-i-n diodes exhibits a remarkable delay in the onset of the steady state double injection current. The delay time varies from a few microseconds up to more than 100 milliseconds, depending on the applied voltage and the defect density. In some cases the current can rise abruptly by more than three orders of magnitude after the delay time. We have performed experiments and numerical modeling in order to understand and characterize the effect [3]. The dependence on defect density made by light soaking and current soaking is shown in figure 3, and provides a new method of measuring the metastable defect density in a-Si:H. Modeling studies identify the origin of the effect as a space charge barrier near the p-type contact which prevents double injection. The barrier is broken down by trapped electrons coming from the n-type contact. The calculations show that the delay time depends strongly on the defect density near the n-type contact, because the delay time is governed by the rate of electron injection. Experiments confirm this prediction by comparing the effect of light-induced defect creation with strongly absorbed illumination at the n-type and p-type contact. When better understood, the forward bias current will be a useful technique for characterizing solar cells.

### **Space Charge Limited Currents in a-Si:H**

Transient and steady state space charge limited current (SCLC) experiments are used to determine the field dependence of mobility and conductivity of a-Si:H [4]. As in doped a-Si:H, the conductivity increases rapidly for fields,  $F$ , above  $10^5$  V/cm, but twice the field has to be applied in hole SCLC experiments to achieve comparable conductivities. Low temperature transient SCLC experiments show features

associated with the transit times, which allow the determination of electron mobilities in the range  $10^{-6}$  -  $10^{-4}$   $\text{cm}^2/\text{Vs}$ . Hole transients, however, decay with a  $t^{-1}$  power law, with no indication of the transit time. The thickness dependent electron mobility reflects the dispersive transport. The field dependence is approximately a power law,  $F^\gamma$  with  $10 < \gamma < 17$ . We show that the enhancement of  $\sigma$  is caused by carrier injection at low field, but is dominated by the rapid increase in carrier mobility at high fields. The tail regions of a-Si:H change from insulating to highly conductive in the presence of high fields, due to field ionization out of localized states, as in resonant tunneling transitions in superlattices. A simple model demonstrates that the inhomogeneous carrier and field distribution typical of the SCLC regime is suppressed by the field dependent mobility.

## Conclusions

Experimental evidence continues to show that hydrogen migration is the underlying origin of defect metastability in a-Si:H. When the detailed interactions between the hydrogen diffusion, defect creation and the electron distribution are better understood, it may be possible to design more stable photovoltaic materials which retain good electronic properties.

## References

1. P. V. Santos, N. M. Johnson, R. A. Street, M. Hack, R. Thompson and C. C. Tsai, *Phys. Rev.*, in press.
2. C. E. Nebel, R. A. Street, N. M. Johnson, and W. B. Jackson, *MRS Symp. Proc.* 258, 395 (1992).
3. M. Hack and R. A. Street, *J. Appl. Phys.*, 72, 2331 (1992).
4. C. E. Nebel and R. A. Street, *Philos. Mag.*, in press.

## Figures

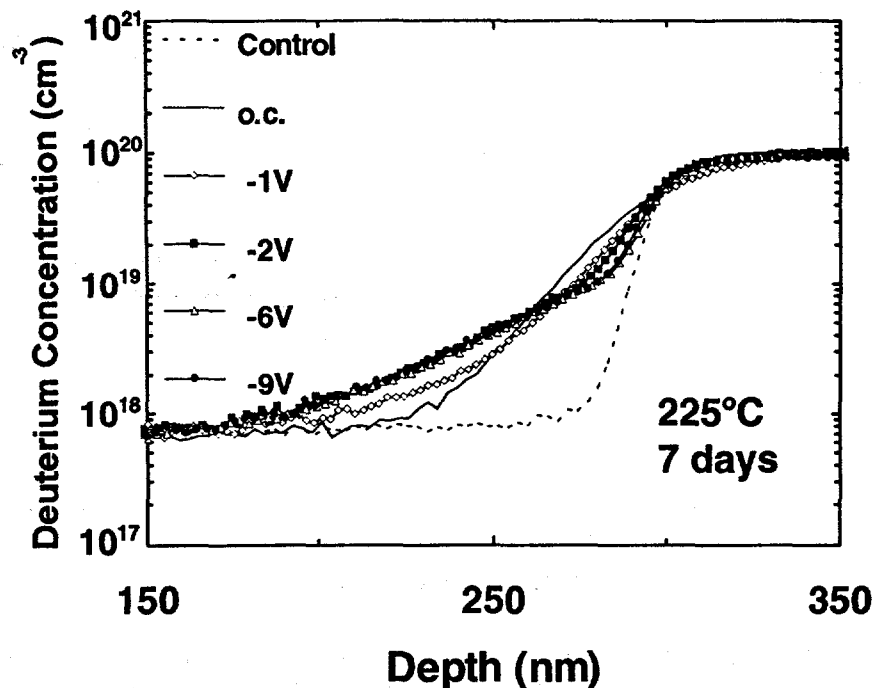


FIG. 1. Deuterium concentration profiles for different reverse bias, compared to open circuit and unannealed samples.

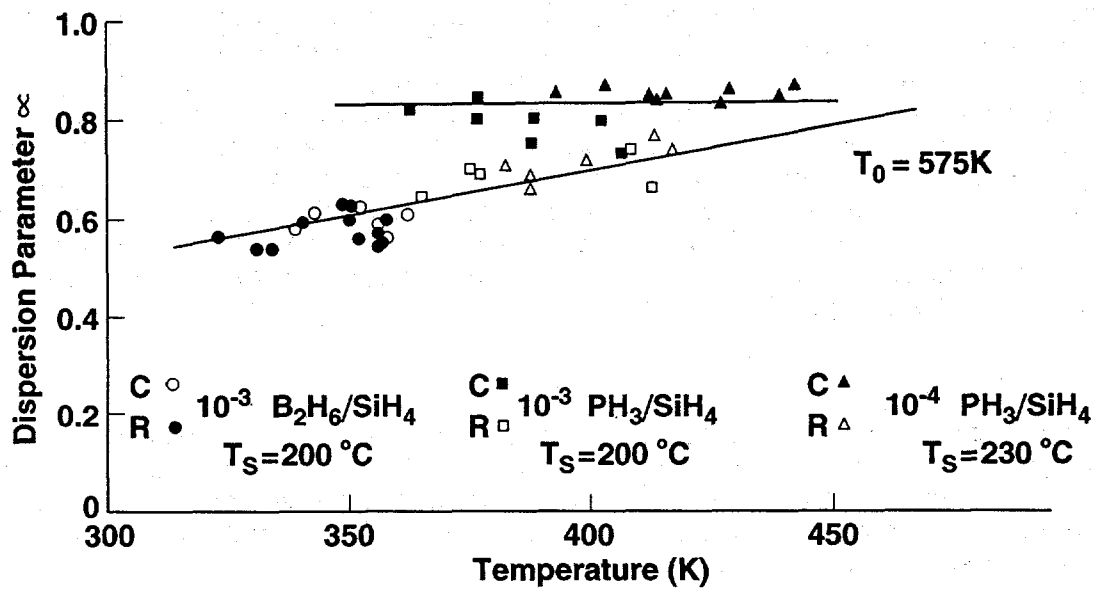


FIG. 2. Measurements showing the different temperature dependence of the dispersion parameter for dopant creation and annealing.

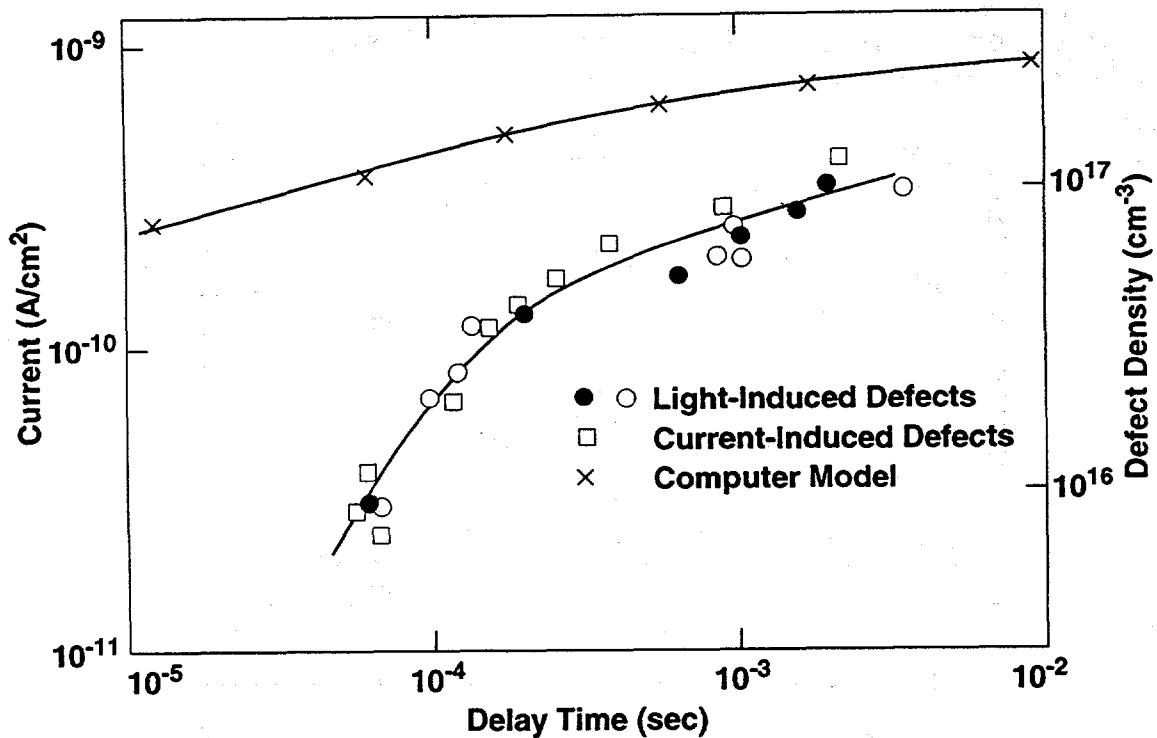


FIG. 3. The delay time for the current versus defect density introduced by light- or current-soaking. Numerical simulations are also shown.



## 5.0 PHOTOVOLTAIC MANUFACTURING TECHNOLOGY (PVMaT) PROJECT

Ed Witt, (Manager)

The PVMaT Project is a government/industry photovoltaic manufacturing research and development (R&D) project composed of partnerships between the federal government (through DOE) and members of the U.S. PV industry. It is designed to assist the U.S. PV industry in improving manufacturing processes, accelerating manufacturing cost reductions for PV modules, increasing commercial product performance, and generally laying the groundwork for a substantial scale up of U.S.-based PV manufacturing plant capabilities.

The project is being carried out in three separate phases, each focused on a specific approach to solving the problems identified by the industrial participants. These participants are selected through competitive procurements. Furthermore, the PVMaT project has been specifically structured to ensure that these PV manufacturing R&D subcontract awards are selected with no intention to either direct funding toward specific PV technologies (e.g., amorphous silicon, polycrystalline thin films, etc.), or spread the awards among a number of technologies (e.g., only one subcontract in each area). Each associated subcontract under any phase of this project is, and will continue to be, selected for funding on its own technical and cost merits.

The Phase 1 portion of the PVMaT program, the problem identification phase, was completed early in 1991. This solicitation was open to any U.S. firm with existing PV manufacturing capabilities, regardless of material or module design. Early in 1991 the competitive selection process for this phase was completed with contracts being awarded to 22 of approximately 40 offerors. Each of these subcontracted efforts was funded at a level of up to \$50,000 and a duration of 3 months. The problems identified by the research in this phase of the program were process-specific in nature and represented opportunities for individual industrial participants to improve their manufacturing processes, reduce manufacturing costs, increase product performance, and/or support a scaleup of U.S.-based manufacturing plant capabilities. These opportunities have since been detailed in the approaches suggested by these organizations for Phase 2 R&D. It is not anticipated that any additional Phase 1 type solicitation will be issued since the Phase 1 was intended to develop initial problem and manufacturing status information and to support the PV industry in preparing for later PVMaT problem solution phases.

Phase 2 of the PVMaT program is now under way, with an expected duration of five years. It consist of multiple competitive procurements over this period and subcontracts awarded under any of these solicitations may be of up to 3 years in duration. The first solicitation under this phase (Phase 2A) was open only to those organizations that received awards in the Phase 1 solicitation. The award selection process is now completed for this solicitation, and seven subcontract awards have been made. Phase 2 of the PVMaT Program is considered the solution phase and addresses the process-specific problems of the specific manufacturer, which were identified under Phase 1 efforts. The subcontracts are highly cost-shared between the U.S. government and U.S. industrial participants. A second, overlapping, and similar process-specific solicitation (Phase 2B) was released in June 1992. Responses to this Phase 2B solicitation are being evaluated now, and subcontracted efforts are planned for later this year. Phase 2B will be open to all U.S. PV industrial firms. Therefore, organizations that were not ready for the first

Phase 2 procurement cycle that was just completed will have another chance to "ramp on" and participate in the solution phase of the program.

There are "general" R&D problems in the PV industry that are relatively common problems to the industry as a whole, a number of companies, or the design and deployment of photovoltaic systems. The PVMaT Program will address these generic problem areas through a teamed research approach. A solicitation on this type of generic manufacturing technology was released in October 1991. Responses to the Phase 3 solicitation are being evaluated now. Participants for these generic research activities may come from either a consortia of industrial companies, individual companies, a university or group of universities, combinations of company and university groups, or other groups with special capabilities for solving a particular problem. These proposed research organizations will focus on module-related R&D problems found to be common to a significant set of PV manufacturers. Teams will also work in tandem with material and component manufacturers to help strengthen the PV industry.

**Title:** Silicon-Film™ Photovoltaic Manufacturing Technology

**Organization:** AstroPower, Inc.  
Newark, Delaware

**Contributors:** William R. Bottenberg, Project Manager; A. M. Barnett, D. A. Brooks,  
D. F. Ford, R. B. Hall, C.L. Kendall, S. M. Lampo, W.P. Mulligan

## Introduction

AstroPower started the first phase of a three year, phased effort to upgrade its facility to produce 1.22m<sup>2</sup> Silicon-Film™ PV modules with an output of 170 Wp. In this program AstroPower will establish a baseline capability for growth of Silicon-Film™ wafers by optimizing present equipment, improving productivity of the Silicon-Film™ machine, improving solar cell performance while decreasing materials consumption, integrating and mechanizing the fabrication process for solar cells, scaling-up cell and module equipment for fabricating larger cells, and minimizing waste stream loads by assessing potential for waste reduction. The key contract milestones are:

Table 1. Silicon-Film™ Manufacturing Technology Milestones

	Phase I	Phase II	Phase III
Wafer Machine			
Production Rate	400 kw/year	1.3 MW/year	3.0 MW/year
Material Use Efficiency	75%	85%	90%
Solar Cell Efficiency	11.0%	12.5%	4.0%
Solar Cell Size a)	100 cm <sup>2</sup>		
b)	675 cm <sup>2</sup>	675 cm <sup>2</sup>	675 cm <sup>2</sup>
Solar Cell Grid Area Coverage	9%	7%	6%
Module	130 W	150 W	170 W

## Approach

The Silicon-Film™ Process is a method for fabricating solar cells by direct growth of a solar cell quality, polycrystalline silicon layer on a low-cost, supporting substrate [1]. This process is designed to significantly reduce silicon cost while retaining the physical and power output characteristics of single crystal silicon. The Silicon-Film™ process has a significant cost advantage over other crystalline silicon technologies because it eliminates ingot sawing, only requires thin layers of active silicon and can make use of lower grades of silicon feedstock. The focus for the Phase I PVMaT-2A project is on establishing the baseline process capability and optimizing the performance of the present machine.

## Results

### Wafer Machine Productivity and Efficiency Results

The first project goal was to establish a baseline wafer machine process capability for production of wafers at a 0.40 MW/year rate. This rate was established and exceeded for production of both 106 cm<sup>2</sup> and 646 cm<sup>2</sup> wafers. The rates were demonstrated by running the machine at rates of 0.57-0.64 m<sup>2</sup>/hour for runs

which produced plank areas of  $0.5 \text{ m}^2$ . Annual operation of the machine for 8000 hours would yield 4600 to  $5100 \text{ m}^2$  of wafer area. Solar cells fabricated from nominally  $100 \text{ cm}^2$  wafers made at these production rates had 1.1 watt power output. Based on these results, rates of 0.48 MW/year were demonstrated for  $106 \text{ cm}^2$  wafers and 0.39 MW/yr for  $646 \text{ cm}^2$  wafers. These results showed a seven-fold improvement for machine throughput during the project to date.

An important measure of wafer machine operation efficiency is the material usage efficiency. This is measured by taking the ratio of silicon in the finished wafer to the amount of silicon applied at the start of the wafer formation process sequence. The goal for Phase I was to establish a material use efficiency of 75%. Runs of 74% were achieved for formation of  $106 \text{ cm}^2$  wafers. The yield is the product of an applicator yield, a trimming yield and a visual/mechanical yield. During this project, we have doubled the material use efficiency by improving the applicator yield from 95% to 99%, by modifications to improve trimming yield, and by process developments to improve the visual/mechanical yield. A driving force for these process developments was the establishment of a wafer specification.

### Solar Cell and Module Results

Silicon-Film™ solar cells were fabricated with 1.1 watts on  $105 \text{ cm}^2$  and 4.8 watts on  $646 \text{ cm}^2$  respectively. The current-voltage curves for these solar cells are shown in Figures 1 and 2. These solar cells were fabricated from wafers made on the production machine using the standard production process.

We assembled four demonstration submodules each employing six  $646 \text{ cm}^2$  solar cells in a series string. These submodules showed the capability to assemble large Silicon-Film™ solar cells into a completed module package. The output of the submodules averaged 20 watts. The current-voltage and power output curves for the best submodule is shown in Figure 3.

### Silicon-Film™ Technology Results

The key determinant of solar cell device performance is the minority carrier diffusion length,  $L_n$ . Typical values for  $L_n$  are in the range of 10-20 microns, as measured by the long wavelength quantum efficiency method. Modeling of short circuit for these devices predicts short circuit currents of 22-27  $\text{mA/cm}^2$ , which are typical for devices made on the production machines. We carried out work to determine what physical properties of the wafers are limiting the diffusion length. There are three primary limiters for  $L_n$ : impurities, defects and residual stress.

Impurity concentration levels were measured in the incoming silicon feedstock and at several stages in the wafer formation process. It was determined that impurity levels in the incoming feedstock for several transition elements could adversely affect the solar cell output. Higher than desired levels of several transition elements were also found to be introduced during the wafer fabrication step. Steps have been taken to eliminate these impurities. Evidence was found for beneficial segregation during the active layer growth step in the case of iron, vanadium, nickel and chromium. It is expected that a silicon feedstock impurity concentration specification will be identified based on the completion of these analyses.

An important task is to measure defect levels on devices and match the observed types and levels to measured QE data and device parameters. We developed a process to fabricate mesa diodes from wafers which could be used to carry out this program. Typical etch pit densities for our wafers are in the range of  $3 - 7 \times 10^5$  dislocations/ $\text{cm}^2$ . We established that defects, as measured by etch pit density, did not appear



to be the limiting factor for diffusion length. As we lower the impurity levels described above we will continue to re-examine the defect level contribution to current collection losses.

Residual stress can remain in the wafer after fabrication, if the thermal profile is not shaped correctly. Measurements of the thermal profile in our machine early in the project indicated a cool region in the profile. Modification of the heating sections eliminated the cool region, with a subsequent decrease in wafer mechanical stress. We are assembling an apparatus to measure residual stress using optical birefringence in the infra-red.

## Conclusions

Phase I of this project has accelerated the advance of Silicon-Film™ manufacturing technology in several important ways. First, the project has led directly to our plans to make an early introduction of a large solar cell product. The successful fabrication of 646 cm<sup>2</sup> wafers and solar cells showed the way for dramatically increasing the power output per solar cell. The examination of tooling and manufacturing issues showed that the jump from 100 cm<sup>2</sup> product to 225 cm<sup>2</sup> product was a logical initial step to capture the manufacturing cost advantages of a larger product. The 225 cm<sup>2</sup> product and module based on it will meet the initial requirements which we see for a utility scale module. This product is scheduled for introduction in the summer of 1993. Work in Phases II and III of this project will carry us to the goal of developing the largest appropriate sized solar cell and module, which we presently believe is a 170 watt module based on 675 cm<sup>2</sup> solar cells.

Another important acceleration of Silicon-Film™ manufacturing Technology has been the establishment of a basis for the design and construction of a 0.6 MW/shift wafer machine. The establishment of a baseline capability and operations database during the first phase is now leading directly to our plans for prototyping this machine.

The putting in place of QA/QC criteria for process steps, particularly in Si raw material feedstock acceptance and preparation, was carried out much faster than we initially thought. We obtained this result by following through on the plans we made for Phase I of the project. These QA/QC criteria are proving crucial for us for meeting our productivity and cost goals.

A fourth important contribution to developing the technology by the PVMaT project was the determination of the importance of H<sup>+</sup> implantation processes for polycrystalline silicon technologies. Cooperative work with National Renewable Energy Laboratory is proving valuable in quickly assessing the benefits to be gained by Kaufmann ion sources and other material enhancement processes.

## References

1. Barnett, A.M., Bledsoe, T.B., Bottenberg, W.R., Brooks, D.S., Ford, D.H., Hall, R.B., Hughes-Lampros, T., Jackson, E.L., Kendall, C.L., Mulligan, W.P., and Shreve, K.P.; "Large Area, Utility Scale Silicon-Film Solar Cell." Prepared for the 26th European Conference, October 1992. Montreaux, Switzerland.

Voc	0.561 volt
Isc	2.586 amp
Vmp	0.474 volt
Imp	2.326 amp
ff	0.761
Pmax	1.103 watt

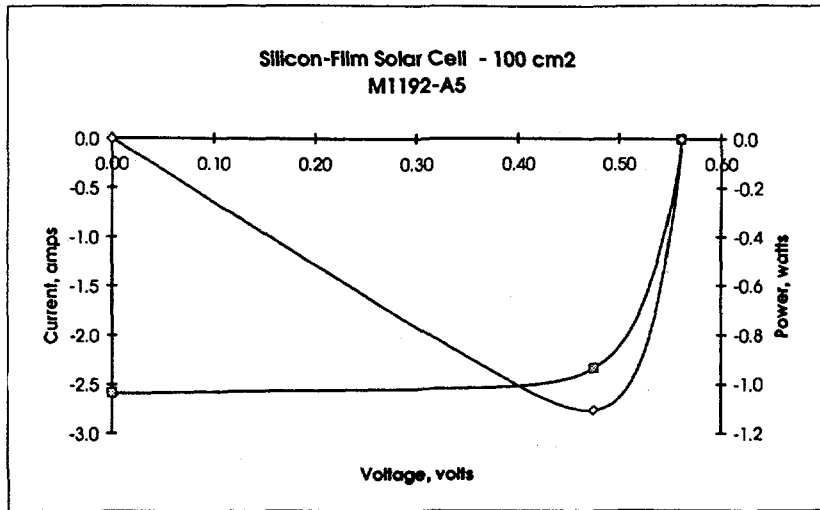


Figure 1. 100 cm<sup>2</sup> Silicon-Film™ Solar Cell Current Voltage Curve, 1.1 watt Solar Cell

Voc	0.526 volt
Isc	13.750 amp
Vmp	0.428 volt
Imp	11.310 amp
ff	0.670
Pmax	4.841 watt

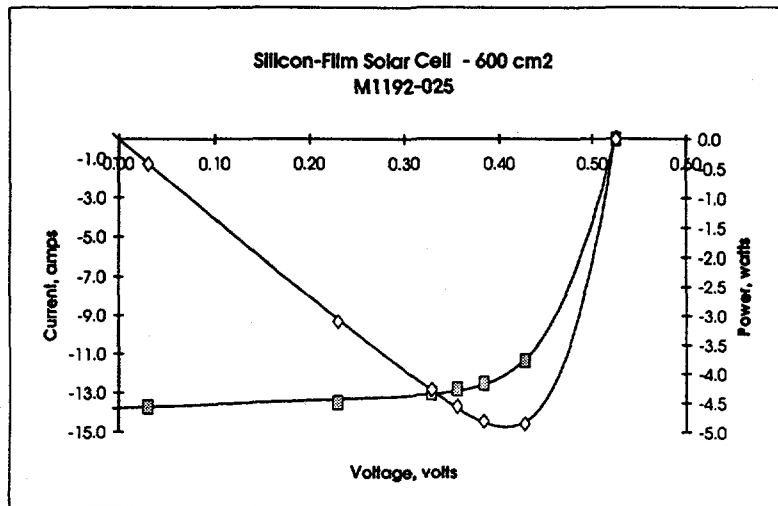
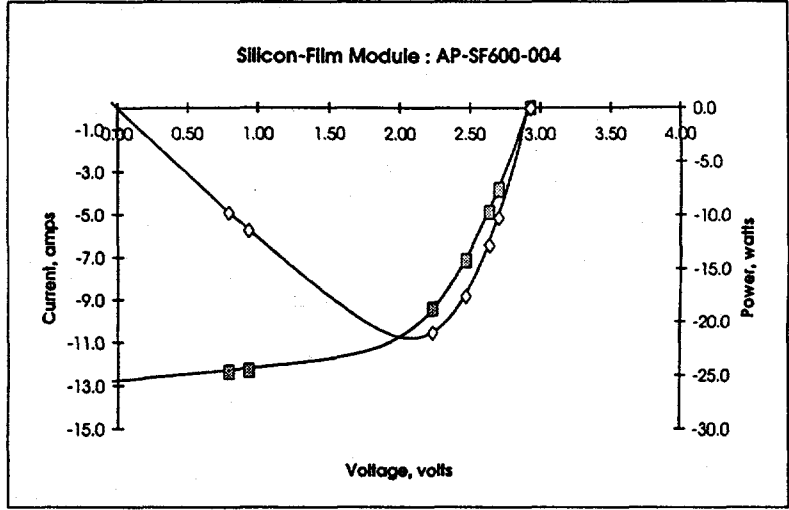


Figure 2. 600 cm<sup>2</sup> Silicon-Film™ Solar Cell Current Voltage Curve, 4.8 watt Solar Cell

Voc	2.915 volt
Isc	12.759 amp
Vmp	2.066 volt
Imp	10.463 amp
ff	0.581
Pmax	21.620 watt



**Figure 3. Large Solar Cell Module Current Voltage Curve**

**Title:** Continuous Roll-to-roll a-Si  
Photovoltaic Manufacturing Technology

**Organization:** Energy Conversion Devices, Inc.  
1675 West Maple Road  
Troy, Michigan 48084

**Contributors:** M. Izu, Principal Investigator, X. Deng, A. Krisko, H.C. Ovshinsky,  
D. Tsu, K. Whelan, R. Young

## **Objectives**

The overall objective of this three year program is to advance ECD's roll-to-roll, triple junction photovoltaic manufacturing technologies, to reduce the module production costs, to increase the stabilized module performance, and to expand the commercial capacity utilizing ECD technology<sup>1</sup>. The specific three year goal is to develop advanced large scale manufacturing technology incorporating ECD's earlier research advances with the capability of producing modules with stable 11% efficiency at a cost of approximately \$1.00 per peak watt.

## **Approaches**

We have performed manufacturing technology development work utilizing our advanced continuous roll-to-roll triple junction a-Si alloy solar cell production line, which was engineered and manufactured by ECD. The production line consists of: 1) a continuous roll-to-roll substrate washing machine; 2) a continuous roll-to-roll back-reflector machine; 3) a continuous roll-to-roll amorphous silicon alloy deposition machine; 4) a continuous roll-to-roll transparent conductor deposition machine.

The production line produces triple junction two band-gap a-Si alloy solar cells consisting of Si/Si/SiGe structure on a 5 mil. thick, 14 inches wide, 700 m stainless steel roll at a speed of 1 ft./min. This production line represents the world's first commercial production line which produces high-efficiency amorphous Si alloy solar cells utilizing multi-junction spectrum splitting cell design and high performance back-reflector.

## **Major Accomplishments**

- A high performance Ag/metal oxide back-reflector system was successfully incorporated in our continuous roll-to-roll commercial production operation for the first time.
- For the first time, the high quality a-SiGe narrow band-gap solar cells have been incorporated in a commercial continuous roll-to-roll manufacturing.
- The world's first 4 ft<sup>2</sup> production PV modules utilizing triple-cell spectrum splitting cell design have been produced in our commercial, continuous roll-to-roll production line.
- The initial aperture area efficiency of the 4 ft<sup>2</sup> module was 8.7%. The stable efficiency after 500 hours light-soaking under 1 Sun at approximately 50°C was 7.2%. The stable efficiency is substantially higher than that of commercially available a-Si 4ft<sup>2</sup> modules, which typically are 5% to 6%. Figure 1 is an I-V characteristic of one 1ft x 4ft module with 8.7% aperture area initial efficiency. In table I, we summarize results of some modules produced in our manufacturing process, measured at ECD and NREL. The performance of a module before and after light soaking for 500 hours under one sun at 50°C is also included in the table.

**Reference**

1. Semi-Annual Report on NREL Subcontract No. ZM-2-11040-7, October 1992.

**Figure 1: I-V Characteristics of a 1ft x 4ft Module with Triple Cell Spectra Splitting Solar Cell Structure Produced in ECD's Continuous Roll-to-Roll Commercial Manufacturing Line. The Aperture Area Module Efficiency is 8.7%.**

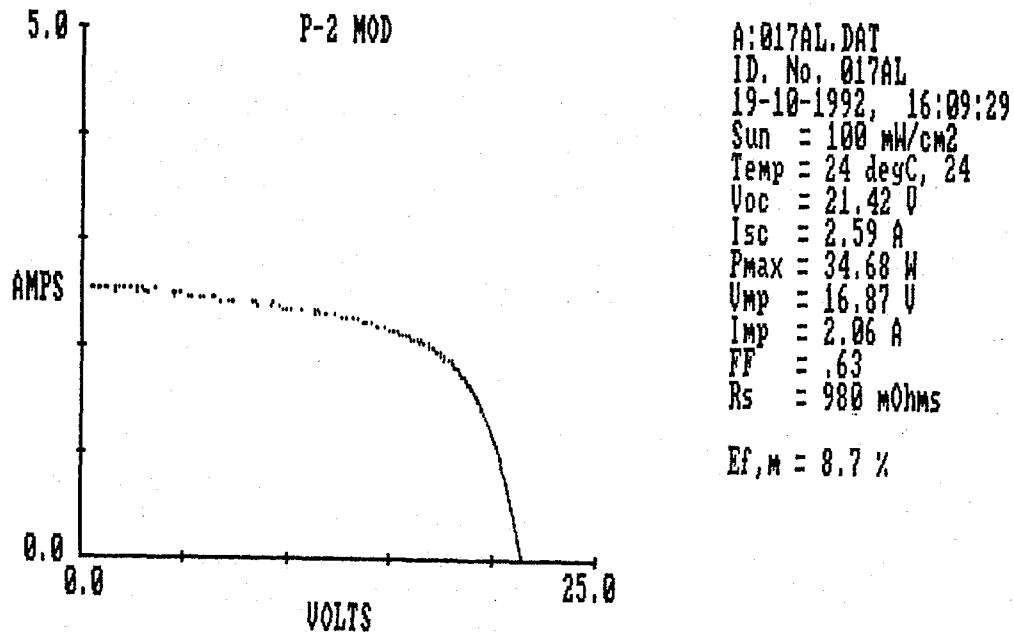


**Table I: I-V Data of ECD's Modules with Triple Cell Spectrum Splitting Solar Cell Structure Produced in ECD's Continuous Roll-to-Roll Manufacturing Line**

Module No.	Measurement Lab	Apert. Area (cm <sup>2</sup> )	Voc (V)	Isc (A)	FF	Pmax (W)	Module Eff. (%)
12	ECD	3970	21.75	2.58	0.6	33.67	8.5
12	NREL	3997	21.79	2.61	0.602	34.21	8.56
17	ECD	3970	21.42	2.59	0.63	34.68	8.7
14	ECD	2182	11.94	2.58	0.61	18.86	8.6
14 after light soaking*	ECD	2182	11.47	2.46	0.56	15.72	7.2

\* This module was light soaked for 500 hours under one sun at 50°C without load.

Title:           **Photovoltaic Manufacturing Technology (PVMaT)  
Improvements for ENTECH's Concentrator Module**

Organization: ENTECH, Inc., Dallas-Fort Worth Airport, Texas

Contributors: M.J. O'Neill, Program Manager  
A.J. McDanal and J.L. Perry

## **Introduction**

With significant assistance from the U.S. Department of Energy (DOE), Sandia National Laboratories (Sandia), and the National Renewable Energy Laboratory (NREL), the ENTECH technical team has been developing, field-testing, refining, and commercializing linear Fresnel lens photovoltaic concentrator technology for the past fifteen years. Figure 1 is a cross-sectional schematic of ENTECH's simple, line-focus, low-concentration module. Table I summarizes ENTECH's technology background, which includes four generations of the line-focus module. ENTECH completed a PVMaT Phase 1 project in FY 1991, and is now performing a PVMaT Phase 2A project.

## **Objective**

The key objective of ENTECH's PVMaT Phase 2A Program, which began in February 1992, is to design, develop, and implement improved manufacturing processes for ENTECH's fourth-generation concentrator module. The improved processes are being engineered to simultaneously achieve enhanced product quality (i.e., improved module efficiency, reliability, and field lifetime), higher production volume (10 MW/year initial rate), and lower production costs (\$1.25/W<sub>peak</sub> goal).

## **Approach**

An outstanding technical team has been assembled to improve the manufacturing processes associated with ENTECH's fourth-generation linear Fresnel lens concentrator module. This team includes technical personnel from NREL (Rick Mitchell, Dave Mooney, et al.), Sandia (Tom Hund, Alex Maish, et al.), 3M (Paul Jaster, DuWayne Radke, et al.), Consumers, Inc. (Arnie Kapitz), Solarex (John Wohlgemuth and Mohan Narayanan), BP Solar (Tim Bruton and Jack Nagle), Siemens Solar (Kim Mitchell and Richard King), Spire Corporation (Mike Nowlan), Integrated Production Systems (Tony Rowley), Texas Instruments (Hugh Wilson), and several key component suppliers, in addition to ENTECH's in-house staff. This team is presently addressing six principal tasks:

**Task 1 - Photovoltaic Cell and Receiver Assembly Automation:** Improved processes are being developed for manufacturing photovoltaic cell assemblies (each comprising one cell, one prismatic cell cover, four copper conductors, two bypass diodes, alumina-loaded silicone encapsulation, all enclosed within a rugged, dielectrically coated aluminum pan). Improved processes are also being developed for manufacturing photovoltaic receiver assemblies (each

comprising 36 interconnected cell assemblies mounted onto one aluminum heat sink with appropriate electrical connectors at each end).

**Task 2 - Prototype Work Station Development:** To verify the key processes being developed under Task 1, prototype work stations are being established for the critical processes, including: cell/diode/conductor soldering; prismatic cell cover application; cell assembly encapsulation; and receiver assembly.

**Task 3 - Prototype Work Station Experimentation:** Process experiments are being conducted with the work stations from Task 2 to optimize and validate the critical production processes.

**Task 4 - Continuous Lens Lamination:** In the past, to make a module-ready lens, ENTECH purchased 0.5 mm thick 3M Fresnel Lensfilm material and laminated it to 3.0 mm thick extruded acrylic sheet, using a methylene chloride solvent lamination process. This process involved a large labor content, poor production yields, low production rates, and considerable safety and health concerns. Under this task, a new process is being developed to continuously laminate the 3M Lensfilm to 1.5 mm thick impact-resistant acrylic (without methylene chloride), forming a continuous roll of module-ready lenses, thereby improving lens quality, reducing lens cost, and precluding a potentially hazardous process.

**Task 5 - Vendor Manufacturing Technology Improvements:** Several parts of ENTECH's concentrator module are manufactured by key vendors. These parts include the solar cells, the extruded aluminum heat sinks, the sheet aluminum housings, etc. These key vendors are improving their manufacturing technologies to provide higher quality parts at larger production rates and reduced unit prices.

**Task 6 - Environmental, Safety, and Health Considerations:** A key issue in developing the manufacturing technologies for ENTECH's fourth-generation concentrator module is to ensure that environmental, safety, and health (ES&H) considerations are fully addressed.

### **Significant Results**

One of the most significant results to date is the successful completion of Task 4, Continuous Lens Lamination. ENTECH's key lens subcontractor, 3M, has delivered a 600-foot long roll of continuously laminated lens material to ENTECH. ENTECH has thoroughly tested the new lens material, and has supplied samples to Sandia and NREL. Sandia has confirmed both excellent optical performance (90% efficiency at 21X concentration) and outstanding hail impact resistance (1 inch at terminal velocity) for the new lens. The new lens provides better optical quality, reduced lens weight, improved hail resistance, better shipping volume, and significantly lower cost, in addition to eliminating the ES&H problems associated with methylene chloride. The new ENTECH-designed lens can be produced in two different versions, with either of the focal plane irradiance profiles shown in Figure 2. Both versions of the 21X line-focus lens are commercially available from 3M, under a patent license arrangement with ENTECH.

Another significant result of the program to date relates to ENTECH's prismatic cell cover, which eliminates gridline shadowing losses for concentrator cells. Under a purchase order from

ENTECH, 3M has delivered continuous prism cover "tape" material in roll form, with each roll containing over 10,000 prism covers! Figure 3 shows the construction of the new prism cover "tape", which includes a very useful disposable liner. The liner provides a rigidizing structure for the silicone rubber prism cover, making the application and alignment of the cover to the cell much easier than it had been in the past without the liner. Furthermore, the liner serves as a mask for the prism cover during later cell assembly encapsulation, keeping the liquid encapsulant off of the optical cover prior to thermal curing of the encapsulant.

Very substantial progress has been made in developing manufacturing processes for the photovoltaic cell assembly. Spire Corporation is developing an automated light-soldering process for the cell/diode/conductor integration step. An extruded aluminum pan has been developed for supporting and enclosing the cell assembly during and after its manufacture. A new dielectric film (DuPont Tefzel) has been incorporated into the cell assembly, dramatically reducing yield losses, while improving production rates. A surplus AT&T electronic power supply encapsulation machine is being modified to encapsulate ENTECH's cell assemblies.

Significant progress has been made in developing manufacturing processes for the photovoltaic receiver assembly. By using thermally conductive tape to mount the new cell assemblies to the heat sink, and crimp-type connectors to make the electrical joints between cell assemblies, photovoltaic receiver manufacture is being dramatically improved in both quality and production rate.

### **Conclusions and Future Plans**

Substantial progress has been made in developing the manufacturing technology needed to produce efficient, reliable, high-quality concentrator modules, at production rates in the 10 MW/year range, with module costs in the \$1.00-1.50/W<sub>peak</sub> range. Unlike many other emerging photovoltaic technologies, the ENTECH fourth-generation concentrator technology requires no further breakthroughs in materials, efficiency, stability, or basic manufacturing processes, to meet the Department of Energy's electrical energy levelized cost goals. High-volume procurement of vendor-furnished parts, coupled with automated assembly of these parts into concentrator modules, will enable this technology to provide 12 cents/kWh electricity in sunny regions of the world. The PVMaT program is addressing the key automated assembly processes. After the six tasks discussed above have been completed, ENTECH's future plan is to implement the automated assembly processes on the factory floor.

### **References**

1. M.J. O'Neill et al., "Photovoltaic Manufacturing Technology Improvements for ENTECH's Concentrator Module - Phase 1 Final Technical Report," NREL/TP-214-4486, Denver, November 1991.
2. M.J. O'Neill et al., "ENTECH's Fourth-Generation Linear Concentrator Module," 1992 DOE/Sandia Crystalline Photovoltaic Technology Project Review Meeting, SAND92-1454, Albuquerque, July 1992.
3. T.M. Bruton et al., "Recent Developments in Concentrator Cells and Modules Using Silicon Laser Grooved Buried Grid Cells," 11th European Photovoltaic Solar Energy Conference and Exhibition, Montreaux, Switzerland, October 1992.
4. M.J. O'Neill, "Fourth-Generation, Line-Focus, Fresnel Lens Photovoltaic Concentrator," 4th Sunshine Workshop on Crystalline Silicon Solar Cells, Tokyo, Japan, November 1992.



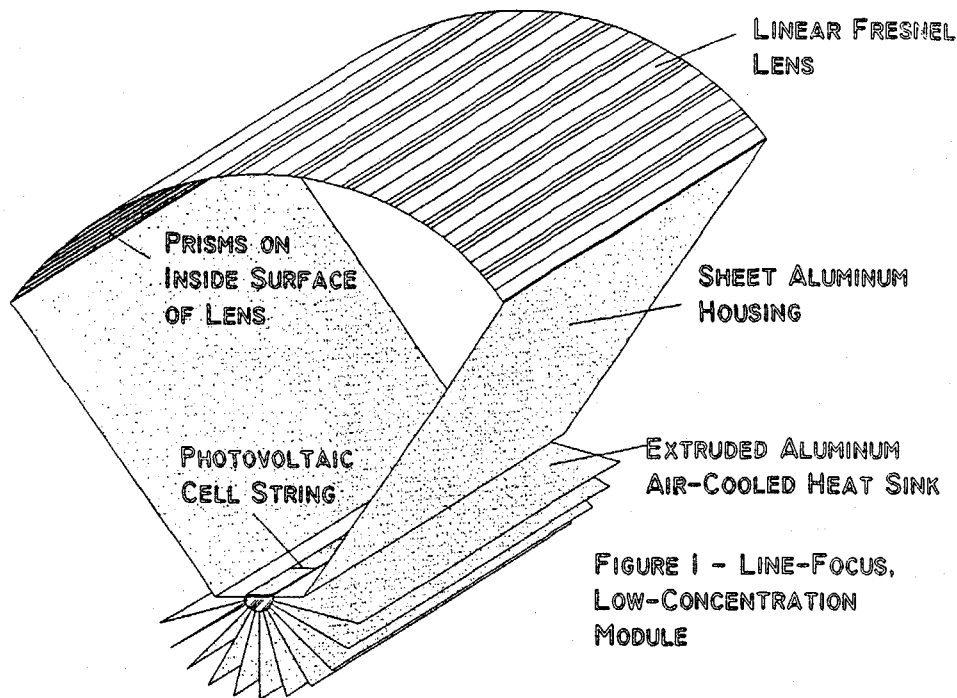


FIGURE 1 - LINE-FOCUS, LOW-CONCENTRATION MODULE

TABLE I - ENTECH'S LINEAR FRESNEL LENS PHOTOVOLTAIC CONCENTRATOR BACKGROUND

Time Period	Module Technology	Production Module Efficiency ( 25C Cell)	Qualification Testing (Sandia)	Systems Deployed
1978-1982	First-Generation 2.2 sq.m. Aperture 25X Concentration Water-Cooled ASEC CZ Si Cells	11-13%	Modules, Lenses, Receivers	25 kW at DFW, TX
1981-1984	Second-Generation 2.8 sq.m. Aperture 40X Concentration Water-Cooled and Air-Cooled Versions ASEC CZ Si Cells	12-14% (Lab Modules 17%)	Modules, Lenses, Cells, Receivers	22 kW at Sandia, NM 5 kW at TVA, TN
1986-87	Third-Generation 2.8 sq.m. Aperture 22X Concentration Air-Cooled Solarex Poly Si Cells Prismatic Cell Covers	13-15%	Modules, Lenses, Cells, Receivers	10 kW at Sandia, NM 1 kW at PG&E, CA
1988-91	Third-Generation 2.8 sq.m. Aperture 22X Concentration Air-Cooled Solarex CZ Si Cells Prismatic Cell Covers	15-17% (Lab Modules 21%)	Modules, Lenses, Cells, Receivers	300 kW at 3M, TX 20 kW at PVUSA, CA
1992-	Fourth-Generation 3.1 sq.m. Aperture 21X Concentration Air-Cooled and Water-Cooled Versions Advanced CZ Si Cells from BP Solar, Solarex, Siemens, Deutsche Aerospace, et al. Prismatic Cell Covers	Higher Each Year	On-Going Now	Utility-Scale > 35 kW (One Tracker = 220 sq.m.) Remote > 1 kW (50 kW Shipped to Date to Southern Africa)

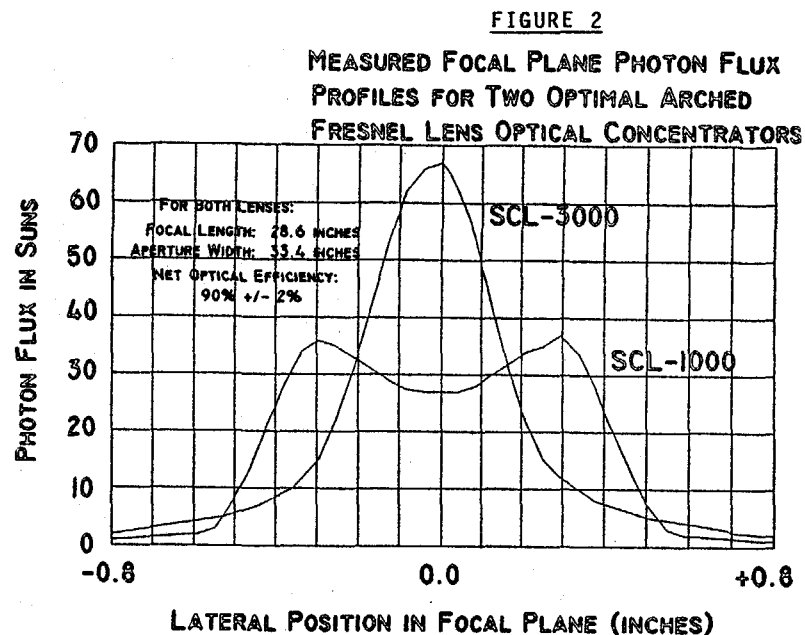
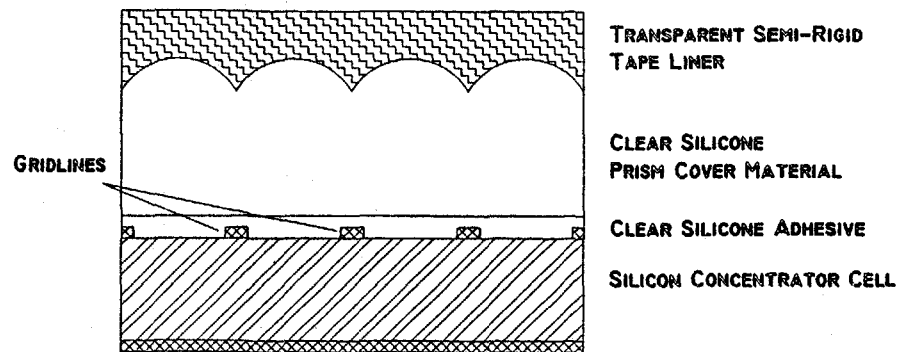


FIGURE 3  
SCHEMATIC OF THE NEW PRISM COVER TAPE MATERIAL APPLIED TO A CELL



Title: THIN EFG OCTAGONS

Organization: Mobil Solar Energy Corporation  
4 Suburban Park Drive  
Billerica, Mass 01821

Contributors: J. P. Kalejs, Program Manager; S. Rajendran,  
Principal Investigator; C. C. Chao.

### Objective

The Mobil Solar program in the DOE/NREL PVMaT Initiative is a three year program directed toward achieving cost reductions in manufacture of wafers of polycrystalline silicon. This is to be accomplished by improving yield and productivity in the growth of 200 micron thick octagons by the Edge-defined Film-fed Growth (EFG) technique, and in laser cutting of the octagons into 10 cm x 10 cm area wafers.

### Introduction

EFG octagon technology [1] allows thin 10 cm x 10 cm polycrystalline wafers to be produced for use as solar cell substrates without the customary need for slicing and grinding of ingots and polishing of wafers. Low cost, high yield and high productivity manufacture of 200 micron thick EFG wafers requires reduction of the thickness of octagon tubes to 200 microns, and increasing of the laser cutting station throughput, while at the same time maintaining or improving process yield and productivity for wafer manufacturing. In the past year, the wafer thickness used in the Mobil Solar pilot production line has been reduced from 400 to 300 microns. The intermediate term objectives for the Phase 1 program are to further reduce wafer thickness to 250 microns and to identify improvements in the octagon crystal growth process and in laser cutting of wafers of this thickness.

Work in progress since the start of the PVMaT program at Mobil Solar in April of this year that is to be described below is concentrated into three tasks: Task 1 - Thin Octagon Growth; Task 2 - Laser Cutting; and Task 3 - Process Control and Product Specification.

### Task 2 - Thin Octagon Growth

A consequence of the advantage gained over ingot growth by the EFG technology, producing thin wafers in the form of silicon sheet, is that stringent measures must be instituted in crystal growth in order to control as-grown material geometry. Variations in octagon tube properties are of several types: thickness nonuniformity, buckling (i.e., deviations from flatness) and residual stress. The Phase 1 goals in this area are to achieve material properties that lead to acceptable wafers for Mobil Solar's pilot production line while reducing their thickness from 300 to 250 microns.

Several crystal growth furnace equipment design reviews were held to develop equipment specifications and to identify approaches for implementation of process improvements that address intermediate goals for octagon growth. The

main elements of these reviews consisted of detailing the requirements for the furnace configuration, control systems and power supply for an improved EFG crystal growth system. Several of these design improvements are aimed at reducing the axial thickness variation along a tube length.

The work in a subtask on improving thickness uniformity around the perimeter of the octagon has identified furnace design changes that can reduce the thickness variation due to heat conduction effects by about a factor of two. These designs are being evaluated for suitability for use in a pilot line setting. The details of this work are reported in the Semiannual Report for this subcontract [2]. Several solutions have been identified to improve ambient control in the furnace and reduce the appearance of oxide deposits that reduce yield and productivity (see Ref. [2] for details). Two and three dimensional magnetic and thermal modelling of the EFG growth process and furnace is under way. These models are being used to study fundamental aspects of heat transfer in the growth process to help define strategies for improving thickness control and reducing thermal stress. They are also being extended for utilization in guiding prototyping of furnace components in order to reduce time and cost of engineering new designs. A separate modeling effort is addressing fundamentals of meniscus shape parameters, which relate to thickness control. This will be used in a later Phase of the work in implementing Intelligent Processing of Materials (IPM) strategies.

The subtask on stress control has investigated, using both theoretical and experimental approaches, the best means by which to manipulate the temperature distribution of the growing octagon tube so as to minimize thermal stress and buckling. A number of design changes have been identified which produce reduced buckling in 250 micron thick octagons [2]. Full implementation of improvements to reduce buckling is held up because of interactive effects related to the temperature distribution between directions needed to improve thickness uniformity and those needed to reduce buckling [2]. Efforts are under way to develop quantitative measurement techniques for monitoring interface region temperature fields and octagon surface deformations, which can be used to help to define solutions for these problems.

Both 300 and 250 micron thick octagons are being grown concurrently in two experimental EFG crystal growth furnaces in order to evaluate the progress made toward program goals on EFG material uniformity with the changes in design variables described above. Typically 5 to 6 octagon tubes are produced per growth run, and then representative tubes cut up to provide wafers for material attribute evaluation on a statistical basis. Other details are in Ref. [2] and material evaluation is described under Task 3.

#### Task 2 - Laser Cutting

The goals of this task are to improve the yield and throughput of the laser cutting technology for producing 200 micron thick EFG wafers. The edge strength of laser-cut EFG wafers is currently limited by microcracks in the sample edge. Two options are being pursued to achieve program goals for increased wafer edge strength: improving existing Nd:YAG lasers, and development of a new generation of high power line focus dye and CO<sub>2</sub> lasers.

Feasibility study phases to study means by which to improve the Nd:YAG and dye laser cut edge quality are under way [2]. Encouraging increases in wafer edge strength have been obtained with a low beam divergence Nd:YAG laser. Future

work will attempt to define whether increased cutting speeds can be obtained with this laser without compromising edge quality. Studies of edge strength as a function of cutting speed are also in progress. Initial results indicate that loss in edge strength occurs with higher laser power levels which are generally required to cut through the entire wafer thickness in one pulse at the cutting speeds needed to meet program goals.

It has been demonstrated for the first time that a dye laser can cut through 300-400 micron thick silicon at rates required to meet throughput goals [2]. This dye laser operates at a wavelength of 585 nm, and is focussed to produce a line cut 5 cm in length.

Throughput goal achievement with the thinner octagon tubes requires concurrent advancement of the octagon tube and wafer handling processes. Engineering design reviews for an advanced laser cutting station have been held, and a number of concepts are being evaluated. The main areas of work include tube and wafer handling equipment, the laser autofocus unit, and computer-based control systems.

### Task 3 - Process Control and Product Specification

Programs in this task are structured to provide support in areas of sensor development for improving crystal growth process control and wafer characterization. The long range objectives in sensor development are to develop and implement advanced concepts of on-line material property monitoring and automated crystal growth process control using Intelligent Processing of Materials (IPM) strategies, which lead to increased yield and productivity in manufacture of 200 micron thick EFG wafers. The second subtask is to develop specifications for EFG wafer thickness uniformity, flatness, residual stress, edge strength and electronic quality needed to achieve acceptance of wafers in the Mobil Solar pilot production line on the basis of yield, as wafer thickness is decreased toward 200 microns. The electronic quality of the thin wafers is to be maintained at a level sufficient to produce 14% efficient solar cells.

Process Control. On-line sensor development has been in progress to obtain equipment to carry out interface temperature field and meniscus shape measurements, buckle mapping and local thickness measurements. Imaging equipment utilizing a CCD camera has been defined that can capture details of the meniscus and solid/liquid interface environment. Separate calibration equipment based on optical pyrometry will be used to provide reference data on the temperature field. These measurements should produce data to allow calculation of the first and second derivatives of the temperature field in the growing octagon within the region 5 mm from the growth interface, which are needed to develop strategies to reduce stress and buckling.

Bench-top feasibility studies of interferometric techniques to map the surface topology of a 10 cm x 10 cm nonflat EFG wafer have been successful. The equipment now has to be configured to produce real time maps of buckle shape as the octagon tube emerges from the furnace. Variations in reflectivity of the octagon tube surface, and local surface irregularities which disrupt fringe patterns have made image analysis difficult.

Eddy current sensors are being studied for their potential to measure on-line local thickness variations in the thin-walled tubes. This sensor will be used in conjunction with coil adjustments in the octagon furnace. On-line

measurement techniques must cope with changing resistivity and polycrystallinity of the material and a varying stand-off distance between the tube and the probe. An operation domain in frequency, probe dimensions and stand-off distance has been defined that is appropriate for the thickness of octagons being grown.

Product Specification. Several approaches are being evaluated to measure residual stress in EFG material. One uses a Shadow-Moire technique, and the other holography to obtain information on strain response of the sheet surface. These studies are at an early stage, and results are not available.

Wafer edge strength after laser cutting is being monitored using the twist test and Weibull statistical analysis. Calibration curves and reference data have been established [2]. The program target is to increase the edge strength from the current 40-50 MPA to 125 MPA.

Laser cutting yields for all experimental tubes are being compiled to establish baseline information. Current cutting yields are typically over 94%. The thinner and more buckled tubes also have cutting yields in this range at their best, but there is a greater variance in the average yields (see Ref. [2] for details). Flatness inspection criteria are being established.

#### Future Work

The Phase 1 goals for process development on EFG wafers require growth of 250 micron thick octagon tubes which produce wafers at a 75% yield through cutting and inspection for flatness. Residual stress less than 10 MPA and wafer edges strengths greater than 125 MPa are to be demonstrated. The work in progress toward Phase 1 program objectives is currently on schedule.

#### Acknowledgements

Contributions to the experimental results described in this report are acknowledged from: A. Menna, R. Stromont, D. Greenlaw C. Caprini, and D. Preston.

#### References

- [1] D. Harvey, "Recent Progress in Octagon Growth Using Edge-defined Film-fed Growth", J. Crystal Growth, 104, 88 (1989).
- [2] Semiannual Progress Report (October 30, 1992) DOE/NREL subcontract No. ZM-2-11040-3, in press.

**Title:** PVMaT Cost Analysis Support

**Organization:** Research Triangle Institute, Center for Semiconductor Research  
3040 Cornwallis Rd., Research Triangle Park, NC 27709

**Contributors:** R. A. Whisnant, Principal Investigator

### **Objective**

The objective of this subcontract is to investigate manufacturing costs for different PV technologies, analyze these costs, and prepare resulting information for utilization by the PVMaT project.

### **Technical Approach**

The work originally defined for this subcontract was designed to assist the PVMaT program in assessing the potential of various PV manufacturing technologies for cost reduction in the PV modules. The information developed is intended to aid the program management in assessing progress and defining directions. The technical approach as defined by the original subcontract consisted of five tasks whose definitions are summarized below.

**Task 1. Initial PV Cost Analysis Methodology Description.** Describe and develop where necessary a photovoltaic cost analysis methodology for comparing different PV manufacturing processes. Such a methodology is to treat the various PV technologies on a non-parochial basis and allow, as much as possible, a uniform set of both input and output parameters (referred to as Characterization Parameters). Develop criteria for prioritizing the technologies based on their promise for reducing PV module manufacturing costs in the future.

**Task 2. Revised PV Cost Analysis Methodology Description.** Make appropriate revisions to the Cost Analysis Methodology of Task 1 using information from subcontractor Phase 1 draft final reports.

**Task 3. Technical Evaluation Panel Support.** Using the Cost Analysis Methodology defined in previous tasks, provide costing analysis support for the SERI Technical Evaluation Panel in its evaluation of proposals for Phase 2.

**Task 4. Methodology Application.** Apply the methodology described in Tasks 1 and 2 to PV manufacturing technology processes to assist in comparing PV module costs. This will include the quantitative specification of Characterization Parameters that characterize the expected module manufacturing costs for each of the process specific technologies to be considered for Phase 2 support.

**Task 5. Summary Report on Cost Analysis Methodology.** Complete a summary report on the relative advantages and disadvantages for the process studied in Task 4.

During the course of completing Tasks 1 and 2, it was decided by the PVMaT program that Tasks 3 through 5 would not be carried out using the Phase 2 proposals as inputs. Tasks 3, 4 and 5 were replaced by an analysis of an amorphous silicon module manufacturing process. This work is being done in collaboration with Dr. Chris Sherring, who is a consultant to the PVMaT project.

## Results

### Tasks 1 and 2.

A Cost Analysis Methodology was completed and provided to NREL. The methodology is contained in a report that defines the criteria for evaluating the status of a technology and its associated manufacturing process.

The largest potential market for PV generation is utility-owned generation. There are a number of other markets for PV capacity that are individually smaller, but in the aggregate they are significant to the emergence of a PV industry. However, a benchmark of utility-owned generation is very useful for examining the potential of PV manufacturing process improvements and comparing their relative merits. The criteria for evaluation are based on the notion that the manufacturing process improvements resulting from the PVMaT project will result in products that come closer to meeting, or exceeding by some amount, the breakeven product price established for utility-owned systems and the modules within those systems. The product that comes closest to meeting, or exceeds by the largest amount, the breakeven price would rank highest, all other criteria being equal. The data available to assess the status of PV technologies varies in terms of availability and accuracy, and so there is uncertainty in any such assessment.

Any PV manufacturing process produces a module that can be characterized by its overall area, its peak power output under specified insolation input (i.e., its efficiency) and by its price to the buyer. Other more detailed specifications include voltage and current at peak output, fill factor, and, of particular importance for a-Si thin film modules, the long-term stability of the output. For the purposes ranking in this methodology, the two key parameters that characterize the module are the module price in  $\$/m^2$  and the achieved stable module conversion efficiency. The module manufacturing process, along with product design, determines price in  $\$/m^2$ . Price is determined by the consumption of materials, and equipment cost, throughput and yield. A process has a throughput expressed in the number of modules produced of a given size in a time period (e.g., a year) that is a function of the design of the module, the process capabilities of the equipment, the process operations performed, and the skill of people in operating that equipment. Processes with high throughput per dollar invested produce products of lower price. Efficiency is a function of both product design and processing proficiency. The efficiency of the modules produced normally is distributed about some mean value, and the mean and standard deviation are resultant process characteristics that are important in comparing and ranking processes. The higher the mean and the smaller the standard deviation, the better the process. These statistics may be difficult to ascertain, especially for processes with little history of production, and they can only be estimated for the proposed improved processes. The standard deviation is therefore perhaps of secondary concern unless it is apparent that certain processes inherently result, for example, in much wider standard deviations than others.

Based on the preceding considerations, a set of quantitative criteria is defined as:

- current price status of the module ( $\$/m^2$ ), actual or computed
- current module efficiency, mean and standard deviation
- projected module price under defined design and process assumptions
- projected module efficiency consistent with the pricing assumptions, mean and standard deviation
- breakeven price for a selected market as a function of system efficiency

The two elements of these criteria that require computation are the breakeven price and the projected module price. A method for calculating breakeven price for the utility market is provided in the report based on a method published by the Electric Power Research Institute. The method proposed for the projected module price uses a manufacturing process cost analysis program previously developed by RTI called STAMPP (STRategic Analysis of Manufacturing Process and Price).

STAMPP models the manufacturing operations of a firm and its overhead and financial structure to calculate a required price of the product produced. It is based on a required revenue (sales) methodology to determine price. The product price provides a specified rate of return on equity investment at a specified annual level of production. Among the outputs of the model are a corporate income statement and balance sheet that allow an assessment of the modeled business in terms of financial and business criteria. These reports are based on accepted accounting procedures. On the manufacturing side, reports are provided that summarize the equipment, labor, materials, floor space, and utilities required in terms of both quantity and cost. Also reported are personnel and associated costs for administrative functions. The result is a complete picture of all aspects of the cost structure underlying the required product price. The STAMPP model provides the capability to identify the impact on required price of changes in the manufacturing process if those changes can be defined in terms of STAMPP input data as defined subsequently.

#### a-Si Process Task

A process was defined for producing a-Si modules that are 2.5' x 5' in size at an annual volume of 2 million square feet. The process used a batch reactor for growing the p-i-n junction. Key process data was defined by Dr. Chris Sherring and RTI used the STAMPP model to estimate a required selling price. Parametric analyses of required price versus key cost drivers were also carried out. The results are preliminary at this time and are being reviewed by NREL.



**Title:** PV Cz Silicon Manufacturing Technology Improvements

**Organization:** Siemens Solar Industries  
Camarillo, California

**Contributors:** Theresa Jester, project manager; Jerry Anderson,  
Robert Probst, David Tanner, and Sergio Vasquez

## **Introduction**

Siemens Solar Industries (SSI) began a three-year, three-phase cost shared contract in March 1992 to demonstrate significant cost reductions and improvements in manufacturing technology. The work is focused on near-term projects for implementation in the SSI Czochralski (Cz) manufacturing facility in Camarillo, California. The key contract milestones are given in Table 1.

## **Approach**

The Cz manufacturing technology development consists of three focused tasks relating to cost reduction. The silicon wafer itself contributes about half of the total module cost and has the most potential for cost reduction. The cell processing costs are about a quarter of the module costs, with cell efficiency results being most important. Module assembly and packaging costs are the balance, with the module design, both materials and labor, contributing significantly.

**Task 1: Silicon Crystal Growth and Thin Wafer Technology.** Crystal growing costs are driven by material growing yields and indirect manufacturing costs such as electricity and machine parts used each time a crystal ingot is fabricated. Wafering costs are driven by labor and the number of good slices yielded per length of crystal processed. This first task of reducing the wafer costs has focused on the graphite usage in the crystal growing machines, the polysilicon material used for ingot growth, and the evaluation of wire saw machines to improve the yielded wafers per inch of ingot.

**Task 2: Silicon Cell Processing.** Cell processing costs are driven by the electrical contacts used, and the labor required for the process steps to clean the wafer, form the semiconductor junction, and the contacts. The second task has been focused on the improvement of the etching bath process for better uniformity, better junction formation, and reduced contact resistance. Studies of process automation for lower labor costs have begun.

**Task 3: Silicon Module Fabrication and Environmental, Safety, and Health Issues.** Module costs are highly sensitive to labor and materials. The module design tasks are driven by high reliability in the field and lower costs. Included in this task is the environmental work to eliminate chlorofluorocarbon (CFC) usage and significantly reduce the caustic waste volumes.

## Results

During FY 1992 (3/13/92 - 9/30/92), several significant manufacturing technology improvements were achieved.

The crystal growing operation improved significantly with a complete redesign of the graphite hot zone parts. This redesign improved the lifetime of these expensive machine parts by more than a factor of three and has resulted in a savings of over \$300,000 annually. This design effort is complete and all the crystal growers at SSI have been retrofitted to include these parts. Crystal growing improvements were also achieved by an on-going study of the polysilicon materials used versus crystal yield. Figure 1 shows a three-month study of various polysilicon remelt runs versus runs with virgin polysilicon chips mixed in. The higher resistivity polysilicon remelt alone shows much higher growing yields, which is believed to be due to the higher state of refinement. This benefit is two-fold, with remelt polysilicon typically much less expensive than the virgin material.

Wafer processing with wire saws is progressing rapidly. The wire saws have proven to yield 30% more wafers per inch in experimental runs. The capacity of a wire saw is much greater than that of an ID saw, resulting in major labor savings for a given manufacturing throughput. The major trade-off with wire saws is an increase in the cost of the slurry cutting media. Figure 2 shows the trade-off of wafers per inch versus slurry use. This has yet to be optimized through development under this contract.

Cell processing improvements have included the implementation of a new etching process with better uniformity across the wafer surface, and a preliminary study of process variations in junction formation and optics versus cell and module performance. A significant result during this preliminary study was the quantification of the sensitivity of certain diffusion processes to humidity exposure. This finding led to implementation of an additional etch step for thorough cleaning of the cell surface prior to contact firing.

Module designs for lower material and labor costs have begun with the focus on a new junction box and less costly framing technique. CFC usage has been significantly reduced in the SSI manufacturing facility under this contract, and has been eliminated in all areas except solder de-fluxing. Alternative solders are currently being tested with a target date of January 1, 1993 for complete elimination of CFC use.

Table 1. Cz manufacturing technology milestones.

	Phase 1	Phase 2	Phase 3
<b>Task 1. Silicon Crystal Growth &amp; Thin Wafer Technology</b>			
A. Increase Cz grower productivity by 25%	10%	15%	25%
B. Demonstrate utility of prototype wire saw Deliver 100 wire sawn wafers	• •		
C. Demonstrate 0.010"-thick wire sawn wafers Deliver 100 0.010" wafers		• •	
D. Reduce wafer cost by 30%		15%	30%
<b>Task 2. Silicon Cell Processing</b> Reduce cell cost by 30% (\$/watt)	10%	20%	30%
<b>Task 3. Silicon Module Fabrication &amp; Environmental, Safety &amp; Health Issues</b>			
A. Reduce module fabrication costs by 35% Deliver modules demonstrating reduced \$/watt	10%	25% 2 modules (20%)	35% 6 modules (25%)
B. Reduce caustic use and waste	Define process and equipment	25% reduction	
C. Replace CFC's	Evaluate CFC alternatives		90% reduction in CFC usage

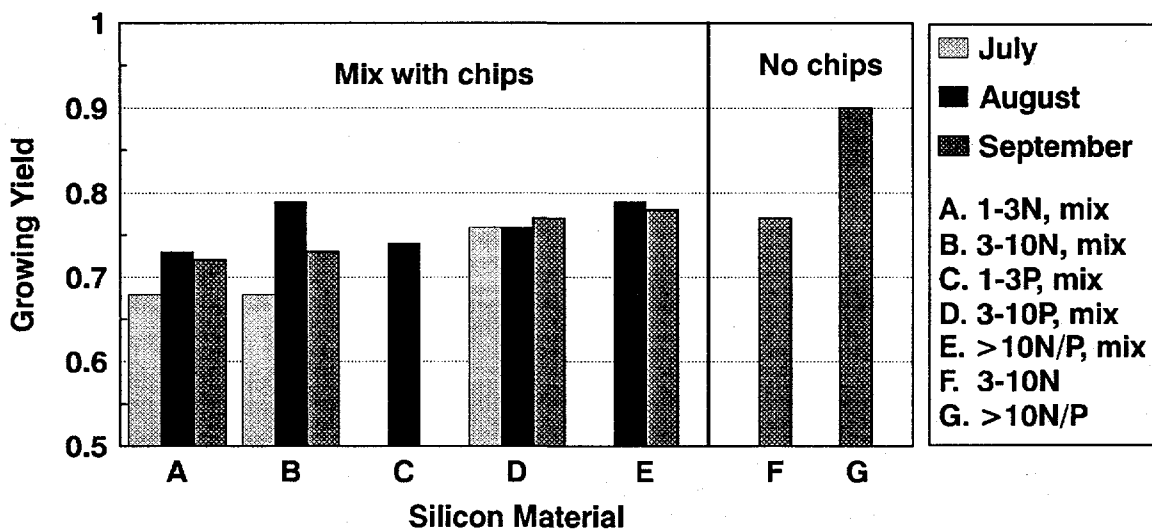


Fig. 1. Effect of various types of silicon mixtures on growing yields.

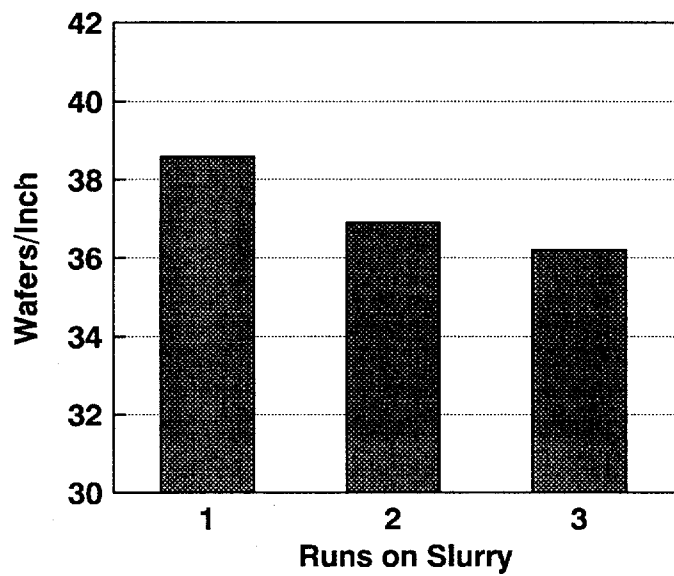


Fig. 2. Yield of wafers per inch versus the number of times the slurry is used.

**Title:** Large Area, Triple-Junction, a-Si Alloy Production Scale-Up\*

**Organization:** Solarex Corporation, Thin Film Division  
826 Newtown-Yardley Road, Newtown, PA 18940

**Contributors:** R. Oswald, Principal Investigator; J. O'Dowd, Program Coordinator; Task Leaders: W. Ashenfelter, K. Jansen, B. Johnson, T. Kloss, E. Twesme, P. Weiss, F. Willing

## **EXECUTIVE SUMMARY**

**Objectives:** The objective of this subcontract over its three year duration is to advance Solarex's photovoltaic manufacturing technologies, reduce its a-Si:H module production costs, increase module performance and expand the Solarex commercial production capacity. Solarex shall meet these objectives by improving the deposition and quality of the transparent front contact; optimizing the laser patterning process; scaling up the semiconductor deposition process; improving the back contact deposition; and scaling up and improving the encapsulation and testing of its a-Si:H modules. In the Phase I portion of this subcontract Solarex shall focus on scaling up components of the chemical vapor deposition system for deposition of the front contact; scaling up laser scribing techniques; formulating triple-junction recipes for module production; and scaling up the metal oxide back contacts.

### **Task 1: Front Contact Development**

Facilitation of a large area (30") CVD belt furnace has been completed and designs for injectors are under consideration. A new gas feed system has been designed for both silicon dioxide and tin oxide deposition including dopant delivery and heated exhaust systems. Designed experiments to study the kinetics of the tin chloride based tin oxide process were performed using the current manufacturing system. Improvements in the optical transmission of the tin oxide were obtained with a process based on the reaction kinetics while still maintaining the optical light scattering and electrical properties for triple-junction devices. (See Figure 1)

---

\* This work was supported under National Renewable Energy Laboratory ZM-2-11040-2.

## **Task 2: Laser Scribing Process Development**

A large area (>6 sq ft) laser scribing station has been designed and a preliminary set-up for scribing four square foot modules was completed. The active area on a four square foot module with this set-up was over 86% with future goals of 94% and 96% when scribe widths and spacings can be reduced. An autofocus system has been designed, built and tested for the large area laser to accommodate glass warpage and improve cutting reliability.

Methods to obtain better coupling between the laser beam and the individual substrate layers are under investigation. Utilizing wavelengths other than the standard green (532nm) has resulted in improved processing speed and more reliable scribes in some applications. Optimization of the parameter space and wavelengths most appropriate for each layer is in progress.

## **Task 3: Amorphous Silicon Based Semiconductor Deposition Process**

The design concept for a five chamber plasma enhanced CVD reactor for deposition of > 6 ft<sup>2</sup> triple-junction modules has been completed. Improvements in the gas distribution, pumping, electrical and substrate heating systems, based on experience with manufacturing systems, have been designed into this large area multi-chamber reactor.

Optimization of the triple-junction device recipe has proceeded in a separate reactor capable of depositions on four square foot substrates. The films made in this reactor have quantum efficiencies that approach those of films made in research systems. Optimization of the diode fill factors is planned next.

## **Task 4: Rear Contact Deposition Process**

The efforts in this task have concentrated on the assembly and test of a large area magnetron sputtering system to deposit the rear contact. A system was partially assembled to test the magnetrons and system design. Several aluminum films were produced and the remainder of the chambers are being assembled in a similar configuration to provide an oxide/metal capability.

## **Task 5: Bus/Wire/Encapsulation/Frame**

An evaluation of possible commercially available indexing systems to allow scale-up of the frit dispensing system and an indexer was selected which could fulfill the requirements for both contact dispensing and laser scribing of large area modules (>6 ft<sup>2</sup>).

A new auto-refill frit delivery valve is undergoing tests. This system would allow larger tolerances to substrate flatness without adversely affecting the deposition thickness, position or width of the bus bar. Evaluations of external connection schemes utilizing both commercially available connectors and new designs are also in progress.

The evaluation and selection of improved encapsulants are in progress. The encapsulant must provide protection of a thin film through prolonged outdoor exposure and provide a high dielectric path to ground for high voltage protection.

### **Task 6: Materials Handling**

A preliminary equipment layout for a plant with a 10 MW output capacity was completed. The layout was constructed based on input from all task leaders and equipment specialists and is consistent with present practices on our manufacturing line. Vendors of glass handling equipment have been contacted and a manual glass transport system designed.

### **Task 7: Environmental Test, Yield, and Performance Analysis**

Environmental and electrical testing capability of large area modules is under development by the Task 7 team. The development of a light (1-SUN) soak station capable of uniformly illuminating a six square foot area at a constant temperature has been completed.

We reviewed the test sequence for the measurement of large area modules ( $\geq 6 \text{ ft}^2$ ) as prescribed in NREL/TR-213-3624. Other equipment available includes a hail tester, dry hi-pot tester, humidity-freeze and thermal cycling chambers. (A review of the wet hi-pot tester procedure was made with NREL personnel to insure that measurements will be consistent.)

# COMPARISON OF TRANSMISSION FOR FRONT CONTACT IN INDEX MATCHING FLUID

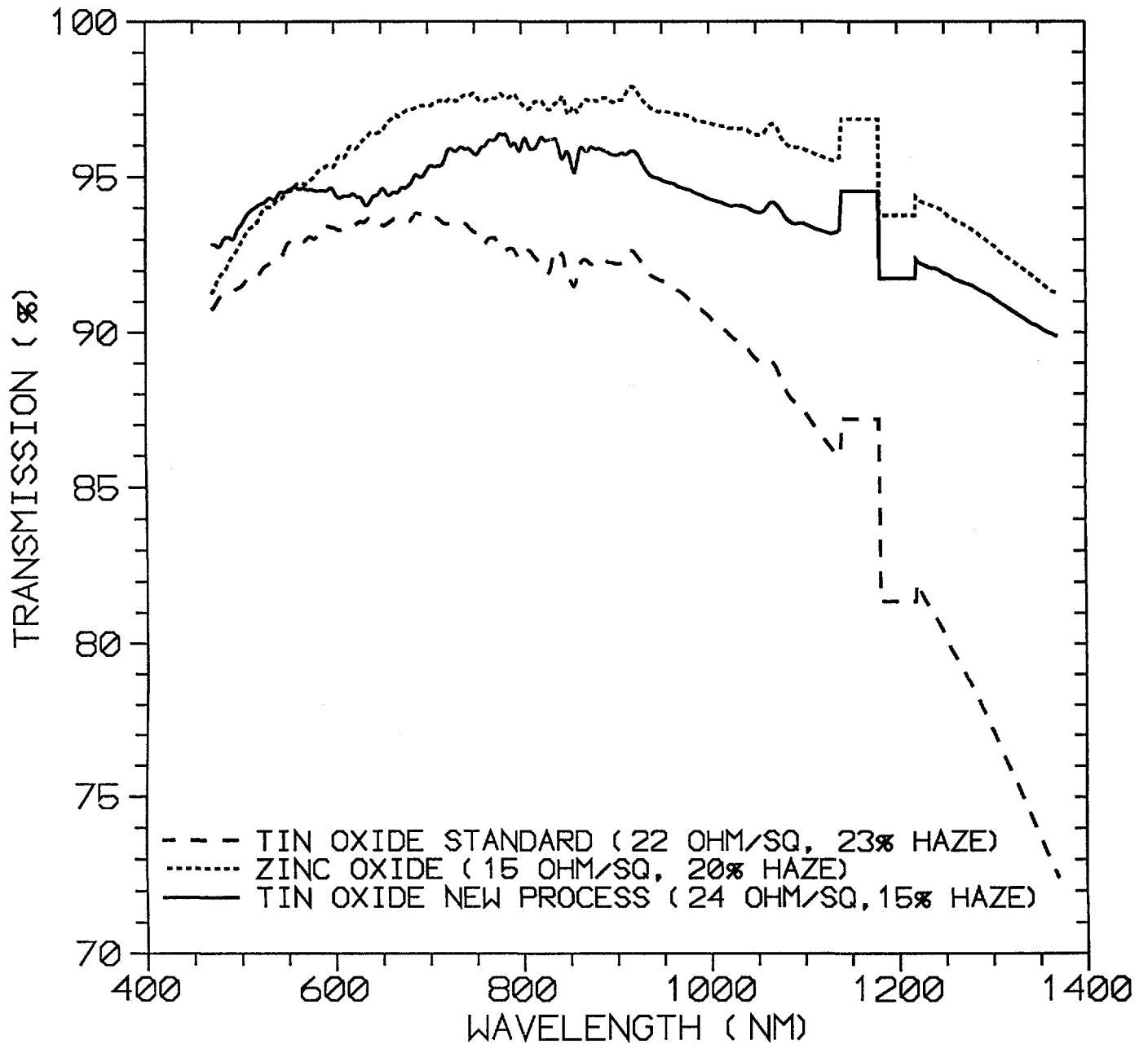


FIGURE 1



Title: Amorphous Silicon Photovoltaic Manufacturing Technology - Phase 2A

Organization: Utility Power Group  
Chatsworth, California

Contributors: G. Duran, principal investigator, K. Mackamul,  
D. Metcalf, C. Miller, M. Stern

### Objective

The objective of this project is to significantly advance the photovoltaic manufacturing technologies, reduce module production costs, increase average module performance, and increase the production capacity existing in Utility Power Group and Advanced Photovoltaic Systems. Areas of focus shall include:

- o Encapsulation
- o Product Design
- o Process and Quality Control
- o Automation

### Progress

#### 1. Task 1 - POWERGLASS Module Encapsulation

Areas of focus include:

- o Materials
- o Application
- o Reliability
- o Cost

The materials considered fall into four main categories:

1. Polyurethanes
2. Epoxies
3. Silicones
4. Plastic Copolymers

The following is a list of the materials investigated to date:

#### Polyurethanes:

- |               |   |                   |
|---------------|---|-------------------|
| Hardman, Inc. | - | Kalex 13361 A/B   |
| Conap, Inc.   | - | Conathane CE-1163 |
|               | - | Conethane CE-1175 |

Chase Humiseal Corp.	-	Humiseal 1A27
	-	Humiseal 1A33
	-	Humiseal 1A20
Epmar Corp.	-	EX165
Epoxy:		
Ameron Corp.	-	Amercoat 385P
Silicone:		
Dow Corning Corp.	-	Q3-6611
	-	577
Chase Humiseal Corp.	-	Humiseal 1C49
General Electric	-	RTV 630
	-	RTV 128
Plastic Copolymer:		
Plastic Flamecoat	-	PF 110
	-	PF 112
	-	PF 160

At the conclusion of the first stage of materials investigation and selection, it was determined that the two most promising encapsulation materials were; Dow Corning 577 Primerless Silicone and Plastic Flamecoat PF 110.

Application techniques being considered include:

- o Airless Spraying
- o Screen Printing
- o Curtain Pouring
- o Brushing
- o Roll Coating

## 2. Task 2 - POWERGLASS Module Termination

The role of module termination is to provide an electrical connection between the module and the external load circuit. The design of an advanced module termination system required optimization of the following criteria:

- o Material Cost
- o Attachment Cost
- o Reliability
- o Adaptability

The current POWERGLASS module termination design was analyzed, and as shown in Table I, the material cost and attachment cost of new terminal designs must not exceed \$1.66 to achieve at least a 50% reduction in POWERGLASS termination cost.

Table I

Item	Cost
Ribbon	\$0.12
Connector	\$0.16
Boot	\$0.46
Pottant	\$0.08
Labor	\$2.50
Total	\$3.32
Design Goal	\$1.66

Four candidate terminal designs have been completed and samples have been fabricated and evaluated in terms of cost and manufacturability. The four candidate terminal designs are; Binding Post, Spring Clip, Wire cage Clamp, and the Threaded Standoff.

The new POWERGLASS module design utilizes a novel "U-turn" concept to allow the positive and negative terminals to be protected by a single enclosure (J-box), thereby eliminating the need for external conductors (busbar ribbons). The idea behind the "U-turn" concept is to have current flow from the bottom terminal of half of the module (submodule) to the top of the submodule, across to the other half of the module (the other submodule), and down to the opposite terminal. Using this technique, the silver paste busbar replaces the busbar ribbon. In addition, this design increases the active area of the module by decreasing the number of interconnects required to attain the desired module voltage.

## APPENDIX: Sub-tier Contractor of UPG

### Amorphous Silicon Photovoltaic Manufacturing Technology - Phase 2A

APS, Inc., Princeton, New Jersey

Principal Investigator, H. Volltrauer, Manager Eureka Line, A. Koniars

#### Objectives

The objectives of this program are to improve the operation of the APS Eureka manufacturing line, to increase its throughput and to reduce manufacturing costs. The effort is divided into four separate tasks: automation of the line; process and quality control; encapsulation; and new module designs. These tasks will be discussed separately.

#### Progress

##### 1. Task 3 - Eureka Module Design

Input from Marketing suggested three directions to pursue for new products. First, the edge connectors used on the modules for PVUSA were thought undesirable; an unobstructed border was requested. Second, a smaller module was needed and third, a module voltage suitable for 12 volt battery charging was deemed necessary. These requirements resulted in three new products.

EP50 - The EP50 produces 50 watts at 38 volts and is the direct replacement for the original EP2. It differs from its predecessor in that the silicone "boot" that was used to protect the connecting point of the foil to the external wires is replaced with a molded junction cover on the back of the module. The connection to the thin-films is made through a hole in the cover glass removed from the edge so as to provide one inch of free perimeter area. In other respects the EP50 is the same as the original EP2.

Manufacturing product specifications (MPS) for this product have been completed and approved for all steps of the encapsulation process. A complete engineering drawing package has been generated and approved. Testing has been carried out that specifically addresses the differences between this product and its predecessor, e.g. static load testing to verify that the holes in the cover glass do not significantly weaken the module; humidity freeze cycling; and thermal cycling. Additional testing is in progress, in part to determine the limits of performance and to test consistency of the process.

EN25 - The EN25 is a half-size module suitable for use in 12 volt systems; its output is 25 watts at nominally 17 volts. The lower voltage is obtained by, first increasing the cell width from 1.11cm to 1.25cm, thus reducing the number of cells and second, by electrically paralleling two halves of the module. This approach requires several new steps in the encapsulation process and some addition to the basic equipment. In part because of the way the lower voltage is obtained, the junction covers are at the center of one end of the module

rather than at the corners as with the EP50. A first cut at equipment modifications was made and several dozen modules produced. Preliminary testing was carried out, again to test the differences between this and previous product. Further testing will take place shortly, when a production run is made. Drawings for this product have been approved and other documentation is in preparation.

EN50 - This 50 watt product is the low voltage version of the EP50. It shares many of the features of the EN25, in that the terminal covers are at the center of one end of the module, and two halves of the module are effectively connected in parallel. Some of the equipment modifications needed for the EN25 apply to this product and a production run for it is also imminent. A draft of a drawing package for this product is being reviewed and as with the EN25, manufacturing product specifications are in preparation.

## 2. Task 4 - Eureka Process and Quality Control

The goal of this task is to improve module quality and throughput and to reduce manufacturing costs by gaining better understanding and control of the process. General areas that are being addressed are process monitoring and control, in-line product performance verification and off-line testing. Specific items that we have made progress in are the following:

Documentation - Manufacturing Process Specifications (MPS) were drafted for the module encapsulation workstations in order to define the process steps, to introduce additional process controls and to obtain essential parametric information. Statistical techniques are being applied to some of these data, both to obtain baseline information on the process and to evaluate and control the process.

IV Measurement Reliability - In large part we judge the quality of our plate or module by its IV measurement; reasonable precision is therefore required. Several steps have been taken to improve these measurements. Light uniformity has been considered as a source of error and steps have been taken to improve it. Because there is some spatial non-uniformity of the thin-film deposits, light intensity variations can interact with deposition variations to give erroneous results. Modifications to the light source placement and careful adjustment of intensities, reduced this problem.

Thin-Film Uniformity - Since start-up of the line, off-line tests have included silicon thickness measurement, consisting of roughly 100 separate determinations per plate. However, these measurements are only carried out on about 1% of the plates made. To better understand variations in film thickness, a prototype in-situ thickness measuring device has been installed. It measures thickness optically by relating the transmission at 600 nm to thickness. Some thickness variations seen from run to run have been attributed to variations in rf power applied to the discharge.

Critical process parameters - A specific goal of this task is to define several process parameters that are critical to the operation.

Several parameters on the thin-film side have been selected for initial study. These include the rf delivered to the chamber, flow rates and pressures of the deposition gases and the effect of base pressure on the electrical quality of product.

In the encapsulation area, two process variables were singled out for initial study. First, a shunt measurement following the border isolation step. In the past, some variation in power loss between plate and module was attributed to this step. The other parameter being investigated is the temperature profile in the terminal cover curing oven. Some preliminary observations suggest that the frequency and size of voids that occasionally occur in the terminal covers are related to the temperature profile of the oven.

### 3. Task 5 - Eureka Power Module and Termination

Two specific goals of this task are to reduce the production cost of the encapsulation process and to reduce the power loss between plate and module.

Cost reduction has focused on reducing labor costs through simplifying and automating the process. While the new molded terminal cover is still applied mostly manually, this step has the potential of being automated in the future.

New dispensing equipment has been tested for applying the terminal cover. This equipment both mixes the components of the material in line as well as dispenses a predetermined amount. Currently, mixing is done as a batch process and dispensing is controlled by the operator.

### 4. Task 6 - Automation in Eureka Manufacturing Line

In the thin-film line the following has been accomplished in the past six months:

**Silicon Deposition** - This step has been automated and is being evaluated in one of our two deposition systems. Based on the initial performance, additional features are contemplated for the update. These deal with additions to the code to add flexibility, safety, self-test features and increased data gathering.

**Encapsulation Area** - The introduction of the new products required changes and equipment additions to this area. To further reduce costs, extensive design work has been applied towards achieving a more fully automated line for the new plant. Most transporting of plates will be automated, as will some of the inline testing.

**Lasers** - This critical equipment has been made more reliable and its throughput increased. To improve reliability, instrumentation has been added to monitor beam quality. Automated inline power measuring equipment has been installed at one station. This measures and stores on disk for later analysis, the laser power prior to lasering each plate. Secondary registration sensors have been added to prevent misalignment of scribes. Water flow and other critical parameters are monitored and cause system shutdown if warranted.

Thin-Film Automation - Unloading of plates from the box carriers after silicon deposition is automated through sputtering. Some steps have been taken to also automate the loading stage. Equipment has been built and auxiliary pieces have been installed, e.g. glass washer transport and rotating stages.

### **Conclusion**

The major accomplishments in the past six months have been the introduction of new products, with the improvements in encapsulation they incorporate. Our emphasis in the next several months will be to refine these products, possibly add new ones and continue the program to more fully automate the encapsulation line. In the process and quality control area, we are working towards networking all the process control computers. This will greatly simplify data analysis.





## 6.0 PHOTOVOLTAIC (PV) MODULE AND SYSTEM PERFORMANCE AND ENGINEERING PROJECT

Richard DeBlasio (Manager)

The PV Module and System Performance and Engineering Project is structured to conduct state-of-the-art PV module, system, and solar radiation research, engineering, testing, evaluation, and analysis tasks, to provide technical results and solutions to technical issues, and to develop PV standards and codes. The project is also designed to maintain and enhance supporting facilities and capabilities that are consistent with DOE's new *Photovoltaics Program Plan FY 1991—FY 1995*, that are complementary to other DOE PV projects, and that ensure that project capabilities and facilities are available resources for cooperative research and utilization by the PV research and development community.

Project activities are managed through the module and systems performance and engineering project management task and organized to address project objectives through the following five primary tasks: 1) cell and module standardized characterization performance; 2) module and system performance testing; 3) module reliability research; 4) solar radiation research; and 5) standards development.

The following subcontract activities represent support for industry/utility PV power projects, domestic and international standards and code development, and PV technology validation at the module/array level of operation.



**TITLE: NATIONAL AND INTERNATIONAL PHOTOVOLTAIC STANDARDS**

**Organizations:** Solar Energy Industries Association,  
Washington, D.C.  
Institute of Electrical Electronic Engineers, Inc.,  
New York, NY  
American National Standards Institute,  
New York, NY

**Contributors:** R.J. Klein, Program Manager; R. DeBlasio; L. Mrig; R. D'Aiello;  
S. Chalmers; J. Anderson; J. Wohlgemuth; D. Feder

**OBJECTIVE**

To assist in technology transfer as an industry aid in the commercialization of PV modules, products and services. To produce photovoltaic standards that will assist U.S. PV industry in improving the manufacturing process, reducing cost and increasing the commercial product performance to maintain a competitive edge in the world market place.

**APPROACH**

To manage and administer secretariat responsibilities for the International Electrotechnical Commission (IEC) Technical Committee 82, Solar Photovoltaic Energy Systems. To maintain continuity of current and future activities through IEEE Standards Coordinating Committee (SCC) 21, Photovoltaics and the United States Technical Advisor Group (USTAG) that is responsible for United States input into the international standards writing arena.

**DISCUSSION OF FY '92 ACTIVITIES**

IEEE SCC 21 had three very productive meetings. During one of those meetings, it was decided that SCC 21 would review Section 690, Grounding of the National Electric Code (NEC), and become involved in attempting to make changes that would improve the applicability of that section to photovoltaics. Progress is also being made on writing an IEEE Standard that addresses "Qualification of Photovoltaic (PV) Modules".

The United States Technical Advisors Group held three meetings during FY '92 and supplied four experts for participation in international standards writing committee meetings along with the committed Secretariat support for the Technical Committee 82 Plenary session held in Tokyo.

During that Tokyo meeting a new chairman, from Japan, nominated by the United States National Committee, was installed to replace the French chairman. During that meeting, TC 82 also decided to supply an expert to become a member of a recently created Joint Working Group (JWG) to deal with battery storage issues, along with IEC TC 21,

Accumulators. TC 82 accepted the symbols "G" and "H" as standard symbols for Irradiance and Irradiation respectively. These symbols will be used in all future TC 82 publications.

This project has also permitted experts to be involved in a government Equal Partners Implementation Committee (EPIC) that is responsible for attempting to get the United States Government Departments (such as GSA, General Services Administration, Commerce and Defense) to use Commercial Standards.

## **SUMMARY**

This year has brought to fruition four IEC publications that includes the all important "Design Qualification and Type Approval of Crystalline Silicon Terrestrial Photovoltaic (PV) Modules" draft. The year has produced four or five other independent publications that should go to proof early in '93.

Continuity with the same experts participating in each working group is most important to produce good technical drafts that may become international standards.

To achieve marketplace acceptance the standard producer must include experts that may be potential users, purchasers, specifiers, regulators and product manufacturers. This project attempts to bring all those experts together to write the best possible photovoltaic standard in each category of the applicable technology.

## **SIGNIFICANT RESULTS**

### **Standards Published:**

#### National:

1. IEEE Publication 928, Recommended Criteria for Terrestrial Photovoltaic Power Systems, reaffirmed 1991.
2. IEEE Publication 929, Recommended Practice for Utility Interface of Residential and Intermediate Photovoltaic Systems, reaffirmed 1991.
3. IEEE Publication 1145, Recommended Practice for Installation and Maintenance of Nickel-Cadmium Batteries for Photovoltaic (PV) Systems.

#### International:

1. IEC Publication 1173, Overvoltage Protection for Photovoltaic (PV) Power Generating Systems - Guide.
2. Addendum to IEC Publication 891, Procedures for Temperature and Irradiance Corrections to Measured I-V Characteristics of Crystalline Silicon Photovoltaic Devices, to include Thin Film devices.

Standards in Proof Stages:

1. IEC Publication 1194, Characteristic Parameters of Photovoltaic (PV) Systems.
2. IEC Publication, Design Qualification and Type Approval of Crystalline Silicon Terrestrial Photovoltaic (PV) Modules.

The publication gives test procedures for Visual Inspection, Damp Heat, Humidity-Freeze, Twist, Insulation, Robustness of Termination, Non-Intrusive Method for Hot-Spot Endurance, Impact of Hailstones, Thermal Cycling, Outdoor Exposure, Mechanical Load, Measurement of Nominal Operating Cell Temperature and Determination of Temperature Coefficients from Module Measurements. This publication specifies methods for determining the electrical and thermal characteristics of modules. It also provides a test sequence designed to demonstrate that a module is capable of withstanding prolonged exposure in general open-air climates. Extreme conditions such as the marine environment are excluded.

Other:

1. Acceptance of Symbols "G" and "H" for Irradiance and Irradiation.
2. Involvement in EPIC.

Additional information can be obtained from:

R.J. Klein  
SEIA Standards Office  
1242 Dartmouth Street  
Scranton, PA 18504  
USA

IEEE and IEC publications available from:

IEEE Customer Service  
445 Hoes Lane  
P.O. Box 1331  
Piscataway, NJ 08855-1331

American National Standards Institute, Inc.  
Sales Department  
11 West 42nd Street, 13th Floor  
New York, NY 10036

Title: Long Term Environmental Effects on Roof-Mounted Photovoltaic Modules

Organization: Southwest Technology Development Institute, Las Cruces, New Mexico 88003

Contributors: A. L. Rosenthal, principal investigator; S. J. Durand, and J. W. Wiles

## Objectives

The objective of this research effort is to characterize the effects of long term exposure to sunlight on fielded photovoltaic (PV) modules. Of particular interest in this effort are the combined effects of high solar flux and high module operating temperatures on module performance.

## Approach

The work on this project was broken down into three tasks. The first task was the preparation of a report summarizing the various photovoltaic roof mount designs in use at the Southwest Region Experiment Station (SWRES) in Las Cruces, NM, along with a commentary on the design tradeoffs and significant performance characteristics of each.

The second task was the compilation of a report that presented all of the historical performance data collected from four photovoltaic arrays at the SWRES. The criteria used for the selection of the four arrays were that, to the extent possible, they should represent different PV technologies (e.g. crystalline, polycrystalline, amorphous, etc.), all should be encapsulated with EVA, and preference should be given to arrays with the longest, continuous set of recorded performance data.

The final task was to instrument 12 modules from each of the selected arrays. This instrumentation provides a resistive load so that each module is operated near its peak power point. In addition, current-voltage (I-V) curves can be automatically taken of all instrumented modules every week for the duration of the contract. Initially, the I-V curves were used to derive normalization coefficients. Summary reports containing normalized curves from each of the instrumented modules will be prepared quarterly

for the duration of the contract. In addition, once each quarter, a single module from each of the selected arrays will be removed and sent to NREL for destructive analysis.

### Results and Discussion of FY '92 Activities

The first task was completed in September 1992 with the delivery to NREL of the report, *The Effects of Photovoltaic Module Mounting on Operating Temperature*. This report compared the effects of integral, direct, standoff, and rack mounting techniques on module operating temperatures. Performance data from the Northeast Region Experiment Station and the Southwest Region Experiment Station were presented to compare roof mount technologies.

The second task was completed in July 1992 with the delivery to NREL of the report, *Photovoltaic Performance Trends -- Module Historical Data*. This report documented the performance histories of several of the PV arrays at the SWRES. It also provided the basis for the selection of the four arrays that now serve in the continuing experimental phase of this work, Task three.

Task three was begun in June and is on-going. The report, *Module Performance Report I*, was delivered to NREL in July. This report presented brief histories of the four selected arrays and I-V curves for 48 modules instrumented within these arrays. This report, therefore, documents the initial conditions of all of the modules at the beginning of the two year test period and provides a baseline against which future performance readings will be compared. The four modules/arrays now under test are:

- Mobil Solar model Ra-180 crystal silicon modules installed in 1983
- Solarex model MIT polycrystalline silicon modules installed in 1981
- Sovonics model P-101 amorphous silicon modules installed in 1989
- Solarex model SA-20 amorphous silicon modules installed in 1988

Figure 1 shows a typical I-V curve for one of the Mobil Ra-180 modules. The figure presents the actual I-V curve obtained during testing and the same curve normalized to conditions of 1000 W/m<sup>2</sup> irradiance and 45°C module temperature. Normalization was performed using coefficients derived according to ASTM standard E1036-85.

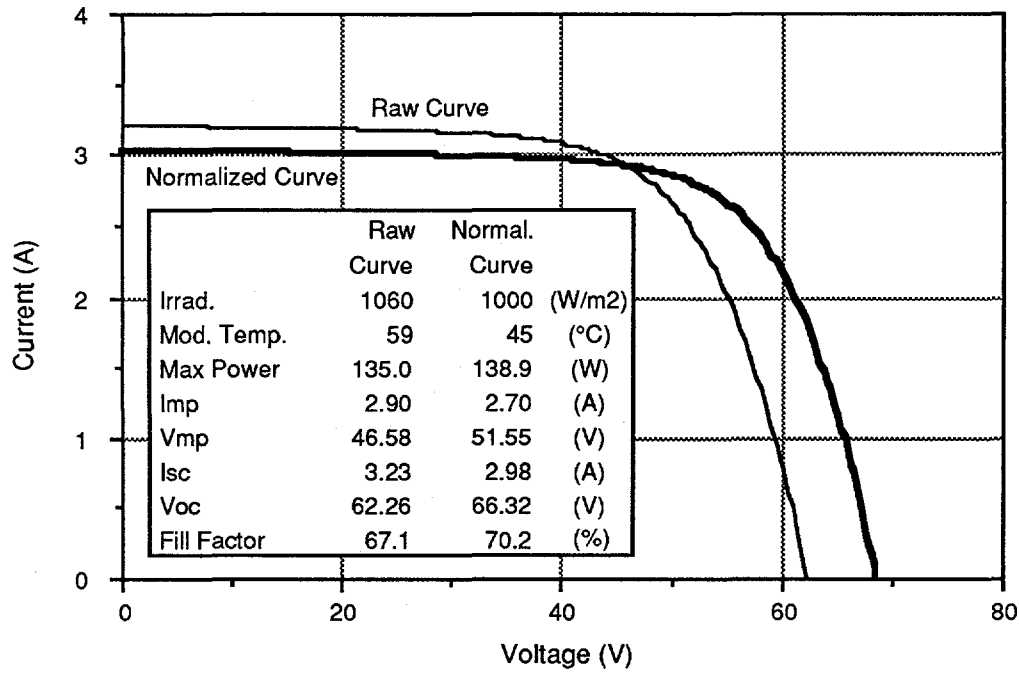


Figure 1. Typical Mobil Ra-180 module I-V curve.

The current contract calls for module performance evaluation reports to be prepared quarterly over a period of two years in an effort to document changes in performance parameters produced by exposure to ambient conditions. In addition, modules will be removed from their arrays and sent to NREL for analysis to correlate observed performance changes with changes in module encapsulant composition.



## 7.0 PV ANALYSIS AND APPLICATIONS DEVELOPMENT PROJECT

Roger W. Taylor (Manager)

The PV Analysis and Applications Development Project was created in May 1992. This new FWP brings together a variety of senior NREL PV personnel to focus additional attention on the growing analytical and applications development needs of the DOE PV Program and the DOE Office of Solar Energy Conversion.

During FY 1992, NREL subcontract activities included six significant efforts as follows:

- Solar Resource, Utility Load Matching Assessment; SUNY-Albany
- Evaluation of DSM Incentive Opportunities for PV; University of Delaware
- Risk-Adjusted IRP Procedures: Reflecting the True Costs of Conventional and Solar Options; University of Massachusetts
- Building-Integrated Photovoltaics: Identification of Issues and Opportunities; Kiss Cathcart Anders Architects
- Design for Photovoltaics: Curriculum Development for North American Architecture School Faculty; AIA/ACSA Research Council
- Brazilian Rural Electrification Pilot Project; Siemens Solar Industries and Centro de Pesquisas de Energia Eletrica (CEPEL).

These projects are described in more detail on the following pages.

In addition to these subcontracts funded directly by NREL, this project has supported the development and implementation of grants and cooperative agreements administered by the DOE NREL Area Office (NAO) that provide for funding U.S. PV market development activities through the new Utility PV Group and the Solar Energy Research and Education Foundation, as well as the major new thrust in PV-Buildings systems through the PV:BONUS program.



Title: Design for Photovoltaics: Curriculum Development for North American Architecture School Faculty

Organization: AIA/ACSA Research Council

Contributors: Deane Evans

## Objective

The objective of the project is to develop guidance for architectural school faculty in North America on how to incorporate information on photovoltaics into the design curriculum. The materials developed over the course of this project will be directly targeted to the 3,000 members and 32,000 students active in North American schools of architecture in any given year.

## Approach

The focus of the work effort will be a comprehensive "resource package" to be made available to all ACSA schools and faculty. The package will be developed by a team of technical advisors with expertise in both research and teaching of energy issues and will consist of the following five elements.

- a basic primer on photovoltaics and their use in buildings, including background materials and teaching aids, in a wide variety of media, suitable for use in teaching;
- a set of guidelines on "how to teach" the information included in the primer, targeted at two different settings;
  - in a lecture course on energy/environmental systems,
  - as part of a studio design course;
- a complementary set of guidelines on linking an architecture school to key energy related organizations who might assist in the educational process, including:

National Renewable Energy Laboratory  
Passive Solar Industries Council  
Solar Energy Industries Association  
Local AIA chapters and members of the AIA Committee on the Environment  
Local utilities  
Local PV manufacturers/distributors;

- a series of case studies on successful use of photovoltaics in buildings;
- case study information on successful teaching of photovoltaics in architecture school curriculum.

In addition to the resource materials developed under the project, a feedback mechanism will also be established whereby successful applications of the information in schools of architecture will be reported to the Research Council and made available to all other ACSA schools on a regular basis as part of an updated resource package. The first schools to provide such reports will be those invited to become members of the Project Team.

**Title:** Building-Integrated Photovoltaics

**Organization:** Kiss Cathcart Anders Architects, P.C.  
New York City, New York

**Contributors:** G. Kiss, principal-in-charge;  
J. Kinkead, principal investigator.

**Objective**

The purpose of this study is to provide an initial analysis from the point of view of the design community of the issues and opportunities for building-integrated PV products for office/commercial and industrial applications. The essence of the study is qualitative and indeed subjective. It is intended as an aid to policy makers and members of the technical community in planning and setting priorities for further study and product development. It is important to remember that the success of a product in the building market depends on acceptance by building owners, managers, regulators, designers, tenants and users, as well as on issues of economics.

**Building Envelope PV Systems**

The study illustrates a selection of building diagrams to show just some of the numerous configurations possible in building-integrated PV systems design (example, *fig. 1*). These configurations are divided into two basic categories: wall and roof systems. They represent a range of advantages and disadvantages in designing for efficient PV performance.

While the primary goal in standalone PV systems layout is to maximize the amount of power generated via optimum array orientation, this goal is tempered in the case of building design by considerations such as construction costs, optimum building floor area, daylight control, thermal performance, and aesthetics. PV panels are usually oriented at an upward tilt to receive the maximum amount of the sun's radiation, but buildings are generally vertical for reasons of economy, efficiency and tradition. Moreover, since cooling is usually the largest consumer of energy in a building, envelopes are often designed to deflect and minimize the amount of radiation falling on a building's surface. This study outlines a discussion of these and other considerations, noting their impact upon PV wall and roof configurations.

Primary considerations discussed include:

- Solar: PV panel performance  
passive solar performance
- Construction: system installation  
panel dimensions  
framing details
- Electrical: wiring accommodation
- Mechanical: envelope ventilation
- Design: PV aesthetics/representation  
economy & engineering  
product opportunities
- Maintenance: cleaning & electrical
- Site/Location: real estate values  
high vs. low rise  
litigation possibilities

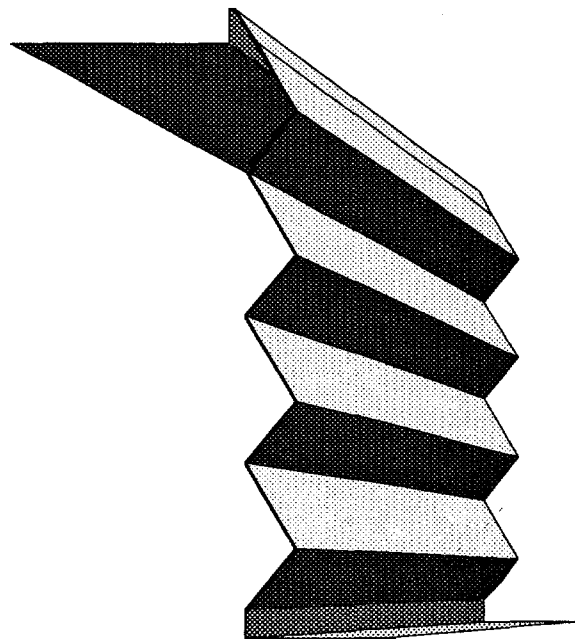


*Fig. 1: PV 'sawtooth' curtain wall diagram.*

Climate:	insulation water penetration wind and other loads lightning
Safety:	thermal stresses glass code requirements
Environmental:	panel disposal/replacement manufacturing

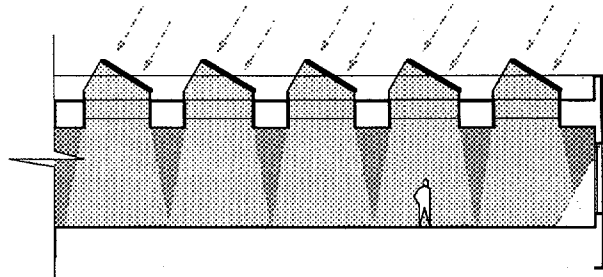


Fig. 2: Partial building section of opaque PV roof monitors.

### Evaluation of PV Building Envelope Performance

The quantitative PV analyses presented in the study do not attempt to evaluate any specific PV technologies. The report assumes devices similar to those available today, or new devices that might reasonably be developed in the next five years such as transparent modules or modules on flexible substrates. Quantitative analyses and prototypical wall sections are based on amorphous cells on a rigid substrate that is waterproof and large enough to fit common construction models. Cell efficiencies used in the analyses are conservatively assumed to be 5%. Higher efficiency cells will improve all the analyses and could lead to different conclusions than those reached in this report.

Quantitative analyses performed include the impact of different planning configurations and vertical wall orientations on PV performance and the impact of multiple wall tilts for the four polar orientations on PV performance. Considerable study is devoted to the self-shadowing effects which occur upon more complex PV wall configurations (sawtooth profile, etc.) as the sun's altitude increases, impacting the performance of the panels during the peak hours of the day (fig. 3, below).

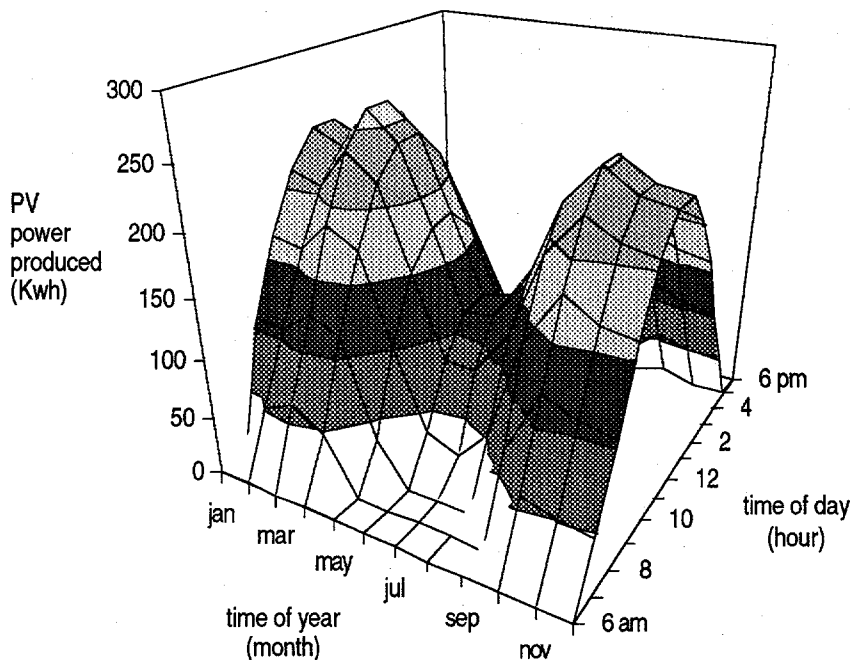


Fig. 3: Hourly/monthly power production of a south-oriented, sawtooth-profile, PV curtain wall. (analysis assumes a 4 story, 100' long wall with 12' flr-to-flr heights, 60° panel tilt, 6'-0" panel length and 5% cell efficiency)

## PVs and Building Systems

The study also presents a brief discussion of building-integrated photovoltaics' impact upon a building's regulatory systems, focusing on the potential for PVs to provide data for controlling these systems. As Figure 4 indicates, there exists a proportional relationship between PV power and typical building loads for a commercial/office occupancy over the course of a day. The 2-3 hour lag with the HVAC load implies a requirement for storage for a standalone system to match the two curves. The DDC control system assumes an intelligent lighting control system using occupancy sensors and/or daylight sensors. This control system for the building could use power data from PVs to adjust lighting levels and equipment control, therefore reducing the overall energy consumption of the building.

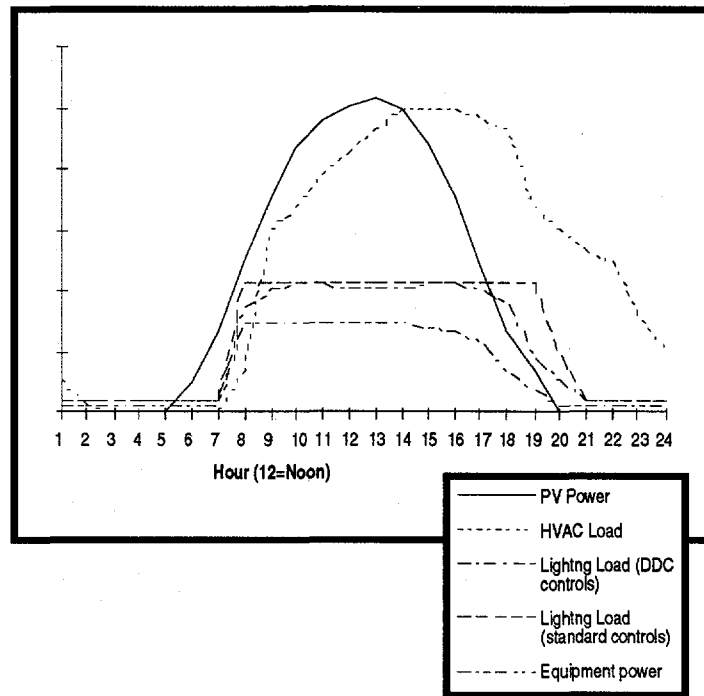


Fig. 4: PV power vs. commercial building load.

## PV-Integrated Building Subsystems

A great number of small scale products can be developed which integrate PVs into building HVAC, lighting or electrical systems. Building-integrated PV panels acting as building sensors for DDC systems offer an opportunity for the panels to play multiple roles in building performance: the panels provide both an envelope (transparent or opaque), they provide power for operating building systems, and they provide the data necessary to regulate those systems.

Some potential PV-integrated products that are evaluated include:

- PV-powered mechanical daylighting systems (fig. 5).
- PV-powered ventilation systems.
- PV-powered emergency lighting systems.
- PV-powered security systems.

## Cost Goals

Costs involved with PV building integration are evaluated for prototypical wall and roof configurations to determine the following:

- Existing building costs without PVs.
- Additional costs for PV integration.
- Additional savings due to PV integration.

## Design Concerns

It is important to recognize that the complexity of the building-integrated PV installations and systems will require the combined efforts of a number of different building trades and product

manufacturers. This study presents a summary list of questions and concerns raised during interviews with multiple members of the building community concerning PV building integration. These members include, but are not necessarily limited to, architects, engineers, developers, owners, facilities managers and building product manufacturers.

### Regulatory Issues

There exist numerous national and state building agencies with energy conservation standards and model energy codes outlined to set minimum requirements for the design of "smart", energy efficient buildings. These codes and regulations are meant to ensure that all new building construction is designed with a concern for minimizing the amount of energy required to operate and occupy a building during its lifetime. As an active energy source (PV-supplied power) and/or a passive energy source (daylight and thermal control), PVs may offset the energy calculations for a building's mechanical and electrical loads. Nevertheless as a physical building element, they fall under the same thermal and weathering requirements of a typical building envelope and must meet specific criteria regarding thermal transmittance and air and water infiltration.

### Conclusions

Solar design (connoting specifically passive solar) has never become a common language among the building community. It has implied fairly rigid design limitations regarding orientation, sloping roof elements and sun spaces, and has exacted penalties in lifestyle to the occupants (having to operate insulating shades or pumps, the inability to put rugs or furniture on a thermal collector floor slab, etc.).

PV buildings introduce a new language to architecture. For the first time a building's skin will do more than keep out the weather and modulate heat and light transmission. It will produce energy (and therefore revenue) instead of losing energy. As an active element of the building, it will be dynamically linked to other systems in ways we cannot fully anticipate. The inherent flexibility of PVs compared to other types of solar collectors (wiring is inherently easier to run than plumbing), combined with a potentially low material cost, raises the possibility that they can be used as a building material first, as a PV device second. Further study of the costs and benefits of PV-integrated building skins and products is warranted. If the economics permit, PVs can be used in any number of building component configurations and without an overriding demand for optimal orientation. More detailed study of the construction cost implications combined with new data on PV and balance of systems costs will indicate whether and when these products will become competitive in the construction market.

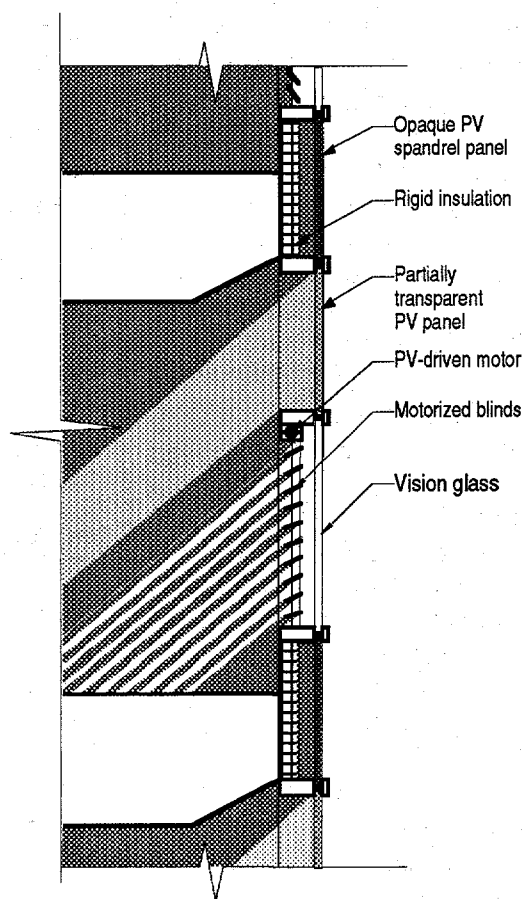


*Fig. 5: PV-integrated window unit with PV-driven motorized blinds.*

Title: Brazilian Rural Electrification Pilot Project

Organization: Siemens Solar Industries (SSI) and Centro de Pesquisas de Energia Eletrica (CEPEL)

Contributors: Bill Howley, Rob Muhn, Antonio Granadero - SSI  
Mauricio Moszkowicz, Luiz Guedes Valente - CEPEL

### **Objective**

To conduct a cooperative joint technology research and development effort to establish and assess the efficiency, operability, and reliability of solar energy based rural electrification in a pilot project in Brazil. In the implementation of this project, CEPEL and NREL will include the cooperation of the states of Ceara and Pernambuco through the state-operated utility companies Companhia Energetica de Ceara (COELCE) and Companhia Energetica de Pernambuco (CELPE), along with the Financing of Studies and Projects Agency (FINEP) and Eletrobras.

### **Approach**

The technology research and development assessment program will consist of two parts. In the first part, NREL will provide equipment to be used in (a) photovoltaic (PV) electric lighting systems to about 200 homes in the Sertao de Sao Francisco region and an additional 150 area lighting systems for the island of Fernando de Noronha in the Brazilian state of Pernambuco; and (b) PV electric lighting systems to about 400 homes, 56 area lighting, and 14 schools in the outback of Ceara. In the second part of the project, an evaluation of the opportunities for a PV-hybrid power system in the fishing village of Jericoacoara, Ceara will be undertaken. This second part is expected to be the subject of a second supply of equipment to CEPEL to provide the necessary key components for this hybrid systems development and demonstration. It is expected that parallel competitive procurements will take place in Brazil, sponsored by the Brazilian entities involved.

NREL is acquiring the appropriate key component equipment from a qualified supplier. Siemens Solar Industries (SSI) has been selected by NREL/DOE to provide the PV modules, batteries, and charge controllers from specifications developed by the project. The subcontract between NREL and SSI provides for the equipment to be supplied by SSI to CEPEL in Rio de Janeiro free of charge. COELCE, CELPE, and CEPEL together are responsible for procuring the balance of system components not provided by NREL and of performing the systems integration, installation, maintenance, and evaluation. COELCE, CELPE, and CEPEL will jointly carry out the implementation and evaluation of the cooperative rural electrification project in Brazil, with the technical collaboration from DOE and NREL. CEPEL will assist NREL, COELCE, and CELPE in the technical evaluation of the program and results reporting.

The program duration is four years, with the installation of the first part of the program to be completed in the first year; it is anticipated that the second part installation for the village of Jericoacoara, Ceara will be defined in the first year and installed in the second year. Following installation, a two-to-three year period of operation, maintenance and performance assessment will be undertaken.



Title: Solar Resource Utility Load Matching Assessment

Organization: Atmospheric Sciences Research Center The University  
at Albany  
State University of New York

Contributors: PI: Richard Perez, co-PI: Ronald Stewart. Other  
Contributors: Robert Seals and Antoine Zelenka

### Objective

To estimate the capability of photovoltaics (PV) to meet the load requirements of electric utilities in the United States based upon insolation data measured by geostationary satellites.

### Approach

This study follows and expands on initial work by the contractor and his colleagues for the New York Power Authority (NYPA) to infer the load matching capability of PV systems with selected northeastern electric utilities. By comparing PV load matching capability estimated from satellite data with that obtained from ground measurements, it was concluded that satellite data can be used to provide a good indication of load carrying capability.

The first task was to confirm these initial conclusions, that is, to confirm, for other US climatic regions, the accuracy of satellite-estimated insolation for the purpose of estimating PV's utility load carrying capability. The second and major task was to estimate the load matching capability of PV for about twenty electric utilities distributed throughout the country, using the satellite-derived data and utility load data for two reference years (1987-88).

### Results and Discussion of Activities completed in FY 92

Task 1 was completed in FY 1992, while the second task is still in progress at the time of this writing. This report presents the findings of the first task.

### METHODS

Climatological vs. Real Data: When evaluating the usefulness of satellites to estimate solar irradiance at the earth surface, it is important to define the needed type of data. Here, we distinguish between (1) climatological data and (2) real data. Climatological data are site-specific but need not be time-specific (e.g., TMY data). Real data are both site and time specific (real-time data are an extreme example of real data). Climatological data may be sufficient to design systems, but not to investigate the interaction between these systems and their intended utilization, if there exists an undetermined relationship between the two: this is the case for PV systems vs. the needs of some electric utilities [1,2]. If a positive relationship exists, PVs may be used in high value peak load reduction applications [3]. However, real insolation data are necessary to characterize and quantify this potential.

Physical vs. End-Use Accuracy: We make a distinction between the satellite's

physical accuracy and its end-use accuracy for a specific task. The physical accuracy is the actual difference between estimated and measured insolation and is benchmarked in terms of mean bias error (MBE) and root mean square error (RMSE). End-use accuracy is task-dependent and is assessed in terms of the error on the end-product of the data analysis. Here, the end product is the load matching capability of PV generation for a given utility.

#### PHYSICAL ACCURACY OF SATELLITE ESTIMATES

Satellite vs. extrapolation from ground measurements: When no insolation data exist for a given site, a common palliative has been to use data from another point, or set of points, where data are available. This approach may be warranted when climatological data are needed, as long as (micro)climatic/environmental differences are small. This is much less true for real data because the time element becomes crucial. A study recently undertaken [4] under the auspices of the International Energy Agency (IEA) dealt specifically with the issue of global irradiance network interpolation/extrapolation. One of its most interesting findings is reported in Fig. 1, where a clearly defined relationship has been established between the extrapolation distance and the resulting RMSE: this increases with the square root of the distance and reaches 20% at 50 km. This trend appears to be universal since it is derived from over 70 measuring station-years in six climatically diverse networks in Switzerland, Germany, Sweden and the northeastern, northwestern and southwestern United States. A similar, although not as readily quantifiable trend, was found for interpolation between stations, with a perceptible but small RMSE reduction when using sophisticated interpolation methods such as kriging [4].

By contrast, the study found that the RMSE of satellite-derived daily global irradiance was of the order of 17-22% for a large number of test sites in Europe, and the US — with a perceptible but overall small dependence on the location, the satellite and on the sophistication of the algorithm [4]. Hence, for real data, satellite-derived insolation becomes preferable to ground extrapolation if distance exceeds 40-50 km.

The IEA results are limited to daily global irradiance. Extrapolation errors are likely to be higher for hourly values since the cause of error, cloud cover inhomogeneities, would no longer be averaged. Our NYPA study [5] showed only a small RMSE increase from a daily to an hourly basis (indeed, the cause of error: determination of turbidity and cloud thickness, is fundamentally different from that of extrapolation and is less affected by the time scale.)

Physical validation of satellite-estimated hourly global direct and tilted irradiance for US sites: We compared satellite-estimated hourly global irradiance, hourly direct irradiance, and simulated PV output, against ground measurements at 6 climatically distinct sites in the US. The test sites are Cape Canaveral, FL (subtropical, humid), Albany, NY (continental, humid), Mesa, AZ, and Carissa Plains, CA (arid), Keystone, CA (semi-arid, mountains) and San Jose, CA (semi-arid/oceanic).

For the satellite we rely on five-to-six global irradiance estimates per day on a 1x1 degree latitude-longitude grid, based on the Justus Tarpley algorithm [6]. Each point is an integrated value of 25 pixels and represents a ground "foot-print" of about 2,500 km<sup>2</sup>. Hourly data are time-extrapolated from these points as explained in [5] and estimates at a specific location are interpo-

lated from the 1x1 grid (extrapolated for coastal sites, since the Justus-Tarpley method is not used over-water). Direct irradiance is further modeled from global [7]. Finally, PV output for a tilted collector is modeled using PVFORM [8]. (Note that ground-reference PV output is also modeled). We point out that this assessment of satellite accuracy is very conservative because: (1) we use the simplest, yet effective, satellite algorithm (the only routinely processed in the US), (2) we rely on time/space inter/extrapolation, (3) we model direct from global, amplifying any error.

Results confirm the preliminary IEA findings for global irradiance: negligible MBE; RMSE ranging from 16% in California to 26% in New York. The scatter is considerably stronger for direct irradiance: while MBEs remain reasonable ( $\pm 10\%$ ), RMSEs are in the 30-50% range. Interestingly, the simulated tilted PV output is little affected by the noise in the direct component: the MBE and RMSE of simulated PV are comparable to that of global irradiance (see Fig. 2). This is because for south facing collectors, any error on the direct tends to be compensated by an opposite error in the anisotropic diffuse component.

#### EFFECTIVE "END-USE" ACCURACY OF SATELLITE-DERIVED INSOLATION FOR INVESTIGATING PHOTOVOLTAIC INTERACTION WITH ELECTRIC UTILITIES

In the second task we use a set of benchmarks to quantify the peak load matching capability of non-dispatchable generating sources (e.g., [1,2]). These benchmarks may be derived from the analysis of time-coincident utility load data and power plant output data. Here, we focus our attention on the accuracy achieved by the satellite for the two most critical benchmarks. The first benchmark is statistical, while the second represents an absolute worst case measure of the PV resource's ability to meet electrical demand.

1. The resource's effective load carrying capability (ELCC) defined as the effective increase in the utility's available capacity due to the added PV resource. If the resource is able to meet all the utility's high loads its ELCC will approach 100%.
2. The minimum buffer energy storage (BUFF), needed to guarantee that the resource will meet all loads above a given threshold. The BUFF is estimated in relation to the total energy storage (TES) that would be needed to meet the same goal in the absence of the PV resource. For an ideally peaking resource,  $BUFF = 0$ . For a resource with no load matching potential,  $BUFF = TES$ .

Our initial study [5] had concluded that the error between satellite and ground-derived benchmarks was not considerable. Here, we extend this evaluation to other climates/utilities, including Florida (Florida Power and Light — FPL), Arizona (Salt River Project — SRP) and California, (Pacific Gas and Electric — PG&E). In each case results are based on two years (1987-88) of ground insolation and satellite data and utility hourly load data.

Figure 3 illustrates the variations of PV's ELCC for each utility in relation to the resource's grid penetration, as derived from both ground insolation data and satellite data. (Note that, in each case, PV's ELCC is much higher than PV's capacity factor — of the order of 20-25% — indicating that PV can effectively contribute to meeting utility peak loads, particularly at low penetration levels). However, the point we want to stress here is the good agreement between satellite and ground derived ELCCs, which confirms and even

strengthen the NYPA findings. In Fig. 4, we compare satellite vs. ground-estimated BUFF requirements for each utility; (note that BUFFs are considerably smaller than TESs). As above, we stress the remarkable agreement between satellite and ground derived BUFF relatively to TES.

## CONCLUSIONS

This study confirms, on a multi-climatic North American scale, the key results of a localized preliminary study [5] while making constructive use of the results of a comprehensive IEA task [4]. These results are:

- (1) the physical accuracy of satellite-derived hourly global irradiance or fixed-tilt south facing irradiance is of the order of 20-25% RMSE and negligible MBE, making the satellite more suitable to real data acquisition than extrapolation beyond 50 km of a ground station.
- (2) Satellite-derived insolation is an effective means of assessing the potential of PV generation in relation to the needs of electric utilities for places with little access to ground data.

Finally, we stress that these results are conservative with respect to the ultimate capabilities of the satellite. Three avenues for future improvement are: (a) higher resolution on-board sensors, (b) combination of satellite for spatial coverage and ground networks for real-time local satellite calibration and (c) stochastic and/or physical improvement of algorithms.

Acknowledgement: This NREL-supported effort (# XR-1111-681) makes effective use of a recently completed IEA Task (Solar Heating and Cooling Program Task 9, subtask 9) supported among others by the Swiss Federal Office of Energy, NYPA and the USDOE. Collaboration with A. Zelenka (leader, IEA subtask 9D) was possible thanks to support from the Mobil Foundation. We thank D. Tarpley of NOAA-NESDIS for providing the satellite data, and T. Hoff, H. Wenger (PG&E), E. Palomino (SRP), L. Greene (FPL), K. Collier (FSEC), J. Bigger (EPRI) and R. Taylor (NREL) for their assistance in obtaining irradiance and utility load data.

## REFERENCE

1. Hoff, T. (1987): Calculating Photovoltaic Value: A Utility Perspective. Proc. 19th IEEE PV Specialists Conference.
2. Perez, R. et al. (1989): PV Load Matching Potential for Metropolitan Utilities and Large Commercial Users..., 9 pp. Proc. 9th European PV Conference, Freiburg, Germany.
3. Wenger H. et al. (1992): PV as DSM Option: Benefits of a Utility-Customer Partnership. World Energy Engineering Congress, Atlanta, GA
4. Zelenka et al., (1992): Rept. of International Energy Agency SHCP Task 9 subtask 9D. IEA, Paris, France
5. Perez, R. et al., (1991): Meeting Utility Load Requirements with Photovoltaics. Proc. ISES World Congress, Denver, Colorado. 6 pp.
6. Justus, C., et al. (1986): Satellite-Measured Insolation Data in the US and Mexico. Remote Sensing Env. 20, pp. 57-83.
7. Perez, R., et al., (1992): Dynamic Global- to-Direct Irradiance Conversion Models. ASHRAE Transactions-Research Series, pp. 354-369
8. Menicucci, D. F. et al., (1988): User's Manual for PVFORM. Report # SAND85-0376-UC-276. Sandia Natl. Labs, Albuquerque, NM.

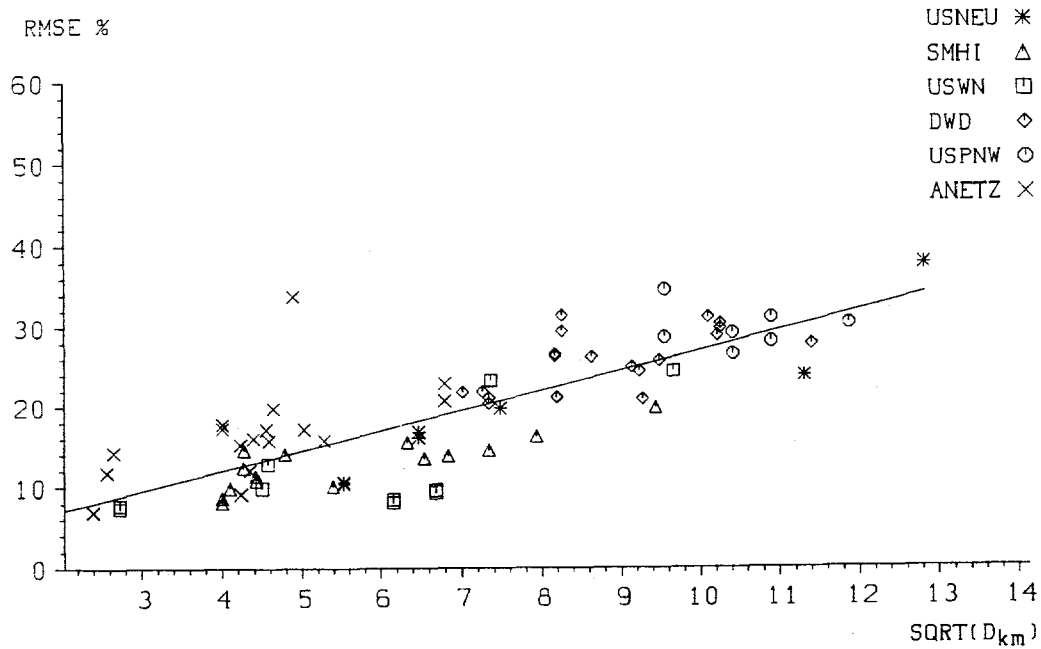


**Figure 1:** Relative RMSE of extrapolation (%), as a function of distance from measuring station (from [4])

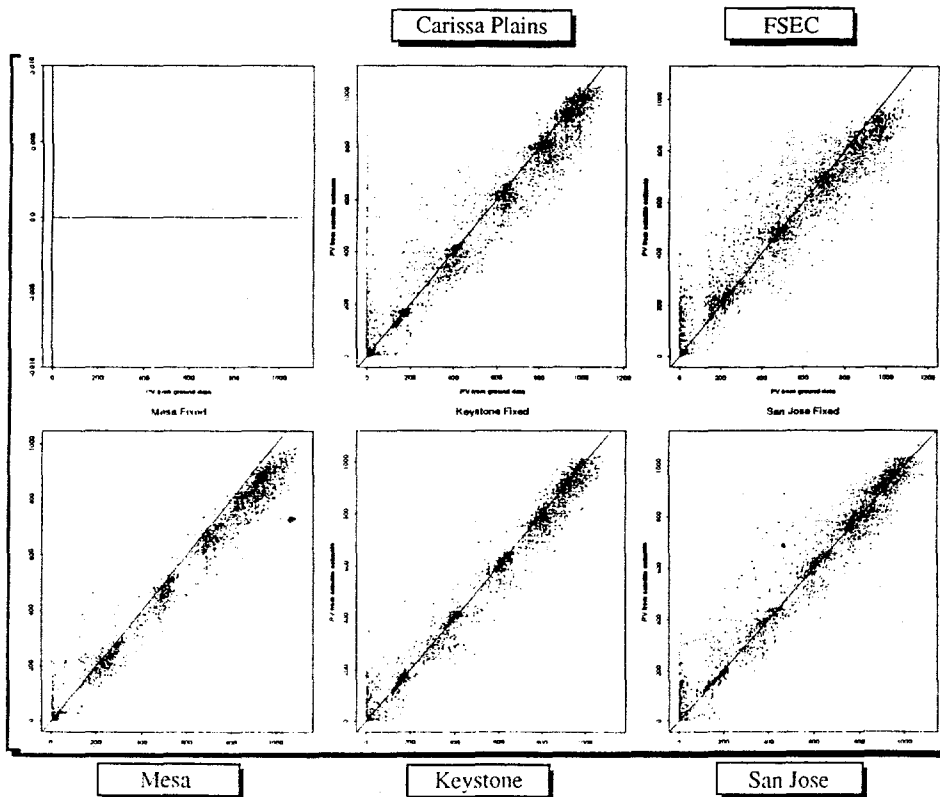


**Figure 2:** Satellite-derived hourly PV output on a fixed-tilt (Y-axis) vs. ground-based values (X-axis)

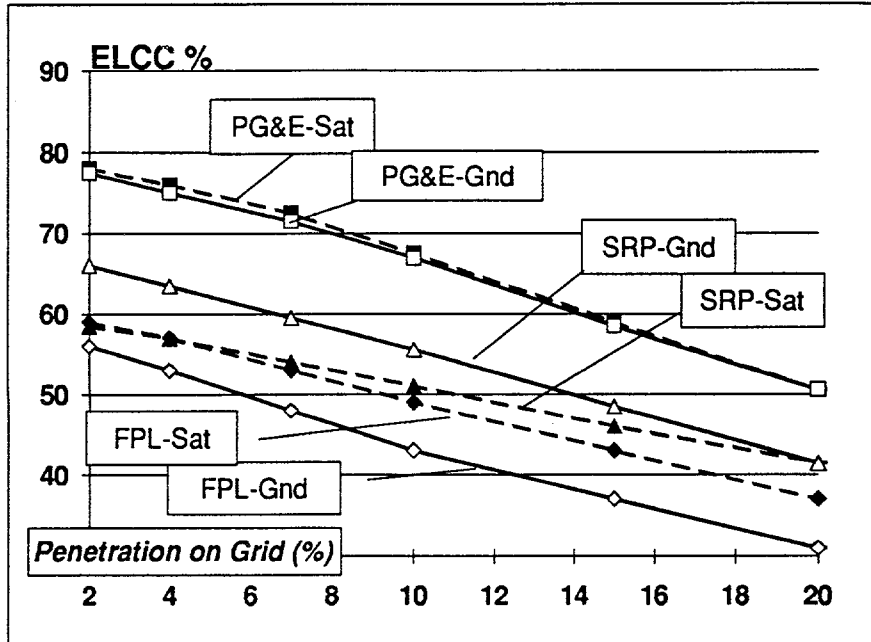


**Figure 3:** Comparison between ground (-Gnd) and satellite-derived (-Sat) ELCC of PV power generation (2-axis tracking) for three US electric utilities as a function of PV grid penetration

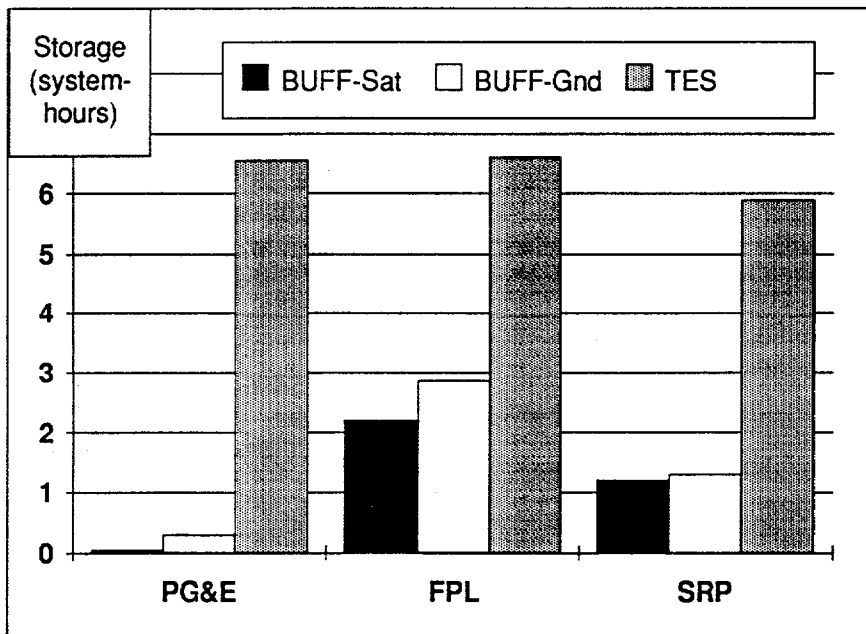


**Figure 4:** Comparison between ground and satellite-derived PV buffer energy storage (MBES) in relation to TES to guaranty a utility peak load reduction of 15%

**Title:** Evaluation of DSM Incentive Opportunities for Photovoltaics

**Organization:** Center for Energy and Urban Policy Research, University of Delaware, Newark, DE 19716

**Contributors:** John Byrne, Principal investigator; Young-Doo Wang and Steven S. Hegedus, investigators; Ralph M. Nigro, project engineer, Delmarva Power; Constantine Hadjilambrinos, C.R. Thulasi Kumar, In-Whan Jung, Bo Shen, Subodh Wagle and Chandrasekhar Govindarajalu, graduate students

## **OBJECTIVES**

The primary objectives of this research have been:

- To evaluate existing residential, commercial and industrial DSM programs with regard to incentive levels and utility avoided costs;
- To analyze the interactions between incentive programs, avoided costs and regulatory influences;
- To describe the role PV could play in residential and commercial DSM programs including the likely incentive levels and the leading utilities and states that could be approached for implementation; and
- To evaluate the technical feasibility of PV-assisted operation as a load reduction strategy equivalent to one commonly used by U.S. utilities in their direct load control (DLC) programs.

## **APPROACH**

To achieve the objectives, the following four tasks have been pursued:

- Task 1: In this task we developed a data base of electric utility DSM incentive programs offered to all customer sectors. The analysis concentrated on 21 utilities that have significant experience with DSM programs.
- Task 2: We analyzed the data collected in Task 1 to estimate an empirical relationship between rebate levels offered by utility DSM programs and electricity (kW) savings using a multivariate approach.
- Task 3: In Task 3 we identified the end-uses which are the most attractive targets for PV-DSM applications. A levelized net present value approach was adopted to perform an economic feasibility test.
- Task 4: A test program for PV-DSM was designed that are consistent with the structure of existing DLC incentive programs in the service territory of Delmarva Power. Testing took place at the University of Delaware's Solar One House in Newark from July through September 1992.

## RESULTS

The following is a review of major results on a task-by-task basis:

### Task 1: Existing DSM Incentive Programs

The 21 utilities analyzed for this research administered 78 different rebate programs in 1991. These programs included end-uses of all types in the residential, commercial and industrial sectors. Most of the residential rebate programs targeted both efficiency improvement and load management involving air conditioning and water heating. Commercial and industrial programs were concentrated in lighting, air conditioning/HVAC, and thermal storage.

The range of rebate values per kW was very broad, varying from \$50 per kW to over \$800 per kW. For individual programs, the total avoided capacity also ranged widely, from ones which saved less than 100 kW to a program with a 1991 savings of 71,500 kW. Considerable variation in pricing existed for several program categories; thus, commercial HVAC rebates extended from \$75 to \$700 and residential water heating rebates varied from \$150 to \$1,500.

### Task 2: DSM Rebate Market: Utility Demand for kW Saved

In the DSM market, rebates represent the prices which utilities are willing to pay customers to encourage their investment in end use efficiency. The upper limit of DSM rebates is set by the cost of buying back capacity from customers compared to generation and purchase power options available to a utility. In this market, demand is typically for kW reductions by utilities during peak periods and the offering price is equal to the rebate amount expressed in \$ per kW saved. The results of a demand analysis performed for this project suggest that the price (rebate) elasticity of demand (kW saved) remained near unity (-1.06) as shown in Figure 1. This indicates that utilities are sensitive to rebate levels in their procurement decisions of peak power (kW saved).

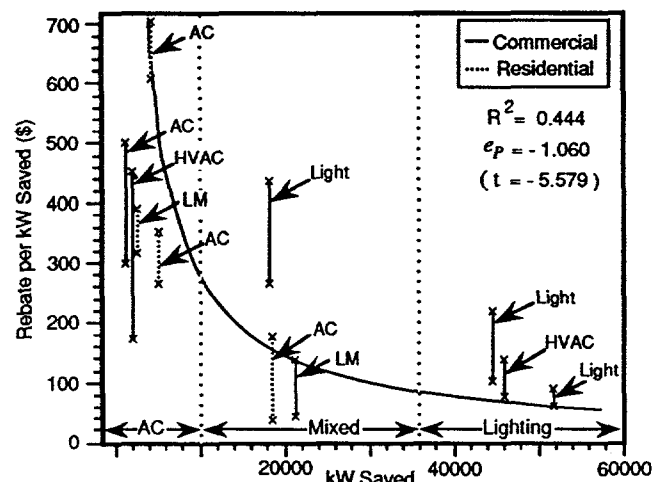


Figure 1. Demand for kW Saved by End-Use

A multivariate analysis was performed to estimate which variables best predicted utility demand for avoided capacity through rebate offers. The effects of utility size (expressed both in operation capacity and sales), fuel mix in generation, financial position (whether there was



surplus or deficit in the utility's net income), SO<sub>2</sub> emissions, regulatory environment (based on an index of DSM cost treatment in state regulation), rebate levels, and rate structure were investigated. The statistically significant predictors were found to be the rebate amount and regulatory environment. SO<sub>2</sub> emissions were the next most efficient predictor, but this variable's impact was found to be statistically insignificant.

### **Task 3: Cost-Effective End-Use Targets for PV-DSM Market**

As shown in Figure 1, the DSM market has two distinguishable segments: one segment mainly involves lighting programs with relatively low rebates (\$100 to \$200) directed exclusively to the commercial and industrial sectors; and the other segment is dominated by programs aimed at reducing peak loads presented by residential and commercial air conditioners (including residential DLC programs) with relatively high rebates (\$200 to \$500). The rebate per kW saved is tantamount to the costs incurred by utilities from acquiring 1 kW of capacity power from the DSM programs, which include incentive payments to customers, equipment costs and other administrative costs. The DLC costs for water heating and air conditioning (LM in the Figure) typically range from \$300 to \$400 per kW saved. These devices belong to the higher rebate range utilities are willing to pay. DSM options in a market segment where utilities are willing to pay higher rebates for avoided power loads enhance PV applicability.

A utility-customer partnership is important for PV-DSM programs to maximize the economic value to the utility and customer, creating a condition in which cost-effective PV-DSM programs could be obtained. Preliminary financial analyses were conducted on the basis of a partnership arrangement in which the utility was assumed to contribute \$300 for PV system costs and the customer would pay \$150 for installation costs of a 50-watt array that would be designed to operate as a DLC device on a residential water heater. The utility's assumed contribution of \$300 is within the domain of incentives currently offered by utilities, particularly in the residential sector.

The preliminary financial analyses of the cost of the PV-DLC water heater program for the Delmarva Power service area suggested that such a program could be competitive with the present DLC program operated by the utility, and its most attractive current supply option of a simple-cycle gas-fired combustion turbine. Levelized present values of revenue requirements (PVRR) were computed for each of these options. Delmarva Power is allowed to include the capital costs of the water heater DLC program in its rate base. This analysis assumes that the same treatment would be allowed for a water heater PV-DLC program. The levelized PVRRs for the water heater DLC program and a gas-fired combustion turbine are \$176 and \$172/kW-Yr, respectively. As a comparison, the levelized PVRR for a PV-DSM water heater program is \$187/kW-Yr. The economics of PV as a DSM tool could be sufficiently attractive to encourage utility interest.

### **Task 4: Technical Feasibility: Solar One House Experiment**

A PV-DLC program for hot water heaters is intended to achieve the same results as the existing water heater DLC program by not only deterring their "on" cycle but also lengthening their "off" cycle during peak periods. The PV array is designed to be connected to heating elements in the customers' hot water tanks to offset heat losses during low hot water demand periods, equivalent to DLC periods. In a PV-DLC system for air conditioning, the circulation fan could

be switched over to a PV power source. Since the circulating fan would run continuously rather than only on thermostat demand, comfort levels in the house might be maintained slightly longer during condensing unit interruptions. The utility would benefit because this would allow the condensing unit "off" cycle to be lengthened, while also shedding the load of the circulating fan.

A test program, in cooperation with Delmarva Power, has been conducted to determine technical feasibilities of both water heater and air conditioning PV-DLC programs. Testing took place at the University of Delaware's Solar One House in Newark from July through September 1992. Preliminary results from the performance data collected under realistic conditions of Delmarva Power's DLC programs indicate that both PV-DLC programs are technically feasible and it would be worthwhile to explore their use as options for existing DLC programs.

## CONCLUSIONS

While it has been recognized that the utility market is the most promising for solar technologies (DOE, 1991), the present cost of photovoltaics (PV) as a generation option is too expensive to stimulate much interest by either electric utilities or state regulatory authorities. PV system costs are currently in the range of 25 to 50¢ per kWh compared to current peak power costs of between 8 to 13¢ per kWh (DOE, 1991). For PV to play an important role in the utility sector at its present price, the best possibility is to penetrate the demand-side management (DSM) markets, functioning as a load management device. The availability and extent of tax benefits, such as exemptions and credits for investment in solar technologies, is a crucial factor in determining the competitive position of PV technology in the DSM market. Perhaps even more critical is the creation of an environment which would allow solar technologies to be routinely evaluated as a DSM option in integrated resource planning (IRP) and DSM plans.

## PUBLICATIONS

More detailed information can be obtained from the following publications which have directly resulted from our NREL-funded research under subcontract, XR-2-11248-1, from October 1991 through September 1992:

1. John Byrne, Young-Doo Wang, Ralph Nigro and Thulasi Kumar. 1992. "Application of Photovoltaic Technology as an Option of Utility Direct Load Control." *Public Utility Fortnightly* (Forthcoming).
2. John Byrne and Constantine Hadjilambrinos. 1992. "DSM Technologies." *1993 ASES White Paper: Progress in Solar Energy Technologies and Applications*. American Solar Energy Society (Forthcoming).
3. John Byrne and Ralph M. Nigro. 1992. *Applying Photovoltaics as A Demand-Side Tool*. Presented at The Delmarva Photovoltaics Conference. October.
4. John Byrne, Constantine Hadjilambrinos and Young-Doo Wang. 1992. "The Role of PV in Demand-Side management: Policy and Industry Challenges." *Proceedings of the 11th Photovoltaic Advanced Research and Development Project Review Meeting*. American Institute of Physics.
5. John Byrne, Constantine Hadjilambrinos, Young-Doo Wang and Ralph M. Nigro. 1992. "An Evaluation of Photovoltaics As a Utility Demand-Side Option in the U.S. Buildings Sector." Presented at the ASHRAE 1992 Annual Meeting, Baltimore MD. June.

**Title:** Risk-Adjusted IRP Procedures: Reflecting the True Costs of Conventional and Solar Options

**Organization:** Finance Department, University of Massachusetts Lowell, Massachusetts

**Contributors:** Shimon Awerbuch, Ph.D., principal investigator

## **Objectives**

This report suggests analytic tools that will improve the quality of decisions made by electric utilities in the Integrated Resource Planning (IRP) Process. It builds on, and extends the widely used revenue requirements method (RRM) to include financial risk considerations for various investments. The report recommends that the RRM not be abandoned but, rather, be enhanced so that it reflects the different levels of expected financial-risk exhibited by alternative resource projects. The procedures are illustrated with a set of illustrative, risk-adjusted, levelized kWh costs for three technologies: coal-fired steam, gas/combined cycle and photovoltaics (PV). In addition to its focus on risk measurement in IRP, the report suggests that overheads, as well as other, less quantifiable costs need to be included in the process.

The report does not advocate that regulated firms undertake unprofitable projects because they are socially desirable. To the contrary-- all of its recommendations are consistent with modern finance theory and its focus on the maximization of investor wealth. The report dispels the notion that only projects with returns in excess of the weighted average cost of capital (WACC) are acceptable. This incorrect notion leads utilities to needlessly reject sound, low-risk, projects thereby needlessly depriving themselves of profit opportunities.

The report recommends that public utility commissions require utilities to reflect differences in financial risk exhibited by alternative capacity choices. This would be done by abandoning the widespread use of the WACC as the singular project hurdle rate. In so doing commissions would recognize that one of the principal inputs of conventional generation, fossil fuels, are commodities whose price cannot be reliably projected over a long period. This means that utilities and regulators need to rely less on fuel price forecasts and more on developing diversified portfolios of generating assets that can perform well under a variety of economic conditions.

## **Background: The Revenue Requirements Method**

Utilities use standard capital budgeting techniques which have changed little since their introduction 40 years ago. That era was marked by a regulatory environment that reflected i) a strong monopoly with low price elasticities of demand coupled with ii) a rather limited menu of fossil-based generating options whose cost and risk properties were quite similar.

In contrast, today's environment is marked by: i) weakened monopoly, ii) a diverse range of

resource options, and, iii) a diverse range of institutional and business options that includes Independent Power Producers (IPP). While the RRM may have worked in the environment of the 1950's it is no longer good enough.

The state-of-the art in project evaluation has also changed over the last three decades, with significant advances in investment analysis and capital theory including the development of the capital asset pricing model (CAPM) and portfolio and options theory. Yet these standard financial techniques have not found their way into utilities' evaluation of capacity additions. In addition, there have been radical advances in cost accounting, performance measurement and manufacturing theory, including better understanding of the benefits of new technology in the production process. These advances can all play a significant role in the IRP process. Public Utility Commissions should require utilities to use state-of-the-art techniques to evaluate resource alternatives.

### **The Problem: IRP Uses Cash Outflows-- Not Net Cash Flows**

The RRM differs from standard Discounted Cash Flow (DCF) project evaluation techniques in one important respect. The DCF technique deals with net cash flows, while the RRM looks only at outflows, the so called 'revenue requirements'. Planners generally select projects with the lowest present worth revenue requirements thereby hoping to minimize rates. It is incorrect to use a discount rate associated with net cash flows to discount the revenue requirements. The WACC is such a discount rate; its use is further invalidated on the basis that it represents the average risk of the firm and not the specific project risk.

Generally, the correct discount rate for any project is its opportunity cost which can be defined in the usual manner as **the rate that could be earned if the funds were invested in another project of similar risk**. Estimating the discount rate therefore involves estimating the risk of a particular project opportunity. Although the WACC "rule-of-thumb" may have sufficed at one time, the crude approximations it yields are not sufficiently refined to provide useful decision support in the case of complex and highly diverse project alternatives. WACC is inappropriate for the revenue requirements under most circumstances because only rarely will it reflect risk correctly.

In an unregulated setting, the WACC can be used for projects whose risk is similar to the overall risk of the firm. However, in IRP, with its focus on the revenue requirements, the WACC doesn't work. The inappropriateness of the WACC as a discount for project outflows is quite settled in the literature and, although not widely recognized, is not a new argument.

### **Recommendations: The Importance of Risk-Adjustment**

Given the range of technological and institutional options available we need to pay closer attention to the discount rate used in the IRP process. The current WACC approach is inherently biased against capital-intensive solar and renewable technologies. It prefers fuel-intensive technologies with low capital and high operating costs.

This report argues that such a bias is not accidental, but is driven largely by the presence of automatic fuel adjustment mechanisms which distort the risks perceived by utilities. Since fuel price variation is largely passed through to customers, it becomes a risk factor that utilities have been able to ignore. This is economically inefficient since customers have considerably less control over the fuel outlays than does the company.

When risky fuel outlays are discounted at a high rate, such as the WACC, their estimated present value is biased downward. Generally, the WACC is too high a discount rate for all but the very *safest* revenue requirements. Its use therefore masks the riskiness of volatile fuel outlays, for example, while overstating the riskiness of the outflows associated with capital. This has the effect of making low-capital/high-fuel investments seem more attractive.

The risk-adjusted discounting procedures described in this report involve grouping the revenue requirements into risk categories and discounting each category by its own, appropriate risk-adjusted discount rate. This differs from the usual RRM practice of discounts all revenue requirements by the WACC. The risk categories used are:

- i) Riskless Cash Flows-- this category consists primarily of the tax shields associated with depreciation and interest deductions;
- ii) Debt-Equivalent Cash Flows-- these outflows include the relatively fixed outlays such as those for property taxes, insurance, fixed O&M, etc. These are presumed to have risk levels similar to the bond interest payments made by the firm.
- iii) Counter-Cyclical (Risky) outflows-- these outflows consist primarily of the fuel outlays, which will generally covary negatively with the stock market or the economy. The cash flow beta estimates for fuel range from -0.25 for coal to about -1.2 for gas and oil. This suggests a discount rate for these outflows in the range of 0.0% to about 4.0% (nominal).
- iv) Cyclical Outflows: This category consists of variable O&M and other expenses which move cyclically.

## Results and Recommendations

Several illustrative risk-adjusted results are developed in the report, using base-case assumptions and data provided the NARUC (National Association of Regulated Utility Commissioners) Finance and Technology Committee. The risk-adjusted kWh costs for coal and gas-based alternatives are higher than the NARUC results-- an outcome that is largely driven by the inclusion of fuel-price risk. The risk-adjusted results can be interpreted as the levelized operating and maintenance costs, plus a guaranteed 30-year price (per kWh) for fuel. This guaranteed price is that stream of annual prices that would have to be pre-specified (agreed to in advance) in order to induce a fuel supplier to deliver the necessary fuel every

year for 30-years without the prospect of reneing or re-negotiation of any sort. The results are summarized below:

NARUC Base-Case vs. Illustrative Risk-Adjusted Results		
TECHNOLOGY	LEVELIZED COST (\$/kWh)	
	NARUC	RISK ADJUSTED
Coal-Fired Steam	\$.077	\$.095
Coal-Fired Steam-AFUDC Adjusted	.082 <sup>a</sup>	.097
Coal-Fired Steam-Carbon Tax in place	---	.128
Combined Cycle (High Fuel Price Risk)	.083	.262
Combined Cycle (Moderate Risk)	.083	.150
Photovoltaics	.246	.207

a. This value is calculated in the report.

There are three additional principal cost areas that affect generation costs: i) flexibility and reversibility, ii) overhead utilization, iii) option values. These cost considerations suggest that if all costs were measured and included, IRP should favor capacity that is flexible and reversible and can be installed with short lead-times over "lumpy" central station capacity. These objectives serve to reduce cost by matching supply with demand continually-- costs are not minimized when even the cheapest kWh units are produced unnecessarily, or the cheapest capacity is idle.

Quantitative flexibility and reversibility measures are not easily applied and must be dealt with qualitatively. By the same token, mathematical measures of risk and overhead utilization are sufficiently developed and can be directly applied to the IRP process. The Report's final recommendations suggest that in evaluating resource alternatives utilities use techniques consistent with state-of-the-art financial and project evaluation techniques which recognize:

- a) Risk differentials among competing alternatives; such risk differentials should typically be reflected through correct discounting procedures.
- b) Other quantitative and qualitative factors that mitigate project risk such as investment modularity, flexibility or reversibility.
- c) The extent to which project alternatives utilize the overhead resources of the firm.
- d) The growth and technology options that may be created for the firm with the adoption of particular technologies.
- e) The extent to which particular fuel and technology choices contribute to the overall cost and risk of the portfolio of generating assets.

Contractor, Principal Investigator, Address	Work Title (Research Activity)	Contract Number	Total Funding (\$K)	FY 1992 Funding (\$K)	Start/End Dates
<u>AMORPHOUS SILICON FY1992</u>					
APS J. McNeil Princeton, NJ 08542	Stable Hi-Eff. a-Si Multijunction Modules	2-11091-1	695.3	695.3	1/91 9/94
Colo School of Mines D. Williamson Golden, CO 80401	Microcrystalline Silicon by Remote Plasma-Enhanced CVD	1-10063-3	143.6	73.0	2/91 1/94
Harvard Harvard R. Gordon Cambridge, MA 02138	Optimization of transparent & Reflecting Films for a-Si Solar Cells	1-11032-1	379.9	67.0	5/91 10/93
Iowa State Univ. V. Dalal Ames, IA 50011	Comprehensive Research on Stability & Electronic Properties of a-Si:H & a-SiGe:H Alloys	1-10063-8	409.3	159.0	3/91 5/94
National Institute of Standards & Tech. A. Gallagher Boulder, CO 80303	Growth Mechanisms & Characterization of a-Si:H Alloy Films	1-11001-1	207.0	87.0	1/91 1/94
Penn. St. Univ R. Collins Univ. Park, PA 16801	In-Situ Characterization of Growth & Interfaces In a-Si Devices	1-10063-10	160.0	60.0	4/91 4/94
Solarex Corp. R. Araya Newtown, PA 18940	Stable Hi-Eff. a-Si Multijunction Modules	0-19033-1	2633.3	534.0	5/90 6/93
Syracuse Univ E. Schiff Syracuse, NY 13244	Research on Defects & Transport to a-Si Based Semiconductors	1-10063-7	121.2	52.0	2/91 4/94
Univ. Delaware-IEC S. Heggadus Newark, DE 19716	Stable Hi-Eff. a-Si Based Solar Cells with Low Hydrogen Content	1-10063-4	667.9	300.0	3/91 4/94
Univ. North Carolina M. Silver Chapel Hill, NC 27599	Recombination & Metastability in a-Si & Si Ge Alloys	1-10063-5	186.8	95.9	2/91 1/94
Univ. of Illinois J. Abelson/N. Maley Champaign, IL 61820	Research on Silicon-Carbon Alloys and Interfaces	1-10063-6	116.0	490.0	2/91 1/94

Contractor, Principal Investigator, Address	Work Title (Research Activity)	Contract Number	Total Funding (\$K)	FY 1992 Funding (\$K)	Start/End Dates
Univ. of Oregon J. Cohen Eugene, OR 97403	Origin of Metastable Light-Induced Changes in a-Si:H	1-10063-1	213.9	107.6	2/91 1/94
United Solar Sys S. Guha Troy, MI 48084	Hi-Eff. Multigap Multijunction a-Si Based Submodules	1-19033-2	1,871.0	349.7	1/91 2/94
Univ. Cal/L.A. E. Johnson Los Angeles, CA 90024	Charge Transport Meas. in Hydrogenated a-Si by Photoconductive Frequency Mixing	2-12201-1	12.5	12.5	6/92 9/92
Xerox Corporation R. Street 3333 Coyote Hill Rd. Palo Alto, CA 94304	Stability, Electronic & Structural Properties of a-Si Silicon Alloys	1-10063-9	281.0	81.0	06/91 5/94
POLYCRYSTALLINE THIN FILMS FY1992					
Astropower, Inc. J. Rand Newark, DE 19711	Dev. of Large-Area Monolithically Integrated Si-Film PV Devices	1-11064-1	898.3	485.6	5/91 2/94
The Boeing Company A. Witzel Seattle, WA 98124	Poly CuGaInSe <sub>2</sub> Thin Films Solar Cells	1-19019-6	242.1	92.0	5/91 5/94
Colorado State Univ. J. Sites Fort Collins, CO 80523	Role of Polycrystallinity in CdTe & CuInSe <sub>2</sub>	0-10046-1	209.0	49.0	4/90 5/93
Colorado School of Mines J. Trefny Golden, CO 80401	CdTe Solar Cells Fabricated by Electro Deposition	2-11036-4	142.0	142.0	3/92 5/95
Energy PV, Inc. (EPV) A. Delahoy Monmouth Jct. NJ 08852	Ultra-thin CIS Devices of Non-HSe	2-12051-1	419.9	419.9	3/92 2/95
Georgia Tech. A. Rohatgi Atlanta, GA 30332	Hi-Eff. CdTe & ZnTe Thin Film Cells	2-11036-3	140.0	140.0	2/92 1/95
ISET V. Kapur Inglewood, CA 90301	Hi-Eff. Thin Film Fabrication CuInSe <sub>2</sub>	0-19019-2	1118.4	350.0	7/90 5/94



Contractor, Principal Investigator, Address	Work Title (Research Activity)	Contract Number	Total Funding (\$K)	FY 1992 Funding (\$K)	Start/End Dates
Martin Marietta M. Misra Denver, CO 80201	Sputtering Techniques for CIS and CdTe Modules	1-11070-1	545.6	150.0	9/91 11/93
Photon Energy (Golden Photon) S. Albright El Paso, TX 79924	Hi-Eff. Large Area CdTe & CdHgTe Panels	0-19019-3	1360.3	699.9	6/90 8/93
Univ. Colorado A. Hermann Boulder, CO 80309	Novel Thin Film CuInSe <sub>2</sub> Fabrication	0-10012-1	105.4	20.0	3/90 10/92
Univ. Delaware R. Birkmire Newark, DE 19716	Polycrystalline Thin Film Materials & Devices	0-10023-1	1742.7	515.0	5/91 2/94
Univ. of S. Florida D. Morel Tampa, FL 33620	Thin Film CdTe, ZnTe, & Hg <sub>1-x</sub> Zn <sub>x</sub> Te Solar Cells	2-11036-1	134.8	134.8	3/92 5/92
Purdue Univ. R. Schwartz W. Lafayette, In 47907	Dev. of Computer Model For Poly Thin Film CuInSe <sub>2</sub> & CdTe Solar Cells	2-11036-2	79.9	79.9	3/92 2/95
Siemens Solar Kim Mitchell Camarillo, CA 93011	CuInSe <sub>2</sub> Modules	1-19019-5	1067.0	367.0	5/91 6/94
Solar Cells Inc. P. Meyers Toledo, OH 43615	Fabrication of Stable Large Area Thin film CdTe PV Modules	1-11059-1	673.3	275.0	5/91 6/94
Solarex R. Arya Newtown, PA 18940	Poly Submodules Based on CuInSe <sub>2</sub> Materials	1-19019-4	1196.0	271.0	11/90 12/93
University of Toledo A. Compaan Toledo, OH 43606	Thin Film Cadmium Telluride Photovoltaic Cells	1-19019-3	412.5	127.0	7/90 1/94
Washington State Univ. L. Olsen Pulman, WA 99164	Investigation of Polycrystalline TF CuInSe <sub>2</sub> Solar Cells Based on ZnSe Windows	2-11036-6	95.0	95.0	2/92 2/95

Contractor, Principal Investigator, Address	Work Title (Research Activity)	Contract Number	Total Funding (\$K)	FY 1992 Funding (\$K)	Start/End Dates
CRYSTALLINE SILICON MATERIALS RESEARCH FY1992					
Duke Univ. U. Goesele Dept. of Mech. Engin. Durham, NC 27706	Point Defects & Their Influence on Solar Cell Related Elec. Properties of Crystalline Silicon	81809701	288.6	44.9	7/88 9/90
Georgia Tech A. Rohatgi Atlanta, GA 30332	Impurity Characterization Support for Silicon	01914501	174.8	30.0	10/89 10/91
N. Carolina St. Univ. G. Lucovsky Box 7214 Raleigh, NC 27695	Microcrystalline Silicon by Remote Plasma-Enhanced CVD	1-10063-2	132999	63.0	2/91 2/94
Suny/Albany J. Corbett Albany, NY 12201	Passivation & Gettering in Solar Cell Silicon	8189703	363.3	57.4	7/88 10/91
Univ. of Southern CA S. Forrest University Park Los Angeles, CA 90089	Electric Characterization Support for Crystalline Silicon	81815401	45.3	19.6	10/88 11/91
ADVANCED HIGH EFFICIENCY FY1992					
Boeing Aerospace B. Stanbery Seattle, WA 98124	New Plasma Source of Hydrides for Epitaxial Growth	1-19142-8	201.5	63.5	4/91 10/92
Colo. State Univ. G. Collins Ft. Collins, Co 80523	Arsine & Hydride Radical Generation for MOCVD Growth	0-19142-9	205.5	60.0	7/90 7/93
Kopin Corp. R. Gale Taunton, MA 02980	Hi-Eff. Thin-Film Solar Cells	0-19142-4	684.5	87.0	7/90 8/93
Purdue Res Found M. Lundstrom W. Lafayette, IN 47907	New III-V Cell Design Approaches for Very High Eff. Cells	0-19142-1	448.7	50.0	8/90 9/93
Rensselaer Ghandhi/Borrenco Troy, NY 12180	MOCVD Crystal Growth	0-19142-10	251.7	100.8	7/90 5/93

Contractor, Principal Investigator, Address	Work Title (Research Activity)	Contract Number	Total Funding (\$K)	FY 1992 Funding (\$K)	Start/End Dates
R.T.I. S. Ghandhi Troy, NY 12180	Materials & structure for Ultra-High-Efficiency Solar Cells	0-19142-3	242.5	44.0	6/90 8/93
Spire Corp. S. Vernon Bedford, MA 01730	GaAs Based Ternary Compounds & Multibandgap Solar Cell Research	0-19142-7	538.5	63.0	8/90 10/93
Univ. S. Cal P. Dapkus Los Angeles, CA	Atomic Layer Epitaxy for Low Temperature Growth of PV Materials	0-19142-6	376.7	70.0	7/90 8/93
Univ. of Utah M. Delong Salt Lake City, UT	Photoluminescence Studies of GaInP <sub>2</sub>	2-12121-1	40.0	40.0	4/92 3/93
VS Corp. J. Werthan Palo Alto, Ca 94303	Metalorganic Vapor Phase Epitaxial Growth of AlGaAs/GaAs GaSGa	1-11095-1	242.3	46.0	5/91 6/93
NEW IDEAS FY1992					
Res. Triangle Inst. M. Timmons R.T.I.	An Inverted AlGaAs/GaAs Patterned Tunnel Junction Cascade Concentrator Cell	0-18110-2	198.1	98.1	1/90 2/92
Univ. of Delaware R. Birkmire Newark, DE 19716	Novel Ways of Depositing ZnTe Films by a Solution Growth Technique	0-18110-1	200.0	100.0	1/90 1/92
Univ. of S. California D. Dapkus Los Angeles, CA 90089	High Efficiency Epitaxial Optical Reflector Cells	0-18110-3	94.8	94.8	1/90 2/91
UNIVERSITY PARTICIPATION PROGRAM FY1992					
No. Carolina St. Univ. S. Bedair Box 7003 Raleigh, NC 27695	New Approaches to Hi-Eff. Solar Cells by MOCVD	9-18141-1	547.2	149.2	7/89 8/92
Stanford University R. Bube Stanford, CA 94305	Ion and Photon-Assisted Growth and Doping of II-VI Compounds	9-18141-4	566.9	136.9	7/89 8/92

Contractor, Principal Investigator, Address	Work Title (Research Activity)	Contract Number	Total Funding (\$K)	FY 1992 Funding (\$K)	Start/End Dates
No. Carolina St. Univ. G. Lucovsky Raleigh, NC 27695	Fundamental Studies of Defect Generation a-Si Alloys Grown by Remote Plasma-enhanced CVD	9-18141-2	438.9	105.5	7/89 12/92
Univ. of Utah C. Taylor 309 Park Bldg. Salt Lake City, UT 84112	Electronic Processes in Thin Film PV Materials	9-18141-3	570.4	136.1	7/89 12/92
PHOTOVOLTAIC MANUFACTURING TECHNOLOGY FY1992					
Entech, Inc. W. Hesse Dallas-Ft. Worth Airport TX 74261	Improvements for ENTECH's Concentrator Module	2-11040-4	1914.3	1276.2	2/92 5/94
Solarex Corp. R. Oswald Newtown, PA 18940	Large Area Triple Junction a-Si Alloy Production Scale-up Project	2-11040-2	1680.2	1120.2	3/92 6/95
Mobil Solar Energy Corp. B. Gillespie Billerica, MA 01821	Thin EFG Octagons	2-11040-3	1294.9	1294.9	4/92 6/95
RTI R. Whisnant R.T. Park, NC 277709	PV Mat Cost Analysis Support	1-11039-1	49.5	49.5	3/91 11/91
Siemens Solar C. Gay Camarillo, CA 93011	PV Manufacturing Technology Phase 2A	2-11040-1	810.0	810.0	3/92 11/94
Astropower, Inc. C. Keith Newark, DE 19716	PV Manufacturing Silicon Film Technology	2-11040-5	1559.9	1559.9	1/92 4/95
Utility Power Group G. Duran Princeton, NJ 08543	a-Si PV Manufacturing Technology Phase 2A	2-11040-6	521.0	521.0	4/92 7/92
E.C.D. Inc. M. Izu Troy, MI 48084	Continuous Roll-to-Roll a-Si PV Manufacturing Technology	2-11040-7	412.3	412.3	4/92 7/92
PV MODULE & SYSTEMS PROJECT					
Florida Energy Center K. Collier Orlando, FL 32816	Evaluation of Roof-Integrated PV Modules Designs & Systems	2-12002-1	49.9	49.9	11/91 5/92

Contractor, Principal Investigator, Address	Work Title (Research Activity)	Contract Number	Total Funding (\$K)	FY 1992 Funding (\$K)	Start/End Dates
SUNY R. Perez Albany, NY 12201	Solar Resource Utility Load Matching Assessment	1-11168-1	106.3	106.3	9/91 3/93
N.M. State Univ. S. Durand Las Cruces, NM 88003	Long Term Environmental Effects on Roof-Mounted Photovoltaics Modules	2-12014-1	50.0	50.0	2/92 1/94
SEIA R. Cline Washington DC 20002	Man and Admin of the IEC/PV/TEC-82 Secratariat and Part. Int'l Stds. Dev.	2-12006-9	45.0	45.0	7/92 11/92
Solar Cells Inc. J. Nolan Toledo, OH 43615	One Kilowatt Photovoltaic System	2-12262-1	15.6	15.6	6/92 12/92
United Solar Sys. Corp L. Slominski Troy, MI 48084	1.8 Kilowatt PV System of a-Si Dual Junction Modules	2-12074-1	20.8	20.8	5/92 8/92
ECD I. Masatsugu Troy, MI 48084	a-Si Utility/Industry Photovoltaic Power Project	2-11061-1	150.0	150.0	7/92 5/94
ANALYSIS & APPLICATIONS					
Univ. of Delaware J. Byrne Newark, DE 19616	Evaluation of DSM Incentive Opportunities for PV	2-11248-1	27.2	27.2	9/92 12/92
Atmos. Sci. Rsch. Cntr Richard Perez State Univ of NY Albany, NY 12222	Solar Resource, Utility Load Matching Assessment	XR-11168-1	106.3	106.3	9/91 9/93



## FY 1992 PV Bibliography

- Albright, S. (November 1991). "Final Report for Photovoltaic Manufacturing Technology Phase I, Final Subcontract Report, 9 January 1991 - 14 April 1991." SERI/TP-214-4569. 15 pp. Work performed by Photon Energy, Inc., El Paso, Texas. Available NTIS: Order No. DE91015032.
- Albright, S.; Ackerman, B.; Chamberlin, R.; Jordan, J. (April 1992). "Module Process Optimization and Device Efficiency Improvement for Stable, Low-Cost, Large Area Cadmium Telluride-Based PV Module Production, Annual Subcontract Report, 1 July 1990 - 31 December 1991." SERI/TP-413-4873. 51 pp. Work performed by Photon Energy Inc., El Paso, Texas. Available NTIS: Order No. DE92010564.
- Banerjee, A.; Chen, E.; Clough, R.; Glatfelter, T.; Guha, S.; Hammond, G.; Hopson, M.; Jackett, N.; Lycette, M.; Noch, J. (April 1992). "Research on Stable, High-Efficiency Amorphous Silicon Multijunction Modules, Annual Subcontract Report, 1 January 1991 - 31 December 1991." SERI/TP-411-4840. 83 pp. Work performed by United Solar Systems Corporation, Troy, Michigan. Available NTIS: Order No. DE92001244.
- Baron, B. N.; Birkmire, R. W.; Phillips, J. E.; Shafarman, W. N.; Hegedus, S. S.; McCandless, B. E. (November 1991). "Polycrystalline Thin Film Materials and Devices, Annual Subcontract Report, 16 January 1990 - 15 January 1991." SERI/TP-214-4502. 73 pp. Work performed by Institute of Energy Conversion, University of Delaware, Newark, Delaware. Available NTIS: Order No. DE92001171.
- Birkmire, R. W.; McCandless, B. E.; Yokimcus, T. A.; Mondal, A. (October 1992). *Novel Ways of Depositing ZnTe Films by a Solution Growth Technique, Final Subcontract Report, 1 January 1990 - 1 January 1992.* SERI/TP-410-4959. 78 pp. Work performed by Institute of Energy Conversion, University of Delaware, Newark, Delaware. Available NTIS: Order No. DE92010591.
- Bottenberg, W. R. (November 1991). "Photovoltaic Manufacturing Technology: Phase I, Final Subcontract Report, 9 January 1991 - 14 April 1991." SERI/TP-214-4568. 20 pp. Work performed by AstroPower, Inc., Newark, Delaware. Available NTIS: Order No. DE91015031.
- Brown, S.; Shen, D. S.; Heeke, N. (November 1991). "Photovoltaic Manufacturing Technology - Phase I, Final Subcontract Report, 9 January 1991 - 14 April 1991." SERI/TP-214-4489. 60 pp. Work performed by Glasstech Solar, Inc., Golden, Colorado. Available NTIS: Order No. DE91015025.
- Brown, J. (November 1991). "Final Technical Report, Phase I, Photovoltaic Manufacturing Technology, Final Subcontract Report, 9 January 1991 - 14 April 1991." SERI/TP-214-4478. 49 pp. Work performed by Solar Cells, Inc., Toledo, Texas. Available NTIS: Order No. DE91015027.
- Catalano, A.; Bennett, M.; Chen, L.; D'Aiello, R.; Fieselmann, B.; Li, Y.; Newton, J.; Podlesny, R.; Yang, L. (August 1992). *Research on Stable, High-Efficiency, Amorphous Silicon Multijunction Modules, Annual Subcontract Report, 1 May 1991-30 April 1992.* SERI/TP-411-4995. 56 pp. Work performed by Solarex Thin Film Division, Newtown,

- Pennsylvania. Available NTIS: Order No. DE92010599.
- Catalano, A. (April 1992) "Recent Advances in a-Si:H Alloy Multi-junction Devices." *Solar Energy Materials* 23, pp. 248-255, Elsevier Science Publishers. Work performed by Solarex Corporation, Thin Films Division.
- Catalano, A.; Arya, R.; Carr, L.; Fieselmann, B.; Lommasson, T.; Podlesny, R.; Russell, L.; Skibo, S.; Rothwarf, A.; Birkmire, R. (May 1992). "Research on Polycrystalline Thin Film Submodules Based on CuInSe<sub>2</sub> Materials, Annual Subcontract Report, 11 November 1990 - 31 October 1991." SERI/TP-413-4906. 72 pp. Work performed by Solarex Corporation, Newtown, Pennsylvania. Available NTIS: Order No. DE92010584.
- Chu, T. L. (April 1992). "Thin Film Cadmium Telluride, Zinc Telluride, and Mercury Zinc Telluride Solar Cells, Final Subcontract Report, 1 July 1988 - 31 December 1991." SERI/TP-413-4791. 96 pp. Work performed by University of South Florida, Tampa, Florida. Available NTIS: Order No. DE92001237.
- Chu, T.L.; Chu, S.S.; Britt, J.; Ferekides, C.; Wang, C.; Wu, C.Q.; Ullal, H.S. (May 1992) "14.6% Efficient Thin-Film Cadmium Telluride Heterojunction Solar Cells." *IEEE Electron Device Letters*, Volume 13, Number 5, p. 303.
- Cohen, J. D. (July 1992). *Microscopic Origins of Metastable Effects in a-Si:H and Deep Defect Characterization in a-Si,Ge:H Alloys, Annual Subcontract Report, 1 February 1991 - 31 January 1992.* SERI/TP-451-4938. 26 pp. Available NTIS: Order No. DE92010588.
- Compaan, A. D.; Bohn, R. G. (April 1992). "Thin Film Cadmium Telluride Photovoltaic Cells, Annual Subcontract Report, 23 July 1990-31 October 1991." SERI/TP-451-4797. 41 pp. Work performed by the University of Toledo, Toledo, Ohio. Available NTIS: Order No. DE92001239.
- Crandall, R. S.; Nelson, B. P.; Moskowitz, P. D.; Fthenakis, V. M. (July 1992). *Safety Analysis Report For the Use of Hazardous Production Materials in Photovoltaic Applications at the National Renewable Energy Laboratory.* SERI/MP-451-4778-A. 167 pp. Available NTIS: Order No. DE92001218.
- Crandall, R. S.; Nelson, B. P.; Moskowitz, P. D.; Fthenakis, V. M. (July 1992). *Safety Analysis Report for the Use of Hazardous Production Materials in Photovoltaic Applications at the National Renewable Energy Laboratory, Volume II: Appendices.* SERI/MP-451-4778-B. 247 pp. Available NTIS: Order No. DE92001218.
- Emery, K.A. "Efficiency Measurements of Photovoltaic Devices", Chapter 3, *Advances in Solar Energy*, 1992..
- Gabor, A.; Hermann, A. (September 1992). *Novel Thin-Film CuInSe<sub>2</sub> Fabrication, Annual Subcontract Report, 1 May 1991 - 30 April 1992.* SERI/TP-451-5014. 19 pp. Work performed by University of Colorado, Boulder, Colorado. Available NTIS: Order No. DE92016440.



- Gale, R. (June 1992). "Advanced High Efficiency Concentrator Cells, Final Subcontract Report, 1 October 1988 - 31 March 1990." SERI/TP-451-4855. Work performed by Varian Research Center, Palo Alto, California. Available NTIS: Order No. DE92010559.
- Gray, J. L.; Schwartz, R. J.; Lee, Y. J. (September 1992) *Development of a Computer Model for Polycrystalline Thin-Film CuInSe<sub>2</sub> and CdTe Solar Cells, Final Subcontract Report: 1 January 1991-31 December 1991.* NREL/TP-413-5092. Work performed by Purdue University, West Lafayette, IN under Subcontract No. XN-0-10013-1.
- Gray, J. L.; Schwartz, R. J.; Lee, Y. J. (April 1992). "Development on the Development of a Computer Model for Polycrystalline Thin-Film CuInSe<sub>2</sub> and CdTe Solar Cells, Annual Subcontract Report, 1 January 1990 - 31 December 1990." SERI/TP-413-4835. 40 pp. Work performed by Purdue University, West Lafayette, Indiana. Available NTIS: Order No. DE92001242.
- Guha, S. (December 1991). "Research on Stable, High-Efficiency Amorphous Silicon Multijunction Modules, Semiannual Subcontract Report, 1 January 1990 - 30 June 1991." SERI/TP-214-4453. 83 pp. Work performed by United Solar Systems Corporation, Troy, Michigan. Available NTIS: Order No. DE92001197.
- Hogan, S. (November 1991). "Photovoltaic Manufacturing Technology Program, Final Subcontract Report, 9 January 1991 - 14 April 1991." SERI/TP-214-4476. 37 pp. Work performed by Spire Corporation, Bedford, Massachusetts. Available NTIS: Order No. DE91015026.
- Jester, T.; Eberspacher, C. (November 1991). "Research on Advanced Photovoltaic Manufacturing Technology, Final Subcontract Report, 1 March 1991 - 4 June 1991." SERI/TP-214-4481. 45 pp. Work performed by Siemens Solar Industries, Camarillo, California. Available NTIS: Order No. DE92001153.
- Kaminar, H.; McEntee, J.; Curchod, D. (November 1991). "Cost Effective Manufacturing of the SEA 10X Concentrator Array, Final Subcontract Report, 9 January 1991 - 14 April 1991." SERI/TP-214-4479. 103 pp. Work performed by Solar Engineering Application Corporation, San Jose, California. Available NTIS: Order No. DE92001151.
- Li, Y.M.; Dawson, R.M.; Collins, R.W.; Wronski, C.R.; Wiedeman, S. (November 1991) "Effect of Surface Recombination on the Spectral Dependence of Photocurrent in Intrinsic Hydrogenated Amorphous Silicon Films." *Applied Physics Letters*, 59(20), p. 2549.
- Luft, W.; Stafford, B.; von Roedern, B.; DeBlasio, R. (1992) "Prospects for Amorphous Silicon Photovoltaics." *Solar Energy Materials and Solar Cells* 26, pp. 17-26, Elsevier Science Publishers.
- Luft, W.; Stafford, B.; von Roedern, B. (May 1992). "Perspective on Photovoltaic Amorphous Silicon." SERI/TP-411-4796. 9 pp. Prepared for the PVAR&D Conference, Denver, Colorado. Available NTIS: Order No. DE92010581.
- Luft, W.; Stafford, B.; von Roedern, B. (November 1991) "The United States Photovoltaic Amorphous Silicon Program: Stabilized Module Performance." *Int. J. Solar Energy*, Vol. 10, pp. 175-183.

- Mitchell, R. L.; Witt, C. E.; Mooney, G. D. (December 1991). "Photovoltaic Manufacturing Technology Project: A Government/Industry Partnership." SERI/TP-214-4588. 7 pp. Prepared for the 1992 ASME International Solar Energy Conference, 4-8 April 1992, Maui, Hawaii. Available NTIS: Order No. DE92001194.
- Mitchell, R. L.; Zweibel, K.; Ullal, H. S. (December 1991). "Polycrystalline Thin-Film Technology: Recent Progress in Photovoltaics." SERI/TP-214-4589. 7 pp. Prepared for the 1992 ASME International Solar Energy Conference, 4-8 April 1992, Maui, Hawaii. Available NTIS: Order No. DE92001195.
- Mooney, G.D.; Hermann, A.M. (March 1992) "Novel Thin-Film CuInSe<sub>2</sub> Fabrication, Annual Subcontract Report, 1 March 1990 - 30 April 1991." TP-411-4752. Work performed by the University of Colorado.
- Nicolet, M.-A. (October 1991). "Investigations of CuInSe<sub>2</sub> Thin Films and Contacts." SERI/TP-214-4433. 13 pp. Work performed at California Institute of Technology, Pasadena, California. Available NTIS: Order No. DE91002192.
- Nolan, J. F.; Meyers, P. V. (September 1992). *Fabrication of Stable, Large-Area, Thin-Film CdTe Photovoltaic Modules, Annual Subcontract Report, 10 May 1991 - 9 May 1992.* SERI/TP-413-5011. 20 pp. Work performed by Solar Cells, Inc., Toledo, Ohio. Available NTIS: Order No. DE92016445.
- NREL Photovoltaic Subcontract Reports: Abstracts and Document Control Information, 1 August 1991 - 31 July 1992.* (August 1992). SERI/TP-410-5008. 61 pp. Available NTIS: Order No. DE92016408.
- NREL Preprints for the 22nd IEEE Photovoltaic Specialists Conference.* (October 1991). SERI/TP-210-4567. 173 pp. Available NTIS: Order No. DE92001154.
- O'Neill, M. J.; McDanal, A. J.; Perry, J. L.; Jackson, M. C.; Walters, R. R. (November 1991). "Photovoltaic Manufacturing Technology (PVMaT) Improvements for ENTECH's Concentrator Module, Final Technical Report, 9 January 1991 - 14 April 1991." SERI/TP-214-4486. 33 pp. Work performed by ENTECH, Inc., DFW Airport, Texas. Available NTIS: Order No. DE92001170.
- Perry, A. J.; Sartwell, B. D.; Valvoda, F.; Rafaja, D.; Williamson, D. L.; and Nelson, A. J. (1992). "Residual Stress and the Effect of Implanted Argon in Films of Zirconium Nitride Made by Physical Vapor Deposition." *Journal of Vacuum Science Technology*, A10(4), p. 1446.
- Photovoltaic Advanced Research and Development Project, Technical Summary Report - June 1992.* (July 1992). SERI/MP-410-5003. 46 pp. Document improperly shows document number as NREL/MP-410-4967, which is the correct number for the May, 1992 Technical Summary Report.
- Photovoltaic Manufacturing Technology Project: Phase I, Subcontractors.* (July 1992). SERI/MK-411-4973. 10 pp Available NTIS: Order No. DE92010597.
- Photovoltaic Advanced Research and Development Project, Technical Summary Report, April 1992.*

- (May 1992). SERI/MP-410-4929. 39 pp.
- Photovoltaic Advanced Research and Development Project, Technical Summary Report, March 1992.* (April 1992). SERI/MP-410-4870. 45 pp.
- PVMaT, History and Current Status - July 1992.* (July 1992). SERI/MK-411-4974. 2 pp. Available NTIS: Order No. DE92010596.
- Rand, J. A.; Bacon, C.; Cotter, J. E.; Lampros, T. H.; Ingram, A. E.; Ruffins, T. R.; Hall, R. B.; Barnett, A. M. (July 1992). *Development of Large-Area Monolithically Integrated Silicon-Film Photovoltaic Modules, Annual Subcontract Report, 1 May 1991 - 15 November 1991.* SERI/TP-413-4996. 25 pp. Work performed by AstroPower, Inc., Newark, Delaware. Available NTIS: Order No. DE92010600.
- Recycling of Cadmium and Selenium from Photovoltaic Modules and Manufacturing Wastes: A Workshop Report.* (September 1992) P.D. Moskowitz and K. Zweibel, Editors. March 11-12, 1992. Published by Brookhaven National Laboratory, Upton, Long Island, New York.
- Rozgonyi, G. A.; Shimura, F.; Buczkowski, A.; Zhon, T.-Q. (December 1991). "Effectiveness and Stability of Impurity/Defect Interactions and Their Impact on Minority Carrier Lifetime, Annual Subcontract Report, 1 August 1990 - 31 July 1991." SERI/TP-214-4503. 61 pp. Work performed by North Carolina State University, Raleigh, North Carolina. Available NTIS: Order No. DE92001172.
- Saifee, S. T.; Konnerth, A., III (November 1991). "Low-Cost Manufacturing of the Point Focus Concentrating Modules and Its Key Component, the Fresnel Lens, Final Subcontract Report, 31 January 1991 - 6 May 1991." SERI/TP-214-4477. 97 pp. Work performed by Solar Kinetics, Inc., Dallas, Texas. Available NTIS: Order No. DE91015028.
- Schiff, E. A.; Antoniadis, H.; Lee, J.-K.; Wang, Q. (April 1992). "Research on Defects and Transport in Amorphous Silicon-Based Semiconductors, Annual Subcontract Report, 20 February 1991 - 19 February 1992." SERI/TP-451-4751. 22 pp. Work performed by Syracuse University, Syracuse, New York. Available NTIS: Order No. DE92001223.
- Schmid, F. (December 1991). "Development of a Fixed Abrasive Slicing Technique (FAST) for Reducing Cost of Photovoltaic Wafers, Final Subcontract Report, 9 January 1991 - 14 April 1991." SERI/TP-214-4485. 64 pp. Work performed by Crystal Systems, Inc., Salem, Massachusetts. Available NTIS: Order No. DE92001165.
- Schmidt, E. (November 1991). "Improved Techniques for Manufacturing the Alpha Solarco Concentrating Photovoltaic System, Final Subcontract Report, 6 January 1991 - 14 April 1991." SERI/TP-214-4498. 36 pp. Available NTIS: Order No. DE91015029.
- SERI Photovoltaic Subcontract Reports: Abstracts and Document Control Information, 1 January - 31 July 1991.* (October 1991). SERI/TP-214-4459. 18 pp. Available NTIS: Order No. DE91015005.
- Silver, M. (July 1992). *Recombination and Metastability in Amorphous Silicon and Silicon Germanium Alloys, Annual Subcontract Report, 1 February 1991 - 31 January 1992.*

- SERI/TP-451-4962. 19 pp. Work performed by University of North Carolina, Chapel Hill, North Carolina. Available NTIS: Order No. DE92010593.
- Sites, J. R. (November 1991). "Role of Polycrystallinity in CdTe and CuInSe<sub>2</sub> Photovoltaic Cells, Annual Subcontract Report, 1 April 1990 - 31 March 1991." SERI/TP-214-4468. 27 pp. Work performed by Colorado State University, Fort Collins, Colorado. Available NTIS: Order No. DE92001168.
- Somberg, H. (November 1991). "Photovoltaics Manufacturing Technology Phase I, Final Subcontract Report, 9 January 1991 - 14 April 1991." SERI/TP-214-4480. 33 pp. Work performed by Global Photovoltaic Specialists, Inc., Canoga Park, California. Available NTIS: Order No. DE92001152.
- Stanbery, B. J. (November 1991). "Manufacturing Technology Development for CuInGaSe<sub>2</sub> Solar Cell Modules, Final Subcontract Report, 9 January 1991 - 14 April 1991." SERI/TP-214-4606. Work performed by Boeing Aerospace & Electronics, Seattle, Washington. Available NTIS: Order No. DE92001176.
- Technical Summary Report - November 1991.* (December 1991). SERI/TP-210-4663.
- Technical Summary Report - October 1991.* (November 1991). SERI/TP-210-4659.
- Technical Summary Report - September 1991.* (October 1991). SERI/MP-210-4584. 36 pp.
- Thakur, R.P.S.; Singh, R.; Nelson, A.J.; Swartzlander, A.B. (1991) "Role of in-situ Rapid Isothermal Processing in Advanced III-V Technology." *Journal of Applied Physics*, 70(7), p. 3857.
- Thornton, J. P. (November 1991). "PV-Related Utility Activities in Colorado." SERI/TP-210-4501. 4 pp.
- Ullal, H. S.; Stone, J. L.; Zweibel, K.; Surek, T. J.; Mitchell, R. L. (December 1991). "Polycrystalline Thin-Film Solar Cells and Modules." SERI/TP-214-4610. 7 pp. Prepared for the 6th International Photovoltaic Science & Engineering Conference, New Delhi, India, 10-14 February 1992. Available NTIS: Order No. DE92001196.
- Whisnant, R. A. (September 1992). *Cost Analysis Methodology Photovoltaic Manufacturing Technology Project, Annual Subcontract Report, 11 March 1991 - 11 November 1991.* SERI/TP-411-5017. 26 pp. Work performed by Research Triangle Institute, Research Triangle Park, North Carolina. Available NTIS: Order No. DE92016441.
- Zweibel, K. (April 1992). "Toward Low Cost CdTe PV." SERI/TP-413-4841. 7 pp. Submitted to the *International Journal of Solar Energy*. Available NTIS: Order No. DE92010552.

<b>Document Control Page</b>	1. NREL Report No. NREL/TP-410-5330	2. NTIS Accession No. DE92000092	3. Recipient's Accession No.
4. Title and Subtitle Annual Report, Photovoltaic Subcontract Program, FY 1992		5. Publication Date March 1993	
		6.	
7. Author(s) Photovoltaics Program, NREL		8. Performing Organization Rept. No.	
9. Performing Organization Name and Address National Renewable Energy Laboratory 1617 Cole Boulevard Golden, Colorado 80401-3393		10. Project/Task/Work Unit No. PV310101	
		11. Contract (C) or Grant (G) No.  (C)  (G)	
12. Sponsoring Organization Name and Address		13. Type of Report & Period Covered Technical report, Annual Progress Report	
		14.	
15. Supplementary Notes			
16. Abstract (Limit: 200 words)  This report summarizes the fiscal year (FY) 1992 (October 1, 1991, through September 30, 1992) progress of the subcontracted photovoltaic (PV) research and development (R&D) performed under the Photovoltaic Advanced Research and Development Project at the National Renewable Energy Laboratory (NREL)—formerly the Solar Energy Research Institute (SERI). The mission of the national PV program is to develop PV technology for large-scale generation of economically competitive electric power in the United States. The technical sections of the report cover the main areas of the subcontract program: the Crystalline Materials and Advanced Concepts project, the Polycrystalline Thin Films project, Amorphous Silicon Research project, the Photovoltaic Manufacturing Technology (PVMaT) project, PV Module and System Performance and Engineering project, and the PV Analysis and Applications Development project. Technical summaries of each of the subcontracted programs provide a discussion of approaches, major accomplishments in FY 1992, and future research directions.			
17. Document Analysis a. Descriptors photovoltaic cells ; amorphous materials ; silicon ; thin films ; deposition ; copper selenide ; cadmium telluride ; gallium arsenide ; efficiency ; semiconductor materials ; solar cells  b. Identifiers/Open-Ended Terms National Renewable Energy Laboratory  c. UC Categories 270			
18. Availability Statement National Technical Information Service U.S. Department of Commerce 5285 Port Royal Road Springfield, VA 22161		19. No. of Pages 349	
		20. Price A15	